Archean to present day evolution of the lithospheric mantle beneath the Kaapvaal craton -

Processes recorded in subcalcic garnets, peridotites and polymict breccia

Dissertation
zur Erlangung des Doktorgrades
der Naturwissenschaften

von
Marina Lazarov
aus Pancevo
(Serbien)

Frankfurt (Juni, 2008)

Archean to present day evolution of the lithospheric mantle beneath the Kaapvaal craton -

Processes recorded in subcalcic garnets, peridotites and polymict breccia

Dissertation
zur Erlangung des Doktorgrades
der Naturwissenschaften

Vorgelegt beim Fachbereich Geowissenschaften/Geographie
der Johann Wolfgang Goethe-Universität
in Frankfurt am Main

von
Marina Lazarov
aus Pancevo
(Serbien)

Frankfurt (Juni, 2008)

Von Fachbereich Geowissenschaften (FB: Mineralogie) der
Johann Wolfgang Goethe-Universität als Dissertation angenommen.

Dekan: Prof. Dr. G. P. Brey

Gutachter: Prof. Dr. G. P. Brey

Prof. Dr. A. B. Woodland

Prof. Dr. F.E. Brenker

Hon.-Prof. Dr. J. Harris

Datum der Disputation: 04. 08. 2008.

Table of contents

Zusammenfassung

Der Erdmantel unter dem Kaapvaal Kraton (Südafrika) hat eine über 3.6 Ga lange und komplexe Geschichte. Er ist zwar der am meisten untersuchte subkratonische Mantel, jedoch sind viele Fragen, bezüglich der Bildung und Modifizierung des Kaapvaal Kratons, immer noch offnen. Ziel dieser Arbeit ist es, die geodynamische, chemische und thermische Entwicklung des Kaapvaal Kratons zu rekonstruieren. Dazu sind 31 grobkörnige Peridotite und 21 einzelne subkalzische Granate aus Schwereminerallkonzentraten der Finsch-Mine, bezüglich ihrer Haupt- und Spurenelement-zusammensetzung und ihrer Lu-Hf und Sm-Nd Isotopensystematik, untersucht worden. Die Prozesse, die in Zusammenhang mit der Förderung von Peridotit-Xenolithen durch Kimberlitschmelzen stehen, sind an polymikten Brekzien untersucht geworden.

Eine kurze Einführung, über den heutigen Kenntnisstand zur Bildung und Modifizierung vom kratonischen Mantel, ist in **Kapitel 1** beschrieben. In diesem Kapitel sind des Weiteren der geologische und tektonische Hintergrund des Kaapvaal Kraton und eine kurze Einführung zur Entstehung von Kimberliten und Diamanten beschrieben. Eine detaillierte Beschreibung der analytischen Methoden, die in dieser Arbeit benutzt werden, bietet **Kapitel 2**. Die Entstehung von subkalzischen Granaten und deren Verhältnis zur Bildung von Diamanten ist im **Kapitel 3** diskutiert. Die petrographiche Beschreibung, Haupt- und Spurenelementkonzentrationen und -Verhältnisse der Finsch-Minerale und -Gesamtgesteine sind in **Kapitel 4** dargestellt. Im selben Kapitel werden auch die Berechnungen von Drücken und Temperaturen (mit Hilfe von Thermobarometrie), sowie der Sauerstofffugazitäten der Peridotite (berechnet aus den Gehalten an 3-wertigem Fe in Granat) diskutiert. Wie für die meisten Niedrigtemperatur-Peridotite vom Kaapvaal Kraton, so wurden auch für die hier untersuchten Finsch-Peridotite niedrige Mg/Si vorgefunden, was auf hohe Orthopyroxengehalte hindeutet. Dies wird ebenfalls in **Kapitel 4**, diskutiert, sowie lithologische Tiefenprofile des Kaapvaal Kratons. Des Weiteren bietet dieses Kapitel eine Diskussion über die Verteilung von Spurenelementen zwischen koexistierenden Mineralphasen. Die Menge an Schmelze, die aus den Peridotiten extrahiert wurde, wird mit Hilfe von Haupt- und Spurenelementgehalten der Finsch Peridotite (**Kapitel 4**) und der subkalzischen Granate (**Kapitel 3**), berechnet. Alle hier bearbeiteten Proben wurden an inkompatiblen Elementen angereichert. Mit Hilfe der Spurenelementmuster können Rückschlüsse über die Art der Anreicherung gezogen werden (**Kapitel 3, 4, 5**). Die Ereignisse, die zu einer partiellen Schmelzbildung im Kapvaal Kraton geführt haben, wurden mit dem Lu-Hf Isotopensystem und die Ereignisse metasomatischer Anreicherung mit dem Sm-Nd Isotopensystem datiert. Diese Datierungen wurden sowohl an subkalzischen Granaten (im **Kapitel 3),** als auch an den (berechneten) Gesamtgesteinen der Peridotite (in **Kapitel 5)** durchgeführt und ergeben ein konsistentes Bild über die Mantelentwicklung des Kaapvaal Kratons.

In polimikten Brekzien aus Kimberley, wurden „subrezente“ metasoamtische Prozesse in Form von Mineralungleichgewichten aufgezeichnet. Diese Ungleichgewichte, die beim Kontakt zwischen der kimberlitischen Schmelze mit den peridotitischen Mineralen entstanden sind, wurden mit Hilfe der Haupt- und Spurenelementgehalte der Minerale untersucht (K**apitel 6**). In diesem Kapitel wird ebenfalls der Mechanismus der Förderung der Xenolithe durch kimberlitische Schmelzen beschrieben.

1. Mantelprozesse – impliziert durch Untersuchungen von Peridotiten und subkalzischen Granaten aus der Finsch-Mine

Alle untersuchte Xenolithe, mit einer Ausnahme von Spinel Peridotit, sind granatführend. Die meisten der untersuchten Proben sind klinopyroxenführende Harzburgite. Dazu kommen vier Lherzolite und vier Dunite (zwei der Letzteren sind klinopyroxenführend und zwei sind klinopyroxenfrei). Nur ein Harzburgit ist klinopyroxenfrei. Ein granatführender Harzburgit ist Rutil- und Phentlanditführend. Sekundäre Minerale, wie z.B. Phlogopit, Amphibol, Klinopyroxen (Kpx) und Spinel, sind sehr selten und nur im Granat-Kelyphit zu finden. Nach der Klassifikation von Harte

(1977), haben die meisten der untersuchten Peridotite mittel- bis grobkörnige (d.h., relativ gleichkörnige) tabulare Texturen.

Minerale aus diesen Proben wurden bezüglich ihrer Haupt- und Spurenelementgehalte, sowie ihrer Lu-Hf und Sm-Nd Isotopensystematik, untersucht und die Ergebnisse werden im Zusammenhang von Bildung und Modifizierung des lithosphärischen Mantels diskutiert.

Die subkalzischen Granate sind durch niedrige Gehalte an Ca und variable Cr-Gehalte charakterisiert. Sie sind nur in Ca-untersättigten Duniten und Harzburgiten zu finden. Die subkalzischen Granate dominieren das Haupt- und Spurenelementbudget in diesen Gesteinen. Deswegen sind 21 subkalzische Granat aus Schwereminералkonzentraten der Finsch-Mine ebenfalls bezüglich ihrer Haupt- und Spurenelementgehalte, sowie der Lu-Hf und Sm-Nd-Isotopensystematik untersucht geworden, um Erkenntnisse über die Prozesse im Kaapvaal Kraton zu gewinnen.

Hauptelementgleichgewichte - Veränderungen im geothermischen Gradient und der Sauerstofffugazität

Der refraktäre Charakter alle Proben wird durch die generell hohen Mg# impliziert (Mg# = 100xMg/(Mg+Fe)): Olivin - Mg# = 91.2 bis 93.7, Orthopyroxen - Mg# = 92.3 bis 94.6, Klinopyroxen – Mg# = 91.8 bis 94.4, Granat – Mg# = 83.2 bis 87.1. Die subkalzische Granate weisen mit noch höheren Mg# (bis 91.9) und Cr# bis 34.3 (Cr# = 100xCr/(Cr+Al)) auf eine noch stärkere Verarmung hin. Die Minerale der meisten Proben haben auch niedrige Gehalte an magmaphilen Elementen (wie: TiO_2, CaO und Na_2O).

Die Minerale von allen Proben haben homogene Hauptelementgehalte. Ausnahmen bilden ein Dunit und ein Harzburgit, die zonierte Klinopyroxene haben. Die Zonierung ist auf die Ränder der Klinopyroxene beschränkt und drückt sich durch erhörte Gehalte von TiO_2, CaO, Mg# und niedrigeren Gehalten von Al_2O_3 und Na_2O aus. Diese Zonierung wurde vermutlich durch eine Reaktion mit dem Kimberlit verursacht.

Durch die Anwendung unterschiedlicher unabhängiger Thermometer wurde getestet, ob sich die Hauptelemente zwischen den Mineralen einer Probe im Gleichgewicht befinden. Innerhalb ihrer Fehler ergaben alle Thermobarometer für eine Probe und einen bestimmten Druck die gleiche Temperatur. Unterschiede können auf die unterschiedliche Kalibrierung der Methoden, beziehungsweise der Vernachlässigung von Fe^{3+}-Gehalten in Mineralen (für die Thermometer, die Mg-Fe Austausch betrachten: T_{Krogh} - Krogh, 1988; $T_{O'Neill}$ - O'Neill and Wood, 1979; T_{Harley} - Harley, 1984) erklärt werden. Das heißt, alle Proben befinden sich bezüglich ihrer Hauptelemente im Gleichgewicht.

Die P-T Bedingungen für Lherzolite und klinopyroxenführende Harzburgite wurden mit dem zwei-Pyroxen Thermometer (T_{BKN} - Brey and Köhler, 1990) und mit dem Granat-Orthopyroxen Barometer (P_{BKN} - Brey and Köhler, 1990) berechnet (Abb. 1). Die P-T Bedingungen der Peridotite ohne Kpx wurden mit dem selbem Barometer und mit dem Granat-Olivin, Fe-Mg Austauschthermometer $T_{O'Neill}$ (O'Neill and Wood, 1979) berechnet. Bei letzteren wurden jedoch nur bei drei Proben die Fe^{3+}-Gehalte mit Mössbauer Spektroskopie bestimmt und bei der Temperaturberechnung entsprechend berücksichtigt (gelbe Quadrate in Abb. 1).

Alle Peridotite kommen aus einem beschränkten Druck- und Temperaturbereich (von 5-6.5 GPa und 1050-1250 °C, Abb. 1). Sie liegen auf dem geothermischen Gradient von 40 mW/m^2 (Chapman and Pollack, 1977) und somit bei niedrigeren Temperaturen als der Kalahari Geotherm (gestrichelte Linie in Abb. 1 - Rudnick and Nayblade, 1999). Auf letzterem liegen die hochtemperierten gescherten Peridotite von Kimberley und Lesotho.

Mössbauer Analysen von Granaten aus Finsch-Peridotiten ergeben einen Bereich für $Fe^{3+}/\Sigma Fe$ von 0.04 to 0.078. Obwohl diese Peridotite aus einem relativ konstanten P-T Bereich stammen, zeigen sie eine große Variabilität in ihrer Sauerstofffugazität ($\Delta \log fO_2$ auf [FMQ]) von -2.5 bis -5.3; Abb. 2). Bei allen Peridotiten ist eine negative Korrelation von Sauerstofffugazität und Druck zu beobachten. Von insgesamt fünf Proben mit leicht höherer Sauerstofffugazität, ist eine der rutilführende Harzburgit (F-12) und die andere, die Probe mit den zonierten Klinopyroxenen (F-3). Diese Finsch-Proben überlappen mit dem hochtemperierten „gescherten" Peridotiten von Lesotho und Kimberley (Woodland and Koch, 2003) (Abb. 2).

Wahrscheinlich führten bestimmte metasomatische Prozessen, im Zusammenhang mit der Anreicherung von Ti und Fe (Probe mit Rutil) oder Reaktionen mit den Kimberliten, zu einer lokalen

Oxidation im Erdmantel. Ähnliche Prozesse führten vermutlich auch zur Genese der „gescherten“ Peridotite, verbunden mit einer Erhöhung des geothermischen Gradienten und lokaler Oxidation des Mantels. Da die Finsch-Peridotite generell diese Merkmale nicht aufweisen, kann man daraus schließen, dass der gesamte lithosphärische Erdmantel des Kaapvaal Kratons vor der Finsch-Kimberliteruption (~ 118 Ma - Smith et al., 1985) auf dem geothermischen Gradienten von 40 mW/m^2 (Chapman und Pollack, 1977) lag und eine negative Korrelation von Sauerstofffugazität und Druck aufwies. Das heißt, die Genese der gescherten Peridotite von Kimberley und Lesotho hat vermutlich nach der Kimberliteruption von Finsch stattgefunden.

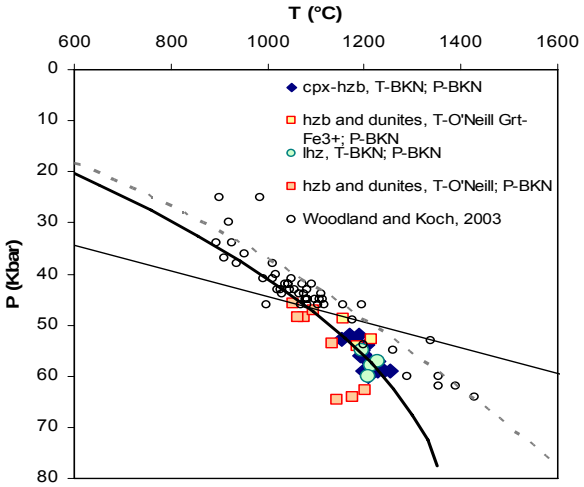

Abb. 1. Die Peridotite von Finsch plotten entlang eines konduktiven geothermischen Gradienten von 40mW/m^2 nach Chapman und Pollack (1977). Die Kalahari Geotherme (Rudnick and Nyblade, 1999) ist mit der gestrickten Linie dargestellt. Die Peridotite aus Lesotho und Kimberley (Woodland und Koch, 2003) sind ebenfalls zum Vergleich dargestellt.

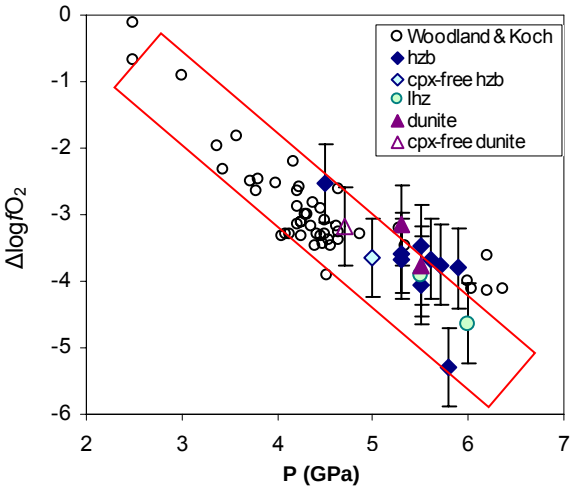

Abb. 2. Variation in Finsch Peridotiten zwischen der Sauerstofffugazität ($\Delta \log fO^2$) und dem Druck (GPa).

Gleichgewicht und Ungleichgewicht von Spurenelementen zwischen Granat und Klinopyroxen und deren Einfluss auf die Nd- und Hf Isotopensysteme

Alle analysierte Minerale aus den Finsch-Peridotiten sind homogen bezüglich ihrer Spurenelemente. Die starken Variationen zwischen den Proben reflektieren die komplexe Geschichte der Peridotite und des subkratonischen Mantels. Die Spurenelementverteilung hängt vom Druck, der Temperatur und der chemische Zusammensetzung der Mineralphasen ab. Die Verteilung der Spurenelemente, sowohl zwischen Granat und Orthopyroxen (Opx) als auch zwischen Granat und Kpx ist, in Übereinstimmung mit der Literatur, von Druck und Temperatur abhängig. Jedoch zeigt die Verteilung der Spurenelemente zwischen Granat und Kpx vor allem eine starke Abhängigkeit vom Cr-Gehalt (Abb. 3), welche sich annähernd durch ein Polynom 2. Grades beschreiben lässt. Diese Korrelation mit dem Cr-Gehalt der Granate ist bei den leichten und mittleren Seltenen Erden (LREE und MREE) besonders stark ausgeprägt, während andere Elemente, wie z.B. Lu und Zr, deutlich stärker streuen. Möglicherweise hat sich für diese Elemente bei einigen Proben kein Gleichgewicht eingestellt, z.B. aufgrund geringer Mobilität und langsamerer inter-granularer Diffusion dieser Elemente, im Vergleich zu den LREE. Alternativ, könnten auch andere kristallchemische Abhängigkeiten, zusätzlich zu der Abhängigkeit vom Cr-Gehalt, bestehen.

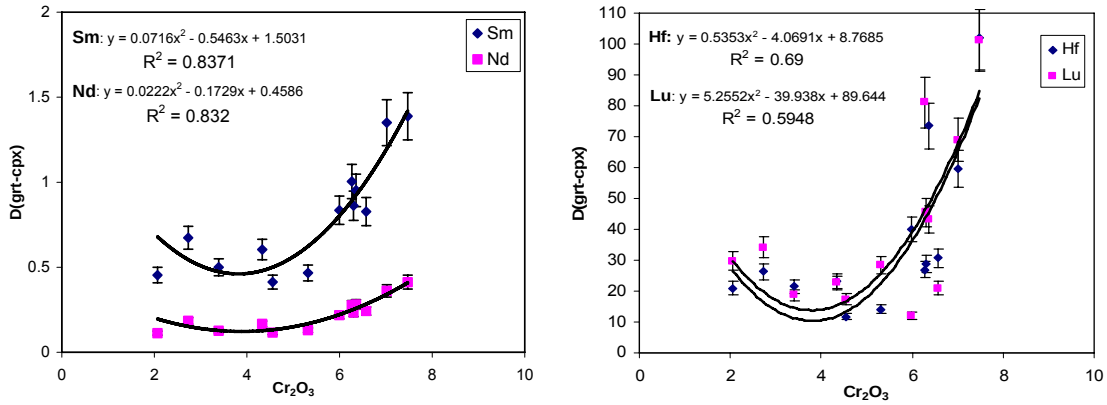

Abb. 3. Verteilung von Sm, Nd, Lu und 10xHf zwischen Granat und Klinopyroxen in Abhängigkeit vom Cr_2O_3-Gehalt (gew-%) in Granat. Die analytischen Fehler betragen ca. 10%.

Die Abhängigkeit der Spurenelementverteilung zwischen Granat und Kpx vom Cr-Gehalt im Granat könnte mit der Größe des Dodekaederplatzes im Zusammenhang stehen, welcher normalerweise von Ca besetzt wird (auch impliziert durch die gute Korrelation von Cr und Ca in Granaten). Die meisten Spurenelemente im Granat sitzen auf diesem Platz. Die Oktaederposition wird von Al belegt, das durch Cr substituiert werden kann. Da Cr einen deutlich größeren Ionenradius hat als Al, könnten hohe Cr-Gehalte die Granatstruktur insgesamt aufweiten, so dass auch auf die Dodekaederposition besser große Ionen passen.

Das etwas unterschiedliche Verhalten verschiedener Spurenelemente bezüglich der Verteilung zwischen Granat und Kpx drückt sich auch in Unterschieden in der Sm-Nd und Lu-Hf Isotopensystematik aus. Alle Sm-Nd Alter an Granat-Kpx Paaren ergeben das Alter der Kimberliteruption von Finsch (~ 118 Ma, Abb. 4). Dies impliziert Gleichgewicht der Spurenelemente (Sm und Nd) und Isotope zwischen den Mineralen. Dies ist für das Lu-Hf System nicht der Fall. Hier geben nur zwei Proben Kimberliteruptionsalter (innerhalb des Fehlers), während die anderen Proben höhere Alter von 180 Ma bis zu 522 Ma ergeben. Eine mögliche Erklärung hierfür mag sein, dass Lu und Hf zwischen Granat und Kpx nicht vollständig equilibriert sind. Dies wird auch durch die extrem variablen Verhältnisse der Lu- und Hf-Verteilungskoeffizienten (D_{Lu}/D_{Hf}) zwischen Granat und Kpx impliziert, während D_{Sm}/D_{Nd} innerhalb ± 10% konstant ist.

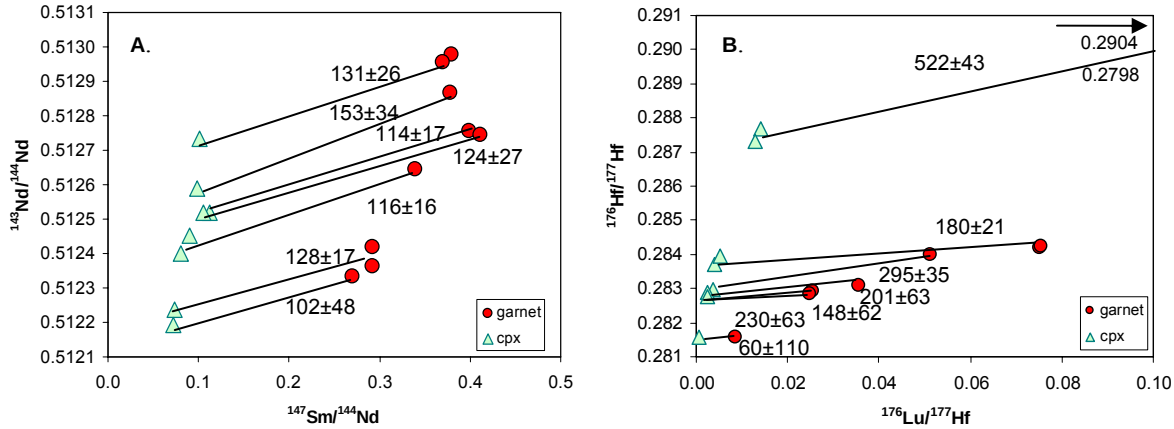

Abb. 4. Isochronendiagramm für Granat und Klinopyroxen Paare für: A. $^{143}Nd/^{144}Nd$ gegen $^{147}Sm/^{144}Nd$; und B. $^{176}Hf/^{177}Hf$ gegen $^{176}Lu/^{177}Hf$.

Datierung und Charakterisierung der partiellen Schmelzbildung im subkratonischen Mantel (von Finsch)

Die anhand von Mineralanalysen berechneten Gesamtgesteinszusammensetzungen wurden benutzt, um die Menge der partiellen Schmelzen zu berechnen. Das Modell von Takazawa et al.

(2000) basiert auf der FeO/MgO Verteilung zwischen Olivin und Schmelze und prognostiziert eine Verarmung der Finsch-Proben zwischen 10 und 48%. Der gleiche Bereich an Verarmung wurde hier durch das Modellieren der schweren Seltenen Erden (HREE) erhalten. Für die Lherzolithe ergibt sich 5 bis 10% Verarmung, während für die Dunite und einige Harzburgite mehr als 30% Verarmung berechnet wurden.

Die Zusammensetzung der subkalzischen Granate impliziert zwei Typen von Protolithen (aus denen die Granate stammen) mit einer unterschiedlichen Geschichte: Granate mit niedrigem C# und variablen und hohen $(Lu/Er)_N$ (= Gruppe-1 Granate) und solche mit variablen und hohen Cr# und niedrigen HREE (= Gruppe-2 Granate). Die Protolithe der Gruppe-2 Granate kann man am besten mit einer ersten Schmelzextraktion (von ca. 25%) bei niedrigem Druck und einer 2. Schmelzextraktion mit Granat im Residuum modellieren. Vermutlich haben auch die meisten der untersuchten Finsch-Peridotite diese beiden Schmelzbildungsereignisse erlebt. Die gesamte Schmelzextraktion kann dabei bis zu 45% betragen. Die Verarmung des Protolithen der Gruppe-1 Granate hat hingegen überwiegend im Granatstabilitätsfeld stattgefunden, jedoch auch in mindestens 2 verschiedenen Ereignissen.

Eine zweistufige Verarmungsgeschichte der subkalzischen Granate und Peridotite wird vor allem durch die Lu-Hf Isotopensystematik impliziert: Sowohl die Gruppe-1 Granate, als auch die Gesamtgesteine der Peridotit-Xenolithe ergeben Lu-Hf Isochronen von ca. 2.5 Ga (Abb. 5A und B). Diese Alter werden als das letzte Schmelzbildungsereignis interpretiert. Beide Isochronen haben positive Initialwerte (von +25ε und 16ε), relativ zum primitiven Mantel von vor 2.5 Ga. Dies deutet auf hohe Lu/Hf Verhältnisse und wenigstens ein Schmelzbildungsereignis einige Zeit vor dem vor 2.5 Ga hin, damit die radiogene Hf-Signatur entstehen kann. Dieses erste Schmelzbildungsereignis könnte vor ca. 3.6 Ga (Abb. 6) stattgefunden haben, aus folgenden Gründen: (i) Die Probe HMCF-Grt29 (der Ausreißer im Isochronendiagramm, Abb. 5B) ergibt ein Modelalter für eine einstufige Verarmung von 3.6 Ga. ii) ein Zeitraum von ca. 1 Ga mit hohen Lu/Hf Verhältnissen ist notwendig, um die radiogene Hf-Isotopie der subkalzischen Granate vor 2.5 Ga zu erklären. iii) Die ältesten Krustenalter des Kaapvaal Kratons liegen bei ca. 3.6 Ga (Kröner and Tegtmeyer, 1994; Kröner, et al., 1996).

Die Gesamtgesteine der Finsch-Peridotite haben etwas niedrigere Hf-Initialwerte (ca. +16 εHf), als die subkalzischen Granate. Dies könnte mit einer geringeren Verarmung der Peridotite beim ersten Schmelzereignis zusammenhängen. Alternativ, könnte die erste Verarmung der Peridotite auch später als die der subkalzischen Granate stattgefunden haben, oder multiple Schmelzbildungs- und Anreicherungsereignisse auf die Peridotite eingewirkt haben. Diese könnten in Zusammenhang mit wichtigen Krustenbildungsereignissen, z.B die Bildung granitischer Gneise vor ca. 3.2 Ga (Poujol et al., 2002; Schmitz et al., 2004) oder dem rhyolitischen und kalkalkalinen Vulkanismus vor ca. 2.9 Ga (Schmitz et al., 2004) stehen.

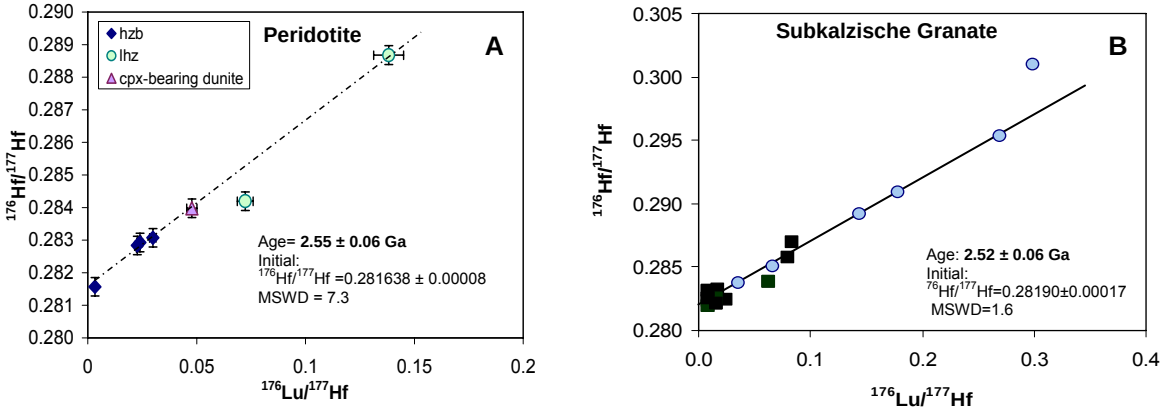

Abb. 5. $^{176}Hf/^{177}Hf$ gegen $^{176}Lu/^{177}Hf$ für: (A) Finsch Gesamtgesteine, die aus den Granat- und Kpx Isotopenzusammensetzungen berechnet wurden, und (B) Subkalzische Granate der Gruppe-1 (hellblaue Punkte). Sowohl die Gesamtgesteine als auch die Gruppe-1 Granate bilden eine Isochrone mit einem Alter von ca. 2.5 Ga (mit je einer Probe, die nicht auf der Isochrone liegt). Die Fehlerbalken in (A) berücksichtigen den möglichen Effekt von Opx bei der Gesamtgesteinsberechnung. Die analytischen Fehler in (A) und (B) liegen innerhalb der Symbolgröße.

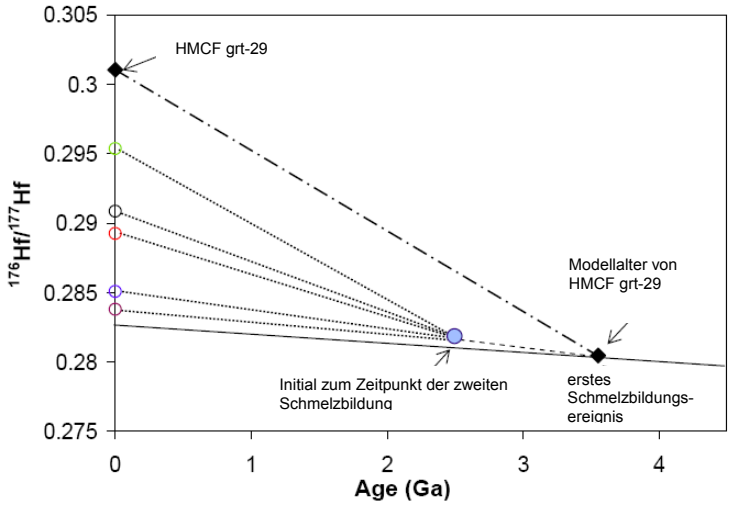

Fig. 7. Hf-Entwicklungsdiagramm für die subkalzischen Granate der Gruppe-1. Die heutigen $^{176}Hf/^{177}Hf$ Verhältnisse sind mit dem Initial der Isochrone (hellblauer Punkt) mit gepunkteten Linien verbunden. Dieses liegt 25 εHf oberhalb des $^{176}Hf/^{177}Hf$ Wertes des primitiven Mantels vor 2.5 Ga. Dies impliziert ein vorheriges Schmelzbildungsereignis für die Protolithe der Gruppe-1 Granate. Dieses könnte vor ca. 3.6 Ga stattgefunden haben, was dem Modellalter der Probe HMCF Grt-29 (schwarzes Karo, die heutige Zusammensetzung ist mit der auf den primitiven Mantel zurückgerechneten mit einer Strich-Punkt-Linie verbunden) entspräche. Die gestrichelte Linie repräsentiert die $^{176}Hf/^{177}Hf$ Entwicklung des Kaapvaal Mantels nach der ersten Schmelzbildung.

Anreicherung von Silizium in den Finsch Peridotiten

Wie die meisten Peridotite des Kaapvaal Kratons, so zeigen auch die meisten Peridotite von Finsch niedrige Olivingehalte relativ zu den gemessenen hohen Werte für Mg#. Deswegen liegen auch die Finsch-Peridotite oberhalb des „Ozeanische Trends“ (Boyd, 1989). Das bedeutet, dass die Peridotite eine Si-Anreicherung erfahren haben und hohe Anteile an Ortopyroxenen besitzen.

Dies kann nicht durch einen Prozess von „Partieller Schmelzbildung“ erklärt werden und eine Reihe von alternativen Modellen wurde bereits entwickelt (Kesson and Ringwood, 1989; Keleman et al., 1992; Herzberg, 1993; Herzberg, 1999; Boyd, 1997; Keleman et al., 1998; Rudnick et al., 1994; Bell et al., 2005; Simon et al., 2007).

Einige Modelle wurden an den Finsch-Peridotiten getestet, unter ihnen die populärste Theorie, die Anreicherung mit einem Si-reichen Fluid (Rudnick et al., 1994; Bell et al., 2005; Simon et al., 2007). Eine solche Anreicherung würde jedoch negative Y und HFSE Anomalien und hohe Gehalte an LILE und LREE produzieren, was nicht in den untersuchten Finsch-Peridotiten beobachtet wurde. Daher müssen andere Prozesse für die Opx-Anreicherung in Betracht gezogen werden. Dies könnten „metamorphe Entmischung (Boyd, 1997) oder kummulative Opx-Anreicherung sein (Herzberg, 1993; Herzberg, 1999, siehe auch die Diskussion in Walter, 1999). Der wahrscheinlichste Prozess bei den Finsch-Peridotiten ist jedoch die Metasomatose mit einer Si-reichen Schmelze.

Datierung und Charakterisierung der metasomatischen Anreicherung von inkompatiblen Elementen

Die sehr variablen Spurenelementgehalte und Hf-Nd Isotopensignaturen der Finsch-Peridotite und subkalzischen Granate deuten auf verschiedene metasomatische Ereignisse zu unterschiedliche Zeiten hin. Peridotite und subkalzische Granate mit niedrigen (positiven oder negativen) εHf- und negativen εNd-Werten, welche mit hohen Gehalten an LILE, LREE und Th gekoppelt sind, deuten auf eine Metasomatose mit einer karbonatitischen oder Si-reichen Schmelze hin. Proben mit sehr negativem εHf und nur leicht negativem εNd und geringfügig angereicherten LILE, LREE aber hohen Gehalten an HFSE, deuten auf eine metasomatische Anreicherung mit einer kimberlitischen Schmelze hin. Die

rutilführende Probe (F-12) mit ihren hohen Gehalten an HFSE und erhöhten Konzentrationen von LILE und LREE ist die einzige in ihrem Modalbestand angereicherte Probe der untersuchten Suite. Die Anreicherung erhöhte den Hf-Gehalt dieser Probe (Abb. 7), was auf eine Fe-Ti-reiche Kimberlitschmelze hindeutet, welche sich in Anwesenheit von Granat im Residuum gebildet hat. Eine weitere Signatur metasomatischer Anreicherung ist in den subkalzischen Granaten der Gruppe-1 aufgezeichnet. Hier weisen hohe Gehalte an LREE und deutlich negative εNd Werte, gekoppelt mit niedrigen Gehalten an HFSE und z.T. extrem positiven εHf-Werten, eindeutig auf eine Anreicherung durch ein Fluid hin, welches vermutlich aus subduzierter Ozeankruste stammt.

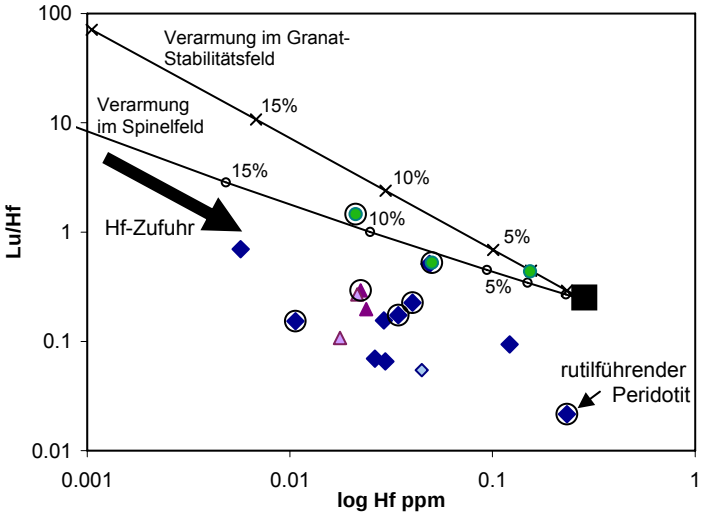

Abb. 7. Lu/Hf Verhältnisse gegen die Hf-Konzentration der Finsch-Peridotite (Gesamtgesteine). Die Linien stellen Modellierungen von nicht-modaler fraktionierender Schmelzbildung (1-20%) eines primitiven Mantels (= schwarzes Quadrat) bei niedrigen Drücken (untere Linie mit Kreisen) und bei hohen Drücken (obere Linie mit Kreuzen) dar. Die Modellierung zeigt, dass alle Harzburgite und Dunite mit Hf (die Richtung der Hf-Anreicherung ist mit dem fetten schwarzen Pfeil angedeutet) oder mit Lu und Hf angereichert wurden. Die höchste Anreicherung an Hf wurde in dem rutilführenden Peridotit beobachtet. Von den sieben eingekreisten Proben wurde auch die Hf- und Nd Isotopie in Granat und Kpx gemessen und von diesen Proben wurde das Lu-Hf Gesamtgesteinsalter bestimmt.

Die Lu/Hf Verhältnisse und Hf-Konzentrationen der Finsch-Peridotite (Abb. 7) zeigen, dass alle Proben Hf-Anreicherung erfahren haben. Dennoch bilden fünf der sieben Proben (eingekreiste Proben Abb. 7) eine Lu-Hf Isochrone (Abb. 5A). Drei dieser Proben haben sogar subchondritische Lu/Hf Verhältnisse und sehr unradiogene $^{176}Hf/^{177}Hf$ Isotopenverhältnisse. Dies impliziert, dass die Proben entweder vor, oder während der letzten vollständigen Reequilibrierung durch partielle Schmelzbildung vor 2.5 Ga, im Zuge der endgültigen Stabilisierung des Kaapvaal Kratons, mit Hf angereichert wurden.

Alle Proben zeigen eine Anreicherung im Nd (und den LREE), welche jedoch nach der letzten Schmelzbildung stattgefunden hat. Die Anreicherung von Hf und Nd durch unterschiedliche metasomatische Ereignisse hat zu einer Entkopplung dieser Isotopensysteme geführt. Im Sm-Nd System bilden die Gesamtgesteine der Peridotite und die subkalzischen Granate „Errorchronen", deren Alter man als Zeitpunkt der Anreicherung interpretieren kann. Für die Peridotit-Gesamtgesteine und die subkalzischen Granate der Gruppe-2 ergibt sich somit ein Metasomatosealter (vermutlich mit einer Schmelze) von ca. 400 Ma (Abb. 8). Für die subkalzischen Granate der Gruppe-1 ergibt die „Errorchrone" ein Alter von ca. 1.3 Ga, welches vermutlich die metasomatische Anreicherung mit einem wässrigen Fluid datiert.

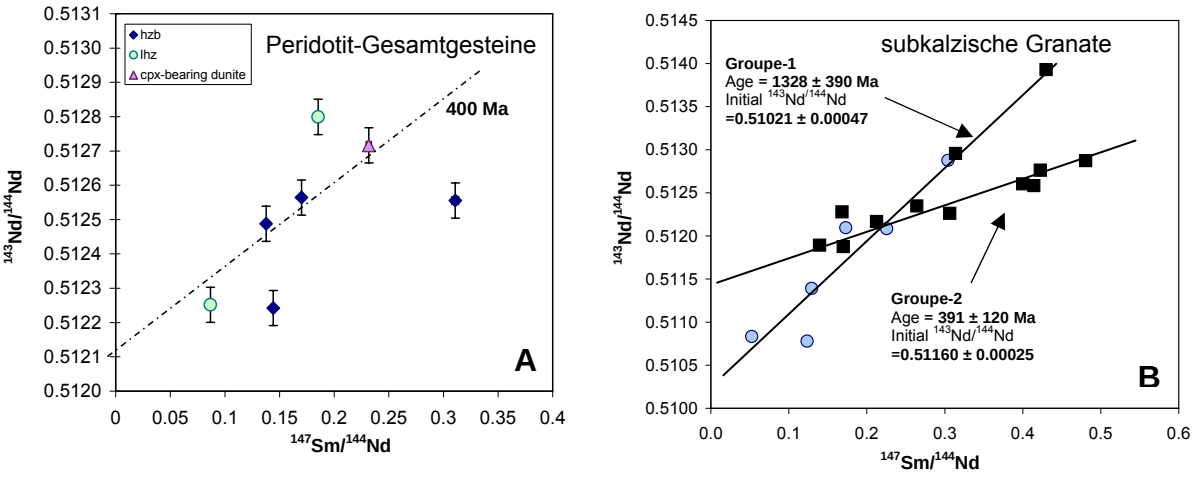

Abb. 8. $^{143}Nd/^{144}Nd$ gegen $^{147}Sm/^{144}Nd$ (A) für die Finsch Peridotit-Gesamtgesteine, welche aus den jeweiligen Daten der Granate und Klinopyroxene berechnet wurden und (B) für die subkalzischen Granate. (A) Die Daten streuen um eine 400 Ma „Errorchrone" mit einem Nd-Isotopeninitialwert, der mit dem der Finsch-Kimberlite übereinstimmt (0.51212, Novell et al., 2004). B) Die Gruppe-1 Granate ergeben ebenfalls eine lineare Korrelation im Nd-Isochronendiagramm, welche einem „Errorchronenalter" von ca. 1.3 Ga (mit relativ großem Fehler) entspricht. Zwei der Gruppe-2 Granate fallen ebenfalls auf diese „Errorchrone". Die anderen Gruppe-2 Granate ergeben ein jüngeres „Errorchronalter" von ca. 400 Ma, in Übereinstimmung mit dem Gesamtgesteins-„Errorchronalter".

2. Die Entwicklung des Kaapvaalkratons

Die älteste Krustenbildung im Kaapvaal Kraton (Südafrika) ist vor ca. 3.6 Ga datiert (Thomas et al., 1993; Kröner und Tegtmeyer, 1994; Kröner et al., 1996 – Abb. 9A). Dieses Alter wurde auch in dieser Studie in Form eines Lu-Hf Modellalter eines hoch-radiogenen subkalzischen Granates beobachtet. Es wird des Weiteren als Zeitpunkt einer ersten Schmelzbildung im Kaapvaal-Mantel durch die hohen Initialwerte der Lu-Hf Isochronen der subkalzischen Granate der Gruppe-1, sowie der Gesamtgesteine impliziert, welche hohe zeitintegrierte Lu-Hf Verhältnisse für eine Dauer von ca. 1 Ga erfordern. Dieses Alter repräsentiert also vermutlich das älteste Schmelzbildungsereignis im Mantel des Kaapvaal Kratons. Die in dieser Studie untersuchten Finsch-Peridotite und subkalzische Granate bilden je eine Lu-Hf Isochrone, welche ein Minimalalter von 2.5 Ga für ein 2. (letztes) Schmelzereignis ergibt. Dieses Alter ist in guter Übereinstimmung mit dem ca. 2.4 Ga Re-Os Alter von Irvine et al. (2001), welches an Sulfiden der Finsch-Peridotite bestimmt wurde. Andere Lokalitäten des Kaapvaal Kratons deuten auf eine letzte Stabilisierung des Kaapvaal Kratons vor bereits 2.7 Ga hin (Walker et al., 1989; Carlson et al., 1999; Menzies et al., 1999; Irvine et al., 2001). Diese Diskrepanz könnte mit methodischen Unsicherheiten zusammenhängen (z.B. durch den Effekt von Orthopyroxen auf die „Pseudo-Gesamtgesteins-Isochronen" der subkalzischen Granate in dieser Studie). Alternativ könnte sie auch mit der geographischen Position der Finsch-Mine zusammenhängen, die weiter westlich als die anderen Lokalitäten (Kimberley, Lesotho und Roberts Victor) und somit weiter von der eigentlichen Kollisionszone entfernt liegt.

Die Schmelzbildung im heutigen Mantel des Kaapvaal Kratons hat in unterschiedlichen Tiefen, entweder bei hohen Drücken mit Granat im Residuum, oder bei niedrigen Drücken im Spinel- oder Plagioklasstabilitätsfeld, stattgefunden. Darauf deuten geochemische Parameter, wie z.B die Cr#, oder HREE-Gehalte und Verhältnisse hin. Insgesamt können Schmelzgrade von bis zu 50% erreicht worden sein, was ein Modell bestätigt, nachdem die frühe kontinentale Kruste durch extrem hohe Schmelzgrade im lithospherischen Mantel gebildet wurde (Card, 1990). Dabei könnte die Schmelzbildung bei niedrigen Drücken an den Mittelozeanischen Rücken stattgefunden haben (Abb. 9A), welche die stark verarmten Peridotite, mit den typischen Signaturen für Residuen aus dem Spinel- bzw. Plagioklas-Stabilitätsfeld, hervorbrachte. Flache Subduktion (prognostiziert von Foley et al., 2003) führten zu früher Kratonisierung und verursachten eine Abschiebung in tiefere Mantelregionen. Dort fand eine weitere partielle Schmelzbildung in Anwesenheit von Granat statt. (Abb. 9B).

Die subchondritischen Lu/Hf Verhältnisse, sowie die unradiogene Hf-Isotopie einiger Peridotite deuten darauf hin, das diese Proben eine metasomatische Anreicherung erfahren haben. Diese Proben wurden wahrscheinlich durch eine Si-reiche Schmelze angereichert (was sich in den hohen Opx-Gehalten widerspiegelt), die auch die Hf-Konzentration und –Isotopie beeinflusste. Da jedoch die meisten dieser Peridotite auch auf der 2.5 Ga Hf-Isochrone liegen, muss diese Anreicherung vor- oder subparallel mit der letzten Schmelzbildung stattgefunden haben – eine spätere Anreicherung hätte die Isochronenbeziehung erheblich gestört. Eine spätere metasomatische Hf-Anreicherung haben vermutlich die subkalzischen Granate der Gruppe-2, sowie die beiden Peridotite erfahren, die unterhalb der Hf-Isochrone liegen.

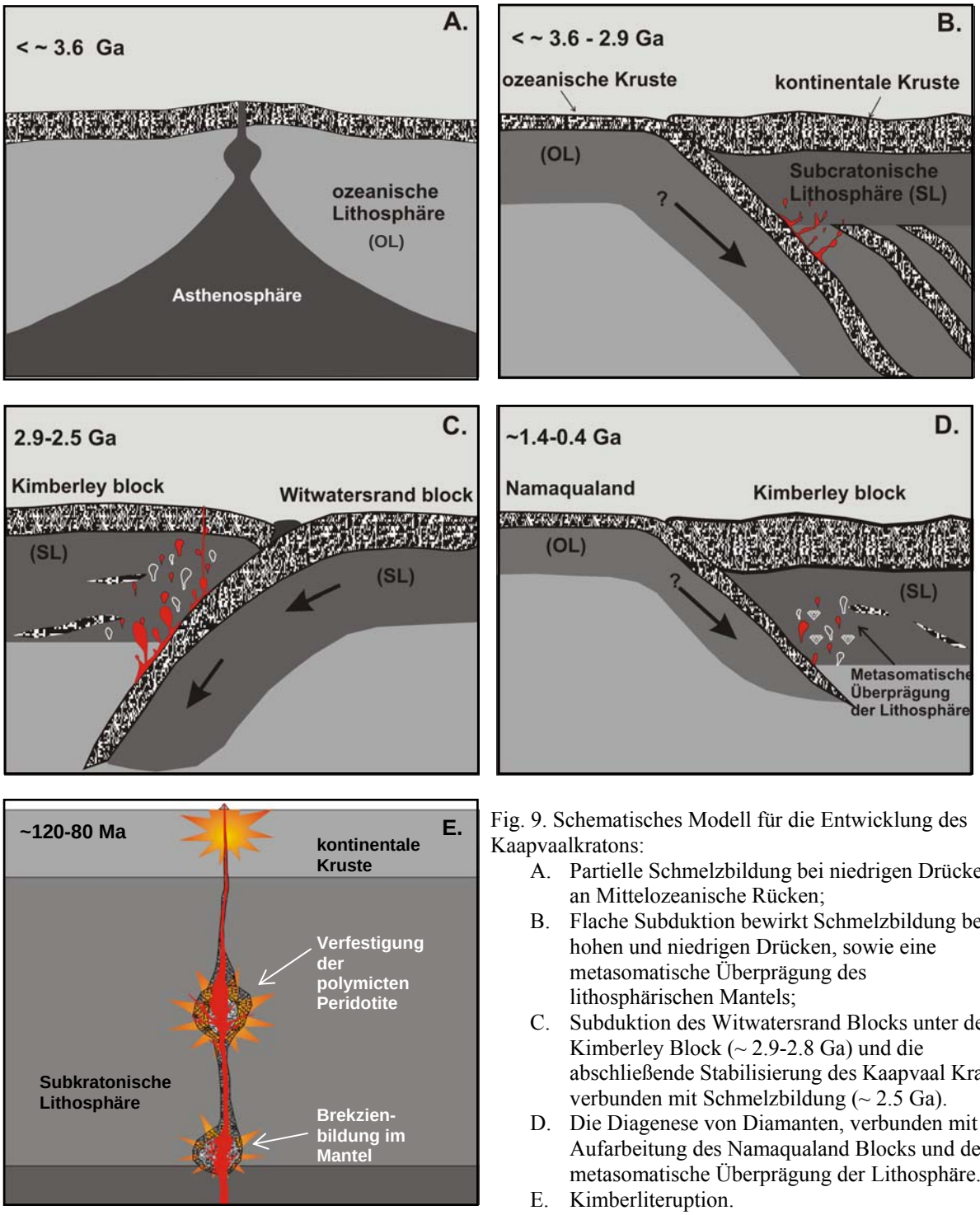

Fig. 9. Schematisches Modell für die Entwicklung des Kaapvaalkratons:

A. Partielle Schmelzbildung bei niedrigen Drücken an Mittelozeanische Rücken;
B. Flache Subduktion bewirkt Schmelzbildung bei hohen und niedrigen Drücken, sowie eine metasomatische Überprägung des lithosphärischen Mantels;
C. Subduktion des Witwatersrand Blocks unter den Kimberley Block (~ 2.9-2.8 Ga) und die abschließende Stabilisierung des Kaapvaal Kraton verbunden mit Schmelzbildung (~ 2.5 Ga).
D. Die Diagenese von Diamanten, verbunden mit der Aufarbeitung des Namaqualand Blocks und der metasomatische Überprägung der Lithosphäre.
E. Kimberliteruption.

Wenigstens zwei metasomatische Ereignisse haben die Sm-Nd Isotopensystematik, nach der partiellen Schmelzbildung vor 2.5 Ga, stark beeinflusst (Abb. 9C). Die subkalzischen Granate der Gruppe-1 deuten darauf hin, dass vor ca. 1.3 Ga eine Metasomatose durch ein wässriges Fluid stattfand (Abb. 9D). Dieses Ereignis hatte keinen Einfluss auf die Lu-Hf Isotopensystematik. Deutlich später, vor ca. 300-500 Ma, fand eine Metasomatose statt, welche sowohl die Nd, als auch die Hf Isotopie beeinflusste und sich in den subkalzischen Granaten der Gruppe-2 und einigen Peridotiten widerspiegelt (Abb. 9D). Beide metasomatischen Ereignisse stehen vermutlich mit der Akkretion und der Aufarbeitung des Namaqualand Gürtels in Zusammenhang, die auf den west-südwestlichen Teil des Kaapvaal Kratons einwirkten (Thomas et al., 1993; Schmitz and Bowring, 2003).

Während der partiellen Aufschmelzung werden Kohlenstoffphasen von der Schmelze gelöst und somit dem Mantel entzogen. Von daher sollten sich Diamanten, die bereits vor der letzten Schmelzbildung vor 2.5 Ga gebildet wurden, bei diesem Ereignis wieder aufgelöst haben. Kohlenstoff für das Diamantwachstum muss dann anschließend wieder durch Metasomatose, in Zusammenhang mit subduziertem Material, eingebracht worden sein. Die Sm-Nd Isotopensystematik von subkalzischen Granaten impliziert, dass diese Metasomatose nicht vor ca. 1.3 Ga stattgefunden hat. Dies impliziert spätes (postarchaisches) Diamantwachstum in Finsch.

„Rezente“ (120-90 Ma) Anreicherungsereignisse, welche mit der „Gruppe II Kimberlitmetasomatose“ oder mit dem „Gruppe I Kimberlitvorläufer“ (Simon et al., 2003) in Zusammenhang stehen, sind nicht in Finsch-, jedoch in Kimberley Peridotiten zu sehen (Abb. 9E). Diese rezenten Ereignisse wurden in der hier untersuchten polymikten Brekzie aufgezeichnet. Sie haben vermutlich auch die „gescherten Strukturen“ verursacht, die in den Hochtemperatur-Peridotiten von Kimberly und Lesotho zu sehen sind (Rudnick and Nyblade, 1999; Woodland and Koch, 2003; Bell et al., 2003; Simon et al., 2003), jedoch in den früher eruptierten Hochtemperatur-Peridotiten von Finsch fehlen (Bell et al., 2003; diese Studie). Daher ist in den Finsch-Peridotiten noch ein älterer geothermischer Gradient, welcher dem 40 mW/m^2 Geotherm von Chapman and Pollack (1977) entspricht, sowie auch eine negative Korrelation der Sauerstofffugazität mit der Tiefe erhalten – im Gegensatz zu den später gebildeten relativ oxidierten gescherten Peridotiten von Kimberley und Lesotho, wo dies nicht mehr der Fall ist.

3. Die Bildung polymikter Peridotite und der Aufstieg kimberlitischer Schmelzen

Eine polymikter Peridotit, welcher in der Kimberley-Mine gefunden wurde, stellt eine mechanische Mischung von Klasten und Mineralen (Opx, Kpx, Granat und Olivin) verschiedener Lithologien des oberen Mantels dar, welche durch feinkörnigen Olivin und geringe Mengen an Picro-Ilmenit, Phlogopit, Rutil und Sulfid zementiert wurde. Durch Temperaturbestimmungen mit dem „Ni-in-Granat“ Thermometer konnte gezeigt werden, dass die einzelnen porphyroklastischen Granate beim Aufstieg der Kimberlitschmelze entlang einer stratigraphischen Mantelsäule von ca. 100 km (von ca. 250 bis 120 km Tiefe) aufgesammelt wurden. Dabei hat die Schmelze mit den porphyroklastischen Mineralen reagiert und an den Rändern Neoblastische Minerale gebildet, z.B. neoblastischer Opx um Opx- und Kpx-Porphyroklasten und neoblastischer Granat um Granat-Porphyroklasten. Analysen dieser neoblastischen Minerale deuten darauf hin, dass die Mantelminerale durch eine volatil-reiche, kimberlitische Schmelze gesammelt und der Xenolith amalgamisiert wurde.

Die Förderung der Mantelklasten begann vermutlich mit einer explosiven Brekzienbildung, als der Sättigungsgehalt für CO_2 in kimberlitischen Schmelzen bei einem Druck von ca. 6-7 GPa erreicht wurde und somit der Liquidus für Mg-Karbonate überschritten wurde. Dieses Schockereignis fragmentierte den umliegenden lithosphärischen Mantel und verursachte Störungen, entlang denen Material in höher gelegene Mantelbereiche transportiert wurde (Abb. 9E). Während des Transports, begannen die Porphyroklasten sich in der Schmelze zu lösen. Jedoch erfolgte der Schmelztransport sehr schnell und die Bildung der Neoblasten an den Mineralrändern verhinderte ein weiteres Lösen der Porphyroklasten. Bei einer Tiefe von ca. 120 km (impliziert von den 1150 °C und 3.5 GPa der Granatneoblasten) viel die aufsteigende Schmelze unterhalb den Liquidus, vermutlich verursacht durch Entgasung. Das Wachstum von Neoblasten und Matrixolivin unter den entsprechend niedrigeren Temperaturbedingungen führte schließlich zur Verfestigung des polymikten Peridotits. Da die Matrix der Brekzie hauptsächlich aus den Mg-reichen Anteilen der Schmelze (Olivin) besteht, kann man schließen, dass eine volatilreiche Komponente fehlt, die vermutlich weiter aufgestiegen ist. Da

zwischen den Mineralen der polymikten Brekzie ein Ungleichgewicht erhalten geblieben ist, muss diese relativ kurz nach ihrer Verfestigung weiter an die Oberfläche transportiert worden sein, möglicherweise mit dem nächsten Puls kimberlitischer Schmelze.

Der gesamte Prozess der explosiven Brekzienbildung, des turbulenten Transports und der Mischung der Porphyroklasten, ihr teilweises Anlösen und die Neoblastbildung muss sehr schnell von Statten gegangen sein und war Teil der Kimberlitbildung insgesamt. Diese Prozesse haben mehrere Schmelzbildungen, Differentiationen und Zwischenstopps bei verschiedenen Manteltiefen, als Bestandteil der Entwicklung kimberlitischer Schmelzen, hervorgerufen. Der hier untersuchte polymikte Peridotit repräsentiert vermutlich ein eingefrorenes Beispiel all dieser Prozesse, die schließlich zu einer Kimberliteruption vor ca. 90 Ma in Kimberley führten.

Summary and conclusions

The Earth's mantle underneath the Kaapvaal craton (South Africa) is the most extensively studied subcratonic lithospheric mantle. Yet many open questions remain concerning its formation and modification during its 3.6 Ga long and complex history. In this work, efforts were made to constrain the geodynamic processes and the chemical and thermal evolution of the cratonic root. For this, 31 coarse-grained peridotites and 21 individual subcalcic garnet grains from heavy mineral concentrates (HMC) from the Finsch mine were studied for their major and trace element compositions, and Lu-Hf and Sm-Nd isotope systematics. Furthermore, processes in the Earth's mantle that follow kimberlite sampling and propagation were studied in polymict peridotite breccia from Kimberley.

A short introduction into the state of the art on formation and modification of the cratonic lithospheric mantle is presented in **Chapter 1** together with information on the geological and tectonic background of the Kaapvaal craton and a brief overview on kimberlite and diamond formation. The analytical methods applied in this study are described in detail in **Chapter 2**. In **Chapter 3** the origin of single grain subcalcic garnets, their host rocks and their protoliths and the relationship to diamond formation is discussed. The petrography of the Finsch peridotites and their major and trace element concentrations are presented in **Chapter 4**. This chapter also provides pressure and temperature estimates of the peridotites, applying thermobarometry, and the determination of the intrinsic oxygen fugacity, as calculated from the ferric iron contents of the garnets. As for the majority of the low-T Kaapvaal craton peridotites, a number of Finsch peridotites also show low Mg/Si ratios, with high modal orthopyroxene, respectively, which is also discussed in this chapter. Furthermore, **Chapter 4** provides a discussion on the budget and partitioning of trace elements between the coexisting mineral phases. From this the amount of melt extraction was estimated. All samples have been re-enriched in incompatible elements. The nature of the metasomatic agents for subcalcic garnets (**Chapter 3**) and peridotites (**Chapter 4**) was deduced from these elements. Lithological profiles for the subcratonic Kaapvaal mantle derived from the Finsch peridotites are discussed in **Chapter 4.** Time steps of depletion events were dated with the Lu-Hf and those of enrichment events with the Sm-Nd isotopic system, which were applied on both, subcalcic garnets (in **Chapter 3)** and (calculated) whole rock peridotites (in **Chapter 5)** from Finsch. These isotope systematics provide a consistent picture of mantle evolution for the Kaapvaal craton.

Recent metasomatic processes are discussed in disequilibrium assemblies of the polymict peridotites from Kimberley in **Chapter 6** by using the major and trace element differences produced by the interaction of kimberlitic melt and peridotite minerals. In the same section, the sampling mechanisms of xenocrysts and the propagation of kimberlitic melt is also discussed.

1. Mantle processes – as implied by investigations of peridotites and subcalcic garnets from the Finsch Mine

Except for one spinel peridotite all other xenoliths studied here are garnet peridotites. The majority of the samples are harzburgites, while the other samples include four lherzolites and four dunites (two clinopyroxene (cpx)-bearing and two cpx-free dunites). Only one harzburgite is cpx-free, one harzburgite contains rutile and pentlandite and four harzburgites are diamond bearing. Secondary minerals are rare and comprise phlogopite, amphibole, clinopyroxene and spinel (mostly around garnets and in their kelyphite). According to the classification of Harte (1977) the majority of the samples have medium- to coarse-grained tabular and equant textures.

Constituent minerals were analysed for major and trace elements and for their Lu-Hf and Sm-Nd isotope ratios. The results are discussed in the context of formation and modification of the lithospheric mantle.

Subcalcic garnets are characterised by low CaO compared to Cr_2O_3. They occur in clinopyroxene-free dunites and harzburgites. Since they are the almost exclusive carriers of most trace elements in such rocks they essentially represent the bulk rock compositions. Their analysis, for major and trace elements and Lu-Hf and Sm-Nd isotope compositions (on 21 garnet grains), yield information on the timing and nature of the dynamic processes underneath the Kaapvaal craton.

Major element equilibrium and changes in the thermal gradient and oxygen fugacity

The refractory nature of all peridotite xenoliths is indicated by high Mg# [Mg# = 100xMg/(Mg+Fe)] in the constituent minerals: $Mg\#_{olivine}$ = 91.2 to 93.7, $Mg\#_{orthopyroxene}$ = 92.3 to 94.6, $Mg\#_{clinopyroxene}$ = 91.8 to 94.4 and $Mg\#_{garnet}$ = 83.2 to 87.1. The subcalcic garnets indicate a still more deplete nature by much higher Mg# of up to 91.9 and Cr# (Cr#=100xCr/(Cr+Al)) up to 34.3.

All samples show intra and inter mineral homogeneity, except for zoned clinopyroxenes in one dunite and one harzburgite. The zoning in major and minor elements is restricted to the outermost rims of the grains and is expressed by elevated Mg#, TiO_2, CaO, and lower Al_2O_3 and Na_2O contents. This compositional change may be due to reaction with the host kimberlite magma.

Inter mineral equilibrium was tested by comparing the results from different, independent thermometers. All applied thermobarometers provide identical temperatures for one sample with a given pressure. Observed differences in the thermobarometric calculations can be attributed to the inherent errors of the methods or to the neglect of Fe^{3+} in the garnets for Fe-Mg exchange thermometers (T_{Krogh} - Krogh, 1988; $T_{O'Neill}$ - O'Neill and Wood, 1979; T_{Harley} - Harley, 1984). Accordingly, all samples have reached equilibrium with respect to their major elements.

The P-T conditions for lherzolites and cpx-bearing harzburgites were calculated by P_{BKN} and T_{BKN} (Brey and Köhler, 1990), and those for cpx-free peridotites were calculated by using P_{BKN} and $T_{O'Neill}$. Three of the latter samples (yellow squares in Fig. 1) were calculated using $T_{O'Neill}$ and considering the Fe^{3+} compositions (obtained by Mössbauer) of their garnets.

The peridotites stem from a restricted pressure (depth) range of 5 to 6.5 GPa and a temperature range of 1050-1250°C (Fig. 1). They plot along the 40 mW/m^2 conductive geotherm of Chapman and Pollack (1977) and on the lower temperature side compared to the high-T sheared peridotites from Kimberley and Lesotho (Woodland and Koch, 2003).

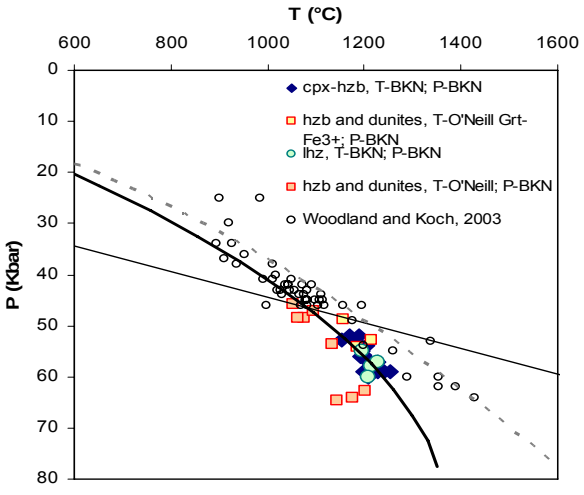

Fig. 1. The peridotites from Finsch plot on a 40 mW/m^2 conductive geotherm of Chapman and Pollack, 1977 (thick line). The Kalahari geotherm (Rudnick and Nyblade, 1999), indicated by the dashed line, is given for comparison. Peridotites from Lesotho and Kimberley (Woodland and Koch, 2003) are also given for comparison.

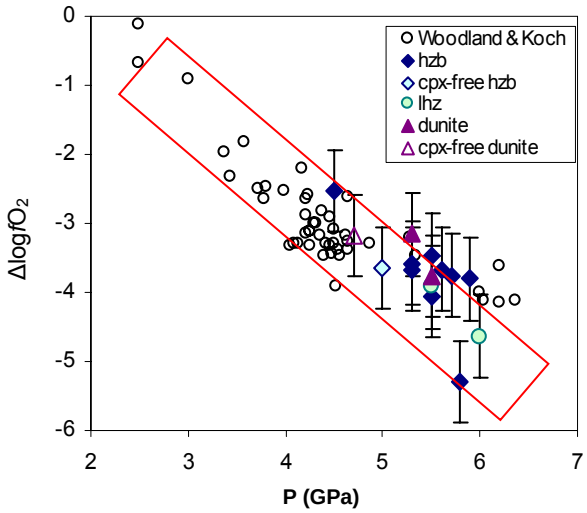

Fig. 2. Co-variation of oxygen fugacity ($\Delta \log fO_2$) and pressure (GPa) of Finsch peridotites. Peridotites from Lesotho and Kimberley (Woodland and Koch, 2003) are also given for comparison.

Mössbauer analyses of garnets from Finsch peridotites show a range in $Fe^{3+}/\Sigma Fe$ from 0.04 to 0.078. Although the temperature and pressure interval of their origin is restricted, the range in oxygen fugacity is rather large with $\Delta \log fO_2$ [relative to FMQ] from -2.5 to -5.3 (Fig. 2). The majority of the samples display a well developed anti-correlation of $\Delta \log fO_2$ with pressure (Fig. 2). Nevertheless, the five samples of this study with slightly higher $\Delta \log fO_2$, for a given pressure, plot above that trend. One of them is a rutile bearing harzburgite and another one is a cpx-bearing dunite with zoned cpx that probably formed during the reaction with the host kimberlite. Those Finsch samples are in good agreement with the high temperature sheared Lesotho and Kimberley samples (Woodland and Koch, 2003) (Fig. 2).

It appears that distinct metasomatic events, like Ti, Fe enrichment (rutile-bearing harzburgite) and reactions with kimberlite (zoned cpx sample) resulted in localised oxidation. In other localities, such as Kimberly, shearing of the coarse-grained peridotites likely produced heating and relatively oxidizing conditions (Fig. 1). This is not observed for the Finsch peridotites. Therefore, the lithospheric mantle before the Finsch kimberlite eruption (~ 118 Ma – Smith et al., 1985) had well equilibrated coarse-grain peridotites that form a linear trend of decreasing oxygen fugacity with depth. Accordingly, shearing observed in the Kimberly and Lesotho peridotites should have happened after the Finsch kimberlite eruption and before those of the Kimberley and Lesotho kimberlite (~ 90 Ma – Smith, 1983) eruptions. This event created sheared textures in peridotites, elevated temperatures and a higher oxidation state of the sub-continental lithospheric mantle.

Equilibrium and disequilibrium of trace element partitioning between garnet and cpx and its influence on the Nd and Hf isotope systems

The minerals of all samples are generally unzoned with respect to their trace element patterns. Variable trace element patterns between minerals of different samples and calculated bulk rocks reflect the complex history of the peridotites and this part of the mantle.

Trace element partitioning between minerals generally depends on pressure, temperature and chemical composition. The trace element partitioning between garnet-opx and opx-cpx shows a pressure and temperature dependence, which agrees with experimental data from the literature for all elements. Garnet/cpx partitioning for the REE also appears pressure and temperature dependent as deduced from the comparison with literature data. However, it also shows a dependency on the Cr content of the garnets (Fig. 3), following a second grade polynomic relationship. This dependency is particular strong for the light and middle REE up to Dy. A good correlation is also observed for Nb, Hf and Sc, while other trace elements, e.g. Lu and Zr, show a relatively large scatter (Fig. 3). This may indicate non-equilibrium in some cases, possibly because of a higher mobility of LREE or slower inter-mineral diffusion of HREE. Alternatively, HREE and HFSE are also in equilibrium between cpx and garnet but depend on other crystal chemical relations, additionally to Cr.

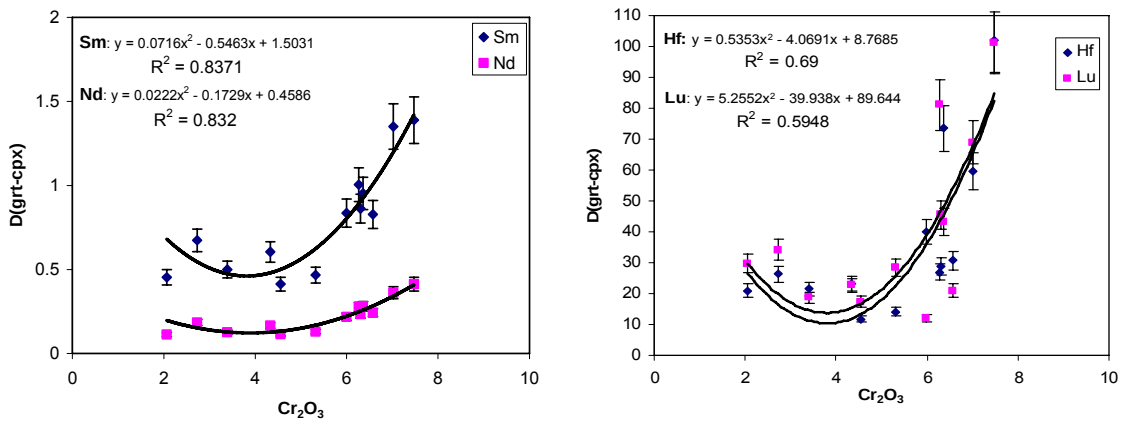

Fig. 3. Partitioning between grt and cpx for Sm, Nd, Lu and 10xHf versus Cr_2O_3 (wt.%) in garnet. Error bars = 10%.

The relationship of the trace element partition coefficients between garnet and cpx and the Cr content in garnet may be related to the size of the dodecahedral position. The majority of the trace elements in garnets are placed on this position (eight fold coordination), which is mostly occupied by the divalent major elements and especially by the large sized Ca. The octaeder position is filled with Al, which can be substituted by Cr. Chromium has a larger ion radius than Al and its presence may expand the garnet structure and with that also the dodecahedral position, allowing incorporation of large sized trace elements, such as the REE.

The different behaviour of different trace elements also appears to affect Sm-Nd and Lu-Hf isotope systematics between garnet and clinopyroxene. All Sm-Nd ages determined on grt-cpx couples give kimberlite eruption ages within uncertainties (~ 118 Ma for Finsch, see Fig. 4A), indicating trace element and isotopic inter-mineral equilibrium of Sm-Nd. This is different for the Lu-Hf system: while two samples give eruption ages within errors, all other samples provide elevated ages between 180 and up to 522 Ma (Fig. 4B). A possible explanation may be in incomplete equilibration of Hf and Lu between garnet and cpx, as also indicated by the highly variable ratio of the partition coefficients of Lu and Hf (D_{Lu}/D_{Hf}) between garnet and cpx, while D_{Sm}/D_{Nd} is constant within ± 10%.

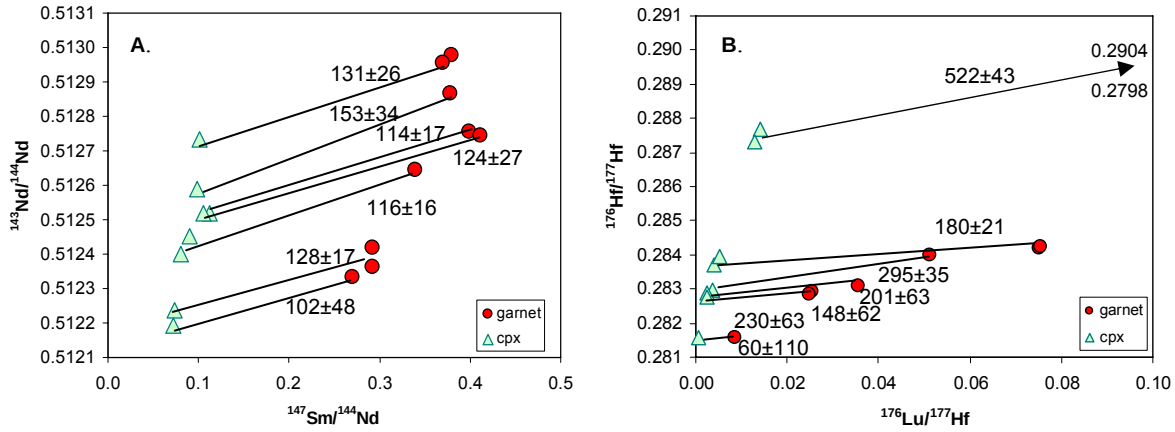

Fig. 4. Isochron diagrams of garnet and cpx pairs for: (A) $^{143}Nd/^{144}Nd$ vs. $^{147}Sm/^{144}Nd$ and (B) $^{176}Hf/^{177}Hf$ vs. $^{176}Lu/^{177}Hf$.

Timing and characterisation of depletion events in the subcratonic mantle

Major and trace element compositions of the Finsch peridotites, recalculated from the modal abundances of the constituent minerals, were used to model the degree of melt extraction. The model of Takazawa et al. (2000) based on the FeO/MgO partitioning between olivine and liquid during partial melting provides degrees of depletion between 10 and 48% for Finsch peridotites. The same range is obtained from the modelling of the HREE. Lherzolites show 5-10% of melt extraction, while dunites and some harzburgites were more than 30% depleted.

The subcalcic garnet compositions reflect two types of host rocks: the samples with variable and high Cr# and low HREE (group-2 garnets) and those with low Cr# and variable and high $(Lu/Er)_N$ (group-1 garnets). Group-2 garnet protoliths can be explained by a first stage (~ 25%) melt extraction at low pressures in the spinel or plagioclase stability field and a second partial melting event in the presence of garnet in the residue. This model may also apply for the majority of the investigated peridotites. The combined degree of partial melting can reach more than 40%. For group-1 garnet protoliths depletion was preferentially in the garnet stability field also in a two stage process (see Lu-Hf isotope systematics).

A two-stage depletion history is most evident from the Lu-Hf isotope systematics: both the group-1 subcalcic garnets and the peridotite xenolith whole rocks yield a Lu-Hf isochron of ~ 2.5 Ga (Fig. 5A,B), which is interpreted as the last depletion age. Both isochrones have highly positive initials of ~ +25 and ~ +16 εHf-units, respectively, relative to the primitive mantle at 2.5 Ga. This indicates at least one depletion event before 2.5 Ga to create the radiogenic Hf isotope signature in the Finsch subcalcic

garnets and peridotites. This first depletion event may have occurred at ~ 3.6 Ga (Fig. 6) for the following reasons: i) HMCF-grt 29 (not a member of the isochron in Fig. 5B) gives a ~ 3.6 Ga model age for single stage depletion, ii) a long time integration period on the order of >1 Ga and high Lu/Hf in the residue are necessary to produce the radiogenic εHf ~ +25 and iii) the oldest crustal ages on the Kaapvaal craton are around 3.6 Ga (Kröner and Tegtmeyer, 1994; Kröner et al., 1996).

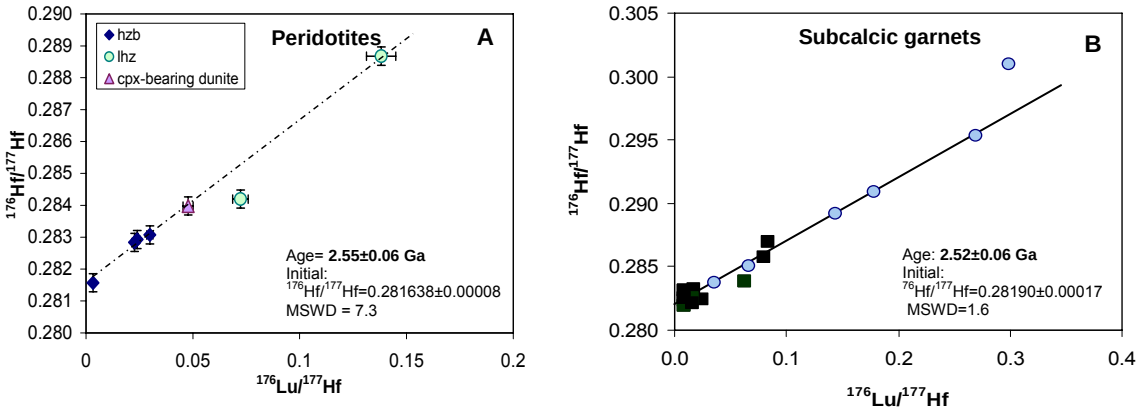

Fig. 5. $^{176}Hf/^{177}Hf$ versus $^{176}Lu/^{177}Hf$ for: (**A**) for the Finsch peridotite whole rocks calculated by grt-cpx isotopic compositions, and (**B**) for group-1 subcalcic garnets (= blue circles; black squares are group-2 garnets). Both, whole rocks and group-1 garnet define an isochron of ~2.5 Ga (with one outlier in both cases). (**A**) Pure analytical errors are within the size of the symbols, and error bars consider the possible effect of opx on whole rock calculations. (**B**) Analytical errors are within the size of the symbols.

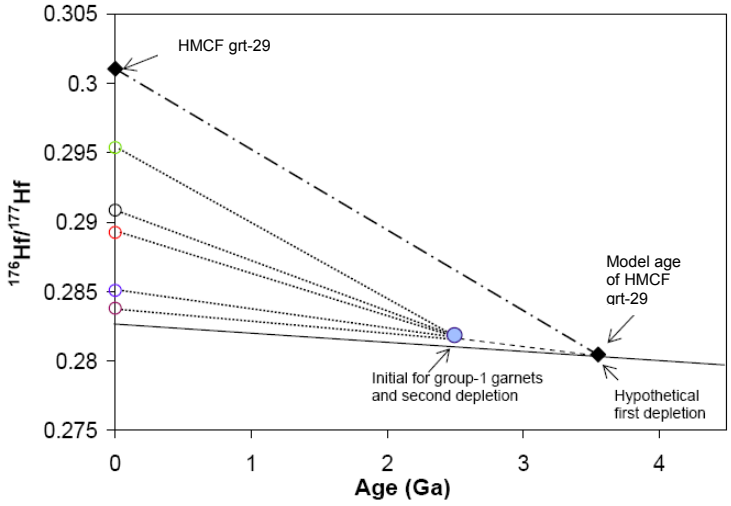

Fig. 6. The Hf evolution diagram for group-1 subcalcic garnets. Present day $^{176}Hf/^{177}Hf$ ratios are connected with their initial (blue circle) by dotted lines. The initial is 25 εHf units higher than the $^{176}Hf/^{177}Hf$ value for the primitive mantle at 2.5 Ga. This indicates a previous depletion event of the group-1 garnet protoliths. It may have occurred at ~ 3.6 Ga, indicated by the model age of HMCF grt-29 (black diamond on the primitive mantle evolution line). The dashed line represents the $^{176}Hf/^{177}Hf$ development after the first partial melting event.

Finsch peridotite whole rocks have lower εHf initials (around +16 εHf) than the subcalcic garnets, which may be explained either by lower depletion of the peridotites compared to the subcalcic garnet precursor rocks, or by pre-depletion later than 3.6 Ga, which is assumed for subcalcic garnets, or by multiple depletion and enrichment processes. Between 3.6 and 2.5 Ga at least two major events occurred in the crust of the Kaapvaal craton i.e. the formation of granitic gneisses at about 3.2 Ga (Poujol et al., 2002; Schmitz et al., 2004) and rhyolitic and calcalkaline volcanism at ~ 2.9 Ga (Schmitz et al., 2004). Thus, multiple partial melting events, as well as re-enrichment in the mantle during these periods cannot be excluded.

Silica enrichment in Finsch peridotites

The majority of the analysed peridotites have, like the majority of the Kaapvaal craton peridotites in general, low modal olivine contents at constant Mg# in olivine, and plot above the oceanic trend as estimated by Boyd (1989). Accordingly, they have high Si-contents or high modal opx contents.

This can not be explained by a simple partial melting process at any conditions in the mantle and a number of alternative models were developed (Kesson and Ringwood, 1989; Kelemen et al., 1992; Herzberg, 1993; Rudnick et al., 1994; Boyd, 1997; Kelemen et al., 1998; Griffin et al., 1999a; Bell et al., 2005; Simon et al., 2007).

Some of these theories were tested on the Finsch peridotites. The most popular speculation is enrichment by Si-rich fluids (Rudnick et al., 1994; Bell et al., 2005; Simon et al., 2007). This would create negative Y and Hf anomalies and high LILE and LREE, which is not observed in the here studied opx-rich peridotites. Thus, other processes must be considered for the opx-enrichment of the Finsch samples. These may include metamorphic unmixing (Boyd, 1997) or cumulative processes (Herzberg, 1993; Herzberg, 1999, see also discussion by Walter, 1999) or, most likely, Si-rich melt metasomatism (Kesson and Ringwood, 1989; Keleman et al., 1992; Keleman et al., 1998).

Timing and characterisation of metasomatic enrichment events

Highly variable trace element compositions and the Hf and Nd isotopic signatures of Finsch peridotites and subcalcic garnets indicate different metasomatic events at different times. Peridotites and subcalcic garnets with low positive or negative εHf and variable negative εNd coupled with high LREE, LILE and Th may indicate carbonatitic or Si-rich melt metasomatism. Samples with strongly negative εHf and small negative εNd and little enriched LILE, LREE and high HFSE indicate metasomatism by kimberlite-like melts. The rutile bearing peridotite with its high HFSE and elevated LILE and LREE is the only modally metasomatized sample in this suite. The enrichment increased the Hf content in this sample (Fig. 7) indicative of a Fe-Ti-rich kimberlite-like melt, which had formed in the presence of garnet. The other clear signature for metasomatic enrichment is recorded in group-1 subcalcic garnets with high LREE and high negative εNd, but low HFSE and positive εHf. This points to a aqueous fluid derived from the subducted plate.

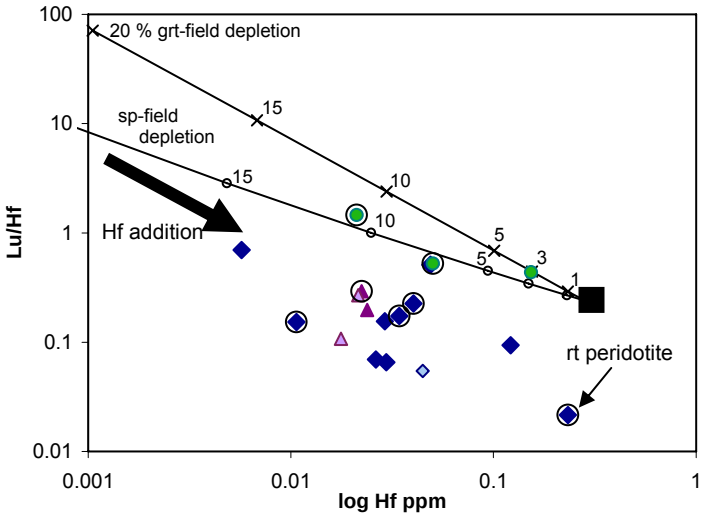

Fig. 7. Lu/Hf ratio versus Hf concentrations (in ppm) in Finsch whole rocks. Modelled non-modal fractional melting curves indicate melting (1-20%) of a primitive mantle (black square) at low pressure (circles) and in the presence of garnet (crosses). The modelling results suggest that all harzburgites and dunites were re-enriched with Hf (indicated with the black arrow), or both Lu and Hf, at some stage. The highest Hf enrichment is observed in a rutile (rt) bearing peridotite (F-12). In the seven encircled samples Hf and Nd isotopes were measured in both cpx and grt, and the Hf data were used to model Lu-Hf whole rock age was determined.

The Lu/Hf ratios and Hf concentrations of Finsch peridotites (Fig. 7) show that all samples are enriched in Hf. Five out of seven samples (encircled in Fig. 7) create an isochron for the Lu-Hf system (Fig. 5A). Three of them have sub-chondritic $^{176}Lu/^{177}Hf$ and very low radiogenic $^{176}Hf/^{177}Hf$ isotopic signatures. This strongly implies that these samples have suffered Hf-enrichment prior to depletion, most likely by a melt. Enrichment in Hf leads to both, to lower Lu/Hf ratios of the rock and the formation of unradiogenic Hf isotopes. Since all those samples were still re-equilibrated at ~ 2.5 Ga this metasomatic event must have occurred either before or synchronously with the last Kaapvaal craton stabilisation event at 2.5 Ga.

All samples show enrichment in Nd (and LREE), which occurred after the final depletion event but not all of them are enriched in Hf. This implies different metasomatic agents at different times and lead to a decoupling of the Hf and Nd isotopes.

The Sm-Nd system yields errorchrons, both for the calculated bulk peridotites and for the subcalcic garnets. The age provided by these errorchrons can be interpreted such that the peridotites and the host rocks of the group-2 subcalcic garnets were cryptically metasomatized at around 400 Ma (Fig. 8), probably by a melt. For group-1 subcalcic garnet the errorchron yields ~ 1.3 Ga (Fig. 9B) and may reflect a metasomatizing event with an aqueous fluid.

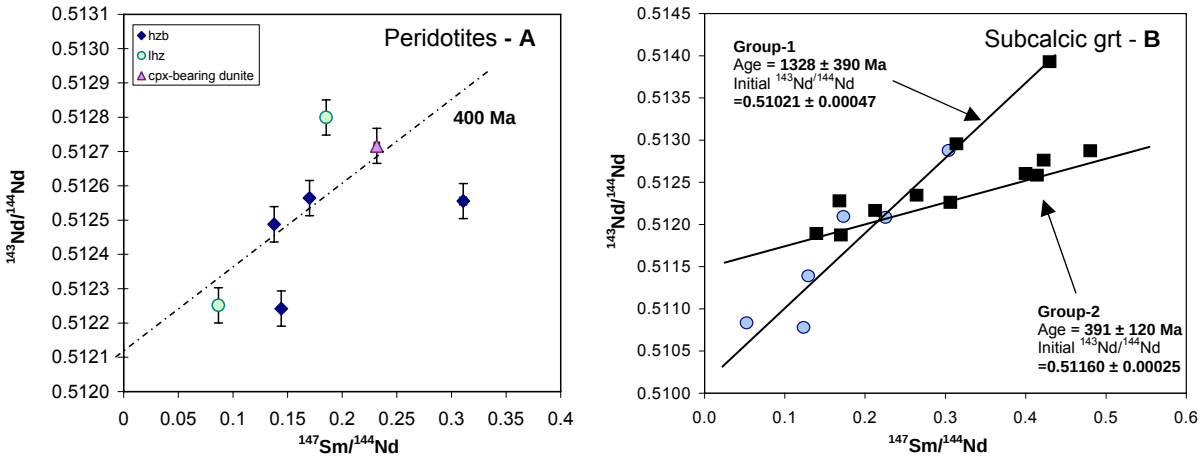

Fig. 8. $^{143}Nd/^{144}Nd$ versus $^{147}Sm/^{144}Nd$ for the Finsch peridotite whole rocks calculated from the isotope compositions of respective garnets and cpx (A) and subcalcic garnets (B). (A) Data plot around a 400 Ma "errorchron" with an initial that agrees with $^{143}Nd/^{144}Nd$ of the Finsch kimberlite (0.51212 - Nowell et al., 2004). (B) Group-1 garnets (circles) define a linear trend with $R^2 = 0.8704$. This correlation gives an errorchron age of around 1.3 Ga with, however, a high uncertainty. Two of the group-2 garnets (squares) also fall on this errorchron. The other group-2 garnets provide a younger errorchron age of around 400 Ma.

2. Evolution of the Kaapvaal craton

The oldest crust formation events in the Kaapvaal craton (South Africa) are dated at around 3.6 Ga (Thomas et al., 1993; Kröner and Tegtmeyer, 1994; Kröner et al., 1996 - Fig. 9A). Such an age is also obtained in this study as a Lu-Hf model age of highly radiogenic subcalcic garnet and is indicated by the high initial of the Lu-Hf isochrons obtained for the Finsch mine subcalcic garnets and for whole rock peridotites, which require high time-integrated Lu/Hf ratios for on the order of around 1 Ga. Accordingly, this age likely represents the oldest depletion event recorded for the Kaapvaal subcratonic mantle. Both subcalcic garnets and peridotites yield an Hf isochron age of 2.5 Ga for the second major depletion event. This minimum age obtained from Finsch peridotites and subcalcic garnets is in good agreement with a Re-depletion age of around 2.4 Ga obtained by Irvine et al. (2001) for sulphides from Finsch peridotites. It may also mark the final craton stabilization. Other localities on the Kaapvaal craton show ages of around 2.7 Ga as the last craton stabilization event (Walker et al., 1989; Carlson et al., 1999; Menzies et al., 1999; Irvine, et al., 2001). This discrepancy may be explained by uncertainties related to the effect of orthopyroxene on the pseudo-whole rock isochron ages, provided by subcalcic garnets in this study. Alternatively, considering the geographic position of Finsch compared to other localities (Kimberley, Lesotho, Roberts Victor, Premier, ...), the Finsch mine

is on the most western side of the Kimberley block, much further away from the two blocks collision zone than the other localities. Possibly, there is a time lag of events between the various localities.

Melting occurred in various pressure regimes either at high pressures in the presence of garnet and at low pressures in the spinel or plagioclase stability field. This can be deduced from geochemical parameters e.g. from the variation of Cr#, HREE and $(Lu/Er)_N$ ratios. The combined degree of partial melting may reach 50%, which supports a model that some Archean cratons were formed by melt extraction of around 50% of the lithospheric mantle (Card, 1990). Depletion at low pressure could have happened in an ocean ridge-like setting (Fig. 9A). It created strongly depleted peridotite residues with spinel/plagioclase field signatures. Shallow subduction processes as proposed by Foley et al. (2003) lead to early craton formation and provided the transport into the deeper upper mantle, where melting occurred in the presence of garnet (Fig. 9B).

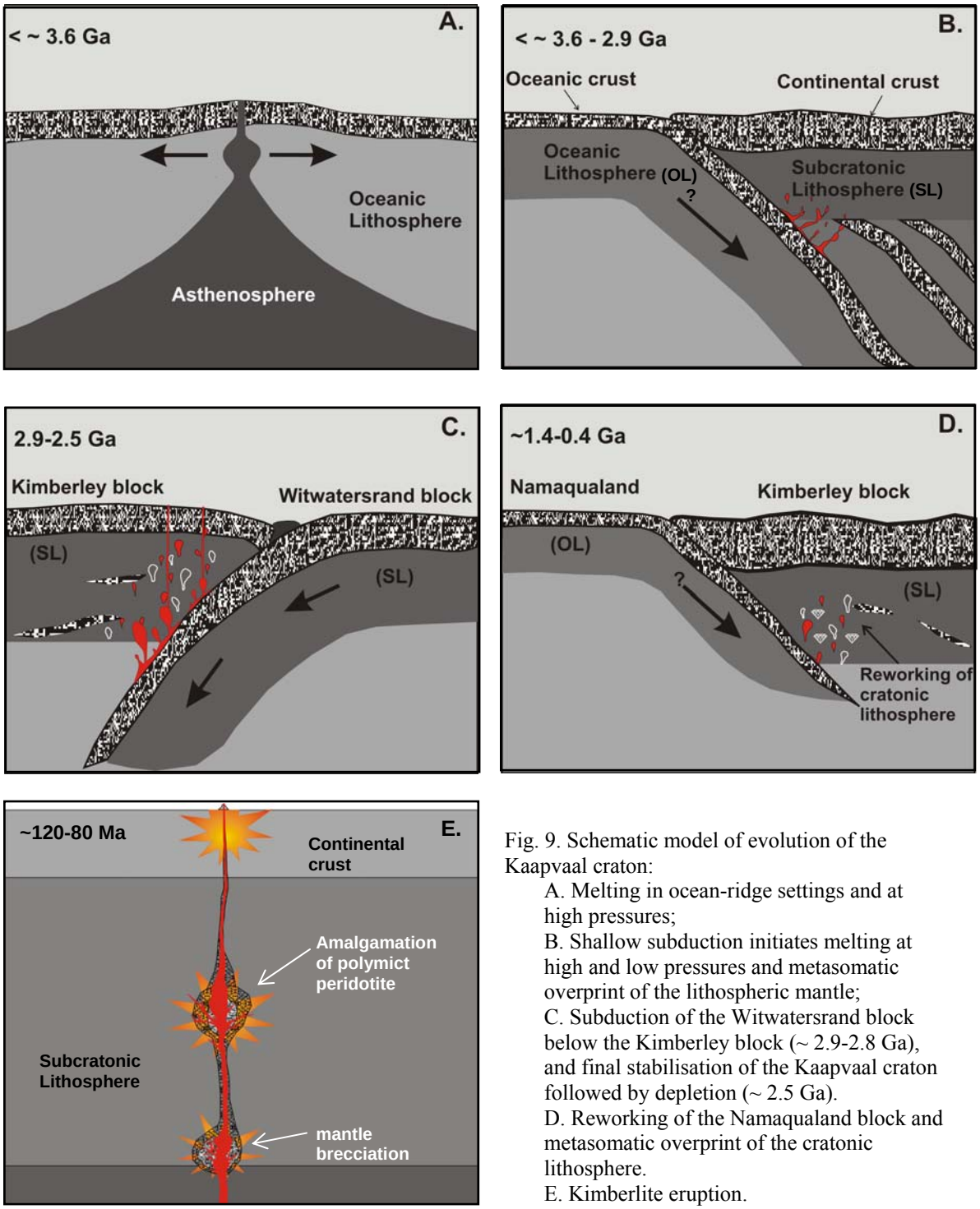

Fig. 9. Schematic model of evolution of the Kaapvaal craton:
A. Melting in ocean-ridge settings and at high pressures;
B. Shallow subduction initiates melting at high and low pressures and metasomatic overprint of the lithospheric mantle;
C. Subduction of the Witwatersrand block below the Kimberley block (~ 2.9-2.8 Ga), and final stabilisation of the Kaapvaal craton followed by depletion (~ 2.5 Ga).
D. Reworking of the Namaqualand block and metasomatic overprint of the cratonic lithosphere.
E. Kimberlite eruption.

The sub-chondritic $^{176}Lu/^{177}Hf$ and very low radiogenic $^{176}Hf/^{177}Hf$ isotopic signatures of some peridotites indicate that these samples were affected by metasomatic enrichment. Finsch samples were likely enriched with a high-Si melt (resulting in high modal opx), which also affected Hf concentrations and isotopes. However, as many of these samples also plot on the Hf isochron, this enrichment must have occurred either before or subparallel to the final depletion event at ~ 2.5 Ga (Fig. 9C), as addition of Hf after that time, would have affected the isochron relationship, significantly. Late Hf-enrichment, connected with more recent metasomatic processes, likely affected the group-2 subcalcic garnets and two peridotites that plot below the Hf isochron.

At least two metasoamatic events have strongly influenced the Sm-Nd isotope systematics after the depletion at 2.5 Ga. Group-1 subcalcic garnets indicate metasomatism by subduction related aqueous fluids at around 1.3 Ga. This event overwhelmed the Sm-Nd contents of the garnets, but its influence on Lu-Hf was negligible. A second metasomatic event happened much later probably between 500 and 300 Ma (Fig. 9D). As defined by the trace elements and Hf and Nd isotope compositions of these samples, different evolving metasomatizing agents were responsible for this event. Both of the metasomatic events may have been connected with the accretion and reworking of the Namaqualand (Thomas et al., 1993; Schmitz and Bowring, 2003) that reworked the west-southwest edge the Kaapvaal craton.

During partial melting any carbon species will be dissolved in the melt and removed from the residue. Therefore, any diamond growth before the last depletion (~ 2.5 Ga) would have been probably completely removed from the lithospheric mantle. Consequently, carbon was apparently reintroduced into the system, i.e. during Metasomatism, and triggered the growth of diamonds. Sm-Nd isotope systematics of the subcalcic garnets of this study indicates that enrichment occurred at ~ 1.3 Ga or later, which implies non-Archean, late diamond growth in Finsch.

Recent, between 120 and 90 Ma old enrichment events connected with the group-II kimberlite metasomatism or with the group-I kimberlite precursor (Simon et al., 2003) are evident in Kimberley peridotites (Fig. 9E). This recent event is recorded in the here studied polymict peridotite.

These late processes have also produced shearing that is evident in high-T Kimberley and Lesotho peridotites (Rudnick and Nyblade, 1999; Woodland and Koch, 2003; Bell et al., 2003; Simon et al., 2003), and is missing in earlier erupted high-T Finsch peridotites (Bell et al., 2003; this study). Therefore, Finsch peridotites record an older thermal gradient that is equal to the 40 mW/m^2 geotherm of Chapman and Pollack (1977), and also show linear decrease of the oxygen fugacity with depth. This is in contrast to the later formed relatively oxidised character of sheared peridotites from Kimberley and Lesotho.

3. Formation of polymict peridotite and the ascent of kimberlitic melt

A polymict peridotite found at the Kimberley mine represents a mechanical mixture of upper mantle clasts and minerals (orthopyroxene, clinopyroxene, garnet and olivine) of different lithologies, cemented by fine-grained olivine and minute amounts of interstitial picro-ilmenite, phlogopite, rutile and sulphide. According to the Ni in garnet thermometry, single porphyroclastic garnets were sampled and mixed during ascent in a 100 km stratigraphic column, starting from ~ 250 km until ~ 120 km. During this ascent, melt has reacted with the porphyroclasts and on the rims neoblastic minerals were formed, i.e. neoblastic orthopyroxene around orthopyroxene porphyroclast, neoblastic garnet around garnet porphyroclast, and neoblastic orthopyroxene around clinopyroxene porphyroclast. Analyses of those neoblastic minerals indicate that volatile-rich, kimberlite-like melt was the agent that collected the mantle minerals and amalgamated this xenolith.

Sampling of single mantle clasts probably started with the “explosive“ brecciation when the saturation point for CO_2-rich kimberlite reached the pressures of 6-7 GPa, by reaching the liquidus of Mg-carbonates. This shock event defragmented the surrounding lithosphere, created dislocations in the cratonic keel, and melt continued upwelling carrying the mantle mixture with it. During this transport, the collected porphyroclasts exhibit minor dissolution. However, rapid transport with the melt, which was only partly in equilibrium with the porphyroclasts, and the development of neoblasts on the rims of the porphyroclasts, stopped any further dissolution. At a depth of around 120 km (indicated by around 1150 °C and 3.5 GPa obtained from neoblastic garnet-opx pare contacts), the ascending melt dropped below the liquidus probably caused by degassing. The growth of neoblasts and precipitation

of matrix olivine at those lower P-T conditions culminated in the consolidation of this polymict peridotite. Since mostly Mg-rich parts of the melt (by the matrix olivine) precipitated to form the polymict peridotite, the volatile-rich part of the melt probably continued upwelling.

Because the whole xenolith preserved inter-mineral disequilibrium, it must have been erupted to the surface shortly after the amalgamation, probably by the next kimberlitic melt impulse.

The whole process of explosive brecciation, turbulent transport and mixing, porphyroclast dissolution and neoblast precipitation happened very fast and was part of the kimberlite formation. It evokes several melt batches with their differentiation and stop overs at various mantle depths as a propagation process of kimberlitic melt. The here studied sample probably represents one frozen part (with variable mantle clasts) of the kimberlitic magma precursor, with kimberlite eruption at ~ 90 Ma years ago in Kimberley.

CHAPTER 1

Introduction

1.1 Research topic and significance

One of the major issues in geology is to understand how the Earth "breathes". Learning about composition and formation of the Earth's interior means learning about processes as far apart as planetary system formation and plate tectonics. Processes in the Earth's mantle are also related to pre-concentration and transfer of precious metals, minerals and gases into crustal levels and the atmosphere, resulting e.g. in the formation of deposits.

Notoriously the Earth's interior is difficult to reach. Seismic tomography, due to its low resolution, provides only a rough picture of the composition and stratigraphy of the Earth's mantle and core. A second indirect possibility to observe the Earth's interior is through igneous eruptions. This samples only a limited depth range and preferentially exotic, plume related magmas. High pressure experiments and computer modelling are mostly working with simplified system and are therefore not capable to resolve fine differences. The discovery of diamonds in 1867 in South Africa initiated many investigations to diamond exploration. It was soon realised that diamonds occur in kimberlites (blue ground), which, besides diamonds, also contains crustal fragments and Earth mantle material (Bonney, 1899). This peridotitic material (mantle xenoliths) gives direct information on the subcontinental lithospheric mantle (SCLM).

In the last four decades mantle xenoliths derived from kimberlites, lamproites and alkali basalts were extensively studied on all continents. They showed that cratonic parts of the continental crust are underlined by a thick, cold and compositionally distinct mantle keel. These lithospheric mantle parts were stabilised in the Archean and isolated from the convecting mantle, and contain direct information on geological and geochemical processes active at that time.

Peridotites from the SCLM are typically depleted in incompatible elements as a result of the primary partial melting events that led to the formation and stabilisation of continental lithospheric mantle (e.g. Jordan, 1988; Boyd, 1989). This depletion event is difficult to decipher by the trace elements and isotopic signatures in the present day rocks because of repeated later chemical overprinting in most samples (Dawson, 1984; Hawkeswort et al., 1984; Harte et al., 1987; Menzies et al., 1987; Simon et al., 2003; Simon et al., 2007). Old metasomatic events generate distinctive isotopic reservoirs in the cratonic mantle (Menzies, 1990; Pearson, 1999; Carlson et al., 1999), whereas younger metasomatism may lead to paradox isotopic compositions since parent-daughter element ratios could not evolve to reflect these changes. Detailed isotope geochemistry into these processes is mostly performed on samples like modally metasomatized peridotites that involves introduction of mineral phases like phlogopite and ilmenite (Harte et al., 1987; Menzies et al., 1987, Erlank et al., 1987) or on the so-called MARID (**m**ica-**a**mphibole-**r**utile-**i**lmenite-**d**iopside) suite (Kramers et al., 1983; Hawkesworth et al., 1990; Konzett et al., 1998; Konzett et al., 2000; Gregoire et al., 2002). Sheared xenoliths preserve chemical and isotopic disequilibria and mantle nodules sampled by "Group I" kimberlitic are also obviously metasomatized and mixed with younger material. This makes them less suitable for a reconstruction of the primary Archean SCLM (Griffin et al., 1989a; Moore and Lock, 2001; Simon et al., 2003; Simon et al., 2007).

Numerous investigations have dealt with the composition, formation, modification and the timing of events in the Earth's lithospheric mantle but the debate is still ongoing:

- What is the origin of the continental upper mantle?
- Which processes led to formation of the first crust? Were they the same as the present day processes?
- What was the ancient geothermal gradient and how high was the oxygen fugacity and which processes influenced their changes?
- Which, why and when different metasomatic events have occurred in the cratonic mantle?

The cratonic mantle underneath southern Africa is unique for having a distinctly higher Si/Mg ratio and therefore higher modal orthopyroxene (opx) contents at a given Mg/Fe ratio than oceanic and most other parts of the upper continental mantle (Boyd, 1989). The reasons and conditions responsible for the enrichment in silica are still debated: 1. extensive melting followed by cooling and metamorphic unmixing of opx and olivine-rich layers (Boyd, 1997); 2. mixing of the residue after

melting with opx-rich cumulate (Herzberg, 1999); 3. re-enrichment of the residue by infiltrating of Si-rich fluids or melts (trondhjemites) derived from low degree melting of subducted oceanic crust (Kesson and Ringwood, 1989; Kelemen et al., 1992, 1998; Rudnick et al., 1994; Walter, 1998).

Insights into the initiation of eruption processes are provided by the rare brecciated polymict peridotites. These samples consist of minerals from practically all different mantle lithologies (Lawless et al., 1979; Dawson et al., 1987; Zhang et al., 2000). They have preserved chemical disequilibrium in their high pressure mineral assemblage and their origin sampling through immediate kimberlite precursors is argued (Lawless et al., 1979; Zhang et al., 2000; Zhang et al., 2001; Zhang et al., 2003).

Diamonds are rare minerals in kimberlites and mantle xenoliths and are interesting not only for economic, but also for scientific reasons. They sometimes have inclusions of minerals from upper and lower mantle and therefore help to understand mantle lithology. Recent teleseismic mapping of the lithospheric mantle beneath the Kaapvaal-Zimbabwe craton shows relatively high P-wave velocities in two prominent but irregularly shaped lobes separated by a broad WNW-trending band of a relatively lower velocity mantle (Fig. 1.1). It appears that Southern African diamonds are stored in such mantle regions with these differences in seismic velocity (Fig. 1.1. - Shirey et al., 2002). This view is still debated as well as the time of diamond formation.

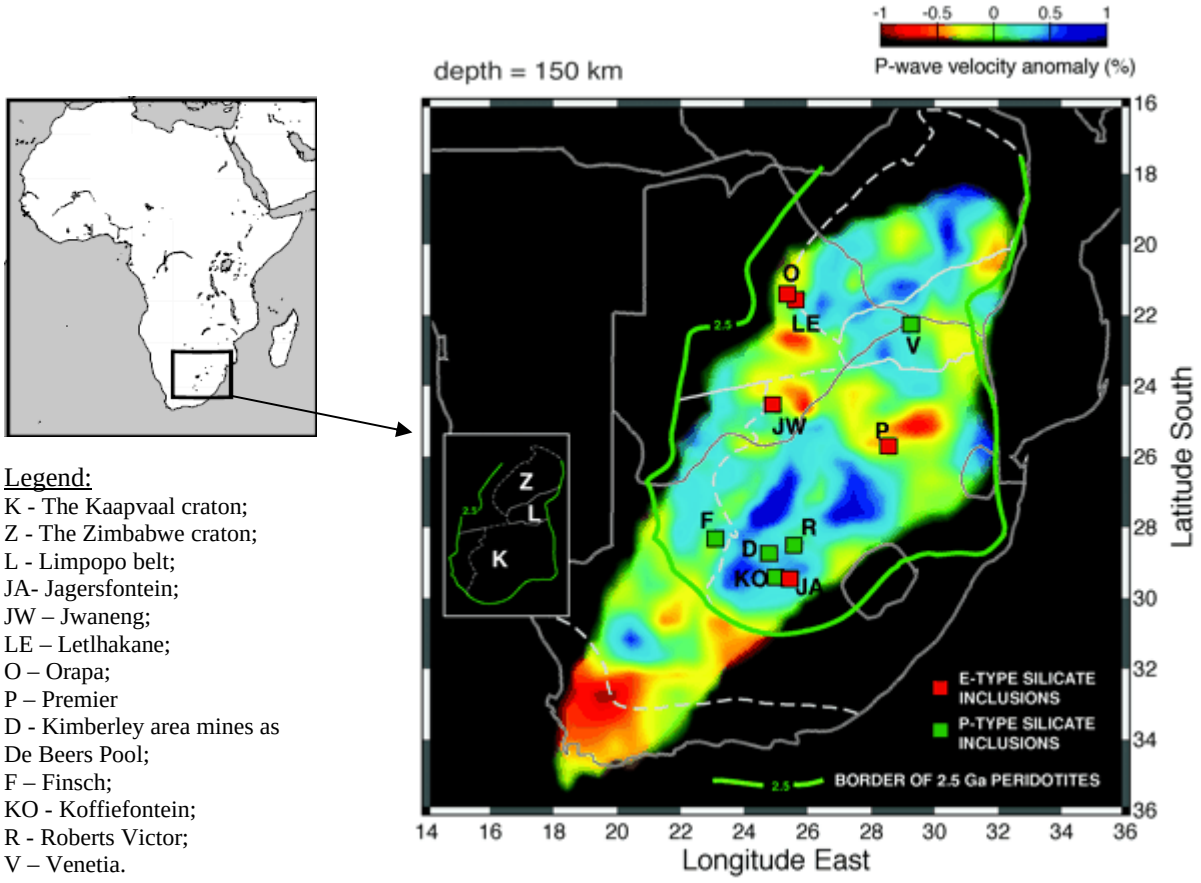

Legend:
K - The Kaapvaal craton;
Z - The Zimbabwe craton;
L - Limpopo belt;
JA- Jagersfontein;
JW – Jwaneng;
LE – Letlhakane;
O – Orapa;
P – Premier
D - Kimberley area mines as De Beers Pool;
F – Finsch;
KO - Koffiefontein;
R - Roberts Victor;
V – Venetia.

Fig. 1.1. Tomographic image derived from seismic P-wave velocity data of the lithospheric mantle in the diamond stability field (150 km depth) adopted from Shirey et al. (2002). Different colours represent areas with positive and negative P-wave anomalies (see scale). The bold green line indicates the outer boundary of the Kaapvaal-Zimbabwe craton. Coloured squares represent diamond mines as stated in legend, whereby red markes mines with predominantly eclogitic and green with predominantly peridotitic silicate inclusions in diamonds.

The close relationship with mantle xenoliths and diamonds makes kimberlites themselves interesting as a research object. Their complex petrography and geochemistry coupled with the unique eruption within thick cratonic lithosphere has been puzzling scientists for almost a hundred years. The

most intriguing questions are (Girnis et al., 1995; Kelley and Wartho, 2000; Nowell et al., 2004; Keshav et al., 2005; Becker and Le Roex, 2006; Lensky et al., 2006; Gregoire et al., 2006): How and where is kimberlite magma formed? What is the chemical composition of primary kimberlite and how does it change on its way to the Earth's surface? How do kimberlites propagate and how do they collect and carry mantle xenoliths?

The Southern African cratonic mantle (SCLM) is the most studied in the world and a wealth of information is available. For this reason, kimberlite erupted mantle xenoliths from the South African SCLM were chosen to address the questions above.

1.2 Geological setting of the Kaapvaal craton

Surrounded by the Limpopo Belt and the Zimbabwe craton in the north, the Namaqua Natal Belt in the west and south, and by the Indian Ocean in the east (Fig. 1.2), the Kaapvaal Craton is the largest, oldest and best preserved terrain in Southern Africa (Hartnady et al., 1985). It has a one billion year old history, which begins at around 3.6 Ga with the emplacement of gneiss complexes in the Swaziland-Barberton area, and ends with the consolidation of the Kaapvaal craton with the Zimbabwe craton and Limpopo belt at around 2.5 Ga (de Wit et al., 1992; Thomas et al., 1993; Poujol et al., 2002). According to seismic tomography the Kaapvaal craton extends down to ~ 200 km (James et al., 2001; James and Fouch, 2002; Shirey et al., 2002; Priesley et al., 2006) with high velocity roots reaching 250 km (Chevrot and Zhao, 2007). The Moho underneath the Kaapvaal craton is relatively shallow at around ~ 40 km (Nguuri et al., 2001). The Great Colesberg Lineament extends from north to south (Fig. 1.3) and divides the Kaapvaal craton into two blocks: the Kimberley (West) and the Witwatersrand (East) block (de Wit et al., 1992; Thomas et al., 1993; Chevrot and Zhao, 2007). These two blocks had a separate evolution in the Archean up to about 2.7 Ga ago, or, according to a more recent study (Schmitz et al., 2004) until ~ 2.88 Ga ago, when they were amalgamated.

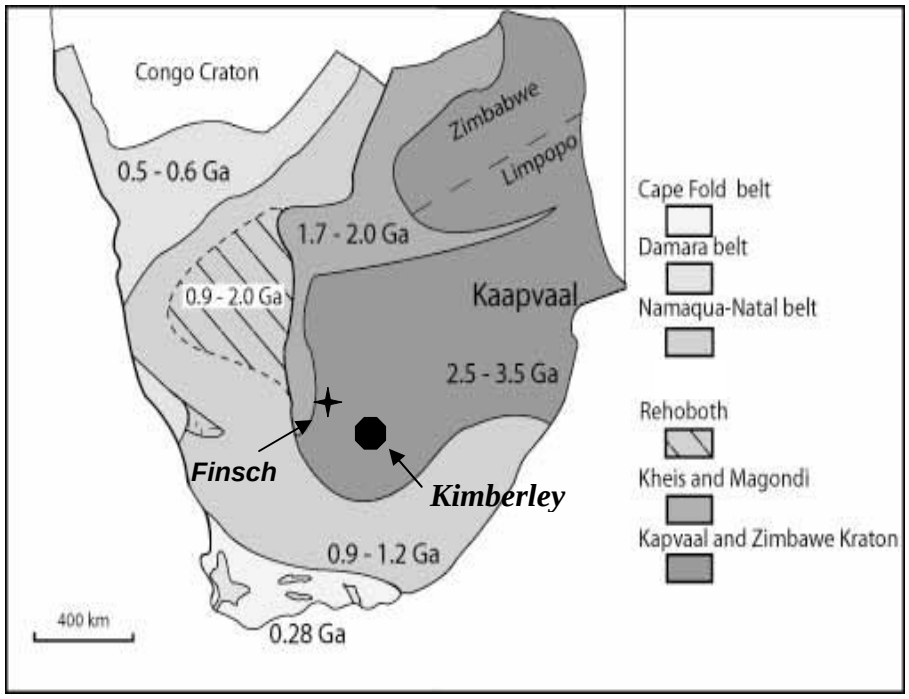

Fig. 1.2. Structural units of southern Africa and locations of Finsch mine and Kimberley pool (Boshof Road dump).

1.2.1 Development of the Kaapvaal craton

Witwatersrand – East block

The crustal section of the Kaapvaal craton consists of 12 terrains of different ages welded together by Archean accretionary events (de Wit et al., 1992, Poujol et al., 2002). The oldest crustal material was formed between 3.7 and 3.3 Ga ago. It consists of at least three tectono-stratigraphic terrains (Ancient gneiss, southern and northern Barberton greenstone terrains), which are all located in the eastern part of the Witwatersrand block (de Wit et al., 1992) (see Fig. 1.3).

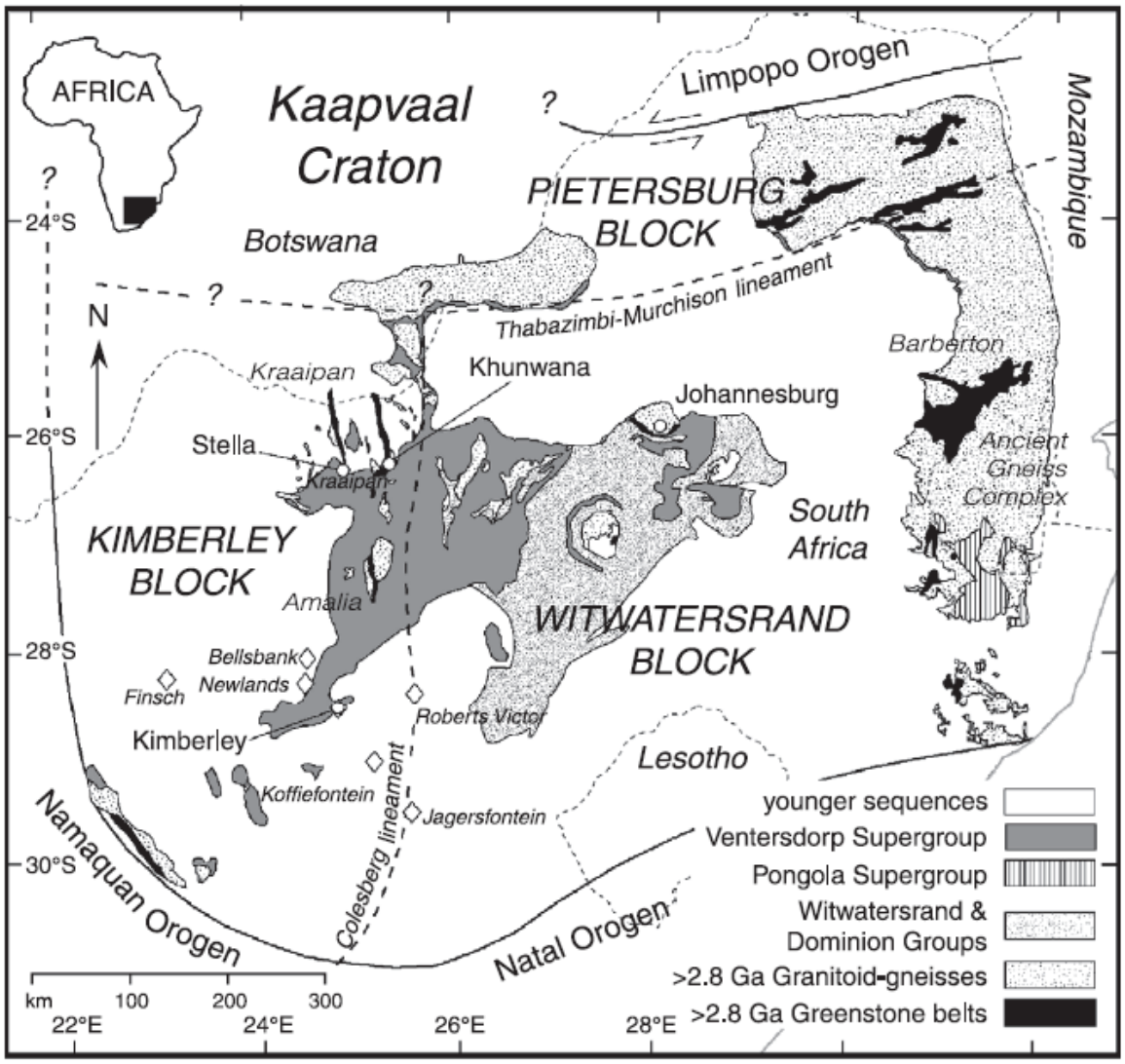

Fig. 1.3. Figure from Schmitz et al. (2004) showing locations of exposed Paleo to Neoarchean crystalline basement and volcano sedimentary basin remnants trough the Kaapvaal craton. Diamonds represent mantle xenolith-bearing kimberlite occurrences.

The Ancient gneiss terrain contains some old (~ 3.6 Ga) tonalitic rocks. The two Barberton terrains are parts of Barberton greenstone belt ranging in age from 3.5-3 Ga. Before 3.5 Ga, the southern Barberton greenstone terrain was developed as a mid-ocean ridge in a shallow-water environment with the difference of a higher heat and fluid flux than today (see de Wit et al., 1992 and ref. therein). It changed into an active arc-like terrain at about ~ 3.4 Ga ago with a trondhjemitic-tonalitic basement that dates back to 3.54 Ga (Armstrong et al., 1990). In the south of the Barberton region the Natal granite-greenstone terrain developed from 3.4 to 3.2 Ga. It was also formed in a shallow marine environment and contains mafic rocks and also boninites and komatiites (e.g. de Wit et al., 1992; Thomas et al., 1993). Thrusting connected with igneous activities at 3.3 -3.2 Ga affected all three terrains. Consequently, de Wit et al. (1992) postulate the formation of the first Witwatersrand

shield before that event. Following as a marker of the final cratonisation of the eastern shield was a transcurrent shearing event at ~ 3.1 Ga with extensive granite formation. After the consolidation of the Witwatersrand block several events occurred until the amalgamation with the Kimberley block: The Dominion Group volcanics heralded the beginning of a sedimentary basin in a continental rift setting (3.09-3.07 Ga) (de Wit et al., 1992; Thomas et al., 1993). This was followed by the development of the Witwatersrand supergroup marine sedimentation from 2.9 until 2.7 Ga (Fig. 1.3). At the same time the Pongola sequence was deposited into the lowest south eastern part of the Witwatersrand block and into the Natal belt. This process was connected with northwest trusting followed by north-south shearing (Armstrong et al., 1990; Robb et al., 1991).

Kimberley – West block

The Kimberley block is placed to the west from the Colesburg Lineament. Its crystalline basement is poorly exposed beneath a cover of Phanerozoic trough Neoarchean sedimentary and volcanic rocks (Drennan et al., 1990; Thomas et al., 1993). Only the small bodies of the Schweizer-Reneke dome and of the Kraaipan, Amalia and Madibe greenstone belts are exposed in the northeast of the Kimberley block (Fig. 1.3) (Thomas et al., 1993; Poujol et al., 2002). They are also closely related to granitic gneisses whose zircons give ages from 3.25 to 2.8 Ga (Robb et al., 1990; Poujol et al., 2002; Schmitz et al., 2004). Formation of the Kraaipan greenstone belt was constrained to 2.93 Ga by the timing of rhyolitic volcanism that preceded calcalkaline volcanism at 2.92 Ga aligned along a north-south trend within the Kraaipan belt. This observation suggests the existence of a volcanic arc and complementary marginal basins on the eastern edge of the Kimberley block (Schmitz et al., 2004). The Kraaipan belt was cross-cut by potassic granitoides at ~ 2.88 Ga that give the time of the suturing of the Kimberley and Witwatersrand blocks (Schmitz et al., 2004). These authors also propose a model in which the Witwatersrand block is the lower plate that is subducted beneath the Kimberley block in a modern style subduction zone scenario.

Shortly after and in the centre of the Kaapvaal craton, i.e. on both blocks, the Ventersdorp supergroup develops (Fig. 1.3). The result of this major rifting was the development of a large sedimentary cover and of intermediate to ultramafic volcanism at around 2.7 Ga (e.g. Schmitz and Bowring, 2003). This cover was deformed during two distinct thrusting events between from 2.7 and 2.55 Ga (Armstrong et al., 1990). At the end of the Archean the Limpopo mobile belt and the Zimbabwe craton were amalgamated with the Kaapvaal craton.

Dating of mantle peridotites by Sm-Nd, Lu-Hf and Re-Os systematics (Walker, et al., 1989; Carlson et al., 1999; Pearson, 1999; Irvine et al., 2001; Simon et al., 2007 and this study – Chapter 3 and 5) gives similar ages between 2.8-2.5 Ga. They consider these ages to corresponding to the final cratonisation and stabilisation of the Kaapvaal craton.

Proterozoic and Phanerozoic development of Kaapvaal craton

Intracratonic extension is the dominating process in the new stabilised Kaapvaal-Limpopo-Zimbabwe block in the early Proterozoic. It produced the Pretoria group basin in the central Transval, the Waterlerg-Soutpansberg Groups in northen Transval and the Matsop Group in the Griqualand. Intra-cratonic igneous activity produced the Buschveld Complex at ~ 2.05 Ga (Thomas et al., 1993). Its activity extends to Botswana and affected the lithospheric mantle underneath the Premier mine. This was constrained by Re-Os isotope data from Premier mantle xenoliths of 2 Ga (Carlson et al., 1999). At the same time, the Vredefort dome was formed as an impact structure within the Kaapvaal craton (Roeting et al., 1990).

During the early and middle Proterozoic the provinces in the eastern and western Namaqualand were formed. The activity started at ~ 2 Ga with the Eburnian orogenic event and continued with the Kheis orogeny which reworked Archean rocks in the west-southwest edge of the Kaapvaal craton at 1.75 Ga (Beukes and Smit, 1987; Alterman and Hölbich, 1991). This zone was reactivated during the Kibaran event at around 1.2 Ga and formed the Namaqualand by the accretion of the Namaqua and Natal terrains (e.g. Schmitz and Bowring, 2003). The end of the Namaqual-Natal orogenesis is marked by a 950-900 Ma mineral cooling age (Thomas et al., 1993).

Formation of the Namaqa-Natal belt is followed by a period of extensive continental fragmentation. It culminates in the late Proterozoic to early Phanerozoic in the "Pan-African" tectonothermal event which is marked by downward fracturing of the cratonic margins to produce the intra-cratonic foreland basins. One of these basins, namely Nama, was formed at Namaqualand closed to the west margin of the Kaapvaal craton. Later from the late Carboniferous until the middle Jurassic, the Karroo basin opened. Sedimentary deposition was followed by the eruption of basalts, which covered large parts of southern Africa (e.g. Thomas et al., 1993). Tectonically, the opening of the Karoo basin is related with the subduction of the paleo-pacific plate underneath the Gondwana plate (Catuneanu et al., 1998). They ascribe the formation of the Karoo flood basalts and the break up of Gondwana to a mantle plume.

The low velocities found in the southeast and the northwest part of the Kaapvaal craton (Fig. 1.1) are attributed to refertilization and/or heating of the mantle keel probably associated with kimberlite activity or related to the Karoo magmatic event and the opening of the South Atlantic ocean (Chevrot and Zhao, 2007).

The Pan-African event established lines of crustal weaknesses that controlled Cretaceous cycles of extension and convergence along the margins of Southern African subcontinent. The fragmentation of Gondwana started at ~ 200 Ma when Australia separated from South Africa. The break up of east and west Gondwana happened between 180-160 Ma (e.g. Fouche et al., 1992). South America separated at ~ 135 Ma which is indicated by the major transform fault on the southeast coast of Southern Africa (Thomas et al., 1993). Parallel to these events kimberlites intruded the Kaapvaal craton.

1.2.2 Kimberlite magmatism

Kimberlites are complex rocks and comprise a clan of volatile-rich, potassic ultrabasic rocks commonly exhibiting a distinctive inequigranular texture with a fine grained matrix. In early days (Wagner, 1914) kimberlites were divided by their petrographic characteristics into basaltic (olivine rich) and micaceous (lamprophyric) kimberlites. These two types are also distinct, geochemically and isotopically, and currently named as Group I (basaltic) and orangeites or Group II (micaceous) kimberlites (see Mitchell, 1995 and Scott Smith, 1996). Group I kimberlites are characterised by relatively high TiO_2, CaO and CO_2 contents whereas Group II are H_2O-rich with comparatively high SiO_2, MgO, K_2O, Al_2O_3 and relatively low TiO_2 (Smith et al., 1985; Scott Smith, 1996). The trace element budget of the primitive kimberlite is highly debated (Smith et al., 1985; Scott Smith, 1996; Gregoire et al., 2003; Becker and Le Roex, 2006). The chemistry of Group I kimberlites is presented in the Chapter 6 of these thesis. The isotope characteristics (Sr, Nd and Hf) of Group I and II kimberlites are discussed in details by Nowell et al. (1999, 2004) and were used for the determination of the origin of kimberlites.

Kimberlite intrusions mostly occur as diatremes on intersections of two or more regional fracture systems. In Southern Africa the distribution of kimberlites is related to the intersection of northeast-southwest, northwest-southeast and east-west crustal fracture trends (Dawson, 1970). The Barkley West field consists of swarm east-west trending sub-parallel feeder dikes, while pipes and root zones like Finsch, Roberts Victor and Elands are rare. In contrast the Kimberley field consists of diatreme facies controlled by northwest-southeast orientated feeder dikes (Mitchell, 1995). The structural aspects of kimberlite emplacement are thought to be related to the uplift of the craton with attendant down warping and faulting along the periphery (Dawson, 1970). However, the distribution of the fields cannot be related in a simple way to any tectonic feature and it is therefore not clear why the region should be a focus for kimberlite magmatism (Mitchell, 1995).

At least eight periods of kimberlite magmatism have been recognised in Southern Africa (Fig. 1.3). The oldest 1.5 and 1.2 Ga are Group I kimberlites erupted in the Kuruman and the Premier field, respectively (Witwatersrand block). They were followed by Group II kimberlites between 200 and 110 Ma, to which the Finsch pipe belongs (Smith, 1983; Smith et al., 1985). Most common on the whole Kaapvaal craton are Group I kimberlites, which have been active in Cretaceous (100 – 85 Ma). The Kimberley pool kimberlites erupted at around 88 Ma and belong to Group I.

1.3 Outline of the thesis

This project focuses on two types of mantle xenoliths from the Kaapvaal craton ordinary coarse peridotites and complex polymict breccia.

The first part considers cold, coarse peridotites from the Finsch mine (Fig. 1.2) and garnets from the Finsch mine heavy mineral concentrates. These mantle xenoliths erupted to the surface from the SCLM by a Group II kimberlite at 118.2 Ma ago (Smith, 1983; Smith et al., 1985). The Finsch kimberlite is placed in the west of the Kimberley block close to the border with the Kheis fold belt (Fig. 1.3). Compared to other kimberlite localities of the Kimberley block that have mostly metasomatized peridotites, the majority of the mantle peridotites sampled by the Finsch kimberlite have a refractory character (Bell et al., 2003; Griffin et al., 2003). It appears that they are not as much affected by the Ventersdorp (2.7 Ga) or the Karoo (~ 180 Ma) volcanism as it is the case for the mantle beneath the Kimberley pool. The latter is also younger (~ 88 Ma years) and may have been overprinted by the earlier kimberlite magmatism at around 120 Ma years. The Finsch peridotites should therefore offer the best possibilities to study ancient processes in the southern African lithospheric mantle.

Another part of this work is devoted to an extremely rare type of peridotites – brecciated polymict peridotites. This kind of samples is so far found only in the Kimberley area (Lawless et al., 1979; Zhang et al., 2000). We were able to collect one complex polymict peridotite from the Boshof Road dump at Kimberley.

Polymict peridotite represents disequilibrium assemblies where the constituent minerals are derived from different mantle lithologies (Zhang et al., 2000; Zhang et al., 2001). This allows the mapping of a profile trough the Kaapvaal SCLM as shown in Chapter 6. The formation of these "exotic" rocks and their relationship with kimberlitic melts is also discussed in Chapter 6. The investigation of the polymict peridotite resulted in a deeper understanding of the formation and propagation of kimberlites as well as of metasomatic processes in the mantle.

1.4 Goals of this study

There are two main objectives of this work; the first one investigates the origin and evolution of the lithospheric mantle beneath the Kaapvaal craton and the second one study processes concerning kimberlite eruption.

This project aims to determine:

- the composition, oxygen fugacity and depth distribution of different mantle lithologies;
- the processes that led to the strong layering of the lithosphere beneath the Kaapvaal craton;
- the refractory character of the Finsch peridotites, and the P-T conditions, at which depletion took place;
- the formation and modification of the Kaapvaal craton with time.

Furthermore, aspects of diamond formation will be addressed.

Polymict peridotites were analysed with the intend to determine:

- the formation of polymict peridotites;
- the formation and propagation of kimberlites;

Chemical characteristics and the metasomatic signature of the kimberlites were also considered.

CHAPTER 2

Methodology

2.1 Samples studied

A total of thirty one mantle peridotites from the Finsch mine were examined during this work, whereby five of them were previously analysed by Skinner (1986) (samples: 695, 882) and by Shee et al. (1982) and Viljoen et al. (1992) (diamond bearing peridotites: 554, 556, and 865) for major and some of them also for trace elements.

After a detailed petrogarphic investigation of samples in thin and/or polished thick sections, major and trace element analyses were preformed on all samples. Analyses were carried out with an **E**lectron **P**robe **M**icro **A**nalyser (EPMA) and with **L**aser **A**blation **I**nductively **C**oupled **P**lasma **M**ass **S**pectrometry (LA-ICP-MS).

The results were used to:

- test major and trace element grain homogeneity, as well as for identification of depletion and enrichment processes;
- test for mineral equilibrium by using different and independent geothermobarometers;
- identify depth and the ambient temperature from which samples were collected;
- check for trace element equilibrium by using known trace element partitioning data.

Garnets from fifteen samples were separated for the Mössbouer spectrometry and the Fe^{2+}/Fe^{3+} ratios of the garnets were used to constrain the variation of the oxygen fugacity with depth.

On the base of the major and trace element data, suitable samples were selected for Lu-Hf and Sm-Nd isotope analysis by **M**ultiple **C**ollector **I**nductively **C**oupled **P**lasma **M**ass **S**pectrometry (MC-ICP-MS). From those, minerals separates were prepared by hand picking. Isotope compositions were analysed from 15 garnets, 7 clinopyroxenes (cpx) and 7 orthopyroxenes (opx).

The geochemical and isotopic study of the single grain, subcalcic garnets from the heavy mineral concentrate (HMC) from the Finsch mine was an independent approach to determine depletion (Lu-Hf) and enrichment (Sm-Nd) ages for the Kaapvaal craton.

The polymict peridotite was cut in half and polished thick and thin sections were made from the whole surface. Major and trace elements of grains from all parts and core to rim profiles were analysed by EPMA and LA-ICP-MS, respectively.

2.2 Major and minor elements

Electron microprobe analyses were carried out in a wavelength-dispersive mode (WDS) with a JEOL JXA 8900RL at the University of Frankfurt. Analyses were performed using an acceleration potential of 15 kV, a beam current of 20 nA and a spot size of 3 µm. The spot size was 1 µm for interstitial minerals and for amphibole, clinopyroxene and spinel from the garnet kelyphite rims. Silicates were analysed by 3-15 spots (depending on the grain size) to test for compositional homogeneity. For Al, Cr, Fe, Ti and Ni integration time of 30 s on peak was used and 20 s for Si, Mg, Ca, Na, K, Mn and P. Back ground measurement were run with an integration time of 10 to 30 s at different distances from the peak depending on which element was measured. Standards were natural minerals and pure oxides and metals. The ZAF algorithm was used for matrix correction. Detection limits (d.l.) for EPM analyses are given in Table 2.1.

***Table 2.1**, Detection limit(d.l.) for EPMA*

Element	ppm	wt.%	
Si	199	0.0426	SiO_2
K	83	0.0100	K_2O
Na	189	0.0255	Na_2O
Ca	126	0.0177	CaO
Mn	157	0.0203	MnO
Mg	144	0.0239	MgO
Ti	203	0.0339	TiO_2
Al	81	0.0153	Al_2O_3
P	199	0.0456	P_2O_5
Fe	177	0.0734	FeO^{tot}
Cr	189	0.0276	Cr_2O_3
Ni	201	0.0256	NiO

Calcium in olivine was also analysed by EPMA in Frankfurt with an accelerator potential of 20 KV and a current of 50 nA and a procedure as outlined by Köhler and Brey (1988). The in house standard San Carlos olivine SC/KA (Th. Köhler) was repeatedly checked during the measurements. Integration times of 40 s on peak and 20 s on back ground assured very good counting statistics. Small olivines in some samples limited the spot size to 3 µm while for larger grains a spot size of 10 µm was used.

2.3 Determination of Fe^{3+} in garnet

The ^{57}Fe resonant absorption spectra of hand-picked garnet separates were obtained with the Mössbouer spectrometer at the University of Frankfurt. Sufficient material was finely ground under acetone and packed into a pre-drilled hole of desired dimension in a Pb disc to obtain a sample thickness of ~ 5 mg Fe/cm^2. Sample masses were generally 15-25 mg. Small amounts of sugar were mixed with the samples in order to create a sample that uniformly filled the hole in the holder. A Ta foil with a hole of appropriate diameter was then mounted on the Pb disc to ensure that only gamma rays that had interacted with the sample reached the detector.

Measurements were performed at room temperature and in constant acceleration mode with a nominal 50 mCi ^{57}Co source in an Rh matrix. The spectra were collected over a velocity range of approximately ± 5 mm/s with a 512-channel multichannel analyser. The velocity was calibrated with respect to α-Fe metal at room temperature.

The obtained spectra were fit using the NORMOS software program (written by R.A. Brand and distributed by Wissenschaftliche Elektronik GmbH, Germany). The spectral model included a single Lorentzian doublet each for the Fe^{2+} and Fe^{3+}. The relative peak widths of the Fe^{2+} doublet were left unconstrained to account for asymmetry due to next-nearest neighbour effects. The doublet attributed to octahedrally-coordinated Fe^{3+} was constrained to have equal peak widths. For two samples with low Fe^{3+} content it was necessary to fix either the peak width or to apply quadrupole splitting to obtain a physically meaningful fit. The $Fe^{3+}/\Sigma Fe$ obtained from the room temperature spectra were corrected for recoil-free fraction effects following the method described in Woodland and Ross, 1994). The resulting $Fe^{3+}/\Sigma Fe$ obtained from the Mössbauer spectra are given in (Table 4.7 in App.-3). Uncertainties arising from instrumental errors and the fitting procedure are considered to be ± 0.01 absolute.

2.4 X-ray fluorescence

Hundred and forty lilac and violet grains from heavy mineral concentrate from Finsch mine were analysed by micro X-ray fluorescence (μXRF – EAGLE II) as a non-destructive method for irregularly shaped mineral grains. The garnet grains were fixed to the sample stage with a piece of clay with a flat horizontal area facing upwards. Analytical conditions were 40 kV and 500 nA and a 300 μm beam diameter.

The μXRF was standardised with a set of well-defined in house garnet standards and other well characterized garnets to cover a large range of CaO (1-7 wt.%) and Cr_2O_3 (2-12 wt.%) contents. An accuracy of about 0.5 wt.% for these two elements is achieved, while the accuracy for the other major elements (Si, Mg, Fe, Al) was about 1-2 wt.%.

2.5 Trace element analyses

The trace elements were analysed by LA-ICP-MS using a New Wave Research LUV213^{TM} ultraviolet Nd-YAG laser coupled with a Finnigan Element2 at the University of Frankfurt.

The laser was used at a pulse frequency of 10 Hz and an energy pulse of around 0.6 mJ (corresponding to 60% laser power). For garnets and larger clinopyroxenes spot size of 95 μm was used, for smaller cpx's of 60-30 μm, and 30-20 μm for the zoned polymict garnet grains. Olivines and orthopyroxenes have low concentration of trace elements and a larger spot size (120-200 μm) was used to ablate more material. USGS BIR 1-G and NIST612 glass were used as external standards and Ca contents from EPMA as an internal standard for cpx and garnet. For olivine and opx NIST614 glass with lower trace element content was used as an external standard and Si from EPMA as an internal standard.

Platinum instead of Ni cones were used for garnet analysis to avoid instrumental Ni background from the cones. Accurate Ni values are needed for "Ni in garnet thermometry" (Griffin et al., 1989b; Canil, 1994; Canil, 1999). The values, especially for Ni, were checked against well-characterised synthetic glasses, i.e. the NIST612 and two in-house garnet standards (PT2a and PN2a), which were

always measured several times within the sequence. An analytical accuracy of around 3% on Ni is indicated by multiple analyses on the garnet standards.

Raw data were produced on-line using the GLITTER-software. The concentrations for the BIR 1-G glass were taken from Eggins et al. (1997), for NIST612 from Pearce et al. (1997), for NIST614 from Norman et al. (1996) and values for garnets PT2a and PN2a are kindly supplied by G. Brey.

2.6 Isotope analyses

Mineral separates from 15 peridotites were used for the determination of Lu-Hf and Sm-Nd isotopes. Each xenolith was crushed to small pieces in a Jaw crusher and a hand mortar and sieved. Fractions between 1-0.5 and 0.5-0.35 μm were run trough a magnet separator and fractions of garnet, opx, cpx and, if available, rutile were collected. Mineral separates were hand-picked to optical purity. To remove possible grain surface impurities, the separated grains were leached at room temperature in 6 M HCl in an ultrasonic bath for 30 min, afterwards ultrasoniced three times in MQ H_2O and finally dried down. Where necessary the leaching procedure was repeated for 15-30 min in 6 M HCl. As known from the literature leaching even at high temperatures (up to 120 °C) with 6 M HCl does not fractionate of Lu, Hf, Sm and Nd in silicates (DeWolf et al., 1996; Wittig et al., 2007). After each leaching procedure the grains were re-picked to optical purity. Only grains from two samples (882, 695), provided by H. Grütter, were leached with HF. Ionov et al. (2005a) did not observe fractionation of Nd and Hf under such conditions. Finally, 30 to 80 mg of garnet from 15 samples, 40 to 120 mg of cpx and 250 mg to 1 g of opx from 7 samples were ultrasoniced in MQ H_2O and dried down prior to spiking.

Knowledge of the exact parent-daughter element ratios for low-Hf and Nd in minerals is essential for precise age constrains and therefore all samples were spiked with Lu-Hf and Sm-Nd tracers prior to dissolution. The sample digestion and chromatographic separation of Lu-Hf and Sm-Nd were performed by combining existing protocols for REE, Lu-Hf and Sm-Nd separation (Maboko and Nakamura, 1995; Münker et al., 2001; Pin and Zalduequi, 1997). Samples were dissolved in a Teflon vial in a 3 ml mixture of HF-HNO_3 (2:1) on a hot plate at approximately 110-120 °C for three days during which they were at least twice ultrasonicated for 30 minutes. After drying down fluorides were cracked in 3-5 ml 6 M HCl. In some cases it was necessary to repeatedly treat the samples with 6 M HNO_3 and 6 M HCl to dissolve all remaining fluorides.

Separation of absolutely pure grains was extremely difficult (in particular for opx) and additionally the size of the xenolith was limited in some cases. We therefore decided to perform chromatographic separation of Lu, Hf, Sm and Nd on the same aliquots. Only for a few cases repeated mineral separate analyses were possible (Table 5.1 in App.-4). Most critical for the accuracy of the analyses was the Hf blank because of the low Hf concentrations. Therefore, chromatography was always started with the purification of Lu and Hf from the samples matrix, to keep the Hf blank as low as possible. The separation was based on the procedure of Münker et al. (2001) using Eichrom Ln-spec resin (column 1). However, in contrast to the protocol described in their study, separation of Zr from Hf was omitted, because this may lead to a loss of some 10% Hf during this step. The separation of Zr is not necessary, since it does not affect the precision of the Hf isotope measurement (Blichert-Toft et al., 1997). The Hf and Lu cuts were dried down and taken up in an appropriate volume of 2% HNO_3 for mass spectrometry measurements.

The matrix, including the light and middle REE, was dried down and re-dissolved in 1 ml 2 M HCl and the REE were separated using a cation exchange resin (column 2, Bio Rad 50Wx8). Most important was the separation of the REE from Fe to avoid overloading the Ln-spec resin, which was used for the Sm–Nd separation (column 3, Pin and Zalduequi, 1997). Since we were working with low sample amounts (25-200 mg) it was possible to reduce the conventional column size (5-10 ml) to 1.5 ml. After loading the samples on the column, the matrix was separated with 14 ml of 2.2 M HCl prior to eluting the REE with 10 ml of 6 M HCl (Fig. 2.1). With this procedure it was possible to separate more than 90% of the Fe from the REE without loosing more than 10% of Sm and Nd. Chromatographic separation of Sm and Nd was performed on the same column that was previously used for Lu-Hf purification (column 3 = column 1, Eichrom Ln-spec resin), following the procedure of Pin and Zalduequi (1997).

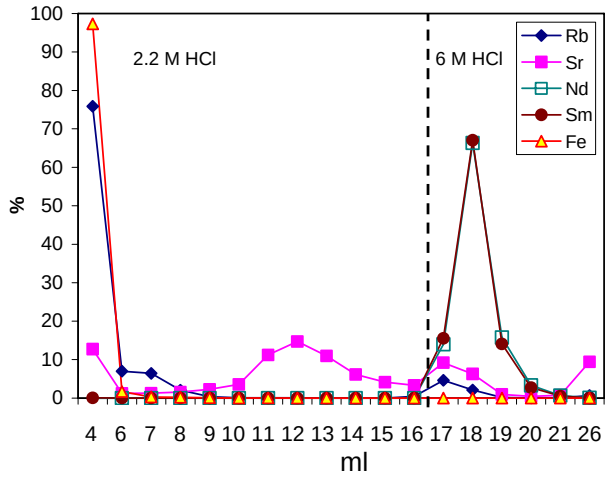

Fig. 2.1. Abundance (in %) of elements eluted with the acid (ml). Separation of REE from matrix on 1.5 ml Bio Rad 50Wx8 column 2. The 2.5 ml of dissolved garnet was loaded on a column, followed by matrix elution with 14 ml 2.2 M HCl and REE were collected with the next 10 ml of 6 M HCl. Dashed line indicate acid change.

All isotopic ratios were analysed in static mode on MC-ICP-MS (Finnigan Neptune) at the University of Frankfurt. Sample aspiration for Hf and Lu was performed using a Cetac-Aridus desolvating nebulizer, whereas Sm and Nd analyses were performed using a dual spray chamber (wet plasma). Hf measurements were performed with the cup configuration, mass bias and interference corrections as described by Blichert-Toft et al. (1997). During our Lu-Hf separation we always collect 30-50% of Yb together with Lu. Therefore, we had to correct for the large mass interference of ^{176}Yb on ^{176} Lu. This was possible with high precision by monitoring the mass bias using the interference-free Yb isotopes^{173}Yb and ^{171}Yb (and assuming a natural ^{173}Yb/ ^{171}Yb = 1.1248, Blichert-Toft et al., 1997).

Sample amounts of Hf were always more than 5 ng, except for some opx samples that contained only 3 ng of Hf. With our instrumental set up we were able to measure such low concentrations of Hf (5 ng - resulting in a signal of ~ 120 mV on ^{176}Hf) with the precision of around 1-2ε (on ^{176}Hf/^{177}Hf). The total blank for Hf was always lower than 30 pg, and for Lu lower than 50 pg. Blank correction was only significant for some extremely low Hf samples. Repeated measurements of the Hf standard JMC475 produced ^{176}Hf/^{177}Hf of 0.282153±0.000014, which is in good agreement with the literature (Blichert-Toft et al., 1997; Chu et al., 2002). Replicate digestion and analyses of BCR-1 yielded ^{176}Lu /^{177}Hf=0.014416±0.00002 and ^{176}Hf /^{177}Hf=0.282879±0.00002. These data are in good agreement with those reported by Bizzarro et al. (2003) and Chu et al. (2002).

The Nd aliquots always contained more than 10 ng Nd, which was measured with a precision of better than 0.5ε, as determined by replicate standard measurements. Procedure blanks were lower than 60 pg for Nd and 40 pg for Sm. Repeated measurements of Nd isotope standards yielded ^{143}Nd/^{144}Nd=0.511722±0.000066 (for the Merck Nd_2O_3) and ^{143}Nd/^{144}Nd=0.511954±0.000026 (for Ames-Nd) respectively, and are in a good agreement with literature values (Deckart et al., 2005; Caro et al., 2006). Replicate digestion and analyses of BCR-1 yielded ^{143}Nd/^{144}Nd=0.512612±0.000016 that is in a good agreement with the literature values (Raczek, et al., 2001; Raczek, et al., 2003).

Uncertainties of Lu-Hf and Sm-Nd ratios and isotope compositions are based on replicate standard measurements and are 1ε for ^{176}Hf /^{177}Hf and ^{143}Nd/^{144}Nd, and 0.5% for ^{176}Lu/^{177}Hf and ^{147}Sm/^{144}Nd.

CHAPTER 3

Time steps of depletion and enrichment in the Kaapvaal craton as recorded by subcalcic garnets from Finsch (SA)

Marina Lazarov, Gerhard P. Brey, Stefan Weyer

Manuscript submitted to Earth and Planetary Science Letters, June 2008

Abstract

Twenty four subcalcic garnets from the Finsch mine (SA) were analysed for major and trace elements and Lu-Hf and Sm-Nd- isotopes. Subcalcic garnets are common inclusions in diamonds and in heavy mineral concentrates from kimberlites where they stem from disrupted (cpx-free) harzburgites and dunites. Their composition defines the chemical budget of most trace elements in such rock types. Thus, the investigation of the trace elements and isotopic composition of subcalcic garnets should directly provide information on the origin, genesis and the age of their host rock.

We were able to distinguish two groups of garnets: group-1 with low Cr# (<11.4), which correlates negatively with CaO and positively with $(Lu/Er)_N$ and group-2 displaying high and variable Cr# (10.9-34.3) but constantly low $(Lu/Er)_N$. These findings imply that group-1 garnets were mainly generated by depletion in the garnet and group-2 garnets by partial melting in the spinel stability field. Group-1 garnets yield a well defined Hf isochron with an age of 2.52±0.059 Ga, likely representing the final depletion of the subcratonic mantle. The high initial of this isochron (εHf ~ +25) indicates that the mantle was already significantly depleted prior to this last depletion event. Group-2 garnets scatter around this isochron at very low Lu/Hf ratios. Sm-Nd does not yield a well defined isochron for either garnet group. Group-1 garnets form an errorchron corresponding to about 1.3±0.39 Ga, while most of group-2 garnets form an errorchron corresponding to 0.4±0.12 Ga.

These findings imply that the present day mantle underneath Finsch (and by inference of the Kaapvaal craton) is the residue of multiple, in situ depletion interfaced with subducted residues of partial melting at low pressures in ocean ridge like settings. The first depletion may have been at around 3.6 Ga for group-1 garnets, mainly in the garnet stability field, and prior 2.5 Ga for group-2 garnets at low pressures in the spinel or plagioclase stability field. The second and final depletion event took place at around 2.5 Ga in the garnet stability field in situ underneath an existing continental crust. This depleted mantle was subsequently metasomatized at least twice. Re-enrichment and presumably diamond formation occurred in two stages, one at around 1.3±0.39 Ga by a subduction related fluid phase and a second at around 0.4±0.12 Ga with melt as metasomatic agent.

Key Words: subcalcic garnet, Archean mantle, Kaapvaal craton, Lu-Hf, Sm-Nd, depletion

3.1 Introduction

Subcalcic, low-Ca, garnets are common inclusions in diamonds and testify the harzburgitic nature of a large proportion of the diamond parent rocks. They occur in rare harzburgitic and dunitic xenoliths and are an important member in heavy mineral concentrates from kimberlite debris. They contribute important information to the origin of diamonds and to the unravelling of the Archean history of the cratonic mantle. Hence, they have been the topic of many investigations (Sobolev et al., 1973; Gurney and Switzer, 1972; Shimizu and Richardson, 1987; Nixon et al., 1987; Viljoen et al., 1992; Boyd et al., 1993; Wang et al., 2000). These lilac to violet garnets have low CaO contents, between 1 and 6 wt.%, together with high Cr_2O_3, mostly between 2 and 15 wt.% (Dawson and Stephens, 1975; Schultze, 2003). Together with high MgO this major element chemistry can only occur in clinopyroxene-free harzburgites and dunites. It also shows that their mantle host rocks are much more depleted than most peridotites from the oceanic lithosphere and from ophiolites. Boyd and Gurney (1986) noted that low-Ca garnets only occur in kimberlites which erupted within Archean cratons but are always absent in off-craton kimberlites.

Low-Ca garnets originate from highly refractory peridotites. These are only minor phases (from 0.5 up to 10 mod.%) in dunites and harzburgites and thus modal abundances of olivine and orthopyroxene (opx) dominate the major element whole rock chemistry. However, garnets are the major carriers of Al_2O_3 and Cr_2O_3 in high pressure peridotites, and their Cr-number (Cr#=100xCr/(Cr+Al)) and Mg-number (Mg#=100xMg/(Mg+Fe)) can be used to describe the residual character of their peridotite host and deduce melting regimes. The majority of trace element is also more compatible in garnets than in orthopyroxene and olivine, i.e. HREE, Y and Zr-Hf budgets are virtually entirely controlled by garnet (Kds in Kelemen et al., 1993; Suhr et al.,1998; Green et al., 2000). Thus, the investigation of the trace elements and isotopic composition (Lu-Hf and Sm-Nd) of low-Ca garnets should directly provide information on the origin, genesis and the age of their host rock.

One of the first attempts to date the timing of diamond formation was the use of the Sm-Nd system on peridotitic garnets pooled from inclusions in diamonds from Finsch and Kimberley

(Richardson et al., 1984). They yielded a model age of 3.2 Ga that was interpreted as the age of formation of the harzburgitic garnets and, by inference, of the diamonds.

Sm-Nd and Rb-Sr isotope studies on subcalcic garnets from heavy mineral concentrates and from harzburgites did not yield any consistent picture nor an age information (Pearson et al., 1995; Jacob et al., 1998). The most recent study by Simon et al. (2007) on peridotitic lithologies mostly from Kimberley shows that the Sm-Nd, Rb-Sr and the Lu-Hf isotopic systems record disequilibrium between the coexisting minerals in this locality. They concluded that the minerals were variously and selectively affected by metasomatic processes. On the other hand, it has been shown by Schmidberger et al. (2002), Ionov and Weiss (2002) and Pearson and Nowell (2004) that the Lu-Hf system is much more resistant to metasomatic processes because metasomatic agents in the deep mantle generally contain very low amounts of Lu compared to the original Lu content of the host rock. Certain metasomatic agents also have low Hf so that the original Lu/Hf ratio may not be affected. In addition, fractionation of Lu (HREE) and Hf (HFSE) between garnet and melt is substantially higher than that between Sm and Nd. This makes Lu-Hf a more suitable isotope system for dating of melt extraction (Scherer et al., 1997; Blicher-Toft et al., 1999). Also, the closure temperature for Lu-Hf is higher than for Sm-Nd (Scherer et al., 2000). Thus, except for Re-Os, the Lu-Hf system is most promising for studying the depletion history of the mantle.

Here, we present major and trace element and Nd and Hf isotopic data of individual subcalcic garnets from a heavy mineral concentrate from the Finsch mine (South Africa) and, in addition, from three garnet separates from harzburgite xenoliths. Based on decoupled Sm-Nd and Lu-Hf isotope systematics, we derive a model on depletion and enrichment events in the subcratonic mantle of South Africa.

3.2 Samples and analytical methods

About 700 single garnet grains of 1 to 6 mm size were collected from a heavy mineral concentrate dump in Finsch. After sorting by colour, 140 lilac and violet grains were analysed by micro X-ray fluorescence (µXRF – EAGLE II) as a non-destructive method for irregularly shaped mineral grains (Table 3.1 in App.-1). The garnets were fixed to the sample stage with a piece of clay with a flat horizontal area facing upwards. Twenty eight garnets between 6 and 127 mg appeared to be of subcalcic character. A few pieces of each grain were mounted in epoxy and polished for detailed major element analysis by Electron probe micro analyser (EPMA) and in situ trace element analysis by LA-ICP-MS. Two of the grains were too small to carry out isotope analysis. The EPMA analysis was done in the WDS mode with a five spectrometer JEOL JXA 8900RL at Frankfurt. The acceleration potential was 15 kV, the beam current 20 nA and the spot size 3 µm. Each grain was randomly analysed on 6-8 spots to ascertain compositional homogeneity (Table 3.2 in App.-1). Seven out of the 28 garnets plotted into the lherzolite field in a CaO-Cr_2O_3 correlation diagram (Fig. 3.1). They were thus excluded from further investigation. The remaining 21 garnets have low CaO but also less than 6 wt.% Cr_2O_3 (Fig. 3.1).

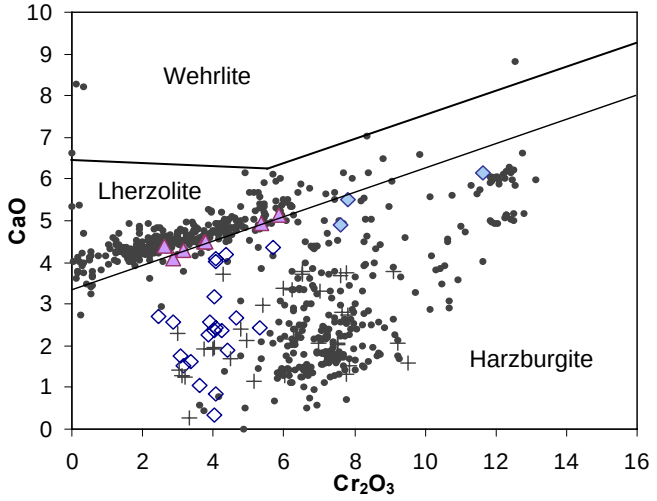

Fig. 3.1. CaO-Cr_2O_3 variation diagram of garnets from heavy mineral concentrates (HMC) and three xenoliths from the Finsch mine, Kimberley. Diamonds are the compositions of the subcalcic garnets used in this study; triangles are lherzolitic garnets not further used in this study (see text). The black dots are HMC garnet (<1 mm) as given by Grütter et al. (2006) and the crosses are those of Gurney and Sweitzer (1972) for grain sizes of more than 2 mm.

Three garnets, solid diamonds in Fig. 3.1, are separates from clinopyroxene free harzburgite and dunite xenoliths from Finsch. (sample 882 - Skinner, 1986 - unpublished honours thesis; samples F-2 and F-7 - Chapter 4). These garnets have more than 5 wt.% Cr_2O_3 and the spinel-garnet harzburgite (882), has 11.6 wt.% Cr_2O_3. Figure 3.1 also shows the whole variability of garnets from Finsch as given by Grütter et al. (2006) and Gurney and Switzer (1972). The comparison shows that our subcalcic garnets mostly overlap with those of Gurney and Switzer (1972), in a field, which is almost separated from that of Grütter et al. (2006). The Grutter data are derived from heavy mineral separates with grain sizes less than 1 mm (personal communication) while the Gurney data are from grain sizes of more than 2 mm, i.e. from the same grain size range as ours. It can be inferred that this reflects a primary correlation of grain size and chemical composition in the mantle where the coarser rock types are lower in Cr.

Trace element analysis

The trace elements were analysed by Laser Ablation Inductively Coupled Plasma Mass Spectrometry (LA-ICP-MS) using a New Wave Research LUV213^{TM} ultraviolet Nd-YAG laser coupled with a Finnigan Element2 at the University of Frankfurt. Platinum- (instead of Ni-) cones were used for analysis, since we were aiming for precise and accurate Ni concentrations in the garnets. Accurate Ni values are needed for "Ni in garnet thermometry" (Griffin et al., 1989b; Canil, 1999). The laser was used at a pulse frequency of 10 Hz and an energy pulse of around 0.6 mJ (corresponding to 60% laser power) for a 95 µm spot size. The USGS BIR-1 glass was used as an external standard and Ca from microprobe analysis for internal normalization. Raw data were produced on-line using the GLITTER-software. The concentrations for the BIR-1 glass were taken from Eggins et al., (1997). The values, especially for Ni, were checked against well-characterised synthetic glasses, i.e. NIST 612 and two in house garnet standards (PT2a and PN2a) which were always measured several times within the sequence. An analytical precision of around 3% on Ni and ~ 10% on REE and Hf is indicated by multiple analyses on standards (Table 3.3 in App.-1).

Isotope analysis

The major fraction of each single subcalcic garnet was used for Lu-Hf and Sm-Nd isotope analysis. Each grain was crushed to smaller pieces in a hand mortar and leached at room temperature in 6M HCl in an ultrasonic bath for 30 min, ultrasonicated three times in MQ H_2O and dried. Samples were then hand-picked to optical purity. If necessary a repeating leaching procedure of 15 min HCl ultrasonication was performed and the grains were re-picked to optical purity. Finally, 25 to 60 mg of garnet separates were ultrasonicated with MQ H_2O and dried prior to spiking. Literature data (DeWolf et al., 1996; Wittig et al., 2006) demonstrate that even a leaching procedure with 6 M HCl at high temperatures (up to 120°C) does not create fractionation of Lu, Hf, Sm and Nd in garnets.

All samples were spiked with Lu-Hf and Sm-Nd tracers prior to dissolution. They were dissolved in a Teflon vial in a 3 ml mixture of HF-HNO_3 (2:1) on a hot plate at approximately 110-120 °C for three days during which they were at least twice ultrasonicated for 30 minutes. After drying down fluorides were repeatedly treated by 3-5 ml 6 M HCl and 6 M HNO_3.

Since most of the garnets have very low concentrations of Lu, Hf, Sm, Nd, (Table 3.3 in App.-1), we had usually only a few nanogram of these elements available for isotope analysis, it was necessary to perform all analyses from one solution. Most critical for the measurements was the low Hf concentration which necessitated a particularly low Hf blank. We started the purification with the separation of Lu and Hf from the sample matrix, using the procedure of Münker et al. (2001) based on Eichrom Ln-spec resin (column 1). However, in contrast to the protocol described in their study, we did not separate Zr from Hf (as Zr does not affect the precision of Hf isotope measurement; Blichert-Toft et al., 1997) because this may have lead to a loss of some 10% Hf and potentially higher blank levels.

The matrix, including the light and middle REE, was dried down and re-dissolved in 1 ml 2M HCl and the REE were separated using a cation exchange resin (column 2, Bio Rad 50Wx8). Most

important was the separation of the REE from Fe to avoid overloading the Ln-spec resin, which was used for the Sm–Nd separation (column 3, Pin and Zalduequi, 1997). Since we were working with low amounts of sample (25-60 mg) it was possible to reduce the conventional column size (5-10 ml) to 1.5 ml. After loading the samples on the column, the matrix was separated with 15 ml of 2.2 M HCl prior to eluting the REE with 10 ml of 6 M HCl. With this procedure it was possible to separate more than 90% of the Fe from the REE without loosing more than 10% of Sm and Nd. Chromatographic separation of Sm and Nd was performed on the same column that was previously used for Lu-Hf purification (column 3=column 1, Eichrom Ln-spec resin), following the procedure of Pin and Zalduequi, 1997.

Isotopic ratios were analysed in a static mode on a multi collector (MC-) ICP-MS (Finnigan Neptune) at the University of Frankfurt. Sample aspiration for Hf and Lu was performed using a Cetac-Aridus desolvating nebulizer, whereas Sm and Nd analyses were performed using a dual spray chamber (wet plasma). Hf measurements were performed with the cup configuration and the mass bias and interference corrections as described by Blichert-Toft et al. (1997). During the Lu-Hf separation 30-50% of the Yb present is always collected together with Lu. Therefore, a correction for the large mass interference of ^{176}Yb on ^{176} Lu is necessary. This was possible with high precision by monitoring the mass bias using the interference free Yb isotopes ^{173}Yb and ^{171}Yb (with ^{173}Yb/ ^{171}Yb=1.1248, Blichert-Toft et al., 1997).

The sample amounts of Hf were always more than 5 ng except for HMCF-grt12 and HMCF-grt29 which contained only 3 ng of Hf. With our instrumental set up we are able to measure such low concentrations of Hf (3 ng result in a signal of ~ 80 mV on ^{176}Hf) with a precision of around 1ε (on ^{176}Hf/^{177}Hf). The total blank for Hf was always lower than 30 pg, and for Lu lower than 50 pg. A blank correction was only necessary for the two lowest Hf samples. Repeated measurements of the Hf standard JMC475 produced ^{176}Hf/^{177}Hf of 0.282153±0.000014, which is in good agreement with the literature (Blichert-Toft et al., 1997; Chu et al., 2002). Replicate digestion and analysis of BCR-1 yielded ^{176}Hf /^{177}Hf =0.282879±0.000024, which is in good agreement with those reported by Bizzarro et al. (2003) and Chu et al. (2002).

Nd-isotope and Sm-ID measurements were also performed by MC-ICP-MS. The Nd aliquots always contained more than 10 ng Nd. Such amounts could be measured with a precision of better than 0.5ε as determined by replicate standard measurements. Procedure blanks were lower than 60 pg for Nd and 40 pg for Sm. Repeated measurements of Nd isotope standards yielded ^{143}Nd/^{144}Nd=0.511722±0.000066 (for Merck Nd_2O_3) and ^{143}Nd/^{144}Nd=0.511954±0.000026 (for Ames-Nd) respectively. They are in a good agreement with literature values (Deckart et al., 2005; Caro et al., 2006). Replicate digestion and analysis of BCR-1 yielded ^{143}Nd/^{144}Nd=0.512612±0.000016.

Uncertainties of Lu-Hf and Sm-Nd ratios and isotope compositions are based on replicate standard measurements and are 1ε for ^{176}Hf /^{177}Hf and ^{143}Nd/^{144}Nd, and 0.5% for ^{176}Lu/^{177}Hf and ^{147}Sm/^{144}Nd.

3.3 Results

3.3.1 Major and trace elements

The range of CaO (0.34-6.14 wt.%) relative to Cr_2O_3 (2.5-11.6 wt.%) places the garnets studied here well within the harzburgitic field (Fig. 3.1; Table 3.2 in App.-1). However, they mostly fall to the lower Cr-side of the mineral concentrate and also of the compositional range of the inclusions in diamonds. Gurney and Switzer (1972) and Viljoen et al. (1992) already noted that Cr-poor garnets are common in the heavy mineral concentrate from Finsch but much less abundant as inclusions in diamonds. Some rare pyroxenite and megacryst garnets also have subcalcic character (Moore and Lock, 2001; Doyle et al., 2004; Schulze, 2003), but they have higher TiO_2 and Ca#, and lower Mg#, which is not observed for Finsch garnets. On contrary high Mg# (85-90) of Finsch garnets rather express their highly refractory nature.

Two groups of garnets are distinguished in Fig. 3.2 with circles and squares. The circles form a negative correlation between Cr# and CaO in Fig. 3.2A on the low Cr# side (<12) of the diagram and a positive correlation with $(Lu/Er)_N$ (Table 3.3 in App.-1) in Fig. 3.2B. These garnets are further referred to as group-1. The second group (group-2) represents a mix of garnets displaying a positive correlation between CaO and Cr# and a tight grouping of compositions between 2 and 3 wt.% CaO and 11 and 15

in Cr#. These garnets have a fairly constant $(Lu/Er)_N$ mostly between 1 and 2 (Fig. 3.2B). This grouping is also noticeable for other elements with similar geochemical behaviour and in Lu-Hf isotope systematics.

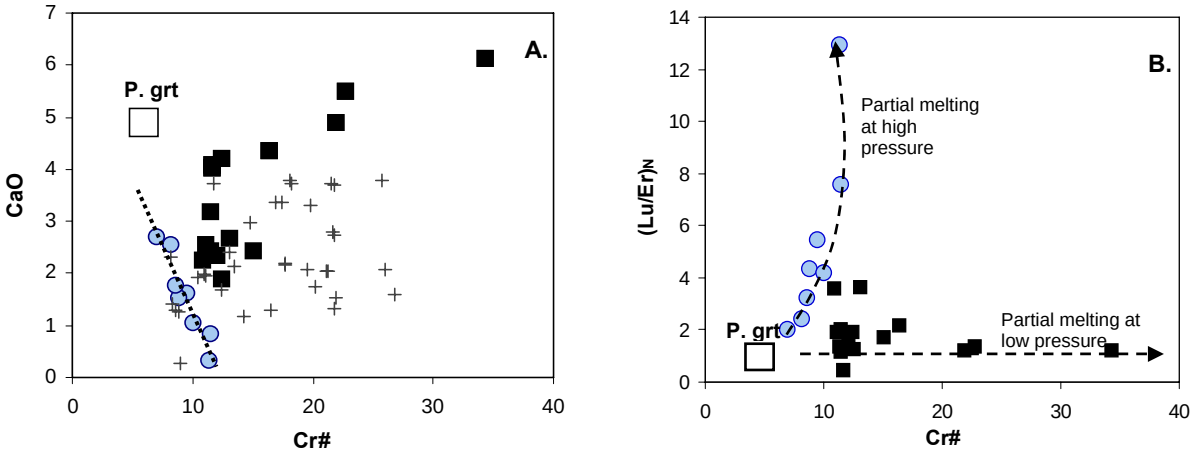

Fig. 3.2. Variation of Cr# (Cr# = molar 100xCr/(Cr+Al)) for single subcalcic garnets from Finsch with (A). CaO (wt.%) and (B). with $(Lu/Er)_N$ ratios (normalized to chondritic C-1 - McDonough and Sun (1995)). Blue circles represent a low-Cr group, further on referred to as group-1 garnets and black squares represent a Cr-richer group and will be referred to as group-2 garnets. Crosses are the subcalcic garnets from Gurney and Switzer (1972). P.grt denotes the composition of a primitive garnet, where Cr# and CaO are from Brey and Köhler (1990) and $(Lu/Er)_N = 1$. the chondritic ratio. Arrows point development of $(Lu/Er)_N$ and Cr# for partial melting in the garnet or in the spinel/plagioclase stability field, respectively.

All garnets have sigmoidal chondrite normalized REE patterns (Fig. 3.3A) similar to those observed by Stachel et al. (1998) and Stachel et al. (2004) for subcalcic garnet inclusions in diamonds. Light to middle REE are bow shaped with the highest values for Nd or Sm in most cases, except for two samples which have the highest values at Ce. The enrichment of the MREE can be up to 30 times relative to chondrite. Similarly as for garnet inclusions in diamonds (Hoal, et al., 1994), the majority of the investigated subcalcic garnets have low $(Sm/Nd)_N$ ratios. The Lu contents vary between one and ten times chondritic with no distinction between the two groups. MREE-enrichment (resulting in the bow-shape pattern) begins for group-1 garnets with Ho, whereas for some group-2 garnets already with Tm. The individual garnets show variable degrees of HREE fractionation and Fig. 3.3 shows that group-1 garnets are more strongly fractionated on average than group-2 garnets.

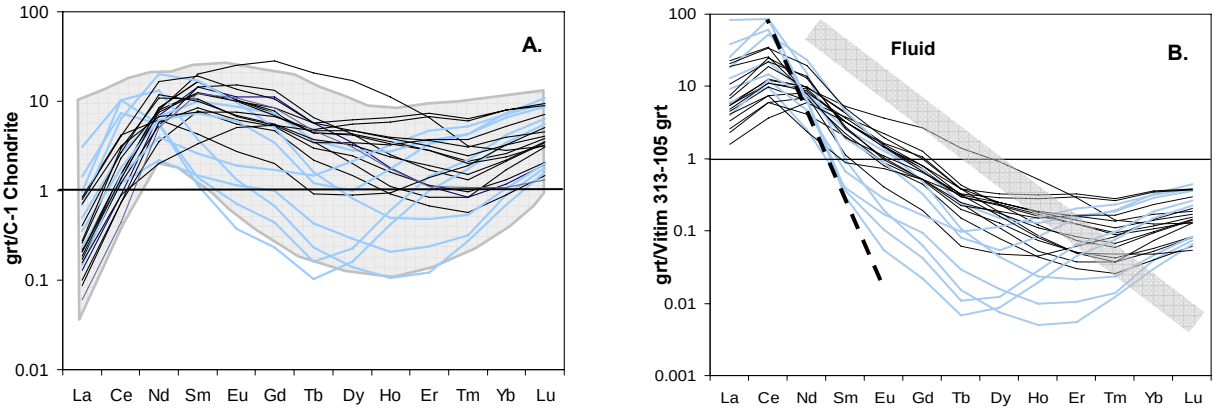

Fig. 3.3. REE pattern of subcalcic garnets from Finsch normalized to (A). Chondrite (C-1, McDonough and Sun, 1995) and (B). Vitim 313-105 garnet (Ionov et al., 2005a). Blue lines show low-Cr, group-1 garnets and thin black lines group-2 garnets. A: The shaded field is an envelope around the compositions of harzburgitic garnet inclusions in diamonds from world wide sources (Stachel et al., 1998, 2004). B: The oblique gray bar indicates the composition of a metasomatic fluid calculated for the strong LREE enrichment of group-1 subcalcic garnets. The dashed line indicates a possible second enrichment process for group-2 garnets.

The normalization of REE of the subcalcic garnets to a garnet from a primitive garnet-lherzolite (Vitim 313-105; Ionov et al., 2005a) removes the sigmoidal shape of the patterns (Fig. 3.3B). It becomes apparent that the pattern consists of mainly two components, one displaying the HREE fractionation with a positive slope of depletion and the other showing the fractionation of the MREE and LREE with a negative slope of enrichment. Group-1 garnets can be distinguished from the group-2 garnets by their stronger fractionated HREE and the higher abundances of the LREE. On contrast, MREE and HREE for the group-2 garnets have higher contents.

Most incompatible trace elements, such as U, Th, Nb, Ta, Sr and LREE concentrations are enriched in all garnets in comparison to those of the primitive garnet from Vitim 313-105 (Ionov et al., 2005a,b). However, the concentrations of Rb and Ba are comparable or lower (Fig. 3.4). Notably, Hf and Zr are mostly higher in the group-2 garnets compared to Vitim, but up to almost two orders of magnitude lower in the group-1 garnets. The group-1 garnets have negative Zr-Hf anomalies and the group-2 garnets either positive or negative Zr-Hf anomalies.

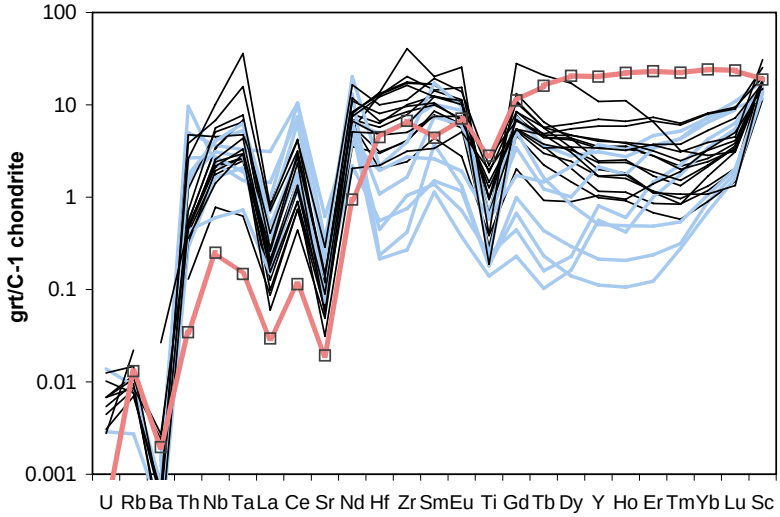

Fig. 3.4. Chondrite normalized spidergram of the subcalcic garnets. Low-Cr, group-1 garnets are represented by blue lines and group-2 with thin black lines. The thick line with squares is the garnet composition from a primitive peridotite (Vitim garnet 313-105, Ionov et al., 2005a,b).

3.3.2 Isotope systematics

We observed a huge spread of εHf and εNd values in Finsch garnets (Fig. 3.5; Table 3.1). Notably, garnets with the most positive εHf values (up to 650) have the most negative εNd values (down to -36). These extremely radiogenic εHf values combined with unradiogenic εNd are characteristic for group-1 garnets. Very high εHf values and also negative εNd-values have already been reported for Kaapvaal craton garnets (Walker et al., 1989; Bedini et al., 2002; Simon et al., 2007). Group-2 garnets have either positive or negative εHf (between -30 and +37) combined with positive or negative εNd (between -15 and +25). All group-2 garnets with positive Zr-Hf anomalies have negative εHf and low $^{176}Lu/^{177}Hf$ ratios, pointing to Hf enrichment by metasomatic processes and therefore to Lu-Hf isotopic disequilibrium. The comparison on Fig. 3.5 shows that Hf and Nd isotopes are decoupled, which is produced by the different behaviour of these four elements during metasomatic enrichment and will be discussed later in detail.

All group-1 garnets except HMCF-grt 29 (the most radiogenic garnet, Fig. 3.2B) display a very good correlation of $^{176}Hf/^{177}Hf$ and $^{176}Lu/^{177}Hf$ (Fig. 3.6A). No correlation is observed for these garnets in a diagram of $^{176}Hf/^{177}Hf$ versus 1/Hf. Thus, the correlation between $^{176}Hf/^{177}Hf$ and $^{176}Lu/^{177}Hf$ can be interpreted as an isochron rather than a mixing line. Garnet HMCF-grt 29 has an extremely low Hf concentration and a larger analytical error (~ 5 ε-units) than that assumed for the other garnets. However, analytical uncertainties cannot explain the offset of this sample from the isochron (~ 150 ε-units), which is defined by the other five group-1 garnets. We therefore interpreted this garnet as the residue of an older partial melting event at ~ 3.6 Ga ago, which is indicated by the model age of this garnet relative to the primitive mantle (see discussion below).

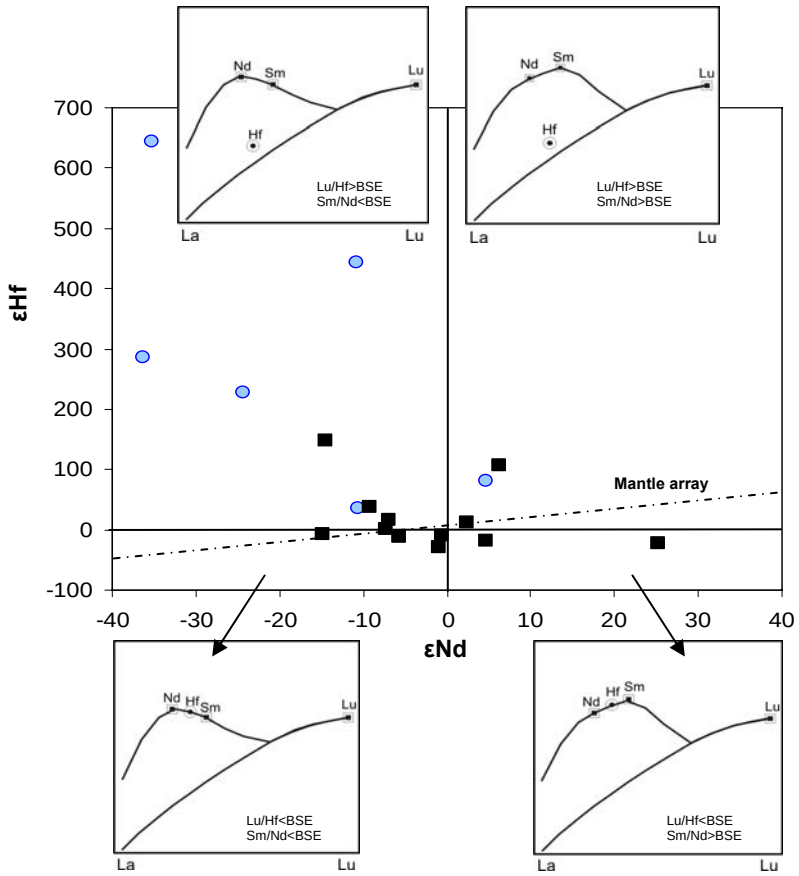

Fig. 3.5. εHf vs. εNd diagram for the subcalcic garnets. Symbols are the same as in Fig. 3.1. The four sketches with the REE patterns schematically depict the abundances of the REE and of Hf as a result of partial melting and subsequent metasomatic overprint. The relative abundances of Nd, Hf, Sm and Lu lead to the highly variable time integrated isotope compositions. The stippled line is the mantle array, which is defined as εHf=1.33xεNd +3.19 (Vervoort et al., 1999). BSE = Bulk Silicate Earth.

Table 3.1*. Lu-Hf and Sm-Nd isotope compositions of subcalcic garnets from the Finsch mine.*

	Sample	Lu (ppm)	Hf (ppm)	$^{176}Lu/^{177}Hf$	$^{176}Hf/^{177}Hf$	εHf	Sm (ppm)	Nd (ppm)	$^{147}Sm/^{144}Nd$	$^{143}Nd/^{144}Nd$	εNd
	HMCF-grt 12	0.04	0.04	0.1435	0.289270	230	0.22	1.02	0.12919	0.511390	-24.3
	HMCF-grt 20	0.20	0.42	0.0668	0.285069	81	1.39	2.75	0.30399	0.512877	4.7
group	HMCF-grt 29	0.13	0.06	0.2987	0.301173	650	0.20	2.26	0.05241	0.510833	-35.2
1	HMCF-grt 38	0.19	0.10	0.2700	0.295332	444	0.80	2.14	0.22548	0.512085	-10.8
	HMCF-grt 43	0.05	0.19	0.0356	0.283760	35	2.66	9.3	0.17296	0.512094	-10.6
	HMCF-grt 58	0.25	0.20	0.1783	0.290882	287	0.47	2.3	0.12347	0.510779	-36.3
	HMCF-grt 3	0.04	0.75	0.0081	0.283102	12	0.85	1.22	0.42242	0.512763	2.4
	HMCF-grt 11	0.07	1.13	0.0089	0.282535	-8	2.15	3.26	0.39981	0.512604	-0.7
	HMCF-grt 13	0.07	0.61	0.0160	0.282814	1	1.68	3.33	0.30628	0.512262	-7.3
	HMCF-grt 14	0.07	1.18	0.0089	0.282289	-17	1.80	2.26	0.48059	0.512874	4.6
group	HMCF-grt 18	0.05	0.47	0.0165	0.282136	-22	1.67	2.35	0.42987	0.513929	25.2
2	HMCF-grt 33	0.12	0.20	0.0839	0.286928	147	0.64	2.77	0.13937	0.511893	-14.5
	HMCF-grt 39	0.01	0.06	0.0173	0.283243	17	1.23	4.42	0.16798	0.512280	-7.0
	HMCF-grt 82	0.11	0.20	0.0800	0.285789	107	0.43	0.84	0.31377	0.512957	6.2
	HMCF-grt 85	0.21	1.18	0.0249	0.282433	-12	1.26	2.89	0.26417	0.512347	-5.7
	F2-grt	0.19	0.43	0.0631	0.283817	37	0.90	2.56	0.21250	0.512167	-9.2
	F7-grt	0.03	0.59	0.0082	0.281932	-30	1.64	2.39	0.41418	0.512585	-1.0
	882-grt	0.10	0.89	0.0166	0.282540	-8	2.35	6.47	0.16976	0.511875	-14.9

Excluding this sample an age of 2.520±0.059 Ga is obtained for group-1 garnets with an initial of $^{176}Hf/^{177}Hf$ = 0.28190±0.00017 and MSWD=1.6 (Fig. 3.6A). Such an age is close to a literature Re-depletion age for the Finsch peridotites (T_{RD}=2.4 Ga) by Irvine et al. (2001). All group-1 garnets conceivably coexisted with orthopyroxene with which they were in isotopic exchange. Assuming opx and garnet preserved their isotopic equilibrium from 2.5 Ga ago, garnets and corresponding whole rocks would provide identical age information. The 2.52 Ga would have to be considered as a minimum age if re-equilibration of garnet and opx occurred after 2.5 Ga, e.g. if the Lu-Hf system remained open on a mineral scale. However, late inter-mineral equilibration would disturb the Lu-Hf isochron, unless the amount of Hf in opx is negligible. Even if considering a small undetectable effect of late equilibrated opx on the Lu-Hf age of the subcalcic garnets, they would likely not exceed the Os-age based on sulphide inclusions in diamonds of ~ 2.6-2.8 Ga (T_{RD}) provided by Walker et al. (1989), Carlson et al. (1999), Menzies et al. (1999) and Irvine et al. (2001). However, they would unlikely reach the proposed craton amalgamation age of 2.9 Ga of Schmitz (2002), Schmitz et al. (2004) and Richardson et al. (2001) or even the 3.2 Ga Sm-Nd model age for garnet inclusions in diamonds by Richardson et al. (1984).

In contrast to the Lu-Hf system, Sm-Nd does not yield a well defined isochron for either garnet group (Fig. 3.6B). The data for group-1 garnets rather scatter around a correlation line corresponding to about 1.3 Ga with a y-axis intercept of 0.5102. Two of the group-2 garnets also fall on this line. Excluding these two, the group-2 garnets form a correlation corresponding to 391±120 Ma with an intercept of 0.51160. This scattering of data is similar to that observed for the Sm-Nd system for subcalcic garnets from Russia (Pearson et al., 1995; Jacob et al., 1998).

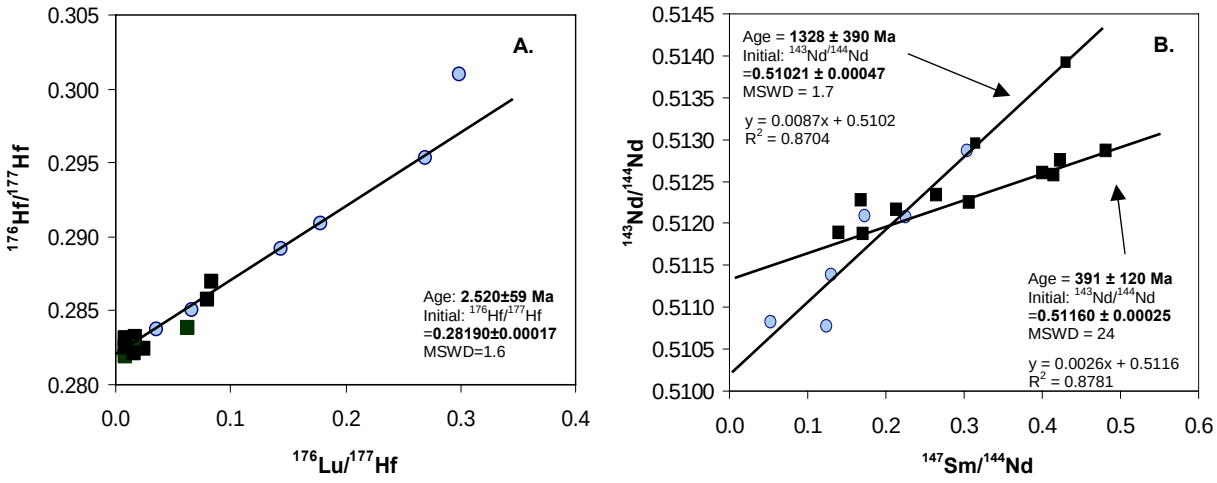

Fig. 3.6. Isochron diagram for the subcalcic garnets from Finsch for: (A). the Lu-Hf system, where group-1 garnets (circles) define an isochron of 2.52 Ga. Garnet HMCGrt 29, which has the highest $^{176}Lu/^{177}Hf$, does not fall on this isochron and is omitted from the age calculation. Most of the group-2 samples (squares) have $^{176}Lu/^{177}Hf$ lower than that of CHUR and scatter around the isochron; (B).the Sm-Nd system, where group-1 garnets (circles) define a linear trend with R^2=0.8704, defining an errorchron age of around 1.3 Ga. Two of the group-2 garnets (squares) also fall on this errorchron. The other group-2 garnets give a younger errorchron age of around 400 Ma.

3.4 Discussion

The complex trace element patterns and ratios as well as the large variation and extreme values of Hf and Nd isotopes of the subcalcic garnets indicate that the present day mantle below the Kaapvaal craton is the product of a number of depletion and enrichment events since its origin in the Archean (Carlson et al., 1999; Irvine et al., 2001; Simon et al., 2007). A possible time sequence will be discussed in the following in conjunction with a model for the origin of the protoliths of the two groups of subcalcic garnets.

Based on their Ni contents (Table 3.3 in App.-1) temperatures from 1011 to 1121 °C and 1022 to 1218 °C are calculated with the Ni-in-garnet thermometers of Canil (1999) and Griffin et al. (1989b) respectively. It can be seen from the comparison of temperatures calculated with the two-pyroxene

thermometer of Brey and Köhler, (1990) for lherzolite xenoliths from Finsch (Chapter 4) with those derived with the two Ni-in-garnet thermometers that T_{Canil} underestimates and $T_{Griffin}$ mostly overestimates temperatures in this T-range. An addition of about 70 °C to the T_{Canil}–temperatures is indicated. This brings the subcalcic garnets to a temperature range between 1080 and 1190 °C corresponding to a depth range of 150-180 km along a cratonic conductive geotherm of 40 mW/m^2 (Chapman and Pollack, 1977). This is at the shallower end of the depth range derived for the Finsch peridotite xenoliths (160-210 km; Viljoen et al., 1992; Chapter 4).

3.4.1 Timing of depletion of the subcalcic garnet protoliths

As previously mentioned, subcalcic garnets can be considered to be the major carrier for Al_2O_3, Cr_2O_3 and a number of trace elements, including MREE-HREE and Zr-Hf. The HREE patterns of such garnets particularly reflect depletion of the peridotites (by one or several partial melting events), as they do not display any alteration by subsequent metasomatic overprint. Group-1 garnets display fractionated HREE up to an extreme of 13 for $(Lu/Er)_N$, a narrow range in Cr# (8-11) and relatively low CaO from 2.7 to 0.3 wt.% (Fig. 3.2). Such strongly fractionated HREE together with very low abundances are difficult to produce by a single stage partial melting event with garnet as a residual phase, as HREE in residual garnets would remain high under such conditions. Low HREE may have been produce by pre-depletion in the spinel stability field prior partial melting in the garnet stability field. In fact, some pre-depletion at low pressure is indicated by the small increase of Cr# for the garnets with high $(Lu/Er)_N$ (Fig. 3.2). However, according to their Cr/Al (Bulatov et al., 1991; Stachel et al., 1998), such pre-depletion can not have exceeded 5-10%, which barely can explain the low HREE. Alternatively, very high degrees of partial melting in the deep mantle may lead to the exhaustion of garnet. Residual orthopyroxene may still have contained a garnet component in this case. Accordingly, garnet would exsolve during cooling and display low Cr/Al ratios and low and highly fractionated HREE, as observed for subcalcic group-1 garnets. Such a scenario may have occurred during a two-stage melting process both within the garnet stability field. Two-stage melting is indicated by the results of the Lu-Hf isotope system which implies partial melting at 2.5 Ga of an already depleted mantle source (εHf ~ +25 at 2.5 Ga). It is also consistent with the high degrees of mantle melting of up to 50%, which are required for craton formation according to Card (1990) and other previous studies.

The highly radiogenic εHf values (Fig. 3.5) are the consequence of high, time integrated $^{176}Lu/^{177}Hf$ ratios which were caused by the dominant role of garnet as a residual phase. The large spread in this ratio results in a well defined Hf isochron with a “minimum age” of 2.5 Ga for the final depletion event (Fig. 3.6A). The initial of the isochron corresponds to εHf ~ +25, which indicates that the mantle was already significantly depleted prior to this last depletion event. Multiple melting is also indicated by the major element composition of the garnets. The correlation of both, group-1 and -2 garnets point to a lower CaO content and a higher Cr# than that of a primitive peridotite (Fig. 3.2A). This indicates that the garnet host rocks cannot be the residues of a single stage partial melting event of a primitive mantle composition.

We place the first depletion event at ~ 3.6 Ga for several reasons (Fig. 3.7): i) HMCF-grt 29 (not a member of the isochron in Fig. 3.6A) gives a ~ 3.6 Ga model age for single stage depletion (Fig. 3.7), ii) a long time period on the order of >1 Ga and high Lu/Hf in the residue are necessary to produce the radiogenic εHf ~ +25 as obtained for the isochron initial and iii) the oldest crustal ages on the Kaapvaal craton are around 3.6 Ga (Kröner and Tegtmeyer, 1994; Kröner, et al., 1996).

In contrast to group-1, group-2 garnets have high Cr# (>11), low $(Lu/Er)_N$ (<3.6) and correspondingly flat HREE patterns and low HREE abundances. These geochemical signatures indicate partial melting in the spinel or plagioclase stability field. Also, most of the group-2 garnets have unradiogenic εHf and εNd (Fig. 3.5). As discussed below, this indicates that both Nd and Hf were strongly affected by metasomatism which dramatically changed the original Sm/Nd and Lu/Hf ratios. Only a few, less metasomatized garnets preserved relatively high Lu/Hf ratios and have therefore radiogenic Hf isotope compositions, while the rest of group-2 garnets scatter around the Hf-isochron, which is defined by the group-1 garnets. This may indicate a similar final depletion age of group-1 and group-2 garnets. However, because of the strong metasomatic effects on Hf of the group-2 garnets, this remains uncertain.

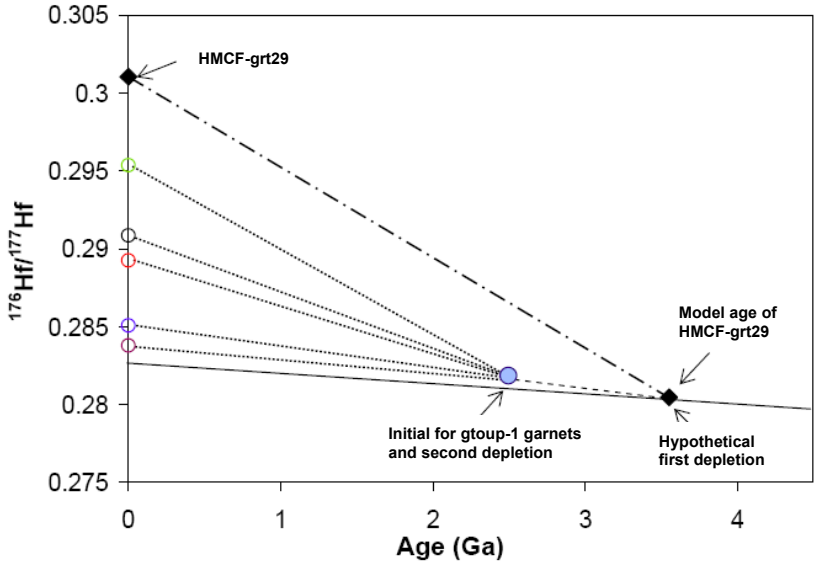

Fig. 3.7. Hf evolution diagram for group-1 garnets. The present day $^{176}Hf/^{177}Hf$ ratios are connected with their initial (blue circle) by dotted lines. The initial is 25 εHf units higher than the $^{176}Hf/^{177}Hf$ value for the primitive mantle at 2.5 Ga. This indicates a previous depletion event of the group-1 garnet protoliths. It may have occurred at ~ 3.6 Ga, the model age of HMCF-grt29 (black diamond on the primitive mantle evolution line). The dashed line represents the $^{176}Hf/^{177}Hf$ development after the first partial melting event.

3.4.2. Timing of re-enrichment of the host rocks

Normalizing the subcalcic garnets from Finsch to the Vitim 313-105 garnet (Fig. 3.3B) shows that they are all re-enriched to various extents in light and middle REE and other incompatible elements. Some samples even appear to be affected by a second enrichment event because of the steepening slope of their LREE compared to MREE (indicated in Fig. 3.3B by the dashed line). All other garnets appear to have a continuous slope from Tb to Ce and the thick grey line in Fig. 3.3B shows the estimated composition of a single stage metasomatizing agent. Since garnets with high $(Lu/Er)_N$ and $^{176}Lu/^{177}Hf$ are highly depleted and have very low Hf concentrations the metasomatizing agent cannot have contained any appreciable amount of Hf. In contrast LREE, such as Sm and Nd, are strongly enriched which is in accord with the low or even negative εNd (Fig. 3.5).

It is well known from experimental work (Kelemen et al., 1993; Suhr et al., 1998; Green et al., 2000) that Hf behaves similar to Sm during partial melting in the mantle with an order $D_{Nd}<D_{Hf}\leq D_{Sm}$. Thus, Hf and other HFSE should be similarly enriched as Sm and Nd by an infiltrating melt. We find low Hf combined with low Ti and Zr and enriched Sm and Nd as a characteristic of all group-1 garnets. Thus the metasomatic overprint cannot be produced by a silicate melt. Metasomatism by a carbonate melt generates low HFSE/LREE ratios (Yaxley et al., 1991; Ionov et al., 1993; Rudnick et al., 1993; Brey et al., 2008) but this is unlikely because this also creates high U contents and high Zr/Hf and Nb/Ta ratios (Ionov et al., 1993; Rudnik et al., 1993), which is not observed in the garnets of this study. Stachel et al. (2004) suggested aqueous fluids as metasomatic agent for the generation of the garnet inclusions in diamonds. This appears to be the most likely way to generate the observed trace element and isotope signatures in group-1 garnets. According to the experimental data of Adam et al. (1997) and Stalder et al. (1998) fluids extracted from subducted, rutile bearing eclogite have strongly fractionated REE pattern with high LREE and LILE, moderate amounts of Nb and Ta, and only insignificant amounts of HREE, Zr, Hf and Ti. Enrichment by such fluids retains the original depleted HREE and leads to high LREE/HFSE, which agrees with the observations for the group-1 garnets.

Metasomatic overprint by subduction related fluids is also in agreement with the negative εNd signature of the group-1 garnets. The highly fractionated REE of the enriching fluids (see Fig. 3.3B) produce low $^{147}Sm/^{144}Nd$ ratios in the garnets and consequently low time integrated $^{143}Nd/^{144}Nd$. This leads to the preservation of very low $^{143}Nd/^{144}Nd$ ratios in some garnets close to the initial of the 1.3 ±

0.4 Ga errorchron (Fig. 3.6B). The low initial is probably the signature of the metasomatizing fluid. Such low values can be best explained as the nature of a fluid emanating 1.3 Ga ago from an old subducted oceanic crust (Fig. 3.8A). The fluid did probably completely overwhelm the Sm and Nd contents and also the Nd isotopic composition of the intruded peridotite, which originally had a highly depleted nature.

Group-1 garnets show a significant correlation (R^2 =0.87) of $^{143}Nd/^{144}Nd$ and $^{147}Sm/^{144}Nd$ (Fig. 3.6B). There is no correlation of $^{143}Nd/^{144}Nd$ with 1/Nd; i.e. mixing of two reservoirs is not indicated. Thus, we interpret the correlation of the Nd isotopes with Sm/Nd as an errorchron, providing age information for the first major enrichment event by aqueous fluids, after the depletion at 2.5 Ga, of the subcratonic mantle at 1.3 ± 0.39 Ga (Fig. 3.8A).

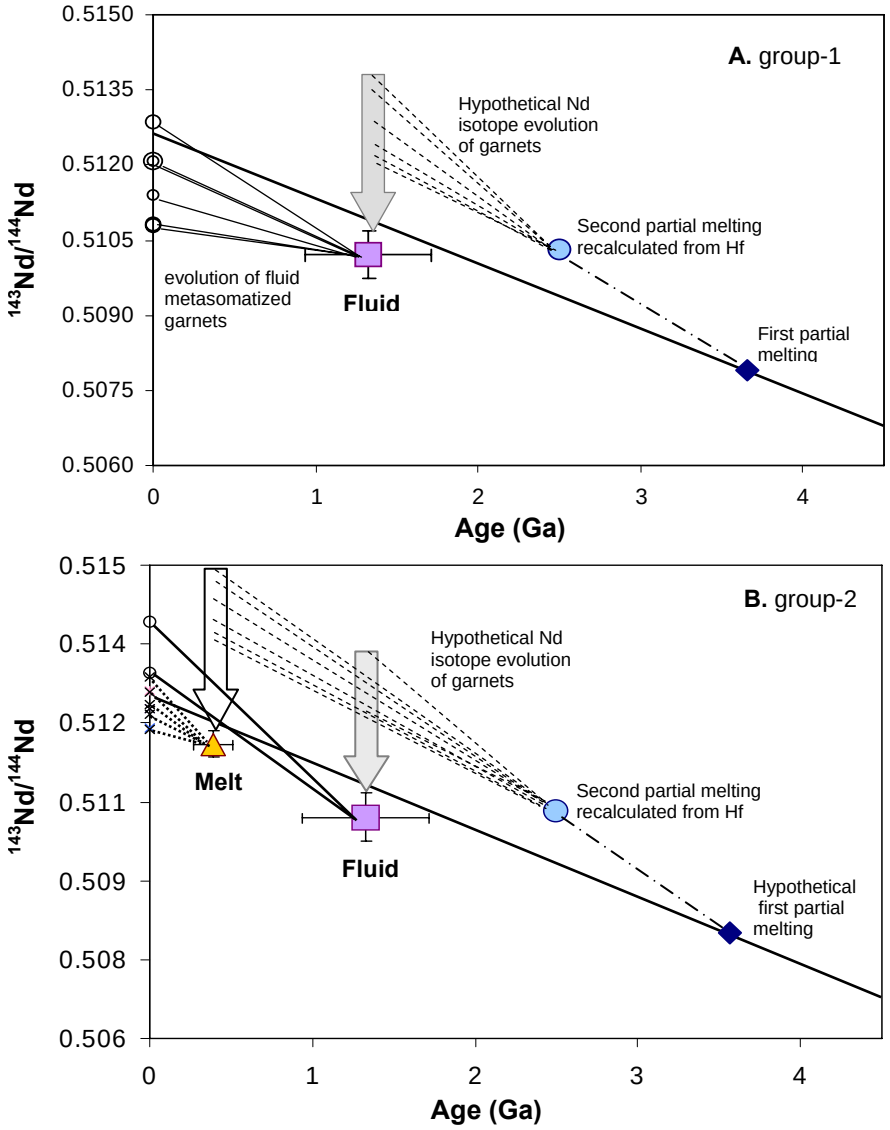

Fig. 3.8. Potential timing of the metasomatic overprint of group-1 (A) and group-2 (B) garnets as indicated by their Nd isotope compositions. The host rocks for group-1 garnets were metasomatized at ~ 1.3 Ga and with the grey arrow pointing to the Nd isotopic composition of the fluid (= initial of the errorchron). B. Host rocks for group-2 garnets were metasomatized mostly at ~ 0.4 Ga with the white arrow pointing to the Nd isotopic composition of the metasomatizing melt (= initial of the errorchron). Two group-2 garnets were presumably only metasomatized by the fluid, which was responsible for the group-1 metasomatism (grey arrow). Depletion ages are taken from Lu-Hf systematics and the corresponding Nd-isotope compositions are calculated from Hf initials, assuming εHf =1.33 x εNd +3.19 (Vervoort et al., 1999).

Group-2 garnets are characterized by high HFSE and, all but two garnets, by a correlation (R^2 = 0.88) of $^{143}Nd/^{144}Nd$ and $^{147}Sm/^{144}Nd$ corresponding to an errorchron age of 391±120 Ma. The

moderate correlation of $^{176}Hf/^{177}Hf$ and $^{176}Lu/^{177}Hf$ (Fig. 3.6A) of the group-2 garnets may be interpreted as a mix of an originally depleted signature and metasomatic enrichment. The different trace element and isotope systematics of these samples indicate that they were enriched by a different event than the group-1 garnets. They are also more consistent with enrichment by a melt. This melt metasomatism generated trace element patterns in the garnets that are higher in both HFSE and REE resulting in disturbed Hf isotope systematics. The timing for the enrichment event may be indicated by the errorchron of 391±120 Ma (Fig. 3.8B), and is thus much later than the enrichment of the group-1 garnets and with a different metasomatizing agent. Only two of the group-2 garnets were apparently mainly affected by the aqueous fluid, which previously affected group-1 garnets at 1.3 Ga ago.

3.4.3 Origin of subcalcic garnets and implications for diamond formation

The origin of subcalcic garnets and their host rocks together with their link to diamond formation was and is highly debated within the last decades (Ringwood, 1977; Boyd and Gurney, 1986; Nixon et al., 1987; Kesson and Ringwood, 1989; Boyd et al., 1993; Malkovets et al., 2007). There are two main classes of models: 1) The protoliths were residues of partial melting at low pressures in a kind of mid-ocean ridge setting which were transformed into garnet harzburgites upon subduction (Ringwood, 1977; Kesson and Ringwood, 1989). The residues consisted of high temperature, clinopyroxene-free spinel harzburgite, which were converted to an olivine + orthopyroxene + subcalcic garnet ± chromite assemblage upon subduction (Bulatov et al., 1991; Stachel et al., 1998). A modified version assumes the garnet harzburgites to be the metamorphic products of strongly serpentinized, subducted oceanic lithosphere, where the serpentinization efficiently removed Ca and added Mg to the oceanic lithosphere (Schulze, 1986). 2). A second class of models assumes that infiltration of carbonatite melt (Griffin et al., 1992) has leached Ca from already depleted garnet or that subcalcic garnets were created by a reaction of Si-rich fluids and grt-free harzburgite at high pressure (Malkovets et al., 2007).

New in the discussion on the origin of subcalcic garnets is that we can distinguish two groups of garnets both by their major and trace element- and by their isotope compositions. Accordingly, they can be generated in two different ways by multiple depletion, either mostly at high pressure (group-1 garnets) or mostly at low pressure (group-2 garnets). Crucial in the interpretation of an origin is the relationship between CaO and Cr# of the garnets and by inference of the bulk rocks. Experimental work shows that partial melting with orthopyroxene and garnet as residual phases barely leads to an increase of Cr# in the bulk residuum and the residual garnet (even at high degrees of partial melting) while CaO in garnet continuously decreases with increasing temperature (Bulatov et al., 1991; Canil and Wei, 1992; Stachel et al., 1998). This is our observation for the group-1 garnets. The constant Cr# and the large range in CaO combined with the highly fractionated HREE (Fig. 3.2) and the high Lu/Hf ratios (which resulted in highly radiogenic Hf-isotope compositions; Fig. 3.5 and 3.6) provide a line of evidence for a high pressure origin of the protoliths as residues of partial melting in the garnet stability field. In contrast, partial melting at low pressure in the spinel/plagioclase stability field is therefore the only way to explain the origin of the protoliths of the group-2 garnets. Bulatov et al. (1991) and Stachel et al. (1998) have shown that partial melting in the spinel stability field leads to high Cr# in the residual peridotite consisting of olivine, high temperature orthopyroxene and chromite. Subduction of such residues leads to the growth of subcalcic garnets with high Cr#, such as displayed by group-2 garnets. Such garnets grow by the metamorphic reaction opx+sp=ol+grt upon subduction and their host rocks should have been the peridotitic part of subducted oceanic lithosphere (Ringwood, 1977; Kesson and Ringwood, 1989).

Diamond growth during partial melting is highly unlikely because it requires a specific combination of redox conditions and fluid compositions at variable P, T conditions. It is much more likely that any carbon species present will be dissolved in the melt and therefore removed from the residuum. Consequently, a carbon species has to be reintroduced into the system, i.e. during metasomatism to allow the growth of diamonds. In fact, depletion and subsequent metasomatic enrichment created the sigmoidal, chondrite normalized REE patterns, which are typical for the garnets from subcratonic peridotites and also typical for the garnet inclusions in diamonds. There is also general agreement that re-enrichment and the sigmoidal patterns are directly connected with diamond growth (e.g. Stachel et al., 2004). Sm-Nd isotope systematics of the subcalcic garnets of this

study indicates that enrichment occurred at ~ 1.3 Ga or later, which implies non-Archean, late diamond growth. In contrast, Sm-Nd and Re-Os model ages of peridotitic garnet and sulphide inclusions in diamonds generally give ages of more than 2.5 Ga and mostly >3 Ga (e.g. Richardson et al., 1984, 1986, 1990, 1993, 2001, Pearson et al., 1998, Shirey et al., 2001, 2004). We deduce from our results that Sm-Nd isotope systematics of the peridotites are likely overwhelmed by that of the metasomatic agents and that diamond formation is not older than 1.5 Ga in Finsch. The Re-Os ages on sulphide inclusions may be interpreted to provide time constraints on partial melting rather than on diamond growth.

Indeed, Sm-Nd two-point garnet-cpx isochron ages of pooled eclogitic inclusions in diamonds from Finsch and the Premier mine range between 1100 and 1600 Ma (Richardson, 1986 and Richardson et al., 1990). This isochron relationship may partially result from mixing and thus may not have strict age significance (Richardson et al., 1993). However, the ages are largely in agreement with our derived metasomatic overprint of the subcalcic garnets at around 1328±390 Ma. Also rare Re-Os isochrones from syngenetic sulphide inclusions provide very young ages of 1 Ga and 70 Ma, which may correspond to real diamond formation ages (Pearson, 1998). Thus, there is substantial evidence for non-Archean diamond growth, as deduced from Sm-Nd systematics of this study on subcalcic garnets.

3.5 Summary and inferences

From the subcalcic garnets we can deduce that the present day mantle underneath Finsch (and by inference of the Kaapvaal craton) is the residue of multiple, in situ depletion interfaced with subducted residues of partial melting at low pressures at ocean ridge like settings. This depleted mantle was subsequently overprinted and re-enriched by two events. The timing of these events can only be partially reconstructed. However, we can reconstruct a scenario for the mantle evolution below the Kaapvaal craton with the following fixed dates:

I) A final depletion event occurred at around 2.5 Ga which probably took place in situ in the garnet stability field underneath an existing continental crust. This event was predated by, at least one earlier depletion, which may have been at around 3.6 Ga.

II) Into this subcontinental mantle, slices of an oceanic lithosphere were injected by a subduction process (Foley et al., 2003), which consisted of depleted peridotite and by inference of its basaltic (picritic?) supplement. These two lithologies were the precursors of the Cr-rich garnet peridotite suite and of eclogite. The time of partial melting at low pressures in the spinel stability field is unknown. However, subduction occurred prior to 2.5 Ga, assuming that the group-2 garnet protoliths experienced a second partial melting event together with group-1 garnet protoliths.

III) Enrichment occurred in 2 stages, at around 1.3±0.39 Ga with a subduction related fluid phase, and at around 0.4±0.12 Ga with a silicic melt as metasomatizing agent. There is no evidence of earlier metasomatic enrichment, after the final depletion at ~ 2.5 Ga. This scenario is in parts similar to the one given by Shirey et al. (2004) for the creation, stabilization and modification of the Archean Kaapvaal-Zimbabwe craton.

Carbon can be juvenile but much of it is also returned to the mantle by subduction. We therefore propose diamond formation during these enrichment events at ~ 0.4-0.5 and ~ 1.3 Ga, although the mantle below the Kaapvaal craton is much older (>2.5 Ga).

CHAPTER 4

Mantle formation and modification based on Finsch mine peridotites (Kaapvaal craton, S.A.)

4.1 Introduction

The major element composition of the Archean sub-continental lithospheric mantle (SCLM) from southern Africa indicates depletion by very high degrees of partial melting, relative to a primitive upper mantle composition (Boyd and Merzman, 1987; Mc Donough and Sun, 1995; Walter, 1998). However, a major proportion is also re-enriched to various extents. A special feature is the Si-enriched character of a substantial part of the South African peridotites, which finds its expression in high modal abundances of orthopyroxene (opx). This feature is still hotly debated (Kesson and Ringwood, 1989; Herzberg, 1993; Rudnick et al., 1994; Kelemen et al., 1998; Walter 1998; Boyd et al., 1997; Herzberg, 1999; Simon et al., 2007). Explanations include e.g. metamorphic differentiation of hot depleted mantle residue (Boyd et al., 1997), and the cumulate addition to the previously depleted lithosphere (Herzberg, 1993; Herzberg, 1999), or the addition of Si-rich melts from subduction zones to the depleted mantle peridotites *(*Rudnick et al., 1994; Kelemen et al., 1998). A recent theory is that opx-rich peridotites form by a reaction of aquatic fluids with depleted peridotites (Zhang et al., 2001; Bell et al., 2005; Simon et al., 2007). Enrichment in incompatible trace elements is ubiquitous and may be accompanied by the growth of new minerals (cryptic versus modal metasomatism – Dawson, 1984; Haggerty, 1987; Menzies et al., 1987; Hoal et al., 1994; Griffin et al., 1999a; Gregoire et al., 2002; Gregoire at al., 2003). The metasomatic processes are believed to be due to the infiltration of different melts or fluids. This may have occurred early in the history of the South African SCLM (Dawson, 1972; Harte et al., 1993) or be related to processes connected with the more recent kimberlite magmatism (Zhang et al., 2000; Simon et al., 2003).

This chapter presents the petrographic characteristics of the Finsch mine peridotite xenoliths as well as the major and trace element chemistry of their constituent minerals. These data will help to constrain the physical conditions (depth, temperature and degree) of the depletion event(s) and the nature of the enriching agent(s). Results from experimental studies on the behaviour of major elements (Bulatov et al., 1991; Walter, 1998, 1999, 2003; Kushiro, 2001) and trace elements (Johnson, 1998; Green et al., 2000) will help to quantify these conditions. The bulk chemistry of the peridotites is recalculated from the modal abundances and chemistry of the constituent minerals.

4.2 Petrography and modal mineralogy

In kimberlite geology garnet peridotites are mainly divided into harzburgites (hzb) and lherzolites (lhz), to distinguish between clinopyroxene (cpx) free and clinopyroxene bearing peridotites. This division was developed for the classification of garnets from heavy mineral concentrates, where in a CaO-Cr_2O_3 diagram garnets differentiate peridotites on Ca –saturated (cpx bearing) and – undersaturated (cpx free) (Fig. 4.1; Sobolev, 1973 Gurney and Switzer, 1972; Schulze, 2003). According to the Streckeisen (1976) nomenclature samples with up to 5 vol.% cpx are named harzburgites and only samples with more than 5 vol.% cpx and suitable content of orthopyroxene (opx) and olivine (ol) are named lherzolites (Fig. 4.2). By this classification olivine rich (> 90%) samples with less than 10 vol. % of cpx and opx together, are determined as dunites. The Streckeisen (1976) nomenclature gives a more detailed aspect on the petrologycal characteristics of samples and therefore will be used in this work. Only where it was important cpx-free samples were also lined out.

All but one, of the 31 analysed peridotite xenoliths from the Finsch mine, kindly supplied by G. Brey, are garnet peridotites. The only exception is sample F-23, a spinel (sp) peridotite. The other samples are: 22 garnet bearing harzburgites, 4 lherzolites, 4 dunites and one garnet and spinel bearing dunite (Fig. 4.2, see also Table 1 in App.-2). Two samples show only olivine and opx in thin section (F-21, F-28) and are calculated by harzburgites. Two of the observed dunites are cpx-free dunites (F-2 and garnet-sp bearing dunite 882 (Skinner, 1986). Only one of the 21 studied harzburgites has Ca-undersaturated garnet and is really cpx-free hzb (F-7). Only those three features with Ca-undersaturated garnet plot in the harzburgite field (Fig. 4.1).

One sample is rutile-pentlandite bearing garnet-harzburgite (F-12). Three cpx-bearing harzburgites (554-XM46, 556-XM48 and 865) are diamond bearing, already described by Shee et al., 1982 and Viljoen et al., 1992. They were made available by F. Viljoen for further analytical work.

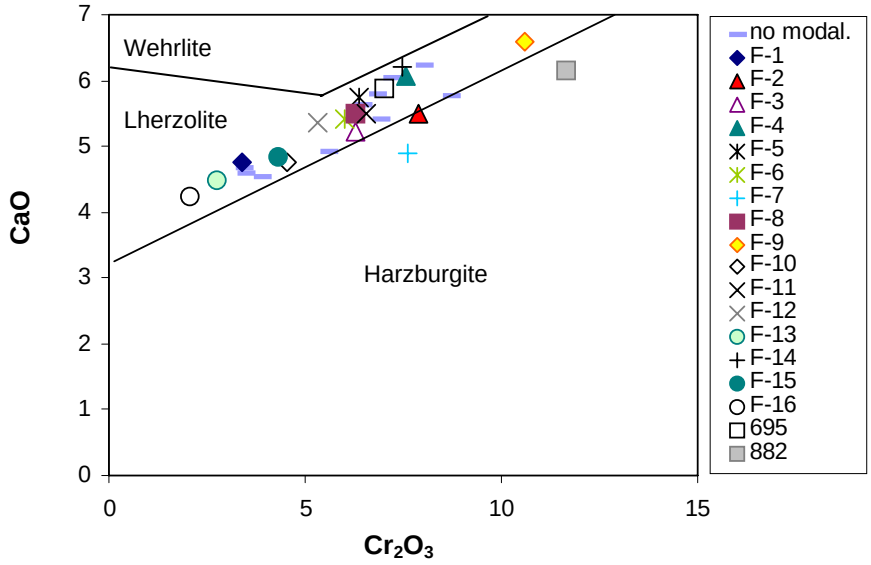

Fig. 4.1. CaO-Cr_2O_3 discrimination diagram (Sobolev 1973; Gurney and Switzer, 1972; Schulze, 2003) for garnets from the Finsch mine peridotites. The garnets are subdivided into harzburgitic (equilibrated only with opx), lherzolitic (equilibrated with opx and cpx) and wehrlitic (equilibrated only with cpx) parageneses.

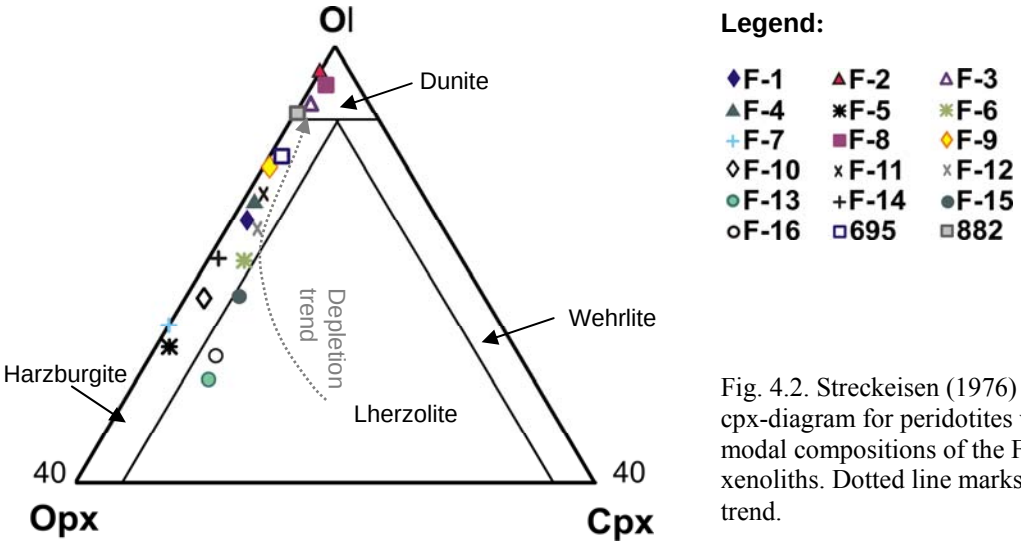

Fig. 4.2. Streckeisen (1976) ol-opx-cpx-diagram for peridotites with the modal compositions of the Finsch xenoliths. Dotted line marks depletion trend.

According to the classification of Harte (1977) the majority of the samples have medium- to coarse-grained tabular to equant textures. Only three have a mosaic-porphyroblastic and five have a porphyroclastic texture (see Appendix App.-2). Some of the samples with porphyroblastic texture have a foliated microstructure. Petrographic details are given in Table 1 in App.-2. The appendix App.-2 also contains information of each xenolith including their petrography, photographs of their thick or thin sections, backscattered electron (BSE) images of interesting features and EDS diagrams of different sulfide features.

"Point-counting" on one or two slices across each xenolith was used to determine the modal mineral abundances in the peridotites. Each slice was copied onto a transparent millimetre paper, the exposed surfaces of identical minerals were added up and the mode was calculated by normalizing to 100% (Fig. A2b in App.-2). For ten samples only thin sections were available and the mineral mode is only a rough approximation.

The averages of olivine, opx, cpx and garnet for all garnet peridotites are 73, 19.4, 5.7 and 1.9 vol.%, respectively (Table 1 in App.-2). In cpx-bearing garnet harzburgites the olivine modes range from 56-85 vol.% (up to 93 vol.% in dunites), the opx modes from 4-39 vol.%, cpx modes from 0.01-

4.3 vol.% and garnet modes from 1-10.2 vol.%. The garnet lherzolites have low and restricted abundances of cpx (5-6.5 vol.%), but higher modal abundances of garnet (9-12.5 vol.%) than the cpx-bearing garnet harzburgites. One cpx-bearing harzburgite (F-12) has around 1 vol.% of rutile and one cpx-free harzburgite (882 – Skinner, 1986) has 0.2 vol.% of chromite. Secondary spinel, cpx and sometimes phlogopite (phl), amphibole (amph) and sulfides (sulf) are present with <0.1 vol.% in some samples (see App.-2).

There is a crude positive correlation of modal olivine and a negative correlation of modal garnet with sample size. Such correlations were studied in coarse-grained cratonic mantle xenoliths by Cox et al. (1987), who attributed them to the close spatial relationship between those two minerals.

Large olivine grains commonly display a euhedral to subhedral tabular habit with straight to curvilinear grain boundaries. In porphyroclastic and especially mosaic-porphyroclastic samples olivines are oval elongated with olivine neoblasts tailings and always show mineral-preferred orientation. Small grains in the same textural type are euhedral with or without preferred mineral orientation. Olivines usually show undulous extinction. In a few samples they are poikilitically enclosed in opx and garnet.

Orthopyroxene is usually subhedral to anhedral with elongated tabular to oval shape. It is occasionally deformed and shows sector undulous extinction. It rarely occurs in irregular form in interstices. Elongated or rounded grains with strongly fractured rims are characteristic of porphyroclastic samples and rim opx neoblasts were also observed in mosaic-porphyroclastic samples. In porphyro- to mosaic-porphyroclastic samples opx has a preferred mineral orientation.

Clinopyroxenes occur as small anhedral or irregular grains with curvilinear grain boundaries. Common are grains with lamellar undulous extinction, and in some samples kink bended cpx is also observed. They are spatially closely related with opx, rarely with garnet. Clinopyroxene neoblasts are observed in mosaic-porphyroclastic samples. It is occasionally included in opx or garnet.

Rounded to equidimensional polygonal shaped garnets prevail, but elongated or irregular shaped grains can also be observed. All samples have garnets with well-developed kelyphite rims of amorphous looking brown material plus small spinels and sometimes related with amphibole, phlogopite and cpx. Garnets are fractured in some samples and the association like in kelyphite fills the cracks. Glaser et al. (1999) attribute the kelyphite rims to decomposition of garnet either related to a decrease in pressure or to the interaction with kimberlite.

Large rutile (0.6-1 mm) occurs in one garnet harzburgite. The subhedral grains occur along garnet grain boundaries and rarely as an interstitial mineral or as an inclusion in garnet. They are occasionally associated with ilmenite and sulfide. Needle like dark coloured exsolutions were observed in all rutile grains.

Spinel is present as secondary mineral in garnet coronas as small (20-200 μm) skeletal or spongy crystals. Large (~ 1.5 mm) subhedral, dark brown spinel is a constituent in the only spinel peridotite and in the only cpx-free garnet bearing dunite.

Occasionally, irregular flakes of sulfides occur in some samples in interstices or in fractures of olivine grains. Rounded spherules are observed as inclusions in garnet and opx. Their compositions vary from sample to sample.

4.3 Results

4.3.1 Mineral major and minor elements

Olivine

Mg# values (Mg#=100xMg/(Mg+Fe)) in olivine range from 91.2 to 93.7 with an average of 92.4. This average is in good agreement with that from the Kimberley samples (Simon et al., 2007) and slightly higher than a value of 92.1 given by Pearson et al. (2003) for the average cratonic mantle. The highest Mg# values are from the cpx-free dunite 882 and the cpx-bearing dunite F-3. The lowest Mg# is observed in lherzolite F-13. Olivines from dunites have Mg# higher than 93 while those from harzburgites and lherzolites vary between 91.2 and 93 (Fig. 4.3). All diamond bearing samples have medium Mg# values in olivine (91.9-92.9).

The NiO content in olivines varies from 0.34 to 0.41 wt.% with two further samples (695 and 882) having less than 0.3 wt.% (Table 4.1 in App.-3). Mg# and NiO appear to correlate in two opposite

ways: a positive correlation of Mg# and NiO wt.% correspond to a trend caused by depletion and a negative correlation which does not correspond to a trend of increasing partial melting, but must be caused by a superimposed process (Fig. 4.3A).

CaO varies in olivine from 0.022 to 0.041 wt.% with a scattering negative correlation with Mg# (Fig. 4.3B, Table 4.1 in App.-3), which is in accord with a partial melting trend.

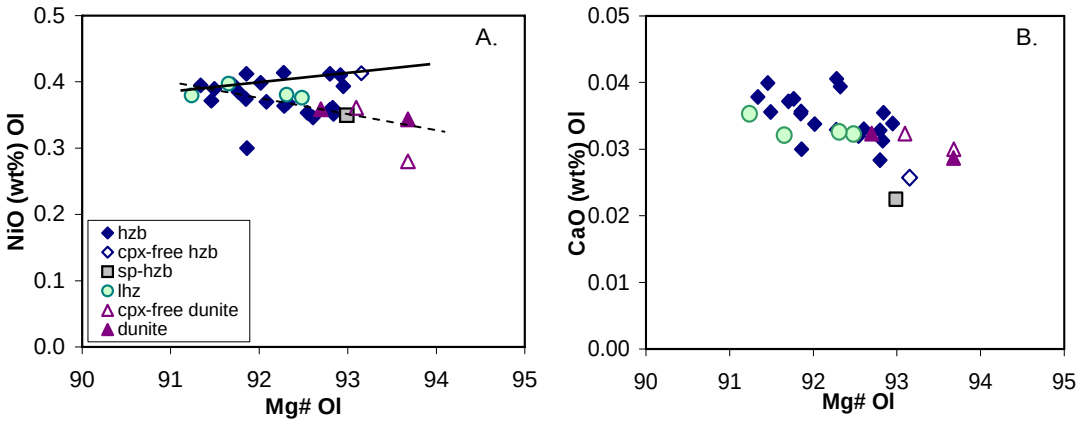

Fig. 4.3. Mg# vs. NiO (A) and CaO (B) in olivine from the Finsch peridotites. (A) Depletion trend is marked with the thick line.

Orthopyroxene

Orthopyroxenes always have slightly higher Mg# than olivine, ranging from 92.3 to 94.6 (Fig. 4.4; Table 4.1 in App.-3). This is in accord with known equilibrium partitioning (Brey and Köhler, 1990). There is a rough positive correlation between Mg# and Cr# (Cr# = 100xCr/(Cr+Al)) with harzburgites having a higher Mg# and Cr# than lherzolites (Fig. 4.4). The average Cr# of 27.3 is considerably higher than for garnet peridotites from Kimberley (24.4 - Simon et al., 2007). The Mg# of opx's shows a rough negative correlation with Al_2O_3, CaO, and Na_2O (Fig. 4.4). That marks strong influence of two processes: sample depletion and inter-mineral temperature equilibration on the chemical composition of opx. There are some out-layers of this trend (marked with the oval-shaped field in Fig. 4.4), like the opx from the dunites (F-2, F-3) and the cpx-bearing harzburgites (F-9, F-21, F-25d), which have relatively high Ca and Na contents for their high depletion factor (Mg#) (Fig. 4.4).

There is a positive co-variation between Al_2O_3 and Na_2O, and negative correlation between Al_2O_3 and Cr_2O_3 in opx (Fig. 4.4). In the Al-Cr space, lherzolites form a trend with dunites and spinel-harzburgite, while cpx bearing harzburgites group on either side of the correlation. Dunites (except for F-2), cpx-free harzburgite and spinel-peridotite have orthopyroxenes, which are most depleted in Ca and Na compared to Al. TiO_2 appears to be elevated in some orthopyroxenes but is far from saturation as demonstrated by the high Ti in opx from the rutile bearing sample F-12. Re-enrichment of Ti is supported by the fact that a correlation between Mg# and TiO_2 is lacking (Fig. 4.4).

The common opx neoblasts along the rims do not differ in major and trace elements from their coarse opx hosts.

Clinopyroxene

Clinopyroxenes generally have Mg# > 91.8 and Cr# > 21.6 (Table 4.1 in App.-3) with a positive correlation between them (Fig. 4.5), whereby those from harzburgites are higher in Cr# than from lherzolites. The Na correlates positively and Ca negatively with Al. Except for the rutile-bearing sample F-12, TiO_2 in cpx is lower than 0.17 wt.% (Fig. 4.5). Noticeable, one cpx from a lherzolite has almost the lowest Ti content.

Chromium and Al in cpx describe two trends, one is a negative correlation dominated by the lherzolites and the other one a positive correlation of the harzburgites. The diamond bearing samples have cpx most depleted in Cr and Al (circled in Fig. 4.5).

The Na_2O ranges from 0.7 to 2 wt.% with no correlation with Mg#. Three samples (F-3, F-10, F-12) with Na_2O > 1.9 wt.% coincide with Type II cpx's of the MARID suite as defined by Gregoire et al. (2003) (Fig. 4.5). These samples also have relatively high Cr contents, a further kinship to the MARID suite (Fig. 4.5; Table 4.1 in App.-3). This implies metasomatic enrichment with a lamproitic

or a Group II kimberlite like melts according to Sweeny (1993), Hamilton et al. (1998), Gregoire et al. (2002) and Gregoire et al. (2003).

Compositional differences in cpx core and rim is noticed in two samples (F-3, F-11), where edges have higher Mg#, Cr#, Ca# and TiO_2 and significantly lower Na_2O and Al_2O_3 (Fig. 4.5).

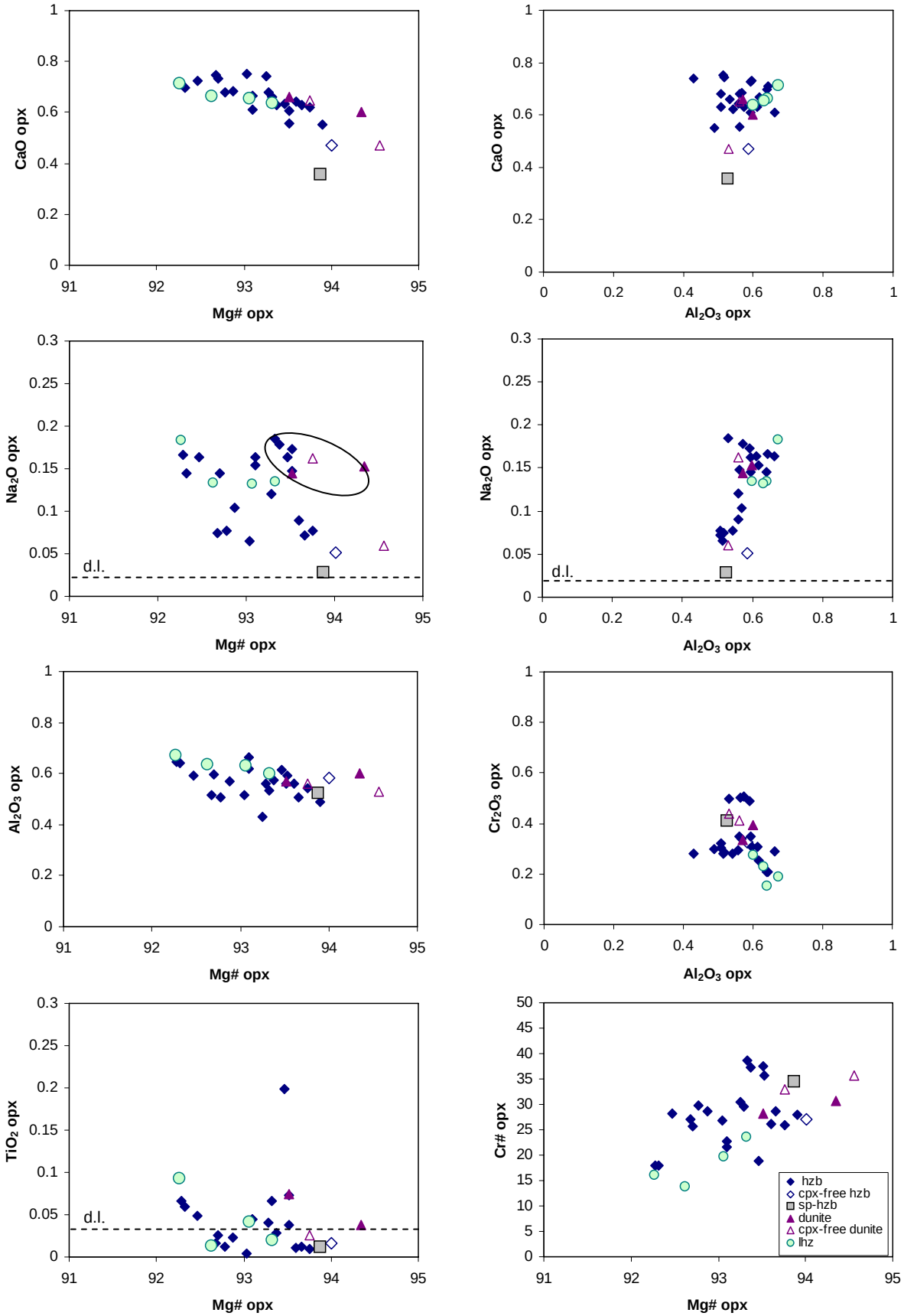

Fig. 4.4. Major element variations in orthopyroxenes from Finsch. d.l.= detection limit.

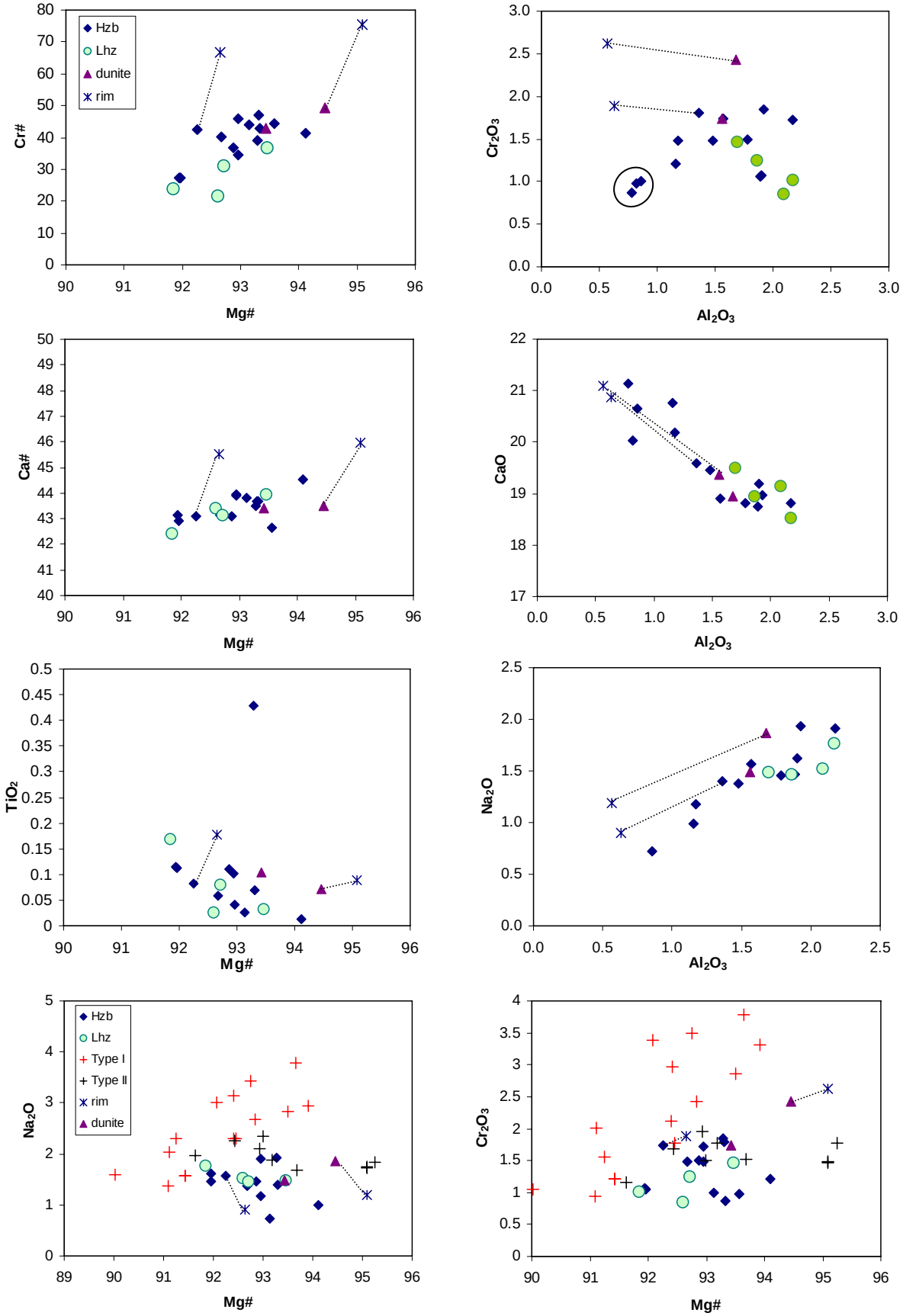

Fig. 4.5. Major element variations in cpx from Finsch peridotites. Clinopyroxenes are homogeneous in composition except for samples F-3 and F-11, where stippled lines connect cores and rims. Crosses in the Mg# vs. Cr_2O_3 and Na_2O diagrams are Type I and Type II clinopyroxenes from the phlogopite bearing and MARID-suite cpx, respectively (Gregoire et al., 2003) (see text for further explanation).

Garnet

In a CaO-Cr_2O_3 diagram (Fig. 4.6) garnets can be divided into those that have equilibrated with opx only (Ca-undersaturated garnets from cpx-free harzburgites), those that coexist with both cpx and opx (Ca-saturated garnets from lherzolites) and those that have equilibrated with cpx only (Ca-oversaturated garnets from wehrlites). Three of the analysed samples have Ca-undersaturated and all others have Ca-saturated garnets. Four of the latter samples are lherzolites and the others cpx-bearing harzburgites and dunites (see petrographic section and App.-2). The Cr# in garnets has a large range from 5.94 to 34.3 with an average of 18.2 (Table 4.1 in App.-3). This is much higher than for the average garnet from the Kimberley area (Simon et al., 2007). The Mg# varies from 83.2 to 87.1 with no correlation between Cr# and Mg#. A major proportion of the garnets show weak negative Cr# - Na_2O correlation (Fig. 4.6). The lherzolithic garnet (F-16) with the lowest Cr# also has relatively low TiO_2 and Na_2O concentrations (Fig. 4.6).

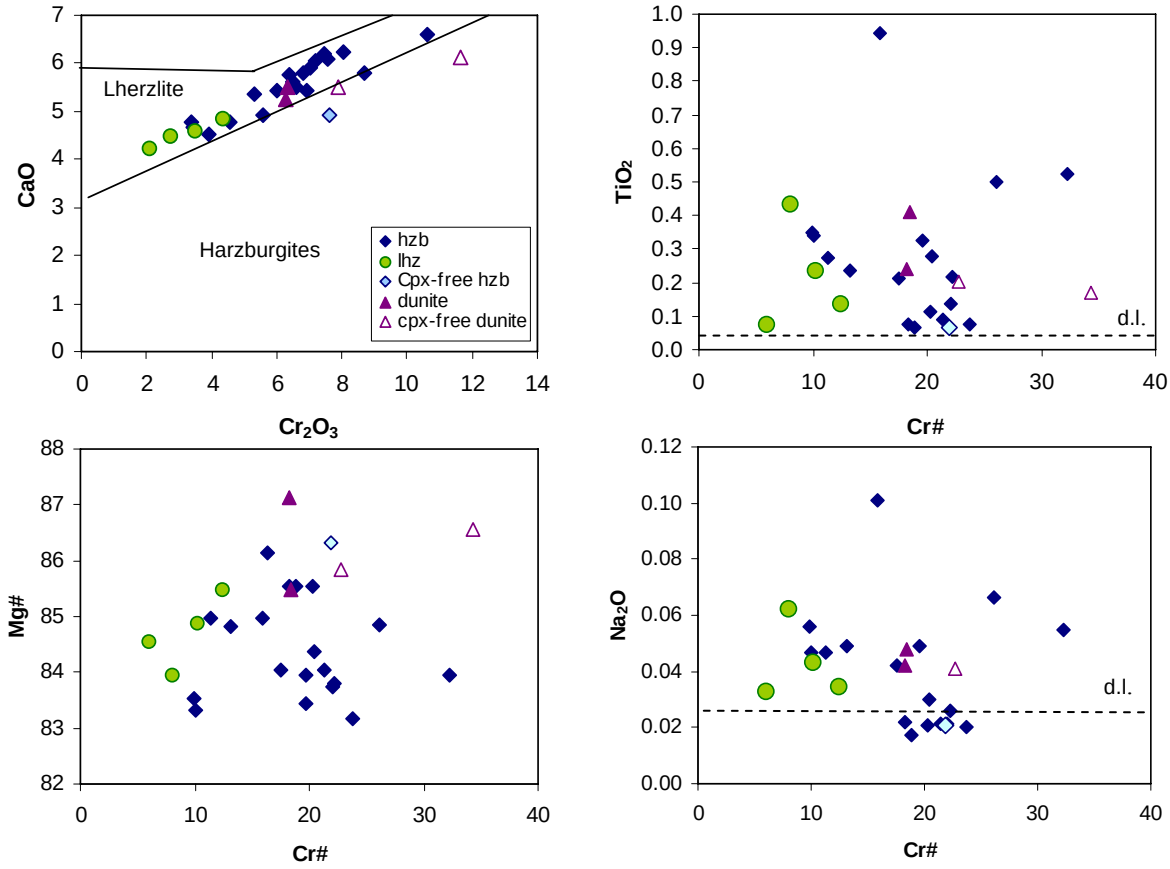

Fig. 4.6. Major and minor element variations in garnets from Finsch peridotites. d.l.=detection limit.

Rutile

Rutile is observed in only one sample (F-12). Its Cr_2O_3 content varies between 2-4.3 wt.%, the FeO between 0.1-0.8 wt.% and Al_2O_3 between 0.1-0.4 wt.% (Table 4.2 in App.-3). Cr- and Fe-rich needle like exsolutions occur in all rutile grains.

Spinel

Only spinel peridotite F-23 and garnet spinel peridotite 882 have primary spinel (chromite) while secondary spinel is ubiquitous in garnet kelyphyte rims. These secondary spinels are highly variable in composition (Table 4.2 in App.-3) and range from 48 to 79.1 in Mg# and from 6.7 to 93.9 in Cr# (see also Fig. 4.7). There is a correspondence of garnet and spinel compositions, i.e. Cr-rich garnets have Cr-rich spinels in their kelyphyte etc.

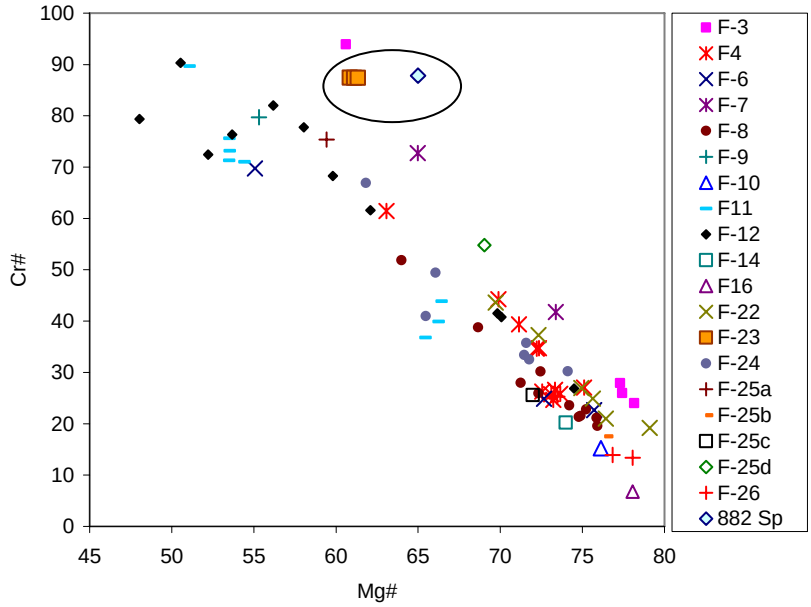

Fig. 4.7. Mg# vs. Cr# in spinels from Finsch peridotites. Primary spinels have higher Cr# than the secondary spinels. Two primary spinels from the spinel-peridotite (F-23) and a grt-sp-dunite (882) are marked with the oval.

Phlogopite, amphibole and secondary cpx

Secondary phlogopite and amphibole occur almost in all samples (see App.-2). They are only present in garnet reaction rims together with secondary cpx and spinel.

The phlogopites range from 80 to 93.8 in their Mg# (Table 4.2 in App.-3). They also have variable TiO_2 (0.125-2.65 wt.%), Al_2O_3 (5.3-18.5 wt.%), FeO (2.7-10.7 wt.%) and K_2O (4.8-10.3 wt.%) (Table 4.2 in App.-3).

Amphiboles are also variable in composition, with Mg# ranging from 81.9 to 92.8, Cr# from 0.3 to 31.4. TiO_2 and K_2O cover a range of 0 to 2.2 wt.% and Na_2O varies from 0 to 1 wt.%.

Secondary cpx in the kelyphytes is highly variable with CaO between 18 and 21 wt.%, Al_2O_3 from 0.5 to 6 wt.% and MgO between 15.5 and 18.8 wt.% (see Table 4.2 in App.-3).

4.3.2 Mineral trace elements

Trace elements are analysed in olivine, opx cpx and garnet from 22 selected peridotites plus rutile from rutile bearing sample. Zoning of trace elements within or between grains was not observed by laser ablation ICP-MS and the average values of up to ten analyses are plotted in the diagrams. All analyses with their averages are given in Table 4.3 in App.-3. To detect potential metasomatic overprints more clearly all trace elements were normalized in the diagrams to the compositions of opx, cpx and garnet from the primitive garnet peridotite Vitim 313-105 (Ionov et al., 2005a, b).

Olivine

Olivines were measured by LA-ICP-MS with a large spot size of 200 µm to account for their low trace element concentrations. This allowed the analysis of Li, Sc, V, Co and Th with an accuracy of about 10%. For Nb, Ta, Zr, Hf and some REE the uncertainties are larger, but it was still possible to determine differences between samples.

The REE contents were two to three orders of magnitude lower than those of the C-1 chondrite (Mc Donough and Sun, 1995) and concentrations of **l**arge **i**on **l**ithophile **e**lements (LILE) was below the detection limit in all olivines from Finsch peridotites. Vanadium and cobalt concentrations are fairly uniform and Sc varies widely (Fig. 4.8). **H**igh **f**ield **s**trength **e**lements (HFSE) show a large variation and high abundances and mostly positive anomalies relative to their neighbouring elements.

The only rutile bearing sample has the lowest Nb and Ta and moderate Zr and Hf abundances (Fig. 4.8). Thorium scatters around the chondritic value and is extremely high in the lherzolite F-15.

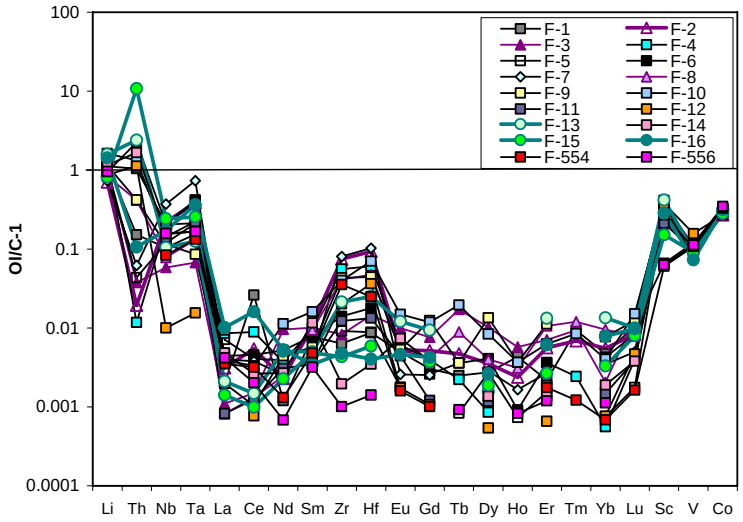

Fig. 4.8. Trace element variations in olivines from Finsch peridotites normalized to C-1 (Mc Donough and Sun, 1995). Triangles = dunites, (open triangles = cpx-free); squares = harzburgites; circles = lherzolites.

Lithium generally correlates negatively with Mg# (Fig. 4.9) as also observed in previous studies for other localities (e.g. Seitz and Woodland, 2000). Accordingly, Li concentrations were interpreted to reflect the depletion event(s) and are not affected by enrichment processes. For two samples (F-3, F-10), where Li in olivine plots above the observed trend with Mg# (Fig. 4.9), this could indicate late stage Li enrichment.

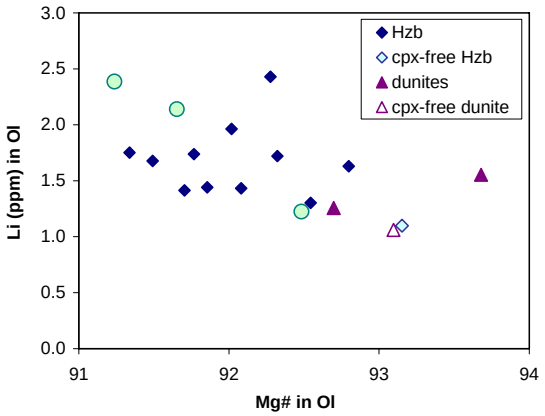

Fig. 4.9. Mg# vs. Li (ppm) content in olivines from Finsch peridotites.

Orthopyroxene

Analytical challenges for opx trace element analysis by LA-ICP-MS are not quite as high as for olivines, therefore spot sizes varying between 120 and 200 µm were employed. However, avoidance of cleavages and deformation lamellae (see App.-2) restricted the placing of the ablation spot. Therefore, several grains could be analysed by only one single spot, rather than the usual 2-3 spots on the same grain. Furthermore, the low trace element concentrations in opx, makes them very sensitive to contamination by a melt, like such from the host kimberlite. Although undetected in major elements some trace element analyses in opx suggest kimberlite alteration, especially when grain discontinuities were involved. Therefore, possible contamination was monitored by tracing elements like Ca, Sr, Rb, Ba, B, Li and Nb during the rendering of single spot analyses by the GLITTER program. Analyses that suffered from contamination (or parts of analyses) were subsequently omitted. Due to the low concentrations of some trace elements in opx, analytical uncertainty with LA-ICP-MS is high.

Accordingly, variation in HREE (which were usually < 0.01ppm and close to the detection limit), Y and Hf could not be resolved in all samples (Table 4.3 in App.-3 and Fig. 4.10).

All orthopyroxenes have sinusoidal C-1 normalized REE patterns with a maximum either on Nd or Sm and lower HREE than LREE (Fig. 4.10). Only the orthopyroxenes from one cpx-bearing harzburgite (F-1) and two lherzolites (F-13, F-16) have almost flat REE and $(La/Lu)_N$ lower than 1. All LREE are one order of magnitude lower than C-1, a few samples have two orders of magnitude lower HREE and the orthopyroxenes from the cpx-bearing harzburgites 554-XM46 (diamondiferous) and F-14 have even three orders of magnitude lower HREE. The diamondiferous peridotites 554-XM46 and 865 have the lowest LREE of all samples. Compared to Kimberley pooled orthopyroxenes (Simon et al., 2007) the Finsch orthopyroxenes have a smaller range in LREE and most middle to heavy REE are lower in Finsch than in Kimberley samples (Fig. 4.10).

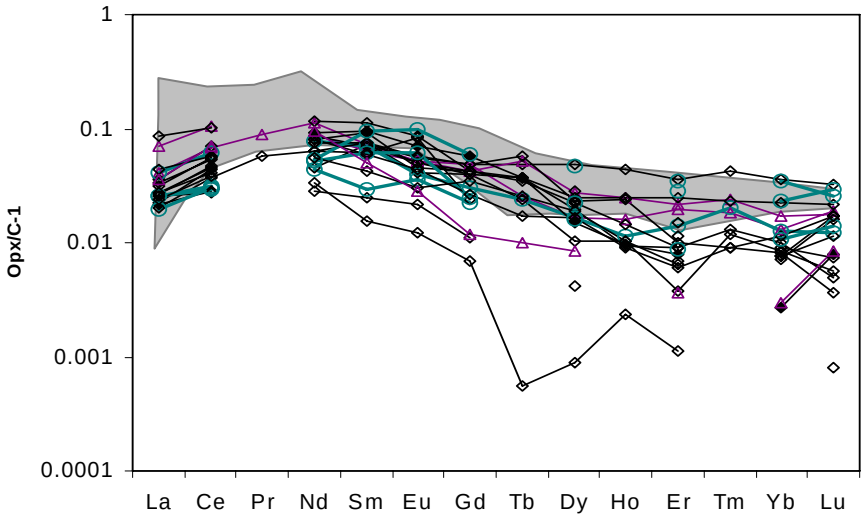

Fig. 4.10. Chondrite (C-1, McDonough and Sun, 1995) normalized REE of orthopyroxenes from Finsch peridotites. Diamonds = harzburgites (field diamond = cpx-free); circles = lherzolites; triangles = dunites.

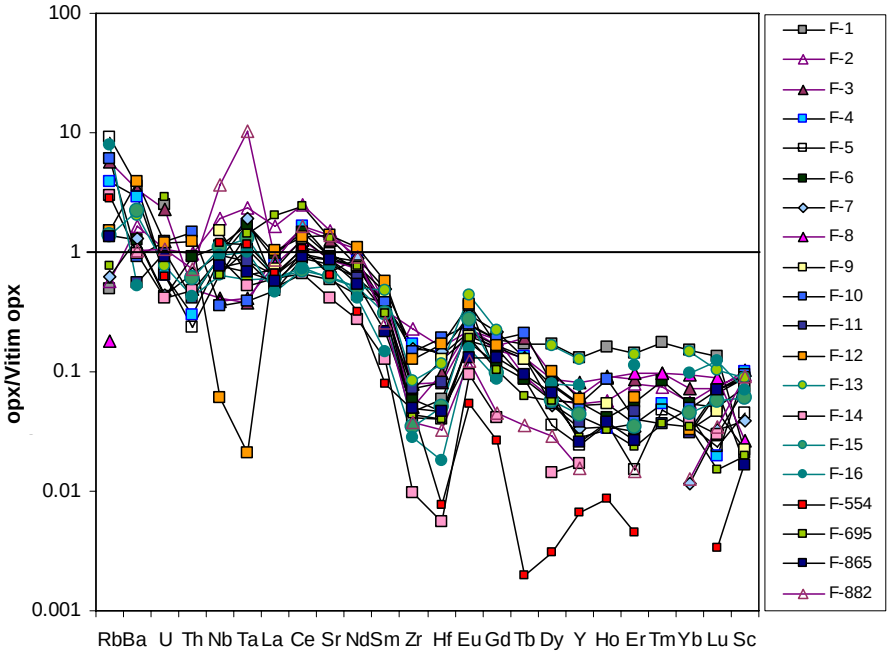

Fig. 4.11. Spidergram of orthopyroxenes from Finsch peridotites. Samples are normalized to opx from the primitive garnet peridotite Vitim 313-105 (Ionov et al., 2005a,b). Triangles = dunites, (open triangles = cpx-free); squares = harzburgites; circles = lherzolites.

Normalizing Finsch orthopyroxenes to opx from the primitive lherzolite Vitim 313-105 (Ionov et al., 2005a,b), shows that most of the Finsch opx's have more than one order of magnitude lower Sc, Hf, Zr, middle and heavy REE (Fig. 4.11). This is an indicator of strong depletion of the Finsch samples compared to the primitive Vitim opx. On the other hand LREE, Rb, Ba, Sr, Nb and Ta are either slightly higher or lower than the Vitim opx. Only three orthopyroxenes have a Nb-Ta trough, with the lowest content in the opx from rutile bearing sample (F-12). All other have a positive Nb-Ta anomaly with the highest values in the cpx-free samples. All opx have a small positive Zr-Hf anomaly and cpx-free harzburgites have the highest values (Fig. 4.11).

Clinopyroxene

According to the small size of cpx usually one or at most two spot analyses (LA-ICP-MS) on a single grain were possible. Therefore, like for opx, several grains were analysed in one sample. Most of the trace elements in cpx were analysed with the accuracy of ~ 10%.

A sinusoidal pattern of C-1 normalised REE with a hump on Nd is characteristic for cpx from Finsch (Fig. 4.12). Only cpx from F-14 shows a continuous increase from Lu to La and therefore the highest $(La/Lu)_N$ ratios (~ 1800 - normalized to chondrite). This cpx is from the most depleted sample with the lowest contents of middle and heavy REE. In analogy to their opx, cpx from harzburgite F-1 and lherzolites F-13 and F-16 have the lowest $(La/Lu)_N$ ~ 10 ratios. With only around 10 times chondritic LREE abundances the clinopyroxenes are low compared to cpx from Kimberley (Fig. 4.12; Pearson et al., 2003; Simon et al., 2007). However, they overlap in their HREE contents with the low temperature Kimberley samples (Fig. 4.12).

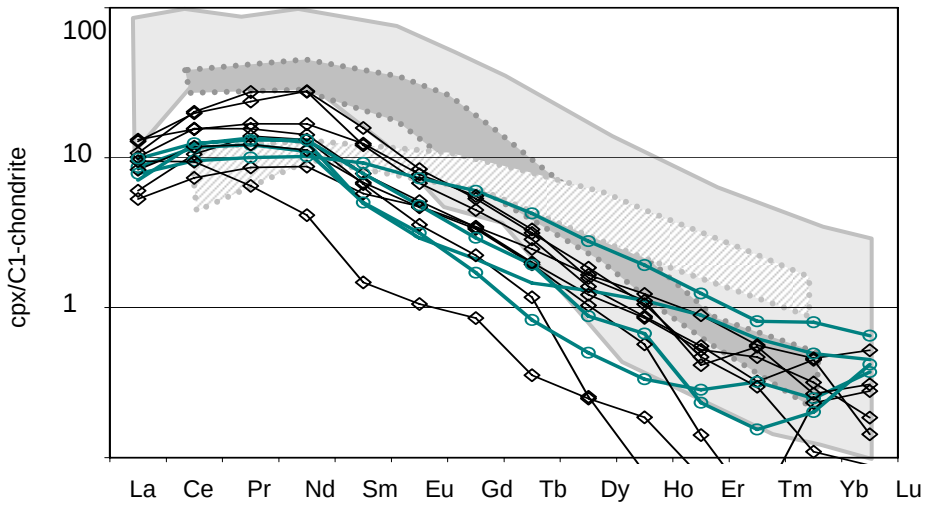

Fig. 4.12. Chondrite normalized REE of cpx from Finsch peridotites. Diamonds = harzburgites; circles = lherzolites. Light grey field = low temperature cpx from Kimberley (Simon et al., 2007); dark grey field = low-T cpx from S.A. (see Pearson et al., 2003); striped field = high-T cpx from S.A. (see Pearson et al., 2003).

All clinopyroxenes have subchondritic Ni and Co and suprachondritic Sc and V contents (Fig. 4.13A, Table 4.3 in App.-3). By contrast the abundances of LILE, REE and HFSE are highly variable. Anyway, all cpx have subchondritic U, Rb and Ba, but only some have subchondritic HFSE.

Normalised to the primitive Vitim 313-105 cpx all Finsch cpx have depleted middle to heavy REE, and enriched LREE (Fig. 4.13B). Contrary to opx, all cpx have well pronounced negative Zr-Hf and Nb-Ta anomalies (Fig. 4.13B) with abundances lower than that of primitive cpx. All Finsch clinopyroxenes have higher Rb, Ba, Sr and U than the primitive Vitim cpx. The Cpx from sample F-14 is the most depleted in REE, Sr and Hf, but has a higher content of Nb, Ta, and also higher U, Th and LILE than the primitive Vitim cpx.

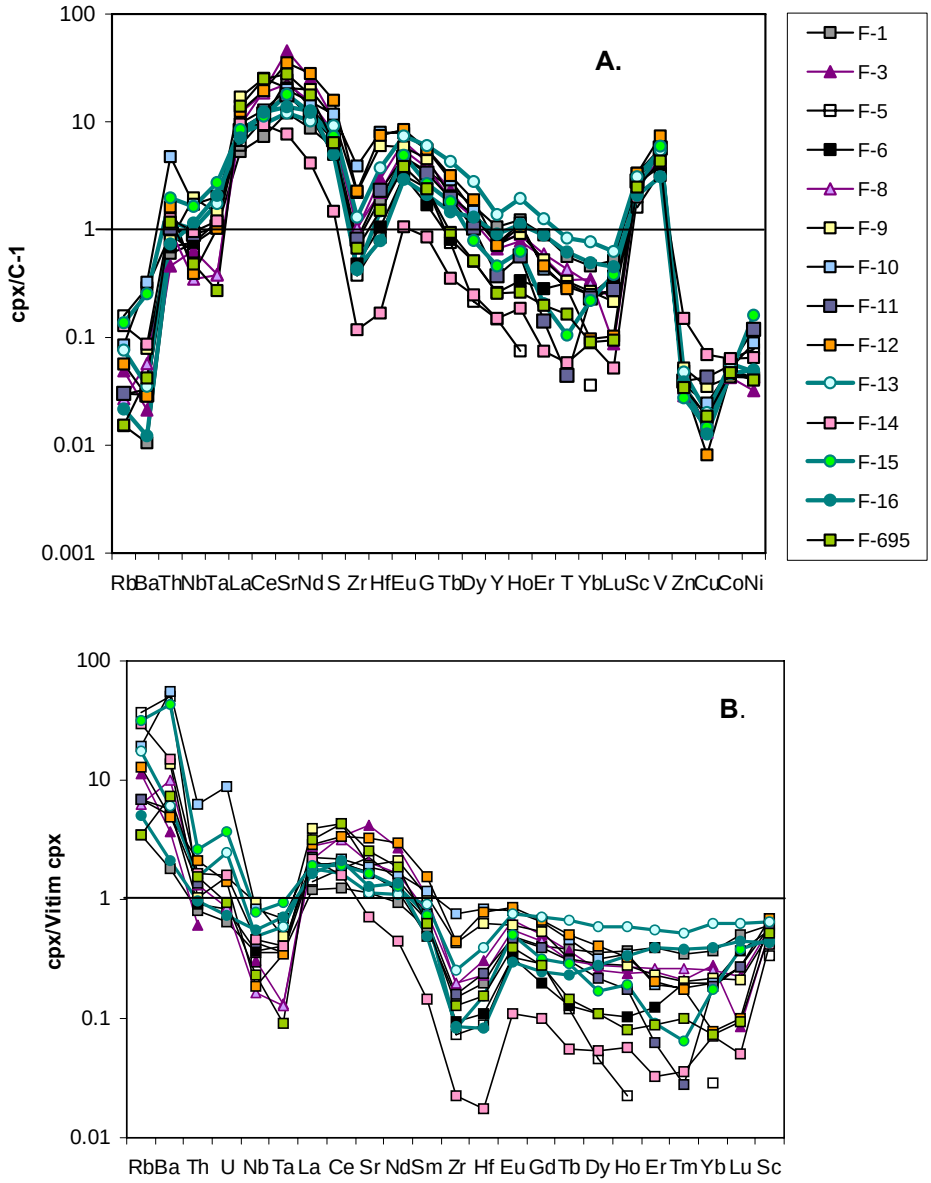

Fig. 4.13. (A) Chondrit (C-1) normalized trace element patterns of cpx from the Finsch peridotites. (B) Primitive cpx (Vitim 313-105, Ionov et al., 2005a,b) normalized trace element patterns of Finsch cpx. Triangles = dunites; squares = harzburgites; circles = lherzolites.

Garnet

At least two analyses were performed on each garnet grain, which confirmed inter-grain trace element homogeneity.

The majority of garnets have a sinusoidal REE pattern with a hump on Sm or Eu (Fig. 4.14). All garnets have low $(La/Lu)_N$ (normalized to chondrite), where the lherzolitic garnets have the lowest values down to 0.004. The cpx-bearing harzburgite (F-1), the dunite (F-8) and the lherzolite (F-13) have a simple, LREE-depleted pattern together with high HREE concentrations. Most enriched in middle and light REE is the spinel, garnet-bearing dunite (882). Harzburgite (F-14) with most depleted cpx has garnet with almost flat REE and very low REE abundances. Overall the Finsch garnets are similar to those from Kimberley (Fig. 4.14).

The highest depletion in HREE, determined as a $(Lu/Er)_N$ ratio, was observed for the garnets from diamondiferous peridotites 554-XM46 and 556-XM48 (2.9 and 2.2, respectively), and the lowest values of 0.6 has garnet from the rutile bearing sample (F-12). The rest garnets have $(Lu/Er)_N$ in the range of 0.8 to 1.8. Garnets from the cpx-free samples F-7 and 882, are mostly enriched in heavy and middle REE with $(Sm/Ho)_N$ ratio ranging between 7 and 4.9.

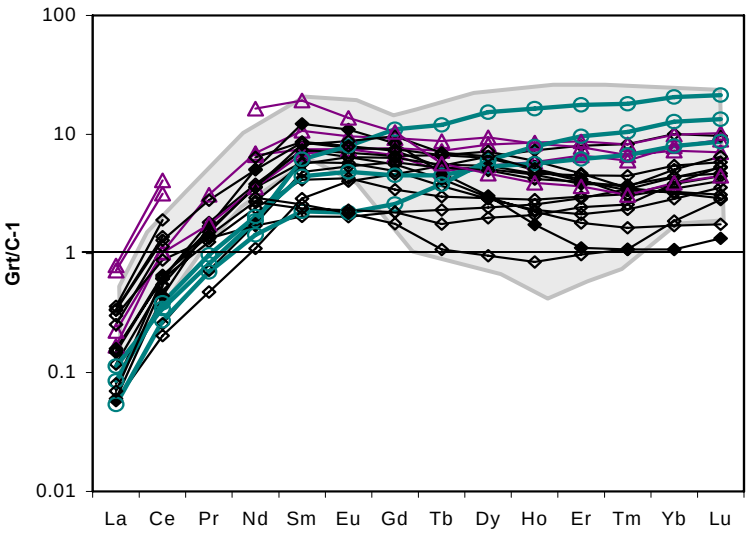

Fig. 4.14. REE of Finsch garnets normalized to chondrite C-1. Diamonds = harzburgites (field diamond = cpx-free); circles = lherzolites, triangles = dunites.

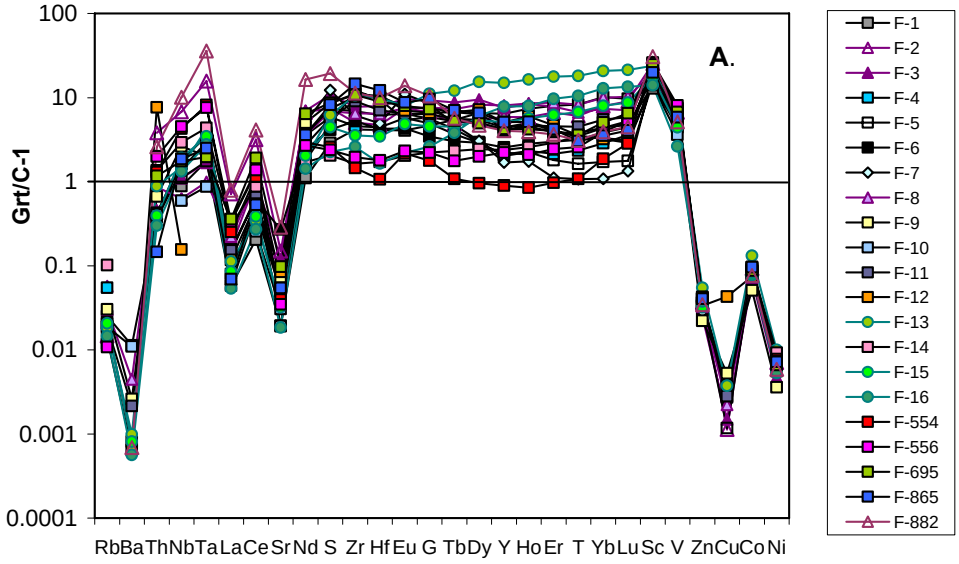

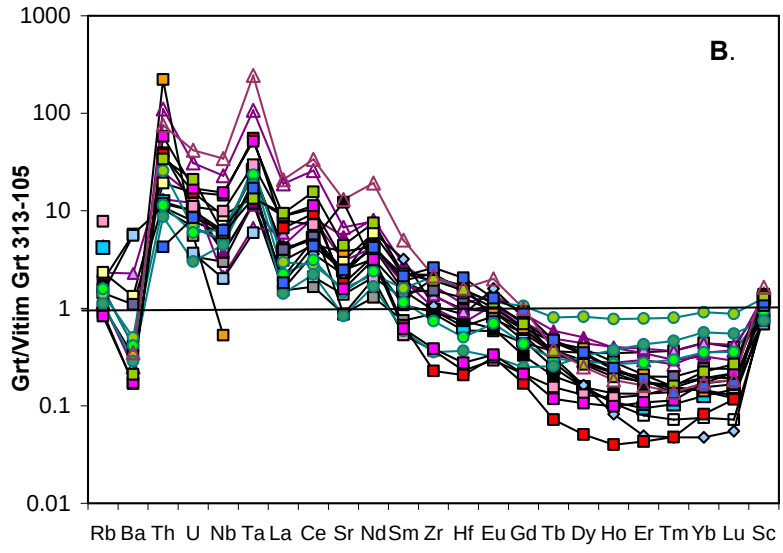

Fig. 4.15. (A) Trace element patterns of Finsch garnets normalized to C-1. (B) Trace element patterns of Finsch garnets normalized to the primitive garnet Vitim 313-105 (Ionov et al., 2005a,b). Triangles = dunites, (open triangles– cpx-free); squares = harzburgites; circles = lherzolites.

Uniformly low abundances of subchondritic Ni and Co and super-chondritic Sc and V is characteristic of all studied garnets (Fig. 4.15A).The majority of garnets have subchondritic HFSE with a strongly pronounced negative Nb-Ta anomaly (Fig. 4.15A). Garnets from cpx-free harzburgites have super-chondritic Th, while the rest has sub-chondritic Th. Cpx-free garnets also have the highest values of Sr, U and Rb, while Ba was below the detection limit. On the other hand, lherzolitic garnets have the most depleted abundances of Sr and U, and relatively high Rb and Ba (Fig. 4.15A).

Normalization to garnet from the primitive peridotite Vitim 313-105 (Ionov et al., 2005a,b) shows depletion of HREE and partly of Zr, Hf and Ba (Fig. 4.15B). Most depleted garnets have even one order of magnitude lower HREE. Here, Zr and Hf have a negative anomaly except for harzburgite F-10. Garnet from the rutile bearing peridotite F-12 has the highest Th contents of all samples, and lowest Nb and Ta (below the detection limit). For all other garnets LILE, LREE, Th, U, Nb and Ta are higher than in the primitive garnet. The Sr, Ba, and Rb make negative anomalies, still majority higher than the primitive grt, and only one garnet (F-6) has a positive Sr anomaly (Fig. 4.15B).

4.4 Discussion

4.4.1 Geothermobarometry and equilibration of major elements

All minerals in the samples are homogeneous in their major element composition except for cpx in F-3 and F-11 where cpx has different core-rim composition. For these, only the core compositions were used for geothermobarometry and for all others the averages of the analyses were taken. The full set of thermobarometers was used as supplied by the in house PTEXEL spreadsheet. The individual results are presented in Table 4.6 in App.-3. and the comparison is discussed below (Figs. 4.17 and 4.18). Samples containing only olivine and opx were omitted, since there was not enough information for their geothermobarometrical calculation.

For the only spinel peridotite temperature was calculated for a preset pressure of 3-5 GPa with the Fe-Mg exchange ol-sp thermometer of O'Neill and Wall (1987). Obtained temperatures of 950 to 990 °C, respectively, clearly point that this sample belongs to the shallowest of the peridotites investigated during this study (Table 4.6 in App.-3).

The results obtained iteratively with the two-pyroxene-thermometer (T_{BKN}) and garnet-opx barometer (P_{BKN}) of Brey and Köhler (1990) are shown in Fig. 4.16 and given in Table 4.6 in App.-3. For cpx-free harzburgites and dunites the combination of the Fe-Mg exchange olivine-garnet thermometer ($T_{O'Neill}$) (O'Neill and Wood, 1979) and P_{BKN} was used. The calculated temperatures range from 1050 to 1250 °C and the pressures from 4.4 to 6.5 GPa (Fig. 4.16; Table 4.6 in App.-3). This implies that all garnet peridotites, except for F-9, were generated in the diamond stability field. The latter is a cpx-free harzburgite, which is, together with all other cpx-free samples, shifted to lower pressures compared to the cpx-bearing samples. For such samples temperatures have to be calculated with the Fe-Mg exchange thermometer of O'Neill and Wood (1979). Its outcome is dependent on the possible presence of Fe^{3+} in garnet which is, however, not considered in these calculations. The absence of Fe^{3+} potentially results in too low temperatures which in turn produces too low pressures. It is therefore quite conceivable that these samples have similar conditions of origin as the cpx-bearing samples and that all samples originated from a restricted depth range between 5 and 6.5 GPa. This is confirmed for three samples (F-2, F-7 and F-9) for which ferric iron composition of garnets were obtained by Mössbauer (Tables 4.6 and 4.7 in App.-3).

All Finsch samples plot on a 40 mW/m^2 conductive geotherm of Chapman and Pollack (1977), at lower temperatures compared to sheared samples from Lesotho (Woodland and Koch, 2003; Simon et al., 2003, Fig. 4.16). Only low temperature harzburgites from Finsch overlap with the Kimberley samples (Rudnick and Nyblade, 1999; Simon et al., 2007, Fig. 4.16).

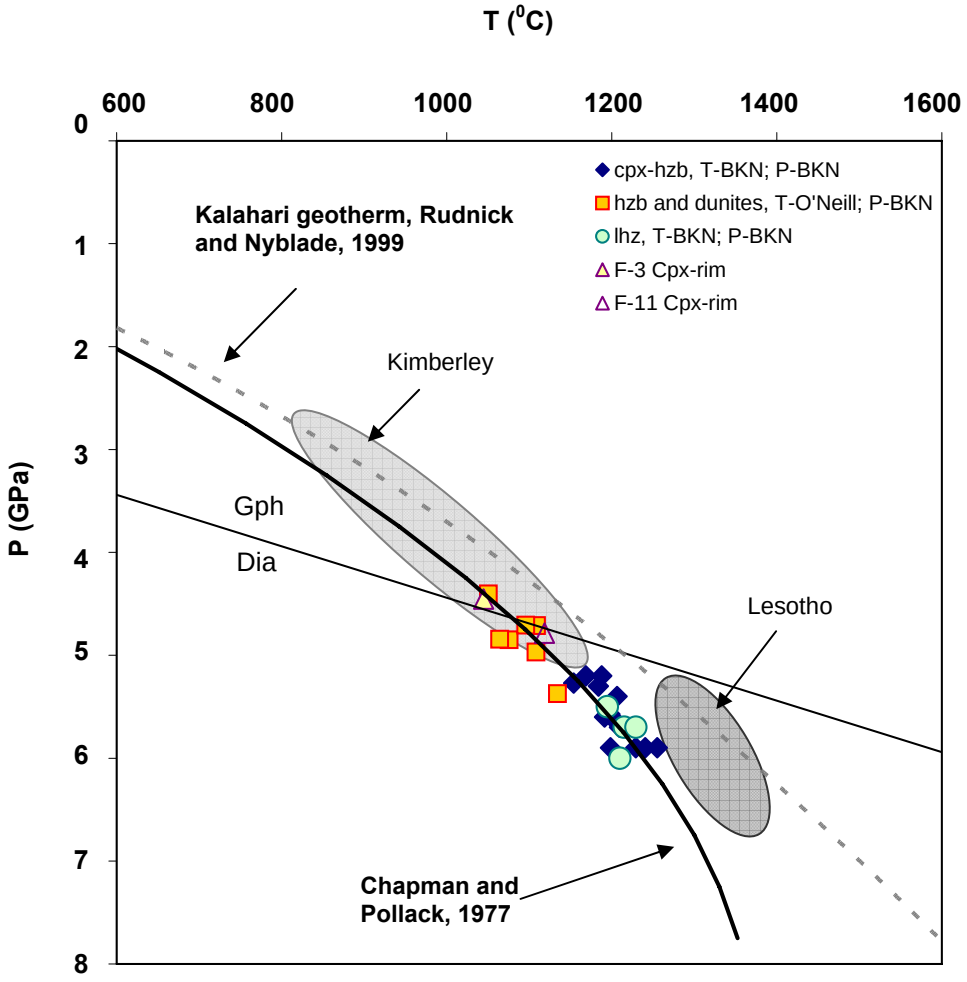

Fig. 4.16. The peridotites from Finsch plot on a 40 mW/m^2 conductive geotherm of Chapman and Pollack (1977). Diamonds (cpx-bearing harzburgites) and circles (lherzolites) calculated with T_{BKN} and P_{BKN}; squares cpx-free harzburgites and dunites calculated with $T_{O'Neill}$ and P_{BKN}. The Kalahari geotherm defined by Rudnick and Nyblade (1999) is given for comparison. Thin line defines P-T conditions for graphite (Gph) - diamond (Dia) transition. The grey ovals envelop the common range of P-T conditions of some xenolith occurrences on the Kaapvaal craton (Rudnick and Nyblade, 1999; Simon et al., 2003, 2007; Woodland and Koch, 2003).

Inter mineral equilibrium can be tested by comparing the results from different, independent thermometers for a given barometer: P_{BKN} was used and compared to the temperatures obtained with, T_{KB} (Köhler and Brey, 1990), $T_{Ca\text{-}in\text{-}opx}$ (Brey and Köhler, 1990), T_{Krogh} (Krogh, 1988), $T_{O'Neill}$ (O'Neill and Wood, 1979), T_{Harley} (Harley, 1984) and T_{cpxNT} (Nimis and Taylor, 2000) with T_{BKN} (Table 4.6 in App.-3 and Fig. 4.17). The Ca-in-olivine thermometer T_{KB} is in excellent agreement with T_{BKN}. The Fe-Mg exchange thermometers T_{Krogh}, $T_{O'Neill}$ and T_{Harley} give systematically lower temperatures than T_{BKN}. This is most probably due to the non-consideration of the oxidation state of Fe, i.e. the neglect of Fe^{3+}. $T_{Ca\text{-}in\text{-}opx}$ also provides lower temperatures than the T_{BKN}, where three samples show temperatures with more than 100 °C difference. However, T_{BKN} temperatures calculated by P_{BKN} are in good agreement (within the 80 °C error of a method) with the T_{NTCpx} obtained iteratively with P_{NTCpx} (Nimis and Taylor, 2000).

Ni-in-garnet is a widely used single crystal thermometer. Two versions exist: a) the experimentally calibrated T_{Canil} (Canil, 1994, 1999) and b) the empirically calibrated $T_{Griffin}$ (Griffin et al., 1989b). These thermometers are based on the temperature dependence of the exchange of Ni between olivine and garnet. Since olivine is overwhelming Ni reservoir in SCLM and is generally fairly constant at around 3000 ppm, Ni temperature changes can be derived from the variable Ni contents in garnet. There is linear correlation between two Ni in garnet thermometers that at lower temperatures (~ 1150 °C) differ from each other within the uncertainties of the methods (not shown).

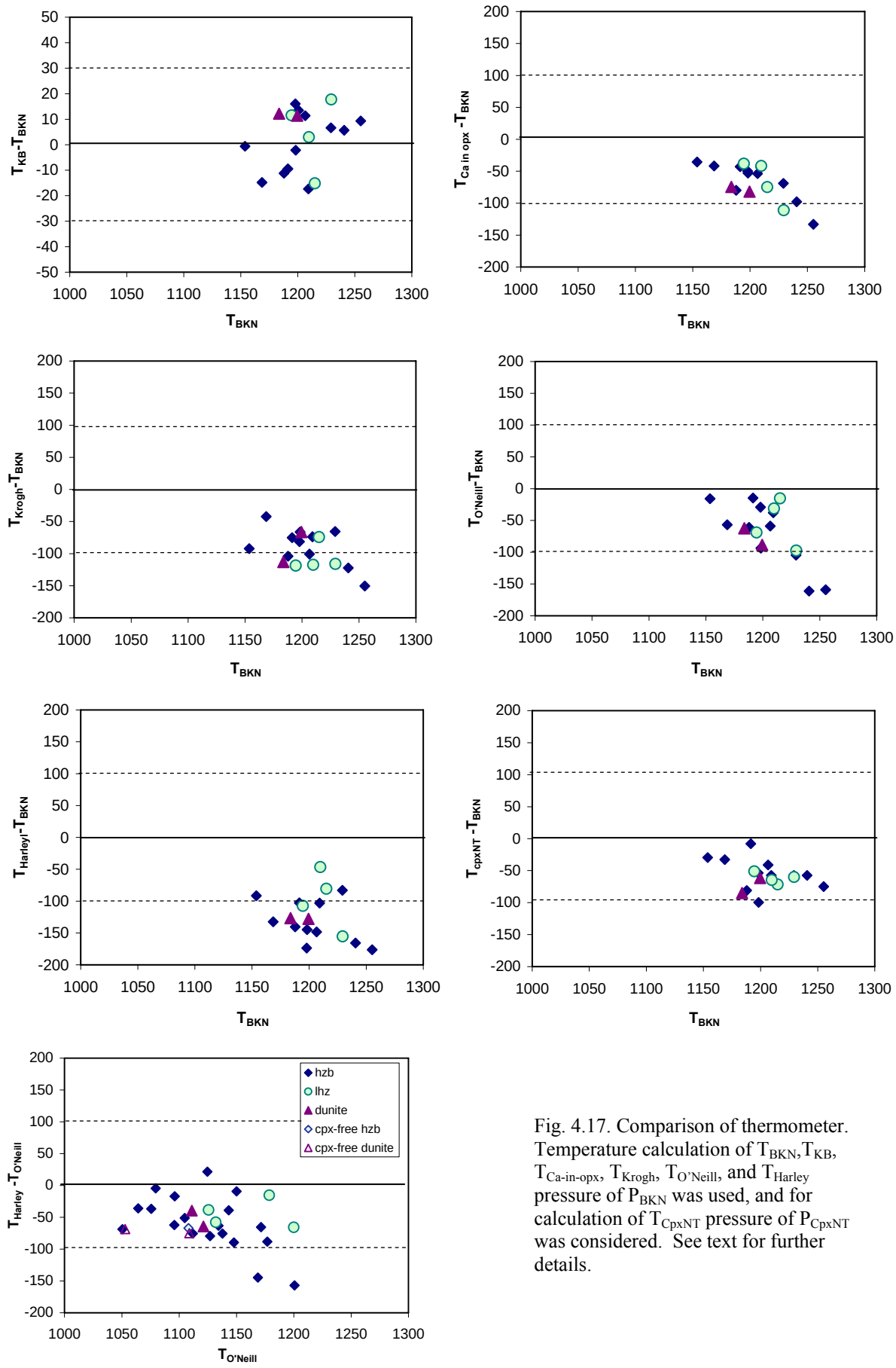

Fig. 4.17. Comparison of thermometer. Temperature calculation of T_{BKN}, T_{KB}, $T_{Ca\text{-}in\text{-}opx}$, T_{Krogh}, $T_{O'Neill}$, and T_{Harley} pressure of P_{BKN} was used, and for calculation of T_{CpxNT} pressure of P_{CpxNT} was considered. See text for further details.

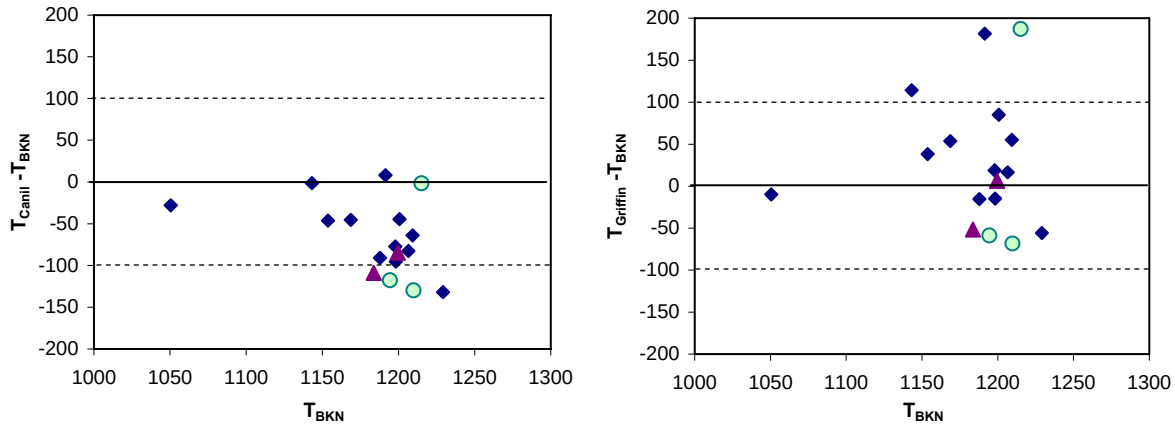

Fig. 4.18. Comparison of T_{Canil} and $T_{Griffin}$ with the T_{BKN}. Symbols as in Fig. 4.17. See text for further details.

The comparison of the two Ni in garnet thermometer versions with T_{BKN} is presented in Fig. 4.18., where they both show relatively good agreement with the T_{BKN}. Tendencially decreasing T_{Canil} temperature with increasing T_{BKN} were observed, where some high temperature samples (>1200 °C) deviate for up to -130 °C from the T_{BKN}. On the other hand T_{BKN} and $T_{Griffin}$ are in good agreement for most of the samples, only unexplainably three samples show anomalously high values (Fig. 4.18; Table 4.6 in App.-3).

The number of independent barometers for garnet peridotites is limited and restricted to P_{BKN} (Brey and Köhler, 1990), P_{KB} (Köhler and Brey, 1990) and P_{NTcpx} (Nimis and Taylor, 2000). The pressures are calculated with T_{BKN} and compared in Fig. 4.19 with P_{KB} and P_{NTCpx}. P_{BKN} and P_{KB} are in good agreement within their respective errors for most of the samples. The comparison between P_{NTcpx} and P_{BKN} indicates an increasing underestimation of P_{NTcpx} with increasing pressure.

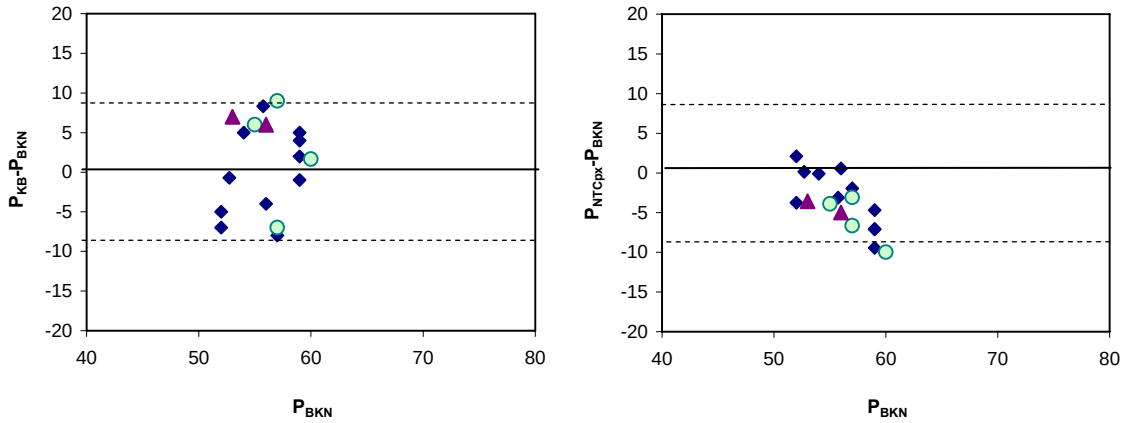

Fig. 4.19. Pressure comparison of Finsch peridotites. Symbols as in Fig. 4.17.

Since observed differences in thermobarometric calculation can be explained by the error of the method or by the neglect of Fe^{3+} in garnet for Fe-Mg exchange thermometers (T_{Krogh}, $T_{O'Neill}$ and T_{Harley}) all observed samples have reached inter mineral major element equilibrium.

4.4.2 Oxygen fugacity

Garnets from 2 dunites, one cpx-free dunite, one cpx-free harzburgite, 9 cpx-bearing harzburgites and 2 lherzolites are analysed by Mössbauer spectroscopy for Fe^{2+} and Fe^{3+}. P-T conditions of mineral equilibrium, needed for determination of Fe^{3+}, taken for all cpx-bearing samples were iteratively solved by P_{BKN} and T_{BKN} (Brey and Köhler, 1990), while for two cpx-free samples the iteration of $T_{O'Neill}$ and P_{BKN} was used (Table 4.7 in App.-3).

Mössbauer analyses show a range in $Fe^{3+}/\Sigma Fe$ from 0.04 to 0.078 (Table 4.7 in App.-3). Most common are samples with the $Fe^{3+}/\Sigma Fe$ ratio of ~ 0.06 which is slightly higher than the reported values of 0.04-0.05 for the peridotites from Kimberly and Lesotho (Woodland and Koch, 2003). This difference may be due to the limited but higher P-T range of the Finsch garnets compared to that of the Kimberley samples. Nevertheless, Finsch garnets have a similar spread of $Fe^{3+}/\Sigma Fe$ vs. T (not shown), like other South African samples (Luth et al., 1990; Woodland and Koch, 2003). An almost linear trend of decreasing Fe^{3+} in garnet and increasing forsterite contents in olivine was observed (Fig. 4.20). A small scatter could be either due to the temperature dependence of Fe^{3+} partitioning between garnet and cpx or because of the incompatible behaviour of Fe^{3+} in garnet during partial melting and melt extraction (Canil and O'Neill, 1996; Woodland and Koch, 2003).

The oxygen fugacity (fO_2) recorded by the Finsch garnets was calculated using the equilibrium between garnet, opx and olivine (Gudmundsson and Wood, 1995) and results are presented in Table 4.7 in App.-3 and in Fig. 4.21. Although these samples represent a small temperature and pressure interval they have a large range in $\Delta\log fO_2$ [relative to FMQ – fayalite-magnetite-quartz oxygen buffer equilibrium] from -2.5 to -5.3. The samples from the greatest depth record low fO_2s close to the Fe-wüstite oxygen buffer. There is a good anti-correlation of $\Delta\log fO_2$ with pressure (Fig. 4.21). The majority of the analysed garnets plot within error (0.6 log unites – Woodland and Koch, 2003) on that trend. The here obtained $\Delta\log fO_2$ for the lower pressure samples are in good agreement with observations made by Woodland and Koch (2003) for the Kimberley garnets. Nevertheless, the five samples of this study with slightly higher $\Delta\log fO_2$, for a given pressure, plot above that trend. One of them is a rutile bearing harzburgite (F-12) and another is a cpx-bearing dunite (F-3) with zoned cpx formed probably during the reaction with host kimberlite. Those Finsch samples are in good agreement with the high temperature sheared Lesotho and Kimberley samples (Woodland and Koch, 2003) (Fig. 4.21). It appears that particular metasomatic events, like Ti, Fe enrichment (rutile-bearing sample) or reactions with kimberlite (zoned cpx sample), as well as the process leading to a sheared texture resulted in localised oxidation.

In conclusion, oxygen fugacity in the sub-cratonic mantle decreases continuously with depth, probably reaching metal saturation at depths >250 km. Only short-lived secondary refertilisation processes like shearing and kimberlite metasomatism created a slightly more oxidising environment in the upper mantle, which with time may have affected large regions.

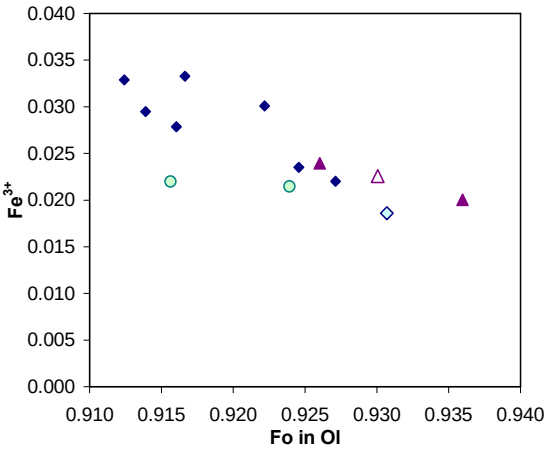

Fig. 4.20. Linear co-variation of Fe^{3+} (cation permformula unit) in garnet and fosterite (Fo) component in olivine.

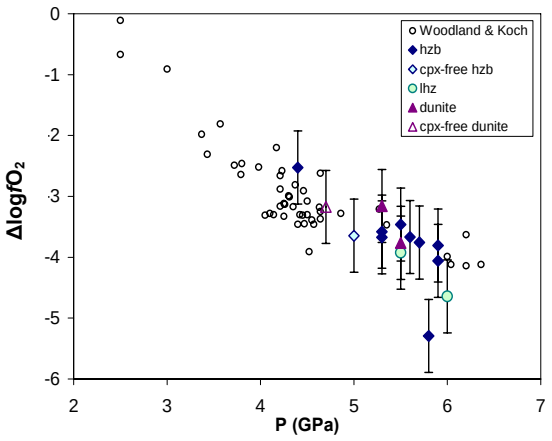

Fig. 4.21. Co-variation of oxygen fugacity ($\Delta\log fO^2$) and pressure (GPa) of Finsch peridotites.

4.4.3 Trace element partitioning

For a valid discussion on trace element relationship and for the reconstruction of whole rocks it was necessary to consider weather minerals have reached trace element equilibrium or not.

Partition coefficients were calculated as D*i* (*i*= element under consideration) for garnet/cpx, garnet/opx and cpx/opx pares and compared with values derived from experiments (Johnson, 1998; Green et al., 2000) and from other natural samples (Van Achterberg et al., 1998; Glaser et al., 1999;

Simon, 2004; Ionov et al., 2005a,b). Trace element partitioning generally depends on pressure, temperature and chemical composition. Literature data show significant scatter and are mostly concern with garnet/cpx pairs from low P and T cratonic peridotites (Van Achterberg et al., 1998; Glaser et al., 1999; Ionov et al., 2005a,b). Our data set extends our knowledge to higher pressures and temperatures and to garnet/opx and cpx/opx trace element partitioning.

Garnet/cpx partitioning

Garnets and clinopyroxenes have the highest trace element contents in harzburgites and lherzolites and were thus the first targets for partitioning studies (see Eggins et al., 1997; Glaser, 1999; Green et al., 2000 and studies referenced therein). General knowledge is that elements like HREE, HFSE, Sc, V and Co preferentially partition into garnet, while LILE, LREE and Ni are preferentially included in cpx. Further more, with increasing equilibrium P and T conditions of the sample, all elements preferentially partition into garnet (as shown by the comparison of low P-T samples of Glaser and Ionov with the high P, T samples of Green and Simon on Fig. 4.22).

Trace element partition coefficients between garnet and cpx for most of the Finsch peridotites are within the range of equilibrated experimental (Green et al., 2000) and natural (Glaser, 1999; Simon, 2004; Ionov et al., 2005a,b) samples. Larger differences between the trace element abundances of the Finsch samples and literature data are observed for LILE, U and Th (Fig. 4.22), which might be due to the low concentrations of these elements in garnets that produced larger analytical errors. It is also evident that garnet/cpx partition coefficients for Zr and Hf of some Finsch samples are higher than those of literature data from samples with similar P and T conditions (see Green = Green et al., 2000 and Simon = Simon, 2004 in Fig. 4.22). This may indicate incomplete garnet-cpx equilibration of these elements. To better constraint the garnet-cpx partitioning, D values for selected elements from Finsch peridotites were compared on Fig. 4.23 with the Cr content of their garnets.

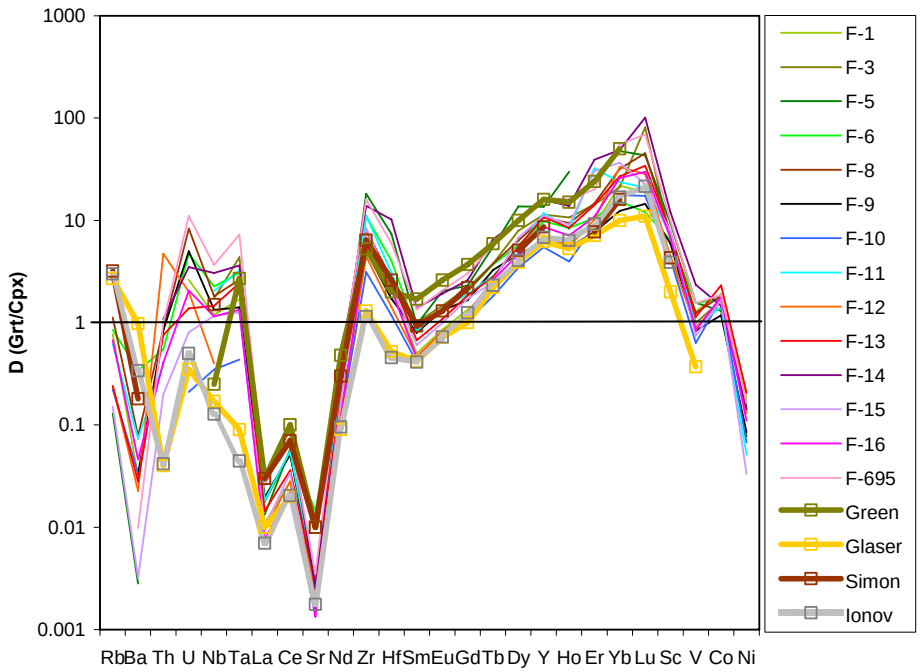

Fig. 4.22. Trace element partitioning between grt and cpx. Literature data: Glaser (T = 1050 °C, P = 2 GPa) = Glaser et al., 1999; Green (T = 1150-1200 °C, P = 4 GPa) = Green et al., 2000; Simon (T =1330 °C, P = 5.7 GPa) = Simon, 2004; Ionov (T = 1030 °C, P = 2 GPa) - Ionov et al., 2005a,b.

Peridotitic garnets are mixtures of preferentially pyrope with variable amounts of almandine, uvarovite and grossular. The majority of the trace elements in garnets are placed in the dodecahedral position (eight fold coordination), which is preferentially occupied by Ca. Therefore, an increase of Ca in garnet should result in an increase of trace element content in garnet. The octaeder position is filled with Al, which can be substituted by Cr. Since Cr has larger ionic radii than Al, this may expand the garnet structure, and with that the dodecahedral position, allowing an easier incorporation of trace

elements. Therefore, increasing of Cr in garnet also results in an increase of garnet/cpx D values for most trace elements (Fig. 4.23).

Garnet/cpx D-values of light and middle REE up to Dy show a perfect second grade polynomic relationship with the Cr content of garnets. A good correlation is also observed for Nb, Hf and Sc, while all other trace elements, such as Lu and Zr show a relatively larger scatter (Fig. 4.23). Either this scatter is produced by other crystal-chemical relations, which operate in addition to the Cr-content, or these elements are not entirely equilibrated between garnet and cpx. Disequilibrium of HREE could be produced by a lower mobility or slower inter-mineral diffusion rates of these elements compared to LREE. Variable equilibration of the REE and HFSE, respectively, is also indicated by the Sm-Nd and Lu-Hf isotope systems. While Sm-Nd have reached equilibrium between garnet and cpx, resulting also in isotopic equilibrium (all garnet-cpx tie line ages yield kimberlite eruption ages, see Chapter 5), the Lu-Hf isotopic system on the other hand did not have reached inter mineral equilibrium for all samples, resulting in variable garnet-cpx Lu-Hf tie-line ages.

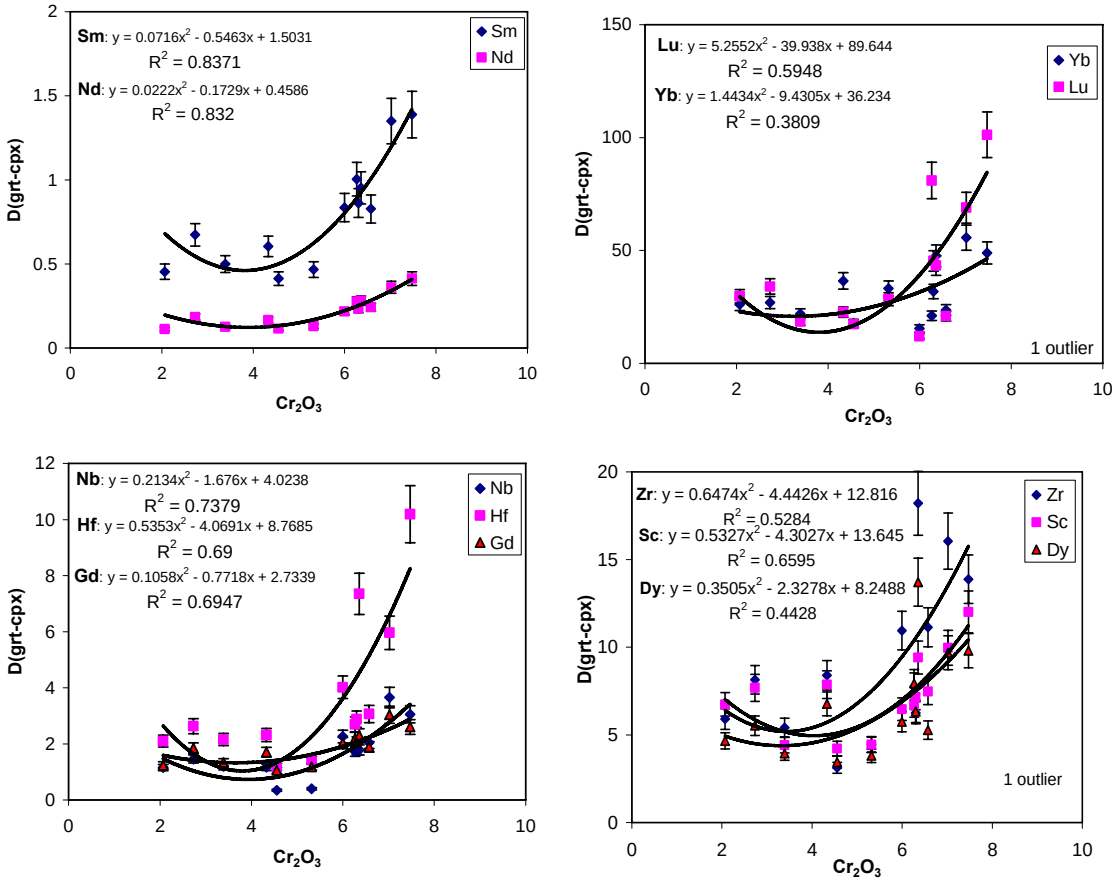

Fig. 4.23. Partitioning between grt and cpx for selected trace elements versus Cr_2O_3 (wt%) in garnet. Error bars indicate 10% analytical uncertainty.

Garnet/opx partitioning

Information on trace element contents in opx and their partitioning with other peridotitic mineral phases is scarce. The studies by Glaser et al. (1999), Simon (2004) and Ionov et al. (2005a,b) are the most comprehensive and their garnet/opx partition coefficients are used here for comparison with our new data. Except for Co, Ni, Ba and Sr all trace elements partition preferentially into garnet with $D^{grt/opx}$ of up to > 100 (Fig. 4.24). A larger scatter and higher D-values for Th, U, Rb and Ba, than observed in other natural samples, may be explained by the larger analytical errors on the opx measurements. It is apparent from the comparison with the low pressure/low temperature data set of Glaser et al. (1999) and Ionov et al. (2005a,b) with Simon (2004) and our data set that increasing pressure and temperature produce higher $D_i^{grt/opx}$. The effect is about one order of magnitude for all elements except for Zr, Hf and Sr (Fig. 4.24). Therefore garnet exsolved from opx would display inherited anomalies of Hf, Zr and Sr.

Most of the Finsch samples have similar partition coefficients as those of Simon (2004). Her sample was derived from 5.7 GPa, i.e. a very similar pressure as that for our samples. However, the temperatures of our samples lie at around 1200 °C, while her samples crystallized at 1330 °C. From this may be concluded that pressure is the decisive factor for the shift of the partition coefficients to higher values, rather than temperature. The partition coefficients are the highest for the sample with the highest Cr garnet (> 11 wt%; 882), which also contains spinel (Fig. 4.24). The other two higher Cr samples also have partition coefficients on the higher side which suggests a Cr effect on the partition coefficient, like observed for garnet-cpx partitioning.

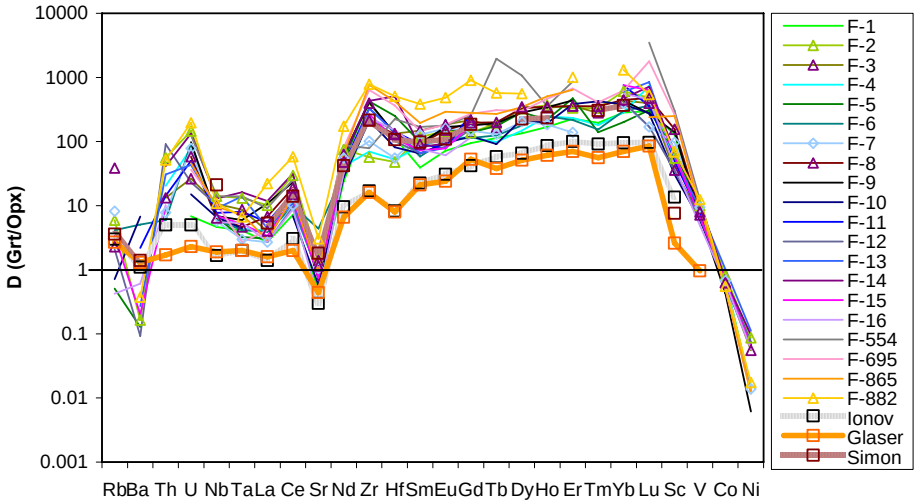

Fig. 4.24. Trace element partitioning between garnet and opx. Legend like in Fig. 4.22.

Cpx/opx partitioning

All trace elements, except for Ni and Co, partition stronger into cpx than opx. In comparison to the literature data a pressure effect may be discerned for the middle to heavy REE, Zr, Hf, Sc and V. All other trace element partition coefficients completely overlap with those of literature data, within their large variations (Fig. 4.25). Larger variation in Nb, Ta, U, Th, Rb and Ba for Finsch and literature data may be explained by the low concentration of these elements in opx that produced large analytical error. The only difference to literature data outside uncertainties (Van Achterbergh et al., 1998) was observed for Sc, which partitions even stronger into cpx.

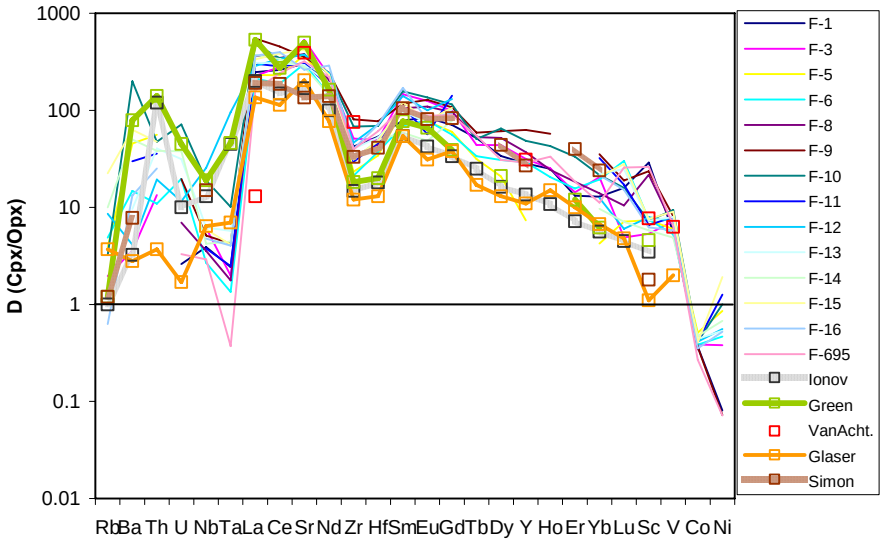

Fig. 4.25. Trace element partitioning between cpx and opx. Legend: Glaser (T = 1050 °C, P = 2 GPa) = Glaser et al., 1999; Green (T = 1050 °C, P = 2 GPa) = Green et al., 2000; Simon (T = 1330 °C, P = 5.7 GPa) = Simon, 2004; Ionov (T = 1030 °C, P = 2 GPa) - Ionov et al., 2005a,b; VanAcht. (T = 1050 °C, P = 4.9 GPa) = Van Achterbergh et al., 1998.

4.4.4 Depletion

The majority of the recalculated Finsch peridotite whole rock compositions yield a positive correlation between Cr_2O_3 and Al_2O_3 (Fig. 4.26, Table 4.4 in App.-3). They all have significantly lower Cr contents than the primitive mantle (square in Fig. 4.26). This may be taken as reflecting a scenario of partial melting where Al and Cr^{3+} behave similarly incompatible. At low pressure, in the spinel stability field, the bulk partition coefficient for Cr is close to zero and only Al is incompatible (Stachel et al., 1998 and ref. therein). This may occur under reduced conditions which were expected to exist during partial melting of the old Archaean lithosphere, as proposed by Canil (2002) for abyssal peridotites. As Cr^{2+} is more compatible, this should result in an increase of the bulk rock Cr content. On the other hand positive correlation between Cr and Al arises on partial melting in the garnet stability field (Fig. 4.26). Furthermore, the high contents of Al indicate that the dunites were not entirely depleted in the spinel stability field. Likely, most of these samples were depleted by a first partial melting event in the spinel stability field, i.e. in a middle ocean ridge (MOR) setting, and subsequently after subduction, a second partial melting event in the garnet stability field. This will be discussed below and also in Chapters 3 and 5.

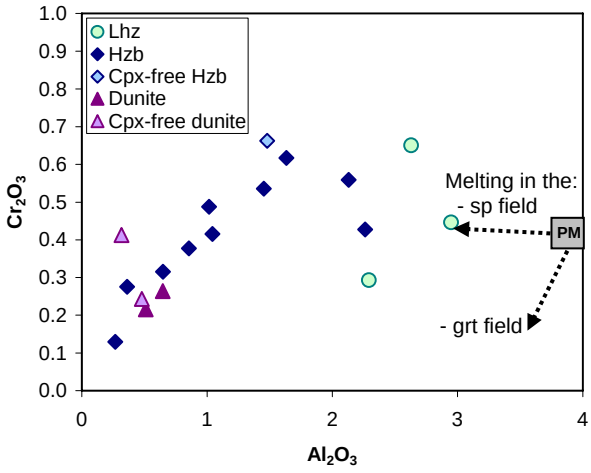

Fig. 4.26. Al_2O_3 - Cr_2O_3 relationship of the Finsch peridotites bulk rock. Grey square – primitive mantle (McDonough and Sun, 1995). Dotted lines point to the depletion at low pressure = "spinel (sp) field" and at high pressure = "garnet (grt) field".

One way to obtain degrees of depletion of natural peridotites is to compare them with experimentally obtained results. Numerous experiments on partial melting of peridotites at various pressures and temperatures are available in the literature (Hirose and Kushiro, 1993; Takahashi et al., 1993; Kushiro, 1998; Walter, 1998; Walter, 1999; Kushiro, 2001). Walter (1998, 1999) designed compositional grids for the estimation of the degree of melt extraction and depth of melting from a primitive, volatile free peridotite based on experiments from 1 to 7 GPa (Fig. 4.27). Calculated bulk rock composition of Finsch peridotites plot irregularly within and outside this grid and at high and low pressures, but always at high degrees of partial melting. Especially SiO_2–FeO plot at high SiO_2 values where half of the samples position outside the grid, demonstrating that this kind of grids cannot be used for peridotites with modal orthopyroxene contents higher than those of the primitive mantle. The cause of the orthopyroxene enhancement has to be accounted for before the application of such grids.

Takazawa et al. (2000) related the FeO and MgO contents in primitive (pyrolite) and in residual peridotites to the degree of partial melting through the FeO/MgO partitioning behaviour between olivine and liquid. This approach is less dependent on the presence or absence of a fluid phase. Using their model the degree of depletion of Finsch peridotites varies between 10 and 48% (Fig. 4.28; Table 4.1). Most harzburgites have been depleted by about 30%, lherzolite F-13 by about 10% and the two other lherzolites by about 26 and 32%. The highest depletion of more than 46% of melt extraction has the opx-rich harzburgite F-5, the cpx-free harzburgite F-7 and the dunite 882.

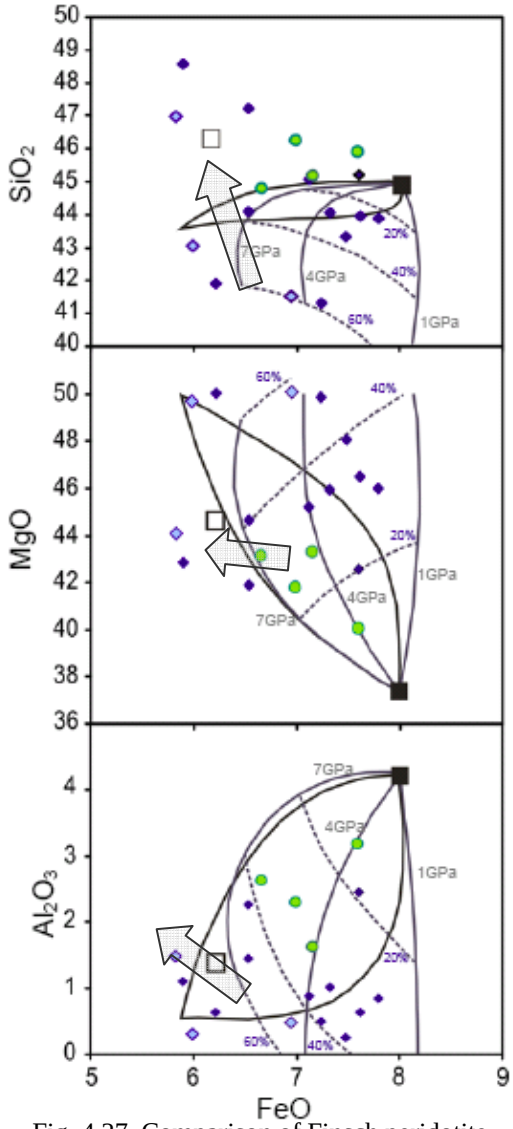

Fig. 4.27. Comparison of Finsch peridotite whole rocks composition with melting grids obtained experimentally (Walter, 1999). Near vertical lines are isobars, marked with pressure in GPa. Dashed lines indicate percentages of melt extraction from a primitive mantle source (black square). Black contours show polybaric fractional melting for different melting intervals (from Walter, 1999). Open square represent average for Kimberley samples (see Walter, 1999). Arrows are Si-addition trend (Walter, 1998).

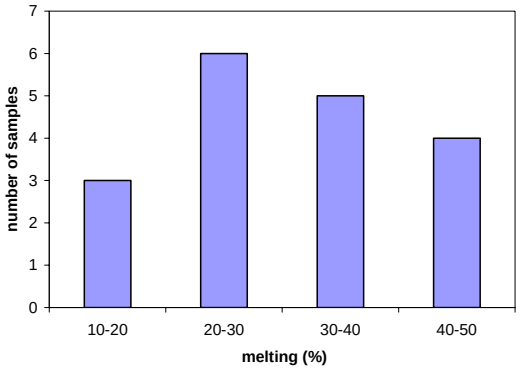

Fig. 4.28. Percent of melt extraction for Finsch peridotites calculated after Takazawa (2000).

Table 4.1. *Amount (in %) of extracted melt from Finsch peridotites calculated after Takazawa et al. (2000).*

sample	% of partial melting
F-1	15.5
F-2	34.3
F-3	44.8
F-4	25.5
F-5	46.2
F-6	25.5
F-7	47.5
F-8	30.4
F-9	27.3
F-10	34.0
F-11	17.4
F-12	37.2
F-13	10.5
F-14	21.4
F-15	32.7
F-16	26.5
695	26.7
882	48.6

Such high amounts of melt extraction obtained from major element relationship should also be reflected in the trace element patterns of the Finsch peridotites. The modelled REE patterns of the reconstructed Finsch peridotite bulk rocks (using the respective mineral abundances and the trace element concentrations of the minerals) are shown in figure 4.29 and given in Table 4.5 in App.-3. As expected from the mineral compositions most of the samples show sigmoidal REE patterns. It is also to be noted that all samples have REE concentrations lower than those of the primitive mantle (except lherzolite F-13, which has slightly elevated HREE). Most of them have HREE more than one order of magnitude lower than the primitive mantle. Secondly, they have middle to heavy REE that follow a

modelled depletion trend, as marked by the dotted line in figure 4.29. Therefore, the fractionation of the HREE from Lu to Tm may be taken as a relict from the partial melting event.

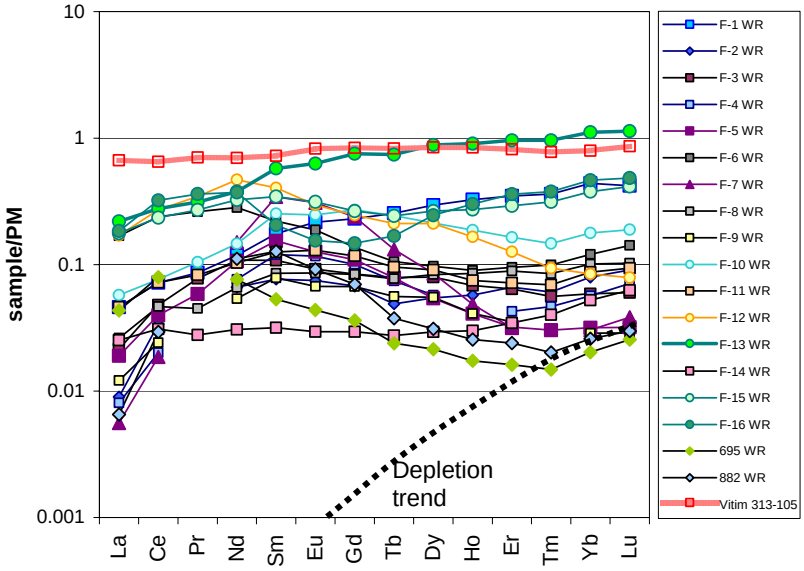

Fig. 4.29. Primitive mantle (PM - Hofmann, 1988) normalized REE of reconstructed whole rocks. Red line is for primitive peridotite Vitim 313-105 (Ionov et al., 2005a). The dotted line marks a modelled depletion trend

Trace element modelling of perfect fractional, non-modal melting of a pyrolite source (McDonough and Sun, 1995) was performed after Johanson et al. (1990) and Hellebrand et al. (2002) to constrain degrees of depletion in Finsch peridotites. Modelling was performed for melting in the garnet stability field using D*i* (distribution coefficient for element *i*) for cpx and garnet from Green et al. (2000) and in the spinel stability field from Kelemen et al. (1993) and Suhr et al. (1998). Melting modes for solid and liquid were taken from Kinzler (1997) and Walter (1998). The modelling results are shown in Fig. 4.30 and are compared with two REE patterns of the apparently “normally” depleted peridotites F-1 and F-13 and the extremely HREE depleted samples 695 and 882.

According to this modelling the least depleted sample lherzolite F-13 was depleted by 5-10% partial melting in the garnet stability field which is in good agreement with the results obtained from major element comparison and calculation (see above Fig. 4.28, and Table 4.1). The second sample with a more “normal”-appearing REE pattern (harzburgite F-1) also seems to be the product of 5-10% depletion, but in the spinel stability field. They both must have experienced a metasomatic overprint which increased the LREE contents (Fig. 4.29), and also elevated other incompatible elements.

Samples 695 and 882 should have been depleted mainly in the spinel stability field to explain their low HREE concentrations. The observed low HREE contents can be achieved e.g. by 25% of melt extraction at low pressure. Secondly, their strongly fractionated HREE also imply the presence of garnet in their residuum (Fig. 4.30). The explanation may lie in a two stage depletion process, as indicated by the Hf isotopes (see Chapter 3 and 5), which occurred at first at low and later on at high pressures with a combined high degree of partial melting of more than 40%. This would be in accord with mayor element modelling after Takazawa et al. (2000). The calculations implicate a similar history for all other samples.

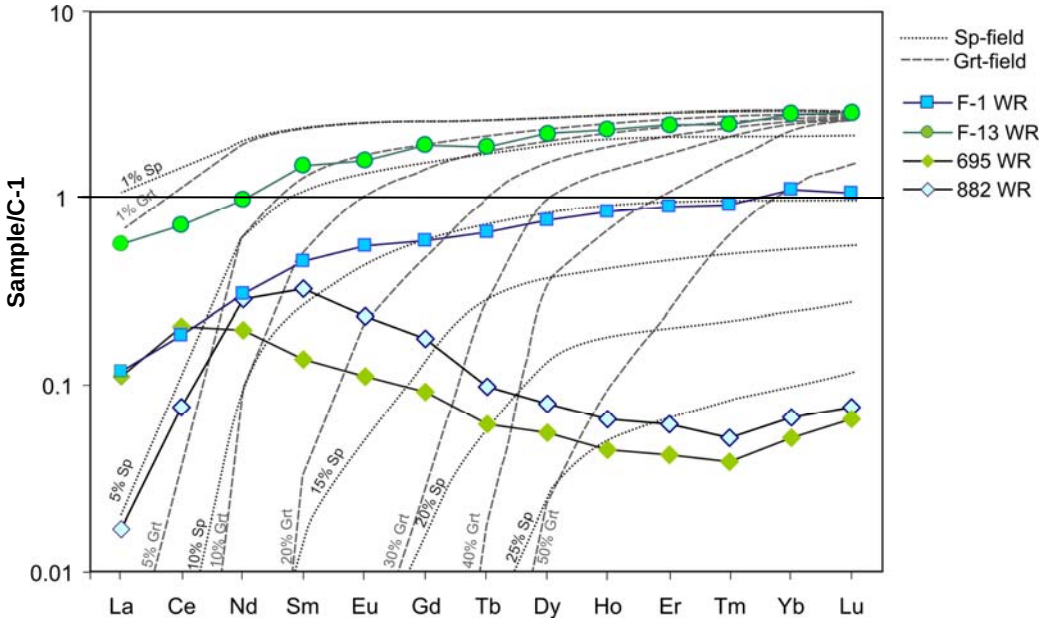

Fig. 4.30. REE depletion in Garnet- (dashed lines) and Spinel- (dotted lines) field compared with some Finsch samples. D*i* (coefficient distribution for element *i*) are taken from (garnet field - Green et al., 2000; spinel-field – Kelemen et al., 1993; Suhr et al., 1998). Melting modes for solid and liquid were taken from Kinzler (1997) (spinel peridotites) and Walter (1998) (garnet peridotites). While melt modes from Walter (1998) for melting in the garnet field preserves garnet even after unrealistically high depletion of 80%, they were modified so that garnet was exhausted from the source after 60% of melting.

4.4.5 Constraints on Si enrichment in Finsch peridotites

In a diagram of Mg# in olivine versus the modal amount of olivine most Finsch peridotites do not follow the oceanic partial melting trend as estimated by Boyd (1989). They rather fall in a field outlined by Boyd (1989) for the Kaapvaal craton (Fig. 4.31) i.e. they have high Si-contents compared to their depletion factor expressed as Mg# in olivine. Additionally, these samples have too high modal abundance of orthopyroxene compared to samples formed by a normal partial melting process. The highest modal opx content is observed for the cpx-bearing harzburgite F-5, but other harzburgites and all lherzolites also plot within the Kaapvaal field as determined by Boyd (1989). As a rare feature for the Kaapvaal craton, four dunites and one harzburgite plot on or close to the "oceanic trend" indicating that they are not enriched in silica.

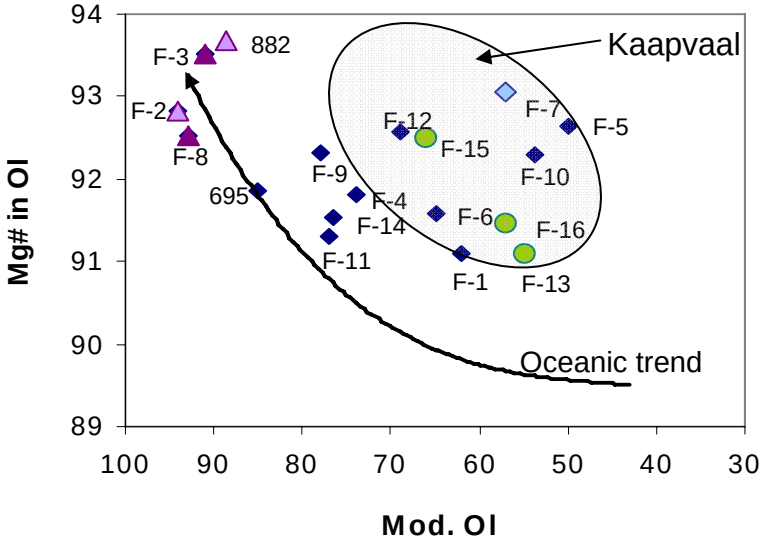

Fig. 4.31. Mg-number (Mg#) in olivine vs. modal olivine (Mod. Ol) for the Finsch peridotites. Arrow represents oceanic trend and Kaapvaal field is for opx rich samples from Kaapvaal craton (Boyd, 1989).

Higher modal opx relative to olivine can be created in peridotites by partial melting up to 20% at low pressures (1.7–2 GPa; Kinzler, 1997; Weng and Presnall, 2001) but further melting would rapidly consume opx. Dry melting at higher pressures also does not shift ol-opx relations in the necessary direction (3-7 GPa, Walter, 1998). The relationship of SiO_2 and MgO/SiO_2 of the bulk rocks shows that half of the Finsch peridotites plot close to the residue trend for dry partial melting of fertile mantle (pyrolite) (Fig. 4.32; Walter, 1998). The highly depleted samples that follow the "oceanic trend" in Fig. 4.31 plot along the ol-opx mixing line in Fig. 4.32, which confirms that these samples are a residue of partial melt extractions. The other samples scatter between the partial melting trend and the ol-opx mixing line. Thus, they are not simple residues from partial melting of a fertile mantle.

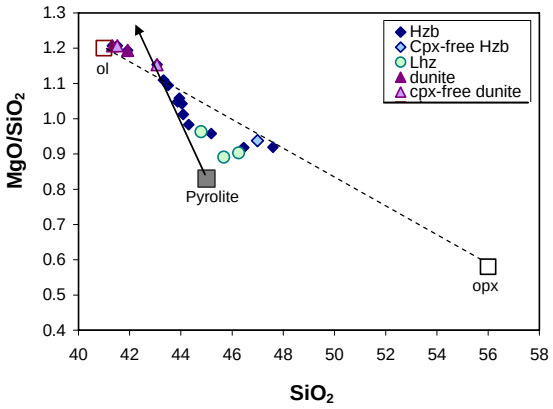

Fig. 4.32. MgO/SiO_2 vs. SiO_2 (wt%) in reconstructed whole rock peridotites. The arrow represents a pyrolite residue trend, and the dashed line is an olivine-opx mixing line, taken from Walter, 1998.

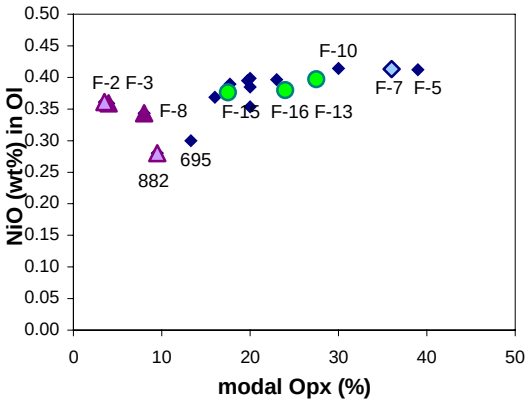

Fig. 4.33. Modal opx against NiO (wt%) in olivine of Finsch peridotites.

A number of authors have addressed this issue and proposed opx enrichment by a complex process of melt extraction followed by Si-enrichment by addition of Si-rich melts or fluids (Kesson and Ringwood, 1989; Kelemen et al., 1992; Rudnick et al., 1994; Kelemen et al., 1998; Griffin et al., 1999a; Bell et al., 2005; Simon et al., 2007), or by metamorphic unmixing (Boyd, 1997), or by cumulate mixing (Herzberg, 1993; Herzberg, 1999).

Most popular is the theory that the high modal opx is due to an enrichment of lithospheric mantle by a Si-rich melt (Keson and Ringwood, 1989; Kelemen et al., 1992; Kelemen et al., 1998) or a fluid (Rudnick et al., 1994; Bell et al., 2005; Simon et al., 2007). Kelemen et al. (1998) used the positive correlation between NiO in olivine and modal opx as a supporting argument for the production of opx at the expense of olivine by the infiltration of a Si-melt/fluid. Since olivine is the main Ni-carrier in the mantle its Ni content must rise if the same original amount of the bulk rock has to be accommodated, as the amount of olivine decreases. Such a correlation is indeed observed for the Finsch peridotites (Fig. 4.33). However, such a correlation also creates if opx would be more refractory than olivine during partial melting.

Nevertheless, high opx contents in the Finsch samples may be explained by Si-enrichment through a melt or fluid. Half of the opx enriched samples (harzburgite F-10, lherzolite F-13, 15 and 16, in Fig. 4.31) appear to show elevated Al content (samples with highest Al contents in Fig. 4.26) compared to other opx enriched samples. Some samples have cpx with elevated Na_2O (F-10, F-12) or garnet with high TiO_2 (F-12). This sample is also rutile and pentlandite bearing. The range in Rb, Ba and Th is rather large and some have elevated Zr and Hf compositions (Fig. 4.34, Table 4.5 in App.-3). All this indicates various kinds of metasomatizing agents, which could be either a fluid or melt. It is unclear, which belongs to the possible opx enrichment process.

The high Si-enriched harzburgite F-5 and the cpx free harzburgite F-7 have many properties in common: they follow the Al-Cr correlation (Fig. 4.26), they are similarly enriched in MREE and LREE and they have small negative Zr-Hf and a positive Nb-Ta anomaly and similar Ba and Th contents; only Sr and Rb are lower in F-7 than in F-5 (Fig. 4.34, Table 4.5 in App.-3). These samples are good candidates to decipher the Si-enriching agents.

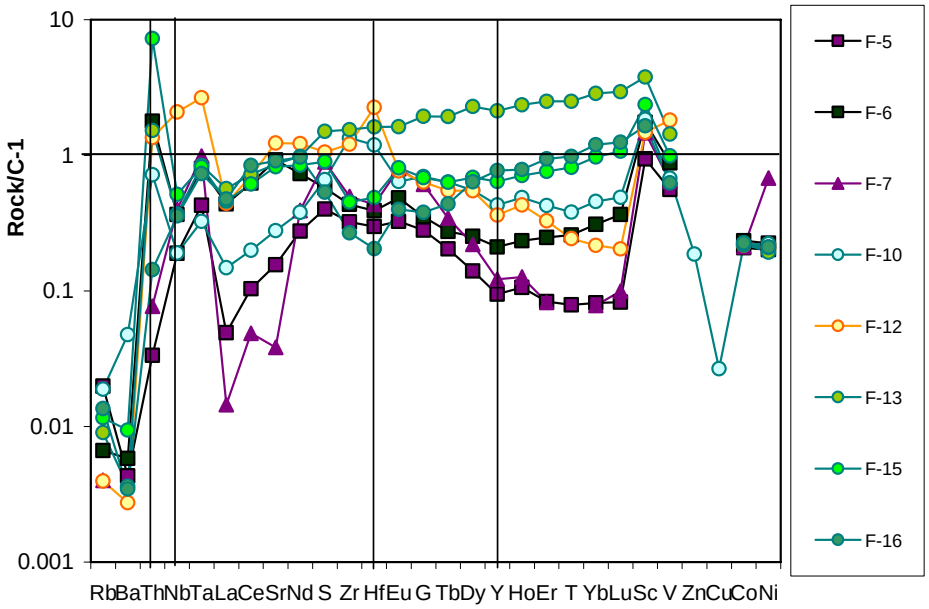

Fig. 4.34. Chondrite (C-1 – McDonough and Sun, 1995) normalized trace element patterns for highly opx enriched Finsch peridotites (samples that plott in the Kaapvaal craton field in Fig. 4.31).

Negative Y and Hf anomalies are indicative of fluid metasomatism (Kessel et al., 2005), but low LILE and Th with Th>Ba point to the opposite (Stalder et al., 1998; Kessel et al., 2005). Also, a positive Nb anomaly with Nb<Ta in these two samples (Fig. 4.34) is contradictory to fluid enrichment. Further more, enrichment of LREE is minor and does not correspond to subduction related fluids (Stalder et al., 1998; Kessel et al., 2005). This leaves strong doubts that these samples were opx-enriched by the Si-rich fluids and other process must be invoked. These may include metamorphic or cumulate processes (Herzberg, 1993; Boyd, 1997; Herzberg, 1999, see also discussion by Walter, 1999) or reaction with a Si-rich melt metasomatism (Kesson and Ringwood, 1989; Keleman et al., 1992; Keleman et al., 1998).

4.4.6 Modal and cryptic metasomatism of the Finsch peridotites

After extraction of more then 30% of partial melt from a regular fertile peridotite, the remaining residue with more than 60% olivine should be clinopyroxene free (e.g. Jaques and Green, 1980; Walter, 1998). Some of the highly depleted peridotites from Finsch that have more than 80% olivine still have small modal cpx (see Table 1 in App.-2). Melt depletion in the present of residual garnet should lead to smooth REE pattern, but most of the Finsch garnets have sinusoidal REE pattern. Furthermore, both garnet and cpx have elevated incompatible elements compared to primitive Vitim 313-105 garnet and cpx, respectively (Ionov et al., 2005a,b; see Figs. 4.15 and 4.13). Therefore, besides partial melting, all here studied samples have undergone secondary process. For mantle peridotites, multi stage evolution is generally recognised, where melt depletion was followed by metasomatic enrichment during interaction with fluids and melts (Dawson, 1982; Menzies and Hawkesworth, 1987; Hoal, 1994).

Two types of metasomatism are generally recognised: modal and cryptic. Modal metasomatism formed by “infiltration” enrichment, where new material is being introduced by volatile bearing melts or fluids percolating through pores in the rocks. It is apparent from the presence of minerals like phlogopite, amphibole, rutile, ilmenite, apatite or carbonates in addition to the common peridotite minerals (Harte, 1983; Erlank et al, 1987; Gregoire et al., 2002). Carbonatitic melts for example may cause the formation of apatite and secondary cpx accompanied by a general enrichment in LREE and LILE (Yaxley et al., 1991; Ionov et al., 1993; Rudnick et al., 1993; Ionov et al., 1996).

The term cryptic metasomatism was proposed for the observed trace element enrichment of peridotites which is apparently unaccompanied by mineralogical changes. This type of metasomatisam

leads to enrichment in incompatible elements and is probably produced by diffusion (Dawson, 1984; Menzies and Hawkesworth, 1987).

Suggested metasomatic agents in mantle peridotites are basaltic (komatiitic), kimberlitic, Si-rich and carbonatitic melts and hydrous fluids (Fig. 4.35B). Modern *Basaltic melts* have relatively flat incompatible trace element patterns with concentrations of up to 10 times chondrite (Mc Donough and Sun, 1995). In the Archaean the equivalent may have been a *komatiitic* melt. The trace elements for Barberton Komatiites are shown in Figs. 4.35 and 4.36 (Lahaye et al., 1995). They have small negative Sr and Zr-Hf anomalies and subchondritic Rb and Ba.

Kimberlite itself, the transport vehicle for peridotites are rich in volatiles and may be responsible for metasomatism either before and/or during the eruption (Gregoire et al., 2002; Gregoire et al., 2003; Simon et al., 2003). Kimberlites have similar HREE contents as komatiites, but are much higher in other incompatible elements (100x chondrite for Rb or Ba and 1000x chondrite for Th or La for Group II kimberlites after Nowel et al. (2004) and Becker and Le Roex (2006). They have positive Ti and Nb anomalies and moderately pronounced negative Zr-Hf and Sr anomalies (Fig. 4.35).

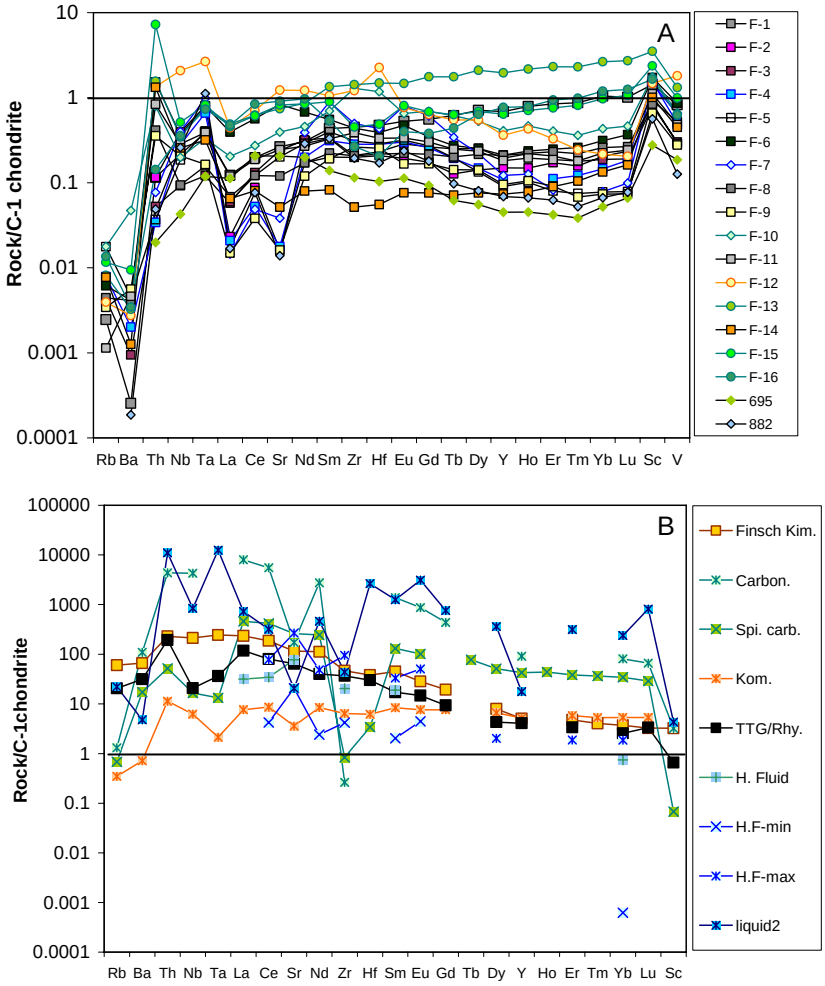

Fig. 4.35. Chondrite normalized (C-1, McDonough and Sun, 1995) trace element of (A) reconstructed whole rocks (WR) of the Finsch peridotites; (B) metasomatic agents: Finsch Kim. = Finsch kimberlite (Becker and Le Roex, 2006); Carbon. = Namibian carbonatite (Nelson et al., 1988); Spi. carb. = Southern African Spickop carbonatite (Ionov and Harmer, 2002); Kom. = Barberton Komatiites (Lahaye et al., 1995); TTG/Rhy. = average **t**onalite-**t**rondhjemite-**g**ranodiorite and rhyolites from Southern Africa (Martin, 1994); H. Fluid- experimentally obtained hydrous fluids (Stalder et al., 1998); H.F.-min and –max = hydrous fluids minimum (min) and maximum (max) values by Bizmis et al., (2000); Liquid = experimentally (at 6 GPa and 1200°C) obtained hydrous fluids and liquids from MORB (**m**iddle **o**cean **r**idge **b**asalts - Kessel et al., 2005).

Si-rich melts during the Archaean comprise the **t**onalite-**t**rondhjemite-**g**ranodiorite (TTG) – suite (Martin, 1994). They have similar contents of HREE as common basalts but have higher LREE and LILE. Their interaction with peridotite would increase these elements and also Na, but would dilute Cr and Mg (Wulff-Pedersen et al., 1999). The proposed origin for these Si-rich melts is partial melting of eclogites (Barth et al., 2001). The concentration of HFSE in these melts is therefore strongly related to the amount of rutile and/or amphibole in the melt source (Fig. 4.35; Foley et al., 2000; Barth et al., 2001).

Even higher LREE/HREE ratios and a restricted range of HFSE/MREE are diagnostic for the interaction of *carbonatitic melts* with peridotites (Ionov et al., 1993; Rudnick, 1993; Ionov et al., 1996; Yaxley, et al., 1998). They have strongly fractionated, but elevated content of REE (>10x chondrite for Lu and >100x chondrite for Lu) and lower LILE than REE (Fig. 4.35). Shown here as an example are carbonatites from South Africa (Spickop – Ionov and Harmer, 2002) and Namibia (Nelson et al., 1988). They differ in strongly incompatible elements (LILE, LREE, Nb, Ta) probably as a result of fractionation. Such differences will be taken into account in the further discussion.

Depletion of HFSE relative to REE points to the interaction with *hydrous fluids*, in which HFSE are less soluble than LREE and MREE (Adam, et al., 1997; Stalder et al., 1998). Such fluids have highly fractionated REE with very low HREE and Y, and high LILE (Fig. 4.35). The origin of such fluids is related to dehydration of the subducted slab and thus, like for the Si-melts, their HFSE contents are also related to the presence of rutile and amphibole in the source (Stalder et al., 1998; Kessel et al., 2005).

The direct use of melt compositions that are observed on the Earth's surface to deduce characteristics of metasomatizing melts and fluids has to be done with caution, since the material derived at the Earth's surface may already be modified by reactions at depth with the peridotite and/or the Earth crust.

Peridotite F-12 contains ~ 1 vol.% of rutile, rare pentlandite and rare phlogopite and was apparently modally metasomatized. This unique sample has the highest contents of V and HFSE (with Ti > Ta > Nb = Hf > Zr) of all samples of the present study. It has elevated MREE and a small positive Sr and a small negative Y anomaly (Fig. 4. 35A). This sample also differs from all others by having very high Hf and a low chondrite normalized Zr/Hf ratio. All these chemical features suggest the involvement of a fluid or a volatile rich melt in formation of Finsch peridotites. Its elevated Na_2O and Cr_2O_3 content of cpx indicate a similarity to the MARID-suite of xenoliths or to peridotites enriched by group II kimberlite (Gregoire et al., 2003). The occurrence of modal rutile and phlogopite implies that kimberlite is the likely candidate for such a melt (as proposed by Gregoire et al., 2002, Gregoire et al., 2003 for MARID suite peridotites). Garnet from this sample (F-12) shows a high sinuosity for REE and volatile bearing phases are poorly abundant. This implies that the volatile rich melt only partly crystallized and reacted with the peridotite while a differentiated melt proportion, more enriched in volatiles and depleted in moderately incompatible elements, continued to percolate through the upper mantle.

If the increased orthopyroxene content is not considered as modal metasomatism, most samples suffered only cryptic metasomatism. According to their positive Zr-Hf anomalies (Fig. 4.35A), the harzburgites F-9, F-10, F-11 and 695 and lherzolite F-13 were likely metasomatized with melt similar to that responsible for metasomatism of the rutile bearing sample. They have positive Nb-Ta anomalies and a positive or not pronounced Sr anomaly that also indicate the same enrichment agent. The degree of interaction, however, is less than in rutile bearing sample, because only cryptic metasomatism occurred.

All other Finsch peridotites have negative or not pronounced Zr-Hf anomalies. Still, their HFSE and REE are elevated compared to an expected normal depletion trend. Niobium and Ta are enriched in all samples with mostly subchondritic Nb/Ta (Fig. 4.35A) with the exception of harzburgite F-9, which has a superchondritic Nb/Ta. Yet their Rb, Ba and Sr are low compared to the LREE. Therefore, most samples were metasomatized by an agent that was enriched in MREE and LREE, and depleted in LILE and had MREE>HFSE.

Comparing concentrations of HFSE (Zr, Hf) with the abundances of middle (Sm) and heavy (Yb, Lu) REE, some enrichment characteristics of the Finsch peridotites were observed in Fig. 4.36A-B. Most of the samples plot in a field with higher $(Sm/Yb)_N$ and $(Zr/Hf)_N$ than those of primitive mantle. These enrichment characteristics are similar to those of the kimberlitic and Si-rich melts. On the other

hand, some peridotites with low $(Sm/Hf)_N$ and $(Lu/Hf)_N$ could also have been enriched with a fluid, and two lherzolites (F-16, F-15) have $(Lu/Hf)_N$ and $(Sm/Hf)_N$ ratios that indicate enrichment by a carbonatitic melt (Fig. 4.36A). The sample F-15 also has high Th, Rb and Ba contents and a small positive Sr anomaly that point to Si-melt enrichment rather than by a carbonatitic melt. Fluids and carbonatitic melts, have significantly lower $(Zr/Hf)_N$, and are strongly enriched in LILE and LREE compared to HREE (Kessel et al., 2005; Stalder et al., 1998), which is not a primary characteristic of the studied samples (Figs. 4.35A, 4.36).

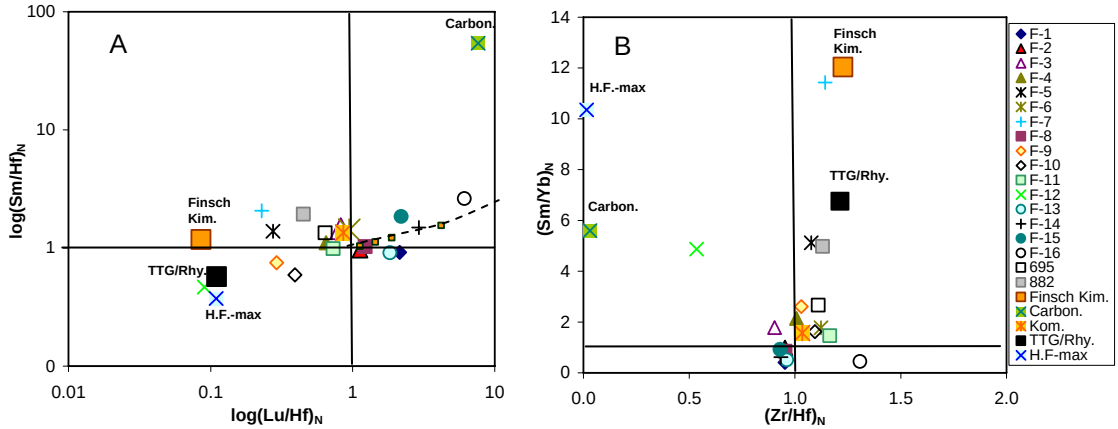

Fig. 4.36. Chondrite normalized (C-1, McDonough and Sun, 1995) trace element ratios of reconstructed whole rocks (WR) of the Finsch peridotites. The dashed line with small squares represents a calculated partial melting trend and the straight lines represent primitive mantle values (Hofmann, 1988).

TTG/Rhy.

From the whole rock trace element chemistry is difficult to be more specific about the kind of metasomatizing agents. These may be mirrored better by the chemistry of specific minerals, especially of garnet. Griffin et al. (1999b) made extensive use from the Y-Zr relationship (Fig. 4.37) to discriminate between fertile, depleted, melt and low-T phlogopite-melt metasomatized garnets. Applying this, all Finsch garnets are either depleted or melt metasomatized peridotites. Two garnets (F-5, F-7) have extremely low Y and Zr concentrations and therefore belong to the depleted group. Yet, they are from orthopyroxene (Si-) rich peridotites, which are supposed to be the product of Si-enrichment (see section 4.4.5. of this chapter). This may imply that the Y-Zr relationship is unsuitable to distinguish between different metasomatizing melts or that the Si enrichment diluted Y and Zr in the peridotites.

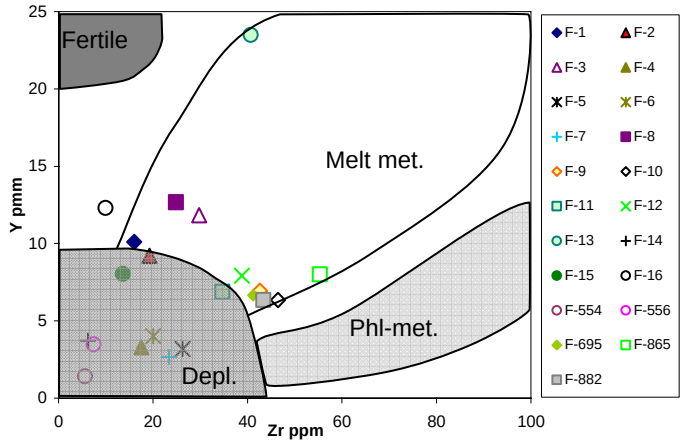

Fig. 4.37. Y and Zr contents of the Finsch garnets. Fields are taken from Griffin et al. (1999b). Phl-met. = low-T phlogopite metasomatism; Melt met. = melt metasomatism; Depl. = depleted peridotites; Fertile = fertile lherzolites.

Following Coltorti et al. (1999) the ratios of $(Ce/Yb)_N$ and $(Zr/Sm)_N$ in garnets and clinopyroxenes are used to discriminate between carbonatitic and Si-melt metasomatism (Fig. 4.38). High $(Ce/Yb)_N$ and low $(Zr/Sm)_N$ are expected for carbonatite metasomatized samples, and low $(Ce/Yb)_N$ combined with high $(Zr/Sm)_N$ for Si-melt metasomatism. As shown by Fig. 4.38 all cpx have relatively low

$(Zr/Sm)_N$ combined with variable $(Ce/Yb)_N$, while garnets have relatively low $(Zr/Hf)_N$ and $(Ce/Yb)_N$. The highest $(Ce/Yb)_N$ in garnets were observed for some cpx-free dunites (F-2, 882) and the harzburgite (F-7), which could be explained by increased LREE in garnets, if cpx does not co-exist. The samples (F-16, F-15), which were suspected to be metasomatized by a carbonatitic melt according to their whole rock trace element contents, show no enrichment of $(Ce/Yb)_N$ in garnet and have the lowest of all $(Ce/Yb)_N$ ratios in cpx. They also do not show strong enrichment of $(Zr/Sm)_N$ and thus have not been metasomatized by a carbonatitic or by a Si-rich melt. While cpx points to a fluid and/or carbonatitic melt, garnets indicate kimberlitic or Si-rich melt metasomatism (Fig. 4.38).Thus, this kind of classification cannot distinguish, which type of metasomatism occurred.

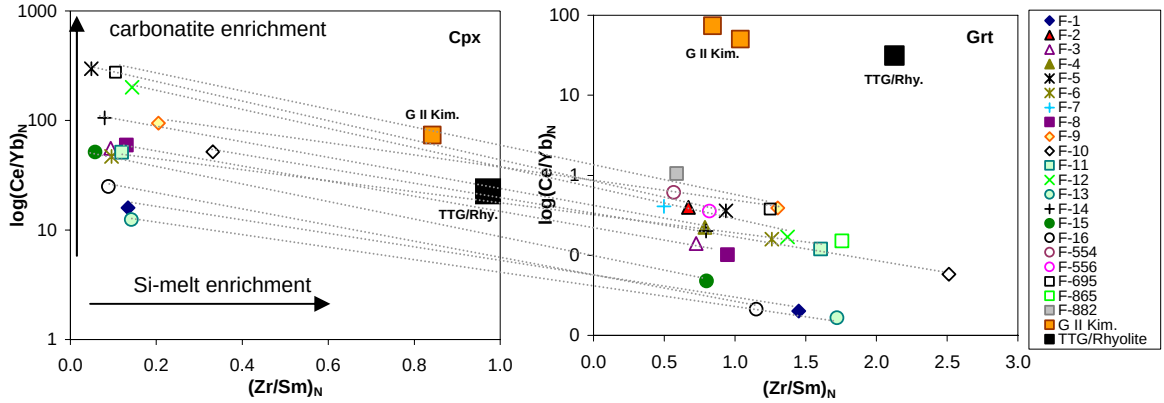

Fig. 4.38. Chondrite (C-1) normalised $(Zr/Sm)_N$ vs. $log(Ce/Yb)_N$ ratios in grt and cpx from the Finsch peridotites. Mineral pares are connected with dotted lines. Several line crosses can be observed, which may indicate incomplete equilibrium between grt and cpx.

All observations indicate that the metasomatic overprint of Finsch peridotites was either produced by a kimberlitic or a Si-rich melt or both. Some samples also show indices for additional reaction with carbonatitic melt or fluid. Those mixed signatures as well as the disagreement of trace element enrichment in bulk rocks and mineral separates could be explained in several ways.

One is not complete trace element equilibrium between minerals. As already indicated by garnet-cpx partitioning (see section 4.4.3) may explain differences observed in the Coltorti, et al. (1999) diagram (Fig. 4.48). This effect is also confirmed with equilibration of isotopic systems of these samples, where Sm-Nd isotopic system is well equilibrated, while Lu-Hf shows disequilibrium between garnet and cpx (see also Chapter 5). Thus, either garnet or cpx was strongly affected by metasomatic enrichment and did not completely re-equilibrate.

A mixed signature of elevated MREE and relatively low LREE and LILE, coupled with various HFSE of Finsch whole rocks could be explained by several factors. One could be that all samples were metasomatized by diffusive exchange with an evolving melt, where complete equilibrium between melt and peridotite was never achieved, as it is proposed by Hoal et al., (1994). This may have created sinusoidal pattern in garnets and different enrichment of other incompatible elements.

The third possibility is that several probably different metasomatic events have subsequently affected these samples. The smooth and relatively small enrichment mostly observed in LREE and LILE could be also explained by a depletion event that followed the enrichment episode(s). For most of the samples two stages of depletion were proposed (section 4.4.4. and Chapters 3 and 5). Therefore, metasomatism could have happened between those two depletion events. In that case strongly enriched samples have afterwards lost some of their LREE and most of the LILE and have created smoother trace element patterns. Isotopic signatures of these samples also indicate multiple enrichments with different metasomatizing agents (see also Chapters 3 and 5). Considering all these effects determination of the metasomatizing agent is very difficult. Thus, Finsch samples have suffered multiple enrichment events with possibly different agents, which were mostly kimberlite like or have Si-rich character as melts derived from the subducted slabs.

4.7.4 Chemical composition - depth relationship

The analysed suite of Finsch peridotites covers only a limited pressure and temperature range (P= 4.5-6 GPa and T=1050-1250°C). Accordingly, sampling is restricted to a depths range of ~ 140 to ~ 210 km. Since P-T conditions of all cpx-free samples were calculating by garnet-olivine ($T_{O'Neill}$ - O'Neill and Wood, 1979) and garnet-opx barometer (P_{BKN} - Brey and Köhler, 1990), which are affected by Fe^{3+} in the minerals (ol, grt), corresponding temperatures are 50-100°C lower (Smith, 1999) than those provided by the two pyroxene thermometer (T_{BKN} - Brey and Köhler, 1990). Correcting for the effect of Fe^{3+} in garnets from cpx-free harzburgites, using Mössbauer spectrometry data (Tables 4.6 and 4.7 in App.-3), the depth range reduce to around 160-210 km.

Although the sampled depth interval is relatively small, little correlation between cpx content in samples and distribution of trace elements in WR and depth can be observed (Fig. 4.39). Lherzolites are samples from the greatest depth, followed by the cpx-bearing harzburgites and dunites, and the cpx-free samples are from the shallowest parts. This depth distribution of the samples is unaffected by the above mentioned temperature correction. The modally metasomatized rutile bearing harzburgite (rt-hzb = F-12) also belongs to the deepest samples of this suite. This sample also records the highest content of incompatible elements (Sr, Nd and Hf).

Lherzolites are enriched in Sr, Nd and Y compared to harzburgites, but contents of these elements are less abundant than of the primitive mantle (PM – Hofmann, 1988). Two of the lherzolites have similarly low Hf contents as the majority of the harzburgites and dunites. These findings imply a negative correlation of trace element concentrations of the Finsch peridotites with depth (Fig. 4.39).

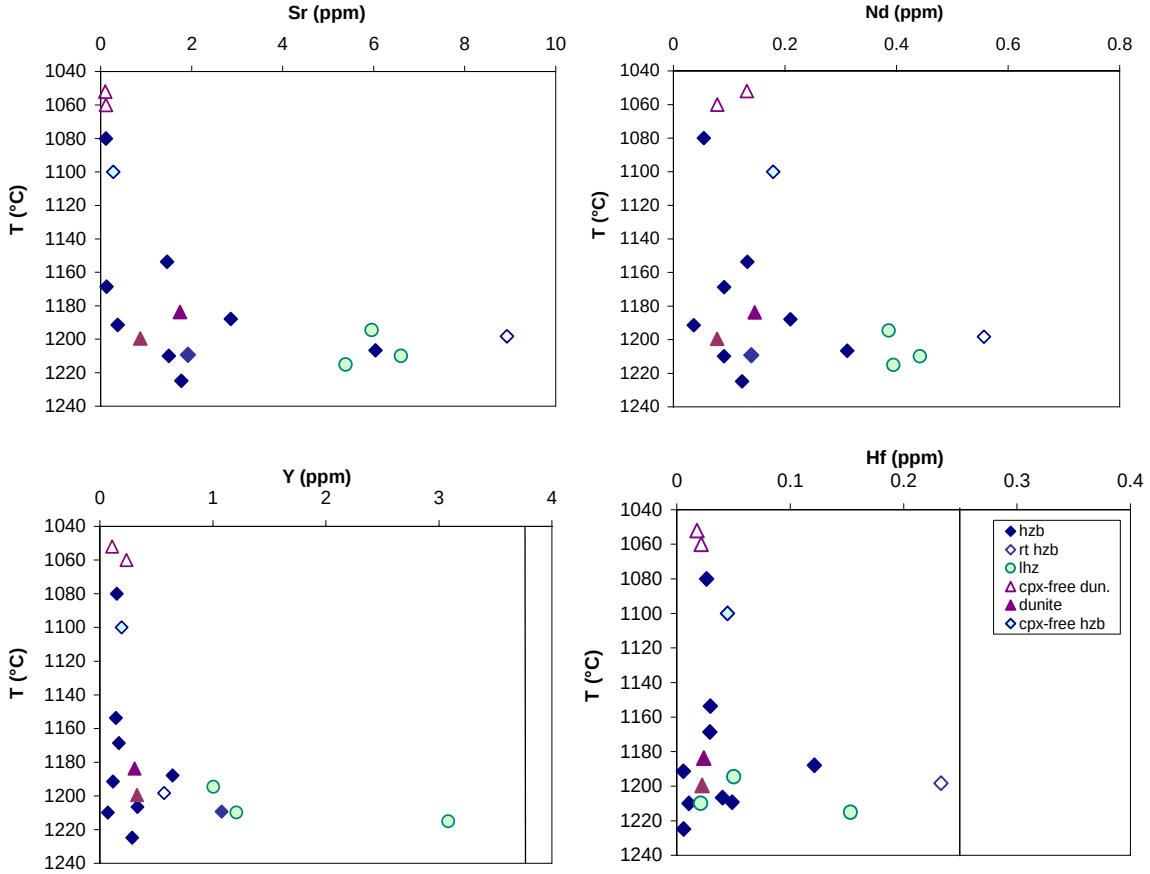

Fig. 4.39. Distribution of the Finsch peridotite trace elements concentrations with depth. Lines point at the value of the primitive mantle (Hofmann, 1988). PM for: Sm=18.2 ppm and Nd =1.19 ppm.

This relationship could be produced by enrichment events (constrained by the subcalcic garnets – Chapter 3 and peridotite isotope compositions – Chapter 5), which likely occurred in situ. As the lherzolite F-15 and the rutile bearing sample F-12 originate from the deepest parts of the mantle, they

should be the first to react with the melt. Accordingly, these samples are the most strongly metasomatized ones. Since metasomatizing melts had only moderate influence on the LREE and LILE (missing water bearing phases – phlogopites and amphibolites in those two samples), it can be assumed, that remaining melts continued percolation and were responsible for the metasomatism of the other samples above. Since the first melt should have been kimberlitic in character (for the rt-bearing hzb) it should, after the reaction with the mantle, have become more volatile- and LREE rich and should have been depleted in Zr and Hf. Such a melt could have brought enough basaltic components (Fe, Al, Ca) to recrystallize cpx in shallower depleted harzburgites and dunites. Probably not much of that reacting melts or fluids reached the shallowest parts, and cpx-free samples kept almost unmetasomatized.

On the other hand, the shallowest cpx-free samples show higher Hf and Nd contents (Fig. 4.39) than some of the deepest cpx-bearing harzburgites. This may indicate to a different metasomatic process at the depth of around 170-180 km than at the higher depths.

To better constraint the relationship of depth and metasomatic enrichment, a larger set of well studied samples from this locality would be required.

4.5 Summary and Conclusions

The suite of analysed Finsch peridotites shows a large diversity in mineral and whole rock major and trace element compositions, leading to the conclusion that complex processes were responsible for their formation. However, mineral major and trace element compositions do not show a large influence of the host kimberlite.

The samples originate from a limited depth range of 160-210 km and have preserved well equilibrated major element compositions from those depths. The oxygen fugacity of garnets from the Finsch samples indicates continuously reducing conditions with increasing depth. In contrast to that trend, rare kimberlite metasomatized samples (rutile bearing) have a relatively oxidised nature.

According to the major and trace element partial melting modelling, most of the observed samples are strongly depleted. Extraction of 30 to 50% of melt is evident for all samples, except two lherzolites, which were only depleted by up to 10%. Most of the samples were firstly depleted at low pressures (spinel or plagioclase stability field), which was followed by depletion at higher pressures in the presence of garnet. Only a few samples display evidence of only one depletion event. The majority of the here studied samples, which have been strongly depleted at the low pressures, have been tectonically re-emplaced into a higher depth in the garnet stability field (Kelemen et al., 1998). During this event, cooling and sub-solidus re-equilibration at the new P-T conditions also involved the extraction of an aluminium phase like grt, maybe also cpx and formation of low-T opx from the aluminium rich high-T opx (Canil, 1992). That is how the ol+opx+grt±cpx±sp assembly has been created.

All samples were metasomatized by different melts or even multiply enriched, or they were metasomatized by diffusion processes of evolving melts. According to the trace element ratios and concentrations of whole rocks and minerals, the most likely metasomatizing agents that reacted with the peridotites were volatile bearing ultramafic (similar to the kimberlite) or silica-rich melts. Beside incompatible trace elements these melts usually also carry other magmaphile elements, like Fe, Ca, Al, Na and Ti. One of these melts was strongly enriched in Ti and sulphides and has modally modified the rutile bearing sample.

Harzburgites are more enriched in highly incompatible elements because they are more permeable than lherzolites, due to their ol-rich character (Toramaru and Fuji, 1986), or because incompatible elements can move faster trough the matrix of refractory peridotites than compatible elements (e.g. Bedini et al., 1997). Therefore, cpx could have been formed by such processes, which is most evident in cpx-bearing dunites (F-3, F-8) and also in some of the cpx-bearing highly depleted harzburgites (695, F-9). That is also supported by the higher content of Ti, Na and LREE in cpx and opx from these samples. Metasomatism by highly volatile bearing Si-rich melts is probably also responsible for the increase of modal opx in the Finsch peridotites.

It can also not be excluded that metasomatism of some samples took place between two depletion events, which may explain the elevated smooth MREE patterns, with low abundance of HFSE and extremely low LILE. However, the following depletion event must also have been occurred at low

pressures, before the final depletion in the garnet stability field (see also Chapters 3 and 5). Otherwise, the low pressure depletion signature would have been entirely erased and these samples, after ~ 20% of melt extraction, would be cpx-free. Thus, extremely small trace elements evidence for metasomatism prior final depletion could have been preserved, and most of the elevated LREE, MREE and LILE signature was formed by re-enrichment after final depletion.

This all indicates a complex development of the Kaapvaal craton connected with the strong multiple depletion followed by several enrichment processes.

CHAPTER 5

Lu-Hf and Sm-Nd dating of mantle depletion and enrichment: a case study on Finsch mine peridotites (Kaapvaal craton - SA)

5.1 Introduction

Processes connected with the formation and modification of the sub-continental lithospheric mantle (SCLM) is mainly recorded in the trace element and isotope signatures of the constituent peridotites. Pioneering work on Sr and Nd isotope signatures and dating on cratonic mantle lithologies started in the 1980s (Menzies and Murthy, 1980; Richardson et al., 1984; Richardson et al., 1985). Since the parent and daughter elements are both incompatible in the Earth mantle for these two isotope systems their ratios and abundances are strongly influenced by depletion and enrichment processes. Further more, Rb is usually extremely depleted in peridotites and is commonly below the detection limit, and both Rb and Sr are very sensitive on kimberlite contamination and surface alteration. This makes the Rb-Sr system not very suitable to date mantle processes prior to the kimberlite eruption. The Sm-Nd system is less sensitive to surface alteration and contamination, but may be fully reset by mantle metasomatism, thus may be a tool to date these processes.

Several years of intensive studies of different isotope systems revealed that the Lu-Hf (Ionov and Weiss, 2002; Schmidberger et al., 2002; Pearson and Nowell, 2004; Wittig et al., 2007) together with the Re-Os system (Pearson et al., 1995; Menzies et al., 1999; Carlson et al., 1999; Irvine et al., 2001; Pearson and Nowell, 2004; Simon et al., 2007) appear to be the reliable isotopic systems for the dating of old, Archaean depletion events. Both the Re-Os and the Lu-Hf system can be robust to mantle metasomatism. However, Re-Os may be affected by the break down of sulfides during low-T secondary oxyhydration during eruption (Lorand, 1990; Pearson et al., 1998).

While Sm-Nd is sensitive to metasomatism with melts and fluids, Lu-Hf can only be affected by the interaction with a significant amount of melt. Therefore, metasomatic enrichment may lead to a decoupling of the Hf and Nd isotopes, whereby Lu-Hf may have preserved information about timing, preconditions and degrees of depletion, while Sm-Nd may provide information about timing and character of enrichment event/s. Mineral separates from Finsch peridotites were therefore analysed for their Sm, Nd, Lu and Hf isotopes. The intention was to obtain depletion ages (using the Lu-Hf isotopic system), as well as to determine the characteristics of enrichment agent/s (resulting in decoupled Lu-Hf and Sm-Nd isotopic systems) and the timing of the enrichment processes (Sm-Nd) from recalculated bulk rock compositions.

5.2 Mineral isotope compositions

The isotopic composition of Lu, Hf, Sm and Nd was analysed on 15 garnets, 7 clinopyroxenes and 7 orthopyroxenes. In three harzburgites (F-11, F-12 and 695) grt, cpx and opx were analysed as well as rutile in one rutile bearing sample (F-12). In one cpx-bearing dunite (F-8), one harzburgites (hzb) (F-6) and two lherzolites (lhz) (F-15, F-16) only grt and cpx pares were measured. For three cpx-free hzb (F-2, F-7 and 882) and one cpx-bearing hzb (F-9) grt and opx were analysed. Further more, garnets from samples F-14, 554, 556 and 865 were also analysed for their Lu, Hf, Sm and Nd isotope composition.

5.2.1 Lu-Hf isotope compositions of opx, cpx and grt

Both, opx and cpx show large variations in $^{176}Lu/^{177}Hf$ 0.00119-0.01414 and 0.00050-0.01303, respectively (Fig. 5.1). These values are much lower compared to the values for cpx from grt-free peridotites (0.012-0.02 - Pearson and Nowell, 2002). However, the range of $^{176}Hf/^{177}Hf$ for opx is limited (0.281961-0.282694), while cpx shows a significantly larger range (0.281566-0.287316; Fig. 5.1; Table 5.1 in App.-4). All clinopyroxenes except that from F12 (rutile bearing) have a positive εHf. The highest values are observed in cpx from lherzolite F-16 (Table 5.1 in App.-4). Clinopyroxene display a strong correlation of $^{176}Lu/^{177}Hf$ and $^{176}Hf/^{177}Hf$ with no correlation between $^{176}Hf/^{177}Hf$ and 1/Hf (Fig. 5.1), the latter excluding a mixing relation. Thus, the correlation between Lu/Hf and the Hf isotope ratios must have age significance.

All orthopyroxenes are sub-chondritic in εHf and show neither correlation between $^{176}Lu/^{177}Hf$ and $^{176}Hf/^{177}Hf$ nor between $^{176}Hf/^{177}Hf$ and 1/Hf (Fig. 5.1).

Garnets dominate the Lu and Hf budgets in four phase peridotites and therefore are governing the Hf isotopic system in such rocks. Their concentrations vary in the Finsch garnets by more than an

order of magnitude (0.014-0.397 ppm and 0.086-1.88 ppm, respectively) with correspondingly high variation in $^{176}Lu/^{177}Hf$ (0.00820-0.27986, Fig. 5.1; Table 5.1 in App.-4). Like for cpx the $^{176}Hf/^{177}Hf$ ratios strongly correlate with Lu/Hf (but not with 1/Hf), again implying an age significance (Fig. 5.1). The large range in Lu/Hf resulted with time in an extreme range for εHf from -42 to +263. Even higher εHf were reported for garnets from other localities from the Kaapvaal craton (Bedini et al., 2002; Simon et al., 2007; Chapter 3). Very low, negative values were not yet reported for peridotites, but are only known from eclogites (Jacob et al., 2005), lamproites and the continental crust (e.g Nowell et al., 1999; Nowell et al., 2004). The most radiogenic value is from lherzolite (F-16) rather than for the more depleted harzburgites. Only five out of the 15 analysed garnets have unradiogenic $^{176}Hf/^{177}Hf$ with the lowest values in garnets from the rutile-bearing harzburgites (F-12; Fig. 5.1; Table 5.1 in App.-4).

Rutile (rt) from F-12 has a similar unradiogenic Hf isotopic signature as the coexisting grt (Table 5.1 in App.-4).

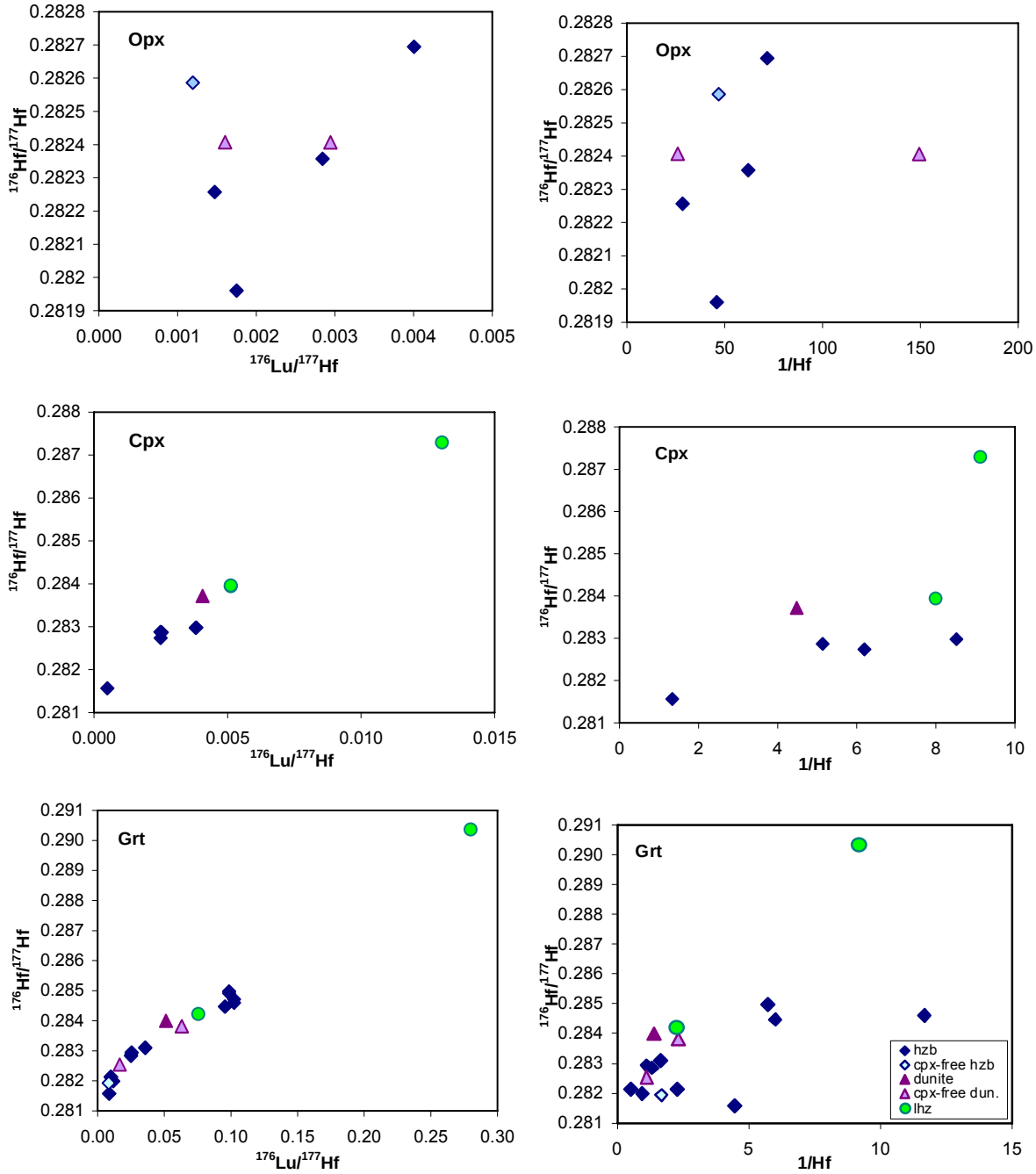

Fig. 5.1. Co-variation of $^{176}Hf/^{177}Hf$ isotope ratios with $^{176}Lu/^{177}Hf$ ratios and 1/Hf (values in ppm) respectively, of the mineral separates (opx, cpx and grt) from selected Finsch peridotites.

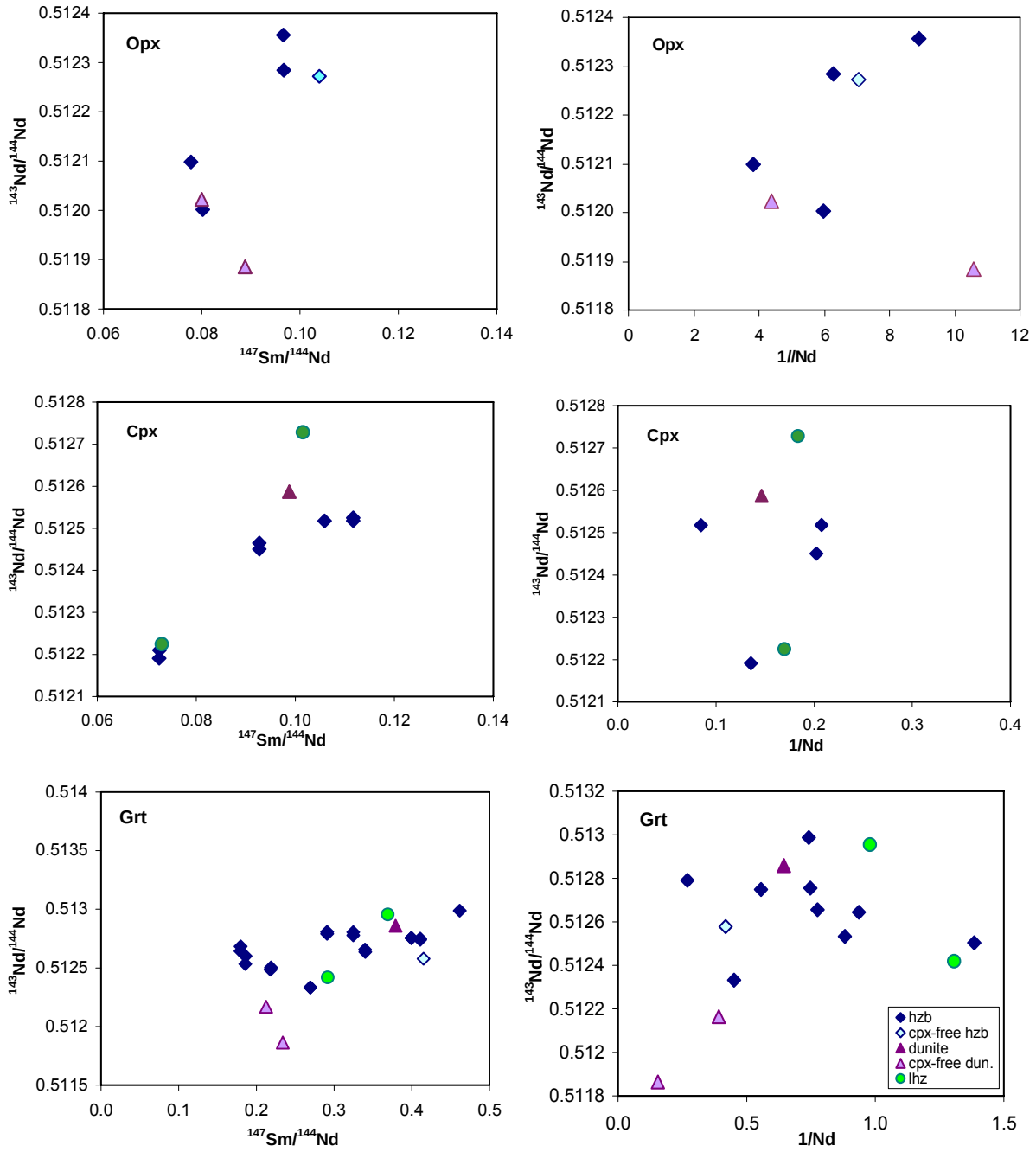

Fig. 5.2. Co-variation of $^{143}Nd/^{144}Nd$ isotope ratios with $^{147}Sm/^{144}Nd$ ratios and 1/Nd (values in ppm) respectively, of the mineral separates (opx, cpx and grt) from selected Finsch peridotites.

5.2.2 Sm-Nd isotope compositions of opx, cpx and grt

All orthopyroxenes (n=7) have sub-chondritic $^{147}Sm/^{144}Nd$ (0.0778-0.1039) and $^{143}Nd/^{144}Nd$ ratios (0.51188-0.512356) (Fig. 5.2; Table 5.1 in App.-4). Accordingly, all have negative εNd from -14.7 to -6.9. Cpx-free harzburgites have the lowest εNd, while cpx-bearing harzburgites have the lowest $^{147}Sm/^{144}Nd$. There is no correlation of the Nd isotope compositions with either Sm/Nd or 1/Nd in opx. Elevated Nd concentrations combined with $^{143}Nd/^{144}Nd$ values close to those of the kimberlites, may imply that the opx mineral separates were contaminated by kimberlitic melt. This possibility will be discussed in more detail below.

Clinopyroxenes have higher concentrations of both Sm and Nd than opx and grt. However, their range in $^{147}Sm/^{144}Nd$ is small (0.0725-0.1117; Fig. 5.2, Table 5.1 in App.-4) and similar to that of opx. Most of the cpx have higher $^{143}Nd/^{144}Nd$ (0.51219-0.512728) than the majority of opx (measured in this study) or Finsch kimberlite (0.51212-0.5122, Nowell et al., 2004). In contrast to the Hf isotope compositions with mostly superchondritic values, all cpx (except F-15) have subchondritic εNd isotopic signatures ranging from -8.7 to -1.

The $^{147}Sm/^{144}Nd$ ratios in garnets vary widely from sub-chondritic to slightly higher than the depleted mantle (0.1795-0.4629; Fig. 5.2; Table 5.1 in App.-4). They also have the largest spread of εNd from all measured mineral phases, ranging from very unradiogenic (-15.5) to radiogenic (+6.8). All Ca-undersaturated garnets have negative εNd with the lowest value obtained for the spinel-bearing, cpx-free harzburgite 882. Such low Nd isotope values were previously reported from the Jagersfontein (Walker et al., 1989) and Kimberley (Simon et al., 2007).

A crude correlation of $^{143}Nd/^{144}Nd$ and $^{147}Sm/^{144}Nd$, but not of $^{143}Nd/^{144}Nd$ and 1/Nd exists between cpx and grt (Fig. 5.2), indicting that variable $^{147}Sm/^{144}Nd$ ratios and Nd isotope compositions are not produced by mixing.

5.3 "Mineral purity" or kimberlite contamination of minerals from the Finsch peridotites

There are two ways that the host kimberlite potentially influences the isotopic signature of minerals in mantle xenoliths. One is direct contamination by chemical reaction with or precipitation of the kimberlitic melt along grain boundaries and fractures and the second one is diffusive inter-mineral re-equilibration because of the high temperature of the melt.

1) Direct kimberlite reaction with the mantle xenolith minerals can happen in two ways: by chemical reaction of the melt with minerals or by precipitation of minerals from the melt or fluids along grain boundaries or fractures (mechanical surface contamination). Chemical reaction will change the major and/or trace element chemistry of minerals and produce zoning (as seen in cpx from samples F-3 and F-11 - see Chapter 4). A consequence will be a resetting of the Hf and Nd isotopic composition of the grain rims or, at the extreme, the whole mineral. The mechanical surface contamination is produced by the percolation of the kimberlitic melt or its derivative fluids along the xenolith mineral grain boundaries, cleavages and fractures. It may there crystallize without significant reaction with the mineral. Such impurities can be avoided by careful hand picking and acid leaching procedures, but, even with outmost care, some un-noticed impurities may escape the attention. This holds especially for opx where the concentration differences between melt and mineral are extremely high (on the order of $1:10^x$) and therefore tiniest amounts of melt may highly affect the opx trace element budget for mass balance reasons.

2) A potentially high temperature of the kimberlite melt may exceed the ambient temperature of the mantle, where the xenoliths originated from. This volatile rich melt may also stimulate element and isotope diffusion processes between xenolith minerals. The temperature may increase significantly above the closure temperature for the Hf and Nd isotope systems with the consequence of at least a partial resetting of the isotope ratios in the minerals. This effect may be stronger for Nd than for Hf as Hf possibly has a slightly higher closure temperature than Nd in garnet (Scherer et al., 2000; Bedini et al., 2004). Therefore, Lu-Hf system seams to be more robust than the Sm-Nd (Ionov and Weiss, 2002; Schmidberger et al., 2002; Pearson and Nowell, 2004; Wittig et al., 2007).

A decisive possibility to check for mechanical contamination by the kimberlitic melt is to compare the isotope dilution (ID) concentrations of mineral separates with concentrations obtained by LA-ICP-MS on carefully selected, clean spots on the same minerals. The results of this procedure are shown in Fig. 5.3 and presented in Table 4.3 in App.-3 for LA-ICP-MS ("in situ" measurements) and in Table 5.1 in App.-4 for MC-ICP-MS (ID –"isotope dilution" analyses). For the majority of the garnets both analytical procedures yield identical results for Nd and Hf within analytical uncertainties.

Only one garnet (F-9) has a higher ID content for Nd and Hf compared to its "in situ" measured value (sample marked with dashed lines in Fig. 5.3). Several (n=7) spot analyses were performed on garnets from this sample (F-9) and all REE and Hf measurements differ by less than 10% from each other. Two batches of garnets from this sample (F-9) were measured by MC-ICP-MS. Only small enrichment of Nd was observed in the first batch, while for Hf the ID measurement of the first batch gives a higher and that of the second batch a lower concentration than in situ measurements. Therefore

it is possible that the first batch of garnets, although no impurities were observed during the hand picking, was contaminated by small amounts of kimberlitic melt.

All measured ID and "in situ" values for clinopyroxene are identical within analytical precision and accordingly plot close to the 1:1 line (Fig. 5.3).

Most problematic are the opx measurements. Both Nd and Hf are extremely low in opx which results in more than 30% error for LA-ICP-MS measurements (see Chapter 4 and Table 4.3 in App.-4). Despite these large uncertainties, the in situ values are significantly lower than the ID values. The most likely explanation is that all opx have suffered from kimberlite contamination, which persisted strong acid leaching (even with concentrated HF acid) and went undiscovered during mineral separation. Therefore, all opx have higher ID Nd and Hf concentrations than the in situ" measurements.

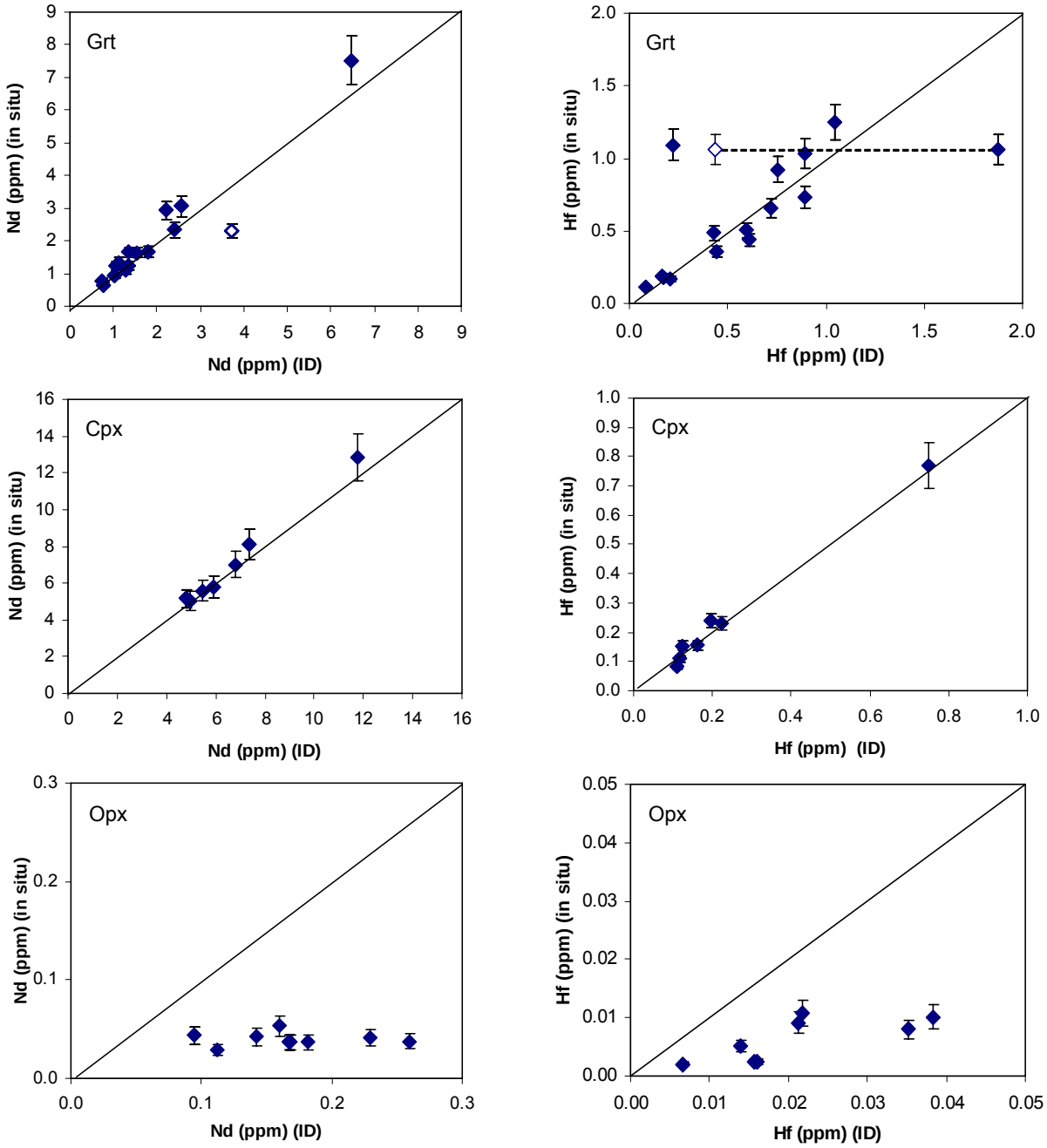

Fig. 5.3. Comparison of Nd and Hf concentrations obtained by "in situ" LA-ICP-MS (Table 4.3 in App.-3) and by isotope dilution (ID) MC-ICP-MS measurements (Table 5.1 in App.-4) of minerals (opx, cpx and grt) from selected Finsch peridotites. Error bars for the LA-ICP-MS are: 10% for Nd and Hf in grt and Nd in cpx, 30% for Hf in cpx and Nd in opx and 50% for Hf in opx. Error bars for the ID measurements are smaller than the size of the symbols. ID measurements of two different garnet separates from the same sample (F-9) are connected with dashed lines.

A clear conclusion can be drawn from these results, i.e. that Nd and Hf in garnets and clinopyroxenes are not affected by the kimberlite melt and can be used for whole rock estimates and age constraints on the xenoliths, while orthopyroxenes are affected and do not represent the original equilibrium composition.

5.4. Discussion

5.4.1 Mineral isochron ages

As described in the previous section mechanical contamination by the kimberlite, during the separation process of opx could not be avoided (Fig. 5.3). Consequently, calculated 2-point garnet-opx tie line ages yield mostly unrealistically high and variable ages, and the Lu-Hf system also gives negative ages (Table 5.1). Only one sample (F-7) gives the eruption age for the Sm-Nd system within analytical errors (which is probably coincidence). Since it was not possible to obtain cleaner separates in large enough amounts for opx analysis, opx was not considered for age constraints.

The Sm-Nd and Lu-Hf ages obtained from grt-cpx pairs are presented in Table 5.1 and in Figs. 5.4 and 5.5.

Lu-Hf isochron ages for garnet-clinopyroxene pairs

The obtained garnet-clinopyroxene isochron ages for Lu-Hf vary between 60 and 521 Ma with relatively large errors between 25 and 110 Ma (Table 5.1, Fig. 5.4). The rutile bearing sample F-12 and the harzburgite F-11 with 60±110 Ma and 148±62, respectively, overlap within analytical errors with the eruption age of the Finsch kimberlite (118.4±2.2 Ma, Smith et al., 1985). If rutile is included in the age calculation for sample F-12 the three points' isochron gives an age of 63±170 Ma. The large errors result from the very unradiogenic $^{176}Hf/^{177}Hf$ and similar $^{176}Lu/^{177}Hf$ ratios in grt and cpx. Three further grt-cpx pairs give ages of around 200±60 Ma, one more lies at around 300 Ma and the highest age is 520 Ma.

If the xenolith has reached inter-mineral Lu-Hf isotope equilibrium, garnet-cpx tie line ages should provide the kimberlite eruption age. However, this is not observed for the Finsch peridotites. From the comparison of LA-ICP-MS and the ID data (Fig. 5.3), as well as from the repeated mineral dissolution and measurements (see Table 5.1 in App.-4), garnet and cpx appear to be essentially unaffected by kimberlite contamination. A potential reason for differing tie-line ages is that they reflect cooling ages following a geological event that affected all phases. As observed by Schmidberger et al. (2002) for Somerset Island xenoliths such cooling ages should correlate with the equilibration temperature. Since all samples display higher temperatures (1150-1250 °C), where grt and cpx probably behaved as an open system for Lu and Hf isotopes (Scherer et al., 2000), they should be chemically and isotopically re-equilibrated. Accordingly, xenoliths from a similar temperature range should yield the same cooling age, which is not observed here for the Lu-Hf system (Fig. 5.5). Another possibility is that Lu-Hf isotopes of xenoliths were affected at different times or that only one mineral phase suffered re-enrichment, and they therefore do not show correlation with the equilibration temperature. On the other hand Lu and Hf have significantly lower diffusion rate in garnets from dry peridotite than Sm and Nd (Ganguly and Tirone, 1999; Bedini et al., 2004), and that may have produced mineral disequilibrium. This is also supported by the partition coefficient behaviour of Lu and Hf between garnet and cpx in the Finsch peridotites (Chapter 4). Very poor correlation between Lu and Hf for grt-cpx partition coefficients and the Cr contents of garnet was observed, while Sm/Nd ratios of garnets relative to cpx are constant within analytical uncertainties (see also Fig. 4.23 in Chapter 4).

In summary, unequilibrated Lu-Hf between cpx and garnet, combined with a different time and amount of Lu and Hf enrichment in the peridotites (like for the rutile bearing sample) may explain diverse grt-cpx Lu-Hf isochron ages.

***Table 5.1**: Garnet-cpx and grt-opx tie-line ages. Value in brackets for F-12 is for grt-cpx-rt assembly.*

	Sm-Nd age (Ma)		Lu-Hf age (Ma)	
Sample	grt-cpx	grt-opx	grt-cpx	grt-opx
F-2		166±35		1165±29
F-6	116±16		201±63	
F-7		133±26		-5027±24
F-8	153±34		295±35	
F-9		501±44		-782±150
F-11	124±27	201±18	148±62	584±81
F-12	114±17	224±30	60±110 (63±170)	-2992±27
F-15	131±26		180±21	
F-16	128±17		522±43	
695	102±48	217±26	230±63	2420±290
882		-33±53		516±41

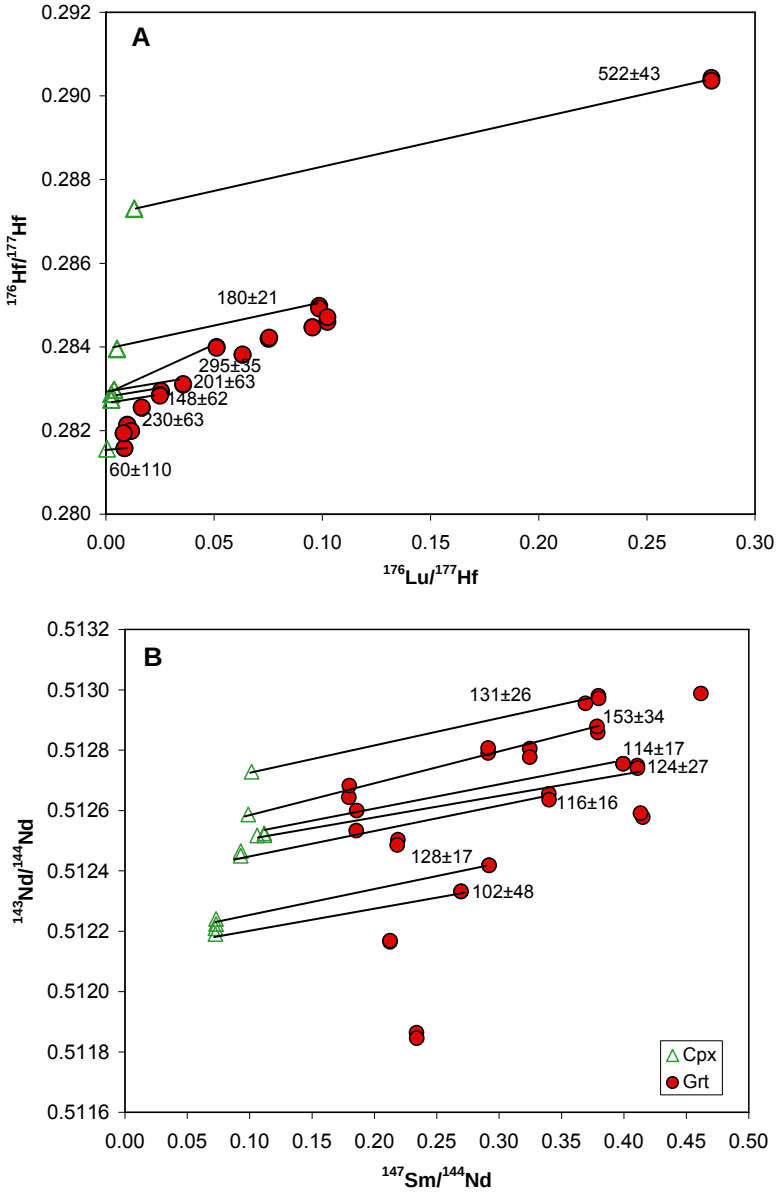

Fig. 5.4. Isochron diagrams for (A): $^{176}Hf/^{177}Hf$ vs. $^{176}Lu/^{177}Hf$ and (B): $^{143}Nd/^{144}Nd$ vs. $^{147}Sm/^{144}Nd$, for the grt-cpx pairs.

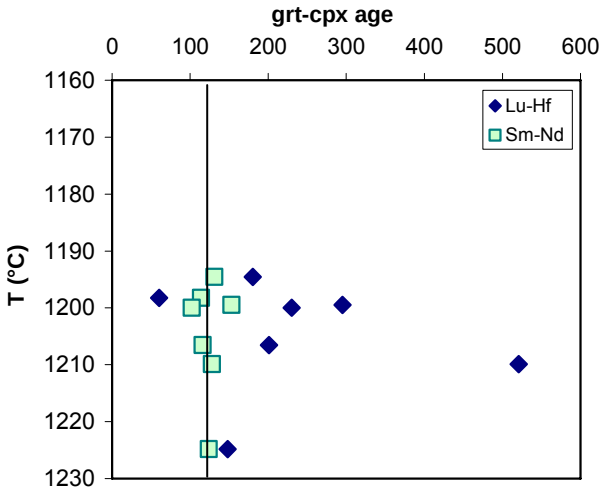

Fig. 5.5. Equilibration temperature and grt-cpx ages. Squares are ages obtained for Sm-Nd system and diamonds for the Lu-Hf system. The vertical line indicates the kimberlite eruption age. The Sm-Nd system yields the eruption age; the Lu-Hf system yields a large age spread at almost identical equilibration temperatures of the xenoliths.

Sm-Nd isochron ages for garnet-clinopyroxene pairs

The garnet-clinopyroxene Sm-Nd ages range between 102 and 153 Ma (Fig. 5.4B; Table 5.1). All ages agree within errors with the eruption age of the Finsch kimberlite (118.4 ± 2.2 Ma, Smith et al., 1985), demonstrating that the Finsch peridotites were in isotopic equilibrium with respect to the Sm-Nd system throughout their geological history until the time of eruption through the kimberlite. Possible explanations for this may include fast diffusion (Ganguly and Tirone, 1999; Bedini et al., 2004) and a stronger influence of metasomatic agents (Ionov and Weiss, 1992; Pearson et al., 1999; Wittig et al., 2007) on Sm-Nd isotope exchange between garnet and cpx, than this is the case for the Lu-Hf system. Therefore, inter-mineral (grt-cpx) equilibrium is reached for Sm-Nd, while the Lu-Hf isotope system still displays disequilibrium (Fig. 5.5).

A well equilibrated Sm-Nd isotope system that yields kimberlite eruption ages is unique compared to previous work from other Southern African localities. The outcome of previous comprehensive studies is dominated by results from xenoliths from the Kimberley pool. Theses samples show a large scatter in Sm-Nd two point isochron ages and do not yield any consistent picture (Richardson, et al., 1985; Pearson et al., 1995; Simon et al., 2007). The difference to the Finsch peridotite suite is that the Kimberley pool kimberlites belong to a younger series of kimberlites at around 90 Ma and that their coarse grained peridotites bear all signs of internal mineral disequilibrium already in their major element compositions (Bell et al., 2003). This disequilibrium may have been inflicted on the subcratonic mantle part by the older kimberlite volcanism at around 120 Ma or was caused by the kimberlite precursor, closely before eruption at 90 Ma.

5.4.2 Whole rock Lu-Hf isotope constraints on the evolution of Finsch SCLM

The whole rock (WR) isotopic composition can be calculated from the modal abundances of garnet, cpx and opx and their respective element concentrations and isotopic ratios. In lherzolites and cpx-bearing harzburgites garnet and cpx are the major carriers of Lu and Hf, while opx contains only minor amounts of these elements, and thus has only a small influence on the whole rock Lu-Hf isotopic signature. As already stated opx was highly affected by the kimberlite melt and it was not possible to prepare contamination free separates (Fig. 5.3). We therefore used only garnet and cpx to calculate the whole rock isotopic compositions. The effect of opx and errors in the calculated modal abundances were accounted for by attributing a correspondingly larger error on the calculated whole rock isotopic composition. Judging from the low contents of Lu and Hf in orthopyroxene obtained by LA-ICP-MS, it may cause a maximal shift of ~ 0.5‰ on $^{176}Hf/^{177}Hf$ and ~ 5% on $^{176}Lu/^{177}Hf$.

The calculated whole rocks show a good correlation between $^{176}Hf/^{177}Hf$ and $^{176}Lu/^{177}Hf$ (Fig. 5.6) corresponding to an isochron age of about 2.5 Ga. Two samples, a lherzolite (F-15) with low $^{176}Hf/^{177}Hf$ and the rutile bearing harzburgite (F-12), with low $^{176}Hf/^{177}Hf$ and $^{176}Lu/^{177}Hf$, plot below this isochron. These samples also show elevated HFSE and the highest Th, Rb and Ba and a positive

Sr anomaly as indicator of strong enrichment (see discussion 4.4.6 in Chapter 4). It was also noticed by the work on subcalcic garnets from Finsch (see Chapter 3) that the SCLM has been metasomatized at least twice after final depletion (at ~ 1.3 and at ~ 0.4 Ga) and that one of these agents brought also Hf with it. Since these samples show slightly enriched Hf compositions, their Lu-Hf isotopic system was probably also recently disturbed. The five remaining samples, form an isochron of 2.55±60 Ga with the MSWD = 7.3 (Fig. 5.6). For the isochron calculation, the pure analytical errors were applied (0.02% on $^{176}Hf/^{177}Hf$ and 0.2% on $^{176}Lu/^{177}Hf$ ratio). The calculated whole rock age is in good agreement with Re-Os ages obtained on sulphides from other Finsch peridotites (T_{RD}= 2.4 Ga, Irvine et al., 2001) and other Kaapvaal craton localities (2.4-2.8 Ga - Walker et al., 1989; Carlson et al., 1999; Menzies et al., 1999) and the 2.52 Ga obtained from Finsch subcalcic garnets (Lazarov et al., 2007; Chapter 3). Irvine et al. (2001) and Lazarov et al. (2007) (see also Chapter 3), consider this age as the final depletion event of the SCLM connected with the cratonisation and stabilisation of the Kaapvaal craton.

The initial of the calculated WR isochron is 16 epsilon units above CHUR at 2.5 Ga. If we assume that the whole rock isochron age represent the only depletion event, this would imply that the initial of this isochron should be equal to $CHUR_{2.5Ga}$ ($^{176}Hf/^{177}Hf$ = 0.28118), and this difference can be barely explained by the effect of opx. This demonstrates that, by 2.5 Ga, Finsch peridotites were already the residuals of a previous depletion event i.e. the present day Finsch peridotites are the products of at least two depletion events. This is identical to what we obtained for the geologic history of the subcalcic garnet host rocks (Chapter 3). It is also in agreement with the major and trace element data of these samples (see Chapter 4) which suggest polybaric depletion for the majority of the studied peridotites.

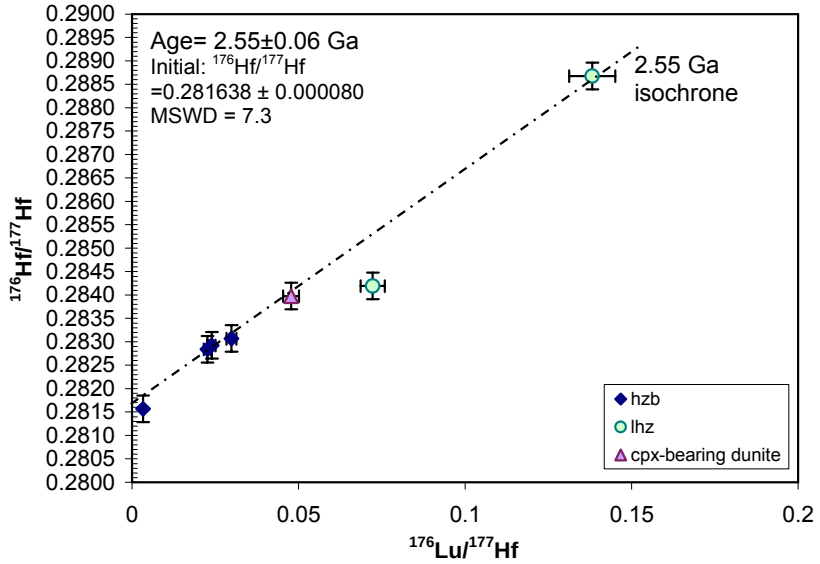

Fig. 5.6. $^{176}Hf/^{177}Hf$ versus $^{176}Lu/^{177}Hf$ for the Finsch peridotite whole rocks calculated by grt-cpx isotopic compositions. Hf isotopic data plot along the 2.5 Ga reference "isochron". Pure analytical errors are with in the size of symbol, and error bars consider the possible effect of opx on whole rock calculations.

Although all five samples plot on the isochron, three of them have sub-chondritic $^{176}Lu/^{177}Hf$ and very low radiogenic $^{176}Hf/^{177}Hf$ isotopic signatures. This strongly implies that these samples have suffered from enrichment prior depletion likely by a melt. Enrichment in Hf leads to both lowering Lu/Hf ratio of the rock and formation of unradiogenic Hf isotopic signature. Since all those samples were still re-equilibrated at ~ 2.5 Ga this metasomatic event should have been either before or synchronously with the last Kaapvaal craton stabilisation event at 2.5 Ga. This is in detail debated below.

5.4.3 Whole rock Sm-Nd isotope constraints on the evolution of Finsch SCLM

Whole rock Sm-Nd isotopic compositions for the Finsch peridotites were calculated by the same procedure and with the same considerations as for the Lu-Hf system. Differently from Lu-Hf, calculated whole rock Sm/Nd isotope ratios do not form an isochron (Fig. 5.7). They plot around a 400

Ma isochron with a very large scatter. This suggests that after the depletion at around 2.5 Ga, the Sm-Nd isotope system experienced multiple overprints. From the work on the subcalcic garnets we know that two such events affected the SCLM underneath Finsch twice, the first time at around 1.3 Ga and the second time at around 400 Ma (see Chapter 3). With the whole rock Sm-Nd data we cannot make such a distinction and can only assume a parallel history of the various lithologies from Finsch from a similar depth range.

A second explanation for the scatter of the Sm-Nd data may be incomplete re-equilibration during metasomatic overprint with different metasomatic agents, with the consequence of a mixed isotopic signature of the old, primary peridotite and new enrichment agent/s. For four of these samples is indicated by the subchondritic Lu/Hf ratios that they were once metasomatized at or before ~ 2.5 Ga. Since they also have Sm-Nd WR disequilibrium with an isotope composition close to the 400 Ma isochron it could be concluded that these samples were enriched twice. Although the latter metasomatism overwhelmed the Nd isotope signature of all samples, but apparently did not have much influence on the more robust Hf isotopic system.

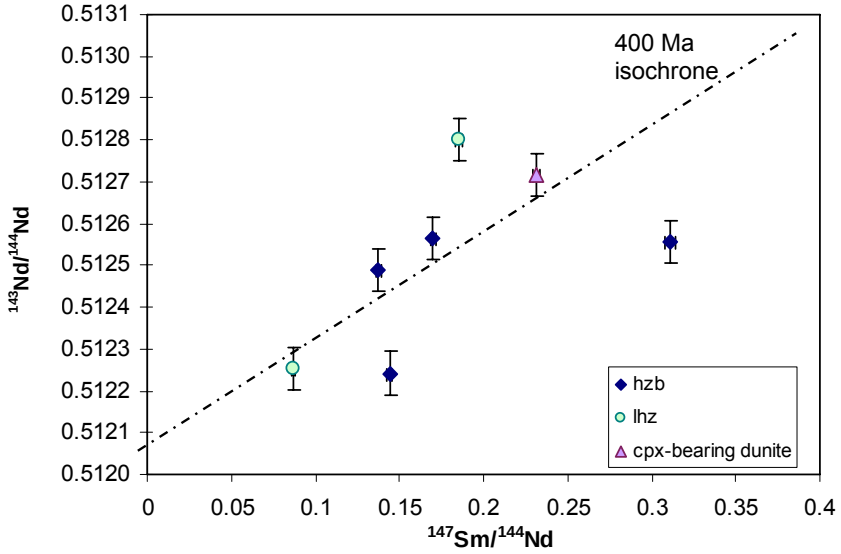

Fig. 5.7. $^{143}Nd/^{144}Nd$ versus $^{147}Sm/^{144}Nd$ for the Finsch peridotite whole rocks calculated from the isotope compositions of respective garnets and cpx. Data plot around a 400 Ma "errorchron" with an initial that agrees with $^{143}Nd/^{144}Nd$ of the Finsch kimberlite (0.51212 - Nowell et al., 2004).

5.4.4 Depletion and enrichment processes recorded in Lu-Hf and Sm-Nd isotope systematic of the Finsch peridotites

During the development of the Kaapvaal craton several events could have influenced the enrichment of the mantle peridotites underneath the Finsch area. These are e.g.: 1. the Archaean metasomatism during the major granitoid formation at ~ 3.2 Ga (Richardson et al., 1993); 2. enrichment during the subduction of the Witwatersrand block underneath the Kimberley block marked by potassic magmatism in the Kraaipan belt (2.88 Ga - Schmitz et al., 2004) or ~ 200 Ma later by the Ventersdorp magmatism (e.g. Schmitz and Bowring, 2003). Although there is no direct information on these events close to the Finsch area, they may have formed melts that have metasomatized the Finsch area, but did not reach the surface; 3. during accretion of the Namaqualand west-southwest edge, the Kaapvaal craton was repeatedly reworked at 1.75 Ga and 1.2 Ga (Thomas et al., 1993; Schmitz and Bowring, 2003); 4. during the Karoo magmatisam (at around 200-110 Ma – Konzet et al., 2000), which was active shortly before the group II kimberlite eruption and during the final kimberlite eruption (at ~ 118 Ma - Smith et al., 1985).

The Sm-Nd and Lu-Hf isotope signatures of the mineral separates from the Finsch peridotites and recalculated whole rock compositions will be used to constrain one or more of the possible enrichment events in this suite of peridotites.

Mineral separates and recalculated whole rocks from the Finsch peridotites plot in all four quadrants of the Hf and Nd isotope space (Fig. 5.8). Differences in the development of Hf and Nd isotopes by partial melting at different pressures may contribute to the large variations observed in εHf

and εNd. Depletion at lower pressure, where cpx and opx budget the trace elements in peridotites, will produce only small differences in εHf and εNd. Melting mainly in such environments formed the "mantle array" (Vervoort et al., 1999), indicated by the dashed line in Fig. 5.8. However, only three garnets and two clinopyroxenes from this study plot close to the "mantle array", while all other peridotites and minerals plot far above or underneath this array (Fig. 5.8). Depletion in the presence of garnet fractionates Lu from Hf more strongly than Sm from Nd. Accordingly, the residue of partial melting in the garnet stability field will lead to peridotite compositions that evolve rapidly with time and develop εHf values above the "mantle array" (Nowell et al., 2004). Further more, the concentration of Lu is controlled by the pressure of the melting regime. While the residue will retain Lu during depletion in the presence of garnet (until garnet is almost exhausted), high degrees of depletion in the spinel stability field will efficiently remove Lu from the residue. This implies that high εHf followed by low Lu concentrations in some Finsch garnets may either be produced by extremely high degrees of depletion in the garnet stability field or it is the product of combined strong depletion in the garnet- and the spinel stability field (see also discussion in Chapter 3 and 4).

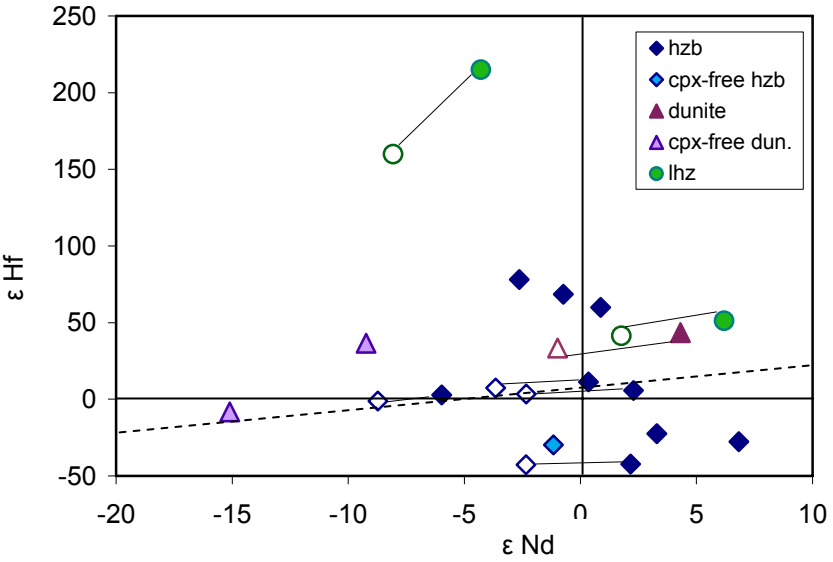

Fig. 5.8. εHf and εNd of cpx and grt from Finsch peridotites. Field symbols are for garnets and open symbols are for cpx. Pares are connected with thin lines. The dashed line represents the mantle array (development of εHf and εNd during the depletion at low pressure) by Vervoort et al. (1999).

Partial melting at both high and low pressures decreases the concentration of Hf and increases the Lu/Hf ratio. Depletion in the spinel stability field has a similar effect, however with a lower slope than in the presence of garnet (Fig. 5.9A). The concentration of Lu may even slightly increase during depletion in the presence of garnet, and decreases only when cpx is exhausted. In contrast, depletion at low pressures removes Lu from the residue. However, depletion of Hf is still stronger, resulting in increasing Lu/Hf ratios (Fig. 5.9B). With the exception of the three lherzolites (which roughly follow the depletion trend line) all Finsch xenoliths have Lu/Hf ratios significantly lower than predicted by any depletion model (indicated by arrow in Fig. 5.9). Consequently, all harzburgites and dunites were re-enriched in Hf at some stage.

Low concentrations of Lu in the whole rocks (mostly 0.03-0.002 ppm - Fig. 5.9A; Table 4.5 in App.-3) coupled with high εHf in some garnets confirm the implications from the major and trace elements (see Chapter 4) that these peridotites were strongly depleted. The very low Lu concentrations imply that most of the investigated samples have suffered 10-20% percent of melting in the spinel stability field (Fig. 5.9), while major and other trace elements imply even more then 30% of melting. This indicates that either between the two depletion events or sub-parallel with the final depletion, all samples were re-enriched in Hf and possibly also slightly in Lu.

Garnets from dunites and cpx–free harzburgites have low or even negative εHf and εNd rather than radiogenic Hf and Nd isotope signatures. Only garnet from one cpx-bearing dunite (F-8) has positive εHf and εNd, but the coexisting cpx has negative εNd. This implies that dunites and highly depleted harzburgites are less resistant to metasomatism than cpx bearing harzburgites and lherzolites. Additionally, as the trace element budget of highly depleted rocks is very low, metasomatic

enrichment has a stronger effect. Since this cpx bearing dunite and other harzburgites show enrichment in Hf, but still, their Lu-Hf whole rocks plot on the last depletion (at ~ 2.5 Ga) isochron, Hf metasomatism must have occurred before or was coupled with final depletion. Samples like the cpx-bearing dunite may also have re-crystallized cpx during this metasomatic event.

Although the three lherzolite samples roughly follow a depletion trend in the spinel stability field (in Fig. 5.9) their composition in the εHf-εNd space is not consistent with low pressure depletion. Both lherzolites (were Hf- and Nd isotope compositions are available) plot significantly above the "mantle array" indicating that these samples suffered either depletion in the garnet stability field, or they inherited radiogenic Hf during metasomatic enrichment.

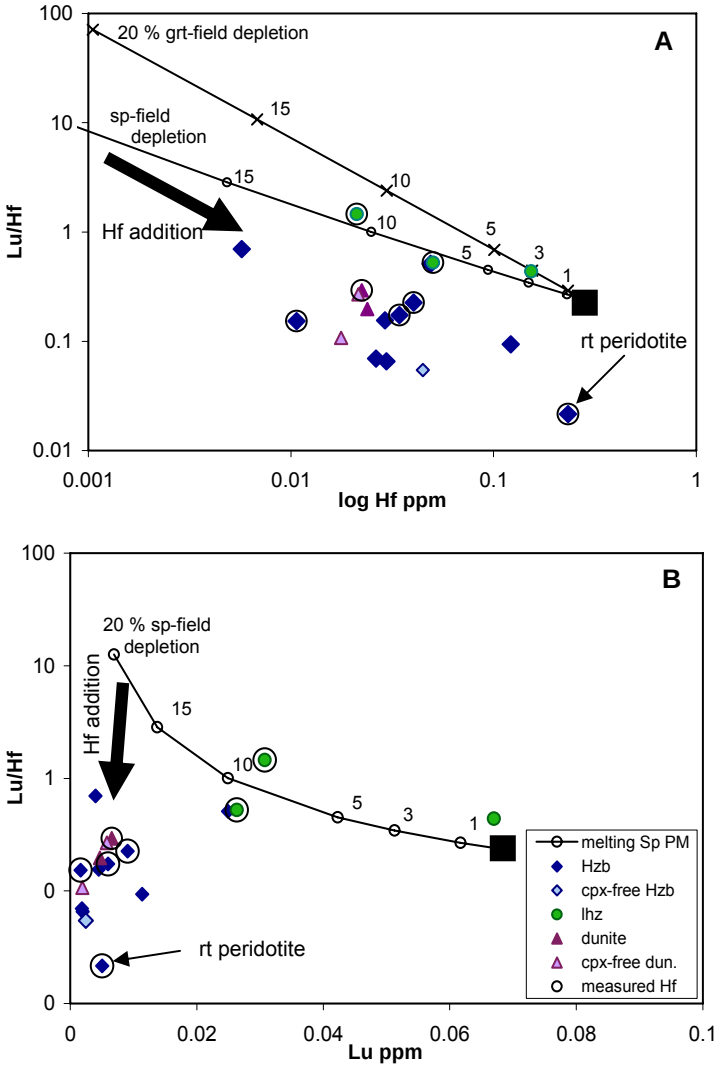

Fig. 5.9. Lu/Hf versus Hf (A) and Lu (B) concentrations in Finsch whole rocks. Modelled non-modal fractional melting curves indicate melting (1-20%) of a primitive mantle (black square) at low pressure (circles) and in the presence of garnet (crosses). The modelling results suggest that 10-20% depletion at low pressures is required to explain the low Lu concentrations of the Finsch peridotites. They also propose that all hzb and dunites were re-enriched with Hf (pointed with the black arrow), or both Lu and Hf, at some stage. The Hf enrichment has a similar slope as the depletion event in the garnet stability field, which suggest enrichment by melt produced at high pressures. Highest Hf enrichment is observed in rutile (rt) bearing peridotite. In the seven encircled samples Hf and Nd isotopes were measured in both cpx and garnet, and from these the Lu-Hf whole rock age was determined in Fig. 5.6.

Both, lherzolite and harzburgite whole rocks as well as garnets from diamond bearing harzburgites that have low or negative εNd, low Sm/Nd ratios, and younger Sm-Nd WR ages, point to the recent enrichment in Nd and Sm. This selective metasomatic enrichment altered Nd but not the Hf isotope compositions as already observed in South African xenoliths (Walker et al., 1989; Bedini et al., 2004) and world wide (Pearson et al., 1999; Ionov and Weiss, 2002; Pearson and Nowell, 2002; Wittig et al.,

2007). This finding strongly implies the existence of at least one metasomatic event after final depletion (at ~ 2.5 Ga ago), which is independent from the kimberlite eruption. Those metasomatic events are recorded by the Nd-isotope composition of subcalcic garnets at around 1.3 and 0.4 Ga (Chapter 3).

Amongst the peridotites from Finsch, three garnets from cpx-bearing harzburgites have positive εNd coupled with negative εHf. The garnet with the most negative εHf belongs to the rutile-bearing harzburgite, and its cpx also shows anomalously negative εHf, coupled with negative εNd. Unradiogenic Hf isotope compositions of cpx may be generated in theory by the infiltration of melts associated with the kimberlite eruption (Simon et al., 2003). However, such low values (as for sample F-12) were not recorded in kimberlites (Nowell et al., 1999; Nowell et al., 2004).

Some rutile bearing eclogites also have low εHf, and therefore melts from them could be the source of a metasomatic agent that has altered e.g. sample F-12. However, melts from eclogites usually create both negative εHf and εNd. This is inconsistent with this sample, which displays only strongly negative εHf. A more likely way to produce this isotope signature is enrichment by a melt from the garnet stability field. Only such melts have highly fractionated εHf and εNd (Fig. 5.10; Nowell et al., 2004) and could therefore be a possible metasomatic agent for this sample. Nowell et al. (1999) proposed that a high negative εHf component was of mantle origin and that it must be ancient in order to deviate significantly from the mantle array (Fig. 5.10). Furthermore, this component must have been isolated from the convecting mantle in order to allow preservation of its distinctive isotope signature (Nowell et al., 1999; Pearson and Nowell, 2002). Possibly, this particular peridotite (F-12) was either formed or strongly modified by such a melt.

Most unusual are garnets with negative εHf and positive εNd. Blitchert-Toft and Albarede (1997) have considered radiogenic Nd coupled with unradiogenic Hf as residue of partial melting in the perovskite stability field. Since all studied samples have suffered enrichment of Hf it is difficult to believe that these samples are primary residues of melting in the presence of perovskite. Additionally, these garnets are also enriched in LREE and other HFSE (Chapter 4). Accordingly, they must have been strongly modified by the later enrichment, anyway. Therefore, the negative εHf signature was likely inherited from the metasomatic agent, similarly to the signature of the rutile bearing sample.

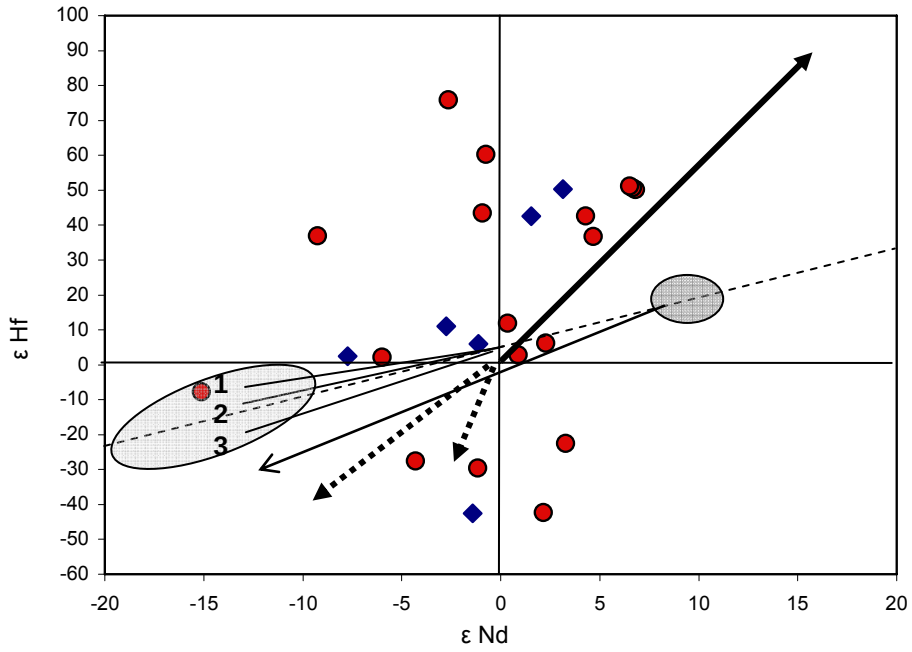

Fig. 5.10. εHf and εNd of whole rocks (diamonds) and garnets (circles) from the Finsch peridotites. The dashed line represents the mantle array (development of εHf and εNd during the depletion at low pressure) by Vervoort et al. (1999). The thick arrow represents a melting residue from partial melting in the garnet stability-field, and the two dotted lines indicate the development of the extracted melt (Nowell et al., 2004). The three thin lines are: 1 = Average carbonate metasomatized spinel peridotite; 2 = MARID-suite peridotite; 3. = Phlogopite K-richterite peridotite (all modelling parameters are taken from Nowell et al., 2004). The dark gray field represents MORB and the arrow pointing to the lower left corner indicates the development of subducted E-MORB (Pearson and Nowell, 2002). The light gray field represents the continental crust (Blichert-Toft and Albarede, 1997).

5.5 Summary and Conclusion

The Lu-Hf and Sm-Nd isotopic composition of Finsch peridotites indicate several depletion and enrichment processes during the evolution of the Kaapvaal craton. According to the Lu-Hf whole rock isotopic data, final depletion coupled with the final cratonisation happened at ~ 2.5 Ga. All samples were depleted at least once before that final cratonisation event. This initial depletion could have happened at lower pressure in an ocean ridge like setting between 3.6 and 3.2 Ga ago. Indicated by the elevated Hf concentrations all samples were metasomatically overprinted between two depletion events. This event may coincide with the re-enrichment during the major granitoid formation at ~ 3.2 Ga proposed by Poujol et al. (2002) and Schmitz et al. (2004). Some samples like for example the cpx-bearing dunite (F-8) could have crystallized cpx during that enrichment. There is a possibility that samples were several times depleted and enriched during that early period of craton evolution. However, this is difficult to resolve, because enrichment and depletion events occurred subsequently and each event at least partially overwhelmed the signatures of the previous one.

After the final depletion (at ~ 2.5 Ga) and before the final kimberlite eruption (at ~ 118 Ma) all samples were additionally metasomatized. This final enrichment event has, for most peridotites, at least partially reset the Sm-Nd isotopic system. However, in most cases it did not have much effect on the Lu-Hf isotope system on a bulk rock scale. This disturbance of the Nd isotope system was most likely produced by a carbonate or Si-rich melt (samples with slightly negative εHf and negative or slightly positive εNd) during the reworking of the Kaapvaal craton at around 400 Ma. Some samples like the rutile-bearing harzburgite (F-12) and other samples with highly unradiogenic Hf were strongly influenced by a melt that was produced by partial melting in the presence of garnet. This enrichment had a strong influence on both the Hf and Nd isotopic signature of the samples. Unradiogenic Hf coupled with a short integration time point out that this metasomatic event also took place shortly before the kimberlite eruption (500-300 Ma).

Older metasomatic events, which were proposed by the Sm-Nd systematics of subcalcic garnets (Chapter 3) and connected with the accretion of the Namaqualand (1.75-1.2 Ga) cannot be excluded. However, these events must have been significantly overprinted by the much younger re-enrichment at around 400 Ma.

CHAPTER 6

Formation of a Polymict Peridotite by Brecciation of Subcontinental Lithospheric Mantle

6.1 Introduction

Mantle xenoliths provide the opportunity to study a range of processes occurring in the Earth mantle at various depths. They are usually the combined products of partial melting and metasomatic enrichment. Lherzolitic, harzburgitic, dunitic, wehrlitic and eclogitic lithologies are parts of the lithospheric mantle erupted to the surface by alkali basalts or kimberlites. Such highly undersaturated and fluid charged melts are not only the transport vehicles for mantle material, they together with carbonatites are also the most likely media responsible for mantle metasomatism because of their low viscosities and wetting angles. Old metasomatic enrichment of the mantle lithology is difficult to constraint if no new formed minerals for example: rutile, ilmenite, phlogopite, etc. were formed (Erlank et al., 1987; Ionov et al., 1993; Ionov et al., 1999; Gregoire et al., 2002) and mantle xenoliths only show variable elevated contents of incompatible elements (Menzies and Hawkesworth, 1987; Griffin et al., 1989a; Rudnick et al., 1993; Simon et al., 2003).

A very rare type of mantle xenoliths, named polymict or brecciated peridotite, provide the rare opportunity to study peridotite-melt reactions. Several of such mantle rocks were found at the De Beers mines in Kimberley, South Africa, and were firstly described by Lawless et al. (1979). These polymict peridotites are mechanical mixtures of upper mantle clasts and minerals cemented by fine-grained olivine and minute amounts of interstitial picro-ilmenite, phlogopite, rutile and sulphide. Further work on these same samples (Zhang et al., 2000, 2001, 2003), lead to the interpretation that polymict peridotites probably represent tectonic rock units that were intermingled in mantle shear fault zones.

Here we present a detailed study of a further polymict peridotite which, through its singular constituency, enables us to put further constraints on explosive processes deep in the mantle. It also gives constraints on the gas charged transport and turbulent mixing of solid mantle material and its halt and solidification as a rock by freezing out the mafic silicate portion of a highly gas charged kimberlitic melt.

6.2 Petrography of the peridotite breccia

6.2.1 Description of hand specimen

Specimen Bosh03-79 was collected from the Boshof Road dump, Kimberley, South Africa. It is a kimberlite derived xenolith and measures approximately 37 x 20 x 16 cm (Fig. 6.1a). The surface shows a brownish alteration colour of olivine interrupted by an irregular dark longitudinal band with black ilmenite (ilm) and green "Granny Smith"-clinopyroxene (cpx). The latter are also set in a patchy groundmass of reddish brown garnet (grt) and light green orthopyroxene (opx). Both ilmenite and Granny Smith clinopyroxene were previously described by Boyd and Nixon (1978) and Boyd et al. (1984) as discrete megacrysts in Kaapvaal craton xenoliths. A cut perpendicular to this band (Fig. 6.1b) shows that this ilm-rich vein-like part (marked with "A" in Fig. 6.1b) makes about one third of this xenolith. Beside it the reddish brown patches consist of small garnet- and the light green of fine-grained orthopyroxene grains occur. Granny Smith clinopyroxene appears in a state of dissolution and is always surrounded by orthopyroxene.

The other two thirds of the xenolith (labelled B and C in Fig. 6.1b) is breccia that consist of olivine (ol), garnet, orthopyroxene and rare clinopyroxene porphyroclasts with differing dimensions, shapes and colours set in a fine grained, slightly serpentinized olivine matrix with rare sulphide patches. The difference in colour is most obvious in the constituent garnets, which vary from orange to violet (Fig. 6.1c). Only difference between parts B and C (Fig. 6.1b) is grain size of the porphyroclasts. These range from 5 to 12 mm in part B and mostly around 3 mm (rarely up to 6 mm) in part C. The porphyroclasts have thin overgrowth rims of their own kind i.e. garnet on garnet, orthopyroxene on orthopyroxene. Only the rare clinopyroxene have orthopyroxene overgrowth. The random assembly of individually

different mantle minerals amalgamated by olivine has previously been described as a polymict peridotite breccia (Lawless et al., 1979; Zhang et al., 2000).

A deformation zone consists almost exclusively of matrix olivine that separates the vein–like parts A from the olivine-rich parts B and C (Fig. 6.1b). Orthopyroxene from part A on that contact zone to part B and C is recrystallized into orthopyroxene neoblasts.

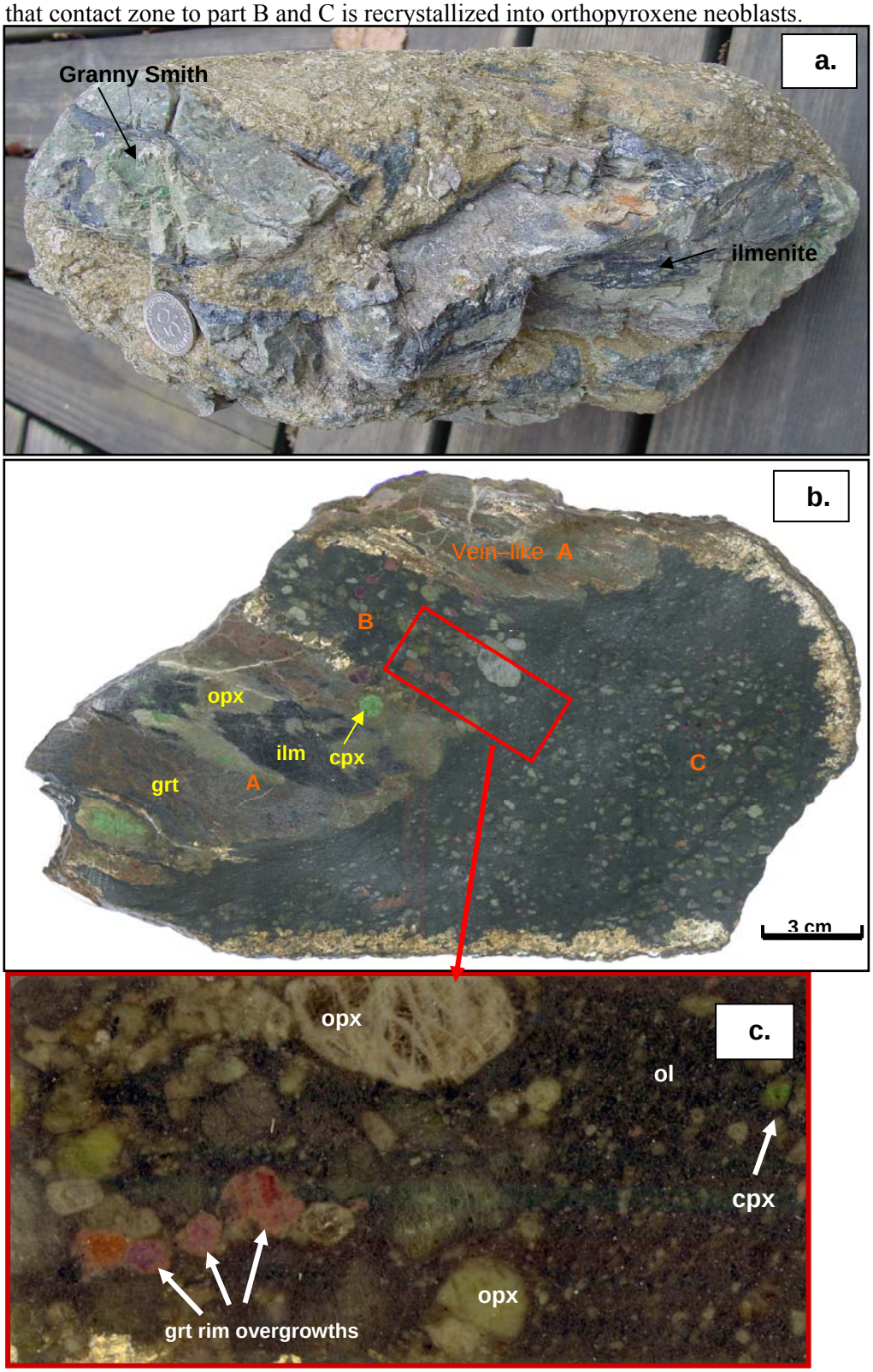

Fig. 6.1 a-c. Polymict peridotite from Kimberley (Bosch03-79). (a). Surface view of the polymict peridotite; (b). crosscut of the polymict peridotite where the vein-like part with ilmenite (ilm) is labelled with A, orthopyroxene (opx), clinopyroxene (cpx) and garnet (grt), and breccia marked with B and C (see Text for details); (c). enlargement of part B, where opx, cpx and differently coloured grt porpyroclasts with reaction rims are amalgamated with fine grain olivine (ol).

6.2.2 Description of thin sections

Description of part A

In the vein-like part A, ilmenite occurs in irregular "layers", displaying polygranular mosaic textures with 120° triple junction grain boundaries. Similar features were already described in Kimberly polymict peridotites by Lawless et al. (1979) and Wyatt and Lawless et al. (1984) and also in the Sloan II pipe in Colorado (Schulze, 1987). In Bosh03-79, these irregular segregations of dark-black ilmenite sometimes envelope up to 1cm long lenses of Granny Smith clinopyroxene. Larger clinopyroxenes sometimes have replacement rims of polygranular mosaic orthopyroxene. The ilmenite vein is surrounded either by anhedral light green orthopyroxene or by a violet-brown garnet mass. Both garnet and opx patches form mosaics of larger crystals surrounded by the fine grain ground mass (Fig. 6.2a). Small (<30 µm) subhedral to anhedral cpx, prismatic to anhedral ilmenite and rutile (<50 µm) are included in mosaic orthopyroxene (Fig. 6.2b). Subhedral chromites up to 0.2 µm in length are very rare interstices in the mosaic orthopyroxene. Irregular patches of anhedral violet garnets with brown-yellow fine-grain garnet overgrowths are sometimes mixed with segregations of ilmenite and orthopyroxene.

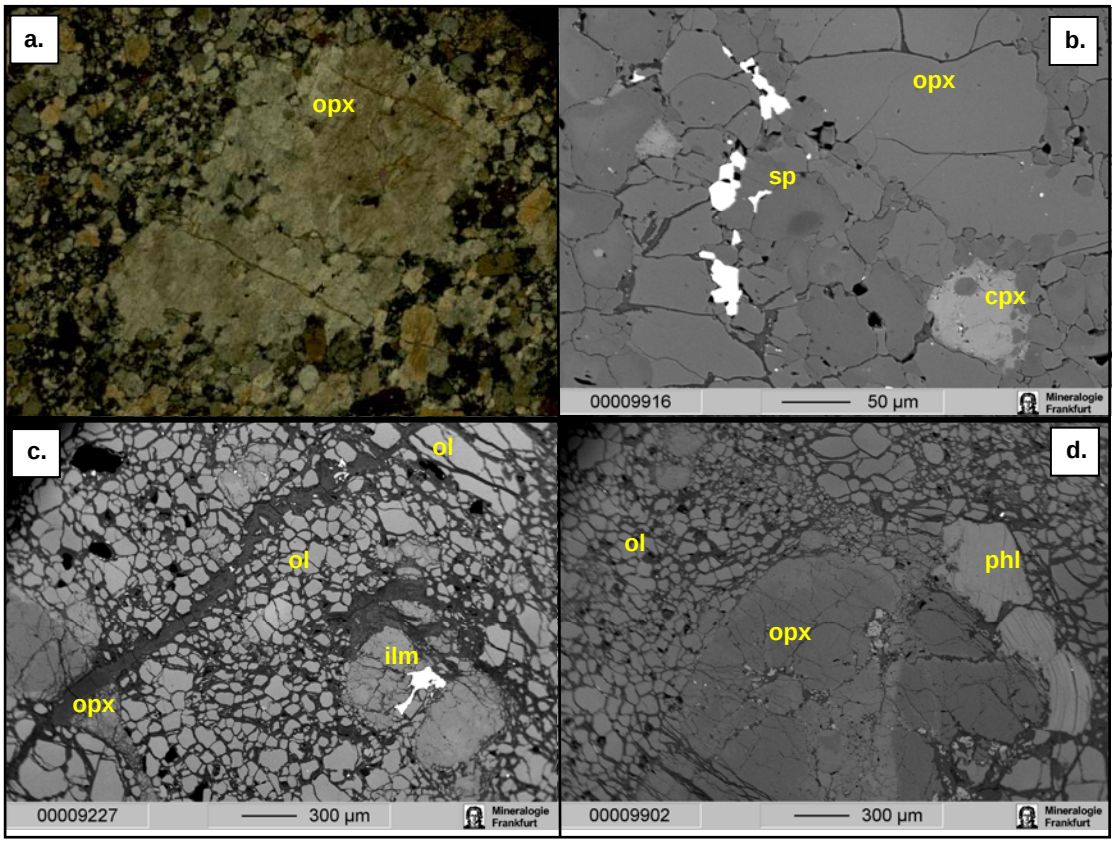

Fig. 6.2 a-d. Micro photographs from the polymict peridotite, including the vein-like part A (a, b), and parts B and C (c, d). (a). Large patchy opx grain in mosaic opx matrix from part A (crosspolars); (b) Back scatter electron (BSE) image of cpx and spinel (sp) in mosaic opx from part A; (c) The opx, ol phenocrysts and ilmenite in fine grain olivine matrix from part C (BSE); (d) The opx phenocryst enveloped with phlogopite (phl) in fine grain olivine matrix from part B (BSE).

Description of parts B and C

With modal 70 to 80%, neoblastic fine-grained **olivine** (0.05 - 0.1 mm) forms the matrix of parts B and C of the polymict peridotite. It increases to almost 100% at the contact of part C and the vein-like part A. There, olivine is oriented parallel to the contact apparently due to

deformation. Small grains of rutile, ilmenite, and sulfide are found as interstices in the olivine matrix (Fig. 6.2c), while rare phlogopite sheets are enveloping porphyroclasts or permeate into grain dislocations (Fig. 6.2d).

Olivine also occurs as anhedral porphyroclasts with undulose extinction and deformation lamellae. Most of these grains are broken into smaller pieces with partial recrystallization into numerous small olivine neoblasts at the rims and in cracks similar as reported by Lawless et al. (1979) and Dawson et al. (2001). Thin serpentine seams are ubiquitous between grain boundaries. Some porphyroclasts show micrometer fine laminations and micrometer scaled exsolutions as parallel, elongated needles (Fig. 6.3). Such laminations and lamellae are observed in impact structure minerals (Ohtani et al., 2006) and interpreted as deformation twining and features due to extremely high stress. Electron microprobe map analysis (Fig. 6.3c) shows that the exsolution wedges have increased concentrations of Cr, Ca and Ti compared to the surrounding olivine, whereby Ca and Cr seem mutually exclusive.

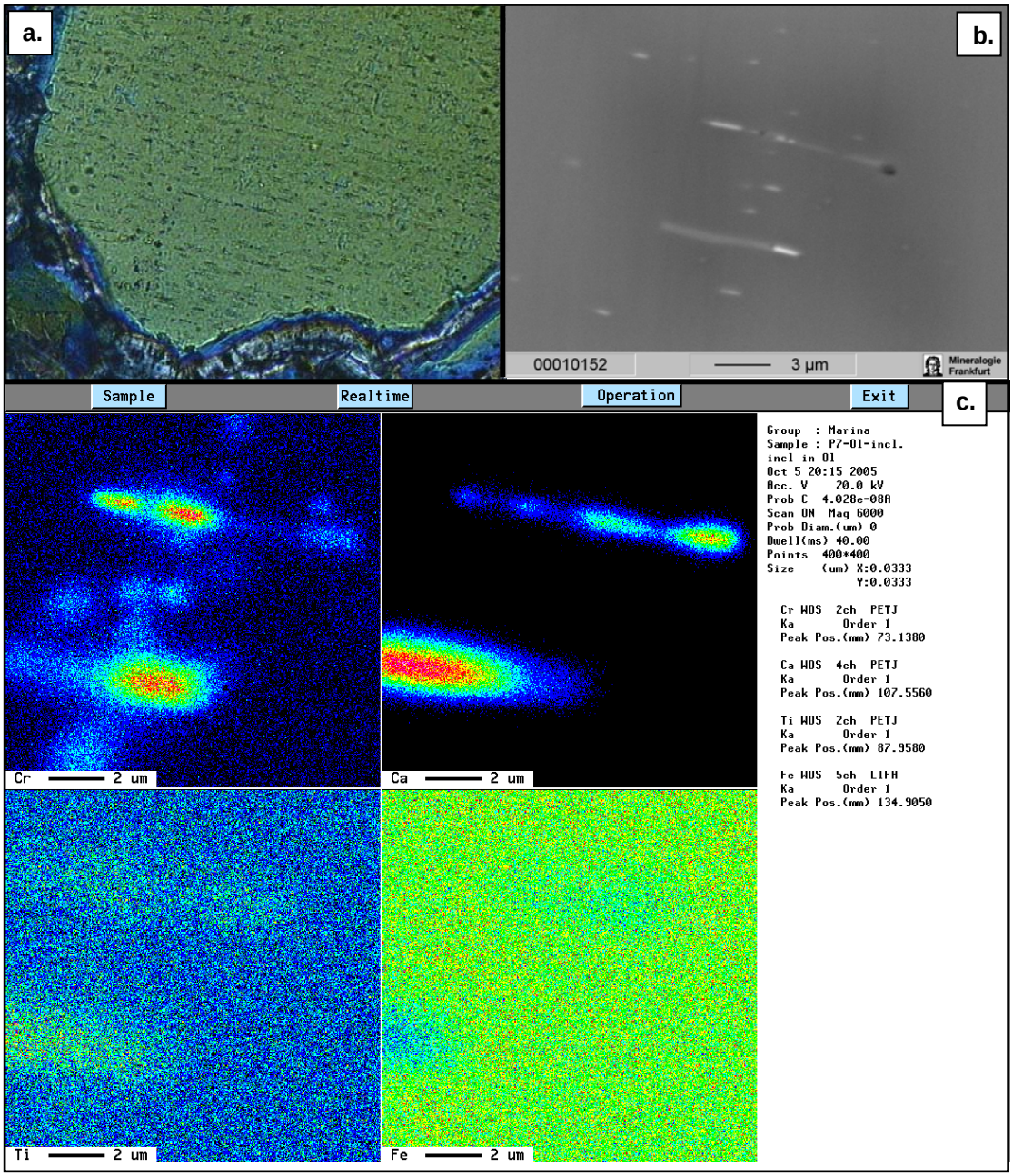

Fig. 6.3 a-c. Exsolution lamely in porphyroclastic olivine from part C of the polymict peridotite. (a) Crosspolarised micro photograph of olivine with the parallel oriented exsolution lamely. (b) BSE image of 1-5µm long exsolution lamely; (c) Map image of exsolution lamely in olivine. Exsolutions are enriched in Ca, Cr and Ti and have lower Fe contents than the host olivine.

Around 60% of the porphyroclasts are differently sized and shaped **orthopyroxenes**. They are usually single grains with newly grown orthopyroxene rims surrounded by the olivine matrix (Figs. 6.2, 6.4 and 6.5).

The size of the orthopyroxene porphyroclasts varies from 0.1 mm to 1 cm, but is mostly between 0.5 and 5 mm. They commonly have irregular grain boundaries and are usually elongated. Some are oval shaped or rounded and sometimes euhedral outlines exist (see esp. Figs. 6.2d, 6.4b, 6.5). They often show undulose extinction due to deformation and some very large orthopyroxenes show kink bending (Figs. 6.2d, 6.4a). The overgrowth orthopyroxenes are generally polycrystalline (Fig. 6.4a-c) but occasionally, broad, monocrystalline, chemically homogeneous rims exist around middle sized (0.5-5 mm) porphyroclasts (Fig. 6.5, left grain). None or only very thin rims are found around a number of middle to large sized (3-10 mm) orthopyroxenes (Figs. 6.4d and 6.5 middle grain). Polycrystalline orthopyroxene neoblasts also occur as reaction rims around very rare clinopyroxene porphyroclasts.

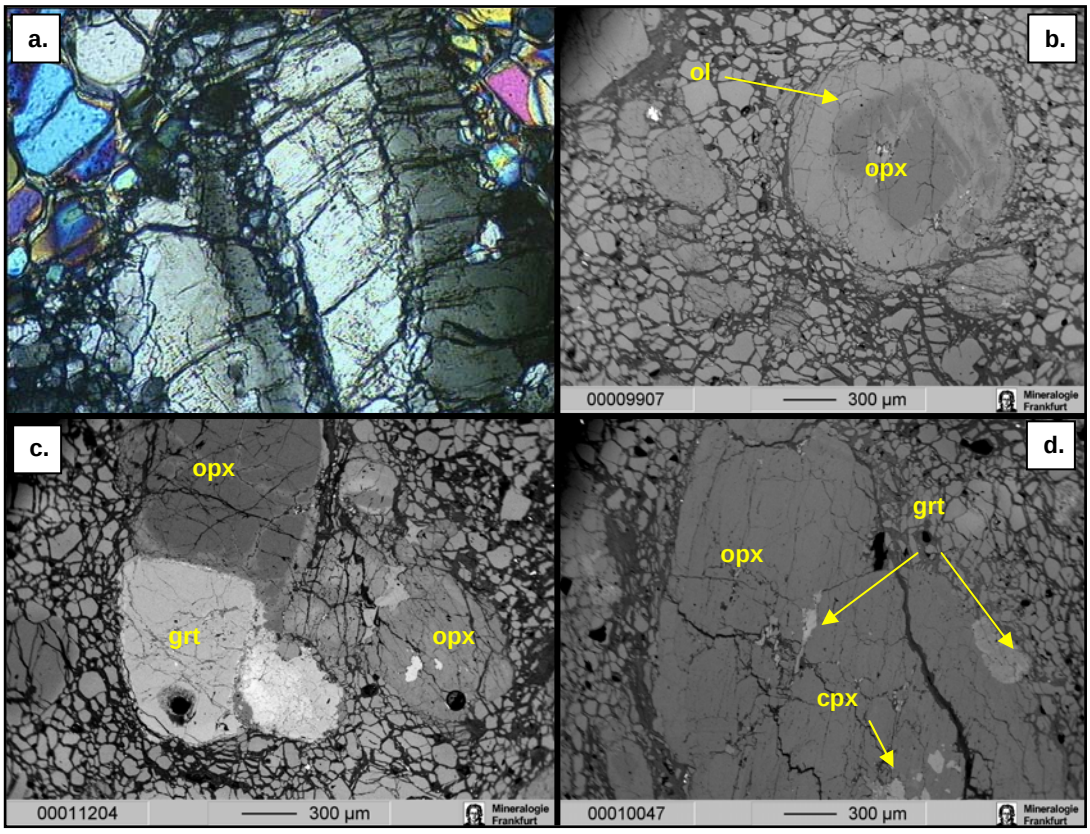

Fig. 6.4 a-d. Variable opx occurrences in parts B and C of the polymict peridotite: (a) cross polarised microphotograph of kink bended opx with fine grain neoblastic opx on the rims; (b) BSE image of euhedral opx that has developed large neoblastic opx crystals. One olivine grain was also enveloped by neoblastic opx; (c) Direct contact of opx and garnet grain marked with neoblastic opx and grt (BSE). (d) Homogeneous, broken opx with grt and cpx on its rim and in discontinuities.

The very rare porphyroclastic **clinopyroxenes** (Cr-diopsides) are always small (<2 mm) with well developed opx overgrowths. Beside them tiny secondary clinopyroxene occurs in dislocations of orthopyroxene porphyroclasts and on garnet rims.

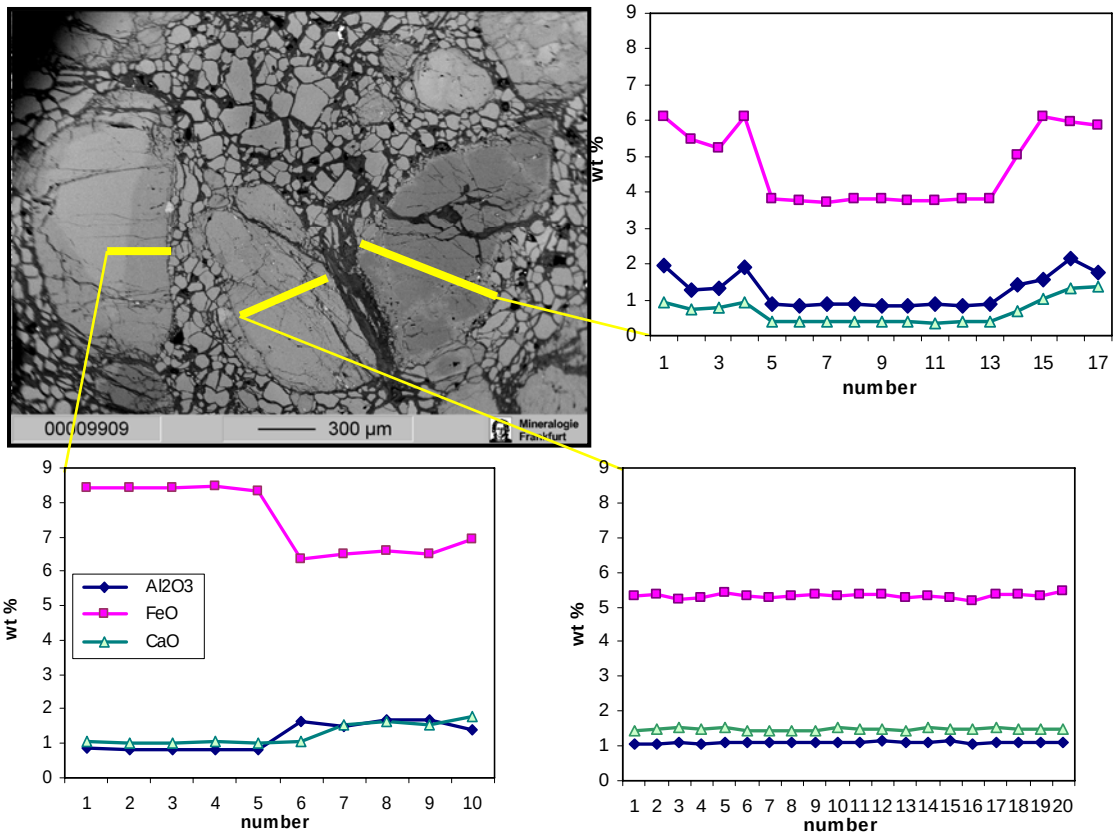

Fig. 6.5. BSE image of three differently changed orthopyroxenes from part C of polymict peridotite. The left grain has developed a reactilon rim, the middle grain did not react at all, and the right grain has developed neoblastic opx grains on its rim. Lines with the numbering of analyses for FeO, Al_2O_3 and CaO (in wt.%) contents are also shown. Note that new reaction rims and neoblastic opx grains reach 6-7 (wt.%) of FeO, up to 2 wt.% of Al_2O_3 and up to 1.5 wt.% of CaO.

The mostly roundish porphyroclastic **garnets** (Fig. 6.6) show a range of colours from eclogitic orange over lherzolitic red or purple and harzburgitic violet to lilac. This spectrum of colors essentially encompasses all types of garnets from kimberlite-borne mantle xenoliths. Most common are light-red colored, probably lherzolitic garnets with 1-5 mm grain size. Violet to lilac, presumably harzburgitic garnets are smaller and on average around 1 mm in diameter. Orange colored, eclogitic garnets with 0.5 to 5 mm in diameter are very rare. Majority of garnets have neoblastic overgrowth rims of polycrystalline garnet, which also extends into the garnet cracks (Fig. 6.6a). Garnets are sometimes zoned and display neoblastic garnet overgrowth (Fig. 6.6b), and very rare are grains with only compositional zoning (Fig. 6.6c). Occasionally, associations of elongated to needle-like clinopyroxene, orthopyroxene, small spinel or ilmenite and phlogopite flakes can be observed in a mixture of chloride and serpentinite around the garnet rims. Rarely, garnet occurs as an inclusion in strongly deformed orthopyroxene porphyroclasts (Fig. 6.4d).

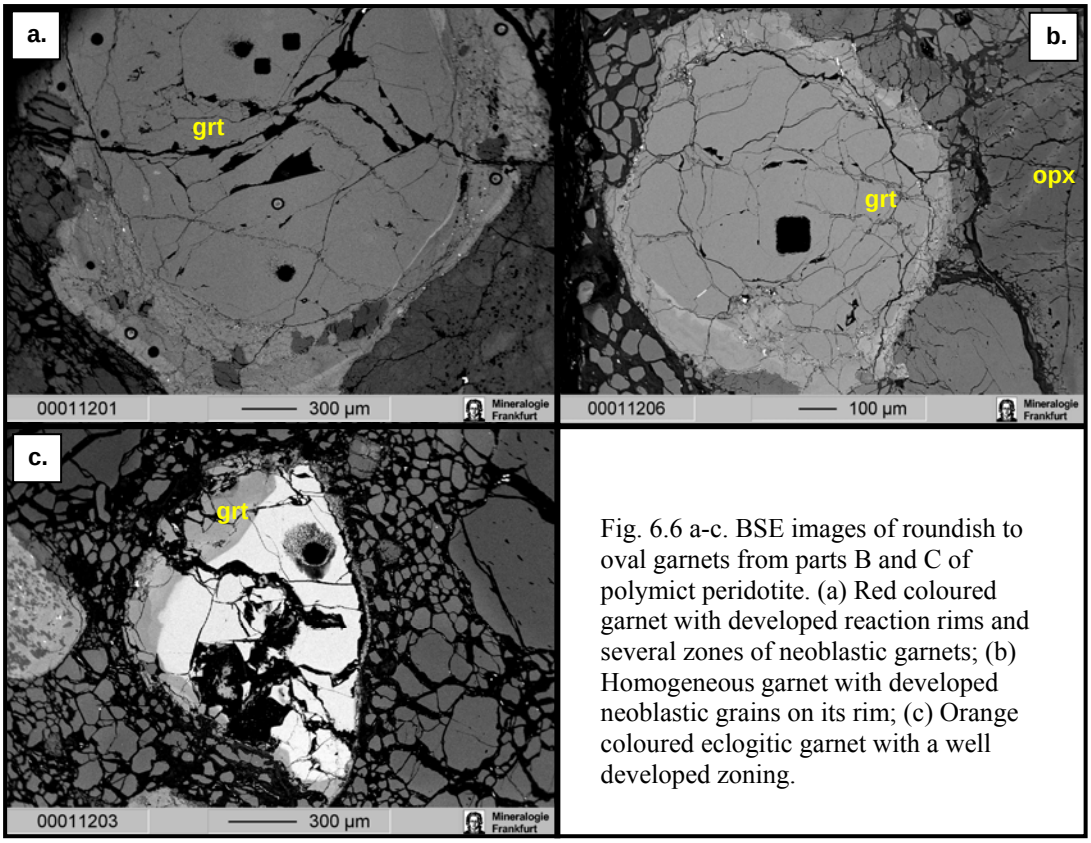

Fig. 6.6 a-c. BSE images of roundish to oval garnets from parts B and C of polymict peridotite. (a) Red coloured garnet with developed reaction rims and several zones of neoblastic garnets; (b) Homogeneous garnet with developed neoblastic grains on its rim; (c) Orange coloured eclogitic garnet with a well developed zoning.

6.3 Chemical composition of porphyroclasts and newly grown rims in parts B and C

6.3.1 Major element chemistry

Olivine

All matrix olivine have similar CaO contents of around 0.037 wt.% (Fig. 6.7), which is lower than for clinopyroxene saturation at the P-T conditions derived for their most likely growth conditions (see below). Their Mg# (Mg# = 100xMg/(Mg+Fe)) range from 88 to 92 with a very pronounced maximum just above 90 (Fig. 6.7).

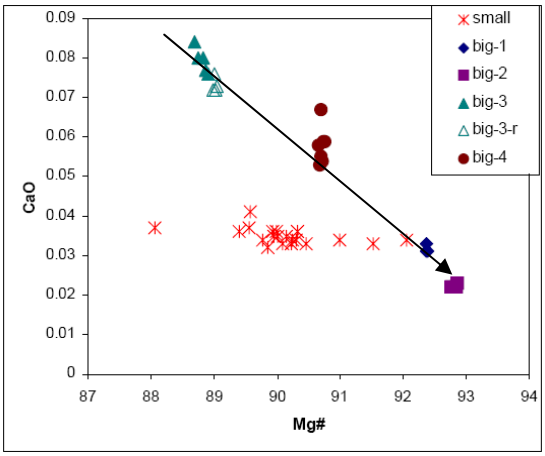

Fig. 6.7. CaO vs. Mg# for Olivine from parts B and C of Polymict peridotite. Small = neoblasts, matrix olivines; Big = porphyroclastic olivines.

The olivine porphyroclasts are quite variable in their major element composition. Each individual grain is homogeneous (except for a small decrease in Mg# and CaO towards the

edges of some clasts). They range in Mg# from 88.5 to 93 corresponding to their origin from primitive to variously depleted mantle peridotites (Table 6.1 in App-5). This is consistent with the negative correlation of Mg# with CaO (Fig. 6.7).

Orthopyroxene

More than 30 analysed orthopyroxene porphyroclasts show a large range in Mg# from 87 to 95 (Fig. 6.8). In this figure (with consecutive numbering of analyses) orthopyroxene rim compositions are encircled and connected by straight lines to their respective porphyroclast, which have very homogeneous compositions, as shown by multiple spot analyses of several grains. Like for the olivine, orthopyroxene Mg-numbers (Mg#) demonstrate that they are derived from fertile to extremely depleted peridotites, whereby those with the lowest Mg# may stem from wehrlites or websterites. In accordance with the variable Mg-numbers the other major elements are also variable with Al_2O_3 from 0.5 to 3 wt.%, CaO from 0.35 to 1.8 wt.%, Cr_2O_3 from 0.03 to 0.5 wt.% and TiO_2 (from below the detection limit up to 0.4 wt.%; Fig. 6.9; Table 6.2 in App-5).

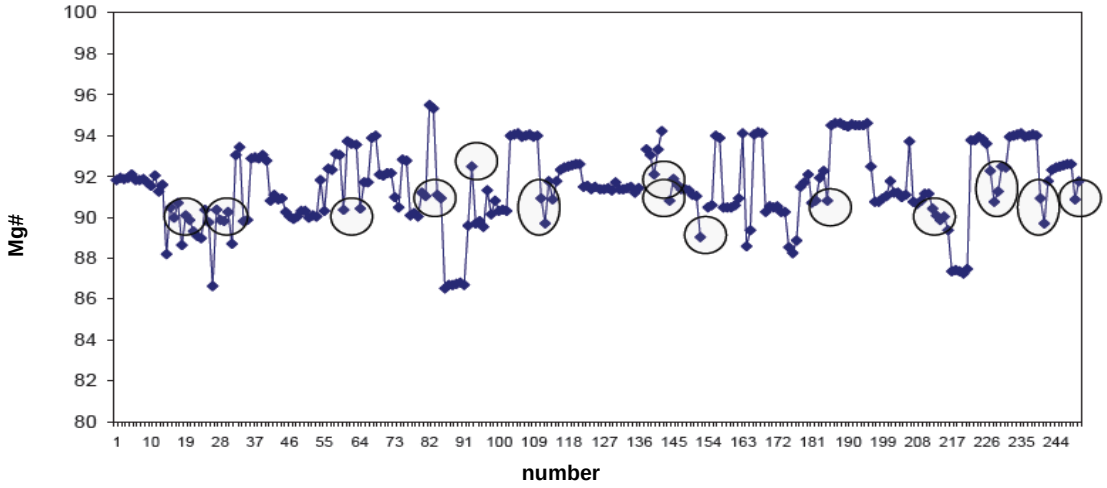

Fig. 6.8. Variation of Mg# in orthopyroxenes from B and C parts of polymict peridotite. Analyses are arranged by consecutive numbering through different opx grains (each grouping is one grain), and circled analyses are for neoblastic opx rims.

Figures 6.8 and 6.9 also show that the neoblastic orthopyroxenes have a much more restricted range of Mg-numbers, which have a maximum somewhat above 90. This is similar like for the neoblastic olivines and demonstrates that the neoblastic phases are in equilibrium. It is also clear from figure 6.8 that there is local chemical equilibrium influenced by the composition of the porphyroclasts and their neoblastic phases. This leads to small local variation in Mg# and Ti, Al and Cr (see also Fig. 6.5). It can also be seen from figure 6.9 that the orthopyroxene neoblasts and reaction rims have a tendency to overlap with the compositions of the megacryst as defined by Mitchell (1986).

Although orthopyroxenes from part A have slightly lower Mg# (89-90), all other elements (Na, Ca, Al, Cr and Ti) have a similar range as neoblastic orthopyroxenes (Fig. 6.9, Table 6.2 in App.-5). They both have lower Na and Ca, and higher Al, Cr and Ti compositions than the porphyroclastic opx or opx from Finsch peridotites. Composition of orthopyroxene from part A completely overlap in Ca and only partly in Al and Cr compositions with kimberlite derived megacrysts (Fig. 6.9).

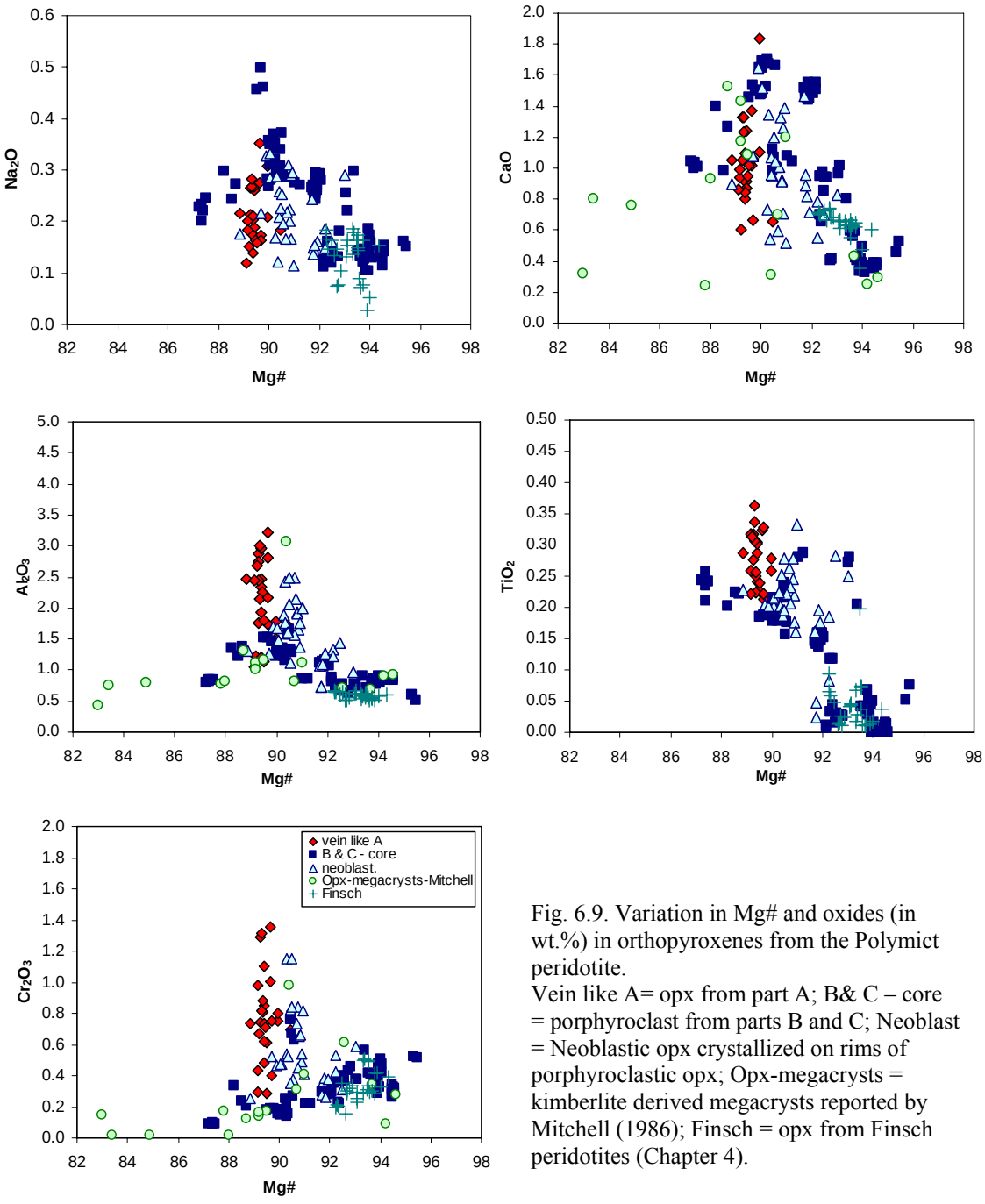

Fig. 6.9. Variation in Mg# and oxides (in wt.%) in orthopyroxenes from the Polymict peridotite.
Vein like A= opx from part A; B& C – core = porphyroclast from parts B and C; Neoblast = Neoblastic opx crystallized on rims of porphyroclastic opx; Opx-megacrysts = kimberlite derived megacrysts reported by Mitchell (1986); Finsch = opx from Finsch peridotites (Chapter 4).

Figure 6.10 is an element map of an orthopyroxene reaction rim in contact with garnet. It shows the garnet, at the top, has a thin secondary reaction and alteration rim with probably chromite as a reaction product and introduction of Na. Garnet appears homogeneous up to its very edge. The polycrystalline overgrowth of opx on opx porphyroclasts appears to be the result of dissolution and precipitation. Orthopyroxene gets dissolved from its rim and from along cracks within the grains with subsequent and immediate overgrowth by the new opx generation. The distribution of Al, Ca, Ti and Fe shows that the new generation is higher in these elements than the porphyroclast and that the new grains still partly contain cores with "old" primary composition.

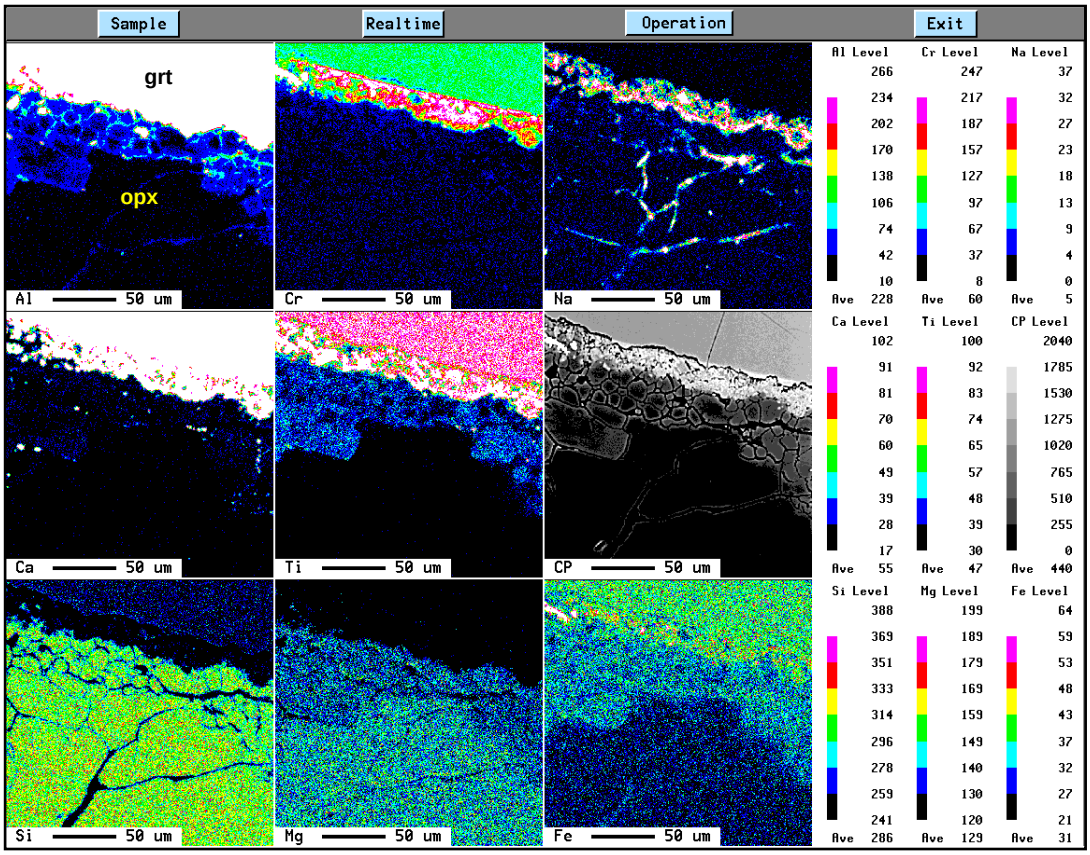

Fig. 6.10. Element map analyses of the contact between garnet (upper grain) and orthopyroxene (lower grain) from part B of the polymict peridotite. The garnet shows a very tin zoning at the very edge of the grain and very small (~ 10 µm) neoblastic grains with higher Cr, Na, and Ti compositions. Opx has larger (10-60 µm) neoblastic opx's on its rim. Neoblasts are enriched in Al, Ti and Fe, and have a lower content of Mg than the porphyroclastic opx

Garnet

The range of Mg-numbers in garnet porphyroclasts is even larger than for olivines and orthopyroxenes and extends from 65 to 90 (Fig. 6.11). Following the description for orthopyroxenes, in Fig. 6.11 garnet rim compositions are encircled in this figure and connected by straight lines to their respective porphyroclasts. The porphyroclasts are analyzed by single or multiple spots across the grain. They are homogeneous in composition and Mg#s indicate garnet derivation from fertile to extremely depleted peridotites and from

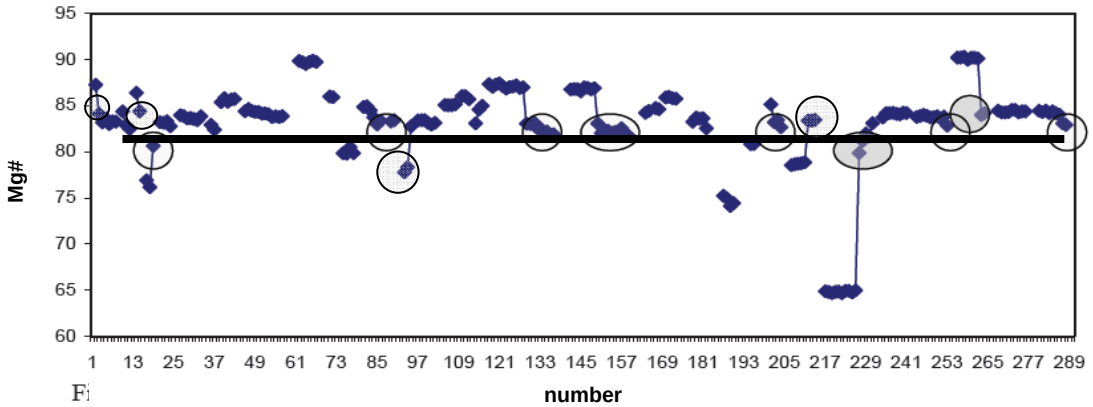

Fig. 6.11. Variation of Mg# in garnets from parts B and C of the polymict peridotite. Analyses are given by consequent numbering, where each grouping represent one garnet grain. Neoblastic garnets are encircled and connected with lines to their porphyroclastic garnets.

eclogites (lowest Mg-numbers). The neoblastic garnets of the overgrowth rims, slightly center on Mg# = 82 (Fig. 6.11).

The whole diversity of the presently analyzed garnet porphyroclasts can be seen in figures 6.11 and 6.12. By their average CaO – Cr_2O_3 contents the majority plots into the lherzolite field (Fig. 6.12a) another larger group into the harzburgite field and one garnet is wehrlitic. The orange-like garnets with lowest Cr contents are eclogitic. A number of the garnets on the lower Cr side have high TiO_2 and some of them may belong to the megacryst suite (Fig. 6.12b; Schulze, 2003). The majority of neoblastic garnets and garnets from part A have subcalcic character (plot in the harzburgitic field in Fig. 6.12a). Neoblastic garnets have quite a range in Cr_2O_3 (< 1 to 5 wt.%) and TiO_2 (0.5 to 1.5 wt.%) but center around 3 and 1 wt.%, respectively. This heterogeneity is probably due to localized, variable chemical composition related to the individual porphyroclast. The high TiO_2 of garnet neoblasts must be a feature of the intruding metasomatizing agent (see below). The relatively low Mg-numbers, the Ca/(Ca+Mg+Fe) ratios and high TiO_2 contents place the neoblastic garnets in the vicinity of the megacryst group as defined by Schulze (2003) (Figs. 6.11 and 6.12).

Like for opx, garnets from part A and neoblastic garnets have similar major element composition (Fig. 6.12; Table 6.3 in App.-5). They are both mostly subcalcic in character, have higher Ti and Na contents than majority of porphyroclastic garnets. By their Cr, Ti and Ca/(Ca+Mg+Fe) ratios all garnets from part A plot into the megacrystic fields as defined by Schultze (2003) (Fig. 6.12).

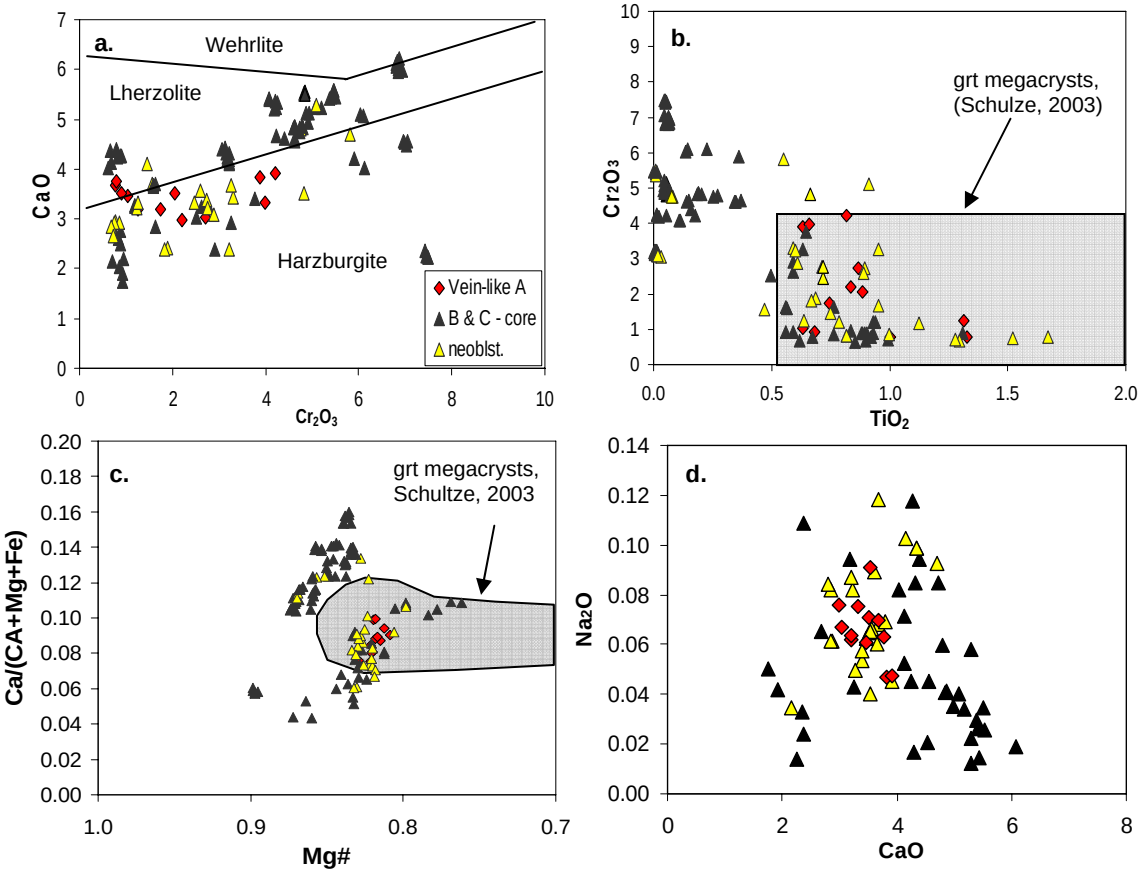

Fig. 6.12. Major element (wt.%) variations of porphyroclastic (B & C-core) and neoblastic garnets (neoblasts.) and garnets from part A (vein-like A). The majority of the neoblastic garnets and garnets from part A have higher Ti and Na and lower Ca, Cr, Mg# and Ca/(Ca+Mg+Fe) ratios than the porphyroclastic garnets. Fields are for kimberlite derived garnet megacrysts (Schultze, 2003).

Clinopyroxene

Only one porphyroclastic clinopyroxene (Cr-diopside) with Mg# at around 91 and Ca# at around 45 was found in the thin sections of the slice cut from the polymict peridotite. This

cpx has relatively high Na_2O (~ 2 wt.%) and low TiO_2 (~ 0.4 wt.%), while a first discontinuous reaction rim of clinopyroxene has higher TiO_2, Cr_2O_3 and Al_2O_3 and lower Mg# then the core (Table 6.4 in App.-5). This in turn is overgrown by an orthopyroxene neoblast rim with compositions similar like neoblastic opx on the rims of porphyroclastic opx.

6.3.2 Trace element chemistry of orthopyroxene and garnet porphyroclasts

Orthopyroxenes

Porphyroclastic orthopyroxenes have fairly simple chondrite normalised REE patterns slightly decreasing from Sm to Lu with a similar slope and concentrations as the orthopyroxene from the primitive peridotite Vitim 313-105 (Ionov et al., 2005a,b). Only Nd, Ce and La of some opx are slightly depleted relative to Sm but always higher than those of the Vitim opx (Fig. 6.13). Porphyroclastic opx have variable Th, U, Nb and LILE that are always higher than those of primitive Vitim opx. Most polymict orthopyroxenes have small negative Sr anomaly, which are, however, not as pronounced as in the primitive mantle opx. The positive Zr-Hf anomaly of the Vitim opx is not observed in opx from the polymict peridotite. The compatible trace elements Ni, Co, Sc and V are always lower than in Vitim opx (see Table 6.5 in App.-5). Finsch opx are enriched in HREE, compared to the orthopyroxenes from Lesotho and Kimberley (Simon et al., 2003, 2007) that show much stronger depletion. The more incompatible elements overlap with the Simon et al. data set beginning with Eu.

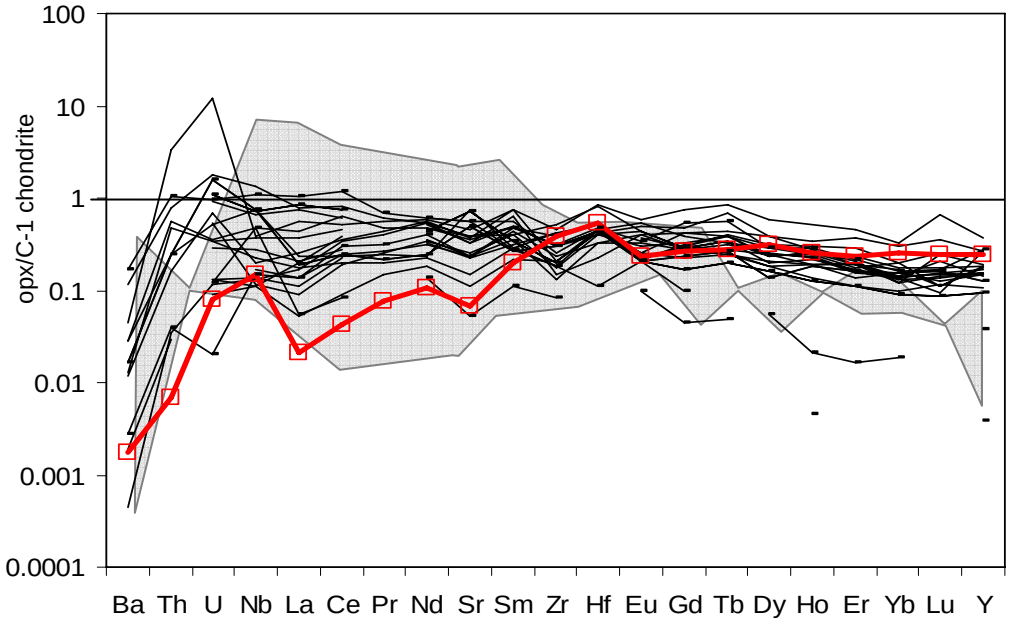

Fig. 6.13. Chondrite (McDonough and Sun, 1995) normalized trace elements from opx from parts B and C of Polymict peridotite. Grey field represent opx from Kimberley and Lesotho (Simon et al., 2003; Simon et al., 2007). Red line with squares mark opx from primitive peridotite Vitim 313-105 (Ionov et al., 2005a,b).

Garnets

Some of the porphyroclastic garnets have REE patterns similar to the garnet from primitive peridotite Vitim 313-105 (Ionov et al., 2005a,b), however, with lower MREE and HREE and somewhat higher LREE (Fig. 6.14). Most garnets, however, have significantly lower HREE (up to 70 times) and sinusoidal chondrite normalised REE patterns. The onset of

the sinusoidal pattern is mostly at Ho and for few at Tm so that almost all more incompatible elements are enriched compared to the Vitim (primitive mantle) garnet. All HFSE, U and Th are higher than those of the primitive Vitim garnet. The Zr and Hf show mostly positive and only in a few cases negative anomalies. Compared to Vitim garnet, the majority of porphyroclastic garnets show similar or lower contents of Rb and Ba, but they all have higher Sr concentrations (Fig. 6.14).

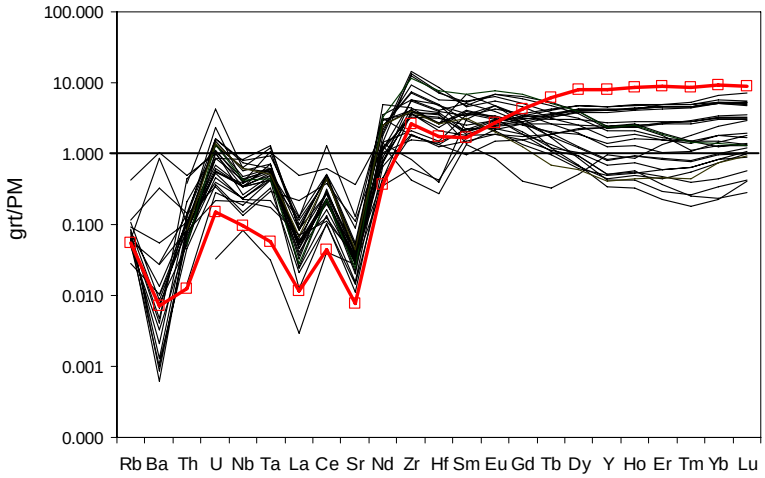

Fig. 6.14. Primitive mantle (PM – Hofmann, 1988) normalized spider-gram for porphyroclastic garnets from B and C. Thicker red line with squares represents grt from the primitive peridotite (Vitim 313-105, Ionov et al., 2005a,b).

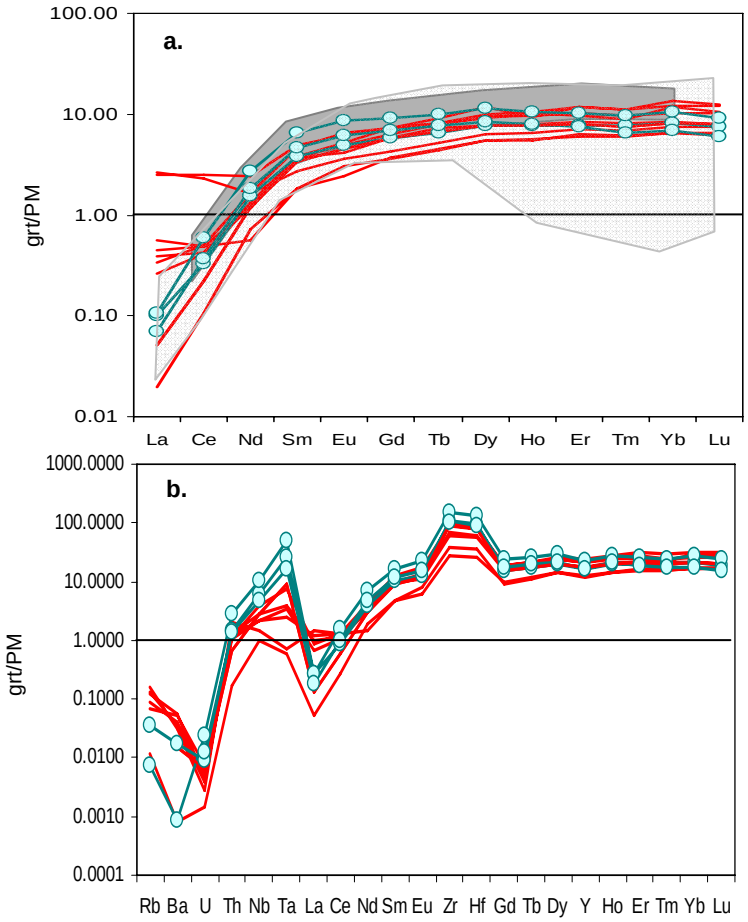

Fig. 6.15. Primitive mantle (PM – Hofmann, 1988) normalized trace element compositions of neoblastic garnets from B and C (red lines) and garnets from part A (green circles): (a) for REE, (light gray field is for porphyroclastic garnets from B and C, and dark grey field is for kimberlite derived megacrystic garnets from Monastery mine - Jones (1987), ; (b) spidergram.

Neoblastic garnets and garnets from part "A" have similarly depleted REE patterns, however, with higher contents than the porphyroclastic garnets from parts B and C (Fig. 6.15a). They overlap with the REE compositions of the kimberlite borne garnet megacrysts from the Monastery mine (Jones, 1987). Both have flat heavy to middle REE patterns, with values around 10x primitive mantle, and the LREE are lower, down to 0.01x primitive mantle. Some elevated La and Ce concentrations of the neoblastic garnets are probably caused by reaction with the pervasive melt that also formed matrix olivine and amalgamated the polymict peridotite. They also show high positive Zr-Hf and Nb-Ta anomalies, while the garnets from part "A" display higher values than the neoblastic garnets (Fig. 6.15b, Table 6.6 in App.-5). Both of them have higher HFSE (up to 100x PM) than the porphyroclastic garnets (up to 10x PM). On the other hand their LILE, U and Th are similar or lower than those of porphyroclastic garnets.

6.4 Thermobarometry

6.4.1 Ni-Thermometry of porphyroclastic garnets

Nickel contents in the peridotitic garnet porphyroclasts ranges from 43 to 150 ppm (Table 6.6 in App.-5). Comparison of the calculated temperatures with the two existing Ni-in-garnet thermometers (Griffin et al., 1989b; Canil, 1999) gives similar results at temperatures between 1000 and 1150 °C (See also Chapter 4). At higher temperatures, the "Griffin-thermometer" gives increasingly higher temperatures compared to Canil (1999). The difference can be more than 300 °C, with up to unrealistically high temperatures of 1600 °C from the "Griffin thermometer".

As observed in Chapter 4 for the Finsch peridotites (T–1050-1250 °C) where the P-T conditions of equilibration were calculated with a number of different thermobarometers (T_{BKN} - Brey and Köhler, 1990; T_{KB} - Köhler and Brey, 1990; T_{ONeil} - O'Neill and Wood 1979; T_{Krogh} - Krogh, 1988; T_{Harley} - Harley, 1984), difference between these thermometers and "Griffin" and "Canil" thermometers exist. The "Canil-thermometer" is decreasingly lower than the T_{BKN}, for temperatures above 1150 °C. On the other hand, the "Griffin-thermometer" sometimes overestimates temperatures, relative to T_{BKN}. Therefore, in this study, the "Canil" thermometer was used, but a correction of ~ 50°C for the high temperature garnets (above 1150 °C) was applied.

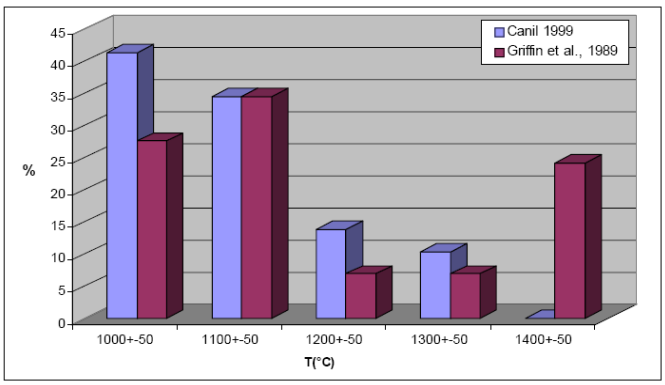

Fig. 6.16. Distribution (in %) of the Ni in garnet temperatures calculated by Canil = blue columns (Canil, 1999) and by Griffin = violet columns (Griffin et al., 1989b)

With the Ni-in-Grt thermometer by Canil (1999), temperatures from around 1050 to more than 1300 °C were estimated (Fig. 6.16, Table 6.7 in App.-5). With the applied correction for the higher values the highest temperature calculations do exceed 1400 °C. Altogether a temperature difference between the porphyroclasts of more than 350 °C is obtained. If we assume that the garnets were equilibrated along a conductive Chapman and Pollack (1977) geotherm of 42 mW/m^2 as observed by Rudnick and Nyblade (1999) and Bell et al. (2003) and if we project derived temperatures onto this geotherm, indicates that the garnets were

sampled from a depth range between ~ 250 and ~ 120 km (Fig. 6.17). This implies that mantle lithologies were disrupted and mingled together by a turbulent process from more than 100 km depth interval within the subcratonic mantle. From the distribution of the (Canil-) temperatures (Fig. 6.16) it appears that increasingly more material was collected from decreasing depths.

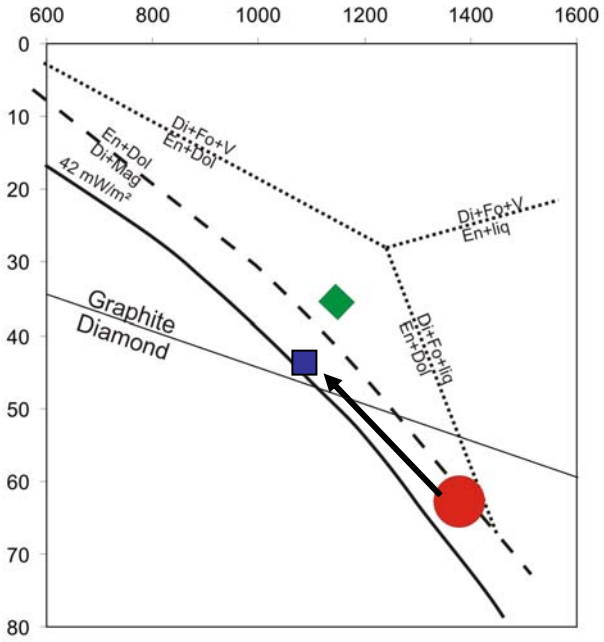

Fig. 6.17. Porphyroclastic garnets were sampled from ~ 1400 °C (red circle in diagram), up to ~ 1100 °C (blue square on diagram) along the 42 mW/m^2 conductive geotherme. Green diamond represents P-T conditions of polymict peridotite amalgamation. Carbonation reactions, calculated – dotted line and experimentally obtained – dashed line, are also presented (Brey et al., 1983).

6.4.2 Thermobarometry of rim overgrowth garnet-opx pairs

The Bosch03-79 sample is a brecciated and olivine-amalgamated xenolith, polymict peridotite, which became part of the solid Earth mantle at some stage in its history. The question is when did this happen and from which depth was it brought to the surface as a xenolith by the kimberlite melt. The latter question may be addressed by applying thermobarometry on suitable mineral assemblages. Solidification and amalgamation must have occurred through partial precipitation of matrix olivine, porphyroclast dissolution and neoblast precipitation by a pervasive ultramafic melt or fluid (see discussion below). The investigation of contacts between orthopyroxene and garnet neoblasts provides the unique possibility to estimate pressures and temperatures of crystallization for such mineral pairs. It is most likely that these assemblages of tens to a few hundreds micrometer grain size have reached local equilibrium or are close to it. We calculated temperatures and pressures of five neoblastic garnet-orthopyroxene pairs with the Fe-Mg exchange thermometer of Harley (1984) and the opx–garnet barometer of Brey and Köhler (1990). They gave averaged temperatures of around 1150 °C and pressures of around 3.5 GPa (Table 6.7 in App.-5).

6.5 Discussion

The disequilibrium porphyroclast assemblage of parts B and C of the polymict peridotite Bosh03-79, most likely contains several mantle lithologies of the subcratonic lithosphere beneath the Kaapvaal craton from a depth interval between 120 and 250 km. The extreme variety of rock types present in such polymict peridotites were already reported by Lawless et

al. (1979) and Zhang et al. (2001, 2003). These authors suggested that a fluid rich melt was responsible for the amalgamation of the breccia and Zhang et al. (2001) interpreted the breccia as the product of tectonic faulting deep in the mantle. The latter is contradicted by the fact that the breccia consist almost exclusively of single grain porphyroclasts and olivine matrix. Furthermore, our findings indicate that these grains were collected from a depth interval of at least 100 km. The crucial facts and questions to be answered are: 1) how did the brecciation initiate and what caused the sampling of a 100 km stratigraphic column of the Earth mantle? 2) How and why did the porphyroclasts preserve their intra grain homogeneity up to the very rims and keep their individual chemical and isotopic identity at the high temperatures of solidification? 3) Why do the compositions of neoblastic orthopyroxenes and garnets coincide with those of matrix orthopyroxene and garnet in part A? 4) How and why did the entire peridotite solidify at mantle depth? 5) What are the characteristics of the melt(s), fluid(s) that collected and solidified the peridotite? The answers to these questions should finally result in a comprehensive model for the formation of the brecciated parts B and C and amalgamation with the part A of the polymict peridotite Bosch03-79.

6.5.1 "Explosive" brecciation at the base of the lithosphere

According to the Ni content in porphyroclastic garnets, grains were sampled from a large depth range of the subcontinental mantle. Beginning at ~ 250 km depth, they were transported to and welded in to peridotite at ~ 120 km. As already mentioned single grain porphyroclast have preserved intra grain homogeneity and have developed neoblasts on their rims as a consequence of melt-mineral reaction. Therefore, the whole process of single grain sampling, mixing, transporting and welding must have been very fast and rapid.

Single grain sampling, through mechanical mixing of a > 100 km stratigraphic column can only be accomplished in a CO_2-rich fluid-melt system with release of a large amount of energy. Mg-rich silicocarbonatites and kimberlites are the partial melting products of carbonated peridotite (lherzolite to harzburgite) at pressures from ~ 6 GPa onwards (Dalton and Presnall, 1998; Brey et al., 2008). Such melts show stepwise devolatilisation at various depths because of the solubility behavior of CO_2 with release of large amounts of CO_2 at each step (Brey and Ryabchikov, 1994).

The first saturation point for CO_2-saturated kimberlites is reached already at pressures of around 6-7 GPa, where a free fluid phase exsolves from the melt (Brey et al., 1983; Ryabchikov et al., 1993) at the base of the cratonic keel. This point is probably already reached at higher pressures for Mg-rich silicocarbonatites (Brey et al., 1983; Fig. 6.17). This is in good agreement with the experimental studies (Girnis et al., 1995), which argue that the eruption of kimberlite is probably triggered by the saturation with CO_2 and degassing at higher depths of around 6 GPa. A great thickness of the cratonic lithosphere create generally under compression of the lithosphere (Zaback and Mooney, 2003) and may together with the small tectonic movements be responsible for the increase of pressure and crack formation at the bottom of the cratonic keel.

These conditions, where a positive volume change connected with the nucleation and growth of fluid bubbles in a melt that was tectonically decompressed, may lead to the initiation of the "explosive" brecciation.

Lensky et al. (2006) estimated that a supersaturation pressure of 0.1-0.2 GPa is needed for the nucleation of CO_2 bubbles in basaltic melts and, according to their calculations, bubble growth following nucleation is very fast. A lowering of pressure would increase the amount of bubbles. Their experiments where carried out at pressures of 1-2 GPa for a basaltic composition, which has a relatively low solubility of CO_2. Here, is assumed that this can be applied in a similar way to kimberlitic and silicocarbonatitic systems at higher pressure because the large effects of pressure on CO_2 compressibility occur below 1 GPa. A further source of CO_2 and a continuous supply during the transport to the surface may be the decrepitating of magnesite (Canil, 1990). The vapour oversaturation may promote crack propagation, which results in a rapid upraise of the fluid-magma-solid mush.

Such an explosive ascent of kimberlite with degassing was also proposed by Dawson (1982). This may also be the explanation for the brecciation of the surrounding rocks, so that the single grains could depart from the peridotites. Furthermore, the observed exsolution lamellae in some porphyroclastic olivines and the kink bending in porphyroclastic orthopyroxenes in this polymict peridotite may testify the "explosive" episode at the base of the continental lithosphere.

6.5.2 Chemical homogeneity of porphyroclasts,

The surface and shape of the majority of the porphyroclasts underneath the overgrowth rims do not show fracturing as a result of brecciation, but rather show dissolution features probably because of direct porphyroclast-melt contact. Experimental observations by Boudier (1991) show that silicate melts produce euhedral corrosion and overgrowth of crystals on anhedral and subhedral xenocrysts. Theses features are often observed by porphyroclast in this polymict peridotite (Fig. 6.4b,c). The reacting melt was presumably of kimberlitic composition (see below). As a partial melting product of peridotitic mantle (Girnis et al., 1995), kimberlitic melts are in equilibrium with these phases at higher pressures, but only with compositions corresponding to their depth of origin below 6 GPa. Mantle phases from lower pressures have to adjust their chemical composition or become dissolved. The dissolution rate will depend on how far the phases are away from equilibrium in terms of their chemical composition and P-T conditions. Experimental observations at the very low pressure of 1.5-2 GPa and temperatures from 1400-1550 °C, show that garnets in direct contact with a kimberlitic melt will be dissolved after only a few hours (Canil and Fedortchouk, 1999). The same holds for orthopyroxene.

The dissolution process and the rapid transport due to the brecciation process (see below) prevent the grains from developing any or larger compositional zoning and the rim overgrowths (neoblastic grains) eventually prevented any further dissolution. Also, the melt-porphyroclast contact was probably a very short time event, as Spera (1984) and Kelley and Wartho (2000) provide compelling evidence that the ascent rate of kimberlites must range from 10-30 m/s. It will be somewhat slower at higher pressures, which are discussed here. The mostly polycrystalline and fine grained nature of the neoblasts and the evenly fine grain size of the olivine matrix indicates high nucleation rates, i.e. by rapid cooling or a fast drop below the liquidus of the melt.

The preferred scenario is that the brecciated porphyroclasts (Fig. 6.18A) were collected at different depths and that the transporting agent, presumably a kimberlite melt, in direct contact with porphyroclasts, dissolved them (Fig. 6.18B), mainly at lower pressures, during the ascent. The growth of the neoblastic rims was that of a dissolution-precipitation process at fairly constant P-T conditions in a fast consolidation process (Fig. 6.18C). This may be due to cooling because of the halt of the breccia at around 3.5 GPa, where ambient temperatures are around 1150 °C, where they substantially dropped below the liquidus. This may be caused by degassing, as there is a discontinuity in the solubility of gases (Brey et al., 1991; Brey and Raybchikov, 1994).

6.5.3. Major and trace element characteristics of pervasive melt

The direct crystallization products from the melt that amalgamated the porphyroclasts in parts B and C of the polymict peridotite are the matrix olivines and the orthopyroxene and garnet overgrowths. Also, tiny rutiles and phlogopites and up to 2 mm sized sulphides are precipitated from the melt. Orthopyroxenes and garnets, normally outside equilibrium at pressures of around 3.5 GPa, grew from a kimberlitic melt as rims on preexisting orthopyroxenes and garnets because of local chemical equilibrium. The neoblastic garnets are subcalcic and clinopyroxene porphyroclasts have opx overgrowths, which demonstrate the Mg-rich character of the melt with a low Ca-activity. The kimberlite borne megacrystic

character of neoblastic opx and garnets is indicated by their major and trace element compositions (see results). Therefore, the pervasive melt was also Fe-, Ca- and Ti-rich, with high contents of REE (with 10x PM of Lu) and HFSE.

This neoblastic mineral assemblage does not represent a melt composition, but is rather a partial precipitate from an Mg-rich melt with a Si-poor, Ca-richer residual, probably silicocarbonatitic melt having left the system. The fractionated part of the melt that left the system was probably also highly enriched in U, Th, LREE and LILE.

Furthermore, based on the previously discussed processes of "explosive" brecciation, as fast ascent and fractionation of the melt was responsible for the polymict formation, this melt should have been volatile-saturated.

These conclusions provide a line of evidences that volatile-rich kimberlite-like melt was responsible for the single grain collection and amalgamation of this polymict peridotite.

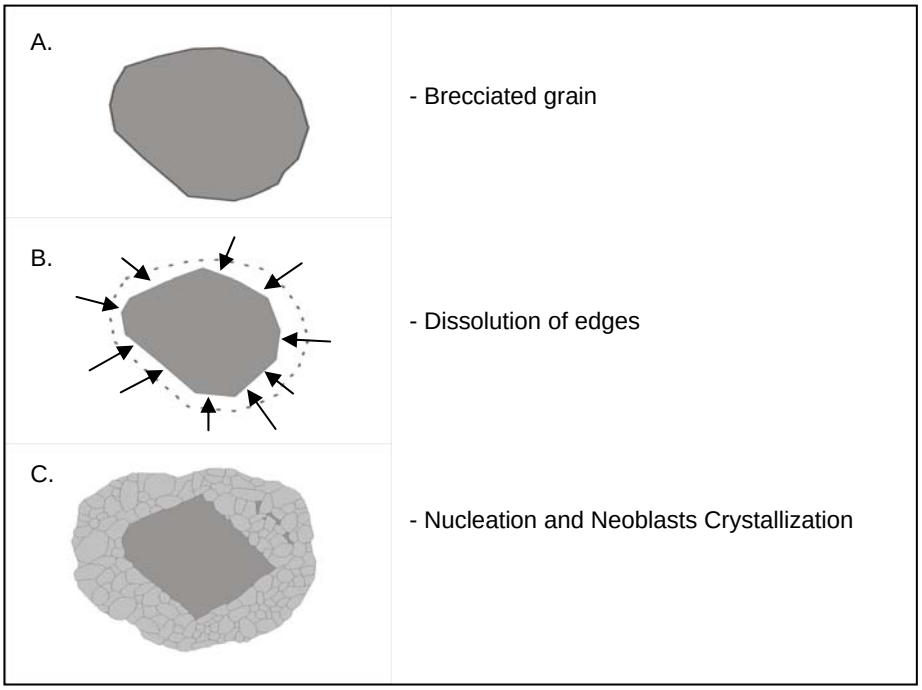

Fig. 6.18. Formation of rim overgrowths on porphyroclastic grains from parts B and C of polymict peridotite. (see text for further discussion).

6.5.4. Conditions of polymict peridotite amalgamation

Temperatures around 1150 °C do not fall on a conductive geotherm of 42mW/m^2 (Chapman and Pollack, 1977) at 3.5 GPa, obtained from neoblastic garnet-opx compositions - they are too high (Fig. 6. 17). At pressures of around 3-4 GPa, the solubility of CO_2 in kimberlite magma changes drastically, causing exsolution of a fluid-phase (Brey et al., 1991). Loss of CO_2 in this depth range would result in intense crystallisation of olivine (Eggler and Wendland, 1979; Brey and Ryabchikov, 1994) and probably consolidation of the whole peridotite.

If the calculated P-T conditions are at equilibrium conditions of amalgamation of the xenolith it must have happened "shortly" before its incorporation into the ascending kimberlite. A prolonged residence of such a hot disequilibrium mantle piece at ambient conditions would lead to cooling, re-crystallization and chemical adjustment of its mineral constituents.

Therefore, the whole process of explosive brecciation, turbulent transport and mixing, porphyroclast dissolution and neoblast precipitation should have happened very fast. It was

therefore probably part of the kimberlite evolution. This sample probably represents one frozen part (with variable mantle clasts) of the kimberlitic magma precursor, of kimberlite that erupted at ~ 90 Ma (Smith, 1983) years ago in Kimberley.

6.5.5 Model of kimberlite propagation and formation of the polymict peridotite

For the formation of such a complex peridotite four events were responsible: 1. brecciation and collection of the porphyroclasts from parts B and C; 2. melt propagation and melt-porphyroclast reaction; 3. amalgamation; and 4. exhumation of the whole polymict peridotite.

In the following, evidence is presented that only kimberlite melt can be responsible for creation and amalgamation of this peridotite. It is well known from experimental and numerical calculations that kimberlites are highly volatile and CO_2-rich melts and that their eruption is very rapid and might consider multiple melt intrusions (Spera, 1984; Artyushkov and Sobolev, 1984; Kelley and Wartho, 2000; Gregoire et al., 2006).

Complex processes of kimberlite melt formation and degassing of the Mg-carbonatites are probably responsible for the "explosive" brecciation of the lithospheric mantle at depths of ~ 250 km (Fig. 6.19A). The brecciation of the surrounding lithospheric mantle causes single grain sampling by the melt. Such melts show stepwise devolatilisation at various depths because of the solubility behavior of CO_2 with release of large amounts of CO_2 at each step (Brey and Ryabchikov, 1994). This together with the small tectonic movements may be responsible for crack formation at the bottom of the cratonic keel. Furthermore, the vapour oversaturation may promote crack propagation, which results in a rapid upraise of the fluid-magma-solid mush.

During the ascent, sampled grains are in disequilibrium with the melt started dissolving them. Due to that fast nucleation caused by rapid cooling, or a fast drop below the liquidus of the melt, neoblastic grains formed on the rims of the porphyroclasts. Experimental data done by Brey and Ryabchikov (1994) emphasized that degassing of the melt with $CO_2 > 10$ wt.% will start at 4-5 GPa. Therefore, the melt will rapidly become less mobile and start cooling down. At pressures around 3-4 GPa, the solubility of CO_2 in kimberlite magma changes drastically, causing exsolution of fluid-phase (Brey et al., 1991). Loss of CO_2 in this depth range would result in intense crystallisation of olivine (Eggler and Wendland, 1979; Brey and Ryabchikov, 1994). That explains the observed crystallized olivine matrix in the polymict peridotite at P-T conditions (1150 °C, 3.5 GPa). Therefore, they mark conditions of the consolidation of the whole polymict peridotite (Fig. 6.19B).

The different size of porphyroclasts in part B, compared to grains in part C, indicates that porphyroclasts were not brought by the same portion of melt, but probably by the several pulses. Therefore, it may be considered that there were at least two subsequent episodes of ascending kimberlite-like melt (probably kimberlite precursors) that created this peridotite. Thus, we can conclude that kimberlite ascent in pulses (two or more), and that they may differentiate at pressures of around 3-4 GPa, corresponding to a depth of 100-120 km. Differentiation of the kimberlite melt probably depends on the concentration of volatiles, and the speed of the ascending. This probably results in variable types of matrix and also variable types of neoblastic rims around porphyroclasts, observed also in different polymict peridotites (Lawless et al., 1979; Dawson et al., 2001; this study).

Since the porphyroclasts are still in disequilibrium and conditions of polymict amalgamation (1150°C, 3.5 GPa) are not in equilibrium with the conductive geotherm, we can conclude that this sample was transported to the surface very shortly after amalgamation. The next pulse of the kimberlite melt may have been responsible for this. Accordingly, this polymict peridotite today represents a part of the Kimberley kimberlite eruption at ~ 90 Ma (Fig. 6.19C).

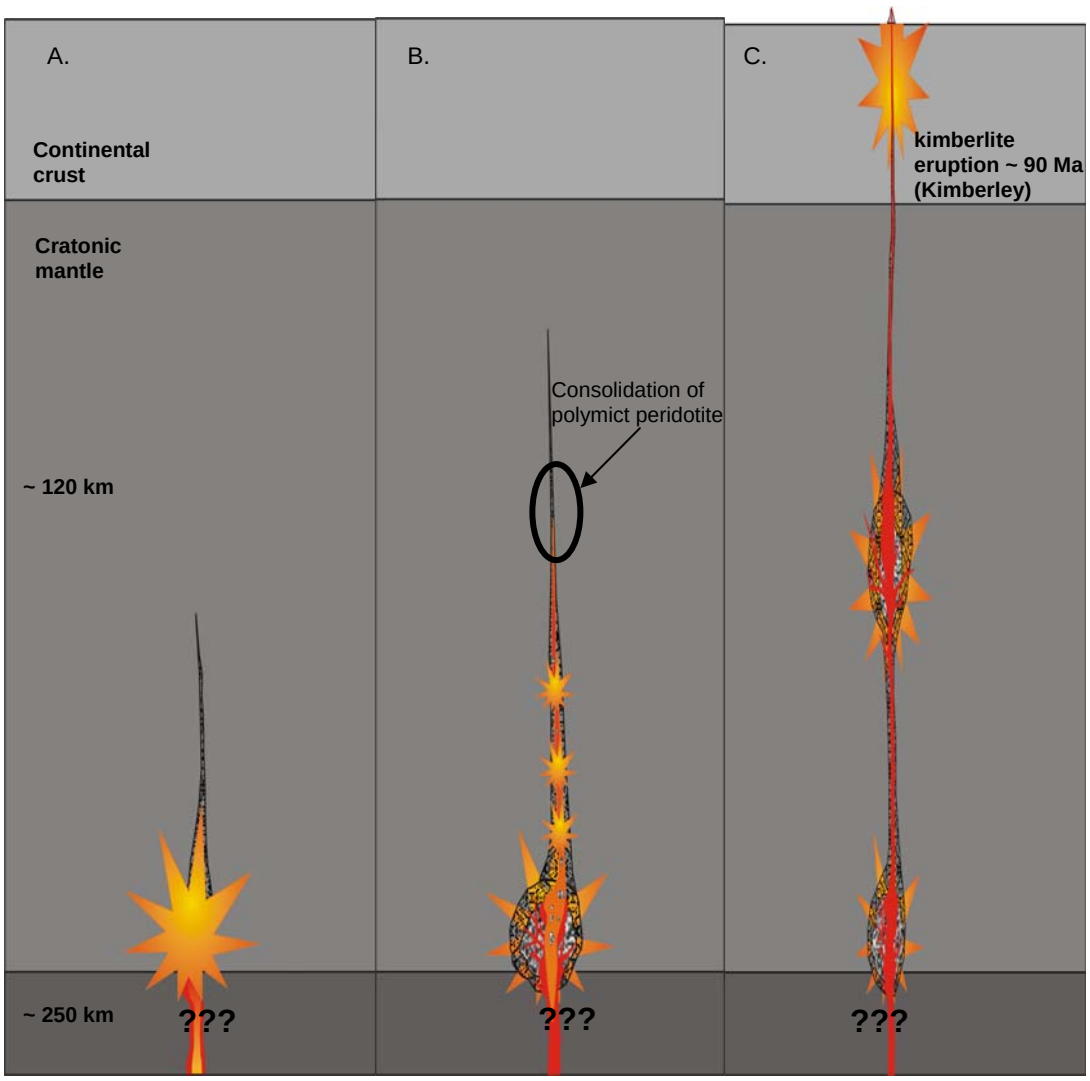

Fig. 6.19. Model for kimberlite propagation and formation of the polymict peridotite. (A) Explosive breciation of the lithospheric mantle at the depth of around 250 km. (B) Single grain sampling by the melt that reaches depths of around 120 km. Due to the degassing whole polymict peridotite consolidates at those depths. (C) Next impulse of a melt brings a polymict peridotite to the surface (see text for further discussion).

6.6. Conclusion

According to the major and trace element composition of neoblastic grains on the rims of the porphyroclast and matrix olivine, and the necessary volatile, especially CO_2, the whole xenolith must have been formed by the kimberlitic melt.

The whole process of explosive brecciation at the bottom of the mantle keel, turbulent transport and mixing of mantle clasts happened very fast. During the melt ascent brecciated porphyroclast dissolve and neoblast precipitate on their rims. That and probably degassing of the melt cased olivine matrix precipitation and amalgamation of the whole xenolith.

This complex process evokes several melt batches with their differentiation and stop-over's at various mantle depths as a propagation process of kimberlitic melt. The here studied sample probably represents one frozen part (with variable mantle clasts) of the kimberlitic magma precursor, with kimberlite eruption at ~ 90 Ma years ago in Kimberley.

REFERENCES

Adam, J., Green, T.H., Sie, S.H., Ryan, C.G., 1997. Trace element partitioning between aqueous fluids, silicate melts and minerals. European Journal of Mineralogy 9, 569-584.

Alterman, W., Hölbich, I.W., 1991. Structural history of the southwestern corner of the Kaapvaal craton and the adjacent Namaqua realm: new observations and s reappraisal. Precambrian Research 52, 133-166.

Armstrong, R.A., Compston, W., Retief, E.A., Williams I.S., Welker, H.J., 1990. Zircin ion microprobe bearing on the age and evolution of the Witwatersrand triad. Precambrian Research 53, 243-266.

Artyushkov, E.V., Sobolev, S.V., 1984. Physics of kimberlite magmatism. In: J. Kornprobst (Editor), Kimberlites I: Kimberlites and related rocks, Proceedingd of the 3th International Kimberlite Conference, ELSEVIER, pp.309-322.

Barth, M. G., Rudnick, R. L., Horn, I., McDonough, W. F., Spicuzza, M. J., Valley, J. W., Haggerty, S. E., 2001. Geochemistry of xenolithic eclogites from West Africa, part I: A link between low MgO eclogites and archean crust formation. Geochimica Et Cosmochimica Acta 65, 1499-1527.

Becker, M., Roex, A.P.L., 2006. Geochemistry of South African On- and Off-craton, Group I and Group II Kimberlites: Petrogenesis and Source Region Evolution. Journal of Petrology 47, 673-703.

Bedini, R.M., Bodinier, J.L., Dautria, J.M. and Morten, L., 1997. Evolution of LILE-enriched small melt fractions in the lithospheric mantle: a case study from the East African Rift. Earth and Planetary Science Letters 153 (1-2), 67-83.

Bedini, R.M., Blichert-Toft, J., Boyet, M. Albarede, F., 2002. Lu-Hf isotope geochemistry of garnet-peridotite xenoliths from the Kaapvaal craton and the thermal regime of the lithosphere. Geochimica Et Cosmochimica Acta 66, A61-A61.

Bedini, R.M., Blichert-Toft, J., Boyet, M., Albarede, F., 2004. Isotopic constraints on the cooling of the continental lithosphere. Earth and Planetary Science Letters 223, 99-111.

Bell, D.R., Schmitz, M.D., Janney, P.E., 2003. Mesozoic thermal evolution of the southern African mantle lithosphere. Lithos 71, 273-287.

Bell, D.R., Gregoire, M., Grove, T.L., Chatterjee, N., Carlson, R.W., Buseck, P.R., 2005. Silica and volatile-element metasomatism of Archean mantle: a xenolith-scale example from the Kaapvaal Craton. Contributions to Mineralogy and Petrology 150, 251-267.

Beukes, N.J., Smit, C.A., 1987. New evidence for thrust faulting in Griqualand West South Africa: implications for stratigraphy and the age of red beds. South African Journal of Geology 90, 378-387.

Bizimis, M., Salters, V.J.M., Bonatti, E., 2000. Trace and REE content of clinopyroxenes from supra-subduction zone peridotites. Implications for melting and enrichment processes in island arcs. Chemical Geology 165, 67-85.

Bizzarro, M., Baker, J.A., Ulfbeck, D., 2003. A new digestion and chemical separation technique for rapid and highly reproducible determination of Lu/Hf and Hf isotope ratios in geological materials by MC-ICP-MS. Geostandards Newsletter-the Journal of Geostandards and Geoanalysis 27, 133-145.

Blichert-Toft, J. Albarede, F., 1997. The Lu-Hf isotope geochemistry of chondrites and the evolution of the mantle-crust system. Earth and Planetary Science Letters 148, 243-258.

Blichert-Toft, J., Chauvel, C., Albarede, F., 1997. Separation of hf and Lu for high precision isotope analysis of rock samples by magnetic sector-multiple collector ICPMS. Contributions to Mineralogy and Petrology 127, 248-260.

Blichert-Toft, J., Albarede, F., Kornprobst, J., 1999. Lu-Hf isotope systematics of garnet pyroxenites from Beni Bousera, Morocco: Implications for basalt origin. Science 283, 1303-1306.

Boudier, F., 1991. Olivine xenocrysts in picritic magmas. Contributions to Mineralogy and Petrology 109, 114-123.

Bonney, T.G., 1899. The parent rock of the diamond in South Africa, R. Soc. London Proc. 65, 235-236.

Boyd, F.R., 1989. Compositional distinction between oceanic and cratonic lithosphere. Earth and Planetary Science Letters 96, 15-26.

Boyd, F., 1997. Correlation of orthopyroxene abundance with the Ni content of coexisting olivine in cratonic peridotites. Transaction of the American Geophysical Union F746.

Boyd, F.R., Nixon, P.H., 1978. Ultramafic nodules from Kimberley pipes, South Africa. Geochimica Et Cosmochimica Acta 42, 1367.

Boyd, F.R., Gurney, J.J., 1986. Diamonds and the African lithosphere. Science 232, 472-477.

Boyd, F.R., Merzman, S.A., 1987. Composition and structure of the Kaapvaal lithosphere, southern Africa. In: B.O. Masen (Editor), Magmatic processes: physicochemical principles. The geochemical Society Special Publications, pp.13-24.

Boyd, F.R., Dawson, J.B., Smith, J.V., 1984. Granny-Smith diopside megacrysts from the Kimberlites of the Kimberley area and Jagersfontain, South-Africa. Geochimica Et Cosmochimica Acta 48, 381-384.

Boyd, F.R., Pearson, D.G., Nixon, P.H., Mertzman, S.A., 1993. Low-calcium garnet harzburgites from Southern Africa – their relations to craton structure and diamond crystallization. Contributions to Mineralogy and Petrology 113, 352-366.

Brey, G.P., Kohler, T., 1990. Geothermobarometry in 4-phase lherzolites. 2. New thermobarometers, and practical assessment of existing thermometers. Journal of Petrology 31, 1353-1378.

Brey, G.P., Ryabchikov, I.D., 1994. Carbon-dioxide in strongly silica undersaturated melts and origin of kimberlite magmas. Neues Jahrbuch Fur Mineralogie-Monatshefte 10, 449-463.

Brey, G., Brice, W.R., Ellis, D.J., Green, D.H., Harris, K.L., Ryabchikov, I.D., 1983. Pyroxene-carbonate reactions in the upper mantle. Earth and Planetary Science Letters 62, 63-74.

Brey, G.P., Kogarko, L.N., Ryabchikov, I.D., 1991. Carbon dioxide in kimberlitic melts. Neues Jahrbuch Fur Mineralogie-Monatshefte 4, 159-168.

Brey, G.P., Bulatov, V.K., Girnis, A.V., Lahaye, Y., 2008. Experimental melting of carbonated peridotite at 6-10 GPa. Journal of Petrology 49, 797-821.

Bulatov, V., Brey, G.P., Foley, S.F., 1991. Origin of low-Ca, high-Cr garnets by crystallization of low-pressure harzburgites. Ext. Abstr. 5Int. Kuimberlite Conf. Araxa, Brazil. CPRM Special Publication 2/91: Rio de Jeneiro, Brazil, 29-31.

Canil, 1990. Experimental study bearing on the absence of carbonate in mantle-derived xenoliths, Geology 18, 1011-1013.

Canil, D., 1994. An experimental calibration of the nickel in garnet geothermometer with applications. Contributions to Mineralogy and Petrology 117, 410-420.

Canil, D., 1999. The Ni-in-garnet geothermometer: calibration at natural abundances. Contributions to Mineralogy and Petrology 136, 240-246.

Canil, D., 2002. Vanadium in peridotites, mantle redox and tectonic environments: Archean to present. Earth and Planetary Science Letters 195, 75-90.

Canil, D., Wei, K.J., 1992. Constraints on the origin of mantle-derived low Ca garnets. Contributions to Mineralogy and Petrology 109, 421-430.

Canil, D., O'Neill, H.S.C., 1996. Distribution of ferric iron in some upper-mantle assemblages. Journal of Petrology 37(3), 609-635.

Canil D., Fedortchouk Y., 1999. Garnet dissolution and the emplacement of kimberlites, Earth and Planetary Science Letters 167, 227-237

Card, K.D., 1990. A review of the superior province of the Canadian shield, a product of Archean accretion. Precambrian Research 48, 99-156.

Carlson, R.W., Pearson, D.G., Boyd, F.R., Shirey, S.B., Irvine, G., Menzies, A.H., Gurney, J.J., 1999. Re-Os systematics of lithospheric peridotites: implications for lithosphere formation and preservation. Proceedings of the 7th International Kimberlite Conference, Cape Town, 1998. Red Roof Design, Cape Town, South Africa, pp. 99-108.

Caro, G., Bourdon, B., Birck, J.L., Moorbath, S., 2006. High-precision Nd^{142}/Nd^{144} measurements in terrestrial rocks: Constraints on the early differentiation of the Earth's mantle. Geochimica Et Cosmochimica Acta 70, 164-191.

Catuneanu, O., Hancox, P.J., Rubidge, B.S., 1998. Reciprocal flexural behaviour and contrasting stratigraphies: a new basin development model for the Karoo retroarc foreland system, South Africa. Basin Research, 10, 417-439.

Chapman, D.S., Pollack H.N., 1977. Regional geotherms and lithospheric thicknesses. Geology 5, 265-268.

Chevrot, S., Zhao, L., 2007. Multiscale finite-frequency Rayleigh wave tomography of the Kaapvaal craton. Geophysical Journal International 169, 201-215.

Chu, N.C., Taylor, R.N., Chavagnac, V., Nesbitt, R.W., Boella, R.M., Milton, J.A., German, C.R., Bayon, G., Burton, K., 2002. Hf isotope ratio analysis using multi-collector inductively coupled plasma mass spectrometry: an evaluation of isobaric interference corrections. Journal of Analytical Atomic Spectrometry 17, 1567-1574.

Coltorti, M., Bonadiman, C., Hinton, R. W., Siena, F., Upton, B. G. J., 1999. Carbonatite metasomatism of the oceanic upper mantle: Evidence from clinopyroxenes and glasses in ultramafic xenoliths of Grande Comore, Indian Ocean. Journal of Petrology 40, 133-165.

Cox, K.G., Smith, M.R., Beswetherick, S., 1987. Textural studies of garnet lherzolites: evidence of exsolution origin from high-temperature harzburgites. In: P.H. Nixon (Editor), Mantle xenolits. John Wiley, Chichester, pp. 537-550.

Dalton, J.A., Presnall, D.C., 1998. The continuum of primary carbonatitic-kimberlitic melt compositions in equilibrium with lherzolite: Data from the system CaO-MgO-Al2O3-SiO2-CO2 at 6 GPa. Journal of Petrology 39, 1953-1964.

Dawson, J.B., 1970. The structural setting of African kimberlite magmatism. in: T.N. Clifford and I.G. Gass (Editors), African Magmatism and Tectonics, Hafner Publ. Co., Darien, Conn., pp. 321-335.

Dawson 1972. Kimberlites and their relationship to the upper mantle. R. Soc. London Philos. Trans. Ser. A. 271, 291-311.

Dawson, J.B., 1982. Kimberlites and their xenoliths. Springer-Verlag, Berlin, 159 pp.

Dawson, J.B., 1984. Constraning types of upper-mantle metasomatism? In: J. Kornprobst (Editor), Kimberlites II: The mantle and the crust-mantle relationschips. Elsevier, pp. 282-331.

Dawson, J.B., 1987. The MARID suite of xenoliths in kimberlite: relationship to veined and metasomatised peridotite xenoliths. In: P.H. Nixon (Editor), Mantle Xenoliths. John Wiley, Chichester, pp. 465-475.

Dawson, J.B., Stephens, W.E., 1975. Statistical classification of garnets from kimberlite and associated xenoliths. The Journal of Geology 83, 589-607.

Dawson, J.B., Hill, P.G., Kinny, P.D., 2001. Mineral chemistry of a zircon-bearing, composite, veined and metasomatized upper-mantle peridotite xenolith from kimberlite. Contributions to Mineralogy and Petrology 140, 720-733.

Deckart, K., Bertrand, H., Liegeois, J.-P., 2005. Geochemistry and Sr, Nd, Pb isotopic composition of the Central Atlantic Magmatic Province (CAMP) in Guyana and Guinea. Lithos 82, 289-314.

de Wit, M.J., de Ronde, C.E.J., Tredoux, M., Roering, C., Hart, R.J., Armstrong, R.A., Green, R.W.E., Peberdy, E., Hart, R.A., 1992. Formation of an Archaean continent. Nature 357, 553-562.

DeWolf, C.P., Zeissler, C.J., Halliday, A.N., Mezger, K., Essene, E.J., 1996. The role of inclusions in U-Pb and Sm-Nd garnet geochronology: Stepwise dissolution experiments and trace uranium mapping by fission track analysis. Geochimica Et Cosmochimica Acta 60, 121-134.

Doyle, P.M., Bell, D.R., Le Roex, A.P., 2004. Fine-grained pyroxenites from the Gansfontein kimberlite, South Africa: Evidence for megacryst magma - mantle interaction. South African Journal of Geology 107, 285-300.

Drennan, G.R., Robb, L.J., Meyer, F.M., Armstrong, R.A., de Bruiyn, H., 1990. The nature of the Archaean basement in the hinterland of the Witwatersrand Basin: II. A crustal profile west of the Welkom Goldfield and comparison with the Vredefort crustal profile. South African Journal of Geology, 93. 41-53.

Eggins, S.M., Woodhead, J.D., Kinsley, L.P.J., Mortimer, G.E., Sylvester, P., McCulloch, M.T., Hergt, J.M., Handler, M.R., 1997. A simple method for the precise determination of >40 trace elements in geological sample by ICPMS using enriched isotope internal standardization. Chemical Geology 134, 311-326.

Eggler, D.H., Wendlandt, R.F., 1979. Experimental studies on the relationship of kimberlite magmas and partial melting of peridotite. In: F.R. Boyd and H.O. Meyer, Editors, Extended Abstracts, 2nd International Kimberlite Conference, American Geophysical Union, pp. 330–338.

Ellis D.J., Green D.H., 1979. An experimental study of the effect of Ca upon garnet — clinopyroxene Fe-Mg exchange equilibria. Contributions to Mineralogy and Petrology 71, 13–22.

Erlank, A.J., Waters, F.G., Hawkesworth, C.J., Haggerty, S.E., Allsopp, H.L., Rickard, R.S., Menzies, M., 1987. Evidence for mantle metasomatism in peridotite nodules from the Kimberley pipes, South Africa. In: M.A. Menzies, C.J. Hawkesworth (Editors), Mantle Metasomatism, Academic Press, London. pp. 221-309.

Fouche, J., Bate, K., van der Merwe, R., 1992. Plate tectonic settings of the Mesozoic basins, southern off-shore, South Africa. In: M.J. de Wit and I.G.D. Ransome (Editores), Inversion tectonics of the Cape Fold Belt, Karoo and Cretaceous basins of southern Africa. Balkema, Rotterdam, pp 33-45.

Foley, S.F., Barth, M.G., Jenner, G.A., 2000. Rutile/melt partition coefficients for trace elemnts and an assessment of the influence of rutile on the trace element characteristics of subduction zone magmas. Geochimica Et Cosmochimica Acta 64, 933-938.

Foley, S.F., Buhre, S., Jacob, D.E., 2003. Evolution of the Archaean crust by delamination and shallow subduction. Nature 421, 249-252.

Ganguly, J., Tirone, M., 1999. Diffusion closure temperature and age of a mineral with arbitrary extent of diffusion: theoretical formulation and applications. Earth and Planetary Science Letters 170, 131-140.

Girnis, A.V., Brey, G.P., Ryabchikov, I.D., 1995. Origin of group 1A kimberlites - fluide-saturated melting experiments at 45-55 Kbar. Earth and Planetary Science Letters 134, 283-296.

Green, T.H., Blundy, J.D., Adam, J., Yaxley, G.M., 2000. SIMS determination of trace element partition coefficients between garnet, clinopyroxene and hydrous basaltic liquids at 2-7.5 GPa and 1080-1200 °C. Lithos 53 (3-4), 165-187.

Glaser, S.M., Foley, S.F., Gunther, D., 1999. Trace element compositions of minerals in garnet and spinel peridotite xenoliths from the Vitim volcanic field, Transbaikalia, eastern Siberia. Lithos 48, 263-285.

Gregoire, M., Bell, D.R., Le Roex, A.P., 2002. Trace element geochemistry of phlogopite-rich mafic mantle xenoliths: their classification and their relationship to phlogopite-bearing peridotites and kimberlites revisited. Contributions to Mineralogy and Petrology 142, 603-625.

Gregoire, M., Bell, D.R., Le Roex, A.P., 2003. Garnet lherzolites from the Kaapvaal craton (South Africa): Trace element evidence for a metasomatic history. Journal of Petrology 44, 629-657.

Gregoire, M., Rabinowicz, M., Janse, A.J.A., 2006. Mantle mush compaction: A key to understand the mechanisms of concentration of kimberlite melts and initiation of swarms of kimberlite dykes. Journal of Petrology 47, 631-646.

Griffin, W.L., Smith, D., Boyd, F.R., Cousens, D.R., Ryan, C.G., Sie, S.H., Suter, G.F., 1989a. Trace-element zoning in garnets from sheared mantle xenoliths. Geochimica Et Cosmochimica Acta 53, 561-567.

Griffin, W.L., Cousens, D.R., Ryan, C.G., Sie, S.H., Suter, G.F., 1989b. Ni in chrome pyrope garnets – a new geothermometer. Contributions to Mineralogy and Petrology 103, 199-202.

Griffin, W.L., Gurney, J.J., Ryan, C.G., 1992. Variation in trapping temperatures and trace-elements in peridotite-suite inclusions from African diamonds – evidence for 2 inclusion suites, and implications for lithosphere stratigraphy. Contributions to Mineralogy and Petrology 110, 1-15.

Griffin, W.L., O'Reilly, S.Y., Ryan, C.G., 1999a. The composition and origin of subcontinental lithospheric mantle. In: Y. Fei, C.M. Bertka and Mysen (Editors), Mantle petrology: Field observation and high-pressure experimentation. Spec Pub No. The Geochemical Society, Washington, pp.13-45.

Griffin, W.L., Shee, S.R., Ryan, C.G., Win, T.T., Wyatt, B.A., 1999b. Harzburgite to lherzolite and back again: metasomatic processes in ultramafic xenoliths from the Wesselton kimberlite, Kimberley, South Africa. Contributions to Mineralogy and Petrology 134 (2-3), 232-250.

Griffin, W.L., O'Reilly S.Y., Natapov, L.M., Ryan, C.G., 2003. The evolution of litospheric mantle beneath the Kalahary Craton ynd its margines. Lithos 71, 215-241.

Grütter, H., Latti, D., Menzies, A., 2006. Cr-saturation arrays in concentrate garnet compositions from kimberlite and their use in mantle barometry. Journal of Petrology 47, 801-820.

Gudmundsson, G., Wood, B.J., 1995. Experimental tests of garnet peridotite oxygen barometry. Contributions to Mineralogy and Petrology 119, 56-67.

Gurney, J.J., Switzer, G.S., 1972. The discovery of garnets closely related to diamonds in the Finsch pipe, South Africa. Contributions to Mineralogy and Petrology 39, 103-116.

Haggerty, S.E., 1987. Mantle metasomes and the kinship between carbonatites and kimberlites. In: K. Bell (Editor) Carbonatites: genesis and Evolution, Uniwin Hyman, London, pp. 546-560.

Hamilton, M.A., Pearson, D.G., Stern, R.A., Boyd, F.R., 1998. Constraints on MARID petrogenesis: SHRIMP II U-Pb zircon evidence for pre-erupption metasomatism at Kampfersdam. Extended Abstracts of the 7th International Kimberlite Conference, Cape Town, RSA, pp. 296-298.

Harley, S.L., 1984. Composition of the garnet-orthopyroxene geobarometer with recent experimental studies, and applications to natural assemblages. Journal of Petrology 25, 697-712.

Harte, B., 1977. Rock nomenclature with particular relation to deformation and recrystallization textures in olivine-bearing xenoliths. The Journal of Geology 85, 279-288.

Harte, B., 1983. Mantle peridotites and processes – the kimberlite samples. In: C.J. Hawkesworth and M.J. Norry (Editors) Continental Basalts and Mantle xenoliths. Shiva, UK, pp. 46-91.

Harte, B., Winterburn, A., Gurney, J.J., 1987. Metasomatic and enrichment phenomena in garnet peridotite facies mantle xenoliths from the Matsoku kimberlite pipe, Lesotho. In: M.A. Menzies, C.J. Hawkesworth (Editors), Mantle Metasomatism, Academic Press, London. pp. 145-220.

Harte, B., Hunter, R.H., Kinny, P.D., 1993. Melt Geometry, Movement and Crystallization, in Relation to Mantle Dykes, Veins and Metasomatism. Philosophical Transactions: Physical Sciences and Engineering 342, 1-21.

Hartnady, C.J.H., Joubert, P., Stowe, C.W., 1985. Proterozoic crustal evolution in aouthwetern Africa. Episodes 8, 236-244.

Hawkesworth, C.J., Rogers, N.W., Vancalsteren, P.W.C., Menzies, M.A., 1984. Mantle enrichment processes. Nature 311, 331-335.

Hawkesworth, C.J., Erlank, A.J., Kempton, P.D., Waters, F.G., 1990. Mantle metasomatism – isotope and trace-element trends in xenoliths from Kimberley, South-Africa. Chemical Geology 85, 19-34.

Hellebrand, E., Snow, J.E., Hoppe, P., Hofmann, A.W., 2002. Garnet-field Melting and Late-stage Refertilization in 'Residual' Abyssal Peridotites from the Central Indian Ridge. Journal of Petrology 43, 2305-2338.

Herzberg, C., 1993. Lithosphere peridotites of the Kaapvaal craton. Earth and Planetary Science Letters 120, 13-29.

Herzberg, C., 1999. Phase equilibrium constraints on the formation of cratonic mantle. In: Y. Fei, C.M. Bertka and Mysen (Editors), Mantle petrology: Field observation and high- pressure experimentation. Spec Pub No.6, The Geochemical Society, Washington, pp. 241-257.

Hirose, K., Kushiro, I., 1993. Partial melting of dry peridotites at high-pressures – determination of compositions of melts segregated from peridotite using aggregates of diamond. Earth and Planetary Science Letters 114, 477-489.

Hoal, K.E.O., Hoal, B.G., Erlank, A.J., Shimizu, N., 1994. Metasomatism of the mantle lithosphere recorded by rare earth elements in garnets. Earth and Planetary Science Letters 126, 303-313.

Hofmann, A.W., 1988. Chemical differentiation of the earth – the relationship between mantle, continental-crust, and oceanic-crust. Earth and Planetary Science Letters 90, 297-314.

Ionov, D., 1998. Trace element composition of mantle-derived carbonates and coexisting phases in peridotite xenoliths from alkali basalts. Journal of Petrology 39, 1931-1941.

Ionov, D., Harmer, R.E., 2002. Trace element distribution in calcite-dolomite carbonatites from Spitskop: inferences for differentiation of carbonatite magmas and the origin of carbonates in mantle xenoliths. Earth and Planetary Science Letters 198, 495-510.

Ionov, D.A., Weiss, D., 2002. Hf isotope composition of mantle peridotites: first results and inferences for the age and evolution of the lithospheric mantle. Abstract, 4th Int. Workshop on Orogenic Lherzolites and Mantle Processes, Samani, Japan, pp. 56-57.

Ionov, D.A., Dupuy, C., O'Reilly, S.Y., Kopylova, M.G., Genshaft, Y.S., 1993. Carbonated peridotite xenoliths from Spitsbergen: implications for trace element signature of mantle carbonate metasomatism. Earth and Planetary Science Letters 119, 283-297.

Ionov, D.A., O'Reilly, S.Y., Genshaft, Y.S., Kopylova, M.G., 1996. Carbonate-bearing mantle peridotite xenoliths from Spitsbergen: Phase relationships, mineral compositions and trace-element residence. Contributions to Mineralogy and Petrology 125, 375-392.

Ionov, D.A., Gregoire, M., Prikhod'ko, V.S., 1999. Feldspar-Ti-oxide metasomatism in off-cratonic continental and oceanic upper mantle. Earth and Planetary Science Letters 165, 37-44.

Ionov, D.A., Blichert-Toft, J., Weis, D., 2005a. Hf isotope compositions and HREE variations in off-craton garnet and spinel peridotite xenoliths from central Asia. Geochimica Et Cosmochimica Acta 69, 2399-2418.

Ionov, D.A., Ashchepkov, I., Jagoutz, E., 2005b. The provenance of fertile off-craton lithospheric mantle: Sr-Nd isotope and chemical composition of garnet and spinel peridotite xenoliths from Vitim, Siberia. Chemical Geology 217, 41-75.

Irvine, G.J., Pearson, D.G., Carlson, R.W., 2001. Lithospheric mantle evolution of the Kaapvaal Craton: A Re-Os isotope study of peridotite xenoliths from Lesotho kimberlites. Geophysical Research Letters 28, 2505-2508.

Jacob, D., Jagoutz, E., Sobolev, N.V., 1998. Neodymium and strontium isotopic measurements on single subcalcic garnet grains from Yakutian kimberlites. Neues Jahrbuch Fur Mineralogie Abh. 172, 357-379.

Jacob, D.E., Bizimis, M., Salters, V.J.M., 2005. Lu-Hf and geochemical systematics of recycled ancient oceanic crust: evidence from Roberts Victor eclogites. Contributions to Mineralogy and Petrology 148, 707-720.

James, D.E., Fouch, M.J., VanDecar, J.C., van der Lee, S., 2001. Tectospheric structure beneath southern Africa. Geophysical Research Letters 28, 2485-2488.

James, D., Fouch, M., 2002. Formation and evolution of Archaean cratons: insight from southern Africa. In: C.M.R. Fowler, C.J. Ebinger and C.J. Hawkesworth (Editors), The Early Earth: Phisical, chemical and Biological development. Special publication of the Geological Society of London, London, pp. 1-26.

Jaques, A.L., Green, D.H., 1980. Anhydrous melting of peridotite at 0-15 Kb pressure and the genesis of tholeiitic basalts. Contributions to Mineralogy and Petrology 73, 287-310.

Johnson, K.T.M., Dick, H.J.B., Shimizu, N., 1990. Melting in the oceanic upper mantle – an ion microprobe study of diopsides in abyssal peridotites. Journal of Geophysical Research-Solid Earth and Planets 95, 2661-2678.

Johnson, K.T.M., 1998. Experimental determination of partition coefficients for rare earth and high-field-strength elements between clinopyroxene, garnet, and basaltic melt at high pressures. Contributions to Mineralogy and Petrology 133, 60-68.

Jones, R.A., 1987. Strontium and neodymium isotopic and rare earth element evidence for the genesis of megacrysts of southern Africa. In: P.H. Nixon (Editor), Mantle xenolits. John Wiley, Chichester, pp. 711-725.

Jordan, T.H. 1988. Structure and formation of the continental tectonosphere. In: M.A. Menzies and K.G. Cox (Editors), Oceanic and continental lithosphere: similarities and differences. Oxford University Press, Oxford.

Kelemen, P.B., Dick, H.J.B., Quick, J.E., 1992. Formation of harzburgite by pervasive melt/rock reaction in the upper mantle. Nature 358, 635-641.

Kelemen, P.B., Shimizu, N., Dunn, T., 1993. Relative depletion of niobium in some arc magmas and the continental crust: partitioning of K, Nb, La and Ce during melt/rock reaction in the upper mantle. Earth and Planetary Science Letters 120, 111-134.

Kelemen, P.B., Hart, S.R., Bernstein, S., 1998. Silica enrichment in the continental upper mantle via melt/rock reaction. Earth and Planetary Science Letters 164, 387-406

Kelley, S.P., Wartho, J.A., 2000. Rapid Kimberlite Ascent and the Significance of Ar-Ar Ages in Xenolith Phlogopites. Science 289, 609-611.

Keshav, S., Corgne, A., Gudfinnsson, G. H., Bizimis, M., McDonough, W. F., Fei, Y. W., 2005. Kimberlite petrogenesis: Insights from clinopyroxene-melt partitioning experiments at 6 GPa in the CaO-MgO-Al_2O_3-SiO_2-CO_2 system. Geochimica Et Cosmochimica Acta 69, 2829-2845.

Kessel, R., Schmidt, M.W., Ulmer, P., Pettke, T., 2005. Trace element signature of subduction-zone fluids, melts and supercritical liquids at 120-180 km depth. Nature 437, 724-727.

Kesson, S.E., Ringwood, A.E., 1989. Slabe-mantle interactions 2. The formation of diamonds. Chemical Geology 78, 97-118.

Kinzler, R.J., 1997. Melting of mantle peridotite at pressures approaching the spinel to garnet transition: Application to mid-ocean ridge basalt petrogenesis. Journal of Geophysical Research-Solid Earth 102, 853-874.

Krogh, E.J., 1988. The garnet-clinopyroxene Fe-Mg geothermometer – A reinterpretation of exsisting experimental data. Contributions to Mineralogy and Petrology 99, 44-48.

Konzett, J., Armstrong, R.A., Sweeney, R.J., Compston, W., 1998. The timing of MARID metasomatism in the Kaapvaal mantle: An ion probe study of zircons from MARID xenoliths. Earth and Planetary Science Letters 160, 133-145.

Konzett, J., Armstrong, R.A., Gunther, D., 2000. Modal metasomatism in the Kaapvaal craton lithosphere: constraints on timing and genesis from U-Pb zircon dating of metasomatized peridotites and MARID-type xenoliths. Contributions to Mineralogy and Petrology 139, 704-719.

Köhler, T., Brey, G.P., 1988. Ca in olivine as a geobarometer for lherzolites. Chemical Geology 70, 10-10.

Köhler, T.P., Brey, G.P., 1990. Calcium exchange between olivine and clinopyroxene calibrated as a geothermobarometer for natural peridotites from 2 to 60 Kb with applications. Geochimica Et Cosmochimica Acta 54, 2375-2388.

Kramers, J.D., Roddick, J.C.M., Dawson, J.B., 1983. Trace-element and isotope studies on veined, metasomatic and MARID xenoliths from bultfontain, South-Africa. Earth and Planetary Science Letters 65, 90-106.

Kröner, A., Tegtmeyer, A., 1994. Gneiss-greenstone reltionships in the Ancient Gneiss Complex of southwestern Swaziland, southern Africa, and implications for early crustal evolution. Precambrian Research 67, 109-139.

Kröner, A. , Hegner, E., Wendt, J.I., Byerly, G.R., 1996. The oldest part of the Barberton granitoid-greenstone terrain, South Africa: evidence for crust formation at 3.5 and 3.7 Ga. Precambrian Research 78, 105-124.

Kushiro, I., 1998. Compositions of partial melts formed in mantle peridotites at high pressures and their relation to those of primitive MORB. Physics of The Earth and Planetary Interiors, 107, 103-110.

Kushiro, I., 2001. Partial melting experiments on peridotites and origin of mid-ocean ridge basalt. Annual Review of Earth and Planetary Sciences 29, 71-107.

Lazarov, M., Brey, G.P., Harris, J.W., Weyer, S., 2007. Timing of mantle depletion and enrichment from single subcalcic garnet grains (Finsch mine, SA). (Abstract) Geochimica Et Cosmochimica Acta 71, A551-A551.

Lahaye, Y., Arndt, N.T., Byerly, G., Chauvel, C., Fourcade, S., Gruau, G. 1995. The influence of alteration on the trace-element and Nd isotopic compositions of komatiites. Chemical Geology 126, 43-64.

Lawless, P.J., Gurney, J.J., Dawson, J.B., 1979. Polymict peridotites from the Bultfontein and De Beers mines, Kimberly, South Africa. The mantle sample: Inclusions in kimberlites and other volcanics. Proceedings of Sec. Int. Kimb. Conf., 2, pp. 145-155.

Lensky, N. G., Niebo, R. W., Holloway, J. R., Lyakhovsky, V., Navon, O., 2006. Bubble nucleation as a trigger for xenolith entrapment in mantle melts. Earth and Planetary Science Letters 245, 278-288

Lorand, J.P., 1990. Are spinel lherzolite xenoliths representative of the abudance of sulphur in the upper mantle? Geochimica Et Cosmochimica Acta 54, 1487

Luth, R.W., Virgo, D., Boyd, F.R., Wood, B.J., 1990. Feric iron in mantle-derived garnets – implications for thermobarometry and for the oxidation-state of the mantle. Contributions to Mineralogy and Petrology 104, 56-72.

Maboko, M.A.H., Nakamura, E., 1995. Sm-Nd garnet ages from the Uluguru granulite complex of Eastern Tanzania: further evidence for post-metamorphic slow cooling in the Mozambique belt. Precambrian Research 74 (4), 195-202.

Malkovets, V.G, Griffin, W.L., O'Reilly, S.Y., Wood, B.J., 2007. Diamond, subcalcic garnets, and mantle metasomatism: Kimberlite sampling patterns define the link. Geology 35, 339-342.

Martin, H., 1994. The Archaean grey gneisses and the genesis of continental crust. In: K.C. Condie (Editor), Archaean Crustal Evolution. Elsevier, Holland, pp. 205-259.

McDonough, W.F., Sun, S.S., 1995. The composition of the Earth. Chemical Geology 120, 223-253.

McGregor, I.D., 1974. The system MgO–Al2O3–SiO2: solubility of Al2O3 in enstatite for spinel and garnet–spinel compositions. Am. Mineral. V.59, 110–19.

Menzies, A.H., Carlson, R.W., Shirey, S.B., Gurney, J.J., 1999. Re-Os systematics of Newlands peridotite xenoliths: Implications for diamond and lithosphere formation. Proceedings of the 7th International Kimberlite Conference, Cape Town, 1998. Red Roof Design, Cape Town, South Africa, 566-573.

Menzies, M.A., 1990. Archean, Proterozoic and Phanerozoic litospheric mantle. In: M.A. Menzies (Editor), Continenttal Mantle, Oxford Univ. Press, pp. 184.

Menzies, M.A., Hawkesworth, C., 1987. Upper mantle processes an composition. In: P.H. Nixon (Editor), Mantle Xenoliths. John Wiley, Chichester, pp. 725-738.

Menzies, M.A., Murthy, R., 1980. Enriched mantle: Nd and Sr isotopes in diopsides from kimberlite nodules. Nature 283, 634-636.

Menzies, M., Rogers, N., Tindle, A., Hawkeswort, C., 1987. Metasomatic and enrichment processes in lithospheric peridotites, an effect of asthenosphere-litosphere interaction. In: M.A. Menzies, C.J. Hawkesworth (Editors), Mantle Metasomatism, Academic Press, London. pp. 313-364.

Mitchell, R.H., 1986. Kimberlites Mineralogy, Geochemistry and Petrology. Plenum Press, London, 442 pp.

Mitchell, R.H., 1995. Kimberlite, Orangeites and Related Rocks. New York: Plenum, 410 pp.

Moore, A.E., Lock, N.P., 2001. The origin of mantle-derived megacrysts and sheared peridotites-evidence from kimberlites in the northern Lesotho Orange Free State (South Africa) and Botswana pipe clusters. South African Journal of Geology 104, 23-38.

Münker, C., Weyer, S., Scherer, E., Mezger, K., 2001. Separation of high field strength elements (Nb, Ta, Zr, Hf) and Lu from rock samples for MC-ICPMS measurements. G-cubed, 2, paper number 2001GC000183.

Nelson, D.R., Chivas, A.R., Chappell, B.W., McCulloch, M.T., 1988. Geochemical and isotopic systematics in carbonatites and implications for the evolution of ocean-island sources. Geochimica Et Cosmochimica Acta 52, 1-17.

Nickel K.G., Green D.H., 1985. Empirical geothermobarometry for garnet peridotites and implications for the nature of the lithosphere, kimberlites and diamonds. Earth. Planet. Sci. Lett. 73,158–170.

Nimis, P., Taylor, W.R., 2000. Single clinopyroxene thermobarometry for garnet peridotites. Part I. Calibration and testing of a Cr-in-Cpx barometer and an enstatite-in-Cpx thermometer. Contributions to Mineralogy and Petrology 139, 541-554.

Nguuri, T.K., Gore, J., James, D.E., Webb, S.J., Wright, C., Zengeni, T.G., Gwavava, O., Snoke, J.A., 2001. Crustal structure beneath southern Africa and its implications for the formation and evolution of the Kaapvaal and Zimbabwe cratons. Geophysical Research Letters 28, 2501-2504.

Nixon, P.H., van Calstern, P.W.C., Boyd, F.R., Hawkesworth, C.J., 1987. Harzburgites with garnets of diamond faces from southern Africa kimberlites. In: P.H. Nixon (Editor), Mantle xenolits. John Wiley, Chichester, pp. 523-535.

Norman, M.D., Pearson, N.J., Sharma, A. and Griffin, W.L., 1996. Quantitative analysis of trace elements in geological materials by laser ablation ICPMSS: instrumental operating conditions and calibration values of NIST glasses. Geostandards and Geoanalytical Research 20, 247-261.

Nowell G.M., Pearson, D.G., Kempton, P.D., Noble, S.R., Smith, C.B., 1999. Origins of kimberlites: A Hf isotope perspective. In: J.J. Gurney, J.L. Gurney, M.D. Pascoe and S.H. Richardson (Editors), Proceedings of the 7th International Kimberlite Conference. Red Roof Design, Cape Town. pp. 616-624.

Nowell, G.M., Pearson, D.G., Bell, D.R., Carlson, R.W., Smith, C.B., Kempton, P.D., Noble, S.R., 2004. Hf Isotope Systematics of Kimberlites and their Megacrysts: New Constraints on their Source Regions. Journal of Petrology 45, 1583-1612.

O'Neill, H.S.C., Wall, V.J., 1987. The Olivine-Orthopyroxene-Spinel Oxygen Geobarometer, the Nickel Precipitation Curve, and the Oxygen Fugacity of the Earth's Upper Mantle. Journal of Petrology 28 (6), 1169-1191.

O'Neill, H.S.C., Wood, B.J., 1979. Experimental-study of Fe-Mg partitioning between garnet and olivine and its calibration as a geothermometer. Contributions to Mineralogy and Petrology 70, 59-70.

Ohtani, E., Kimura, Y., Kimura, M., Kubo, T., Takata, T., 2006. High-pressure minerals in shocked L6-chondrites: constraints on impact conditions. Shock Waves 16, 45-52.

Pearce, N.J.G., Perkins, W.T., Westgate, J.A., Gorton, M.P., Jackson, S.E., Neal, C.R., Chenery, S.P., 1997. A compilation of new and published major and trace element data for the NIST SRM 610 and NIST SRM 612 glass reference materials. Geostandards Newsletter 21, 115-144.

Pearson, D.G., 1999. The age of continental roots. Lithos 48, 171-194.

Pearson, D.G., Nowell, G.M., 2004. Re-Os and Lu-Hf Isotope Constraints on the Origin and Age of Pyroxenites from the Beni Bousera Peridotite Massif: Implications for Mixed Peridotite-Pyroxenite Mantle Sources. Journal of Petrology 45, 439-455.

Pearson, D.G., Shirey, S.B., Carlson, R.W., Boyd, F.R., Pokhilenko, N.P., Shimizu, N., 1995. Re-Os, Sm-Nd, and Rb-Sr isotope evidence for thick Archean lithospheric mantle beneath the Siberian Craton modified by multistage metasomatism. Geochimica Et Cosmochimica Acta 59, 959-977.

Pearson, D.G., Shirey, S.B., Harris, J.W., Carlson, R.W., 1998. Sulphide inclusions in diamonds from the Koffiefontein kimberlite, S Africa: constraints on diamond ages and mantle Re-Os systematics. Earth and Planetary Science Letters 160, 311-326.

Pearson, D.G., Canil, D., Shirey, S.B., 2003. Mantle samples included in volcanic rocks: xenoliths and diamonds. In: Turekian, K.K., Holland, H.D. (Editors), Treatise on Geochemistry, Volume 2: The Mantle and Core, Amsterdam: Elsevier. pp. 171-276.

Pin, C., Zalduegui, J.F.S., 1997. Sequential separation of light rare-earth elements, thorium and uranium by miniaturized extraction chromatography: Application to isotopic analyses of silicate rocks. Analytica Chimica Acta 339, 79-89.

Poujol, M., Robb, L.J., Anhaeusser, C.R., Gericke, B., 2002. Geochronological constrains on the evolution of the Kaapvaal craton, South Africa. Economic Geology Research Institute, information circular 306. 33 pp.

Priestley, K., McKenzie, D., Debayle, E., 2006. The state of the upper mantle beneath southern Africa. Tectonophysics 416, 101-112.

Raczek, I., Stoll, B., Hofmann, A.W., Peter Jochum, K., 2001. High-Precision Trace Element Data for the USGS Reference Materials BCR-1, BCR-2, BHVO-1, BHVO-2, AGV-1, AGV-2, DTS-1, DTS-2, GSP-1 and GSP-2 by ID-TIMS and MIC-SSMS. Geostandards and Geoanalytical Research 25, 77-86.

Raczek, I., Jochum, K.P., Hofmann, A.W., 2003. Neodymium and Strontium Isotope Data for USGS Reference Materials BCR-1, BCR-2, BHVO-1, BHVO-2, AGV-1, AGV-2, GSP-1, GSP-2 and Eight MPI-DING Reference Glasses. Geostandards and Geoanalytical Research 27, 173-179.

Richardson, S.H., 1986. Latter-day origin of diamonds of eclogitic paragenesis. Nature 322, 623-626.

Richardson, S., Gurney, J., Erlank, A., Harris, J., 1984. Origin of diamonds in old enriched mantle. Nature 310, 198-202.

Richardson, S.H., Erlank, A.J., Hart, S.R., 1985. Kimberlite-borne garnet peridotite xenoliths from old enriched subcontinental lithosphere. Earth and Planetary Science Letters 75,116-128.

Richardson, S.H., Erlank, A.J., Harris, J.W., Hart, S.R., 1990. Eclogitic diamonds of Proterozoic age from Cretaceous kimberlites. Nature 346, 54-56.

Richardson, S.H., Harris, J.W., Gurney, J.J., 1993. Three generations of diamonds from old continental mantle. Nature 366, 256-258.

Richardson, S.H., Shirey, S.B., Harris, J.W., Carlson, R.W., 2001. Archean subduction recorded by Re-Os isotopes in eclogitic sulfide inclusions in Kimberley diamonds. Earth and Planetary Science Letters 191, 257-266.

Ringwood, A.E., 1977. Synthesis of pyrope-knorringite solid-solution series. Earth and Planetary Science Letters 36, 443-448.

Robb, L.R., Davis, D.W., Kamo, S.L., 1990. U-Pb ages on single detrital zircon grains from the Witwetersrand Basin: constraints on the age of sedimentation and on the evolution of granite adjacent to the basin. The Journal of Geology 98, 311-328.

Robb, L.R., Davis, D.W., Kamo, S.L., 1991. Chronological framework for the Witwatersrand basin and evolutions: towards a time-constrained depositional model. South African Journal of Geology 94, 86-95.

Roeting, C., Barton, J.M., Winterm H.R.d.l., 1990. The Vredefort structure: a perspective with regard to new tectonic data from adjoining terranes. Tectonophysics 171, 7-22.

Rudnick, R.L., Nyblade, A.A., 1999. The thickness and heat production of Archean lithosphere: constraints from xenolith thermobarometry and surface heat flow. In: Y. Fei, C.M. Bertka and Mysen (Editors), Mantle petrology: Field observation and high- pressure experimentation. Spec Pub No. The Geochemical Society, Washington, pp. 3-12.

Rudnick, R.L., McDonough, W.F., Chappell, B.W., 1993. Carbonatite metasomatism in the northern Tanzanian mantle – petrographic and geochemical characteristics. Earth and Planetary Science Letters 114, 463-475.

Rudnick, R.L., McDonough, W.F., Orpin, A., 1994. Northern Tanzanian xenoliths: a composition with Kaapvaal peridotites and inferences on metasomatic interactions. In: L.O. Meyer HOA (Editor), Kimberlites, related rocks and mantle xenoliths. CPRM Spec Pub Jan/94, Brazilia, pp.336-353.

Ryabchikov, I.D., Orlova, G.P., Senin, V.G., Trubkin, N.V., 1993. Partitioning of rare-earth elements between phosphate-rich carbonatite melt and mantle peridotites. Mineralogy and Petrology 49, 1-12.

Scherer, E.E., Cameron, K.L., Blichert-Toft, J., 2000. Lu-Hf garnet geochronology: Closure temperature relative to the Sm-Nd system and the effects of trace mineral inclusions. Geochimica Et Cosmochimica Acta 64, 3413-3432.

Scherer, E.E., Cameron, K.L., Johnson, C.M., Beard, B.L., Barovich, K.M., Collerson, K.D., 1997. Lu-Hf geochronology applied to dating Cenozoic events affecting lower crustal xenoliths from Kilbourne Hole, New Mexico. Chemical Geology 142, 63-78.

Schmidberger, S.S., Simonetti, A., Francis, D., Gariepy, C., 2002. Probing Archean lithosphere using the Lu-Hf isotope systematics of peridotite xenoliths from Somerset Island kimberlites, Canada. Earth and Planetary Science Letters 197, 245-259.

Schulze, D.J., 1986. Calcium anomalies in the mantle and a subducted metaserpentinite origin for diamonds. Nature 319, 483-485.

Schulze, D.J., 1987. Megacrysts from alkalic volcanic rocks. In: P.H. Nixon (Editor), Mantle xenolits. John Wiley, Chichester, pp. 433-453.

Schulze, D.J., 2003. A classification scheme for mantle-derived garnets in kimberlite: a tool for investigating the mantle and exploring for diamonds. Lithos 71, 195-213.

Schmitz, M.D., Bowring, S.A., 2003. Constraints on the thermal evolution of continental lithosphere from U-Pb accessory mineral thermochronometry of lower crustal xenoliths, southern Africa. Contributions to Mineralogy and Petrology 144, 592-618.

Schmitz, M.D., Vervoort, J.D., Bowring, S.A., Patchett, P.J., 2002. Decoupling of the Lu-Hf and Sm-Nd isotopic systems in granulitic lower crust beneath southern Africa. Geochimica Et Cosmochimica Acta 66, A682-A682.

Schmitz, M.D., Bowring, S.A., de Wit, M.J., Gartz, V., 2004. Subduction and terrane collision stabilize the western Kaapvaal craton tectosphere 2.9 billion years ago. Earth and Planetary Science Letters 222, 363-376.

Scott Smith, B.H., 1996. Kimberlites, in R.H. Mitchell (Editor), Undersaturated alkaline rocks: mineralogy, petrology and economic potential, Mineral association of Canada, pp. 217-243.

Seitz, H.-M., Woodland, A.B., 2000. The distribution of lithium in peridotitic and pyroxenitic mantle lithologies-an indicator of magmatic and metasomatic processes. Chemical Geology 166, 47-64.

Shee, S.R., Gurney, J.J., Robinson, D.N., 1982. Two diamond-bearing peridotitic xenoliths from the Finsch kimberlite, South Africa. Contributions to Mineralogy and Petrology 81 (2), 79–87.

Shimizu, N., Richardson, S.H., 1987. Trace-element abundance patterns of garnet inclusions in peridotite-suite diamonds. Geochimica Et Cosmochimica Acta 51, 755-758.

Shirey S.B., Carlson, R.W., Richardson, S.H., Menzies, A.H., Gurney, J.J., Pearson, D.G., Harris, J.W., Wiechert, U., 2001. Archean emplacement of eclogitic components into the lithospheric mantle during formation of the Kaapvaal Craton. Geophysical Research Letters 28, 2509-2512.

Shirey, S.B., Harris, J.W., Richardson, S. H., Fouch, M. J., James, D. E., Cartigny, P., Deines, P., Viljoen, F., 2002. Diamond genesis, seismic structure, and evolution of the Kaapvaal-Zimbabwe craton. Science 297, 1683-1686

Shirey S.B., Richardson, S.H., Harris, J.W., 2004. Integrated model of diamond formation and craton evolution. Lithos 77, 923-944.

Simon, N.S.C., 2004. The formation and modification of cratonic litospheric roots: A petrological and geochemical study of xenoliths from the Kaapvaal craton. PhD Thesis, Vrije University, Vrije, 251 pp.

Simon, N.S.C., Irvine, G.J., Davies, G.R., Pearson, D.G., Carlson, R.W., 2003. The origin of garnet and clinopyroxene in "depleted" Kaapvaal peridotites. Lithos 71, 289-322.

Simon, N.S.C., Carlson, R.W., Pearson, D.G., Davies, G.R., 2007. The Origin and Evolution of the Kaapvaal Cratonic Lithospheric Mantle. Journal of Petrology 48, 589-625.

Skinner, C.P., 1986. A study of the peridotite nodule suite from the Finsch kimberlite, South Africa. Unpubl. Hons. Thesis, Univ. Cape Town, 38 pp.

Smith, C.B., 1983. Pb, Sr and Nd isotopic evidence for sources of southern African Cretaceous kimberlites. Nature 304, 51-54.

Smith, D., 1999. Temperatures and pressures of mineral equilibration in peridotite xenoliths: Review, discussion, and implications. In: Y. Fei, C.M. Bertka and Mysen (Editors), Mantle petrology: Field observation and high- pressure experimentation. Spec Pub No.6, The Geochemical Society, Washington, pp. 171-188.

Smith C.B, Allsopp, H.L., Kramers, J.D., Hutchinson, G., Roddick, J.C., 1985. Emplacement ages of Jurassic-Cretaceous South African kimberlites by the Rb-Sr method on phlogopite and hole rock samples. Trans. of the Geol. Soc. South Africa 88, pp 249-287.

Suhr, G., Seck, H.A., Shimizu, N., Gunther, D., Jenner, G., 1998. Infiltration of refractory melts into the lowermost oceanic crust: evidence from dunite- and gabbro-hosted clinopyroxenes in the Bay of Islands ophiolite. Contributions to Mineralogy and Petrology 131, 136-154.

Stalder, R., Foley, S.F., Brey, G.P., Horn, I., 1998. Mineral aqueous fluid partitioning of trace elements at 900-1200 degrees C and 3.0-5.7 GPa: New experimental data for garnet, clinopyroxene, and rutile, and implications for mantle metasomatism. Geochimica Et Cosmochimica Acta 62, 1781-1801.

Stachel, T., Viljoen, K.S., Brey, G., Harris, J.W., 1998. Metasomatic processes in lherzolitic and harzburgitic domains of diamondiferous lithospheric mantle: REE in garnets from xenoliths and inclusions in diamonds. Earth and Planetary Science Letters 159, 1-12.

Stachel, T., Aulbach, S., Brey, G.P., Harris, J.W., Leost, I., Tappert, R., Viljoen, K. S., 2004. The trace element composition of silicate inclusions in diamonds: a review. Lithos 77, 1-19.

Streckeisen, A., 1976. To each plutonic rock its proper name. Earth-Science Reviews 12, 1-33.

Sobolev, N.V., Lavrente, Yg., Pokhilen. Np., Usova, L.V., 1973. Chrome-rich garnets from kimberlites of Yakutia and their parageneses. Contributions to Mineralogy and Petrology 40, 39-52.

Spera, F.J., 1984. Carbon dioxside in petrogenesis III: role of volatiles in the ascentof alkaline magma with special reference to xenolith bearing mafic lavas. Contributions to Mineralogy and Petrology 88, 217-232.

Sweeny, R.J., Thompso, A.B., Ulmer, P., 1993. Phase relations of a natural MARID composition and implication for MARID genesis, lithospheric mantle and mantle somatism. Contributions to Mineralogy and Petrology 141, 397-414.

Takazawa, E., Frey, F.A., Shimizu, N., Obata, M., 2000. Whole rock compositional variations in an upper mantle peridotite (Horoman, Hokkaido, Japan): are they consistent with a partial melting process? Geochimica et Cosmochimica Acta, 64(4): 695-716.

Thomas, R.J., von Veh, M.W., McCourt, S., 1993. The tectonic evolution of southern Africa: an overview. Journal of African Earth Sciences 16, 5-24.

Toramaru, A., Fuji, N., 1986. Connectivity of a melt phase in a partially molten peridotite. Journal of Geophysical Research 91, 9239-9252

Van Achterbergh, E., Griffin, W., Shee, S., Wyatt, B., Sharma, A., 1998. Natural trace element coefficients for garnet, clinopyroxene and orthopyroxene: variation with the temperautere and pressure, Abstr. 7th International Kimberlite conference, Cape Town, pp. 934-936.

Vervoort, J.D., Patchett, P.J., Blichert-Toft, J., Albarède, F., 1999. Relationships between Lu-Hf and Sm-Nd isotopic systems in the global sedimentary system. Earth and Planetary Science Letters 168, 79-99.

Viljoen, K.S., Swash P.M., Otter, D.J., Schulze D.J., Lawless, P.J., 1992. Diamondiferous garnet hartzburgites from the Finsch kimberlite, Northern Cape, South Africa. Contributions to Mineralogy and Petrology 110, 133-138.

Wagner P.A., 1914. The diamond fields of southern Africa. Transvaal Leader, Johannesbutg, 347 pp.

Walker, R.J., Carlson, R.W., Shirey, S.B., Boyd, F.R., 1989. Os, Sr, Nd and Pb isotope systematics of southern African peridotite xenoliths: Implications for the chemical evolution of subcontinental mantle. Geochimica Et Cosmochimica Acta 53, 1583-1595.

Walter, M.J. 1998. Melting of garnet peridotite and the origin of komatiite and depleted lithosphere. Journal of Petrology 39, 29-60.

Walter, M.J., 1999. Melting residues of fertile peridotite and the origin of cratonic lithosphere. In: Y. Fei, C.M. Bertka and Mysen (Editors), Mantle petrology: Field observation and high- pressure experimentation. Spec Pub No.6, The Geochemical Society, Washington, pp. 225-239.

Walter, M.J., 2003. Melt extraction and compositional variability in mantle lithosphere. In: Turekian, K.K., Holland, H.D. (Editors), Treatise on Geochemistry, Volume 2: The Mantle and Core, Amsterdam: Elsevier. pp. 363-395.

Wang, W.Y., Sueno, S., Takahashi, E., Yurimoto, H., Gasparik, T., 2000. Enrichment processes at the base of the Archean lithospheric mantle: observations from trace element characteristics of pyropic garnet inclusions in diamonds. Contributions to Mineralogy and Petrology 139, 720-733.

Weng, Y.-H., Presnall, D.C., 2001. The system diopside-forsterite-enstatite at 5.1 GPa: A Ternary model for melting of the mantle. Can. Mineral. 39, 299-308.

Wittig, N., Baker, J.A., Downes, H., 2006. Dating the mantle roots of young continental crust. Geology 34, 237-240.

Wittig, N., Baker, J.A., Downes, H., 2007. U-Th-Pb and Lu-Hf isotopic constraints on the evolution of sub-continental lithospheric mantle, French Massif Central. Geochimica Et Cosmochimica Acta 71, 1290-1311.

Woodland, A.B., Ross, C.R., 1994. A crystallographic and Mossbauer-spectroscopy study of $Fe^{2+}{}_3Al_2Si_3O_{12}$–$Fe^{2+}{}_3Fe^{3+}{}_2Si_3O_{12}$, (almandine-skiagite) and $Ca_3Fe^{3+}{}_2Si_3O_{12}$–$Fe^{2+}{}_3Fe^{3+}{}_2Si_3O_{12}$, (andradite-skiagite) garnet solid-solutions. Physics and Chemistry of Minerals 21, 117-132.

Woodland, A.B., Koch, M., 2003. Variation in oxygen fugacity with depth in the upper mantle beneath the Kaapvaal craton, Southern Africa. Earth and Planetary Science Letters 214, 295-310.

Wulff-Pedersen, E., Neumann, E.R., Vannucci, R., Bottazzi, P., Ottolini, L., 1999. Silicic melts produced by reaction between peridotite and infiltrating basaltic melts: ion probe data on glasses and minerals in veined xenoliths from La Palma, Canary Islands. Contributions to Mineralogy and Petrology 137, 59-82.

Wyatt, B.A., Lawless, 1984. Ilmenite in polymict xenoliths from the Bultfontein and De Beers Mines, South Africa. In: J. Kornprobst (Editor), Kimberlites II: The mantle and crust-mantle relationships, Proceedingd of the 3th International Kimberlite Conference, ELSEVIER, pp. 43-56.

Yaxley, G.M., Crawford, A.J., Green, D.H., 1991. Evidence for carbonatite metasomatism in spinel peridotite xenoliths from western Victoria, Australia. Earth and Planetary Science Letters 107, 305-317.

Yaxley, G.M., Green, D.H., Kamenetsky, V., 1998. Carbonatite metasomatism in the southeastern Australian lithosphere. Journal of Petrology 39, 1917-1930.

Zaback. M.L., Mooney, W.D., 2003. Lithospheric buoyancy and continental intraplate stresses. International Geology Review 45, 95-118.

Zhang, H. F., Mattey, D. P., Grassineau, N., Lowry, D., Brownless, M., Gurney, J. J., Menzies, M. A., 2000. Recent fluid processes in the Kaapvaal Craton, South Africa: coupled oxygen isotope and trace element disequilibrium in polymict peridotites. Earth and Planetary Science Letters 176, 57-72.

Zhang, H.F., Menzies, M.A., Gurney, J.J., Zhou, X.H., 2001. Cratonic peridotites and silica-rich melts: Diopside-enstatite relationships in polymict xenoliths, Kaapvaal, South Africa. Geochimica Et Cosmochimica Acta 65, 3365-3377.

Zhang, H.F., Menzies, M.A., Mattey, D., 2003. Mixed mantle provenance: diverse garnet compositions in polymict peridotites, Kaapvaal craton, South Africa. Earth and Planetary Science Letters 216, 329-346.

APPENDICES

Table 3.1.
Major element data of garnets from heavy mineral concentrates (HMC) from the Finsch mine, obtained by μ-XRF.

sample	SiO_2	CaO	MnO	MgO	Cr_2O_3	FeO	Al_2O_3	TiO_2	Total
HMCF-grt-1	43.16	4.93	0.33	19.64	4.30	6.84	19.62	0.08	98.9
HMCF-grt-2	42.95	5.31	0.32	21.05	4.86	7.18	20.57	0.04	102.4
HMCF-grt-3	43.21	2.77	0.36	21.35	6.17	6.59	17.97	0.04	98.4
HMCF-grt-4	43.81	4.66	0.34	21.13	4.41	7.42	20.87	0.04	102.6
HMCF-grt-5	40.99	4.82	0.32	20.07	4.62	6.49	18.89	0.02	96.2
HMCF-grt-6	42.85	4.87	0.34	19.31	5.57	6.31	17.35	b.d.l.	96.5
HMCF-grt-7	41.06	4.56	0.32	21.01	3.93	6.80	19.67	0.08	97.3
HMCF-grt-8	42.48	5.53	0.36	19.19	5.91	6.75	18.75	0.00	98.9
HMCF-grt-9	42.78	4.59	0.34	20.62	3.82	7.28	20.32	0.03	99.8
HMCF-grt-10	44.81	5.84	0.34	21.02	6.17	7.02	19.88	0.05	105.2
HMCF-grt-11	42.24	2.71	0.32	22.15	4.64	6.61	19.93	0.06	98.7
HMCF-grt-12	44.03	1.14	0.32	25.31	5.21	6.50	20.08	b.d.l.	102.6
HMCF-grt-13	43.41	3.11	0.33	22.45	5.53	6.79	20.39	0.02	102.0
HMCF-grt-14	43.48	3.63	0.33	23.38	4.71	6.72	21.07	0.05	103.4
HMCF-grt-15	44.20	4.84	0.33	21.79	3.16	7.78	22.23	0.06	104.4
HMCF-grt-16	41.36	5.26	0.32	19.57	6.26	6.44	16.76	0.42	96.4
HMCF-grt-17	43.43	5.10	0.32	17.52	5.11	7.09	17.11	0.05	95.7
HMCF-grt-18	41.80	4.45	0.33	21.02	5.95	6.37	18.16	0.02	98.1
HMCF-grt-19	42.74	4.97	0.35	17.00	5.49	7.39	19.77	0.09	97.8
HMCF-grt-20	47.95	2.83	0.30	19.30	3.36	6.95	18.41	0.05	99.2
HMCF-grt-21	42.87	4.89	0.32	20.45	4.64	6.55	19.64	0.29	99.7
HMCF-grt-22	43.13	6.62	0.34	18.27	8.28	7.04	17.16	0.19	101.1
HMCF-grt-23	43.26	4.95	0.35	19.60	6.16	6.68	17.73	0.15	98.9
HMCF-grt-24	43.24	5.29	0.32	20.25	4.79	7.22	19.11	0.04	99.9
HMCF-grt-25	42.10	4.60	0.32	21.41	3.96	7.36	20.55	0.05	100.4
HMCF-grt-26	42.07	4.71	0.32	21.53	3.68	7.34	21.44	0.02	101.1
HMCF-grt-27	42.61	5.17	0.33	20.29	2.62	8.07	21.54	0.00	100.6
HMCF-grt-28	41.00	1.86	0.30	25.01	3.69	6.68	20.85	b.d.l.	99.4
HMCF-grt-29	41.11	1.76	0.31	23.62	3.50	6.82	20.38	b.d.l.	97.5
HMCF-grt-30	42.16	4.17	0.34	21.18	4.40	7.18	20.17	b.d.l.	99.6
HMCF-grt-31	41.26	2.51	0.33	23.31	4.78	6.38	19.68	b.d.l.	98.3
HMCF-grt-32	46.83	2.69	0.33	20.97	5.08	7.19	18.33	0.04	101.5
HMCF-grt-33	43.82	2.64	0.33	20.67	4.71	7.33	19.29	0.03	98.8
HMCF-grt-34	43.72	4.92	0.35	20.53	4.35	7.09	19.84	0.03	100.8
HMCF-grt-35	48.55	0.95	0.34	16.13	5.49	7.52	19.69	0.04	98.7
HMCF-grt-36	42.79	4.67	0.32	20.25	3.95	7.36	20.01	0.01	99.4
HMCF-grt-37	43.20	2.87	0.32	22.29	4.83	6.96	20.04	0.07	100.6
HMCF-grt-38	44.46	2.05	0.31	22.39	3.42	6.32	19.36	b.d.l.	98.3
HMCF-grt-39	42.73	2.25	0.29	21.36	5.89	6.44	19.38	0.10	98.4
HMCF-grt-40	51.58	4.85	0.32	14.28	3.68	7.55	15.29	0.01	97.6
HMCF-grt-41	41.50	4.19	0.32	20.74	2.48	7.99	21.01	b.d.l.	98.2
HMCF-grt-42	43.48	4.50	0.32	17.94	3.74	7.63	20.26	0.04	97.9
HMCF-grt-43	45.12	1.42	0.31	21.77	4.50	6.95	18.11	0.00	98.2
HMCF-grt-44	41.64	4.46	0.33	21.88	3.24	7.21	21.24	b.d.l.	100.0
HMCF-grt-45	41.21	4.45	0.32	22.01	4.03	6.74	20.55	0.14	99.5
HMCF-grt-46	42.14	4.26	0.34	20.66	2.45	8.21	21.96	0.05	100.1
HMCF-grt-47	41.07	4.17	0.33	21.01	2.40	7.79	22.36	b.d.l.	99.1
HMCF-grt-48	43.54	4.68	0.31	18.99	3.45	7.23	18.73	0.07	97.0
HMCF-grt-49	42.02	4.18	0.33	22.98	1.75	7.64	23.56	0.01	102.5

Table 3.1. *(continued)*

sample	SiO_2	CaO	MnO	MgO	Cr_2O_3	FeO	Al_2O_3	TiO_2	Total
HMCF-grt-50	41.04	4.18	0.34	20.61	2.38	7.99	21.31	0.01	97.9
HMCF-grt-51	41.65	4.40	0.31	22.15	3.48	7.14	21.35	0.42	100.9
HMCF-grt-52	44.63	4.27	0.32	20.49	2.60	8.12	20.26	0.07	100.7
HMCF-grt-53	41.85	4.32	0.32	20.30	2.77	7.77	20.60	0.08	98.0
HMCF-grt-54	42.50	4.23	0.32	20.48	2.90	7.60	19.62	0.09	97.5
HMCF-grt-55	41.45	4.16	0.32	22.21	2.57	7.26	21.98	0.10	100.0
HMCF-grt-56	42.61	4.73	0.32	22.56	3.09	7.30	22.32	0.13	103.1
HMCF-grt-57	41.60	4.18	0.31	20.55	2.63	7.49	20.28	0.06	97.1
HMCF-grt-58	42.89	2.97	0.30	23.11	2.66	6.71	22.07	0.11	100.8
HMCF-grt-59	40.94	4.17	0.33	22.02	2.78	7.37	21.68	0.13	99.4
HMCF-grt-60	41.52	3.92	0.32	21.22	2.73	7.10	20.63	0.21	97.7
HMCF-grt-61	47.28	4.49	0.32	18.71	3.35	7.64	18.29	0.04	100.1
HMCF-grt-62	42.77	4.41	0.34	21.32	2.27	8.61	22.31	0.06	102.0
HMCF-grt-63	45.26	4.57	0.35	18.29	2.43	8.75	21.74	0.07	101.5
HMCF-grt-64	45.37	4.62	0.36	19.66	2.98	8.47	20.57	0.07	102.1
HMCF-grt-65	43.20	4.32	0.35	19.64	2.79	8.37	20.10	0.02	98.8
HMCF-grt-66	42.70	4.32	0.32	23.49	2.65	7.53	22.79	0.04	103.8
HMCF-grt-67	42.69	2.82	0.32	23.44	4.23	6.64	20.62	0.12	100.9
HMCF-grt-68	48.36	4.49	0.34	18.07	2.43	8.46	20.12	0.07	102.4
HMCF-grt-69	44.28	4.24	0.33	19.23	2.73	8.13	19.47	0.07	98.4
HMCF-grt-70	41.40	4.35	0.32	21.76	3.14	7.37	21.43	0.09	99.8
HMCF-grt-71	42.27	4.40	0.33	22.44	2.87	7.40	22.24	0.17	102.1
HMCF-grt-72	41.85	4.30	0.34	22.38	2.84	8.16	22.08	0.03	102.0
HMCF-grt-73	42.29	4.30	0.32	21.16	2.99	7.46	20.50	0.06	99.1
HMCF-grt-74	40.72	4.22	0.31	22.55	2.86	6.85	21.41	0.11	98.6
HMCF-grt-75	44.76	4.38	0.33	19.15	3.64	7.38	18.91	0.03	98.4
HMCF-grt-76	43.01	4.67	0.33	20.33	3.63	7.31	19.98	0.09	99.4
HMCF-grt-77	43.24	4.91	0.34	19.61	4.41	7.60	20.56	0.15	100.8
HMCF-grt-78	41.72	4.35	0.33	21.28	2.62	8.05	21.58	0.12	100.0
HMCF-grt-79	42.82	4.72	0.39	20.65	3.71	7.84	20.64	0.12	100.9
HMCF-grt-80	41.63	4.23	0.32	21.31	2.96	7.86	20.67	0.03	99.0
HMCF-grt-81	43.04	4.75	0.33	20.45	4.53	6.87	19.37	0.18	99.5
HMCF-grt-82	41.95	4.23	0.32	20.83	4.42	7.10	19.61	0.16	98.6
HMCF-grt-83	41.80	4.61	0.32	21.93	3.49	6.80	21.23	0.27	100.4
HMCF-grt-84	42.88	3.88	0.34	21.25	2.79	7.90	19.85	0.10	99.0
HMCF-grt-85	43.90	4.50	0.35	20.12	4.57	7.20	20.28	0.16	101.1
HMCF-grt-86	42.96	4.72	0.38	19.95	2.62	9.07	22.12	0.17	102.0
HMCF-grt-87	44.02	4.28	0.32	19.92	2.36	7.72	20.01	0.19	98.8
HMCF-grt-88	42.96	4.30	0.32	20.37	2.59	7.72	20.42	0.15	98.8
HMCF-grt-89	41.56	4.47	0.32	21.42	2.82	7.50	21.07	0.14	99.3
HMCF-grt-90	41.29	4.08	0.30	22.16	2.40	7.36	21.72	0.09	99.3
HMCF-grt-91	41.26	4.18	0.34	21.67	2.44	7.50	21.44	0.16	99.0
HMCF-grt-92	42.35	4.12	0.31	21.98	2.28	7.43	21.53	0.09	100.1
HMCF-grt-93	48.12	4.20	0.34	17.13	2.53	7.33	17.01	0.19	96.8
HMCF-grt-94	43.94	4.31	0.32	19.82	2.94	7.69	20.25	0.09	99.4
HMCF-grt-95	43.84	4.59	0.32	19.98	3.69	6.91	19.17	0.22	98.5
HMCF-grt-96	42.90	4.24	0.31	22.71	2.21	7.67	22.74	0.11	102.8
HMCF-grt-97	42.47	4.24	0.32	21.54	2.39	7.94	21.91	0.10	100.9
HMCF-grt-98	43.25	3.96	0.29	20.38	1.32	7.26	20.89	0.02	97.4
HMCF-grt-99	42.22	4.19	0.32	22.03	2.28	7.85	21.99	0.13	101.0

Table 3.1. *(continued)*

sample	SiO_2	CaO	MnO	MgO	Cr_2O_3	FeO	Al_2O_3	TiO_2	Total
HMCF-grt-100	42.16	4.29	0.33	20.15	2.64	7.60	20.23	0.20	97.6
HMCF-grt-101	45.25	4.45	0.32	21.65	2.42	8.14	22.28	0.09	104.6
HMCF-grt-102	43.17	4.40	0.32	19.84	3.06	7.46	18.95	0.11	97.3
HMCF-grt-103	41.89	4.30	0.32	20.92	2.18	7.96	21.17	0.07	98.8
HMCF-grt-104	41.36	4.13	0.32	22.67	2.20	7.83	22.25	0.09	100.8
HMCF-grt-105	41.92	4.24	0.33	21.72	2.39	7.86	21.50	0.09	100.0
HMCF-grt-106	40.83	4.23	0.32	20.88	2.57	7.75	20.72	0.12	97.4
HMCF-grt-107	43.74	4.07	0.32	21.53	2.23	8.08	21.55	0.10	101.6
HMCF-grt-108	42.08	3.98	0.29	22.74	2.25	7.88	22.91	0.08	102.2
HMCF-grt-109	42.61	4.16	0.31	21.58	2.45	7.73	21.61	0.12	100.5
HMCF-grt-110	42.99	4.25	0.38	19.73	2.92	7.60	19.53	0.15	97.5
HMCF-grt-111	41.44	4.20	0.31	22.88	2.34	6.75	22.11	0.09	100.1
HMCF-grt-112	43.64	4.60	0.36	19.97	2.91	8.53	21.27	0.10	101.4
HMCF-grt-113	46.47	4.67	0.32	19.21	3.68	7.97	18.07	0.06	100.5
HMCF-grt-114	41.01	4.31	0.33	21.49	2.98	7.49	21.23	0.10	98.9
HMCF-grt-115	42.41	4.36	0.32	23.05	2.80	7.55	22.90	0.06	103.3
HMCF-grt-116	41.10	4.10	0.31	22.09	2.41	7.42	22.02	0.08	99.5
HMCF-grt-117	41.86	4.29	0.30	20.90	3.25	7.68	20.70	0.06	99.0
HMCF-grt-118	41.28	4.03	0.31	20.74	2.54	7.27	20.25	0.11	96.5
HMCF-grt-119	40.76	4.35	0.33	21.53	3.16	7.27	21.33	0.19	98.9
HMCF-grt-120	45.50	4.21	0.31	19.07	2.91	7.22	18.78	0.10	98.1
HMCF-grt-121	50.83	4.50	0.33	14.90	3.34	8.24	17.53	0.09	99.8
HMCF-grt-122	42.36	4.34	0.31	20.80	3.16	7.32	19.66	0.14	98.1
HMCF-grt-123	41.90	4.24	0.32	22.39	2.49	7.64	22.15	0.10	101.2
HMCF-grt-124	41.53	4.66	0.33	22.15	3.70	6.86	21.07	0.27	100.6
HMCF-grt-125	43.03	4.15	0.31	21.46	2.40	7.54	21.21	0.16	100.2
HMCF-grt-126	42.25	4.26	0.32	22.80	2.68	7.42	22.42	0.04	102.2
HMCF-grt-127	42.71	4.63	0.33	21.98	3.25	7.72	22.15	0.15	102.9
HMCF-grt-128	42.28	4.09	0.31	21.16	2.39	7.59	21.24	0.06	99.1
HMCF-grt-129	42.44	4.43	0.33	21.61	3.22	7.25	20.79	0.27	100.1
HMCF-grt-130	41.28	4.17	0.32	22.52	2.57	7.48	22.00	0.06	100.2
HMCF-grt-131	45.32	4.40	0.33	17.99	2.88	8.17	19.59	0.11	98.8
HMCF-grt-132	40.72	4.21	0.29	22.80	3.30	7.57	21.84	0.14	100.9
HMCF-grt-133	42.27	4.61	0.32	20.27	3.93	7.78	20.26	0.19	99.6
HMCF-grt-134	41.68	4.33	0.31	21.32	3.85	7.49	20.41	0.19	99.6
HMCF-grt-135	41.27	4.12	0.31	21.61	2.41	7.44	20.90	0.13	98.2
HMCF-grt-136	44.14	4.32	0.32	21.50	2.70	7.76	21.49	0.08	102.3
HMCF-grt-137	40.88	4.07	0.35	22.23	2.06	7.00	21.64	0.09	98.3
HMCF-grt-138	41.73	4.38	0.34	22.67	2.96	7.42	21.98	0.09	101.6
HMCF-grt-139	43.32	4.11	0.32	20.02	2.22	7.70	20.78	0.09	98.5
HMCF-grt-140	45.47	4.43	0.32	19.91	2.42	8.31	20.70	0.07	101.6
HMCF-grt-141	41.57	4.42	0.36	20.29	2.32	8.74	21.86	0.16	99.7

***Table 3.2**. Major and minor element compositions of subcalcic garnets from the Finsch mine, obtained by EPMA. Values are in wt%.*

	Sample	SiO_2	Na_2O	CaO	MnO	MgO	Cr_2O_3	FeO	Al_2O_3	TiO_2	Total	Mg#	Ca#	Cr#
	HMCF-grt 12	43.03	0.02	0.83	0.24	25.40	4.09	5.05	21.22	0.02	99.92	90.0	2.3	11.4
	HMCF-grt 20	42.97	0.04	2.55	0.24	23.85	2.89	5.52	21.84	0.05	100.01	88.5	7.2	8.1
	HMCF-grt 28	43.01	0.02	1.62	0.27	24.23	3.35	5.86	21.54	0.01	99.93	86.9	4.6	9.5
group	HMCF-grt 29	43.03	0.02	1.53	0.27	24.28	3.14	5.82	21.73	0.02	99.86	88.1	4.3	8.8
1	HMCF-grt 35	43.14	0.02	0.34	0.24	25.87	4.04	4.98	21.26	0.01	99.91	89.9	0.9	11.3
	HMCF-grt 38	43.19	0.04	1.77	0.23	24.81	3.06	5.02	21.96	0.04	100.14	89.8	4.9	8.5
	HMCF-grt 43	43.10	0.05	1.05	0.25	25.32	3.61	5.09	21.72	0.02	100.29	89.9	2.9	10.0
	HMCF-grt 58	43.11	0.04	2.69	0.25	23.71	2.46	5.57	22.12	0.05	100.03	88.3	7.7	6.9
	HMCF-grt 3	42.42	0.03	2.42	0.28	23.61	5.33	5.66	20.11	0.08	100.00	88.1	6.9	15.1
	HMCF-grt 11	42.65	0.04	2.38	0.28	23.88	4.03	5.55	21.25	0.07	100.19	88.5	6.7	11.3
	HMCF-grt 13	42.63	0.04	2.66	0.27	23.43	4.64	5.64	20.64	0.04	100.06	88.1	7.5	13.1
	HMCF-grt 14	42.62	0.05	3.18	0.29	23.15	4.05	5.65	21.06	0.05	100.17	87.9	9.0	11.5
	HMCF-grt 18	42.28	0.02	4.35	0.28	21.90	5.68	6.05	19.48	0.03	100.13	86.6	12.5	16.4
	HMCF-grt 30	42.36	0.04	4.02	0.36	21.62	4.09	6.61	20.86	0.02	100.09	87.9	11.8	11.6
group	HMCF-grt 32	42.78	0.02	2.35	0.29	23.78	4.25	5.77	20.77	0.07	100.12	88.9	6.6	12.1
2	HMCF-grt 33	42.80	0.03	2.26	0.27	23.76	3.86	5.80	21.20	0.02	100.04	87.9	6.4	10.9
	HMCF-grt 37	42.77	0.05	2.43	0.26	23.73	4.06	5.59	21.05	0.08	100.09	90.9	6.8	11.5
	HMCF-grt 39	42.95	0.05	1.88	0.23	24.53	4.42	4.94	20.91	0.10	100.07	89.9	5.2	12.4
	HMCF-grt 67	42.86	0.04	2.56	0.27	23.59	3.90	5.60	21.02	0.13	100.02	91.9	7.2	11.1
	HMCF-grt 82	42.33	0.05	4.10	0.31	21.53	4.07	6.82	20.67	0.17	100.08	84.9	12.0	11.7
	HMCF-grt 85	42.28	0.05	4.21	0.35	21.69	4.36	6.36	20.51	0.16	100.00	85.9	12.2	12.5
	F2-grt	41.99	0.04	5.50	0.32	20.97	7.80	6.17	17.80	0.20	100.85	85.2	15.9	22.7
	F7-grt	41.99	0.02	4.90	0.31	21.70	7.59	6.13	18.16	0.07	100.93	85.7	14.0	21.9
	882-grt	40.93	b.d.l.	6.14	0.33	20.22	11.63	5.59	14.96	0.17	99.97	86.6	17.9	34.3

***Table 3.3**. LA-ICP-MS analyses of trace element concetration of subcalcic garnets from the Finsch mine. Values are averages of several spot analyses (in ppm). The $(Lu/Er)_N$ ratios are normalized to C-1 chondrite (McDonough and Sun, 1995).*

Abbreviations: n – number of spot analyses; b.d.l.- below detection limit; n.a. – not analysed; T (°C) Canil – temperatures calculated by Ni in garnet thermometer from Canil (1999) and T(°C) Griffin - temperatures calculated by Ni in garnet thermometer from Griffin et al. (1989).

	group-1							
n	**2**	**4**	**2**	**3**	**2**	**3**	**2**	**3**
sample	**HMCF-gtr 12**	**HMCF-gtr 20**	**HMCF-gtr 28**	**HMCF-gtr 29**	**HMCF-gtr 35**	**HMCF-gtr 38**	**HMCF-gtr 43**	**HMCF-gtr 58**
B	0.28	0.32	0.29	0.32	0.30	0.35	0.27	0.55
Sc	83	92	89	95	79	107	82	69
V	174	186	253	278	187	177	185	192
Co	44	47	46	52	44	56	43	42
Ni	56	55	48	54	50	65	43	52
Cu	b.d.l.	0.12	b.d.l.	b.d.l.	b.d.l.	0.08	b.d.l.	0.06
Zn	9.5	9.6	9.6	10.4	8.7	11.3	8.5	9.5
Ga	4.2	3.9	4.6	4.6	3.8	4.4	3.3	4.5
Rb	b.d.l.	b.d.l.	0.02	b.d.l.	b.d.l.	b.d.l.	b.d.l.	0.01
Sr	0.71	0.94	1.4	4.5	2.51	0.53	1.58	1.01
Y	0.3	4.9	0.9	1.3	0.2	3.3	0.8	5.8
Zr	2.9	25	1.0	4.0	1.6	6.3	15	10.4
Nb	0.39	1.0	0.56	0.87	0.65	0.74	0.98	0.14
Mo	0.16	0.40	0.39	0.44	0.23	0.39	0.19	0.26
Ba	0.01	0.03	0.02	0.03	0.03	0.01	0.02	0.01
La	0.05	0.12	0.34	0.74	0.23	0.08	0.16	0.04
Ce	0.74	1.6	4.5	6.4	6.3	1.1	3.9	0.92
Nd	1.0	3.1	2.5	2.6	6.0	2.9	9.2	1.8
Sm	0.2	1.5	0.2	0.2	0.6	1.1	2.5	0.4
Eu	0.07	0.49	0.02	0.04	0.07	0.34	0.54	0.11
Gd	0.20	1.5	0.05	0.09	0.13	0.68	1.0	0.34
Tb	0.02	0.13	0.00	0.01	0.01	0.04	0.06	0.05
Dy	0.07	0.69	0.04	0.06	0.03	0.25	0.20	0.53
Ho	0.01	0.15	0.02	0.03	0.01	0.10	0.03	0.18
Er	0.04	0.58	0.16	0.23	0.02	0.54	0.08	0.74
Tm	0.01	0.11	0.04	0.05	0.01	0.11	0.01	0.13
Yb	0.14	1.0	0.55	0.68	0.11	1.2	0.17	1.2
Lu	0.04	0.22	0.13	0.16	0.04	0.27	0.05	0.23
Hf	0.06	0.50	0.02	0.05	0.02	0.11	0.22	0.20
Ta	0.03	0.07	0.02	0.04	0.03	0.04	0.09	0.01
W	0.01	b.d.l.	0.01	b.d.l.	b.d.l.	0.01	0.92	0.01
Pb	0.01	0.21	0.01	0.01	0.01	0.01	0.02	0.01
Th	0.01	0.04	0.28	0.14	0.08	0.05	0.05	0.01
U	0.01	0.05	0.10	0.10	0.17	0.11	0.16	0.02
$(Lu/Er)_N$	7.6	2.4	5.5	4.3	13.0	3.2	4.2	2.0
T (C°)								
Griffin	1142	1123	1077	1113	1088	1195	1041	1133
Canil	1075	1070	1042	1065	1050	1107	1023	1067

Table 3.3. *(continued)*

	group-2															
n	**2**	**2**	**2**	**3**	**2**	**3**	**2**	**2**	**3**	**2**	**2**	**3**	**3**	**4**	**5**	**3**
Sam.	**HMCF-gtr 3**	**HMCF-gtr11**	**HMCF-gtr13**	**HMCF-gtr14**	**HMCF-grt18**	**HMCF-grt30**	**HMCF-grt32**	**HMCF-grt33**	**HMCF-grt37**	**HMCF-grt39**	**HMCF-grt67**	**HMCF-grt82**	**HMCF-grt85**	**F2-grt**	**F7-grt**	**882-grt**
B	0.32	0.24	0.34	0.30	0.15	0.28	0.30	0.29	0.32	0.29	0.29	0.28	0.30	0.51	1.95	0.46
Sc	119	110	101	107	68	109	88	88	105	111	101	104	117	150	107	182
V	211	261	259	226	185	161	188	248	253	192	201	203	259	375	303	288
Co	51	54	46	45	28	50	49	44	52	51	47	50	44	46	40	38
Ni	69	59	49	49	44	41	69	46	57	59	55	61	50	74	59	61
Cu	0.12	b.d.l.	b.d.l.	0.07	0.04	b.d.l.	0.08	b.d.l.	0.06	0.07	0.11	0.16	0.07	0.14	b.d.l	b.d.l.
Zn	12.1	10.7	9.0	8.1	5.5	9.2	12.9	9.1	10.1	10.4	10.9	11.3	9.5	11.3	8.8	10.7
Ga	5.0	3.0	2.8	2.4	2.0	2.5	4.7	5.1	3.0	4.4	5.0	5.1	5.4	7.6	n.a	5.4
Rb	b.d.l.	0.03	b.d.l.	0.02	b.d.l.	0.07	0.02	b.d.l.	0.02	b.d.l.	0.02	0.02	0.02	0.03	0.05	b.d.l.
Sr	0.52	0.58	0.41	0.47	0.44	0.40	0.62	0.86	0.56	1.02	0.99	0.23	0.65	1.08	0.36	2.09
Y	3.1	5.3	1.8	3.9	1.6	17	2.6	1.6	5.5	3.7	5.3	6.6	11.0	9.2	2.7	6.3
Zr	30	67	38	77	16	155	15	9.3	65	32	37	12.0	62	19	23	43
Nb	0.42	0.80	0.53	0.51	0.19	0.58	0.46	1.1	0.82	1.22	1.35	0.52	0.62	1.63	0.34	2.43
Mo	0.34	0.33	0.33	0.45	0.19	0.51	0.45	0.35	0.35	0.33	0.35	0.45	0.55	0.41	b.d.l	0.51
Ba	b.d.l	0.01	0.02	0.01	b.d.l	0.60	0.01	0.01	0.05	0.01	0.01	0.01	0.06	0.01	b.d.l	0.02
La	0.03	0.05	0.05	0.04	0.02	0.06	0.02	0.20	0.05	0.10	0.07	0.04	0.04	0.17	0.01	0.19
Ce	0.55	0.93	0.85	0.74	0.45	1.4	0.45	2.6	0.93	1.7	1.8	0.55	0.82	1.9	0.27	2.5
Nd	3.2	3.8	3.6	2.5	1.6	3.7	2.7	2.9	3.8	5.4	5.0	0.9	3.4	3.1	2.3	7.5
Sm	2.1	2.5	1.8	2.1	1.1	3.0	1.3	0.6	2.5	1.5	1.6	0.5	1.8	1.1	1.8	2.9
Eu	0.64	0.57	0.59	0.87	0.32	1.4	0.35	0.16	0.56	0.40	0.38	0.29	0.57	0.42	0.62	0.78
Gd	2.2	1.5	1.5	2.6	0.93	5.6	1.0	0.40	1.4	1.1	1.1	1.1	1.7	1.3	1.7	2.1
Tb	0.20	0.16	0.13	0.24	0.08	0.75	0.11	0.03	0.16	0.14	0.12	0.17	0.21	0.18	0.17	0.21
Dy	0.84	1.03	0.50	1.06	0.36	4.2	0.60	0.22	1.1	0.80	0.86	1.1	1.5	1.3	0.75	1.2
Ho	0.10	0.18	0.06	0.14	0.05	0.61	0.09	0.05	0.19	0.13	0.18	0.21	0.36	0.32	0.10	0.21
Er	0.18	0.45	0.14	0.27	0.11	1.0	0.19	0.22	0.45	0.30	0.60	0.51	1.17	1.07	0.18	0.59
Tm	0.02	0.05	0.02	0.03	0.01	0.08	0.02	0.05	0.05	0.04	0.09	0.06	0.16	0.15	0.03	0.08
Yb	0.19	0.42	0.27	0.35	0.14	0.46	0.21	0.53	0.39	0.36	0.85	0.52	1.3	1.3	0.17	0.63
Lu	0.05	0.09	0.08	0.08	0.04	0.08	0.05	0.12	0.08	0.09	0.18	0.10	0.23	0.22	0.03	0.11
Hf	0.59	1.4	0.65	1.31	0.31	1.4	0.32	0.21	1.3	0.69	0.83	0.23	1.3	0.48	0.51	1.0
Ta	0.03	0.09	0.04	0.04	0.01	0.04	0.04	0.06	0.09	0.09	0.11	0.04	0.06	0.21	0.04	0.49
W	0.56	b.d.l.	0.01	0.01	b.d.l.	0.02	b.d.l.	3.9	b.d.l.	0.01	b.d.l.	b.d.l.	b.d.l.	0.03	b.d.l	0.02
Pb	0.01	0.01	0.02	0.01	b.d.l.	0.01	0.03	0.01	0.01	0.02	0.02	0.01	b.d.l.	0.03	0.25	0.01
Th	0.01	0.02	0.01	0.01	b.d.l.	0.01	0.01	0.14	0.02	0.04	0.02	0.01	0.01	0.11	0.01	0.08
U	0.03	0.05	0.06	0.03	0.03	0.07	0.02	0.11	0.05	0.08	0.08	0.04	0.05	0.09	0.02	0.13
$(Lu/Er)_N$	1.7	1.4	3.6	2.0	2.2	0.5	1.8	3.6	1.2	1.9	1.9	1.3	1.3	1.4	1.2	1.2
T (C°) Griffin	1213	1165	1095	1079	1047	1022	1218	1061	1141	1152	1126	1170	1090			
Canil	1119	1086	1047	1047	1024	1013	1118	1034	1079	1086	1069	1092	1053			

Table 1. in App.-2

Sample	Content	Modal mineral content					Type	texture/structure
		ol	opx	cpx	grt	other		
F-1	ol, opx, cpx, grt	68	19.7	2.1	10.2	sp, cc	harzburgite	mosaic-porphyroclastic
F-2	ol, opx,grt	94	3.5	/	2.5	phl, sp, am-cpx	cpx-free dunite	coarse-grain tabular
F-3	ol, opx, cpx, grt	89	8	0.5	2.5	phl, sp, sulf, am-cpx	cpx-bearing dunite	coarse-grain tabular
F-4	ol, opx, cpx, grt	74	20	1	5	am-cpx sp	harzburgite	mosaic-porphyroclastic/foliated
F-5	ol, opx, cpx, grt	56	39	0.7	4.3	am-cpx sp	harzburgite	porphyroclastic
F-6	ol, opx, cpx, grt	65	23	4.3	7.7	phl, sp, am-cpx	harzburgite	coarse-grain equant
F-7	ol, opx,grt	57	36	/	7	phl,am, sp,sulf	cpx-free harzburgite	coarse-grain tabular
F-8	ol, opx, cpx, grt	93	4	0.5	2.5	phl, sp, am-cpx,	cpx-bearing dunite	coarse-grain tabular
F-9	ol, opx, cpx, grt	82	16	0.01	2	phl, sp, sulf	harzburgite	coarse-grain equant
F-10	ol, opx, cpx, grt	58.8	30	1.8	9.4	am-cpx, phl, sp	harzburgite	medium to coarse-grain to porphyroclastic/foliated
F-11	ol, opx, cpx, grt	77	17.7	1.3	4	phl, sp, am-cpx	harzburgite	coarse-grain tabular
F-12	ol, opx, cpx, grt, rt	69	20	3.4	6.6	rt ~1 wt%, sp, sulf	harzburgite	coarse-grain tabular
F-13	ol, opx, cpx, grt	57.5	24	6	12.5	phl, sulf	lherzolite	fine-grain equant to porphyroclastic/foliated
F-14	ol, opx, cpx, grt	76.5	20	0.5	3	am-cpx, phl, sp	harzburgite	coarse-grain equant
F-15	ol, opx, cpx, grt	66	17.5	4.5	12	am, phl, sulf.	lherzolite	carse-grain tabular
F-16	ol, opx, cpx, grt	57	27.5	6.5	9	am-cpx, sp, sulf	lherzolite	coarse-grain equant
F-21	ol, opx			?	?	-	harzburgite	coarse-grain tabular
F-22	ol, opx,grt, (cpx)					sp, am	harzburgite	medium- to coarse-grain equant
F-23	ol, opx, sp			?	sp	-	harzburgite	medium- to coarse-grain/foliated
F-24	ol, opx,grt, (cpx)					phl, sp, am-cpx	harzburgite	coarse-grain tabular
F-25-1a	ol, opx,grt, (cpx)					am-cpx, sp	harzburgite	coarse-grain tabular
F-25-1b	ol, opx, cpx, grt					sp, phl, am-cpx	harzburgite	mosaic porphyroclastic
F-25-1c	ol, opx, cpx, grt					am-cpx, phl, sp	harzburgite	porphyroclastic
F-25-1d	ol, opx,grt, (cpx)					am-cpx, phl, sp	harzburgite	coarse-grain tabular
F-26	ol, opx, cpx, grt					am-cpx, phl, sp	lherzolite	porphyroclastic/foliated
F-28	ol, opx,			?	?	-	harzburgite	coarse-grain tabular

Modal analyses thick sections were performed by counting mineral surfaces of 1 or 2 sample cross cuts sketched on transparent millimetre paper (as it is shown on Fig 2b). For samples from F-21 to F-28 only thin samples were available and therefore no modal analyses were calculated.

ol-olivine, opx-orthopyroxene, cpx-clinopyroxene, grt-garnet; sp-spinel; rt-rutile; am-amphibole; phl-phlogopite; sulf-sulfide; cc-calcite;

"(cpx)"- cpx is not observed, but garnet is Ca-saturated pointing its existence;

"?"- not observed in thin section and not sure if exist;

Finsch F-1:

Sample F-1 is a garnet bearing harzburgite with not more than 2 vol.% cpx. Fine grain (100-400 µm) strongly serpentinised neoblastic olivine makes more than half of the rock volume resulting in a mosaic-porphyroclastic texture of this peridotite (Fig. A1a,b). Usually associating, both, diopside and enstatite have tabular elongated to oval elongated shape (Fig. A1b,c,e). Less abundant diopsides are smaller (up to 2 mm length) than enstatite, while the average size of enstatite is between 5-6 mm. Opx shows strong irregular undulose extinction while cpx has thin lamely undulose extinction. Light green diopside is sometimes strongly deformed with severe kink bending (Fig. A1c). The opx-cpx contact is marked with serpentine and small recrystallized cpx grains are also present (Fig. A1c).Garnets are slightly fractured rounded or irregular grains (3-6 mm) with relatively thin kelyphite rims (Fig. A1d). Octahedral spinels are common minerals in garnet reaction rims. Beside sp and am, Ca-carbonates (?) occur in garnet kelyphite.

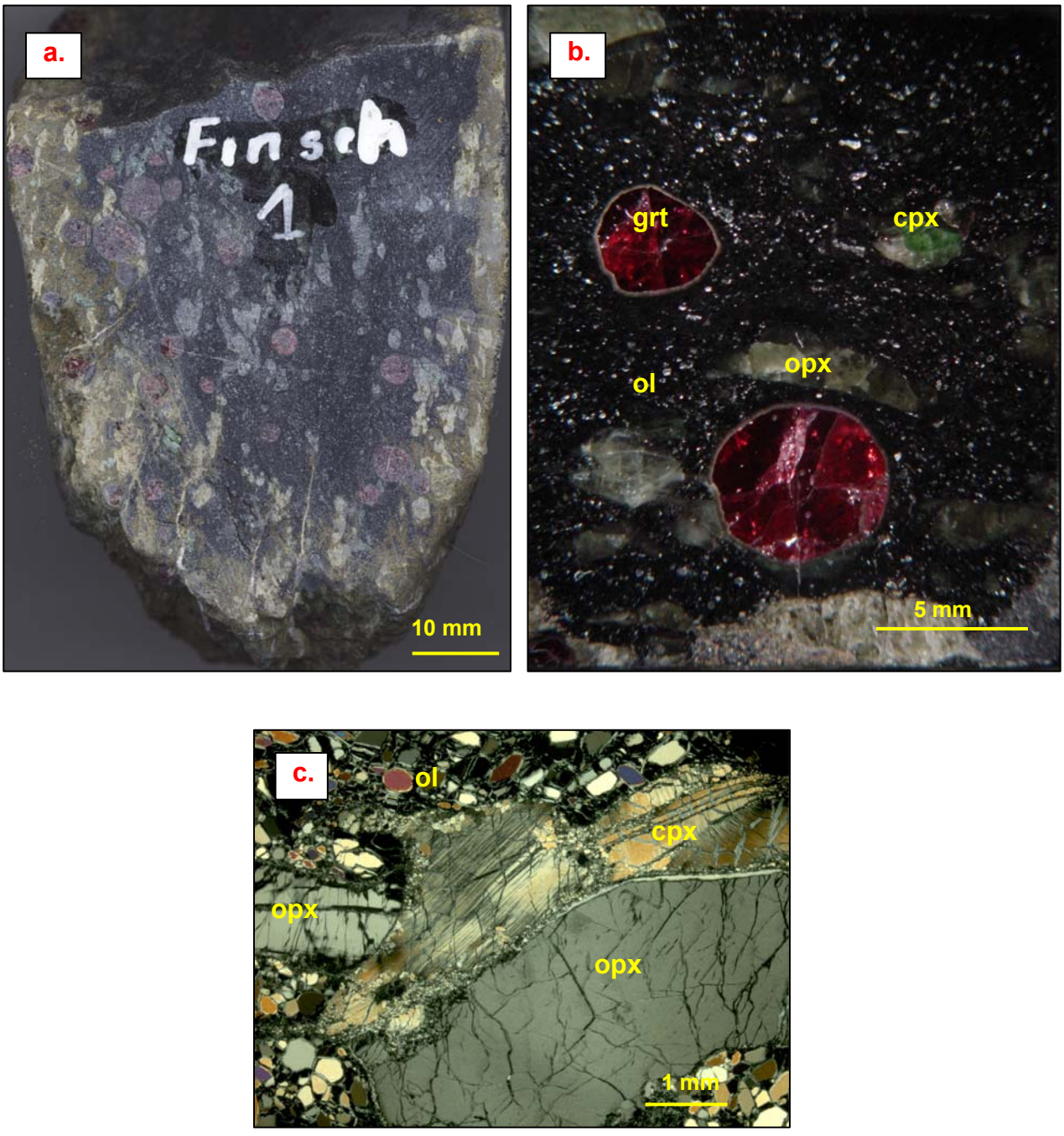

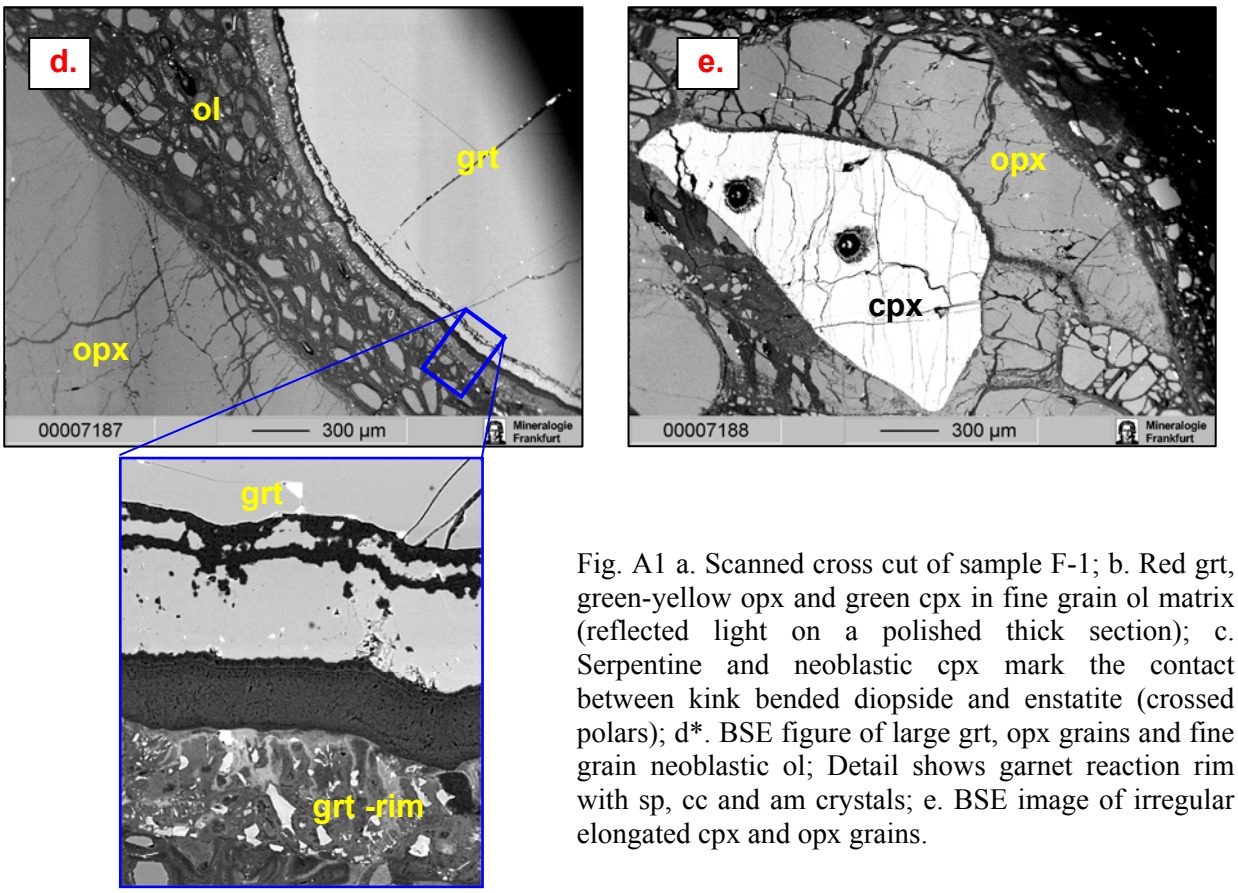

Fig. A1 a. Scanned cross cut of sample F-1; b. Red grt, green-yellow opx and green cpx in fine grain ol matrix (reflected light on a polished thick section); c. Serpentine and neoblastic cpx mark the contact between kink bended diopside and enstatite (crossed polars); d*. BSE figure of large grt, opx grains and fine grain neoblastic ol; Detail shows garnet reaction rim with sp, cc and am crystals; e. BSE image of irregular elongated cpx and opx grains.

* Dark stripes on BSE image is due to the EPMA scanning mode.

Finsch F-2:

The cpx-free harzburgite F-2 has a coarse tabular texture. Large (7-10 mm), strongly serpentized olivine makes more than 80 vol-% of this peridotite. The grains are tabular with curved grain boundaries (Fig. A2a,c). Small, up to 500 µm in length, interstitial olivine grains are also observed. Some opx grains form anhedral and elongated lath. Such grains are occasionally in contact with garnet. Dark violet garnets are elongated to irregular in shape (3-5 mm) and have thick reaction rims (up to 2 mm) (Fig. A2c). Octahedral Cr-spinel (20-30 µm), small phlogophite flakes, amphibol and serpentine are associated with garnet reaction rims and garnet grain dislocations (Fig. A2d). Olivine is sometimes present as an inclusion in garnet.

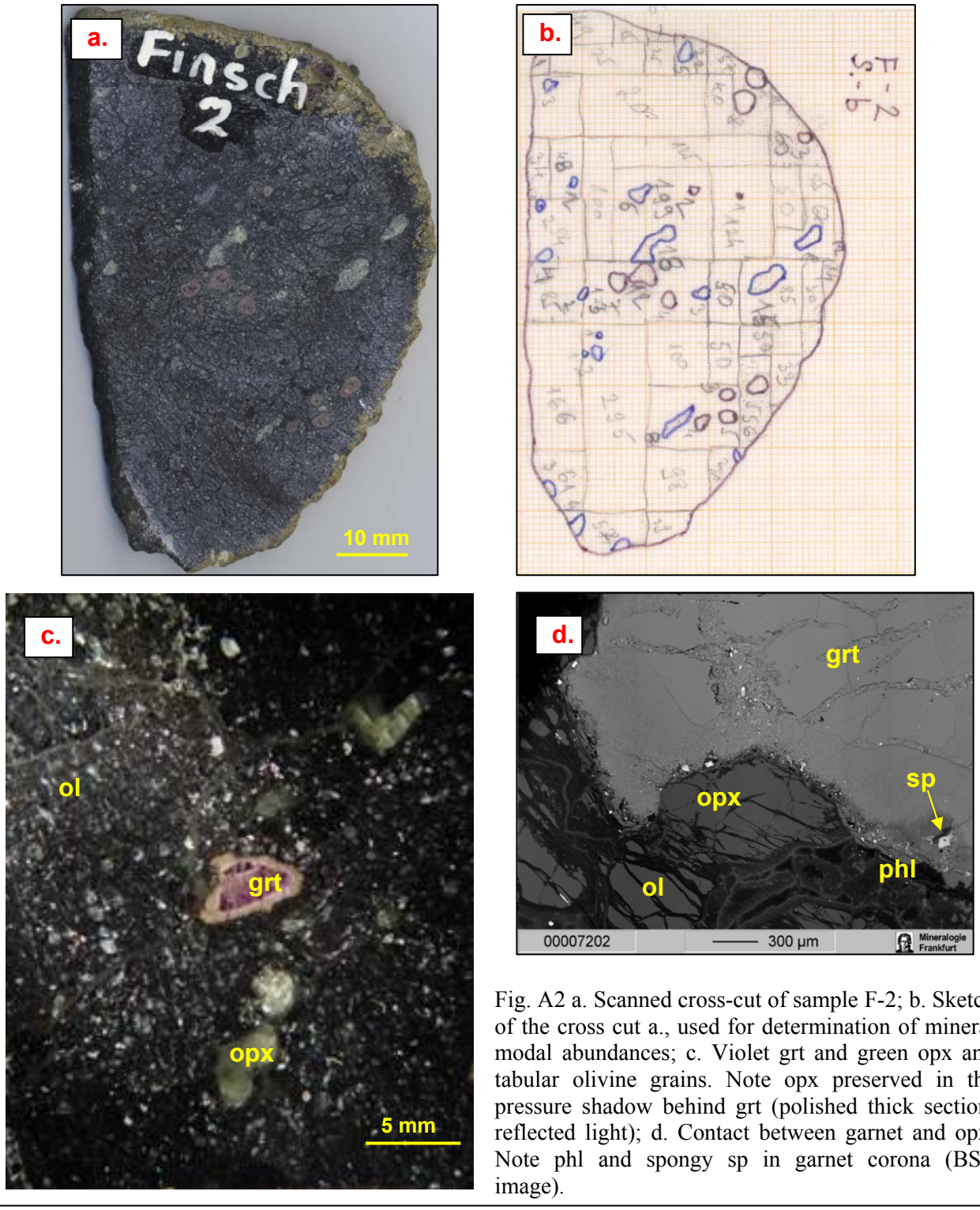

Fig. A2 a. Scanned cross-cut of sample F-2; b. Sketch of the cross cut a., used for determination of mineral modal abundances; c. Violet grt and green opx and tabular olivine grains. Note opx preserved in the pressure shadow behind grt (polished thick section, reflected light); d. Contact between garnet and opx. Note phl and spongy sp in garnet corona (BSE image).

Finsch F-3:

A coarse grain tabular texture is characteristic for this four phase dunite. Olivine is tabular prismatic to elongate in shape and range in size from 3 to 6 mm length and 1 to 5 mm width. Rare interstitial neoblastic olivine grains (<300µm) are observed around opx, cpx and grt grains. Orthopyroxenes have elongated tabular habitus with rounded edges (Fig. A3a,b). Usually, they are 4 to 6 mm across and have partly fractured rims. Oval olivines are sometimes included in opx grains. Cpx are very rare minerals in this rock. They have irregular shape and are strongly deformed (Fig. A3c). Large (6 to 9 mm), rounded garnet grains have extremely thick (up to 3 mm) reaction rims (Fig. A3a,b). This four phase peridotite also contains small irregular sulfide grains (Fig. A3d). They are interstitial minerals between olivine grains.

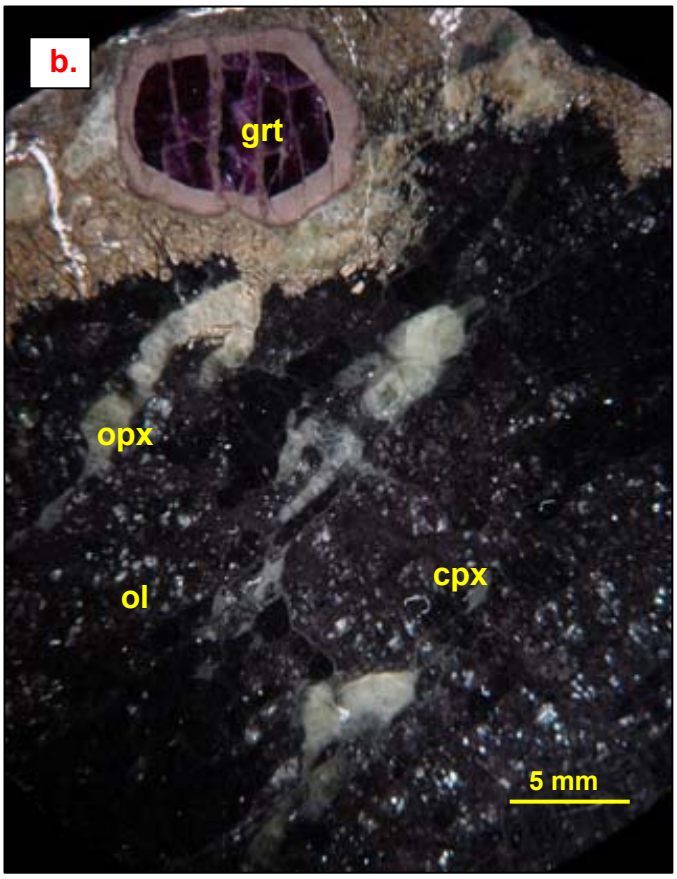

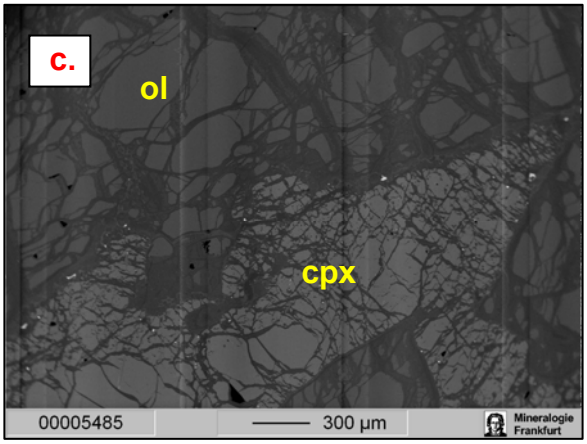

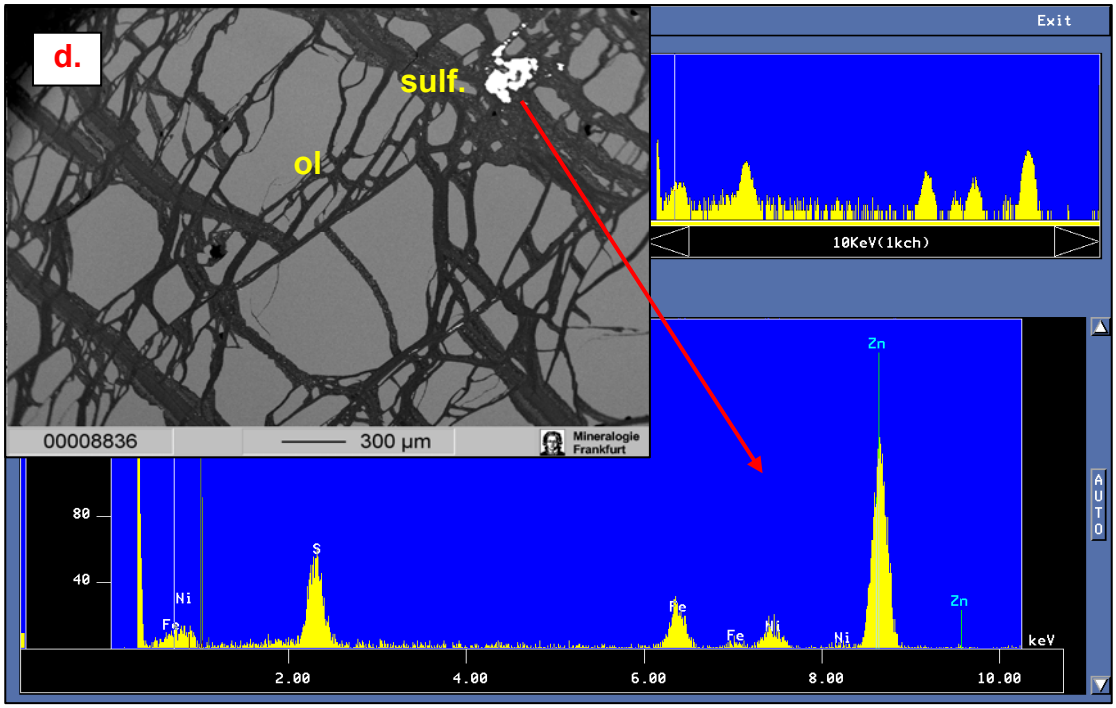

Fig. A3 a. Scanned cross cut of sample F-3; b. Elongated tabular ol and opx, and round grt with thick reaction rim. Cpx appears as interstices among ol (reflected light on a polished thick section); c*. BSE image of irregular shaped cpx with fractured edges; d. Irregular interstitial sulfide grain. Note the Zn peak on the EDS image of this sulfide.

* Dark stripes on BSE image is due to the EPMA scanning mode.

Finsch F-4:

Sample F-4 has a mosaic–porphyroclastic texture. It represents a four phase harzburgite with around 1 vol.% cpx. Small (10-200 µm) olivine grains are the most abundant minerals (Fig. A4a,c). All porphyroclastic grains, except grt, are aligned in the same direction (Fig. A4a,b). Large 2 to 4 mm elongated olivine grains are rare. They always show tailing of small neoblastic olivine grains in the direction of the grain elongation. Opx with a length of up to 7 mm are the largest grains in this sample (Fig. A4a,b). Opx and rare cpx are also elongated and show extremely undulose extinction. Both opx and cpx have neoblastic opx and cpx, respectively, on their rims, (Fig. A4c,d). Garnets are round or oval, partly deformed, and have thick reaction rims (Fig. A4e). The 30-40 µm long sp and am grains have crystallized in garnet kelyphite rims (Fig. A4f).

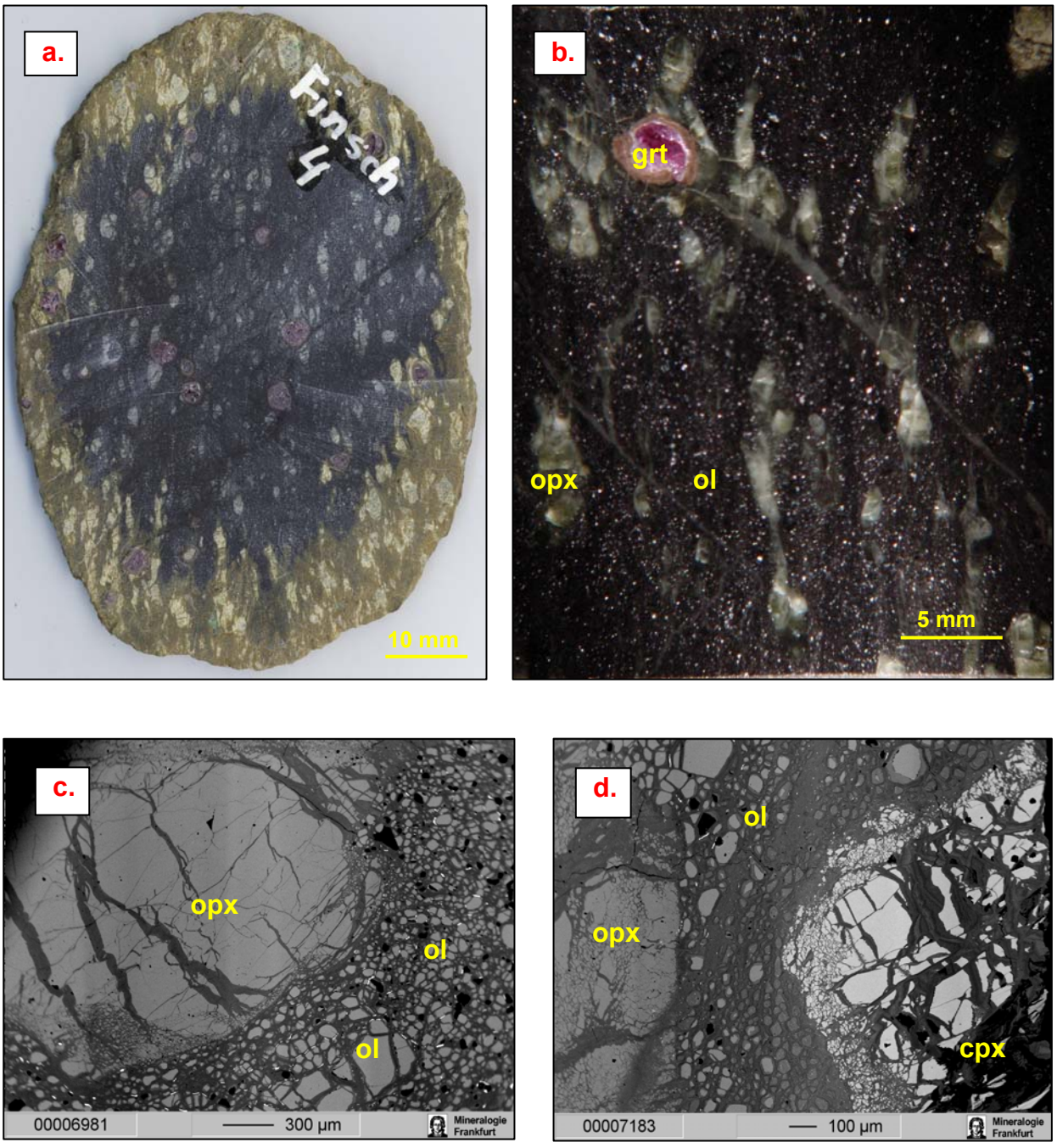

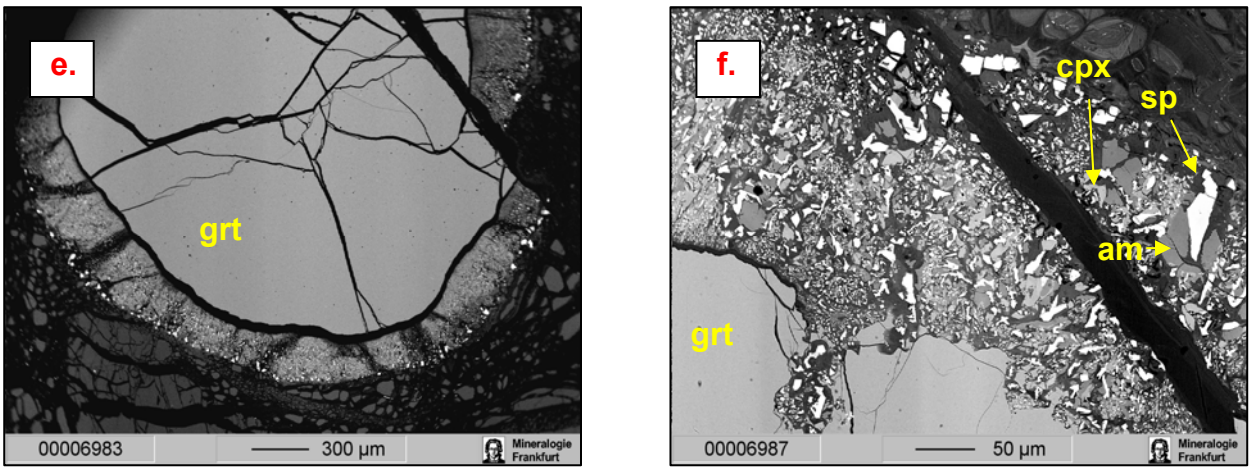

Fig. A4 a. Scanned cross cut of sample F-4; b. Elongated opx grains mark foliation of this rock (reflected light on a polished thick section); c.* BSE image opx and ol porphyroclasts in fine grain ol neoblast; d. Recristallized rims of opx and cpx grains (BSE); e. Rounded garnet with the secondary fracture (BSE); f. Needle like sp, skeletal Al-rich am and cpx in a garnet kelyphite rim (BSE).

* Dark stripes on BSE image is due to the EPMA scanning mode.

Finsch F-5:

All ol, opx and cpx grains in this garnet bearing harzburgite are around 1 to 3 mm long (Fig. A5a, b). Only garnets may be up to 5 mm in diameter. Olivines are tabular to oval and have undulose extinction. Opx is the most abundant mineral in this peridotite. They are equedimensional with a completely irregular shape and curved linear grain boundaries. Only smaller opx grains show sector undulose extinction. Olivine is a common inclusion in opx grains (Fig. A5c,d). Garnets are round or slightly elongated with the thin reaction rims (Fig. A5b,d). Cpx can also be small up to 300 µm and have interstitially irregular shape.

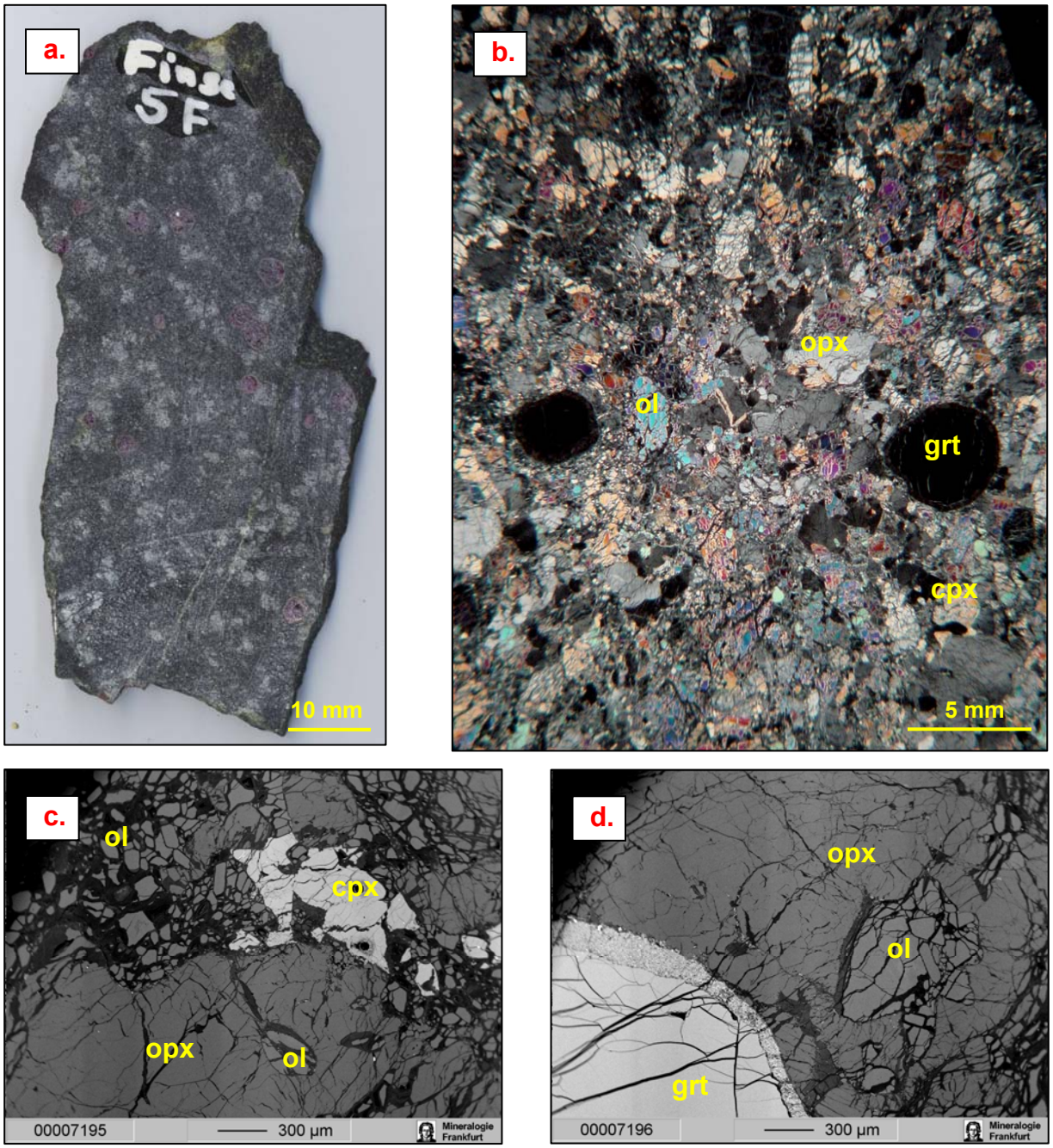

Fig. A5 a. Scanned cross-cut of sample F-5; b. Medium- to course- grain equant texture of sample F-5 (Thin section, crossed polars); c. BSE image of the opx and cpx contact. Note the irregular shape of cpx and the oval olivin inclusion in opx; d. Garnet in contact with irregular opx. Note the way opx envelope the olivin grain (BSE).

Finsch F-6:

Common triple-junctions give a coarse grain texture to this harzburgite (Fig. A6a,b). Olivine is regularly tabular, but some rare ovoid grains are also observed. Their size varies from 1 to 5 mm, but most common are 2 mm long grains. Extremely rare are small ~10 µm neoblastic olivines around cpx and grt grains. Opx are mostly elongated and tabular in shape, rarely irregular (Fig. A6b,c). Larger opx grains (up to 3 mm) sometimes have olivine inclusions. Cpx are smaller (~ 1 mm) than opx and elongate amoeboid in shape (Fig. A6c). Fine twin lamely were observed on some cpx grains. They are deformed and have neoblastic cpx on their rims. Garnets are rounded with 3 to 5 mm across. Sp, am, serp and rare phl are associated in garnet reaction rims.

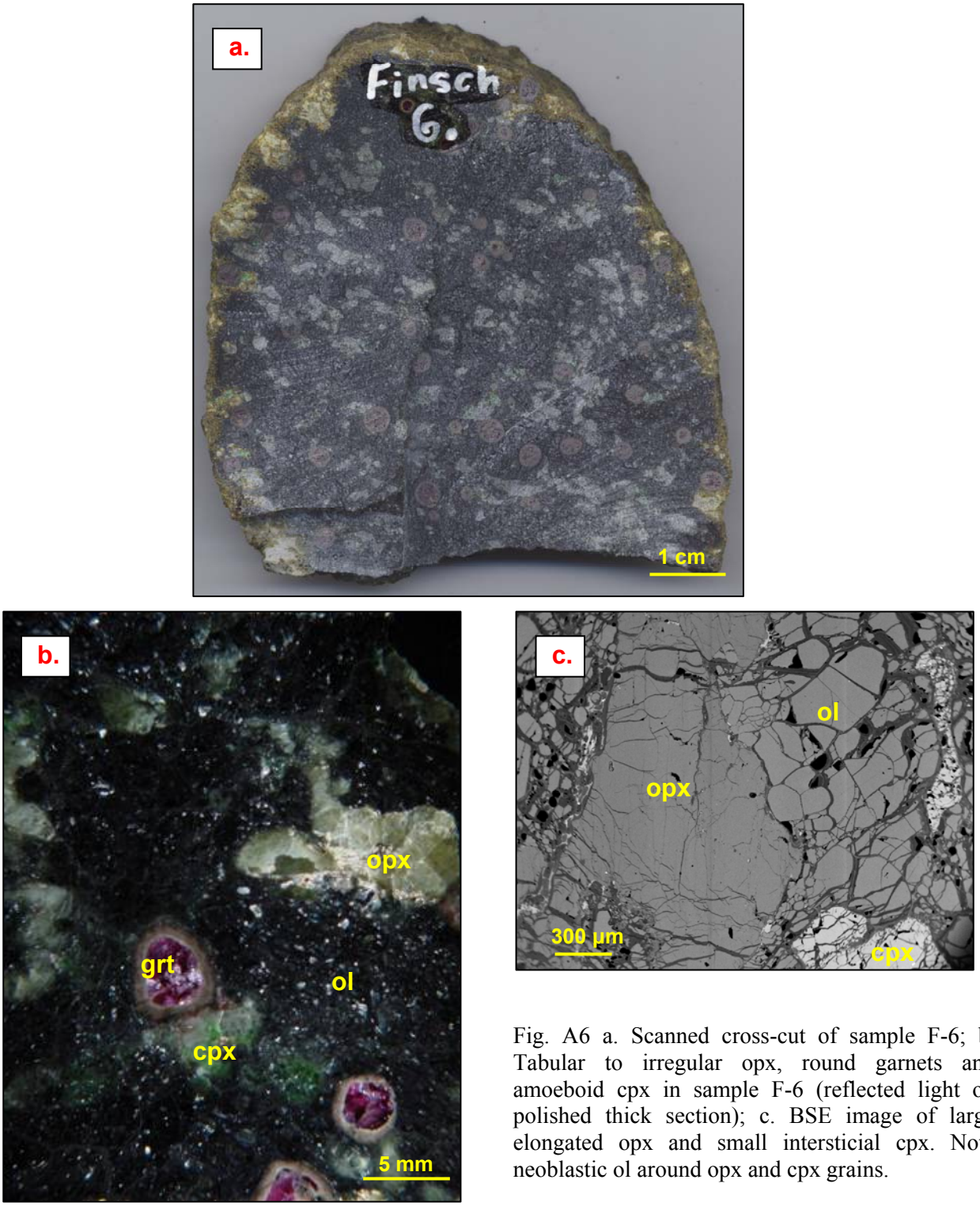

Fig. A6 a. Scanned cross-cut of sample F-6; b. Tabular to irregular opx, round garnets and amoeboid cpx in sample F-6 (reflected light on polished thick section); c. BSE image of large elongated opx and small intersticial cpx. Note neoblastic ol around opx and cpx grains.

Finsch F-7:

A coarse grain tabular texture is characteristic of sample F-7 (Fig. A7a,b). This cpx-free harzburgite has around 40 vol. % opx. Large 5 to 10 mm olivine grains are tabular, while smaller (2-5 mm) grains are oval in shape. Rare small neoblastic olivines (~10 µm) are filling the interstices. Opx are tabular with straight grain boundaries to elongate amoeboid in shape (Fig. A7b,c,d). The size of opx varies from 1 to 12 mm in length, and most common are 5 mm long grains. Rare, neoblastic opx were observed on opx rims (Fig. A7c). During hand picking of opx, grains with sulfide inclusions were found. Garnets are elongated or round with 4-7 mm across.

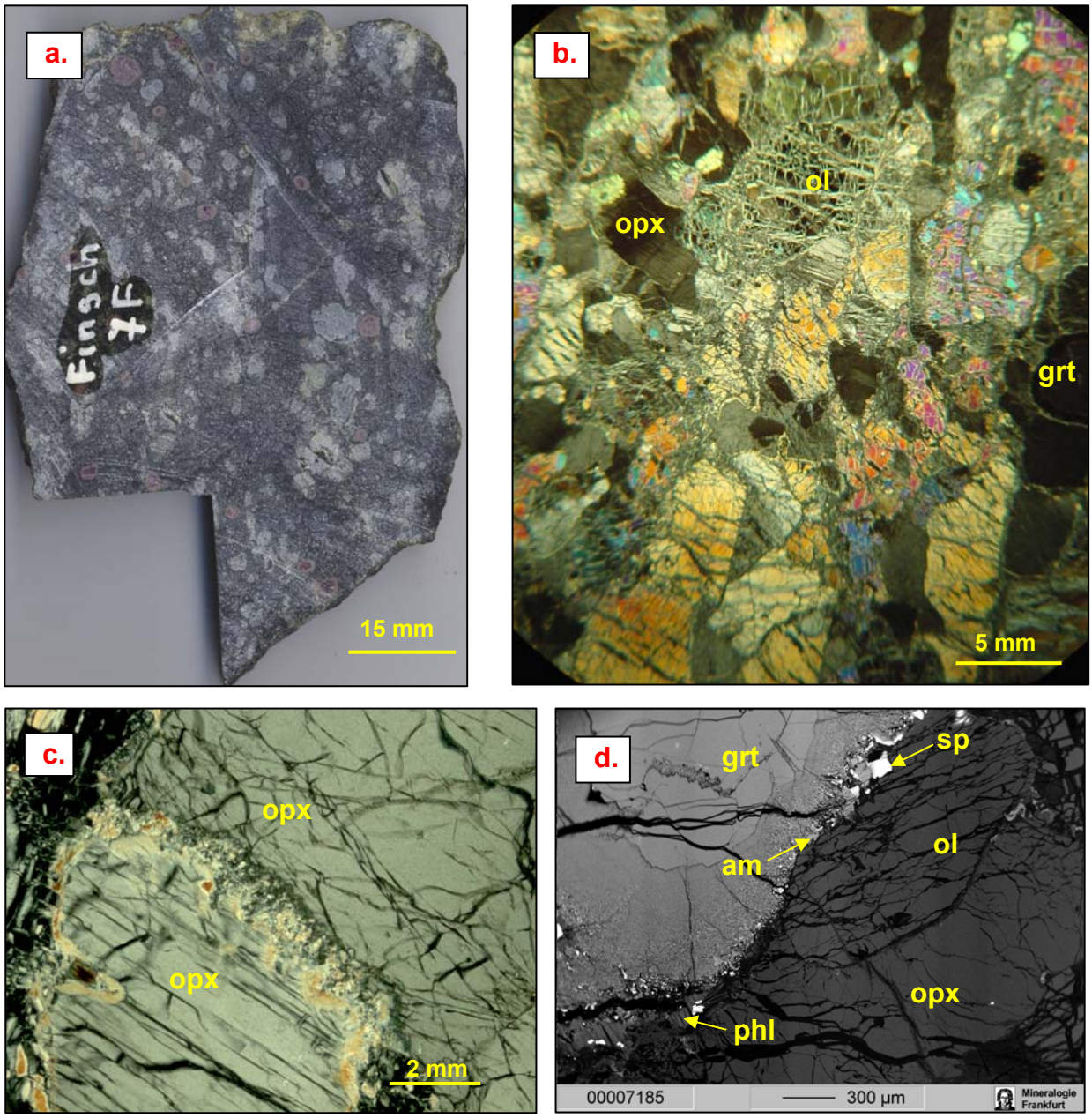

Fig. A7 a. Scanned cross-cut of sample F-7; b. Common triple junctions in course tabular texture of F-7 (crossed polars); c. Two occurrences of opx. Note neoblastic opx grains on the rim of the lower grain (crossed polars); d. BSE image of grt-opx contact. Sp and am show gradation of grain size in kelyphite and larger grains occure together with phl on the edge of garnet. Note straight ol-opx grain boundaries.

Finsch F-8:

Olivine is the most common mineral in this coarse-grain tabular four phase peridotite. Opx and cpx are extremely rare in this dunite, and together make not more than 5 vol.% (Fig. A8a,b). Most abundant are large (up to 10 mm) tabular olivines, and rarely smaller grains are observed (Fig. A8b). Opx are angular, sometimes elongated (up to 7 mm long) and partly deformed (Fig. A8c). Cpx are strongly deformed and mostly in contact with garnet (Fig. A8d). the size of the garnets varies from 1 to 8mm across. Some garnets are rounded and some are "irregular" shaped. There is no connection between shape and size of the garnet grains. When garnet is not in direct contact with cpx, phl flakes are enveloping garnet rim.

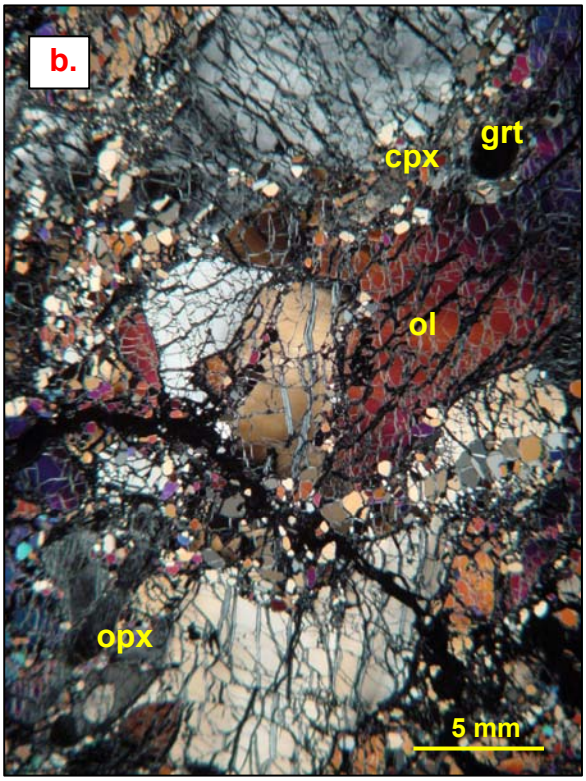

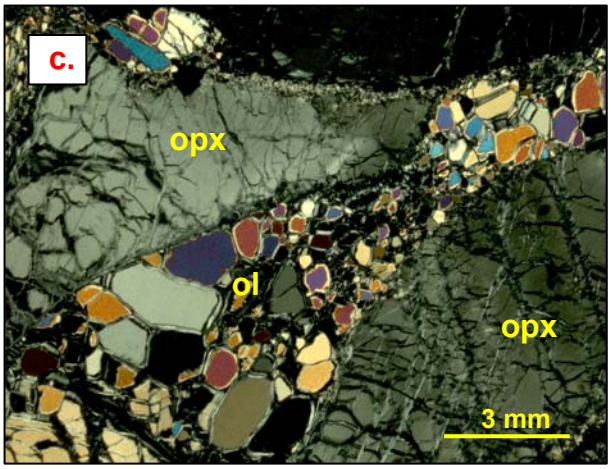

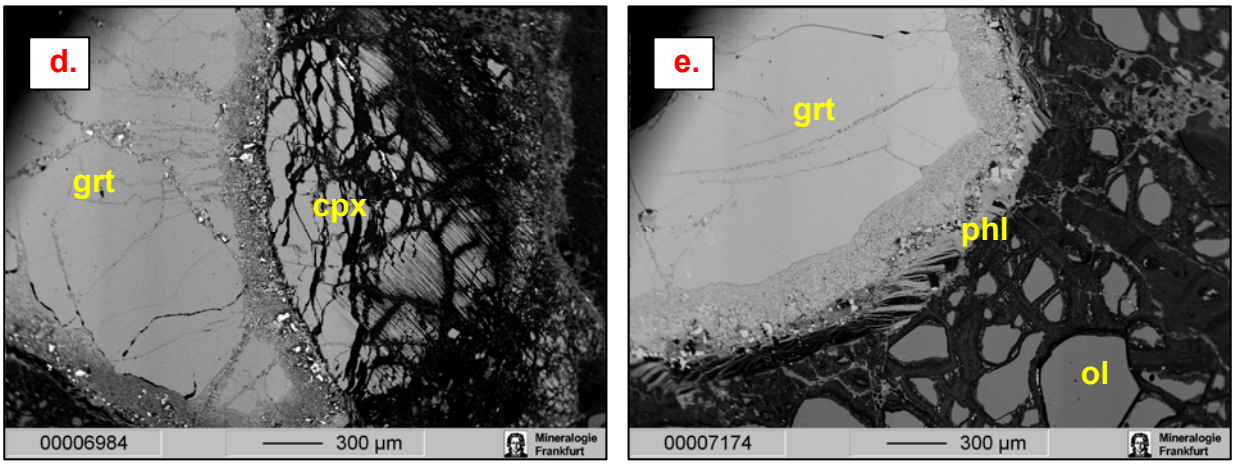

Fig. A8 a. Scanned cross-cut of sample F-8; b. Angular opx and elongated garnets between coarse olivine grains (reflected light on a polished thick section); c. Partly deformed opx with straight grain boundaries and fine grain olivine. Note neoblastic opx at the rim of a large opx grain; d.* BSE image of cpx in a garnet pressure shade; e.* BSE figure of sp and phl flakes at grt rims.

*Dark stripes on BSE images are due to the EPMA scanning mode.

Finsch F-9:

The sample F-9 is a coarse equant garnet harzburgite (Fig. A9a). Olivines are elongated tabular or oval and vary from 1 to 7 mm in length. Opx are elongated irregular shape and sometimes have fractured edges (Fig. A9b,c). Garnets have a round-angular shape and range in size from 2 to 8 mm in diameter. All garnets have up to 1mm thick reaction rims (Fig. A9b,c). The CaO and Cr_2O_3 contents of garnet indicate that this sample contains cpx. Careful hand picking of grained sample yielded a couple of cpx grains.

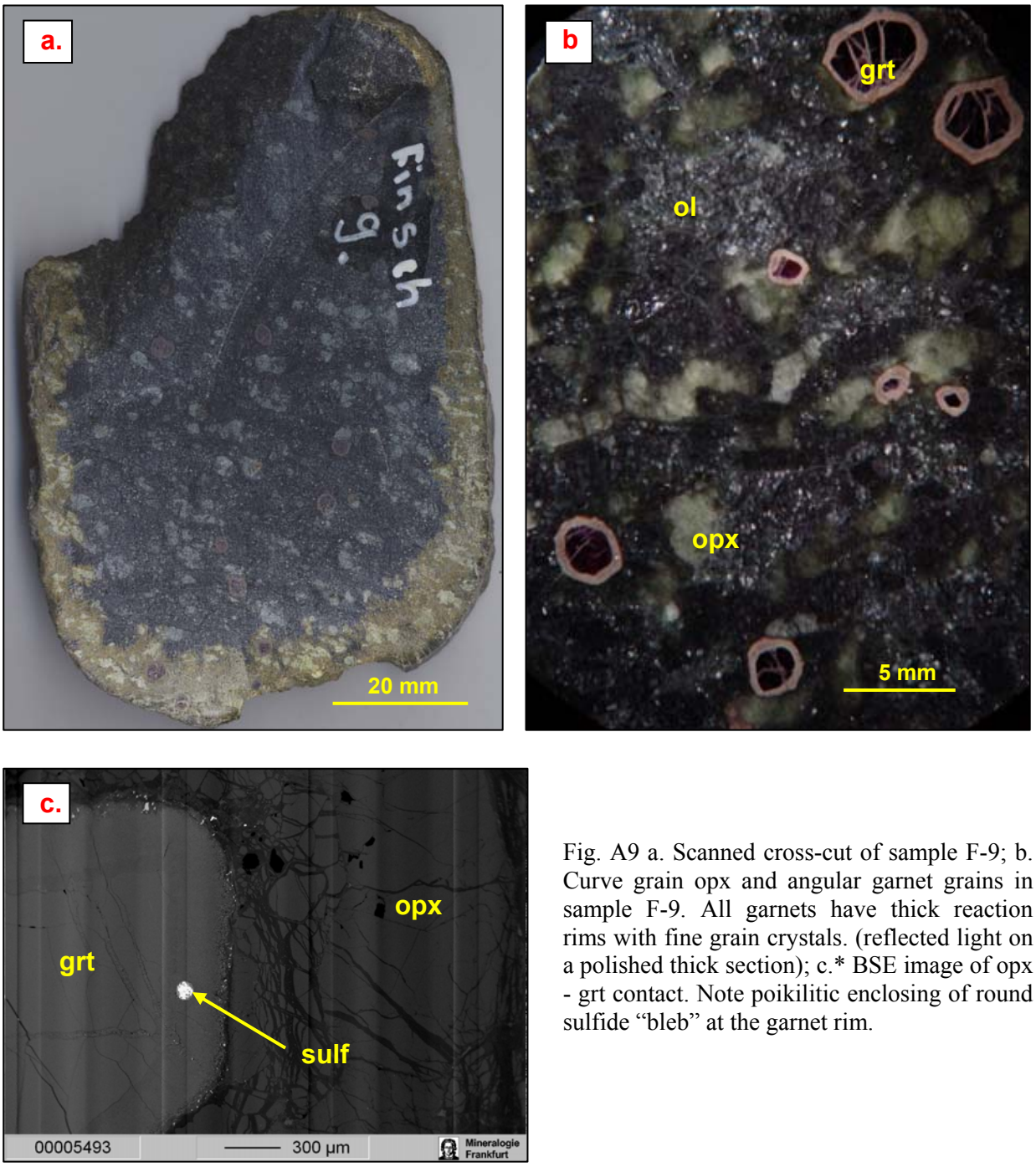

Fig. A9 a. Scanned cross-cut of sample F-9; b. Curve grain opx and angular garnet grains in sample F-9. All garnets have thick reaction rims with fine grain crystals. (reflected light on a polished thick section); c.* BSE image of opx - grt contact. Note poikilitic enclosing of round sulfide "bleb" at the garnet rim.

*Dark stripes on BSE images are due to the EPMA scanning mode.

Finsch F-10:

This four phase garnet peridotite has porphyroclastic texture. All grains are deformed and all except garnet are elongated (Fig. A10a,b). The grain orientation marks foliation of this peridotite. Olivine is mostly represented by fine grain (20-200 µm) neoblasts (Fig. A10c). Larger (1-3 mm) oval olivines are rare. Some opx have sector undulouse extinction. Small oval olivines are sometimes included in opx grains. Cpx is less fractured than the other grains. It appears in elongated prismatic, or oval shape (Fig. A10c,d). Cpx have line undulose extinction and sometimes also neoblastic cpx at their rims (Fig. A10c). Garnets are strongly fractured and the cracks as well as grain rims are filled with a mixture of phl, sp, am, secondary cpx and serpentine. Ol and cpx are frequent poikilitic inclusions in garnets (Fig A10a,b).

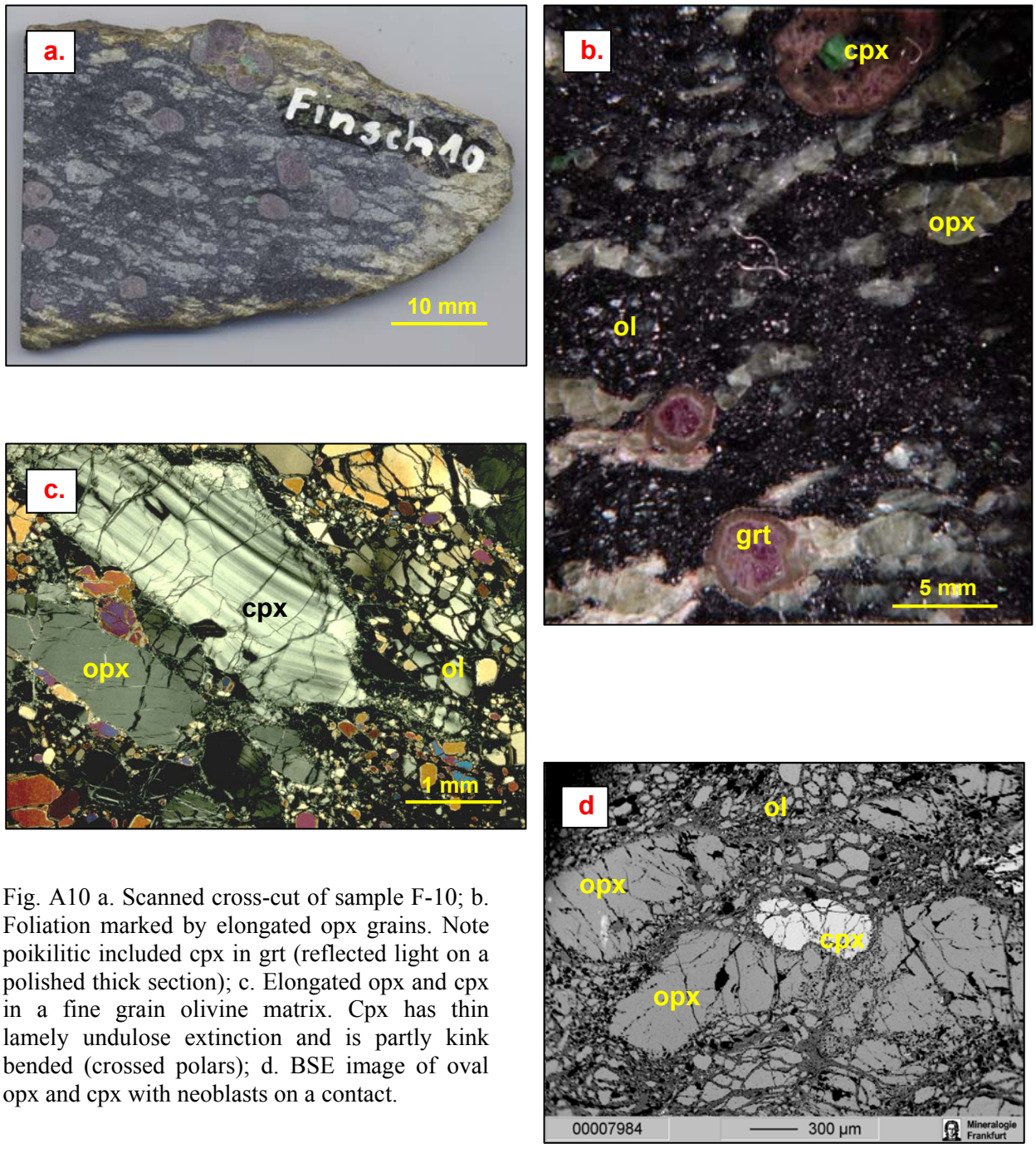

Fig. A10 a. Scanned cross-cut of sample F-10; b. Foliation marked by elongated opx grains. Note poikilitic included cpx in grt (reflected light on a polished thick section); c. Elongated opx and cpx in a fine grain olivine matrix. Cpx has thin lamely undulose extinction and is partly kink bended (crossed polars); d. BSE image of oval opx and cpx with neoblasts on a contact.

Finsch F-11:

The garnet bearing harzburgite F-11, has a coarse grain tabular texture (Fig. A11a,b). Olivin is large and strongly serpentinized, so that in thin section all together looks like one large grain. Opx are oval or rounded and strongly fractured (Fig. A11c,d). Cpx are irregular elongated grains with the twining lamely. They are only slightly deformed and partially or completely changed to chlorite (Fig. A11b,c). Garnets are rounded from 2 to 7 mm in diameter. They have thick (up to 2 mm) reaction rims with around 100 µm long sp and around 200 µm long am, serp and chl (Fig. A11d,e).

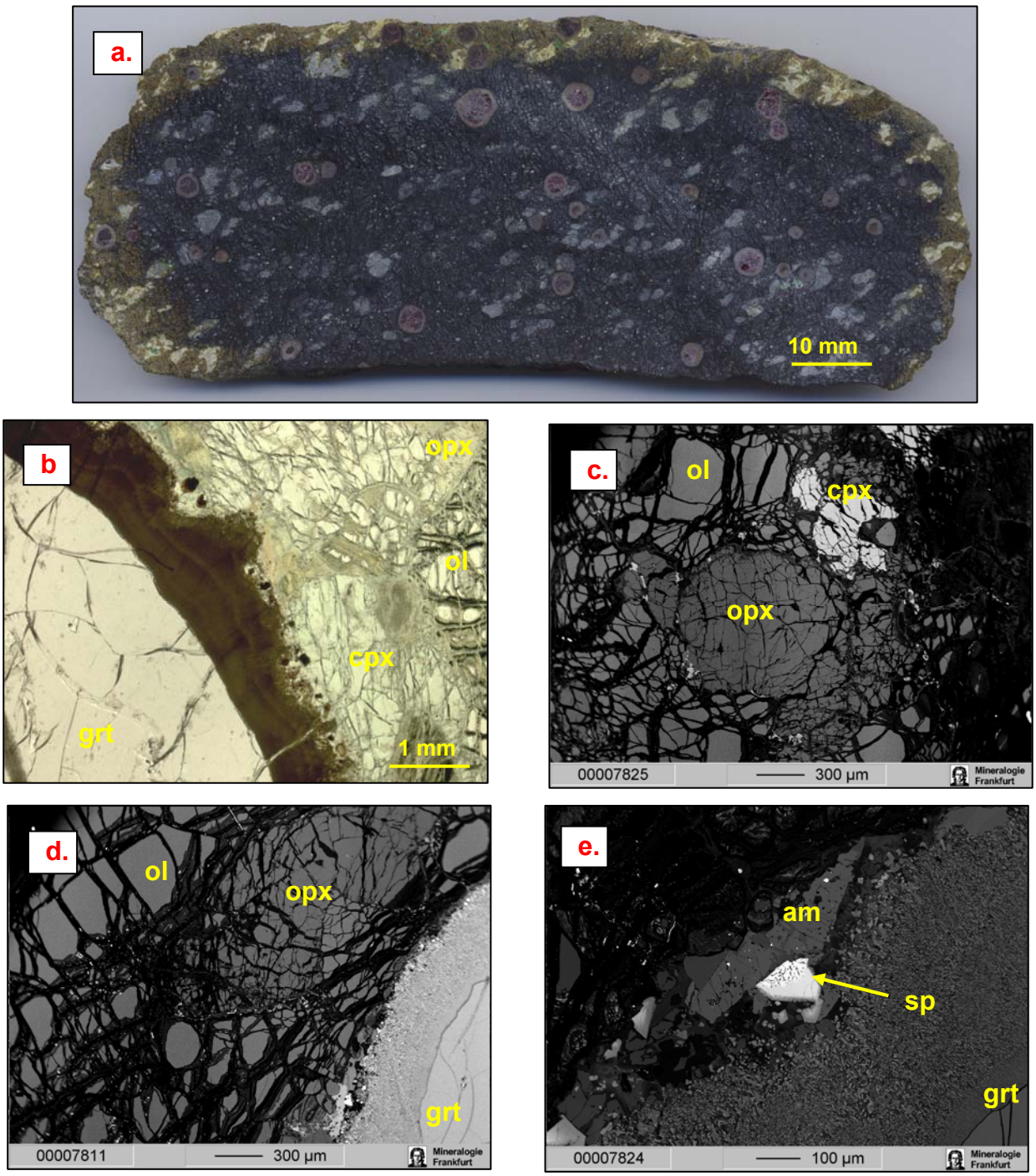

Fig. A11 a. Scanned cross-cut of sample F-11; b. Ol, opx and cpx building 120° contact (crossed polars); c. BSE image of fractured rounded opx and interstitial cpx; d. Strongly fractured opx grain. Grt has thick reaction rim consist of sp, am, and secondary cpx (BSE); e. BSE figure of spongy sp and elongated am at grt kelyphite.

Finsch F-12:

The sample F-12 is a rutile bearing garnet harzburgite with a coarse tabular texture. This sample has well developed 120° grain contacts (Fig. A12a,b). Large elongated opx grains are partly fractured. Olivines are common inclusions in opx (Fig. A12f). Tabular to elongated amoeboid cpx grains are partly fractured (Fig. A12b,g). Garnets are oval or angular with curved sharpe boundaries. They have 1 to 2 mm thick reaction rims with octahedral sp and prismatic opx (Fig. A12b,f,g). Garnet kelyphite are enveloped with phl lamely. Orange to brown coloured rhombic rutiles are found as interstitial mineral and as inclusions in garnets but, the most common and largest (~1 mm) rutiles are found at garnet rims together with sulfide and ilmentite (Fig. A12b,c,f). All rutile grains have dark needle like exsolutions of Cr-rich spinel (Fig. A12d). Pentlandite (?) appears as rounded blebs with a well developed Fe–richer sulfide at the rims and quenched, needle like pentlandite (?) and Ni-rich pyrite (?) in the middle (Fig. A12d,e). Those blabs appear as inclusions in garnets and sometimes also at the garnet-rutile contact (Fig. A12b).

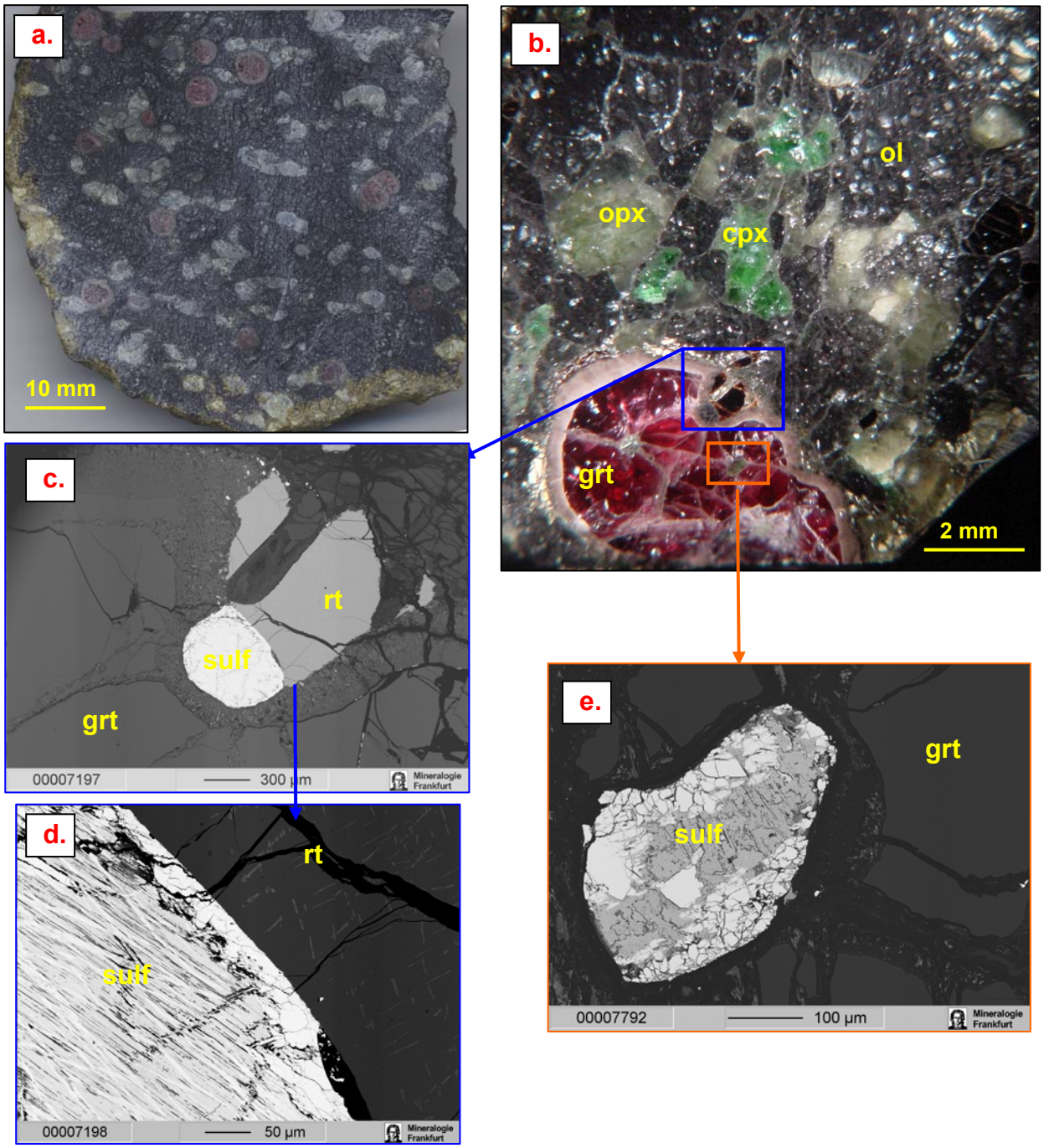

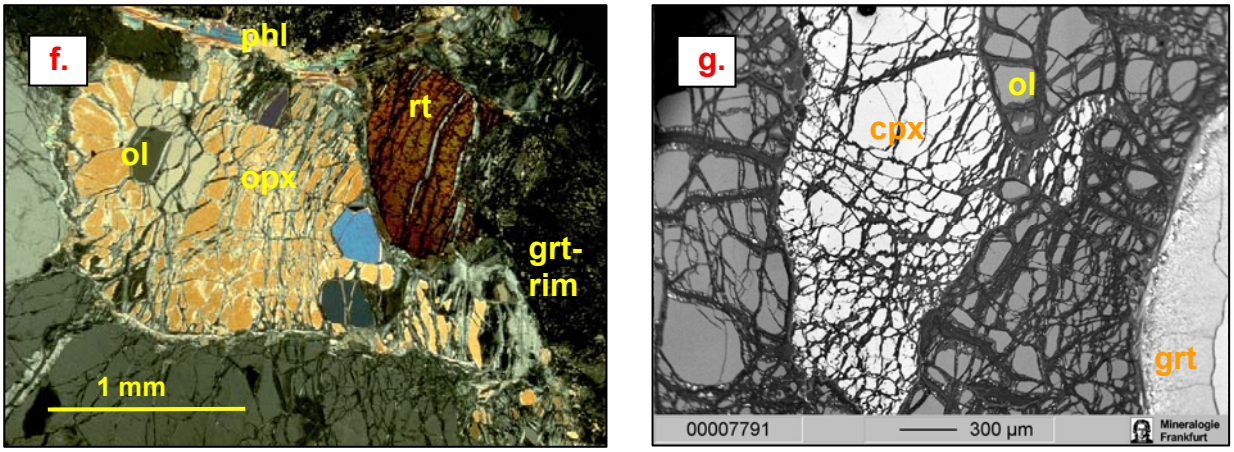

Fig. A12 a. Scanned cross-cut of sample F-12; b. Coarse grain tabular ol, opx and cpx in a sample F-12. Note the orange rutile grain and the gray sulfide grain on the garnet rim (blue rectangle). Two gray sulfide blebs are included in the same garnet grain (orange rectangle) (reflected light on a polished thick section); c. BSE image of the garnet-sulfide-rutile contact. d. Large magnification of the rutile-sulfide contact from c. (BSE). Note light coloured needle exolutions in the rutile grain. The sulfide blab has a thicker rim of Fe richer sulfide and quenched needle like Fe-Ni-sulfide (pentlandite?) in the centre; e. BSE figure of sulfide inclusion in garnet. Gray crystals are Fe-rich, while bright pats are Fe-Ni sulfides; f. Fractured opx with olivine inclusions at the contact with rutile and garnet (crossed polars). Note phl flakes on the garnet rim; g. BSE image of interstitial form of elongated cpx.

Finsch F-13:

Fine grain ol, opx and cpx create a middle to fine-grain equant to porphyroclastic texture for lherzolite F-13 (Fig. A13a,b). Most of the olivines have sizes between 20-100 µm, and longer 0.5-1 mm grains are very rare. Opx are often idiomorph prismatic, but some have an irregular habitus (Fig. A13b,c). Rare irregular opx grains have neoblastic opx rims. All opx and cpx grains are from 0.5 to 2 mm long. Cpx are mostly irregular in shape, and rarely have a prismatic habitus. Sometimes prismatic cpx have lamellar undulose extinction (Fig. A13b). Some cpx grains also have neoblastic cpx at their rims. With up to 10 mm across, garnets are the largest grains in this peridotite. They are rounded and have thin or no kelyphite rims (Fig. A13b,c). As accessories, elongated sulfide grains were observed. Sulfides are 50-100 µm long and consist of pyrite and pentlandite (?) (Fig. A13d,e).

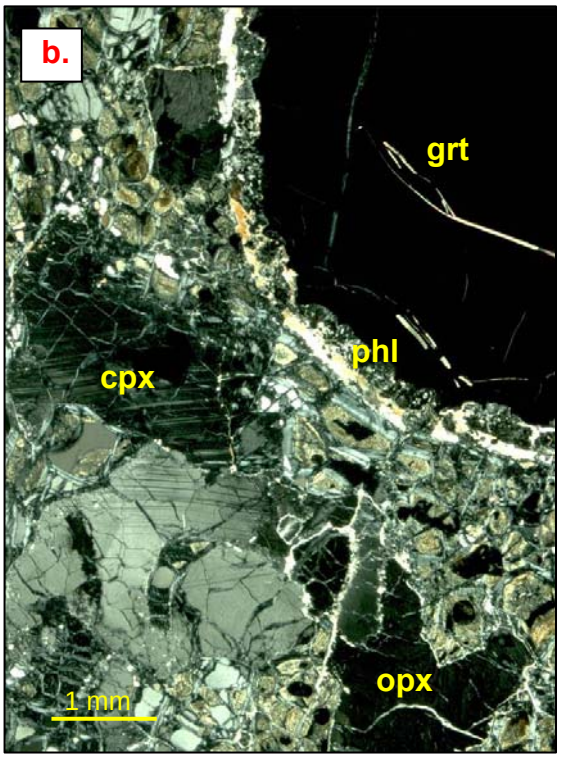

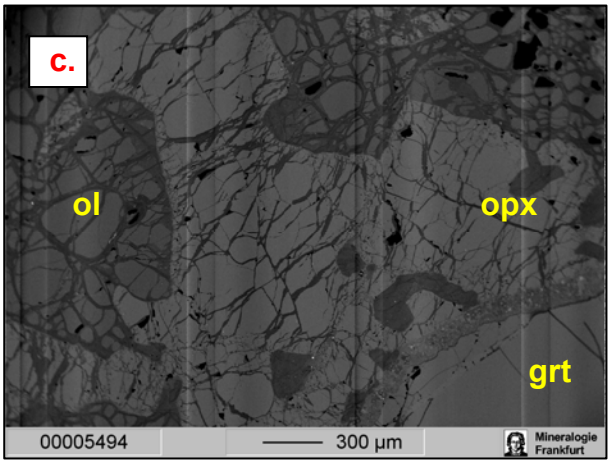

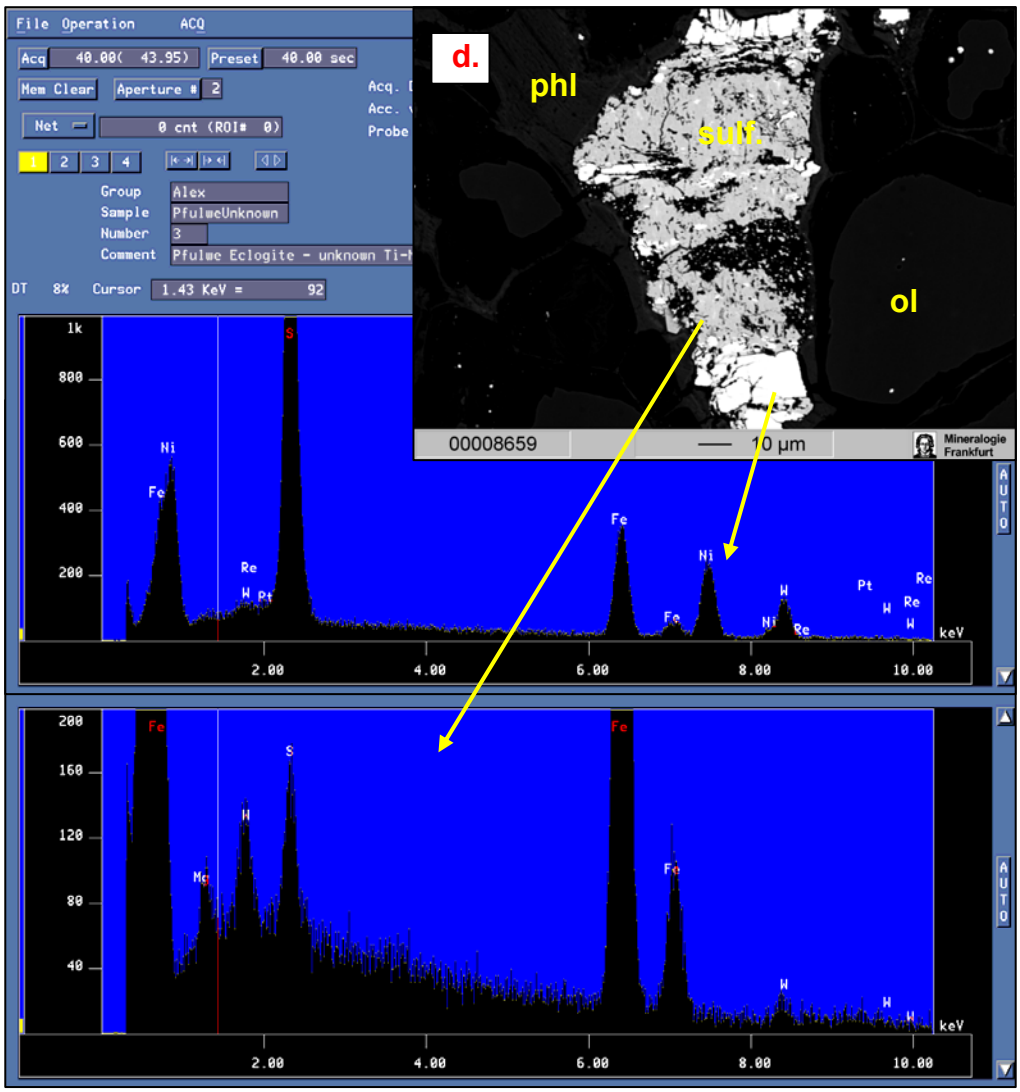

Fig. A13 a. Scanned cross-cut of sample F-13; b. Lamellar undulose extinction of prismatic and irregular cpx grains. Note colourful phl shists around the garnet grain (crossed polars); c.* BSE image of olivine inclusions in a irregular opx grain. Note the thin reaction rim of the garnet grain; d. BSE figure of interstitial sulfide; EDS images showing that the light coloured part (on BSE) is Fe-Ni-sulfide (Pentlandite?) and the gray coloured parts (on BSE) are Fe–rich (pyrite ?). Note the W peak for the gray coloured crystals.

*Dark stripes on BSE images are due to the EPMA scanning mode.

Finsch F-14:

The coarse equant texture is characteristic of this garnet bearing four phase peridotite. All minerals are slightly elongated and vary in size from 1 to 5 mm. Most common are grains around 2mm across (Fig. A14a,b). Opx and cpx have irregular shape and are partly fractured (Fig. A14c). Garnets are angular, elongated and all have reaction rims. Some are also strongly deformed (Fig. A14b,d). A mixture of fine grain sp and am feats the fractures of the garnet grains and is together with phl present in garnet kelyphites (Fig. A14d).

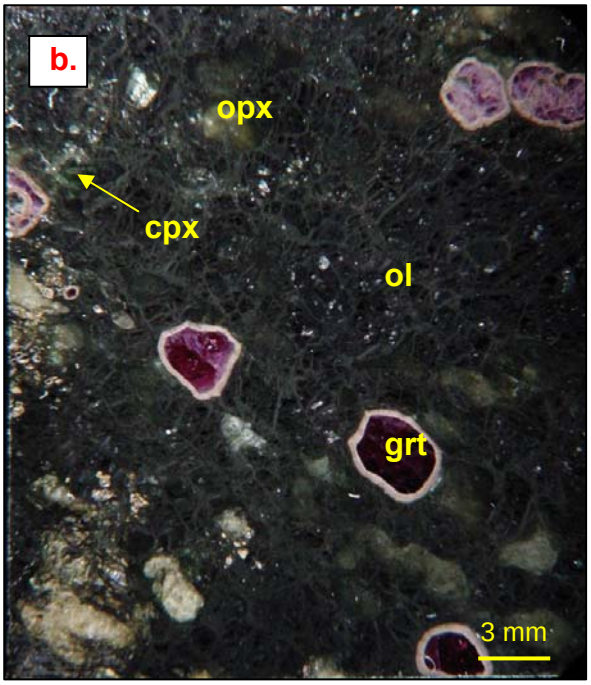

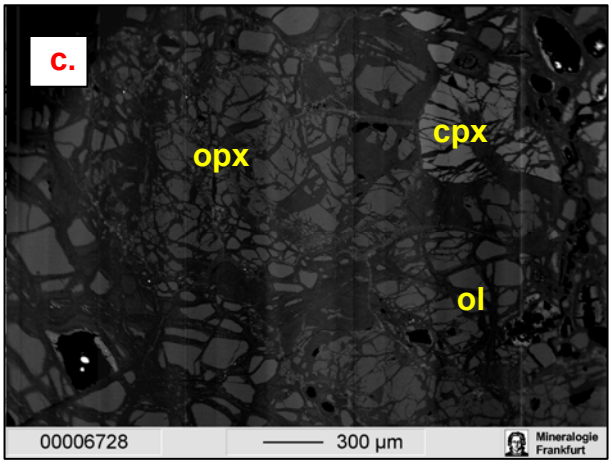

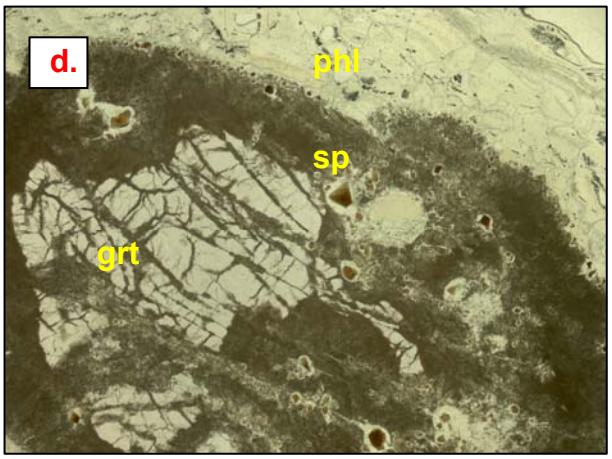

Fig. A14 a. Scanned cross-cut of sample F-14; b. Angular grt and elongated opx in sample F-14 (reflected light on a polished thick section); c.* BSE image of fractured opx and cpx. d. Strongly deformed garnet with sp crystals at kelyphite rims and phl enveloping the grain (crossed polars).

* Dark stripes on BSE image is due to the EPMA scanning mode.

Finsch F-15:

The sample F-15 is a garnet bearing lherzolite with a coarse tabular texture (Fig. A15a,b,e). Olivines are tabular to slightly oval in shape. Dimensions vary from 1 to 8 mm in length. Opx and cpx are oval or elongated, whereas opx is always larger (2-5 mm) than cpx (1-3 mm long) (Fig. A15c,d). Both are partly fractured. Cpx has either sector or lamely undulose extinction (Fig. A15c,d). Larger cpx have neoblastic cpx grains on rims (Fig. A15d). Garnets are rounded with 3 to 8 mm in diameter. They have thin kelyphit rims (Fig. A15e). Some iron sulfides and pentlandites are found as interstitial minerals in this sample.

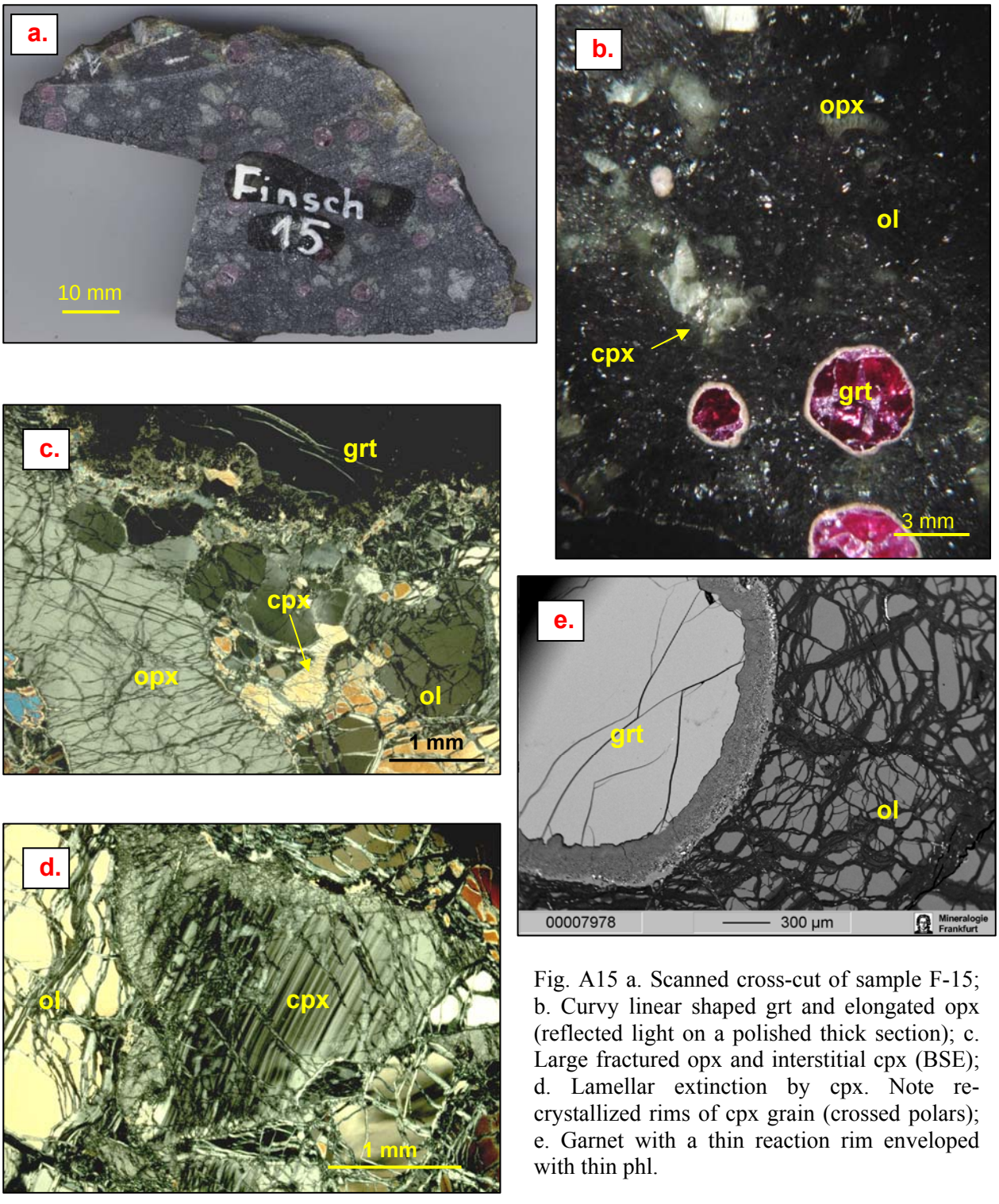

Fig. A15 a. Scanned cross-cut of sample F-15; b. Curvy linear shaped grt and elongated opx (reflected light on a polished thick section); c. Large fractured opx and interstitial cpx (BSE); d. Lamellar extinction by cpx. Note re-crystallized rims of cpx grain (crossed polars); e. Garnet with a thin reaction rim enveloped with thin phl.

Finsch F-16:

The garnet lherzolite F-16 has a coarse equant texture. Most of the ol, opx and cpx have a similar grain size of ~2 mm. Only grt can reach up to 7 mm in diameter (Fig. A16a,b). Opx are oval or irregular shaped (Fig. A16c,d,e). They all show undulose extinction, but only some are deformed (Fig. A16d,e). Cpx are idiomorph prismatic to irregular in shape and display twinning (Fig. A16c,f,g). Garnets are rounded in shape and have thick reaction rims. Compared to all here analysed samples, in garnet reaction rim from F-16 the largest sp (up to 200 µm long) were observed (Fig. A16c,g). Ol often appears as inclusion in opx, cpx and grt (Fig. A16a,e,f,g).

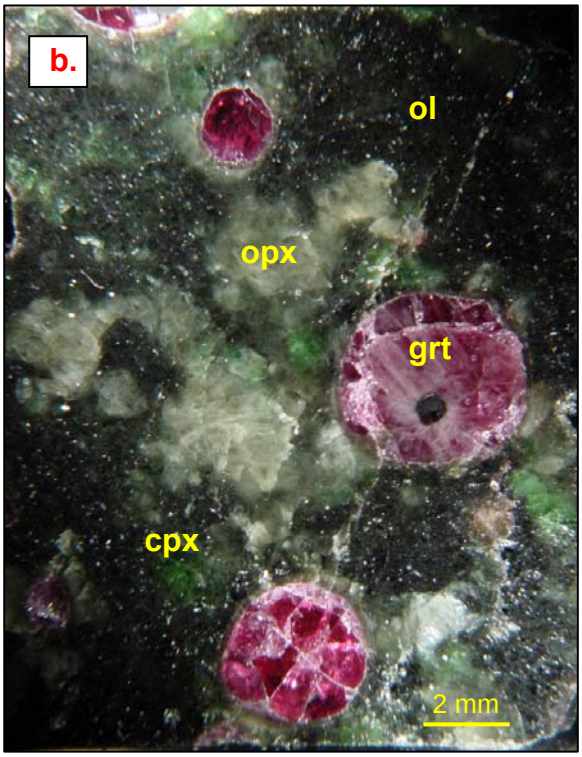

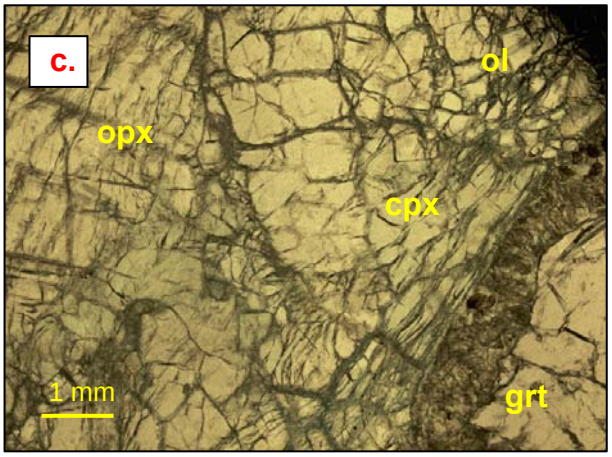

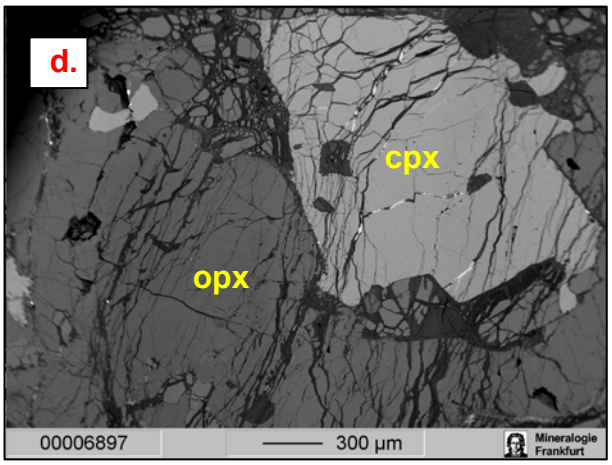

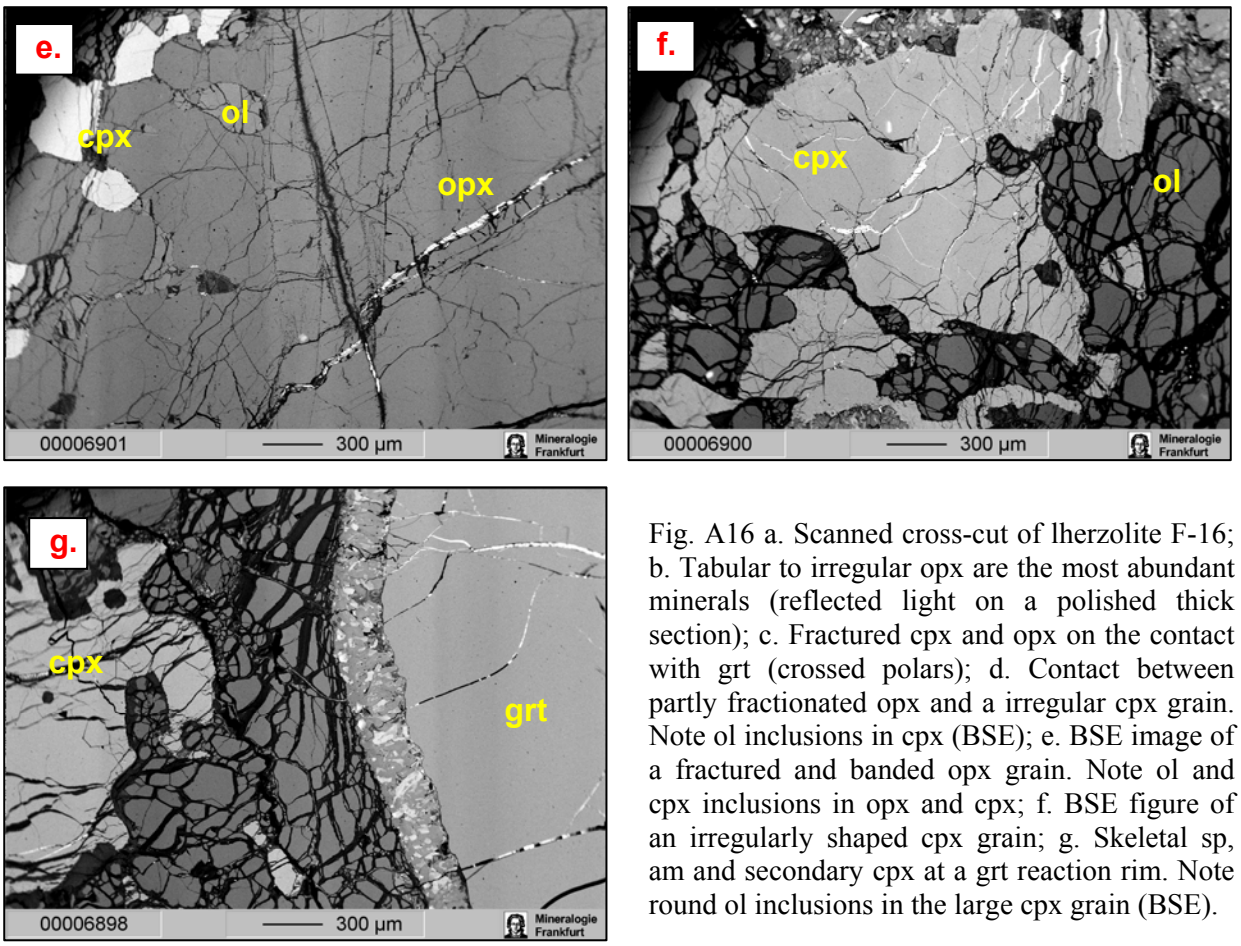

Fig. A16 a. Scanned cross-cut of lherzolite F-16; b. Tabular to irregular opx are the most abundant minerals (reflected light on a polished thick section); c. Fractured cpx and opx on the contact with grt (crossed polars); d. Contact between partly fractionated opx and a irregular cpx grain. Note ol inclusions in cpx (BSE); e. BSE image of a fractured and banded opx grain. Note ol and cpx inclusions in opx and cpx; f. BSE figure of an irregularly shaped cpx grain; g. Skeletal sp, am and secondary cpx at a grt reaction rim. Note round ol inclusions in the large cpx grain (BSE).

Finsch F-21:

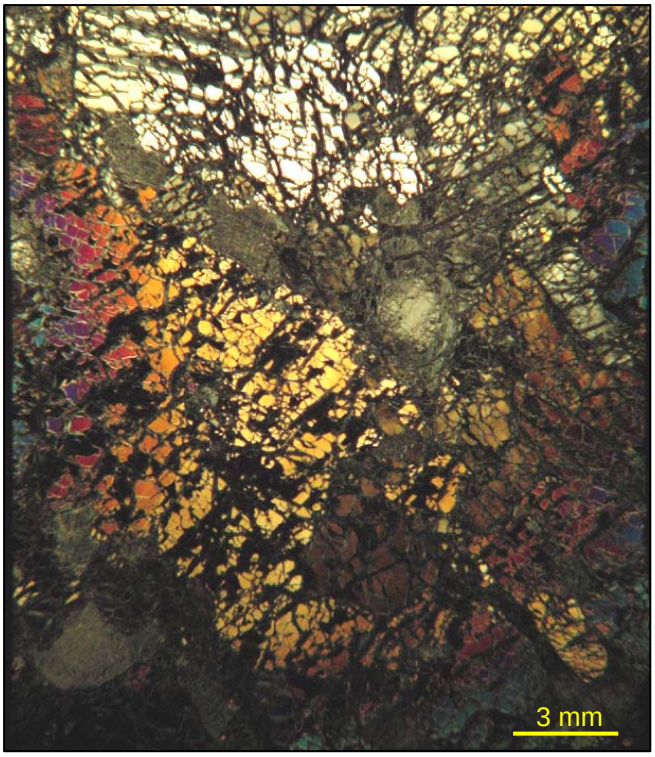

Sample F-21 is a coarse-grain tabular peridotite. Large (5-10 mm long) tabular ol grains have undulose extinction. Opx are smaller 2 to 5 mm in diameter. They are rounded, oval or irregular in shape, with strongly fractured rims. Neither cpx nor grt was found in this thin section.

Finsch F-22:

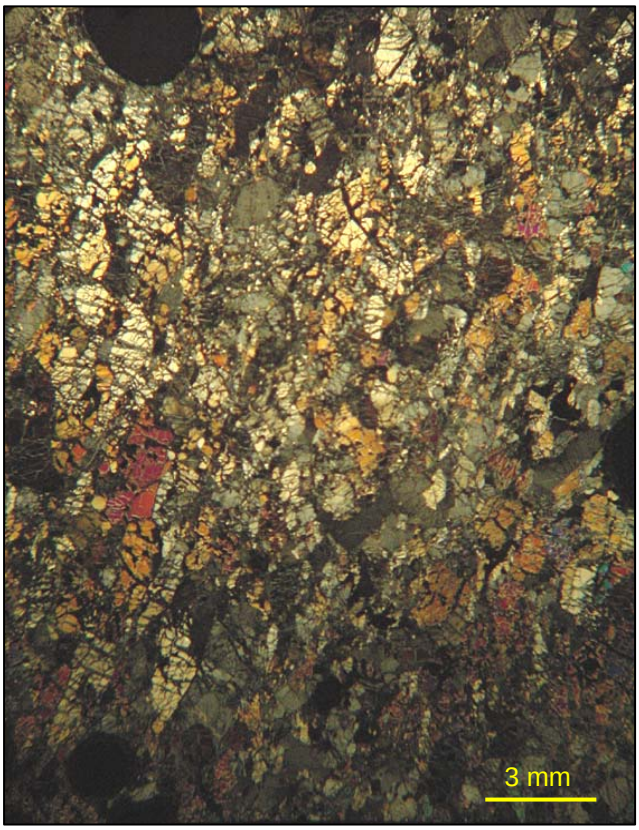

Middle to coarse grain texture is characteristic of this garnet bearing peridotite. Olivine and opx grains have subhedral elongated shape, while garnets are rounded. Poorly developed foliation is marked by grain elongation. Grain size of ol and opx varies from 0.5 to 4 mm in length. Most common are 2 mm long grains. Interstitial ol neoblasts ~50 µm long are rare. Garnets can have up to 5 mm in diameter. They have 0.5 mm thick reaction rims with tenuous crystals.
According to the CaO-Cr_2O_3 content of grt, this peridotite also contains cpx, which is, however, not observed in the thin section.

Finsch F-23:

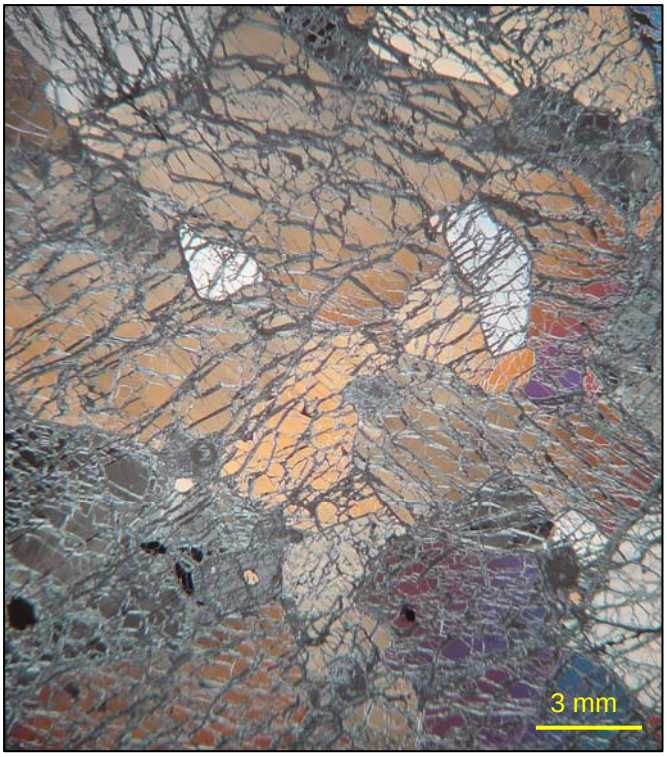

This spinel peridotite has a coarse grain tabular texture. Olivines are the most common minerals in this rock. They are large (up to 1.2 cm), with idiomorphic tabular shape. Largest grains show undulose extinction. Opx are also tabular to slightly oval in shape. They are strongly fractured and chloritized. Rare rounded olivines are included in opx grains. Spinel are octahedral with rounded or zig-zag angles. The size of the spinel grains reaches up to 1.5 mm. Spinel has a dark-orange to brown colour.

Finsch F-24:

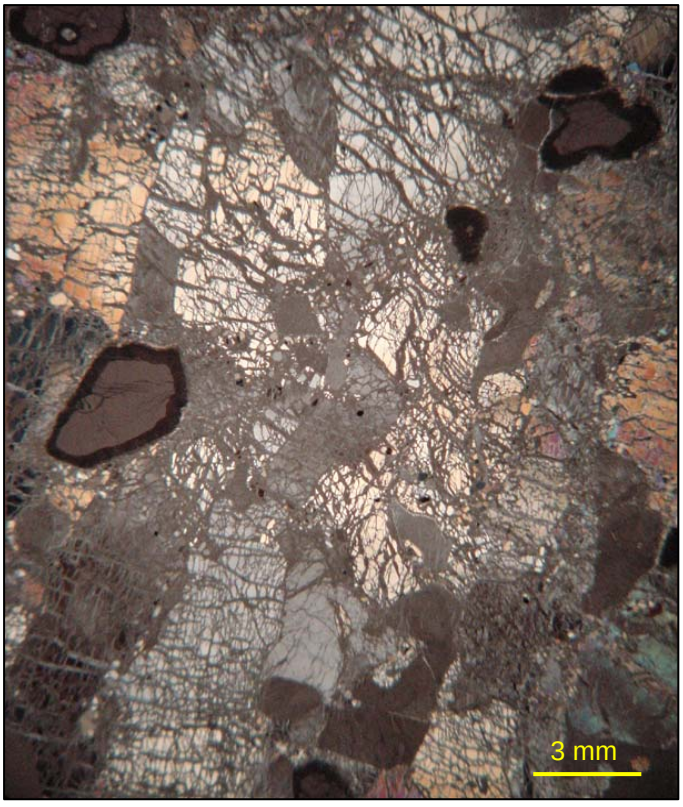

Common triple junctions mark coarse tabular texture of this rock. Olivines are tabular with oval grain boundaries and can be from 2 to 7 mm long. Opx have a variable shape from prismatic angular to irregular elongated with rounded edges. Rounded opx are very rare. Cpx are rare and generally smaller than opx. They are filling intersticies and therefore are irregular in shape. Size of garnets can extend 5 mm. They are elongated, angular to irregular in shape. Garnets have up to 1mm thick spinel-rich reaction rims. Olivine is a common inclusion in garnet and opx.

Finsch F-25a:

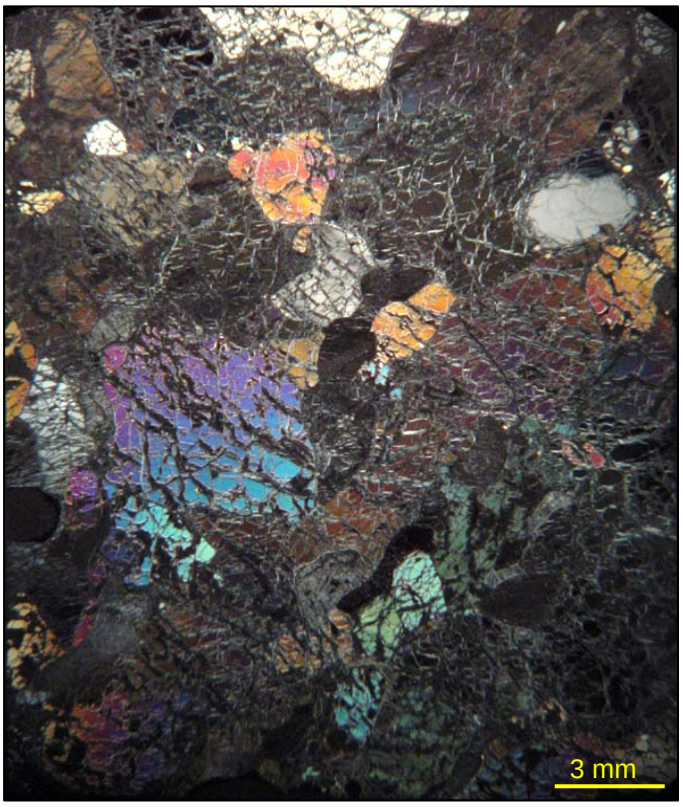

This garnet bearing lherzolite has a coarse-grain tabular texture. Equant grain olivines are with a length of 7 mm the largest grains in this peridotite. Opx and Cpx are subhedral elongared with rounded edges or irregular in shape. Some opx are strong fractured and some have only deformed edges. Rare cpx show twinning lamely. Only one round garnet with 3 mm in diameter was observed in thin section. This garnet grain has a thin reaction rim.

Finsch F-25b:

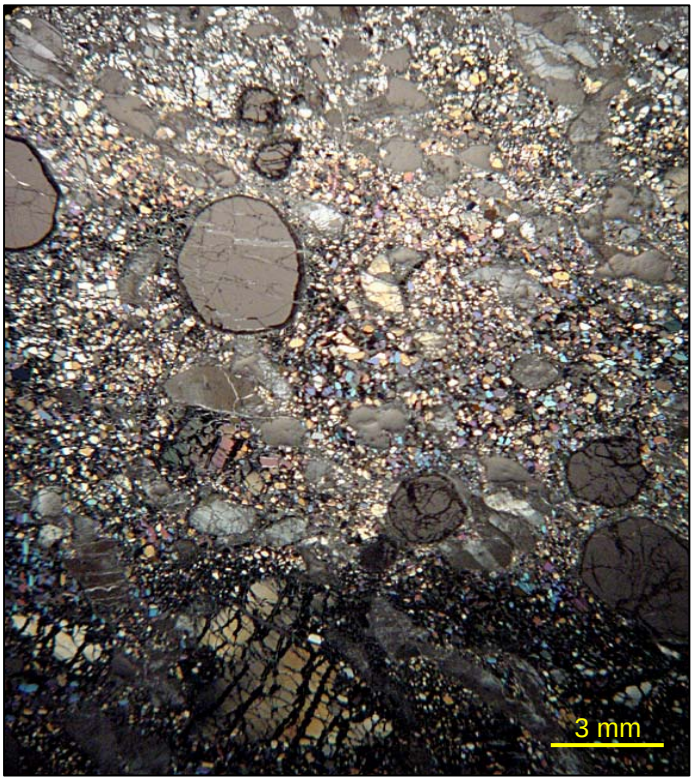

Larger opx and grt porphyroclasts in a fine grain 10-50 µm olivine matrix create the porphyroclastic texture of this peridotite. olivines grains larger than 5 to 10 mm in length are rare. Opx are either prismatic or strongly elongated in shape. Those grains can reach up to 8 mm length. Cpx are small, rounded to oval in shape and have neoblastic cpx on their rims. Some cpx have twinning lamely. Garnets are oval or irregular, and smaller grains are more deformed than larger ones. They have thin reaction rims. Sp, amph and phl is associated with garnet keliphytes and garnet fractures.

Finsch F-25c:

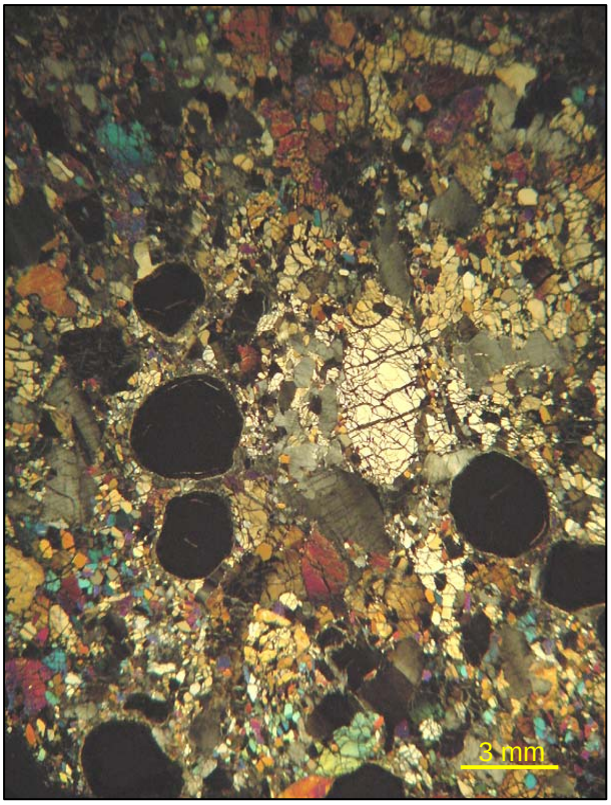

Sample F-25c is a porphyroclastic garnet bearing peridotite. Some olivine grains are large from 2-5 mm long tabular to elongated, but most of them occur as oval fine-grain (50-200 µm) matrix olivine. Large opx are subhedral prismatic, while smaller grains have anhedral to irregular shape. Larger opx grains are partially deformed. They all have undulose extinction. Garnets are angular and rarely completely rounded. Spinel, amph and phl are associated with garnet thick keliphyte. Some garnets are partially deformed and cracks are filled with phl. Cpx were not observed in thin section, but based on garnet Ca-Cr compositions this peridotite is a cpx-bearing harzburgite.

Finsch F-25d:

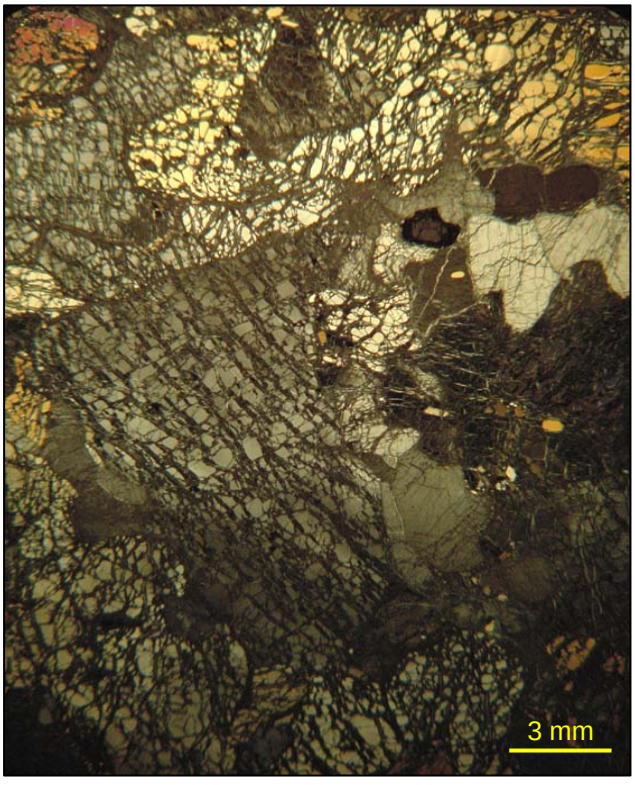

Large olivine grains dominate in this coarse-grain tabular garnet-bearing peridotite. Subhedral, tabular olivine with curvilinear boundaries have undulouse extinction. Tabular subhedral to irregular opx grains are evidently smaller than olivine. Curvilinear opx boundaries are commonly fractured. Opx shows sector unulouse extinction. Oval olivines are sometimes included in opx. Irregular Grt grains have thick reaction rim. Spinel, am, cpx and phl are products of garnet break-down reactions.

In thin-section only fine grain cpx (20-50 µm) is observed at opx crosses. Garnet from this sample is Ca-saturated that constrains coexistence with cpx.

Finsch F-26:

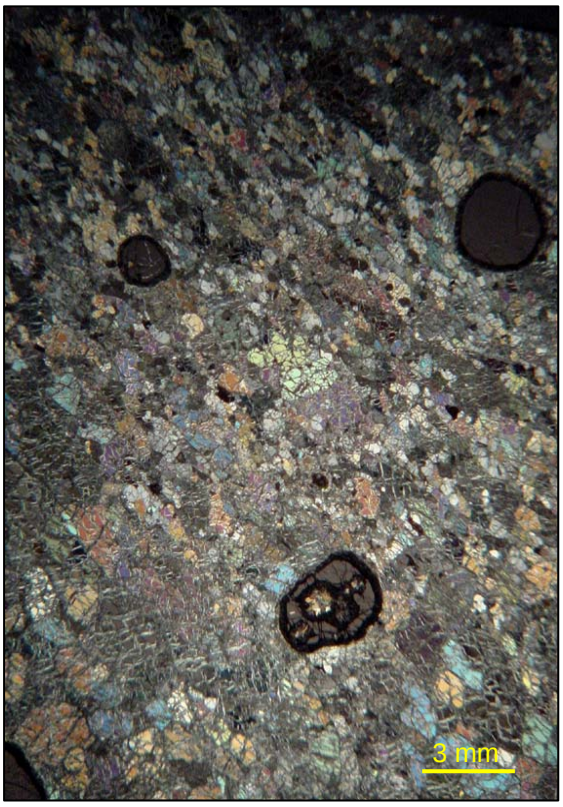

This lherzolite has a porphyroclastic texture, where grain elongation marks foliation (all grains except grt). Olivine, opx, and cpx occur as similarly 0.2 to 1 mm elongated grains, with the most common fraction of around 0.5 mm. Olivine is rarely up to 3 mm long. Opx and cpx show undulose extinction. Garnets are round and up to 5 mm in diameter. Fine grain phl, sp sometimes larger cpx and am are on grt reaction rims. Phlogopite also occurs in grt fractures.

Finsch F-28:

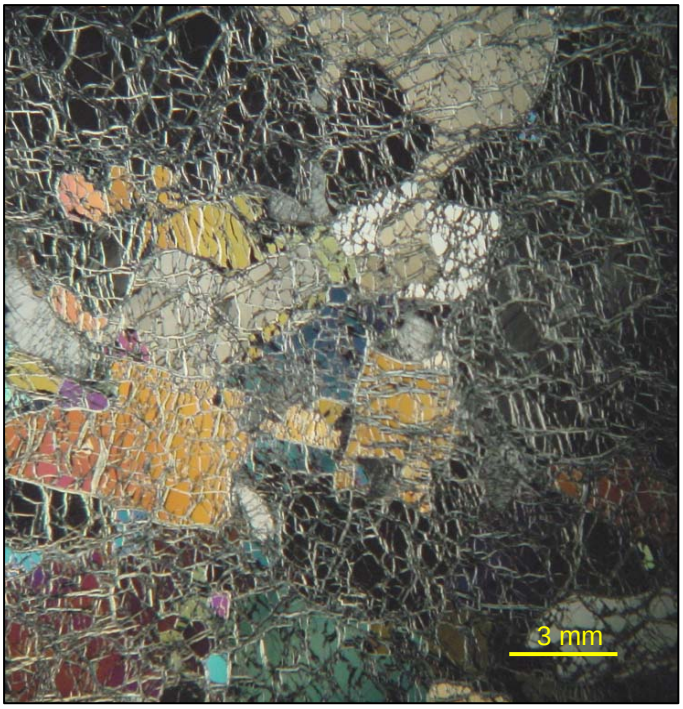

Only olivine and opx are observed in this coarse-grain tabular peridotite. Olivine is the dominant mineral and waries in shape and size. They are euhedral tabular or subhedral elongated and can have 1 to 10 mm in length. Opx are smaller than ol, maximal 4 mm long. They are elongated to irregular in shape and strongly fractured. Both, olivine and opx display undulose extinction.

Table 4.1 *Major element compositions of olivine (ol), orthopyroxene (opx), clinoproxene (cpx) and garnet (grt) from Finsch peridotites (EPMA)*

	Olivine																											
Sample	**F-1**		**F-2**		**F-3**		**F-4**		**F-5**		**F-6**		**F-7**		**F-8**		**F-9**	**F-10**		**F-11**		**F-12**		**F-13**		**F-14**		**F-15**	
comment		Ca in ol		Ca in ol		Ca in ol		Ca in ol		Ca in ol		Ca in ol		Ca in ol		Ca in ol			Ca in ol		Ca in ol		Ca in ol		Ca in ol		Ca in ol
n	12	10	13	8	19	15	10	12	14	16	16	12	13	18	17	12	40	6	10	25	12	22	9	17	12	24	15	20	13
SiO_2	41.07	40.84	41.39	41.46	40.79	41.14	41.06	41.20	41.48	41.48	41.19	41.24	41.23	41.56	40.97	41.21	40.55	41.19	41.09	40.94	41.32	40.37	41.20	40.15	40.74	40.88	41.00	41.23	41.45
Na_2O	0.03		0.03		0.02		0.02		0.02		0.02		0.01		0.02		0.03	0.02		0.02		0.02		0.02		0.01		0.02	
CaO	0.05	0.04	0.03	0.03	0.03	0.03	0.04	0.03	0.04	0.03	0.04	0.04	0.03	0.03	0.04	0.03	0.04	0.04	0.03	0.04	0.04	0.03	0.03	0.04	0.04	0.04	0.04	0.04	0.03
MnO	0.12	0.10	0.10	0.09	0.09	0.09	0.12	0.10	0.10	0.09	0.11	0.11	0.10	0.09	0.10	0.10	0.11	0.09	0.09	0.12	0.11	0.10	0.09	0.11	0.10	0.11	0.11	0.11	0.10
MgO	50.83	49.95	52.02	51.56	52.72	52.00	51.47	50.52	52.12	51.08	51.26	50.27	52.22	51.31	51.95	51.30	51.82	51.90	51.24	50.53	49.97	51.19	51.16	50.97	49.70	51.15	50.56	52.26	50.82
Cr_2O_3	0.03		0.04		0.04		0.04		0.04		0.05		0.04		0.04		0.07	0.02		0.05		0.03		0.02		0.04		0.04	
FeO*	8.85	8.44	7.15	6.81	6.51	6.26	8.19	7.81	7.38	7.06	8.40	8.11	6.94	6.72	7.49	7.20	7.68	7.73	7.64	8.58	8.28	7.33	7.35	8.88	8.50	8.45	8.09	7.55	7.36
Al_2O_3	0.02		0.02		0.02		0.03		0.02		0.02		0.02		0.02		0.02	0.02		0.02		0.02		0.02		0.02		0.02	
NiO	0.40	0.39	0.38	0.36	0.36	0.34	0.41	0.40	0.41	0.41	0.40	0.40	0.41	0.41	0.38	0.36	0.37	0.40	0.41	0.39	0.39	0.34	0.35	0.40	0.38	0.39	0.38	0.38	0.38
Total	101.43	99.77	101.19	100.33	100.59	99.86	101.39	100.07	101.65	100.16	101.52	100.16	101.03	100.12	101.03	100.21	100.72	101.44	100.52	100.71	100.11	99.48	100.19	100.63	99.45	101.12	100.17	101.66	100.13
4 O																													
Si	0.9900	0.9983	0.9920	0.9998	0.9821	0.9949	0.9875	1.0006	0.9910	1.0027	0.9899	1.0019	0.9893	1.0036	0.9859	0.9970	0.9807	0.9880	0.9937	0.9925	1.0048	0.9864	0.9976	0.9775	0.9990	0.9870	0.9964	0.3287	1.0035
Na	0.0012		0.0012		0.0010		0.0009		0.0009		0.0009		0.0006		0.0009		0.0012	0.0011		0.0010		0.0010		0.0011		0.0006		0.0003	
Ca	0.0012	0.0010	0.0008	0.0008	0.0008	0.0007	0.0010	0.0009	0.0010	0.0008	0.0010	0.0010	0.0008	0.0007	0.0010	0.0009	0.0010	0.0011	0.0008	0.0010	0.0009	0.0008	0.0008	0.0012	0.0010	0.0011	0.0010	0.0003	0.0008
Mn	0.0024	0.0021	0.0021	0.0019	0.0018	0.0018	0.0024	0.0022	0.0021	0.0019	0.0023	0.0022	0.0021	0.0018	0.0021	0.0021	0.0023	0.0018	0.0019	0.0024	0.0022	0.0021	0.0019	0.0022	0.0021	0.0024	0.0023	0.0008	0.0020
Mg	1.8265	1.8200	1.8587	1.8534	1.8924	1.8746	1.8453	1.8292	1.8561	1.8409	1.8365	1.8206	1.8680	1.8467	1.8637	1.8502	1.8682	1.8555	1.8471	1.8262	1.8112	1.8642	1.8464	1.8499	1.8169	1.8413	1.8320	0.6210	1.8338
Cr	0.0007		0.0007		0.0008		0.0008		0.0007		0.0008		0.0007		0.0008		0.0013	0.0004		0.0009		0.0006		0.0005		0.0008		0.0003	
Fe^{tot}	0.1785	0.1726	0.1435	0.1374	0.1310	0.1265	0.1647	0.1587	0.1474	0.1429	0.1688	0.1647	0.1392	0.1357	0.1507	0.1458	0.1553	0.1550	0.1546	0.1741	0.1684	0.1498	0.1488	0.1808	0.1745	0.1705	0.1644	0.0504	0.1490
Al	0.0007		0.0006		0.0004		0.0007		0.0007		0.0006		0.0006		0.0005		0.0006	0.0006		0.0006		0.0005		0.0006		0.0005		0.0002	
Ni	0.0077	0.0078	0.0074	0.0070	0.0070	0.0067	0.0079	0.0078	0.0079	0.0080	0.0078	0.0077	0.0080	0.0080	0.0073	0.0070	0.0072	0.0077	0.0081	0.0076	0.0076	0.0068	0.0069	0.0078	0.0075	0.0077	0.0075	0.0024	0.0073
Total	3.0094	3.0017	3.0075	3.0004	3.0176	3.0052	3.0117	2.9994	3.0083	2.9972	3.0092	2.9981	3.0097	2.9965	3.0133	3.0030	3.0184	3.0114	3.0063	3.0068	2.9952	3.0128	3.0024	3.0219	3.0011	3.0123	3.0036	1.0044	2.9965
Mg#	91.10	91.34	92.84	93.10	93.52	93.68	91.81	92.02	92.64	92.80	91.58	91.70	93.07	93.15	92.52	92.70	92.32	92.29	92.28	91.30	91.49	92.56	92.54	91.10	91.24	91.52	91.77	92.50	92.48
Fo	90.99	91.24	92.74	93.01	93.44	93.60	91.70	91.92	92.54	92.71	91.48	91.60	92.97	93.07	92.42	92.60	92.22	92.21	92.19	91.19	91.39	92.47	92.46	91.00	91.14	91.42	91.66	92.39	92.39

"Ca in ol" - longer measurement on Ca peak (see Chapter 2 for details)

n - number of analyses

* - Total Fe as FeO

4, 6, 12 O - formula calculated on 4, 6, 12 oxigen;

Table 4.1 *(continued)*

	Olivine																										
Sample	**F-16**		**F-21**		**F-22**		**F-23**		**F-24**		**F-25a**		**F-25b**		**F-25c**		**F-25d**		**F-26**		**F-28**		**554XM46**	**556XM48**	**695**	**865**	**882**
comment		Ca in ol		Ca in ol		Ca in ol		Ca in ol		Ca in ol		Ca in ol		Ca in ol		Ca in ol		Ca in ol		Ca in ol		Ca in ol			Ca in ol		Ca in ol
n	25	13	30	12	24	8	39	12	29	9	33	8	41	12	37	12	30	10	27	9	28	13	5	6	12	10	7
SiO_2	40.58	40.78	40.96	40.98	41.14	41.04	41.05	40.94	41.07	41.17	40.70	40.89	40.79	40.87	40.90	40.86	40.94	41.16	40.83	41.12	40.84	41.06	40.73	40.75	40.78	41.36	41.42
Na_2O	0.02		0.02		0.02		0.01		0.01		0.01		0.02		0.02		0.02		0.02		0.02						
CaO	0.04	0.03	0.03	0.03	0.03	0.03	0.02	0.02	0.04	0.04	0.04	0.04	0.04	0.04	0.04	0.04	0.03	0.03	0.03	0.03	0.03	0.03		0.04	0.03		0.03
MnO	0.10	0.10	0.11	0.10	0.10	0.09	0.11	0.10	0.10	0.10	0.12	0.11	0.11	0.10	0.11	0.10	0.11	0.10	0.11	0.10	0.11	0.10	0.09	0.11	0.12	0.08	0.09
MgO	50.75	50.23	51.22	50.89	51.78	51.25	51.64	51.20	51.54	51.24	50.52	50.27	50.53	50.10	50.96	50.72	51.42	51.11	51.14	50.86	51.14	50.90	51.40	50.41	50.46	50.78	51.63
Cr_2O_3	0.02		0.06		0.04		0.05		0.04		0.04		0.03		0.03		0.05		0.02		0.05		0.00	0.03		0.06	0.05
FeO*	8.44	8.15	7.49	7.24	7.17	6.93	7.09	6.88	7.26	7.05	8.26	7.95	8.70	8.34	7.85	7.56	7.30	7.04	7.87	7.55	7.40	7.04	7.88	7.97	7.97	6.90	6.21
Al_2O_3	0.02		0.02		0.02		0.02		0.02		0.02		0.02		0.02		0.02		0.02		0.02		0.00	0.02		0.05	
NiO	0.42	0.40	0.36	0.35	0.39	0.39	0.36	0.35	0.36	0.35	0.38	0.37	0.39	0.37	0.37	0.36	0.35	0.36	0.38	0.38	0.37	0.36	0.37	0.41	0.30	0.41	0.28
Total	100.40	99.69	100.27	99.60	100.71	99.74	100.36	99.50	100.45	99.95	100.11	99.63	100.66	99.82	100.32	99.65	100.27	99.79	100.45	100.04	100.00	99.48	100.47	99.75	99.66	99.64	99.71
4 O																											
Si	0.9871	0.9966	0.9924	0.9979	0.9912	0.9966	0.9920	0.9964	0.9922	0.9979	0.9916	0.9985	0.9902	0.9979	0.9921	0.9961	0.9913	0.9990	0.9897	0.9981	0.9920	0.9997	0.9871	0.9947	0.9957	1.0042	1.0017
Na	0.0008		0.0010		0.0007		0.0005		0.0006		0.0007		0.0011		0.0009		0.0010		0.0008		0.0011						
Ca	0.0011	0.0008	0.0008	0.0009	0.0009	0.0009	0.0006	0.0006	0.0010	0.0009	0.0010	0.0009	0.0011	0.0010	0.0011	0.0011	0.0008	0.0008	0.0009	0.0009	0.0008	0.0007		0.0009	0.0008		0.0008
Mn	0.0021	0.0020	0.0022	0.0021	0.0020	0.0019	0.0023	0.0021	0.0021	0.0020	0.0024	0.0023	0.0023	0.0021	0.0022	0.0021	0.0022	0.0020	0.0022	0.0020	0.0023	0.0021	0.0018	0.0022	0.0025	0.0016	0.0018
Mg	1.8404	1.8296	1.8498	1.8471	1.8595	1.8555	1.8601	1.8576	1.8561	1.8515	1.8349	1.8300	1.8287	1.8235	1.8429	1.8433	1.8560	1.8493	1.8477	1.8402	1.8519	1.8475	1.8570	1.8347	1.8367	1.8380	1.8614
Cr	0.0003		0.0011		0.0007		0.0009		0.0007		0.0007		0.0005		0.0006		0.0009		0.0004		0.0010			0.0015		0.0012	0.0010
Fe^{tot}	0.1716	0.1666	0.1518	0.1475	0.1445	0.1408	0.1434	0.1400	0.1466	0.1428	0.1682	0.1624	0.1767	0.1703	0.1593	0.1542	0.1479	0.1428	0.1596	0.1533	0.1503	0.1434	0.1597	0.1627	0.1627	0.1401	0.1256
Al	0.0006		0.0005		0.0005		0.0005		0.0005		0.0004		0.0006		0.0006		0.0005		0.0006		0.0005			0.0006		0.0014	
Ni	0.0082	0.0078	0.0070	0.0068	0.0076	0.0077	0.0069	0.0068	0.0070	0.0069	0.0075	0.0074	0.0075	0.0073	0.0072	0.0071	0.0069	0.0071	0.0074	0.0074	0.0072	0.0070	0.0072	0.0081	0.0059	0.0080	0.0054
Total	3.0125	3.0035	3.0070	3.0023	3.0081	3.0033	3.0074	3.0036	3.0072	3.0021	3.0079	3.0016	3.0093	3.0022	3.0073	3.0039	3.0080	3.0010	3.0097	3.0019	3.0075	3.0004	3.0129	3.0047	3.0043	2.9945	2.9978
Mg#	91.47	91.65	92.41	92.61	92.79	92.95	92.84	92.99	92.68	92.84	91.60	91.85	91.19	91.46	92.05	92.28	92.62	92.83	92.05	92.31	92.49	92.80	92.08	91.86	91.86	92.92	93.68
Fo	91.37	91.56	92.31	92.51	92.70	92.86	92.74	92.89	92.58	92.74	91.49	91.74	91.08	91.36	91.94	92.19	92.52	92.74	91.95	92.22	92.39	92.70	92.00	91.75	91.75	92.84	93.59

Table 4.1 *(continued)*

	opx																										
Sample	**F-1**	**F-2**	**F-3**	**F-4**	**F-5**	**F-6**	**F-7**	**F-8**	**F-9**	**F-10**	**F-11**	**F-12**	**F-13**	**F-14**	**F-15**	**F-16**	**F-21**	**F-22**	**F-23**	**F-24**	**F-25a**	**F-25b**	**F-25c**	**F-25d**	**F-26**	**F-28**	**554XM46**
comment																											
n	22	12	14	18	22	14	20	6	18	12	19	24	7	30	16	20	32	24	39	29	33	41	37	30	27	28	4
SiO_2	58.11	58.43	57.70	57.76	58.53	58.27	58.30	58.05	57.41	58.09	57.75	56.88	57.03	58.04	58.44	57.58	57.60	58.03	57.71	57.91	57.45	57.66	57.65	57.63	57.61	57.49	56.71
K_2O					0.01					0.01											0.01						
Na_2O	0.17	0.16	0.15	0.10	0.09	0.15	0.05	0.14	0.19	0.16	0.16	0.16	0.18	0.07	0.14	0.13	0.18	0.08	0.03	0.07	0.08	0.15	0.15	0.17	0.13	0.15	
CaO	0.71	0.65	0.60	0.68	0.64	0.73	0.47	0.66	0.66	0.61	0.73	0.63	0.71	0.74	0.64	0.66	0.63	0.62	0.36	0.63	0.68	0.70	0.67	0.61	0.66	0.56	0.74
MnO	0.13	0.11	0.10	0.13	0.11	0.14	0.11	0.12	0.13	0.11	0.14	0.11	0.13	0.13	0.12	0.12	0.12	0.11	0.12	0.11	0.13	0.12	0.12	0.12	0.12	0.12	0.10
MgO	35.50	36.11	36.55	35.96	36.40	35.82	36.61	36.16	36.01	35.48	35.22	35.71	35.47	35.79	35.71	35.57	35.51	36.18	36.45	36.08	35.37	35.27	35.56	35.59	35.60	35.65	36.05
Cr_2O_3	0.21	0.41	0.40	0.34	0.30	0.31	0.32	0.33	0.50	0.29	0.35	0.31	0.19	0.29	0.28	0.15	0.51	0.28	0.41	0.30	0.32	0.21	0.25	0.49	0.23	0.50	0.28
FeO*	5.29	4.29	3.91	4.92	4.43	5.03	4.16	4.47	4.59	4.68	5.11	4.45	5.30	5.04	4.55	5.05	4.49	4.29	4.24	4.35	4.91	5.23	4.70	4.39	4.73	4.41	4.65
Al_2O_3	0.64	0.56	0.60	0.57	0.56	0.60	0.58	0.57	0.53	0.66	0.59	0.61	0.67	0.52	0.60	0.64	0.57	0.54	0.53	0.51	0.51	0.64	0.62	0.59	0.63	0.56	0.43
TiO_2	0.07	0.03	0.04	0.02	0.01	0.03	0.02	0.07	0.07	0.05	0.05	0.20	0.09	0.02	0.02	0.01	0.03	0.01	0.01	0.01	0.01	0.06	0.04	0.07	0.04	0.04	
NiO	0.12	0.11	0.10	0.14	0.12	0.12	0.13	0.12	0.11	0.12	0.12	0.10	0.13	0.13	0.11	0.12	0.10	0.12	0.10	0.11	0.11	0.11	0.11	0.11	0.11	0.12	0.12
Total	100.95	100.87	100.15	100.63	101.20	101.18	100.76	100.71	100.20	100.26	100.22	99.39	99.93	100.77	100.62	100.05	99.75	100.27	99.97	100.10	99.58	100.15	99.89	99.78	99.87	99.60	99.08
6 O																											
Si	1.9790	1.9824	1.9704	1.9718	1.9800	1.9782	1.9780	1.9754	1.9675	1.9879	1.9803	1.9699	1.9654	1.9784	1.9882	1.9765	1.9795	1.9801	1.9747	1.9804	1.9805	1.9787	1.9792	1.9788	1.9783	1.9778	1.9548
K					0.0003					0.0002											0.0004						
Na	0.0110	0.0107	0.0101	0.0069	0.0059	0.0096	0.0034	0.0095	0.0123	0.0109	0.0108	0.0109	0.0122	0.0049	0.0089	0.0089	0.0119	0.0051	0.0019	0.0048	0.0052	0.0097	0.0102	0.0115	0.0088	0.0098	
Ca	0.0259	0.0236	0.0220	0.0250	0.0233	0.0266	0.0171	0.0241	0.0242	0.0223	0.0267	0.0233	0.0263	0.0272	0.0233	0.0244	0.0232	0.0227	0.0131	0.0231	0.0251	0.0256	0.0245	0.0224	0.0242	0.0205	0.0273
Mn	0.0037	0.0032	0.0029	0.0037	0.0032	0.0039	0.0031	0.0035	0.0037	0.0032	0.0040	0.0032	0.0038	0.0037	0.0033	0.0034	0.0036	0.0032	0.0036	0.0032	0.0039	0.0035	0.0034	0.0035	0.0034	0.0035	0.0029
Mg	1.8021	1.8263	1.8603	1.8302	1.8355	1.8126	1.8516	1.8345	1.8400	1.8018	1.8004	1.8363	1.8221	1.8188	1.8111	1.8202	1.8189	1.8405	1.8591	1.8390	1.8177	1.8045	1.8199	1.8215	1.8221	1.8282	1.8525
Cr	0.0056	0.0111	0.0107	0.0091	0.0079	0.0082	0.0087	0.0090	0.0136	0.0078	0.0094	0.0058	0.0052	0.0077	0.0075	0.0041	0.0138	0.0076	0.0112	0.0082	0.0087	0.0056	0.0069	0.0133	0.0063	0.0136	0.0076
Fe^{tot}	0.1508	0.1216	0.1116	0.1404	0.1255	0.1427	0.1180	0.1273	0.1316	0.1335	0.1466	0.1283	0.1529	0.1437	0.1296	0.1450	0.1291	0.1226	0.1214	0.1244	0.1415	0.1501	0.1349	0.1261	0.1359	0.1268	0.1340
Al	0.0258	0.0224	0.0241	0.0229	0.0223	0.0239	0.0234	0.0229	0.0215	0.0266	0.0240	0.0249	0.0273	0.0208	0.0240	0.0258	0.0232	0.0218	0.0212	0.0205	0.0206	0.0259	0.0250	0.0239	0.0255	0.0228	0.0175
Ti	0.0017	0.0006	0.0010	0.0006	0.0003	0.0007	0.0004	0.0019	0.0017	0.0012	0.0012	0.0078	0.0024	0.0004	0.0005	0.0003	0.0007	0.0002	0.0003	0.0003	0.0003	0.0015	0.0012	0.0019	0.0011	0.0010	
Ni	0.0033	0.0031	0.0027	0.0037	0.0034	0.0034	0.0034	0.0032	0.0030	0.0033	0.0033	0.0029	0.0037	0.0034	0.0031	0.0034	0.0028	0.0032	0.0027	0.0029	0.0031	0.0031	0.0031	0.0029	0.0031	0.0033	0.0033
Total	4.009	4.005	4.016	4.014	4.007	4.010	4.007	4.011	4.019	3.999	4.007	4.013	4.021	4.009	4.000	4.012	4.007	4.007	4.009	4.007	4.007	4.008	4.008	4.006	4.009	4.007	4.000
Mg#	92.28	93.76	94.34	92.87	93.60	92.70	94.01	93.51	93.33	93.10	92.47	93.47	92.26	92.68	93.32	92.62	93.37	93.76	93.87	93.66	92.78	92.32	93.10	93.52	93.06	93.51	93.25
Ca#	1.42	1.28	1.17	1.35	1.25	1.45	0.92	1.30	1.30	1.22	1.46	1.26	1.42	1.47	1.27	1.32	1.26	1.22	0.70	1.24	1.36	1.40	1.33	1.21	1.31	1.11	1.45
Cr#	17.89	33.05	30.70	28.55	26.19	25.60	27.12	28.14	38.69	22.73	28.23	18.81	16.09	26.98	23.69	13.79	37.30	25.84	34.55	28.55	29.71	17.87	21.66	35.66	19.76	37.42	30.40

Table 4.1 *(continued)*

	opx				cpx																	
Sample	**556XM48**	**695**	**865**	**882**	**F-1**	**F-3**	**F-3**	**F-4**	**F-5**	**F-6**	**F-8**	**F-10**	**F-11**	**F-11**	**F-12**	**F-13**	**F-14**	**F-15**	**F-16**	**F-26**	**F-25b**	**F-25c**	**695**
comment						core	rim						core	rim									
n	7	5	5	4	18	7	8	13	9	14	18	12	10	8	16	17	17	9	27	10	32	31	3
SiO_2	57.43	58.57	57.76	59.03	55.46	54.76	54.34	55.14	55.55	55.49	54.95	55.32	55.39	54.77	55.25	54.33	55.26	55.66	54.90	54.96	54.87	54.92	55.31
K_2O					0.04	0.11	0.01	0.09	0.12	0.09	0.07	0.07	0.08		0.07	0.06	0.08	0.04	0.03	0.05	0.03	0.07	0.09
Na_2O	0.07	0.12	0.08	0.06	1.63	1.87	1.19	1.18	0.99	1.38	1.49	1.91	1.57	0.90	1.93	1.77	0.72	1.49	1.52	1.46	1.46	1.46	1.40
CaO	0.75	0.68	0.55	0.47	19.18	18.94	21.09	20.18	20.77	19.45	19.37	18.82	18.90	20.87	18.96	18.53	20.66	19.51	19.14	18.95	18.75	18.81	19.58
MnO	0.12	0.11	0.10	0.10	0.11	0.08	0.08	0.10	0.09	0.11	0.10	0.10	0.11	0.11	0.10	0.11	0.10	0.09	0.09	0.10	0.10	0.10	0.12
MgO	35.19	35.86	35.93	36.76	18.16	17.68	17.84	18.49	18.59	18.43	18.15	17.27	17.93	17.94	17.70	18.08	19.05	17.90	17.95	17.94	17.94	17.92	18.13
Cr_2O_3	0.28	0.35	0.30	0.44	1.07	2.43	2.62	1.48	1.21	1.48	1.73	1.72	1.73	1.89	1.84	1.02	1.00	1.46	0.86	1.25	1.06	1.49	1.80
FeO*	4.69	4.60	4.13	3.77	2.84	1.85	1.64	2.50	2.07	2.59	2.28	2.33	2.68	2.54	2.27	2.86	2.50	2.23	2.56	2.52	2.80	2.45	2.32
Al_2O_3	0.51	0.56	0.55	0.53	1.90	1.68	0.57	1.18	1.16	1.48	1.56	2.17	1.57	0.63	1.92	2.17	0.86	1.69	2.09	1.86	1.89	1.78	1.36
TiO_2		0.04	0.05		0.11	0.07	0.09	0.04	0.01	0.06	0.10	0.10	0.08	0.18	0.43	0.17	0.03	0.03	0.03	0.08	0.11	0.11	0.07
NiO	0.13		0.13		0.06	0.05	0.04	0.07	0.08	0.06	0.06	0.07	0.07	0.05	0.05	0.06	0.06	0.05	0.06	0.06	0.06	0.05	
Total	99.19	100.89	99.46	101.16	100.57	99.51	99.52	100.46	100.65	100.62	99.86	99.90	100.11	99.90	100.54	99.17	100.34	100.16	99.24	99.24	99.09	99.16	100.18
6 O																							
Si	1.9852	1.9871	1.9840	1.9885	1.9868	1.9833	1.9789	1.9832	1.9899	1.9881	1.9836	1.9925	1.9940	1.9860	1.9804	1.9749	1.9876	1.9982	1.9892	1.9917	1.9920	1.9913	1.9884
K					0.0017	0.0049	0.0005	0.0040	0.0056	0.0039	0.0031	0.0031	0.0039		0.0032	0.0027	0.0039	0.0020	0.0014	0.0023	0.0016	0.0033	0.0041
Na	0.0044	0.0079	0.0054	0.0039	0.1130	0.1310	0.0843	0.0821	0.0686	0.0959	0.1043	0.1337	0.1091	0.0635	0.1342	0.1249	0.0504	0.1036	0.1070	0.1028	0.1030	0.1002	0.0976
Ca	0.0278	0.0247	0.0193	0.0170	0.7363	0.7350	0.8231	0.7778	0.7971	0.7467	0.7494	0.7261	0.7290	0.8110	0.7283	0.7218	0.7963	0.7503	0.7431	0.7359	0.7293	0.7344	0.7542
Mn	0.0034	0.0032	0.0030	0.0029	0.0033	0.0026	0.0024	0.0031	0.0028	0.0033	0.0029	0.0031	0.0032	0.0035	0.0029	0.0032	0.0032	0.0026	0.0029	0.0030	0.0032	0.0030	0.0037
Mg	1.8133	1.8137	1.8400	1.8460	0.9700	0.9545	0.9681	0.9914	0.9928	0.9844	0.9765	0.9273	0.9621	0.9700	0.9454	0.9796	1.0217	0.9577	0.9695	0.9692	0.9708	0.9701	0.9716
Cr	0.0077	0.0094	0.0081	0.0117	0.0302	0.0697	0.0754	0.0422	0.0342	0.0420	0.0494	0.0489	0.0493	0.0545	0.0523	0.0293	0.0285	0.0416	0.0245	0.0358	0.0303	0.0430	0.0512
Fe^{tot}	0.1357	0.1305	0.1177	0.1062	0.0850	0.0561	0.0501	0.0751	0.0622	0.0778	0.0687	0.0703	0.0808	0.0770	0.0681	0.0870	0.0753	0.0671	0.0775	0.0763	0.0849	0.0744	0.0697
Al	0.0210	0.0224	0.0225	0.0210	0.0804	0.0716	0.0244	0.0498	0.0489	0.0625	0.0663	0.0924	0.0664	0.0271	0.0813	0.0929	0.0364	0.0716	0.0892	0.0795	0.0808	0.0740	0.0576
Ti		0.0010	0.0012		0.0031	0.0020	0.0024	0.0011	0.0003	0.0016	0.0028	0.0027	0.0022	0.0049	0.0116	0.0046	0.0007	0.0009	0.0007	0.0022	0.0030	0.0031	0.0019
Ni	0.0037		0.0036		0.0017	0.0014	0.0012	0.0020	0.0022	0.0018	0.0017	0.0021	0.0019	0.0014	0.0015	0.0018	0.0018	0.0013	0.0017	0.0018	0.0018	0.0015	
Total	4.002	4.000	4.005	3.997	4.011	4.012	4.010	4.012	4.004	4.008	4.009	4.002	4.002	3.999	4.009	4.023	4.006	3.997	4.007	4.000	4.001	3.998	4.000
Mg#	93.04	93.29	93.90	94.56	91.95	94.45	95.08	92.96	94.11	92.68	93.42	92.95	92.26	92.65	93.28	91.85	93.14	93.46	92.60	92.71	91.96	92.87	93.30
Ca#	1.51	1.34	1.10	0.91	43.15	43.50	45.95	43.96	44.54	43.13	43.42	43.91	43.11	45.54	43.51	42.42	43.80	43.93	43.39	43.16	42.90	43.09	43.70
Cr#	26.83	29.54	27.99	35.77	27.31	49.34	75.56	45.86	41.17	40.20	42.70	34.62	42.59	66.83	39.15	24.00	43.91	36.74	21.57	31.06	27.28	36.73	47.03

Table 4.1 *(continued)*

	garnet																				
Sample	**F-1**	**F-2**	**F-3**	**F-4**	**F-5**	**F-6**	**F-7**	**F-8**	**F-9**	**F-10**	**F-11**	**F-12**	**F-13**	**F-14**	**F-15**	**F-16**	**F-22**	**F-24**	**F-25a**	**F-25b**	**F-25c**
comment																					
n	28	8	9	17	13	10	14	15	17	9	23	13	16	9	18	16	15	24	14	19	28
SiO_2	42.48	41.99	41.61	41.54	42.27	42.09	41.99	41.76	40.58	42.29	41.68	42.06	41.80	41.56	42.55	42.32	41.89	41.80	41.26	42.13	42.23
K_2O		0.01				0.01				0.01		0.01									
Na_2O	0.06	0.04	0.04	0.03	0.02	0.04	0.02	0.05	0.05	0.05	0.05	0.10	0.06	0.02	0.03	0.03	0.02	0.02	0.02	0.05	0.05
CaO	4.77	5.50	5.23	6.08	5.75	5.42	4.90	5.50	6.60	4.76	5.50	5.37	4.49	6.20	4.85	4.23	5.62	5.42	6.24	4.68	4.54
MnO	0.33	0.32	0.30	0.35	0.32	0.34	0.31	0.33	0.37	0.32	0.36	0.32	0.31	0.35	0.31	0.30	0.31	0.32	0.37	0.33	0.31
MgO	21.42	20.97	21.63	20.24	21.08	20.91	21.70	21.28	19.50	21.11	20.54	21.01	21.77	20.36	21.42	21.87	20.75	20.87	19.42	20.90	21.48
Cr_2O_3	3.39	7.90	6.26	7.55	6.36	6.00	7.59	6.30	10.62	4.56	6.57	5.32	2.73	7.47	4.33	2.07	6.47	6.93	8.03	3.43	3.90
P_2O_5	0.02	0.03		0.02	0.05	0.03	0.03	0.02	0.02	0.04	0.03	0.02	0.03		0.02	0.02	0.04			0.02	0.02
FeO*	7.53	6.17	5.70	6.97	6.35	7.08	6.13	6.44	6.64	6.74	7.26	6.63	7.41	7.05	6.49	7.13	6.25	6.28	7.00	7.46	6.77
Al_2O_3	20.66	17.80	18.87	17.69	19.03	18.88	18.16	18.68	14.95	20.10	18.04	18.95	21.03	17.77	20.44	21.94	18.70	18.29	17.27	20.58	20.42
TiO_2	0.35	0.20	0.24	0.22	0.08	0.21	0.07	0.41	0.52	0.24	0.32	0.94	0.43	0.14	0.13	0.07	0.07	0.11	0.08	0.34	0.27
NiO	0.01	0.01	0.02	0.02	0.01	0.01	0.01	0.02	0.02	0.01	0.02	0.01	0.02	0.01	0.02	0.02	0.01	0.01	0.01	0.01	0.01
Total	101.02	100.85	99.92	100.71	101.32	101.02	100.93	100.78	99.87	100.22	100.37	100.74	100.09	100.95	100.60	100.00	100.12	100.08	99.73	99.91	100.01
12 O																					
Si	3.0024	3.0043	2.9843	2.9930	2.9988	3.0015	2.9938	2.9827	2.9859	3.0117	3.0027	2.9972	2.9764	2.9890	3.0127	2.9972	3.0073	3.0066	3.0088	3.0089	3.0075
K		0.0006				0.0004				0.0005		0.0004									
Na	0.0076	0.0057	0.0058	0.0036	0.0030	0.0058	0.0028	0.0066	0.0078	0.0067	0.0068	0.0140	0.0086	0.0030	0.0047	0.0046	0.0024	0.0029	0.0029	0.0065	0.0065
Ca	0.3614	0.4219	0.4021	0.4696	0.4374	0.4141	0.3746	0.4209	0.5206	0.3633	0.4249	0.4101	0.3429	0.4778	0.3680	0.3211	0.4322	0.4179	0.4873	0.3580	0.3463
Mn	0.0197	0.0194	0.0181	0.0213	0.0192	0.0208	0.0187	0.0197	0.0229	0.0190	0.0219	0.0192	0.0189	0.0214	0.0186	0.0182	0.0189	0.0194	0.0227	0.0198	0.0186
Mg	2.2574	2.2369	2.3125	2.1742	2.2296	2.2222	2.3071	2.2658	2.1386	2.2412	2.2062	2.2323	2.3107	2.1828	2.2603	2.3088	2.2199	2.2376	2.1110	2.2250	2.2798
Cr	0.1894	0.4411	0.3552	0.4299	0.3566	0.3380	0.4279	0.3558	0.6177	0.2566	0.3744	0.2997	0.1538	0.4250	0.2424	0.1157	0.3674	0.3940	0.4631	0.1938	0.2195
P	0.0011	0.0020		0.0015	0.0028	0.0018	0.0021	0.0013	0.0013	0.0025	0.0020	0.0009	0.0015		0.0012	0.0012	0.0023			0.0012	0.0012
Fe^{tot}	0.4454	0.3691	0.3417	0.4202	0.3769	0.4219	0.3656	0.3845	0.4086	0.4015	0.4374	0.3953	0.4416	0.4242	0.3843	0.4221	0.3751	0.3781	0.4273	0.4455	0.4033
Al	1.7213	1.5010	1.5948	1.5021	1.5913	1.5868	1.5263	1.5722	1.2963	1.6869	1.5320	1.5920	1.7647	1.5063	1.7058	1.8319	1.5824	1.5509	1.4846	1.7331	1.7141
Ti	0.0186	0.0109	0.0130	0.0118	0.0040	0.0114	0.0035	0.0220	0.0289	0.0126	0.0176	0.0505	0.0233	0.0075	0.0072	0.0040	0.0036	0.0061	0.0042	0.0182	0.0147
Ni	0.0008	0.0007	0.0014	0.0009	0.0007	0.0004	0.0008	0.0009	0.0010	0.0008	0.0010	0.0007	0.0010	0.0005	0.0010	0.0009	0.0006	0.0004	0.0006	0.0005	0.0008
Total	8.0256	8.0136	8.0301	8.0283	8.0206	8.0252	8.0235	8.0327	8.0298	8.0033	8.0270	8.0122	8.0434	8.0383	8.0065	8.0260	8.0123	8.0150	8.0137	8.0106	8.0125
Mg#	83.52	85.84	87.12	83.80	85.54	84.04	86.32	85.49	83.96	84.81	83.45	84.96	83.96	83.73	85.47	84.54	85.54	85.54	83.17	83.32	84.97
Ca#	13.80	15.87	14.81	17.76	16.40	15.71	13.97	15.67	19.58	13.95	16.15	15.52	12.92	17.96	14.00	12.21	16.30	15.74	18.75	13.86	13.19
Cr#	9.91	22.71	18.21	22.25	18.31	17.56	21.90	18.46	32.27	13.20	19.64	15.84	8.02	22.01	12.44	5.94	18.84	20.26	23.78	10.06	11.35

Table 4.1 *(continued)*

	garnet						
Sample	**F-25d**	**F-26**	**554XM46**	**556XM48**	**865**	**695**	**882**
comment							
n	10	22	6	4	7	5	6
SiO_2	41.15	42.24	40.92	41.15	41.52	41.25	40.93
K_2O							
Na_2O	0.07	0.04	0.02	0.02	0.04	0.03	
CaO	5.78	4.58	6.21	6.04	4.91	5.89	6.14
MnO	0.35	0.32	0.36	0.34	0.31	0.35	0.33
MgO	20.18	21.33	19.80	19.90	21.52	20.15	20.22
Cr_2O_3	8.71	3.50	7.40	7.21	5.98	7.02	11.63
P_2O_5	0.03	0.03		0.02			
FeO*	6.43	6.78	6.79	6.72	6.01	6.66	5.59
Al_2O_3	16.51	20.76	17.66	17.79	19.15	18.34	14.96
TiO_2	0.50	0.23	0.11	0.09	0.204	0.28	0.17
NiO	0.01	0.01	0.02	0.01			
Total	99.74	99.82	99.42	99.29	99.67	99.97	99.97
12 O							
Si	2.9986	3.0093	2.9845	3.0011	3.0505	2.9757	2.9887
K							
Na	0.0094	0.0060	0.0030	0.0030	0.0060	0.0042	
Ca	0.4514	0.3498	0.4515	0.4720	0.3774	0.4552	0.4804
Mn	0.0216	0.0192	0.0215	0.0207	0.0188	0.0214	0.0204
Mg	2.1925	2.2654	2.1397	2.1629	2.2385	2.1669	2.2010
Cr	0.5018	0.1969	0.3916	0.4157	0.3165	0.4004	0.6714
P	0.0019	0.0017		0.0010			
Fe^{tot}	0.3918	0.4039	0.4094	0.4103	0.3606	0.4018	0.3414
Al	1.4183	1.7432	1.6018	1.5292	1.6192	1.5592	1.2874
Ti	0.0275	0.0125	0.0061	0.0050	0.0146	0.0152	0.0093
Ni	0.0007	0.0005	0.0009	0.0009			
Total	8.0157	8.0087	8.0100	8.0222	8.0022	8.0000	8.0000
Mg#	84.84	84.87	83.94	84.05	86.13	84.36	86.57
Ca#	17.07	13.37	17.42	17.91	14.43	17.36	17.91
Cr#	26.13	10.15	19.65	21.37	16.35	20.43	34.28

Table 4.2 *Major element composition of phlogopite, amphibole sec. Cpx, spinel, rutile from Finsch peridotites*

	rt																				sp
Sample	F12-rt1	F12-rt2	F12-rt3	F12-rt4	F12-rt5	F12-rt6	F12-rt7	F12-rt8	F12-rt9	F12-rt10	F12-rt11	F12-rt12	F12-rt13	F12-rt14	F12-rt15	F12-rt16	F12-rt17	F12-rt18	F12-rt19	F12-rt20	F-12	F3sp-1
comment																						
SiO_2	0.02	0.04	0.02	0.04	0.03	0.04	0.01	0.02	0.03	0.05	0.04	0.03	0.04	0.02	0.02	0.04	0.06	0.04	0.03	0.02	0.03	0.08
K_2O																						
Na_2O														0.04	0.02	0.02		0.02				
CaO																		0.02				0.02
MnO	0.02	0.01	0.01	0.01	0.01	0.02	0.01	0.01	0.01	0.02	0.01	0.02	0.01	0.03	0.01	0.04	0.02	0.01	0.02	0.03	0.02	0.27
MgO	0.03	0.20	0.25	0.02	0.02	0.03	0.03	0.06	0.03	0.04	0.01	0.02	0.02	0.02	0.02	2.90	0.01	0.02	0.02	0.02	0.19	14.28
Cr_2O_3	3.53	3.42	3.39	3.39	3.19	3.09	4.35	3.88	4.14	4.44	2.85	3.25	3.07	2.78	2.88	14.60	2.89	2.94	2.75	2.91	3.89	64.73
P_2O_5								0.02		0.02												
FeO*	0.26	0.76	0.89	0.23	0.34	0.19	0.44	0.83	0.38	0.54	0.14	0.13	0.17	0.15	0.12	4.65	0.13	0.16	0.20	0.21	0.54	16.56
Al_2O_3	0.15	0.44	0.36	0.17	0.12	0.09	0.12	0.12	0.11	0.17	0.10	0.12	0.29	0.08	0.10	4.09	0.35	0.20	0.19	0.08	0.37	2.80
TiO_2	97.64	96.71	95.42	97.42	96.85	96.96	96.08	95.28	96.38	95.22	101.38	101.36	101.27	101.60	102.04	77.67	101.22	101.32	101.72	101.41	97.75	1.34
NiO		0.03	0.01	0.05		0.05		0.02	0.03	0.02	0.05			0.01	0.03	0.07			0.05		0.03	0.14
Total	101.68	101.59	100.34	101.34	100.58	100.49	101.07	100.24	101.11	100.53	104.60	104.93	104.88	104.74	105.23	104.09	104.70	104.74	104.98	104.70	102.82	100.233
12 O																						
Si	0.0014	0.0028	0.0013	0.0029	0.0025	0.0035	0.0010	0.0017	0.0020	0.0041	0.0034	0.0019	0.0033	0.0014	0.0017	0.0029	0.0045	0.0031	0.0019	0.0017	0.0025	0.0079
K																						
Na														0.0053	0.0029	0.0036		0.0022				
Ca																		0.0014				0.0021
Mn	0.0016	0.0007	0.0007	0.0006	0.0006	0.0012	0.0010	0.0005	0.0008	0.0016	0.0008	0.0012	0.0004	0.0022	0.0006	0.0024	0.0012	0.0005	0.0016	0.0022	0.0011	0.0231
Mg	0.0032	0.0234	0.0297	0.0022	0.0024	0.0031	0.0040	0.0075	0.0036	0.0043	0.0010	0.0024	0.0027	0.0024	0.0022	0.3460	0.0011	0.0027	0.0027	0.0024	0.0225	2.1390
Cr	0.2210	0.2140	0.2150	0.2130	0.2020	0.1960	0.2740	0.2470	0.2610	0.2820	0.1730	0.1970	0.1860	0.1690	0.1740	0.9250	0.1750	0.1780	0.1660	0.1770	0.2423	5.1430
P								0.0011		0.0010												
Fe^{tot}	0.0172	0.0501	0.0598	0.0150	0.0225	0.0126	0.0291	0.0556	0.0252	0.0360	0.0092	0.0081	0.0111	0.0096	0.0076	0.3120	0.0085	0.0102	0.0126	0.0136	0.0363	1.3910
Al	0.0144	0.0408	0.0336	0.0154	0.0110	0.0086	0.0111	0.0112	0.0099	0.0165	0.0089	0.0105	0.0260	0.0076	0.0085	0.3860	0.0316	0.0179	0.0170	0.0068	0.0347	0.3320
Ti	5.8100	5.7680	5.7670	5.8140	5.8240	5.8320	5.7670	5.7710	5.7790	5.7490	5.8530	5.8370	5.8300	5.8570	5.8550	4.6790	5.8340	5.8410	5.8500	5.8510	5.7584	0.1010
Ni		0.0016	0.0006	0.0034		0.0031		0.0010	0.0021	0.0014	0.0028			0.0005	0.0017	0.0047			0.0033		0.0022	0.0109
Total	6.0719	6.1014	6.1078	6.0692	6.0678	6.0631	6.0895	6.0983	6.0847	6.0981	6.0533	6.0591	6.0602	6.0558	6.0542	6.6627	6.0589	6.0581	6.0561	6.0563	6.0998	9.1529
Mg#																						60.59
Cr#																						93.94

* - Total Fe as FeO

12 O - formula calculated on 12 oxigen;

Table 4.2 *(continued)*

	sp																			
Sample	F3sp-2	F3sp-3	F3sp-4	F4sp-1	F4sp-2	F4sp-3	F4sp-4	F4sp-5	F4sp-6	F6sp-1	F6sp-2	F6sp-3	F7sp-1	F7sp-2	F8sp-1	F8sp-2	F8sp-3	F8sp-4	F8sp-5	F9sp-1
comment																				
SiO_2	0.38	0.08	0.49	0.86	0.13	0.13	0.13	0.15	0.12	0.13	0.14	0.10	0.12	0.13	0.19	0.34	0.23	0.55	0.10	0.16
K_2O																		0.02	0.02	0.01
Na_2O					0.02		0.02	0.02						0.02	0.02			0.02		
CaO	0.28	0.16	0.16		0.01	0.02	0.01	0.03	0.01	0.02	0.03	0.07	0.01	0.01	0.17	0.11	0.09	0.06	0.03	0.06
MnO	0.29	0.32	0.31	0.26	0.30	0.24	0.26	0.25	0.26	0.40	0.30	0.32	0.23	0.23	0.46	0.28	0.32	0.36	0.31	0.41
MgO	19.60	19.42	19.34	19.66	15.46	17.72	18.06	18.57	18.55	13.79	20.45	19.13	18.62	15.62	15.36	20.11	19.31	18.83	19.33	13.55
Cr_2O_3	22.14	23.87	25.41	23.84	48.38	37.15	33.74	30.18	30.45	51.10	20.75	22.54	36.21	56.40	42.32	19.56	19.82	26.59	21.38	55.29
P_2O_5																				
FeO*	9.76	10.09	10.12	11.61	16.14	13.61	13.06	12.72	12.63	20.06	11.69	12.83	12.03	15.01	15.41	11.39	11.53	12.76	11.98	19.51
Al_2O_3	46.90	45.55	43.91	43.03	20.35	31.39	34.86	38.22	38.41	14.87	47.48	45.63	33.87	14.17	26.32	48.86	48.37	41.27	46.42	9.43
TiO_2	0.10	0.07	0.08	0.13	0.23	0.08	0.12	0.10	0.07	1.00	0.06	0.10	0.14	0.61	0.58	0.22	0.24	0.18	0.18	1.56
NiO				0.18	0.13	0.16	0.12	0.16	0.15	0.12	0.08	0.09	0.07	0.15	0.03	0.02			0.06	0.06
Total	99.46	99.57	99.84	99.59	101.14	100.49	100.37	100.40	100.67	101.51	100.97	100.82	101.33	102.35	100.87	100.89	99.95	100.64	99.84	100.05
12 O																				
Si	0.0304	0.0068	0.0398	0.0707	0.0117	0.0110	0.0107	0.0124	0.0099	0.0120	0.0108	0.0083	0.0103	0.0122	0.0168	0.0269	0.0186	0.0451	0.0084	0.0158
K																		0.0017	0.0025	0.0015
Na					0.0036		0.0024	0.0024						0.0037	0.0036			0.0038		
Ca	0.0246	0.0143	0.0141		0.0011	0.0014	0.0010	0.0023	0.0009	0.0023	0.0021	0.0058	0.0007	0.0007	0.0164	0.0095	0.0081	0.0050	0.0028	0.0067
Mn	0.0197	0.0223	0.0216	0.0181	0.0230	0.0177	0.0188	0.0178	0.0181	0.0317	0.0201	0.0220	0.0168	0.0180	0.0347	0.0190	0.0219	0.0250	0.0214	0.0345
Mg	2.3690	2.3630	2.3600	2.4140	2.1130	2.2960	2.3030	2.3300	2.3220	1.9149	2.4249	2.3028	2.3550	2.1610	2.0450	2.3900	2.3230	2.3230	2.3500	1.9880
Cr	1.4190	1.5410	1.6440	1.5520	3.5070	2.5530	2.2820	2.0090	2.0210	3.7634	1.3049	1.4390	2.4300	4.1380	2.9880	1.2330	1.2650	1.7400	1.3790	4.3020
P																				
Fe^{tot}	0.6620	0.6890	0.6930	0.8000	1.2370	0.9890	0.9340	0.8960	0.8870	1.5627	0.7776	0.8664	0.8540	1.1650	1.1510	0.7600	0.7790	0.8830	0.8170	1.6060
Al	4.4810	4.3840	4.2360	4.1780	2.1990	3.2150	3.5150	3.7930	3.8000	1.6325	4.4509	4.3424	3.3890	1.5500	2.7700	4.5930	4.6010	4.0250	4.4630	1.0940
Ti	0.0062	0.0040	0.0049	0.0081	0.0157	0.0052	0.0079	0.0060	0.0047	0.0699	0.0035	0.0062	0.0090	0.0424	0.0388	0.0130	0.0146	0.0113	0.0111	0.1152
Ni				0.0120	0.0096	0.0111	0.0083	0.0111	0.0101	0.0090	0.0051	0.0059	0.0049	0.0113	0.0022	0.0010			0.0037	0.0043
Total	9.0127	9.0254	9.0147	9.0552	9.1207	9.0995	9.0831	9.0809	9.0764	9.0000	9.0000	9.0000	9.0722	9.1023	9.0675	9.0471	9.0340	9.0630	9.0609	9.1701
Mg#	78.16	77.42	77.30	75.11	63.07	69.89	71.15	72.23	72.36	55.06	75.72	72.66	73.39	64.97	63.99	75.87	74.89	72.46	74.20	55.31
Cr#	24.05	26.01	27.96	27.09	61.46	44.26	39.37	34.63	34.72	69.75	22.67	24.89	41.76	72.75	51.89	21.16	21.56	30.18	23.60	79.73

Table 4.2 *(continued)*

	sp																			
Sample	F10sp-1	F11sp-1	F11sp-2	F11sp-3	F11sp-4	F11sp-5	F11sp-6	F11sp-7	F12sp-1	F12sp-2	F12sp-3	F12sp-4	F12sp-5	F12sp-6	F12sp-7	F12sp-8	F12sp-9	F14sp-1	F16sp-1	F16sp-2
comment																				
SiO_2	0.11	0.16	0.12	0.15	0.16	0.15	0.14	0.15	0.04	0.09	0.11	0.14	0.18	0.05	0.04	0.09	0.12	0.45	0.07	0.10
K_2O													0.04							
Na_2O	0.01		0.03	0.02	0.01	0.01	0.02	0.01	0.03			0.02				0.01	0.02	0.03	0.01	0.01
CaO	0.03	0.01	0.01	0.01	0.05	0.01	0.03	0.01		0.02		0.01	0.03	0.01		0.01	0.03	0.12	0.01	0.02
MnO	0.26	0.39	0.41	0.37	0.37	0.39	0.38	0.37	0.32	0.36	0.35	0.46	0.35	0.18	0.19	0.27	0.28	0.27	0.23	0.21
MgO	20.38	13.53	13.58	13.65	17.20	13.87	17.18	17.12	13.09	15.92	15.09	13.83	14.55	12.80	10.93	17.74	19.29	19.63	20.52	20.73
Cr_2O_3	14.55	53.33	50.68	51.91	36.40	50.80	33.17	30.80	50.60	43.91	46.70	55.13	53.02	49.73	43.45	33.76	23.37	18.72	6.47	6.55
P_2O_5					0.02														0.02	
FeO*	11.39	20.95	21.05	21.11	15.49	20.70	15.62	16.10	22.83	17.33	18.08	19.22	18.74	19.69	17.83	13.66	11.77	12.30	10.75	10.39
Al_2O_3	54.23	11.52	13.68	12.77	31.28	13.89	33.47	35.53	3.63	18.35	14.53	8.10	10.16	10.33	11.08	31.91	42.67	49.50	60.92	60.46
TiO_2	0.11	1.39	1.29	1.35	0.40	1.26	0.35	0.32	6.98	2.98	3.52	3.25	3.02	7.42	16.41	1.12	0.56	0.10	0.05	0.08
NiO		0.08	0.06	0.07	0.06	0.07	0.05	0.05	0.21	0.09	0.11	0.11	0.13	0.13	0.13	0.12	0.11	0.02	0.05	0.11
Total	101.08	101.36	100.90	101.41	101.44	101.15	100.40	100.47	97.75	99.06	98.50	100.27	100.21	100.33	100.06	98.70	98.21	101.15	99.09	98.67
12 O																				
Si	0.0085	0.0150	0.0110	0.0140	0.0141	0.0142	0.0119	0.0126	0.0042	0.0089	0.0109	0.0137	0.0174	0.0047	0.0036	0.0082	0.0097	0.0359	0.0055	0.0079
K													0.0044							
Na	0.0015		0.0056	0.0034	0.0014	0.0021	0.0025	0.0010	0.0060			0.0032				0.0018	0.0027	0.0052	0.0014	0.0020
Ca	0.0025	0.0015	0.0007	0.0013	0.0045	0.0011	0.0030	0.0010		0.0015		0.0015	0.0035	0.0011		0.0010	0.0022	0.0103	0.0011	0.0020
Mn	0.0169	0.0318	0.0332	0.0300	0.0273	0.0312	0.0276	0.0268	0.0284	0.0283	0.0283	0.0383	0.0285	0.0144	0.0151	0.0201	0.0199	0.0183	0.0149	0.0137
Mg	2.3613	1.9500	1.9480	1.9550	2.2220	1.9790	2.2210	2.1950	2.0160	2.2280	2.1660	2.0260	2.1060	1.8420	1.5350	2.3240	2.4100	2.3172	2.3620	2.3940
Cr	0.8941	4.0760	3.8540	3.9450	2.4950	3.8440	2.2740	2.0950	4.1350	3.2590	3.5560	4.2850	4.0710	3.7950	3.2370	2.3460	1.5480	1.1720	0.3950	0.4010
P					0.0012														0.0012	
Fe^{tot}	0.7403	1.6940	1.6930	1.6970	1.1230	1.6570	1.1320	1.1590	1.9730	1.3600	1.4560	1.5800	1.5230	1.5900	1.4050	1.0040	0.8250	0.8145	0.6940	0.6730
Al	4.9675	1.3130	1.5510	1.4460	3.1950	1.5670	3.4210	3.6030	0.4420	2.0310	1.6500	0.9380	1.1630	1.1760	1.2310	3.3050	4.2140	4.6195	5.5430	5.5210
Ti	0.0063	0.1012	0.0932	0.0977	0.0258	0.0906	0.0226	0.0207	0.5420	0.2100	0.2550	0.2410	0.2200	0.5390	1.1630	0.0739	0.0351	0.0061	0.0027	0.0049
Ni		0.0065	0.0048	0.0051	0.0043	0.0054	0.0034	0.0036	0.0176	0.0067	0.0083	0.0087	0.0101	0.0099	0.0098	0.0085	0.0071	0.0010	0.0028	0.0067
Total	9.0000	9.1891	9.1945	9.1955	9.1146	9.1916	9.1190	9.1188	9.1652	9.1345	9.1315	9.1354	9.1480	8.9721	8.5995	9.0935	9.0747	9.0000	9.0237	9.0262
Mg#	76.13	53.51	53.50	53.53	66.43	54.43	66.24	65.44	50.54	62.10	59.80	56.18	58.03	53.67	52.21	69.83	74.50	73.99	77.29	78.06
Cr#	15.25	75.64	71.30	73.18	43.85	71.04	39.93	36.77	90.34	61.61	68.31	82.04	77.78	76.34	72.45	41.51	26.87	20.24	6.65	6.77

Table 4.2 *(continued)*

	sp																			
Sample	F16sp-3	F22sp-1	F22sp-2	F22sp-3	F22sp-4	F22sp-5	F22sp-6	F23sp-1	F23sp-2	F23sp-3	F23sp-4	F23sp-5	F26sp-1	F24sp-2	F24sp-3	F24sp-4	F24sp-5	F25asp-1	F25bsp-1	F25csp-1
comment																				
SiO_2	0.11	0.24	0.11	0.07	0.08	0.40	4.49	0.17	0.16	0.15	0.19	0.17	0.15	0.15	0.09	0.09	0.16	7.63	0.16	0.12
K_2O																		2.79		
Na_2O		0.01		0.02	0.01	0.03				0.01		0.02		0.02	0.02	0.01	0.01	0.74	0.01	0.02
CaO	0.01	0.27	0.10	0.09	0.09	0.09	0.07	0.01	0.01	0.01		0.02	0.02		0.03	0.02	0.06	3.50	0.03	0.04
MnO	0.21	0.36	0.33	0.29	0.32	0.29	0.28	0.27	0.27	0.30	0.26	0.30	0.35	0.36	0.32	0.26	0.50	0.41	0.21	0.30
MgO	20.37	16.55	17.57	18.81	19.17	19.91	21.09	14.02	13.71	14.14	13.55	13.76	16.57	16.69	18.34	19.43	14.02	13.96	20.34	19.11
Cr_2O_3	9.55	37.55	32.87	24.76	23.01	19.49	16.34	65.93	66.06	65.95	65.90	65.94	40.58	34.48	29.19	26.90	52.39	36.65	16.41	22.55
P_2O_5		0.02		0.01		0.03		0.02		0.01						0.03		0.41	0.02	
FeO*	10.70	12.82	11.97	11.21	11.00	10.95	9.93	14.96	15.76	14.94	15.54	15.61	15.17	15.68	13.05	12.10	15.44	16.99	11.21	13.27
Al_2O_3	57.61	32.57	37.07	45.01	46.56	49.22	46.15	6.35	6.42	6.31	6.35	6.37	27.83	33.29	39.04	41.60	17.35	8.03	51.81	43.96
TiO_2	0.05	0.05	0.07	0.01	0.03	0.02	0.01	0.06	0.06	0.07	0.10	0.07	0.09	0.05	0.06	0.13	0.54	1.26	0.12	0.12
NiO	0.12	0.04	0.11	0.03	0.04	0.03	0.12	0.10	0.05	0.10	0.10	0.07	0.01	0.00	0.03	0.05	0.03	0.49	0.09	0.10
Total	98.73	100.48	100.20	100.31	100.32	100.47	98.49	101.88	102.50	101.99	101.99	102.33	100.79	100.72	100.20	100.63	100.51	92.87	100.41	99.58
12 O																				
Si	0.0088	0.0205	0.0095	0.0053	0.0067	0.0318	0.3590	0.0161	0.0155	0.0149	0.0185	0.0162	0.0134	0.0133	0.0079	0.0071	0.0148	0.7780	0.0123	0.0100
K																		0.3620		
Na		0.0014		0.0030	0.0011	0.0045				0.0017		0.0046		0.0033	0.0027	0.0016	0.0010	0.1472	0.0019	0.0035
Ca	0.0011	0.0254	0.0086	0.0082	0.0081	0.0077	0.0060	0.0011	0.0010	0.0014		0.0017	0.0020		0.0025	0.0019	0.0058	0.3820	0.0025	0.0035
Mn	0.0138	0.0265	0.0235	0.0198	0.0219	0.0196	0.0190	0.0221	0.0221	0.0244	0.0215	0.0243	0.0260	0.0264	0.0225	0.0184	0.0398	0.0353	0.0138	0.0210
Mg	2.3800	2.1340	2.2200	2.2910	2.3170	2.3700	2.5130	2.0290	1.9780	2.0440	1.9640	1.9870	2.1880	2.1560	2.3010	2.3930	1.9560	2.1220	2.4010	2.3600
Cr	0.5920	2.5680	2.2030	1.5990	1.4750	1.2310	1.0330	5.0610	5.0550	5.0570	5.0660	5.0520	2.8410	2.3630	1.9430	1.7570	3.8750	2.9540	1.0270	1.4770
P		0.0017		0.0010		0.0022		0.0012		0.0010						0.0018		0.0352	0.0011	
Fe^{tot}	0.7010	0.9270	0.8490	0.7660	0.7460	0.7310	0.6640	1.2140	1.2750	1.2120	1.2640	1.2650	1.1240	1.1370	0.9190	0.8360	1.2080	1.4490	0.7420	0.9190
Al	5.3230	3.3210	3.7050	4.3330	4.4500	4.6330	4.3480	0.7270	0.7320	0.7220	0.7280	0.7280	2.9050	3.4000	3.8740	4.0500	1.9130	0.9650	4.8340	4.2920
Ti	0.0029	0.0030	0.0047	0.0009	0.0018	0.0012	0.0007	0.0041	0.0044	0.0048	0.0071	0.0052	0.0059	0.0032	0.0040	0.0083	0.0380	0.0968	0.0072	0.0072
Ni	0.0075	0.0026	0.0076	0.0017	0.0028	0.0018	0.0075	0.0078	0.0039	0.0076	0.0076	0.0055	0.0009	0.0000	0.0023	0.0031	0.0020	0.0405	0.0055	0.0063
Total	9.0301	9.0311	9.0319	9.0290	9.0314	9.0346	8.9514	9.0835	9.0869	9.0918	9.0775	9.0896	9.1086	9.1022	9.0819	9.0792	9.0549	9.3670	9.0498	9.0996
Mg#	77.25	69.72	72.34	74.94	75.64	76.43	79.10	62.57	60.81	62.78	60.84	61.10	66.06	65.47	71.46	74.11	61.82	59.42	76.39	71.97
Cr#	10.01	43.61	37.29	26.96	24.89	20.99	19.20	87.44	87.35	87.51	87.44	87.40	49.44	41.00	33.40	30.26	66.95	75.38	17.52	25.60

Table 4.2 *(continued)*

	sp						phl														
Sample	F25csp-2	F25dsp-1	F-26	F-27	F-28	882	F2phl-1	F3phl-1	F3phl-2	F3phl-3	F3phl-4	F5phl-1	F5phl-2	F6phl-1	F6phl-2	F6phl-3	F6phl-4	F7phl-1	F8phl-1	F8phl-2	F8phl-3
comment																					
SiO_2	0.14	1.77	0.23	10.48	0.13	0.12	38.20	39.43	41.16	39.52	38.18	38.62	36.66	38.74	39.27	35.34	38.74	40.85	39.57	39.68	37.65
K_2O	0.01	0.51	0.01	0.01	0.02		9.21	7.68	9.52	9.48	9.39	6.87	4.98	4.83	7.14	6.29	4.83	9.90	9.38	9.33	9.96
Na_2O	0.01	0.04		0.09			0.18	0.29	0.32	0.32	0.30	0.21	0.14	0.14	0.18	0.09	0.14	0.16	0.59	0.46	0.43
CaO	0.06	0.20	0.08	3.77	0.04	0.05	0.03	0.08	0.02	0.06	0.09	0.09	0.41	0.93	0.11	0.45	0.93	0.03	0.04	0.02	0.03
MnO	0.32	0.46	0.24	0.26	0.31	0.41	0.04	0.08	0.03	0.05	0.05	0.07	0.70	0.34	0.11	0.36	0.34	0.04	0.06	0.07	0.07
MgO	19.85	16.71	21.09	19.85	19.58	14.26	23.03	25.04	23.58	22.48	23.51	28.14	26.87	25.26	27.89	22.54	25.26	24.72	22.14	22.92	21.44
Cr_2O_3	18.23	42.67	12.87	10.88	22.63	64.14	2.14	1.46	2.07	3.40	0.31	0.15	0.10	2.08	1.58	3.16	2.08	2.36	3.99	2.68	2.84
P_2O_5		0.03		0.02									0.12	0.09		0.22	0.09				
FeO*	12.10	13.36	11.32	9.94	12.59	13.69	2.86	4.05	2.76	2.89	3.01	4.76	7.00	6.42	3.40	10.70	6.42	3.02	3.74	3.76	4.04
Al_2O_3	49.39	23.58	53.31	47.13	44.83	5.97	12.65	13.37	14.45	16.04	16.65	12.64	13.35	14.65	12.21	12.83	14.65	13.40	14.88	14.10	17.26
TiO_2	0.02	0.58	0.09	0.11	0.07	0.52	1.18	1.69	1.40	1.20	2.65	0.16	0.26	0.32	0.82	0.32	0.32	0.56	0.85	0.92	0.90
NiO	0.10	0.03	0.02	0.06	0.05		0.14	0.17	0.17	0.11	0.10	0.06	0.09	0.03	0.11		0.03	0.18	0.08	0.08	0.02
Total	100.23	99.93	99.25	102.60	100.24	99.16	89.67	93.35	95.47	95.55	94.23	91.76	90.69	93.81	92.83	92.29	93.81	95.22	95.31	94.01	94.62
12 O																					
Si	0.0114	0.1583	0.0178	0.7870	0.0105	0.0118	5.7549	5.6714	5.7883	5.5835	5.4470	5.6377	5.4582	5.5392	5.6583	5.3614	5.5392	5.7946	5.6420	5.7172	5.4232
K	0.0007	0.0581	0.0009	0.0008	0.0018		1.7701	1.4092	1.7079	1.7087	1.7090	1.2794	0.9459	0.8810	1.3124	1.2174	0.8810	1.7915	1.7062	1.7150	1.8302
Na	0.0012	0.0076		0.0128			0.0532	0.0798	0.0862	0.0882	0.0833	0.0580	0.0410	0.0394	0.0500	0.0259	0.0394	0.0429	0.1620	0.1282	0.1193
Ca	0.0052	0.0188	0.0064	0.3030	0.0033	0.0053	0.0047	0.0125	0.0027	0.0092	0.0135	0.0144	0.0657	0.1420	0.0176	0.0723	0.1420	0.0046	0.0063	0.0025	0.0040
Mn	0.0215	0.0351	0.0158	0.0166	0.0212	0.0342	0.0052	0.0100	0.0033	0.0054	0.0059	0.0088	0.0884	0.0409	0.0139	0.0465	0.0409	0.0052	0.0070	0.0083	0.0083
Mg	2.3770	2.2340	2.4930	2.2240	2.3900	2.0940	5.1722	5.3692	4.9434	4.7347	5.0001	6.1238	5.9639	5.3843	5.9907	5.0977	5.3843	5.2275	4.7060	4.9231	4.6038
Cr	1.1580	3.0250	0.8070	0.6460	1.4650	4.9953	0.2549	0.1660	0.2302	0.3798	0.0345	0.0167	0.0113	0.2351	0.1800	0.3790	0.2351	0.2647	0.4498	0.3053	0.3234
P		0.0024		0.0013									0.0107	0.0029		0.0131	0.0029				
Fe^{tot}	0.8130	1.0020	0.7510	0.6250	0.8630	1.1278	0.3603	0.4872	0.3246	0.3415	0.3591	0.5811	0.8716	0.7677	0.4097	1.3575	0.7677	0.3583	0.4460	0.4531	0.4867
Al	4.6760	2.4920	4.9830	4.1740	4.3270	0.6931	2.2460	2.2665	2.3950	2.6708	2.7996	2.1747	2.3426	2.4688	2.0735	2.2940	2.4688	2.2402	2.5005	2.3943	2.9301
Ti	0.0014	0.0391	0.0053	0.0064	0.0045	0.0385	0.1337	0.1828	0.1478	0.1278	0.2843	0.0170	0.0296	0.0339	0.0885	0.0359	0.0339	0.0600	0.0914	0.0992	0.0971
Ni	0.0065	0.0020	0.0015	0.0038	0.0030		0.0174	0.0194	0.0189	0.0123	0.0115	0.0068	0.0107	0.0029	0.0131		0.0029	0.0131	0.0087	0.0092	0.0017
Total	9.0719	9.0744	9.0817	8.8007	9.0894	9.0000	15.773	15.674	15.648	15.662	15.748	15.918	15.829	15.535	15.808	15.888	15.535	15.810	15.726	15.755	15.828
Mg#	74.51	69.04	76.85	78.06	73.47	65.00	93.49	91.68	93.84	93.27	93.30	91.33	87.25	87.52	93.60	78.97	87.52	93.59	91.34	91.57	90.44
Cr#	19.85	54.83	13.94	13.40	25.29	87.82	10.19	6.83	8.77	12.45	1.22	0.76	0.48	8.70	7.99	14.18	8.70	10.57	15.25	11.31	9.94

Table 4.2 *(continued)*

	phl																					
Sample	F8phl4	F8phl5	F10phl1	F11phl1	F11phl2	F11phl3	F11phl4	F11phl5	F11phl6	F11phl7	F13phl1	F13phl2	F13phl3	F13phl4	F15phl1	F15phl2	F15phl3	F15phl4	F15phl5	F15phl6	F15phl7	F25bphl1
comment																						
SiO_2	38.55	39.32	40.07	39.62	39.86	40.16	40.92	39.85	40.20	40.47	38.87	38.91	39.18	36.59	37.52	41.39	39.35	38.31	38.15	38.67	39.57	38.44
K_2O	9.93	10.04	9.25	9.28	8.72	8.94	9.79	10.15	9.10	9.50	9.47	9.08	9.73	8.79	9.06	9.51	9.80	9.26	9.16	9.68	9.22	5.69
Na_2O	0.44	0.36	0.19	0.26	0.22	0.18	0.13	0.14	0.11	0.22	0.36	0.60	0.44	0.69	0.51	0.10	0.20	0.12	0.11	0.28	0.30	0.11
CaO			0.04	0.01	0.02		0.06	0.03	0.02		0.03	0.01		0.10	0.03	0.01	0.02	0.02	0.01	0.02	0.03	0.07
MnO	0.09	0.05	0.04	0.06	0.06	0.03	0.05	0.04	0.07	0.04	0.04	0.03	0.05	0.15	0.08	0.05	0.06	0.07	0.07	0.08	0.07	0.21
MgO	22.28	23.27	25.69	22.66	24.49	24.91	23.49	22.82	23.94	22.90	23.15	22.86	22.86	21.70	22.51	24.73	22.97	21.22	20.49	22.69	22.15	28.37
Cr_2O_3	3.08	2.98	3.65	2.42	2.19	2.12	2.21	2.29	2.10	2.34	2.00	1.95	1.76	1.35	2.60	2.01	3.52	4.00	6.15	3.65	3.35	2.18
P_2O_5				0.02						0.02			0.02		0.02		0.02		0.03			0.02
FeO*	4.04	3.85	3.33	3.72	4.01	4.05	4.11	4.47	4.19	4.54	3.99	4.22	4.16	4.48	3.77	3.81	3.89	4.47	4.16	3.85	3.92	4.00
Al_2O_3	17.26	14.93	12.08	14.80	12.98	12.50	13.26	14.57	13.84	14.85	15.10	15.49	14.12	18.47	17.28	12.62	14.97	16.95	16.95	16.34	15.90	12.51
TiO_2	1.02	0.93	1.07	1.41	0.94	0.92	1.49	1.04	0.96	1.09	0.95	0.98	1.60	1.02	0.53	1.33	0.83	0.31	0.26	0.60	0.69	0.18
NiO	0.07	0.13	0.08	0.18	0.13	0.14	0.25	0.12	0.13	0.13	0.13	0.11	0.13	0.08	0.05	0.21	0.17	0.05		0.05	0.07	0.02
Total	96.76	95.85	95.48	94.43	93.62	93.95	95.75	95.52	94.65	96.10	94.09	94.25	94.06	93.44	93.95	95.78	95.80	94.77	95.54	95.91	95.27	91.79
12 O																						
Si	5.4265	5.5892	5.6972	5.6727	5.7507	5.7803	5.7979	5.6831	5.7400	5.7091	5.6024	5.5916	5.6649	5.3081	5.4095	5.8401	5.5945	5.4980	5.4502	5.4862	5.6208	5.5824
K	1.7832	1.8207	1.6778	1.6950	1.6049	1.6415	1.7696	1.8466	1.6576	1.7097	1.7413	1.6646	1.7947	1.6268	1.6664	1.7119	1.7775	1.6953	1.6694	1.7520	1.6708	1.0542
Na	0.1204	0.0978	0.0513	0.0719	0.0604	0.0488	0.0368	0.0387	0.0310	0.0604	0.1003	0.1658	0.1233	0.1952	0.1420	0.0271	0.0543	0.0323	0.0296	0.0767	0.0818	0.0313
Ca			0.0056	0.0021	0.0032		0.0088	0.0041	0.0024		0.0049	0.0018		0.0160	0.0042	0.0017	0.0035	0.0028	0.0015	0.0024	0.0052	0.0106
Mn	0.0105	0.0057	0.0049	0.0067	0.0073	0.0039	0.0056	0.0043	0.0081	0.0045	0.0048	0.0038	0.0066	0.0182	0.0099	0.0059	0.0077	0.0084	0.0083	0.0094	0.0088	0.0262
Mg	4.6754	4.9311	5.4452	4.8366	5.2672	5.3449	4.9617	4.8515	5.0959	4.8159	4.9741	4.8973	4.9273	4.6929	4.8381	5.2019	4.8684	4.5399	4.3638	4.7989	4.6905	6.1420
Cr	0.3428	0.3349	0.4103	0.2739	0.2498	0.2413	0.2476	0.2582	0.2371	0.2610	0.2279	0.2216	0.2012	0.1551	0.2964	0.2242	0.3957	0.4539	0.6947	0.4094	0.3762	0.2503
P				0.0013						0.0019			0.0019		0.0013		0.0010		0.0023			0.0014
Fe^{tot}	0.4756	0.4577	0.3960	0.4454	0.4838	0.4875	0.4870	0.5331	0.5003	0.5356	0.4809	0.5072	0.5030	0.5435	0.4546	0.4496	0.4625	0.5365	0.4970	0.4568	0.4657	0.4858
Al	2.8634	2.5012	2.0243	2.4974	2.2071	2.1204	2.2143	2.4489	2.3290	2.4690	2.5650	2.6235	2.4061	3.1579	2.9362	2.0987	2.5084	2.8669	2.8539	2.7322	2.6619	2.1412
Ti	0.1083	0.0996	0.1141	0.1514	0.1017	0.0997	0.1584	0.1117	0.1025	0.1154	0.1025	0.1058	0.1741	0.1117	0.0579	0.1413	0.0888	0.0329	0.0283	0.0639	0.0735	0.0192
Ni	0.0079	0.0144	0.0093	0.0205	0.0155	0.0160	0.0280	0.0139	0.0147	0.0149	0.0152	0.0123	0.0152	0.0093	0.0054	0.0243	0.0191	0.0058		0.0056	0.0079	0.0022
Total	15.814	15.852	15.836	15.674	15.752	15.784	15.716	15.794	15.719	15.696	15.819	15.795	15.816	15.835	15.821	15.727	15.780	15.673	15.597	15.793	15.663	15.745
Mg#	90.77	91.51	93.22	91.57	91.59	91.64	91.06	90.10	91.06	89.99	91.18	90.62	90.74	89.62	91.41	92.04	91.32	89.43	89.78	91.31	90.97	92.67
Cr#	10.69	11.81	16.85	9.88	10.17	10.22	10.06	9.54	9.24	9.56	8.16	7.79	7.72	4.68	9.17	9.65	13.62	13.67	19.58	13.03	12.38	10.47

Table 4.2 *(continued)*

	phl			am-cpx																	
Sample	F25cphl1	F25dphl1	F26phl1	F2-1	F2-2	F2-3	F2-4	F2-5	F2-6	F3-1	F3-2	F3-3	F3-4	F3-5	F4-1	F4-2	F4-3	F4-4	F4-5	F4-6	F5-1	F5-2
comment																						
SiO_2	38.65	38.82	39.63	35.13	38.83	39.26	35.61	36.99	36.20	48.19	48.18	44.51	49.10	48.02	48.97	46.63	51.17	50.12	46.43	45.86	39.72	35.25
K_2O	8.45	9.94	4.85	0.03	0.04	0.02	0.05		0.02	0.01		0.02		0.01					0.01		0.01	
Na_2O	0.28	0.30	0.07	0.10	0.09	0.08	0.12	0.10	0.11	0.02	0.01	0.08	0.03	0.14	0.04	0.35	0.05	0.72	0.42	0.04	0.18	0.19
CaO	0.12	0.01	0.23	6.12	4.12	3.23	4.53	3.63	4.80	1.10	1.10	15.16	1.25	19.25	1.17	19.73	2.59	18.22	18.86	1.58	9.38	8.40
MnO	0.05	0.05	0.20	0.37	0.37	0.34	0.40	0.41	0.43	0.31	0.31	0.31	0.29	0.25	0.40	0.33	0.42	0.28	0.36	0.42	0.33	0.30
MgO	22.33	22.80	26.12	23.95	26.15	28.46	25.23	26.24	25.17	28.87	29.32	16.05	29.64	16.02	28.46	14.19	28.67	16.81	13.93	27.55	22.45	22.24
Cr_2O_3	2.23	2.72	0.17	8.35	8.35	6.80	8.86	8.23	8.14	2.69	2.86	4.94	2.89	2.83	4.06	4.44	2.83	2.85	4.76	4.22	5.51	7.90
P_2O_5			0.02			0.04	0.04	0.03			0.05	0.05				0.02	0.02		0.02		0.02	0.03
FeO*	3.94	3.32	9.77	6.16	6.64	5.89	6.80	6.59	6.55	5.71	5.62	3.77	5.69	3.10	6.89	3.65	7.17	4.03	3.76	7.09	5.99	6.23
Al_2O_3	12.37	15.63	9.96	17.89	15.73	15.41	16.87	16.26	16.40	12.33	12.45	13.97	11.12	8.83	10.50	10.18	7.64	7.10	10.75	10.34	15.08	18.67
TiO_2	1.23	0.99	0.66	0.21	0.16	0.13	0.16	0.15	0.17	0.14	0.13	0.48	0.15	0.35	0.08	0.29	0.16	0.25	0.38	0.13	0.05	0.10
NiO	0.18	0.12	0.05	0.02			0.01	0.01		0.01				0.01	0.03		0.03			0.01		
Total	89.82	94.71	91.73	98.33	100.48	99.65	98.67	98.63	98.01	99.38	100.02	99.34	100.16	98.81	100.60	99.81	100.74	100.38	99.67	97.25	98.72	99.31
12 O																						
Si	5.8156	5.5623	5.8600	5.0510	5.4131	5.4657	5.1053	5.2621	5.2060	6.4869	6.4497	6.2433	6.5628	6.7766	6.5763	6.5832	6.8674	6.9683	6.5553	6.4198	5.6497	5.0413
K	1.6220	1.8169	0.9149	0.0055	0.0073	0.0041	0.0086		0.0044	0.0024		0.0027		0.0022					0.0011		0.0011	
Na	0.0823	0.0836	0.0198	0.0287	0.0241	0.0202	0.0320	0.0281	0.0318	0.0039	0.0031	0.0228	0.0078	0.0369	0.0115	0.0947	0.0141	0.1946	0.1141	0.0117	0.0499	0.0535
Ca	0.0187	0.0021	0.0369	0.9428	0.6154	0.4818	0.6958	0.5533	0.7396	0.1584	0.1571	2.2783	0.1792	2.9106	0.1678	2.9844	0.3724	2.7141	2.8529	0.2370	1.4295	1.2871
Mn	0.0059	0.0061	0.0247	0.0453	0.0432	0.0399	0.0482	0.0488	0.0527	0.0356	0.0354	0.0365	0.0325	0.0293	0.0452	0.0396	0.0474	0.0324	0.0426	0.0494	0.0396	0.0357
Mg	5.0089	4.8701	5.7578	5.1335	5.4345	5.9066	5.3923	5.5648	5.3962	5.7934	5.8512	3.3561	5.9061	3.3702	5.6976	2.9865	5.7360	3.4841	2.9319	5.7493	4.7604	4.7416
Cr	0.2653	0.3081	0.0195	0.9492	0.9203	0.7485	1.0043	0.9257	0.9255	0.2863	0.3027	0.5478	0.3054	0.3158	0.4311	0.4956	0.3003	0.3133	0.5313	0.4671	0.6196	0.8933
P			0.0013			0.0032	0.0035	0.0022			0.0043	0.0058				0.0012	0.0017		0.0015		0.0013	
Fe^{tot}	0.4958	0.3978	1.2082	0.7407	0.7741	0.6857	0.8153	0.7840	0.7878	0.6428	0.6292	0.4422	0.6360	0.3659	0.7738	0.4309	0.8047	0.4686	0.4440	0.8300	0.7125	0.7451
Al	2.1937	2.6394	1.7358	3.0316	2.5844	2.5284	2.8505	2.7262	2.7797	1.9561	1.9643	2.3095	1.7517	1.4686	1.6619	1.6938	1.2084	1.1634	1.7888	1.7059	2.5280	3.1469
Ti	0.1387	0.1070	0.0731	0.0228	0.0170	0.0136	0.0172	0.0160	0.0180	0.0143	0.0129	0.0507	0.0155	0.0369	0.0076	0.0304	0.0158	0.0260	0.0401	0.0139	0.0058	0.0104
Ni	0.0215	0.0137	0.0059	0.0019			0.0009	0.0011		0.0009				0.0010	0.0029		0.0028			0.0016		
Total	15.668	15.807	15.657	15.953	15.833	15.894	15.970	15.910	15.942	15.381	15.405	15.290	15.397	15.314	15.375	15.339	15.369	15.365	15.302	15.486	15.796	15.955
Mg#	90.99	92.45	82.66	87.39	87.53	89.60	86.87	87.65	87.26	90.01	90.29	88.36	90.28	90.21	88.04	87.39	87.70	88.15	86.85	87.38	86.98	86.42
Cr#	10.79	10.45	1.11	23.84	26.26	22.84	26.05	25.35	24.98	12.77	13.35	19.17	14.85	17.70	20.60	22.64	19.90	21.22	22.90	21.49	19.69	22.11

Table 4.2 *(continued)*

	am-cpx																					
Sample	F5-3	F6-1	F6-2	F6-3	F6-4	F6-5	F7-1	F7-2	F8-1	F8-2	F8-3	F8-4	F10-1	F10-2	F10-3	F10-4	F10-5	F10-6	F10-7	F14-1	F14-2	F15-1
comment																						
SiO_2	38.82	45.67	38.35	45.35	44.04	44.17	35.53	35.53	42.28	53.51	51.15	49.74	49.98	44.06	42.34	54.84	51.22	49.16	46.90	31.59	37.67	44.33
K_2O	0.05	0.03	0.39	0.20	0.06	0.92	0.04	0.04	0.02		0.01	0.01	1.65	2.20	0.05	0.04	0.01	0.03	0.04	0.97	0.13	0.92
Na_2O	0.11	0.07	0.10	0.07	0.15	0.09	0.05	0.05	0.28	0.09	0.07	0.71	0.29	0.29	0.12	0.08	0.02	0.03	0.24	0.15	0.09	0.49
CaO	4.58	7.29	5.29	1.96	10.04	2.24	1.45	1.45	14.16	1.09	1.40	18.75	9.53	3.49	2.70	1.75	1.25	1.59	13.29	6.58	2.97	10.56
MnO	0.34	0.37	0.39	0.37	0.36	0.41	0.40	0.40	0.40	0.38	0.37	0.29	0.33	0.31	0.35	0.32	0.20	0.39	0.32	0.37	0.37	0.34
MgO	26.58	25.46	24.03	28.47	22.41	28.83	28.86	28.86	18.18	32.07	30.47	16.30	19.09	20.35	27.58	33.26	34.58	28.86	19.65	20.80	26.01	21.04
Cr_2O_3	6.17	3.90	6.28	3.75	4.14	3.36	9.12	9.12	4.68	1.29	2.61	2.63	2.70	4.76	4.23	0.31	0.32	2.95	3.43	11.80	7.86	2.99
P_2O_5	0.02					0.02						0.02	0.05	0.04					0.03	0.02	0.03	
FeO*	6.32	6.72	7.49	7.13	5.69	6.43	7.09	7.09	4.61	6.25	6.00	3.47	4.79	6.14	7.39	6.24	6.18	6.93	4.81	8.21	7.95	4.94
Al_2O_3	16.08	9.79	17.40	11.59	10.74	11.99	16.35	16.35	12.03	6.01	8.11	7.55	10.71	17.71	16.53	3.26	6.33	11.35	11.68	18.12	15.73	10.75
TiO_2	0.04	0.18	0.20	0.11	0.24	0.14	0.08	0.08	0.75	0.04	0.09	0.34	0.29	0.23	0.17	0.14	0.16	0.22	0.45	0.17	0.10	0.29
NiO	0.07			0.02	0.04				0.03	0.02	0.02	0.04		0.01	0.03	0.03	0.15	0.03		0.01	0.02	
Total	99.17	99.50	99.93	99.03	97.91	98.60	98.98	98.98	97.42	100.75	100.30	99.86	99.41	99.59	101.48	100.27	100.42	101.54	100.84	98.78	98.93	96.65
12 O																						
Si	5.4529	6.3529	5.3899	6.2521	6.2611	6.1380	5.0501	5.0501	6.1057	7.0791	6.8313	6.9449	6.8912	6.0832	5.7343	7.2873	6.8246	6.5307	6.4482	4.6735	5.3571	6.3803
K	0.0084	0.0060	0.0699	0.0345	0.0100	0.1631	0.0074	0.0074	0.0041	0.0000	0.0017	0.0020	0.2902	0.3875	0.0090	0.0071	0.0020	0.0046	0.0075	0.1829	0.0239	0.1686
Na	0.0291	0.0200	0.0275	0.0198	0.0424	0.0232	0.0132	0.0132	0.0776	0.0231	0.0186	0.1925	0.0762	0.0771	0.0310	0.0211	0.0062	0.0088	0.0642	0.0416	0.0243	0.1353
Ca	0.6893	1.0865	0.7966	0.2895	1.5293	0.3335	0.2208	0.2208	2.1909	0.1542	0.2003	2.8049	1.4078	0.5163	0.3918	0.2492	0.1784	0.2263	1.9577	1.0430	0.4525	1.6284
Mn	0.0408	0.0437	0.0468	0.0436	0.0429	0.0486	0.0480	0.0480	0.0488	0.0429	0.0423	0.0345	0.0387	0.0364	0.0404	0.0359	0.0220	0.0440	0.0376	0.0465	0.0443	0.0419
Mg	5.5659	5.2797	5.0348	5.8512	4.7496	5.9725	6.1152	6.1152	3.9138	6.3248	6.0665	3.3928	3.9239	4.1885	5.5684	6.5887	6.8686	5.7155	4.0275	4.5874	5.5142	4.5144
Cr	0.6852	0.4289	0.6978	0.4088	0.4654	0.3692	1.0249	1.0249	0.5343	0.1348	0.2756	0.2903	0.2943	0.5196	0.4529	0.0320	0.0332	0.3098	0.3729	1.3802	0.8838	0.3402
P	0.0014					0.0013						0.0015	0.0043	0.0027					0.0023	0.0016	0.0024	
Fe^{tot}	0.7424	0.7818	0.8803	0.8220	0.6765	0.7473	0.8428	0.8428	0.5567	0.6915	0.6701	0.4052	0.5523	0.7089	0.8370	0.6934	0.6886	0.7699	0.5531	1.0158	0.9455	0.5946
Al	2.6620	1.6050	2.8822	1.8832	1.7996	1.9637	2.7389	2.7389	2.0475	0.9371	1.2765	1.2424	1.7404	2.8818	2.6385	0.5106	0.9940	1.7770	1.8926	3.1594	2.6365	1.8235
Ti	0.0041	0.0192	0.0215	0.0113	0.0258	0.0148	0.0084	0.0084	0.0809	0.0035	0.0090	0.0358	0.0298	0.0239	0.0168	0.0135	0.0159	0.0215	0.0467	0.0189	0.0110	0.0313
Ni	0.0079			0.0018	0.0043				0.0029	0.0021	0.0017	0.0049		0.0013	0.0029	0.0031	0.0163	0.0030		0.0007	0.0026	
Total	15.888	15.624	15.847	15.618	15.607	15.774	16.070	16.070	15.563	15.393	15.394	15.350	15.245	15.425	15.723	15.442	15.650	15.411	15.408	16.150	15.896	15.659
Mg#	88.23	87.10	85.12	87.68	87.53	88.88	87.89	87.89	87.55	90.14	90.05	89.33	87.66	85.52	86.93	90.48	90.89	88.13	87.93	81.87	85.36	88.36
Cr#	20.47	21.09	19.49	17.83	20.55	15.82	27.23	27.23	20.70	12.58	17.76	18.94	14.47	15.28	14.65	5.91	3.23	14.85	16.46	30.40	25.11	15.72

Table 4.2 *(continued)*

	am-cpx																					
Sample	F16-1	F16-2	F16-3	F16-4	F16-5	F16-6	F22-1	F22-2	F22-3	F22-4	F22-5	F22-6	F25b-1	F25b-2	F25b-3	F25b-4	F25b-5	F25b-6	F26-1	F26-2	F26-3	F26-4
comment																						
SiO_2	47.59	47.82	51.22	49.33	48.85	49.32	48.30	51.47	37.63	39.96	39.53	36.64	42.37	47.71	45.49	37.97	34.01	36.20	34.15	37.53	54.06	52.59
K_2O		0.01	0.01	0.01	0.02		0.49		0.06	0.08	0.14	0.46		0.02	0.79	0.90	0.01	0.03	0.07	0.20		
Na_2O	0.40	0.37	0.14	0.06	0.04	0.04	0.29	0.04	0.23	0.14	0.11	0.13	0.02	0.45	0.51	0.25	0.07	0.25	0.28	0.13	0.08	0.58
CaO	19.31	19.77	17.95	1.92	1.21	1.27	17.95	1.66	10.21	5.91	6.25	6.83	3.17	18.36	15.65	7.25	2.71	6.29	7.07	4.86	2.21	14.39
MnO	0.26	0.27	0.37	0.32	0.31	0.31	0.27	0.29	0.38	0.40	0.41	0.42	0.25	0.32	0.35	0.56	0.40	0.55	0.56	0.46	0.45	0.48
MgO	15.23	14.90	17.82	28.42	28.59	28.70	16.85	30.89	20.79	24.00	23.96	22.20	28.15	15.35	18.01	22.92	24.65	23.28	21.72	24.79	31.23	20.96
Cr_2O_3	0.28	0.20	0.38	0.07	0.05	0.06	2.90	1.11	7.93	5.84	6.54	7.76	2.41	2.65	3.96	6.98	12.44	9.38	9.50	8.37	1.34	1.34
P_2O_5		0.02	0.06				0.04					0.02	0.02	0.06	0.05	0.05		0.04	0.02		0.02	
FeO*	4.14	4.05	5.06	7.22	7.09	7.03	3.43	5.93	6.05	5.59	6.22	6.55	5.20	4.18	4.37	5.39	7.93	6.61	6.41	6.43	6.55	4.90
Al_2O_3	10.71	10.65	5.49	10.48	11.78	11.31	8.77	7.28	15.76	13.22	14.48	16.75	15.59	9.77	7.72	12.83	18.16	15.17	16.63	14.32	3.92	3.63
TiO_2	1.73	0.96	0.19	1.76	1.50	2.01	0.15	0.02	0.09	0.07	0.13	0.12	0.24	0.56	0.33	0.49	0.38	0.49	0.51	0.44	0.11	0.07
NiO	0.05			0.02	0.01	0.02	0.03	0.09	0.02	0.01	0.03		0.01	0.02	0.03		0.02					0.02
Total	99.71	99.02	98.70	99.62	99.45	100.07	99.46	98.78	99.14	95.22	97.80	97.88	97.43	99.45	97.27	95.58	100.79	98.29	96.92	97.54	99.95	98.97
12 O																						
Si	6.6517	6.7259	7.2110	6.6452	6.5701	6.5928	6.7809	6.9517	5.4009	5.8304	5.6545	5.3024	5.8894	6.7130	6.6046	5.6211	4.8235	5.2436	5.0401	5.4238	7.2438	7.3292
K		0.0011	0.0014	0.0021	0.0026		0.0879		0.0104	0.0156	0.0261	0.0855		0.0036	0.1467	0.1698	0.0024	0.0055	0.0122	0.0371		
Na	0.1092	0.1009	0.0368	0.0154	0.0096	0.0104	0.0781	0.0092	0.0643	0.0393	0.0297	0.0365	0.0051	0.1236	0.1444	0.0726	0.0201	0.0711	0.0810	0.0353	0.0195	0.1567
Ca	2.8917	2.9792	2.7075	0.2771	0.1742	0.1819	2.7000	0.2402	1.5701	0.9239	0.9579	1.0590	0.4721	2.7678	2.4345	1.1499	0.4118	0.9762	1.1180	0.7525	0.3173	2.1487
Mn	0.0309	0.0322	0.0445	0.0365	0.0354	0.0348	0.0317	0.0328	0.0457	0.0492	0.0496	0.0509	0.0291	0.0383	0.0434	0.0697	0.0479	0.0670	0.0695	0.0563	0.0505	0.0565
Mg	3.1734	3.1242	3.7400	5.7073	5.7323	5.7193	3.5265	6.2197	4.4483	5.2203	5.1093	4.7894	5.8331	3.2198	3.8981	5.0583	5.2117	5.0271	4.7788	5.3408	6.2384	4.3547
Cr	0.0313	0.0222	0.0427	0.0079	0.0057	0.0059	0.3219	0.1182	0.8999	0.6737	0.7396	0.8879	0.2649	0.2948	0.4546	0.8170	1.3949	1.0742	1.1085	0.9564	0.1416	0.1477
P		0.0016	0.0053				0.0031					0.0014	0.0014	0.0051	0.0039	0.0042		0.0028	0.0011		0.0012	
Fe^{tot}	0.4839	0.4764	0.5957	0.8134	0.7975	0.7859	0.4027	0.6698	0.7262	0.6821	0.7441	0.7927	0.6045	0.4919	0.5306	0.6673	0.9406	0.8007	0.7912	0.7771	0.7340	0.5711
Al	1.7643	1.7654	0.9109	1.6639	1.8673	1.7818	1.4511	1.1588	2.6659	2.2733	2.4411	2.8569	2.5539	1.6202	1.3210	2.2385	3.0355	2.5898	2.8926	2.4391	0.6191	0.5962
Ti	0.1818	0.1019	0.0203	0.1783	0.1517	0.2021	0.0158	0.0022	0.0098	0.0075	0.0139	0.0125	0.0253	0.0588	0.0361	0.0540	0.0410	0.0537	0.0570	0.0481	0.0107	0.0073
Ni	0.0051			0.0023	0.0014	0.0016	0.0030	0.0093	0.0021	0.0008	0.0035		0.0012	0.0025	0.0029		0.0022					0.0017
Total	15.323	15.329	15.311	15.349	15.348	15.316	15.400	15.412	15.844	15.716	15.769	15.874	15.679	15.334	15.617	15.918	15.932	15.909	15.949	15.867	15.375	15.370
Mg#	86.77	86.77	86.26	87.53	87.79	87.92	89.75	90.28	85.97	88.44	87.29	85.80	90.61	86.75	88.02	88.35	84.71	86.26	85.80	87.30	89.47	88.41
Cr#	1.74	1.24	4.48	0.47	0.31	0.33	18.16	9.26	25.24	22.86	23.25	23.71	9.40	15.39	25.60	26.74	31.49	29.32	27.71	28.17	18.62	19.85

Table 4.2 *(continued)*

	am-cpx				
Sample	F26-5	F26-6	F26-7	F26-8	F26-9
comment					
SiO_2	53.64	52.74	52.10	46.53	47.13
K_2O	0.01			0.01	0.01
Na_2O	0.53	0.38	0.04	0.77	0.05
CaO	14.92	17.19	1.35	18.62	1.28
MnO	0.35	0.42	0.31	0.33	0.34
MgO	21.32	19.86	31.08	13.90	27.90
Cr_2O_3	0.57	0.55	0.55	3.55	3.41
P_2O_5		0.02			
FeO*	4.76	4.34	6.16	3.75	6.66
Al_2O_3	3.45	3.64	8.02	10.44	12.10
TiO_2	0.09	0.12	0.17	0.42	0.17
NiO			0.06		0.04
Total	99.64	99.25	99.83	98.32	99.10
12 O					
Si	7.3982	7.3465	6.9445	6.6394	6.4198
K	0.0012			0.0016	0.0017
Na	0.1425	0.1026	0.0101	0.2127	0.0124
Ca	2.2048	2.5655	0.1924	2.8466	0.1872
Mn	0.0410	0.0492	0.0345	0.0394	0.0389
Mg	4.3836	4.1241	6.1758	2.9568	5.6655
Cr	0.0624	0.0602	0.0582	0.4005	0.3672
P		0.0012			
Fe^{tot}	0.5490	0.5056	0.6867	0.4475	0.7587
Al	0.5608	0.5976	1.2599	1.7557	1.9425
Ti	0.0093	0.0123	0.0165	0.0447	0.0172
Ni			0.0065		0.0041
Total	15.353	15.364	15.385	15.345	15.415
Mg#	88.87	89.08	89.99	86.86	88.19
Cr#	10.01	9.16	4.41	18.57	15.90

Table 4.3 *Trace element compositions of the constituent minerals in Finsch peridotites (LA-ICP-MS)*

	F-1 olivine					average	F-1 orthopyroxene				average	F-1 clinopyroxene			average	F-1 garnet					average	F-2 olivine		
Element	F1-Ol3	F1-Ol4	F1-Ol1	F1-Ol2	F1-Ol3	**ol F-1**	F1opx2	F1opx2	F1opx3	F1opx4	**opx F-1**	F1cpx1	F1cpx4	F1cpx5	**cpx F-1**	F1-Gt1	F1-Gt2	F1-Gt3	F1-Gt4	F1-Gt5	**grt F-1**	F2-Ol-3	F2-Ol-4	F2-ol2
Li	n.a.	n.a.	1.72	1.81	1.72	**1.75**	0.95	1.51	1.44	1.08	**1.25**	1.37	0.45	bdl	**0.91**	0.298	bdl	bdl	0.070	0.114	**0.161**	0.950	0.960	1.19
B	1.24	1.13	1.14	0.91	1.00	**1.08**	0.770	0.910	1.010	0.980	**0.918**	2.36	1.47	1.90	**1.91**	4.08	3.58	3.33	2.90	3.23	**3.42**	1.36	1.32	n.a.
Sc	0.364	0.393	0.392	0.416	0.390	**0.391**	0.580	0.600	0.608	0.581	**0.592**	17.2	17.0	17.4	**17.2**	74.8	76.4	79.1	75.6	74.2	**76.0**	n.a.	n.a.	2.16
V	6.99	6.91	6.51	6.79	6.40	**6.72**	38.5	40.9	40.4	40.2	**40.0**	226	221	214	**220**	285	287	296	281	278	**285**	6.48	6.53	5.80
Co	156	158	164	173	168	**164**	80.0	63.0	63.4	64.2	**67.7**	25.5	24.8	24.3	**24.9**	49.3	47.3	46.2	47.4	47.3	**47.5**	138	139	133
Ni	n.a.	n.a.	n.a.	n.a.	n.a.	**n.a.**	n.a.	n.a.	n.a.	n.a.	**n.a.**	441	422	408	**424**	80.0	76.3	75.7	75.3	74.7	**76.4**	n.a.	n.a.	n.a.
Cu	n.a.	n.a.	n.a.	n.a.	n.a.	**n.a.**	n.a.	n.a.	n.a.	n.a.	**n.a.**	1.82	2.03	1.30	**1.72**	0.413	0.450	0.480	0.473	0.439	**0.451**	n.a.	n.a.	n.a.
Zn	n.a.	n.a.	n.a.	n.a.	n.a.	**n.a.**	n.a.	n.a.	n.a.	n.a.	**n.a.**	12.5	12.1	11.6	**12.1**	11.8	11.0	11.4	11.5	11.7	**11.5**	n.a.	n.a.	n.a.
Ga	0.151	0.160	0.223	0.219	0.213	**0.193**	2.02	2.00	2.03	2.00	**2.01**	n.a.	n.a.	n.a.	**n.a.**	n.a.	n.a.	n.a.	n.a.	n.a.	**n.a.**	0.113	0.111	n.a.
Ge	0.628	0.635	0.547	0.542	0.563	**0.583**	1.29	1.45	1.44	1.43	**1.40**	n.a.	n.a.	n.a.	**n.a.**	n.a.	n.a.	n.a.	n.a.	n.a.	**n.a.**	0.546	0.568	n.a.
Rb	bdl	0.0017	bdl	bdl	bdl	**0.0017**	0.003	bdl	0.010	0.002	**0.005**	0.027	0.036	0.043	**0.035**	0.041	0.033	0.013	0.021	0.027	**0.027**	bdl	0.0084	bdl
Sr	0.0039	0.0037	0.0067	0.0055	0.0092	**0.0058**	0.258	0.256	0.379	0.267	**0.290**	85.4	88.6	89.6	**87.8**	0.124	0.147	0.156	0.137	0.139	**0.141**	0.012	0.0096	bdl
Y	0.0044	0.0037	0.0039	0.0031	0.0023	**0.0035**	0.043	0.054	0.052	0.051	**0.050**	1.67	1.64	1.68	**1.66**	9.5	10.2	11.0	10.1	9.7	**10.1**	0.0028	0.0022	0.0104
Zr	0.023	0.030	0.025	0.016	0.027	**0.024**	0.061	0.078	0.069	0.070	**0.070**	2.93	2.98	2.95	**2.95**	15.2	16.1	17.5	15.8	15.4	**16.0**	0.298	0.273	0.348
Nb	0.023	0.030	0.022	0.021	0.029	**0.025**	0.043	0.046	0.048	0.046	**0.046**	0.181	0.185	0.170	**0.179**	0.208	0.206	0.220	0.218	0.215	**0.213**	0.067	0.061	0.036
Mo	n.a.	n.a.	n.a.	n.a.	n.a.	**n.a.**	n.a.	n.a.	n.a.	n.a.	**n.a.**	n.a.	n.a.	n.a.	**n.a.**	n.a.	n.a.	n.a.	n.a.	n.a.	**n.a.**	n.a.	n.a.	n.a.
Cs	n.a.	n.a.	n.a.	n.a.	n.a.	**n.a.**	n.a.	n.a.	n.a.	n.a.	**n.a.**	bdl	bdl	0.0044	**0.0044**	bdl	bdl	bdl	bdl	bdl	**bdl**	n.a.	n.a.	bdl
Ba	n.a.	n.a.	n.a.	n.a.	n.a.	**n.a.**	n.a.	n.a.	n.a.	n.a.	**n.a.**	0.228	0.247	0.231	**0.235**	bdl	bdl	bdl	0.0074	bdl	**0.0074**	n.a.	n.a.	bdl
La	bdl	bdl	0.0003	bdl	0.0007	**0.0005**	0.0043	0.0042	0.0079	0.0038	**0.0051**	1.23	1.27	1.27	**1.26**	bdl	bdl	0.011	bdl	0.017	**0.014**	0.0010	0.0007	bdl
Ce	0.037	0.040	bdl	bdl	bdl	**0.039**	0.017	0.016	0.021	0.015	**0.017**	4.36	4.61	4.50	**4.49**	0.109	0.128	0.135	0.128	0.125	**0.125**	0.0029	0.0015	0.0085
Pr	n.a.	n.a.	n.a.	n.a.	n.a.	**n.a.**	n.a.	n.a.	n.a.	n.a.	**n.a.**	0.805	0.786	0.809	**0.800**	0.045	0.038	0.049	0.042	0.046	**0.044**	n.a.	n.a.	n.a.
Nd	0.0006	0.0003	0.0003	0.0009	0.0006	**0.0005**	0.019	0.024	0.022	0.019	**0.021**	4.10	3.95	3.92	**3.99**	0.455	0.486	0.590	0.514	0.479	**0.505**	0.0008	bdl	0.0017
Sm	bdl	0.0013	bdl	bdl	0.0010	**0.0011**	0.009	0.012	0.012	0.011	**0.011**	0.810	0.940	0.810	**0.853**	0.454	0.441	0.444	0.467	0.328	**0.427**	bdl	bdl	0.0017
Eu	bdl	0.0006	0.0001	0.0001	bdl	**0.0003**	0.0025	0.0030	0.0040	0.0032	**0.0032**	0.266	0.272	0.262	**0.267**	0.242	0.211	0.249	0.225	0.214	**0.228**	0.0003	0.0005	bdl
Gd	0.0007	0.0003	0.0006	0.0012	0.0002	**0.0006**	0.0090	0.0086	0.0121	0.0094	**0.0098**	0.720	0.690	0.660	**0.690**	0.890	0.875	1.091	0.885	0.873	**0.923**	0.0010	0.0008	0.0014
Tb	0.0001	0.0001	0.0001	bdl	0.0001	**0.0001**	0.0017	0.0016	0.0019	0.0017	**0.0017**	0.090	0.095	0.082	**0.089**	0.191	0.211	0.208	0.191	0.181	**0.196**	0.0001	0.0002	n.a.
Dy	0.0011	0.0011	0.0004	0.0007	0.0001	**0.0007**	0.010	0.014	0.011	0.013	**0.012**	0.411	0.406	0.404	**0.407**	1.51	1.59	1.74	1.65	1.55	**1.61**	0.0011	0.0001	0.0019
Ho	0.0005	0.0001	0.0002	0.0002	0.0002	**0.0002**	0.0018	0.0024	0.0031	0.0022	**0.0024**	0.068	0.065	0.069	**0.067**	0.367	0.417	0.456	0.393	0.378	**0.402**	bdl	0.0001	n.a.
Er	0.0006	bdl	0.0002	0.0004	0.0002	**0.0003**	0.0050	0.0066	0.0066	0.0046	**0.0057**	0.150	0.138	0.140	**0.143**	1.23	1.32	1.45	1.20	1.21	**1.28**	0.0006	0.0001	0.0018
Tm	0.0004	bdl	0.0001	bdl	bdl	**0.0002**	0.0008	0.0010	0.0011	0.0013	**0.0011**	0.016	0.015	0.010	**0.014**	0.183	0.213	0.233	0.199	0.198	**0.205**	bdl	0.0002	n.a.
Yb	0.0012	bdl	0.0004	0.0007	0.0007	**0.0008**	0.0040	0.0058	0.0075	0.0056	**0.0058**	0.080	0.060	0.082	**0.074**	1.62	1.59	1.73	1.63	1.54	**1.62**	0.0010	0.0008	0.0010
Lu	0.0003	0.0004	bdl	0.0001	0.0002	**0.0003**	0.0008	0.0009	0.0008	0.0008	**0.0008**	bdl	0.013	bdl	**0.013**	0.231	0.233	0.258	0.236	0.234	**0.238**	bdl	0.0001	bdl
Hf	0.0014	0.0007	0.0008	0.0010	0.0006	**0.0009**	0.0027	0.0043	0.0038	0.0039	**0.0037**	0.200	0.211	0.180	**0.197**	0.411	0.430	0.461	0.439	0.382	**0.425**	0.0111	0.0099	0.0115
Ta	0.0022	0.0032	0.0015	0.0014	0.0022	**0.0021**	0.0055	0.0060	0.0056	0.0063	**0.0058**	0.0134	bdl	0.0149	**0.0142**	0.019	bdl	0.028	0.025	0.025	**0.024**	0.0062	0.0054	0.0038
W	n.a.	n.a.	n.a.	n.a.	n.a.	**n.a.**	n.a.	n.a.	n.a.	n.a.	**n.a.**	n.a.	n.a.	n.a.	**n.a.**	n.a.	n.a.	n.a.	n.a.	n.a.	**n.a.**	n.a.	n.a.	n.a.
Pb	n.a.	n.a.	bdl	bdl	bdl	**bdl**	n.a.	n.a.	n.a.	n.a.	**n.a.**	1.98	8.76	0.24	**3.66**	0.91	0.15	0.22	5.86	0.22	**1.47**	n.a.	n.a.	0.053
Th	bdl	0.0044	bdl	bdl	bdl	**0.0044**	n.a.	n.a.	n.a.	n.a.	**n.a.**	0.0137	0.0166	0.0221	**0.0175**	bdl	bdl	bdl	bdl	bdl	**bdl**	bdl	0.0006	bdl
U	bdl	0.0003	bdl	bdl	0.0001	**0.0002**	bdl	bdl	0.0053	bdl	**0.0053**	bdl	0.0041	0.0037	**0.0039**	0.0065	0.0119	0.0124	0.0103	0.0099	**0.0102**	0.0001	bdl	0.0002

bdl - below detection limit
n.a. - not analysed

Table 4.3 *(continued)*

	F-2 olivine				F-2 orthopyroxene					F-2 garnet						F-3 olivine							F-3 orthopyroxene	
				average					**average**						**average**							**average**		
Elemen	F2-ol3	F2-ol4	F2-ol5	**ol F-2**	F2opx-1	F2opx-2	F2opx-4	F2opx3	**opx F-2**	F2-Grt1a	F2-Grt2a	F2-Gt-1b	F2-Gt-2b	F2-Gt-3b	**grt F-2**	F3-ol2	F3-ol5	F3-ol7	F3-ol10	F3-ol11	F3-ol12	**ol F-3**	F3opx-1	F3opx1
Li	1.14	1.14	1.10	**1.06**	1.92	1.88	0.91	0.49	**1.30**	bdl	bdl	bdl	0.510	bdl	**0.510**	1.36	1.76	1.72	1.53	1.45	1.44	**1.54**	bdl	0.748
B	n.a.	n.a.	n.a.	**1.34**	0.940	1.010	0.980	n.a.	**0.977**	0.600	0.570	0.490	0.466	0.412	**0.508**	n.a.	0.636	0.579	0.588	0.572	0.561	**0.587**	0.490	0.600
Sc	2.14	2.11	2.10	**2.15**	n.a.	n.a.	n.a.	2.71	**2.71**	147	147	151	157	147	**150**	2.51	2.18	2.08	2.02	2.01	2.00	**2.13**	3.09	2.95
V	5.77	5.51	5.33	**6.15**	38.6	38.0	37.2	36.0	**37.4**	370	387	375	370	372	**375**	4.07	6.40	6.36	5.99	5.96	5.87	**5.78**	42.3	38.9
Co	133	134	136	**136**	57.0	57.6	57.5	55.4	**56.9**	45.4	45.2	48.0	46.0	47.5	**46.4**	127	144	144	133	132	131	**135**	56.4	55.2
Ni	2999	2981	3003	**2999**	n.a.	n.a.	n.a.	n.a.	**n.a.**	73.4	72.9	77.8	72.0	74.2	**74.0**	n.a.	3488	3412	3134	3127	3098	**3252**	765	936
Cu	n.a.	n.a.	n.a.	**n.a.**	n.a.	n.a.	n.a.	n.a.	**n.a.**	bdl	bdl	bdl	0.135	0.137	**0.136**	n.a.	3.29	3.00	2.78	2.78	2.72	**2.91**	0.89	2.52
Zn	n.a.	n.a.	n.a.	**n.a.**	n.a.	n.a.	n.a.	n.a.	**n.a.**	13.0	11.9	11.0	10.2	10.6	**11.3**	n.a.	59.9	65.0	57.3	58.5	57.8	**59.7**	29.4	31.7
Ga	n.a.	n.a.	n.a.	**0.112**	1.41	1.47	1.39	n.a.	**1.42**	7.85	7.71	7.96	7.01	7.37	**7.58**	n.a.	n.a.	n.a.	n.a.	n.a.	n.a.	**n.a.**	1.64	n.a.
Ge	n.a.	n.a.	n.a.	**0.557**	1.29	1.32	1.38	n.a.	**1.33**	n.a.	n.a.	n.a.	n.a.	n.a.	**n.a.**	n.a.	n.a.	n.a.	n.a.	n.a.	n.a.	**n.a.**	n.a.	n.a.
Rb	bdl	bdl	bdl	**0.0084**	0.0023	0.0091	bdl	bdl	**0.0057**	0.023	0.027	0.048	0.040	0.031	**0.034**	bdl	bdl	bdl	bdl	bdl	bdl	**bdl**	0.114	0.046
Sr	0.187	bdl	0.136	**0.069**	0.752	0.725	0.714	0.776	**0.742**	0.96	0.97	1.20	1.17	1.11	**1.08**	bdl	bdl	0.0089	bdl	bdl	bdl	**0.0089**	0.913	0.548
Y	0.0028	0.0028	0.0032	**0.0045**	0.015	0.017	0.027	0.026	**0.021**	9.27	9.16	8.75	9.74	9.13	**9.21**	0.0022	0.0038	0.0058	bdl	bdl	0.0037	**0.0039**	0.017	0.026
Zr	0.218	0.305	0.309	**0.284**	0.251	0.216	0.416	0.470	**0.338**	18.9	19.5	20.3	19.3	18.2	**19.2**	0.040	0.023	0.032	0.035	0.030	0.032	**0.032**	0.086	0.072
Nb	0.048	0.055	0.057	**0.053**	0.131	0.134	0.121	0.079	**0.116**	1.83	1.74	0.99	1.78	1.80	**1.63**	0.014	0.015	0.015	0.015	0.013	0.014	**0.014**	0.029	0.024
Mo	n.a.	n.a.	n.a.	**n.a.**	n.a.	n.a.	n.a.	n.a.	**n.a.**	0.480	0.430	0.453	0.411	0.287	**0.412**	n.a.	n.a.	n.a.	n.a.	n.a.	n.a.	**n.a.**	0.081	n.a.
Cs	bdl	bdl	bdl	**bdl**	n.a.	n.a.	n.a.	bdl	**n.a.**	0.0025	bdl	bdl	bdl	bdl	**0.0025**	bdl	bdl	bdl	bdl	bdl	bdl	**bdl**	n.a.	bdl
Ba	bdl	bdl	bdl	**bdl**	n.a.	n.a.	n.a.	0.067	**0.067**	0.011	bdl	bdl	bdl	bdl	**0.011**	bdl	bdl	n.a.	bdl	bdl	bdl	**bdl**	n.a.	0.463
La	0.0005	0.0007	0.0004	**0.0007**	0.021	0.017	0.016	0.013	**0.017**	0.164	0.164	0.158	0.188	0.174	**0.170**	bdl	bdl	0.0004	0.0002	bdl	bdl	**0.0003**	0.013	0.006
Ce	0.0004	0.0028	0.0010	**0.0033**	0.064	0.067	0.058	0.074	**0.065**	1.92	1.93	1.93	1.95	1.99	**1.94**	0.0012	bdl	0.0020	0.0004	0.0004	bdl	**0.0010**	0.055	0.029
Pr	n.a.	n.a.	n.a.	**n.a.**	n.a.	n.a.	n.a.	n.a.	**n.a.**	n.a.	n.a.	n.a.	n.a.	n.a.	**n.a.**	n.a.	bdl	0.0005	0.0002	bdl	bdl	**0.0004**	n.a.	0.007
Nd	0.0006	0.0022	bdl	**0.0010**	0.041	0.029	0.039	0.055	**0.041**	2.89	2.96	3.19	3.17	3.06	**3.05**	bdl	bdl	0.0062	bdl	bdl	bdl	**0.0062**	0.049	0.041
Sm	bdl	0.0020	bdl	**0.0017**	0.0092	0.0046	0.0130	0.0110	**0.0095**	1.03	1.08	1.15	1.21	1.07	**1.11**	0.0018	0.0015	bdl	0.0011	0.0016	bdl	**0.0015**	0.011	bdl
Eu	0.0002	bdl	bdl	**0.0003**	0.0028	0.0021	0.0038	0.0029	**0.0029**	0.392	0.414	0.442	0.44	0.421	**0.422**	bdl	0.0002	bdl	0.0014	0.0004	0.0003	**0.0006**	0.0032	bdl
Gd	bdl	bdl	0.0006	**0.0010**	0.0086	0.0097	0.0087	0.0118	**0.0097**	1.31	1.32	1.39	1.37	1.26	**1.33**	bdl	bdl	bdl	bdl	0.0015	0.0006	**0.0011**	0.0059	0.0047
Tb	n.a.	n.a.	n.a.	**0.0002**	0.0012	0.0006	0.0010	n.a.	**0.0009**	0.174	0.166	0.179	0.186	0.176	**0.176**	n.a.	0.0007	0.0006	0.0004	bdl	bdl	**0.0006**	0.0010	0.0018
Dy	0.0004	bdl	bdl	**0.0009**	0.0022	0.0026	0.0054	0.0064	**0.0041**	1.35	1.33	1.32	1.44	1.31	**1.35**	bdl	bdl	0.0035	bdl	bdl	bdl	**0.0035**	0.0052	0.0051
Ho	n.a.	n.a.	n.a.	**0.0001**	0.0011	0.0006	0.0010	n.a.	**0.0009**	0.327	0.316	0.301	0.338	0.318	**0.320**	n.a.	0.0006	0.0002	0.0001	0.0003	0.0003	**0.0003**	0.0007	0.0016
Er	0.0011	bdl	bdl	**0.0009**	bdl	0.0036	0.0031	0.0029	**0.0032**	1.08	1.08	0.96	1.16	1.05	**1.07**	0.0008	bdl	bdl	0.0017	bdl	bdl	**0.0012**	0.0025	0.0027
Tm	n.a.	n.a.	n.a.	**0.0002**	0.001	0.000	bdl	n.a.	**0.0005**	0.158	0.145	0.136	0.162	0.145	**0.149**	n.a.	0.0003	0.0003	0.0002	0.0002	bdl	**0.0002**	bdl	bdl
Yb	0.0007	0.0022	0.0010	**0.0009**	0.003	0.003	0.002	0.001	**0.0021**	1.33	1.27	1.18	1.40	1.23	**1.28**	0.0002	0.0005	bdl	bdl	bdl	bdl	**0.0003**	bdl	0.002
Lu	0.0003	0.0003	0.0001	**0.0002**	bdl	bdl	bdl	bdl	**bdl**	0.229	0.226	0.205	0.232	0.220	**0.222**	0.0001	0.0003	bdl	bdl	bdl	bdl	**0.0002**	bdl	bdl
Hf	0.0058	0.0118	0.0126	**0.0096**	0.005	0.005	0.017	0.013	**0.010**	0.470	0.502	0.509	0.490	0.453	**0.485**	0.0026	0.0005	bdl	0.0024	bdl	bdl	**0.0018**	0.0071	0.0048
Ta	0.0056	0.0077	0.0067	**0.0052**	0.017	0.015	0.016	0.018	**0.016**	0.213	0.212	0.182	0.235	0.227	**0.214**	0.0011	bdl	0.0009	0.0011	0.0009	bdl	**0.0010**	0.0023	0.0022
W	n.a.	n.a.	n.a.	**n.a.**	0.0028	0.0006	0.0014		**0.0016**	0.020	bdl	bdl	bdl	0.032	**0.026**	n.a.	n.a.	n.a.	n.a.	n.a.	n.a.	**n.a.**	0.024	n.a.
Pb	0.030	0.027	0.078	**0.042**	n.a.	n.a.	n.a.	0.132	**0.132**	0.012	0.024	0.037	0.058	0.038	**0.034**	0.091	0.236	0.408	0.148	0.159	0.197	**0.206**	n.a.	0.150
Th	0.723	0.048	0.052	**0.206**	n.a.	n.a.	n.a.	0.0020	**0.0020**	0.110	0.112	0.104	0.112	0.115	**0.111**	0.0014	0.0016	0.0030	0.0002	0.0003	bdl	**0.0013**	n.a.	0.0012
U	bdl	0.0001	0.0002	**0.0002**	bdl	0.0010	bdl	0.0007	**0.0008**	0.077	0.078	0.101	0.101	0.106	**0.093**	bdl	0.0002	bdl	0.0002	bdl	bdl	**0.0002**	0.0010	0.0016

Table 4.3 *(continued)*

	F-3 orthopyroxene					average	F-3 clinopyroxene		average	F-3 garnet				average	F-4 olivine						average	F-4 orthopyroxene		
Elemer	F3opx3	F3opx4	F3opx5	F3opx7	F3opx9	**opx F-3**	F3cpx3	F3cpx4	**cpx F-3**	F3-Gt2a	F3-Gt1	F3-Gt2	F3-Gt3	**grt F-3**	F4-Ol-1	F4-Ol-2	F4-Ol-3	F4-ol2	F4-ol4	F4-ol5	**ol F-4**	F4opx3	F4opx4	F4opx5
Li	0.865	0.712	0.95	0.844	0.811	**0.822**	0.810	bdl	**0.810**	bdl	bdl	bdl	bdl	**bdl**	n.a.	n.a.	n.a.	2.28	1.94	1.67	**1.96**	n.a.	0.666	0.775
B	0.430	0.442	0.341	0.341	0.422	**0.438**	3.63	4.27	**3.95**	4.29	4.30	3.92	3.91	**4.11**	1.65	1.46	1.45	n.a.	n.a.	n.a.	**1.52**	n.a.	n.a.	n.a.
Sc	2.86	2.8	2.85	2.81	2.78	**2.88**	15.6	15.3	**15.4**	98	104	109	103	**103**	n.a.	n.a.	n.a.	2.37	2.16	2.08	**2.20**	2.89	2.91	2.80
V	38.7	39.3	39.1	39.4	39.9	**39.7**	289	279	**284**	294	301	249	287	**283**	6.89	6.62	6.67	4.76	5.64	5.48	**6.01**	33.1	33.3	33.5
Co	54.3	55.5	54.6	55.0	54.5	**55.1**	20.9	21.6	**21.3**	35.7	37.4	31.8	35.0	**35.0**	178	169	165	146	148	144	**159**	65.8	65.0	65.3
Ni	902	910	896	890	892	**884**	326	350	**338**	50.0	53.1	37.9	56.2	**49.3**	n.a.	n.a.	n.a.	3325	3327	3235	**3296**	1000	980	995
Cu	1.88	2.35	1.98	1.95	1.95	**1.93**	n.a.	2.02	**2.02**	0.179	bdl	bdl	bdl	**0.179**	n.a.	n.a.	n.a.	n.a.	n.a.	n.a.	**n.a.**	n.a.	n.a.	n.a.
Zn	30.5	33.2	32.6	32.1	32.2	**31.7**	7.69	10.21	**8.95**	8.36	7.49	7.40	7.51	**7.69**	n.a.	n.a.	n.a.	n.a.	n.a.	n.a.	**n.a.**	n.a.	n.a.	n.a.
Ga	n.a.	n.a.	n.a.	n.a.	n.a.	**1.64**	n.a.	n.a.	**n.a.**	n.a.	n.a.	n.a.	n.a.	**n.a.**	0.132	0.117	0.117	n.a.	n.a.	n.a.	**0.122**	n.a.	n.a.	n.a.
Ge	n.a.	n.a.	n.a.	n.a.	n.a.	**n.a.**	n.a.	n.a.	**n.a.**	n.a.	n.a.	n.a.	n.a.	**n.a.**	0.675	0.646	0.622	n.a.	n.a.	n.a.	**0.648**	n.a.	n.a.	n.a.
Rb	0.026	0.026	0.152	0.027	0.206	**0.085**	0.104	0.122	**0.113**	0.294	0.089	0.058	0.085	**0.131**	bdl	bdl	0.0043	bdl	bdl	0.0064	**0.0054**	bdl	0.065	0.050
Sr	0.591	0.567	0.730	0.529	1.430	**0.758**	329	332	**331**	0.853	0.865	0.848	0.920	**0.872**	0.021	0.004	0.018	bdl	0.059	bdl	**0.025**	0.283	0.449	0.470
Y	0.026	0.024	0.029	0.026	0.026	**0.025**	1.02	1.07	**1.04**	11.2	12.0	12.5	11.7	**11.8**	0.0017	0.0012	0.0019	0.0025	0.0015	bdl	**0.0017**	0.015	0.020	0.020
Zr	0.066	0.076	0.085	0.069	0.102	**0.079**	3.95	3.72	**3.84**	28.1	30.2	31.6	29.1	**29.8**	0.199	0.187	0.222	0.257	0.206	0.206	**0.213**	0.260	0.277	0.284
Nb	0.024	0.023	0.033	0.022	0.052	**0.030**	0.167	0.140	**0.154**	0.258	0.283	0.239	0.283	**0.266**	0.052	0.049	0.050	0.053	0.048	0.041	**0.049**	0.073	0.055	0.050
Mo	n.a.	n.a.	n.a.	n.a.	n.a.	**0.081**	n.a.	n.a.	**n.a.**	n.a.	n.a.	n.a.	n.a.	**n.a.**	n.a.	n.a.	n.a.	n.a.	n.a.	n.a.	**n.a.**	n.a.	n.a.	n.a.
Cs	bdl	bdl	bdl	bdl	0.0077	**0.0077**	bdl	bdl	**bdl**	bdl	bdl	bdl	bdl	**bdl**	n.a.	n.a.	n.a.	bdl	0.0018	bdl	**0.0018**	bdl	0.0048	0.0027
Ba	0.138	0.017	0.161	0.009	0.848	**0.273**	0.465	0.487	**0.476**	bdl	bdl	bdl	bdl	**bdl**	n.a.	n.a.	n.a.	bdl	0.029	bdl	**0.029**	0.020	0.173	0.157
La	0.011	0.0037	0.025	0.0052	0.065	**0.019**	2.21	2.23	**2.22**	0.039	0.040	0.032	0.048	**0.040**	0.0027	0.0003	0.0011	0.0053	bdl	0.0008	**0.0020**	0.0061	0.0080	0.0090
Ce	0.042	0.028	0.075	0.040	0.198	**0.067**	11.6	12.1	**11.9**	0.64	0.644	0.588	0.652	**0.631**	0.0072	0.0012	0.0066	0.0148	0.0007	0.0022	**0.0055**	0.027	0.036	0.048
Pr	0.009	0.006	0.013	0.006	0.0239	**0.011**	2.32	2.48	**2.40**	0.285	0.291	0.273	0.305	**0.289**	n.a.	n.a.	n.a.	n.a.	n.a.	n.a.	**n.a.**	n.a.	n.a.	n.a.
Nd	0.067	0.047	0.063	0.044	0.105	**0.059**	11.7	11.4	**11.5**	3.1	3.28	3.22	3.15	**3.19**	0.0024	0.0008	0.0018	0.0030	0.0012	0.0009	**0.0017**	0.028	0.036	0.036
Sm	0.009	0.012	0.011	0.012	bdl	**0.011**	1.47	1.69	**1.58**	1.48	1.67	1.55	1.64	**1.59**	bdl	0.0015	bdl	bdl	bdl	0.0014	**0.0015**	0.0078	0.0068	0.0097
Eu	0.002	0.003	bdl	0.002	0.00359	**0.0029**	0.394	0.345	**0.370**	0.534	0.578	0.537	0.521	**0.543**	bdl	bdl	0.0003	bdl	bdl	bdl	**0.0003**	0.0020	0.0018	0.0034
Gd	0.013	bdl	0.013	0.0083	bdl	**0.0089**	0.785	0.900	**0.843**	1.85	1.89	1.84	1.81	**1.85**	bdl	bdl	0.0004	0.0012	bdl	bdl	**0.0008**	0.004	0.007	0.013
Tb	0.0018	0.0008	0.0013	0.0025	0.00179	**0.0016**	0.066	0.102	**0.084**	0.326	0.316	0.332	0.292	**0.317**	bdl	0.0001	bdl	n.a.	n.a.	n.a.	**0.0001**	n.a.	n.a.	n.a.
Dy	0.0052	0.0063	0.0117	0.0056	0.0048	**0.0063**	0.308	0.279	**0.294**	2.15	2.35	2.50	2.31	**2.33**	0.0002	bdl	bdl	bdl	bdl	bdl	**0.0002**	0.0011	0.0055	0.0054
Ho	0.0014	0.0025	0.0011	0.0009	0.00183	**0.0014**	0.041	0.045	**0.043**	0.442	0.451	0.492	0.445	**0.458**	bdl	bdl	bdl	n.a.	n.a.	n.a.	**bdl**	n.a.	n.a.	n.a.
Er	0.0046	0.0037	bdl	bdl	0.0028	**0.0033**	0.085	0.091	**0.088**	1.19	1.35	1.20	1.27	**1.25**	0.0003	0.0002	bdl	0.0013	bdl	bdl	**0.0006**	bdl	bdl	0.0018
Tm	0.0007	0.0007	bdl	0.0008	bdl	**0.0008**	0.004	0.0128	**0.008**	0.164	0.166	0.165	0.166	**0.165**	bdl	bdl	bdl	n.a.	n.a.	n.a.	**bdl**	n.a.	n.a.	n.a.
Yb	bdl	0.0025	bdl	bdl	bdl	**0.0022**	0.051	0.061	**0.056**	1.06	1.24	1.18	1.24	**1.18**	bdl	bdl	bdl	bdl	bdl	bdl	**bdl**	bdl	0.001	bdl
Lu	bdl	0.0008	0.0002	0.0008	bdl	**0.0006**	0.0014	0.0029	**0.0022**	0.157	0.182	0.188	0.170	**0.174**	0.0001	0.0001	0.0001	0.0002	bdl	bdl	**0.0001**	bdl	bdl	bdl
Hf	0.0059	0.0068	0.0054	0.0091	0.0041	**0.0062**	0.286	0.323	**0.305**	0.792	0.833	0.869	0.783	**0.819**	0.0045	0.0051	0.0066	0.0095	0.0047	0.0069	**0.0062**	0.004	0.011	0.012
Ta	0.0031	0.0019	0.0034	0.0035	0.0055	**0.00312**	0.0025	0.0080	**0.0053**	0.022	0.024	n.a.	n.a.	**0.023**	0.0051	0.0046	0.0049	0.0058	0.0061	0.0066	**0.0055**	0.016	0.013	0.012
W	n.a.	n.a.	n.a.	n.a.	n.a.	**0.024**	n.a.	n.a.	**n.a.**	n.a.	n.a.	n.a.	n.a.	**n.a.**	n.a.	n.a.	n.a.	n.a.	n.a.	n.a.	**n.a.**	n.a.	n.a.	n.a.
Pb	0.114	0.174	0.127	0.136	0.191	**0.149**	1.64	1.83	**1.74**	0.137	0.146	0.188	0.152	**0.156**	n.a.	n.a.	n.a.	0.015	0.042	0.054	**0.037**	0.112	0.159	0.055
Th	0.0007	0.0014	0.0014	0.0003	0.0067	**0.0019**	0.014	0.013	**0.013**	0.011	bdl	bdl	0.015	**0.013**	bdl	bdl	0.0005	0.0005	bdl	bdl	**0.0005**	0.0004	0.0008	0.0006
U	0.0011	0.0014	0.0020	0.0011	0.0055	**0.0020**	bdl	bdl	**bdl**	0.036	0.038	0.029	0.041	**0.036**	0.0003	bdl	bdl	0.0005	bdl	0.0001	**0.0003**	0.0003	0.0002	0.0004

Table 4.3 *(continued)*

cont.	F-4 opx		F-4 garnet				F-5 olivine				F-5 orthopyroxene							F-5 clinopyroxene			F-5 garnet				
		average				**average**				**average**							**average**								**average**
Element	F4opx-1	**opx F-4**	F4-Gt1	F4-Gt2	F4-Gt3	**grt F-4**	F5-Ol-2	F5-Ol-3	F5-ol2	**ol F-5**	F5opx-1	F5opx-2	F5opx-3	F5opx1	F5opx2	F5opx4	**opx F-5**	F5cpx1	F5cpx2	**cpx F-5**	F5-Gt1	F5-Gt2	F5-Gt3	F5-Gt4	**grt F-5**
Li	0.890	**0.777**	bdl	bdl	bdl	**bdl**	n.a.	n.a.	1.45	**1.45**	0.150	0.460	0.170	1.185	0.799	0.747	**0.910**	1.13	1.22	**1.18**	0.169	0.231	bdl	bdl	**0.200**
B	1.16	**1.16**	3.31	2.85	3.17	**3.11**	1.24	1.39	n.a.	**1.32**	0.960	0.980	1.01	n.a.	n.a.	n.a.	**0.983**	13.0	7.1	**10.1**	1.47	2.47	2.32	2.2	**2.12**
Sc	n.a.	**2.87**	134	128	154	**139**	n.a.	n.a.	1.74	**1.74**	n.a.	n.a.	n.a.	2.32	2.133	2.087	**2.18**	9.55	9.22	**9.39**	85.1	90.8	92.5	91.2	**89.9**
V	33.1	**33.2**	357	338	321	**339**	5.33	5.30	4.92	**5.18**	32.6	32.6	32.1	31.4	30.8	32.3	**32.0**	191	192	**192**	304	301	291	298	**299**
Co	66.3	**65.6**	44.9	43.5	41.5	**43.3**	152	151	143	**149**	63.5	63.2	62.6	59.2	60.4	60.5	**61.6**	31.6	25.5	**28.6**	42.5	41.7	40.4	40.7	**41.3**
Ni	n.a.	**992**	74.3	71.4	65.7	**70.5**	n.a.	n.a.	3326	**3326**	n.a.	n.a.	n.a.	953	966	951	**956**	816	639	**728**	66.2	63.4	61.0	62.1	**63.2**
Cu	n.a.	**n.a.**	0.353	0.280	0.674	**0.436**	n.a.	n.a.	n.a.	**n.a.**	n.a.	n.a.	n.a.	n.a.	n.a.	n.a.	**n.a.**	bdl	1.7	**1.7**	0.141	bdl	bdl	bdl	**0.141**
Zn	n.a.	**n.a.**	12.2	11.7	10.2	**11.4**	n.a.	n.a.	n.a.	**n.a.**	n.a.	n.a.	n.a.	n.a.	n.a.	n.a.	**n.a.**	15.2	9.50	**12.4**	9.77	9.59	9.24	8.62	**9.31**
Ga	1.34	**1.34**	n.a.	n.a.	n.a.	**n.a.**	0.068	0.071	n.a.	**0.070**	0.833	0.812	0.791	n.a.	n.a.	n.a.	**0.812**	n.a.	n.a.	**n.a.**	n.a.	n.a.	n.a.	n.a.	**n.a.**
Ge	1.44	**1.44**	n.a.	n.a.	n.a.	**n.a.**	0.438	0.444	n.a.	**0.441**	1.03	1.10	1.04	n.a.	n.a.	n.a.	**1.06**	n.a.	n.a.	**n.a.**	n.a.	n.a.	n.a.	n.a.	**n.a.**
Rb	0.003	**0.039**	0.166	0.122	0.090	**0.126**	bdl	bdl	bdl	**bdl**	bdl	0.005	0.074	0.105	0.157	0.122	**0.093**	0.364	0.215	**0.290**	0.049	0.049	0.050	0.040	**0.047**
Sr	0.615	**0.454**	0.356	0.441	0.378	**0.392**	0.036	0.013	bdl	**0.024**	0.336	0.352	0.475	0.675	0.541	0.509	**0.481**	178	240	**209**	0.353	0.371	0.368	0.335	**0.3568**
Y	0.013	**0.017**	3.03	3.17	3.68	**3.29**	bdl	bdl	0.0013	**0.0013**	0.0088	0.0087	0.0088	0.0103	0.0115	0.0094	**0.0096**	0.233	0.253	**0.243**	2.98	3.15	3.30	3.24	**3.17**
Zr	0.192	**0.253**	17.1	16.3	19.3	**17.5**	0.030	0.036	0.039	**0.035**	0.061	0.052	0.063	0.062	0.069	0.065	**0.062**	1.44	1.26	**1.35**	24.6	26.5	27.1	26.9	**26.2**
Nb	0.043	**0.055**	0.468	0.36	0.367	**0.398**	0.028	0.030	0.028	**0.029**	0.041	0.040	0.044	0.041	0.042	0.038	**0.041**	0.149	0.112	**0.131**	0.240	0.297	0.269	0.257	**0.2658**
Mo	n.a.	**n.a.**	n.a.	n.a.	n.a.	**n.a.**	n.a.	n.a.	n.a.	**n.a.**	n.a.	n.a.	n.a.	n.a.	n.a.	n.a.	**n.a.**	n.a.	n.a.	**n.a.**	n.a.	n.a.	n.a.	n.a.	**n.a.**
Cs	n.a.	**0.0038**	bdl	bdl	bdl	**bdl**	n.a.	n.a.	n.a.	**n.a.**	n.a.	n.a.	n.a.	0.0058	0.0091	0.0100	**0.0083**	0.027	0.024	**0.025**	bdl	bdl	bdl	bdl	**bdl**
Ba	n.a.	**0.117**	bdl	bdl	bdl	**bdl**	n.a.	n.a.	0.03	**0.030**	n.a.	n.a.	n.a.	0.132	0.205	0.089	**0.142**	6.47	n.a.	**6.47**	0.024	0.017	0.021	0.012	**0.018**
La	0.011	**0.0086**	0.037	0.036	0.032	**0.035**	0.0021	0.0013	bdl	**0.0017**	0.0028	0.0026	0.0025	0.0181	0.0081	0.0032	**0.0062**	1.43	1.42	**1.43**	0.016	0.023	0.018	0.020	**0.019**
Ce	0.059	**0.043**	0.400	0.389	0.388	**0.392**	0.0048	0.0023	0.0004	**0.0025**	0.022	0.020	0.020	0.051	0.033	0.025	**0.028**	6.54	6.39	**6.47**	0.381	0.380	0.374	0.373	**0.377**
Pr	n.a.	**n.a.**	0.142	0.148	0.150	**0.147**	n.a.	n.a.	n.a.	**n.a.**	n.a.	n.a.	n.a.	n.a.	n.a.	n.a.	**n.a.**	1.31	1.27	**1.29**	0.166	0.175	0.166	0.170	**0.169**
Nd	0.059	**0.040**	1.78	1.50	1.63	**1.64**	0.0026	0.0010	bdl	**0.0018**	0.028	0.031	0.037	0.041	0.033	0.037	**0.035**	6.19	5.87	**6.03**	1.66	1.74	1.82	1.75	**1.74**
Sm	0.018	**0.010**	0.835	0.803	0.950	**0.863**	bdl	bdl	bdl	**bdl**	0.016	0.007	0.011	0.011	0.011	0.011	**0.011**	1.14	0.836	**0.988**	1.09	1.10	1.09	1.06	**1.09**
Eu	0.0042	**0.0028**	0.321	0.309	0.338	**0.323**	0.0001	0.0001	0.0001	**0.0001**	0.0021	0.0026	0.0022	0.0019	0.0029	0.0022	**0.0023**	0.179	0.223	**0.201**	0.343	0.384	0.374	0.354	**0.364**
Gd	0.010	**0.0086**	0.980	0.950	1.020	**0.983**	bdl	bdl	bdl	**bdl**	0.0065	0.0056	0.0093	0.0107	0.0076	0.0084	**0.0080**	0.482	0.407	**0.445**	1.06	1.15	1.09	1.15	**1.11**
Tb	0.0014	**0.0014**	0.119	0.137	0.143	**0.133**	bdl	bdl	bdl	**bdl**	0.0010	0.0006	0.0011	n.a.	n.a.	n.a.	**0.0009**	0.027	0.057	**0.042**	0.136	0.147	0.169	0.156	**0.152**
Dy	0.0072	**0.0048**	0.653	0.673	0.800	**0.709**	0.0004	0.0009	bdl	**0.0007**	bdl	0.0031	0.0029	0.0033	0.0011	0.0023	**0.0026**	0.053	0.072	**0.063**	0.744	0.725	0.702	0.741	**0.728**
Ho	0.0005	**0.0005**	0.107	0.118	0.154	**0.126**	bdl	bdl	bdl	**bdl**	0.0007	0.0003	0.0007	n.a.	n.a.	n.a.	**0.0006**	0.0041	0.0046	**0.0044**	0.119	0.129	0.120	0.121	**0.123**
Er	0.0011	**0.0015**	0.338	0.305	0.383	**0.342**	bdl	0.0003	0.0002	**0.0002**	bdl	0.0007	bdl	0.0009	0.0008	0.0002	**0.0006**	bdl	0.0054	**0.0054**	0.296	0.288	0.297	0.271	**0.288**
Tm	0.0003	**0.0003**	0.055	0.060	0.059	**0.058**	n.a.	n.a.	n.a.	**n.a.**	bdl	bdl	0.0003	n.a.	n.a.	n.a.	**0.0003**	bdl	bdl	**bdl**	0.040	0.040	0.043	0.039	**0.040**
Yb	0.0023	**0.0016**	0.443	0.413	0.530	**0.462**	bdl	bdl	bdl	**bdl**	bdl	0.0017	0.0011	bdl	bdl	bdl	**0.0014**	0.0058	bdl	**0.0058**	0.242	0.305	0.290	0.268	**0.276**
Lu	bdl	**bdl**	0.081	0.090	0.094	**0.088**	bdl	bdl	bdl	**bdl**	bdl	0.0001	0.0002	bdl	bdl	bdl	**0.0001**	bdl	bdl	**bdl**	0.044	0.051	0.042	0.037	**0.043**
Hf	0.0081	**0.0086**	0.405	0.480	0.479	**0.455**	0.0012	0.0007	0.0009	**0.0009**	0.0021	0.0026	0.0027	0.0025	0.0031	0.0023	**0.0025**	0.087	0.103	**0.095**	0.611	0.655	0.646	0.645	**0.639**
Ta	0.0061	**0.012**	0.056	0.050	0.049	**0.052**	0.0024	0.0032	0.0030	**0.0029**	0.0067	0.0060	0.0060	0.0085	0.0081	0.0090	**0.0074**	bdl	0.0048	**0.0048**	0.018	0.026	0.022	0.028	**0.024**
W	0.0030	**0.0030**	n.a.	n.a.	n.a.	**n.a.**	n.a.	n.a.	n.a.	**n.a.**	0.0035	bdl	0.0005	n.a.	n.a.	n.a.	**0.0020**	n.a.	n.a.	**n.a.**	n.a.	n.a.	n.a.	n.a.	**n.a.**
Pb	n.a.	**0.108**	0.233	0.098	0.061	**0.131**	n.a.	n.a.	0.0491	**0.049**	n.a.	n.a.	n.a.	0.079	0.061	0.254	**0.131**	1.08	0.883	**0.981**	3.11	1.27	1.21	0.06	**1.41**
Th	n.a.	**0.0006**	0.012	0.012	0.013	**0.012**	0.0020	0.0017	0.0002	**0.0013**	n.a.	n.a.	n.a.	0.0005	0.0001	0.0009	**0.0005**	0.026	0.023	**0.025**	bdl	bdl	bdl	bdl	**bdl**
U	0.0007	**0.0004**	0.032	0.027	0.030	**0.030**	bdl	bdl	bdl	**bdl**	0.0004	0.0004	0.0003	0.0004	0.0005	0.0003	**0.0004**	bdl	0.010	**0.010**	0.037	0.032	0.025	0.033	**0.032**

Table 4.3 *(continued)*

	F-6 olivine							average	F-6 orthopyroxene						average	F-6 clinopyroxene							average	F-6 garnet
Element	F6-Ol-1	F6-Ol-2	F6-ol1	F6-ol2	F6-ol3	F6-ol4	F6-ol5	**ol F-6**	F6opx1	F6opx2	F6opx4	F6Opx1	F6Opx3	F6opx5	**opx F-6**	F6cpx3	F6cpx4	F6cpx5	F6cpx8	F6cpx9	F6cpx1(	F6cpx1:	**cpx F-6**	F6-Gt1
Li	n.a.	n.a.	1.63	1.19	1.38	1.47	1.40	**1.41**	0.910	0.730	0.800	0.670	bdl	0.830	**0.788**	bdl	bdl	bdl	bdl	bdl	0.417	bdl	**0.417**	0.440
B	1.98	1.82	n.a.	n.a.	n.a.	n.a.	n.a.	**1.90**	n.a.	n.a.	n.a.	1.09	1.07	n.a.	**1.08**	n.a.	2.07	1.87	1.78	1.96	1.90	1.32	**1.82**	2.34
Sc	2.22	2.10	2.21	2.18	2.22	2.20	2.18	**2.19**	3.07	2.93	2.98	n.a.	n.a.	n.a.	**2.99**	16.4	16.1	16.2	16.1	15.7	15.7	15.4	**16.0**	100
V	6.54	6.59	6.80	6.68	6.21	6.15	6.47	**6.46**	39.4	40.9	40.7	41.5	42.1	39.6	**40.9**	212	216	216	218	217	213	214	**215**	353
Co	n.a.	n.a.	149	152	151	153	152	**151**	63.9	64.3	63.2	68.1	67.8	62.2	**65.5**	25.3	25.5	25.7	24.8	25.1	24.9	25.3	**25.2**	44.3
Ni	n.a.	n.a.	3256	3288	3272	3281	3274	**3274**	956	943	937	n.a.	n.a.	927	**941**	438	444	450	437	442	434	437	**440**	77.8
Cu	n.a.	n.a.	n.a.	n.a.	n.a.	n.a.	n.a.	**n.a.**	n.a.	n.a.	n.a.	n.a.	n.a.	n.a.	**n.a.**	1.92	2.76	2.58	1.83	1.94	1.86	2.41	**2.19**	0.433
Zn	n.a.	n.a.	n.a.	n.a.	n.a.	n.a.	n.a.	**n.a.**	n.a.	n.a.	n.a.	n.a.	n.a.	n.a.	**n.a.**	11.3	10.7	11.3	10.3	11.9	11.3	11.4	**11.2**	11.4
Ga	0.146	0.132	n.a.	n.a.	n.a.	n.a.	n.a.	**0.139**	n.a.	n.a.	n.a.	1.53	1.49	n.a.	**1.51**	n.a.	n.a.	n.a.	n.a.	n.a.	n.a.	n.a.	**bdl**	bdl
Ge	0.662	0.668	n.a.	n.a.	n.a.	n.a.	n.a.	**0.665**	n.a.	n.a.	n.a.	1.45	1.45	n.a.	**1.45**	n.a.	n.a.	n.a.	n.a.	n.a.	n.a.	n.a.	**bdl**	bdl
Rb	bdl	bdl	0.0060	bdl	bdl	0.0051	bdl	**0.0056**	0.0111	0.030	0.0052	bdl	0.010	0.0331	**0.01395**	0.086	0.051	0.052	0.046	0.073	0.106	0.062	**0.068**	0.142
Sr	bdl	0.005	0.056	0.157	0.041	bdl	0.160	**0.084**	0.390	0.512	0.440	0.335	0.540	0.520	**0.443**	134	132	135	132	132	134	134	**133**	bdl
Y	0.0019	bdl	0.0081	0.0020	0.0025	0.0018	0.0046	**0.0035**	0.021	0.022	0.020	0.015	0.013	0.018	**0.021**	0.429	0.420	0.409	0.419	0.398	0.401	0.394	**0.410**	3.93
Zr	0.031	0.029	0.122	0.037	0.040	0.044	0.073	**0.054**	0.072	0.101	0.087	0.059	0.062	0.090	**0.087**	1.92	1.87	1.81	1.75	1.88	1.83	1.75	**1.83**	20.0
Nb	0.051	0.050	0.027	0.057	0.056	0.055	0.052	**0.050**	0.059	0.074	0.073	0.069	0.066	0.070	**0.068**	0.215	0.185	0.186	0.178	0.165	0.179	0.174	**0.183**	0.421
Mo	n.a.	n.a.	n.a.	n.a.	n.a.	n.a.	n.a.	**n.a.**	n.a.	n.a.	n.a.	n.a.	n.a.	n.a.	**n.a.**	n.a.	n.a.	n.a.	n.a.	n.a.	n.a.	n.a.	**n.a.**	n.a.
Cs	n.a.	n.a.	0.0013	bdl	bdl	bdl	bdl	**0.0013**	bdl	bdl	bdl	n.a.	n.a.	bdl	**bdl**	0.005	bdl	bdl	bdl	bdl	0.007	bdl	**0.006**	bdl
Ba	n.a.	n.a.	0.049	bdl	bdl	bdl	0.043	**0.046**	0.034	bdl	0.067	n.a.	n.a.	0.230	**0.050**	0.831	0.656	0.689	0.695	0.755	0.86	0.716	**0.743**	0.761
La	0.0003	0.0005	0.0004	0.0003	0.0003	0.0007	0.0048	**0.0010**	0.0074	0.016	0.009	0.006	0.010	0.011	**0.010**	2.09	2.05	2.07	2.03	2.01	2.04	2.01	**2.04**	0.044
Ce	0.0009	0.0011	0.0023	0.0011	0.0015	0.0022	0.0104	**0.0028**	0.036	0.054	0.041	0.027	0.033	0.046	**0.038**	7.28	7.05	7.25	7.17	7.03	7.21	7.13	**7.16**	0.357
Pr	n.a.	n.a.	n.a.	n.a.	n.a.	n.a.	n.a.	**n.a.**	n.a.	n.a.	n.a.	n.a.	n.a.	n.a.	**n.a.**	1.17	1.13	1.16	1.12	1.12	1.14	1.11	**1.14**	0.114
Nd	bdl	bdl	0.0021	0.0010	0.0013	0.0013	0.0063	**0.0024**	0.037	0.041	0.038	0.026	0.033	0.041	**0.035**	5.23	5.06	5.13	4.92	5.05	5.07	4.88	**5.05**	1.10
Sm	bdl	bdl	0.0012	bdl	0.0012	0.0009	0.0013	**0.0012**	0.010	0.012	0.011	0.008	0.012	0.013	**0.011**	0.780	0.710	0.740	0.690	0.760	0.740	0.740	**0.737**	0.700
Eu	bdl	bdl	bdl	bdl	bdl	bdl	bdl	**bdl**	0.0012	0.0035	0.0017	0.0019	0.0031	0.0019	**0.0023**	0.184	0.181	0.172	0.163	0.186	0.176	0.181	**0.178**	0.261
Gd	0.0003	0.0001	0.0009	0.0004	0.0005	bdl	0.0009	**0.0005**	0.0036	0.0076	0.0053	0.0069	0.0068	0.0101	**0.0060**	0.393	0.345	0.362	0.283	0.315	0.337	0.331	**0.338**	0.703
Tb	bdl	0.0001	n.a.	n.a.	n.a.	n.a.	n.a.	**0.0001**	n.a.	n.a.	n.a.	0.0010	0.0008	n.a.	**0.0009**	0.029	0.030	0.033	0.017	0.041	0.019	0.036	**0.029**	0.110
Dy	bdl	0.0003	0.0009	0.0015	bdl	bdl	0.0014	**0.0010**	0.0037	0.0053	0.0049	0.0027	0.0037	bdl	**0.0040**	0.135	0.129	0.12	0.095	0.13	0.081	0.181	**0.124**	0.736
Ho	bdl	bdl	n.a.	n.a.	n.a.	n.a.	n.a.	**bdl**	n.a.	n.a.	n.a.	0.0004	0.0009	n.a.	**0.0006**	0.020	0.022	0.018	0.012	0.016	0.019	0.022	**0.018**	0.164
Er	0.0006	0.0004	0.0015	0.0002	0.0001	bdl	0.0007	**0.0006**	0.0020	0.0026	0.0036	0.0021	0.0009	0.0041	**0.0022**	0.052	0.046	0.035	0.049	0.032	bdl	0.058	**0.045**	0.488
Tm	bdl	bdl	n.a.	n.a.	n.a.	n.a.	n.a.	**n.a.**	n.a.	n.a.	n.a.	0.0003	0.0007	n.a.	**0.0005**	bdl	bdl	bdl	bdl	bdl	bdl	0.0079	**0.0079**	0.077
Yb	bdl	0.0006	0.0009	0.0008	bdl	bdl	0.0004	**0.0007**	0.0012	0.0013	0.0021	0.0028	0.0029	0.0013	**0.0021**	0.040	bdl	bdl	0.041	bdl	bdl	0.039	**0.040**	0.562
Lu	0.0002	0.0002	0.0002	bdl	0.0002	0.0001	bdl	**0.0002**	0.0003	0.0006	0.0003	0.0002	0.0002	0.0008	**0.0003**	0.0075	bdl	bdl	bdl	bdl	bdl	0.0108	**0.0092**	0.111
Hf	0.0005	0.0006	0.0051	0.0013	0.0023	0.0017	0.0015	**0.0018**	0.0030	0.0038	0.0035	0.0022	0.0021	0.0025	**0.0029**	0.116	0.091	0.111	0.123	0.089	0.115	0.117	**0.109**	0.472
Ta	0.0051	0.0040	0.0045	0.0071	0.0054	0.0069	0.0069	**0.0057**	0.013	0.014	0.015	0.009	0.008	0.011	**0.012**	0.019	0.017	0.015	bdl	0.012	0.021	0.011	**0.016**	0.031
W	n.a.	n.a.	n.a.	n.a.	n.a.	n.a.	n.a.	**n.a.**	n.a.	n.a.	n.a.	0.0003	0.0013	n.a.	**0.0008**	n.a.	n.a.	n.a.	n.a.	n.a.	n.a.	n.a.	**n.a.**	n.a.
Pb	n.a.	n.a.	1.0500	0.0270	0.0228	0.0184	0.0222	**0.228**	0.044	0.521	0.023	n.a.	n.a.	0.073	**0.196**	1.70	0.311	0.357	0.347	0.328	0.327	0.438	**0.544**	0.127
Th	bdl	0.001	0.197	0.000	0.002	0.188	0.001	**0.065**	0.0008	0.0024	0.0023	n.a.	n.a.	0.130	**0.0018**	0.022	0.023	0.024	0.016	0.021	0.017	0.019	**0.020**	0.015
U	bdl	bdl	0.0159	0.0002	0.0001	bdl	bdl	**0.0054**	0.0001	0.0002	0.0001	0.0003	0.0005	0.0001	**0.0003**	0.0068	bdl	0.0051	0.0036	bdl	0.0044	0.0049	**0.0050**	0.024

Table 4.3 *(continued)*

	F-6 garnet				average	F-7 olivine								average	F-7 orthopyroxene						average	F-7 garnet		
Element	F6-Gt2	F6-Gt3	F6-Gt4	F6-Gt5	**grt F-6**	F7-Ol1	F7-Ol2	F7-ol1	F7-ol2	F7-ol3	F7-ol4	F7-ol5	F7-ol6	**ol F-7**	F7Opx1	F7Opx2	F7Opx3	F7opx2	F7opx4	F7opx5	**opx F-7**	F7-Gt1	F7-Gt2	**grt F-7**
Li	bdl	bdl	bdl	0.358	**0.399**	1.00	bdl	1.31	1.29	1.24	1.14	1.08	0.631	**1.10**	bdl	bdl	bdl	0.250	0.497	0.539	**0.429**	0.497	bdl	**0.497**
B	2.24	2.06	1.90	1.29	**1.97**	1.70	1.58	n.a.	n.a.	n.a.	n.a.	n.a.	n.a.	**1.64**	1.16	1.15	1.05	n.a.	n.a.	n.a.	**1.12**	2.17	1.72	**1.95**
Sc	102	105	105	103	**103**	0.318	0.357	1.92	1.98	1.99	1.98	1.91	1.91	**1.55**	n.a.	n.a.	n.a.	1.87	1.91	2.02	**1.93**	107	107	**107**
V	342	330	328	317	**334**	6.10	6.05	4.71	5.19	4.91	5.19	4.97	5.30	**5.30**	31.5	32.2	32.8	31.9	31.8	33.1	**32.2**	302	305	**303**
Co	44.4	42.6	42.3	40.8	**42.9**	157	149	140	142	139	141	140	136	**143**	59.2	60.1	59.7	59.5	59.7	59.1	**59.5**	40.3	40.1	**40.2**
Ni	73.4	69.7	68.5	64.6	**70.8**	n.a.	n.a.	3317	3349	3302	3323	3369	3452	**3352**	n.a.	n.a.	n.a.	950	954	937	**947**	59.1	59.1	**59.1**
Cu	bdl	bdl	0.220	bdl	**0.327**	n.a.	n.a.	n.a.	n.a.	n.a.	n.a.	n.a.	n.a.	**n.a.**	n.a.	n.a.	n.a.	n.a.	n.a.	n.a.	**n.a.**	bdl	bdl	**bdl**
Zn	10.4	10.3	10.0	10.1	**10.4**	n.a.	n.a.	n.a.	n.a.	n.a.	n.a.	n.a.	n.a.	**n.a.**	n.a.	n.a.	n.a.	n.a.	n.a.	n.a.	**n.a.**	8.83	8.75	**8.79**
Ga	n.a.	n.a.	n.a.	n.a.	**n.a.**	0.078	0.067	n.a.	n.a.	n.a.	n.a.	n.a.	n.a.	**0.072**	0.681	0.669	0.675	n.a.	n.a.	n.a.	**0.675**	n.a.	n.a.	**n.a.**
Ge	n.a.	n.a.	n.a.	n.a.	**n.a.**	0.490	0.487	n.a.	n.a.	n.a.	n.a.	n.a.	n.a.	**0.489**	1.12	1.11	1.07	n.a.	n.a.	n.a.	**1.10**	n.a.	n.a.	**n.a.**
Rb	0.036	0.040	0.041	0.031	**0.058**	bdl	bdl	0.0058	bdl	0.0048	bdl	bdl	0.0075	**0.0060**	0.0053	bdl	bdl	bdl	0.0071	0.0050	**0.0058**	0.054	0.048	**0.051**
Sr	0.277	0.288	0.423	0.317	**0.326**	bdl	0.006	bdl	bdl	0.330	bdl	bdl	0.352	**0.229**	0.386	0.267	0.336	0.326	0.377	0.465	**0.360**	0.381	0.330	**0.356**
Y	3.91	4.07	4.04	4.08	**4.01**	0.0022	0.0016	0.0029	0.0022	0.0021	0.0024	0.0016	0.0024	**0.0022**	0.017	0.009	0.018	0.010	0.013	0.026	**0.015**	2.63	2.68	**2.66**
Zr	19.5	20.3	20.4	19.9	**20.0**	0.238	0.285	0.336	0.331	0.342	0.336	0.331	0.275	**0.309**	0.202	0.205	0.228	0.264	0.260	0.320	**0.247**	23.2	23.6	**23.4**
Nb	0.390	0.420	0.438	0.402	**0.414**	0.085	0.093	0.089	0.082	0.097	0.093	0.091	0.073	**0.088**	0.050	0.063	0.051	0.065	0.068	0.058	**0.059**	0.332	0.347	**0.340**
Mo	n.a.	n.a.	n.a.	n.a.	**n.a.**	n.a.	n.a.	n.a.	n.a.	n.a.	n.a.	n.a.	n.a.	**n.a.**	n.a.	n.a.	n.a.	n.a.	n.a.	n.a.	**n.a.**	n.a.	n.a.	**n.a.**
Cs	bdl	bdl	bdl	bdl	**n.a.**	n.a.	n.a.	bdl	0.0010	bdl	bdl	0.0043	bdl	**0.0027**	n.a.	n.a.	n.a.	bdl	bdl	bdl	**bdl**	bdl	bdl	**bdl**
Ba	0.008	0.012	0.233	bdl	**0.254**	n.a.	n.a.	0.064	0.067	bdl	bdl	bdl	0.097	**0.076**	bdl	bdl	bdl	0.062	0.042	0.091	**0.065**	bdl	bdl	**bdl**
La	0.035	0.033	0.045	0.032	**0.038**	bdl	0.0008	0.0004	bdl	bdl	0.0005	0.0005	0.0025	**0.0009**	0.0048	0.0046	0.0054	0.0061	0.0056	0.0082	**0.0053**	0.012	0.017	**0.014**
Ce	0.366	0.387	0.392	0.378	**0.376**	0.0004	0.0029	0.0014	0.0004	0.0037	0.0009	0.0026	0.0064	**0.0023**	0.027	0.022	0.028	0.030	0.027	0.041	**0.029**	0.268	0.272	**0.270**
Pr	0.118	0.114	0.119	0.116	**0.116**	n.a.	n.a.	n.a.	n.a.	n.a.	n.a.	n.a.	n.a.	**n.a.**	n.a.	n.a.	n.a.	n.a.	n.a.	n.a.	**n.a.**	0.155	0.160	**0.157**
Nd	1.20	1.09	1.13	1.01	**1.10**	bdl	bdl	0.0002	bdl	bdl	0.0011	bdl	0.0031	**0.0015**	0.039	0.038	0.042	0.045	0.047	0.050	**0.043**	2.32	2.34	**2.33**
Sm	0.602	0.626	0.577	0.574	**0.616**	bdl	bdl	bdl	bdl	0.0008	bdl	0.0004	bdl	**0.0006**	0.016	0.013	0.016	0.011	0.015	0.019	**0.015**	1.81	1.82	**1.82**
Eu	0.241	0.237	0.239	0.229	**0.241**	0.0002	bdl	bdl	bdl	0.0001	bdl	bdl	bdl	**0.0001**	0.0042	0.0030	0.0055	0.0024	0.0045	0.0059	**0.0042**	0.595	0.647	**0.621**
Gd	0.711	0.699	0.672	0.641	**0.685**	bdl	0.0002	0.0008	0.0010	0.0007	bdl	0.0002	0.0005	**0.0006**	0.013	0.008	0.010	0.012	0.015	0.016	**0.012**	1.60	1.76	**1.68**
Tb	0.109	0.121	0.107	0.096	**0.109**	bdl	bdl	n.a.	n.a.	n.a.	n.a.	n.a.	n.a.	**n.a.**	0.0014	0.0009	0.0017	n.a.	n.a.	n.a.	**0.0013**	0.170	0.171	**0.171**
Dy	0.675	0.742	0.718	0.712	**0.717**	bdl	bdl	0.0003	0.0009	0.0014	0.0002	bdl	bdl	**0.0007**	0.0036	0.0030	0.0056	0.0038	0.0024	0.0049	**0.0039**	0.735	0.766	**0.751**
Ho	0.151	0.152	0.160	0.145	**0.154**	0.0001	0.0001	n.a.	n.a.	n.a.	n.a.	n.a.	n.a.	**0.0001**	0.0002	0.0002	0.0012	n.a.	n.a.	n.a.	**0.0005**	0.095	0.095	**0.095**
Er	0.460	0.486	0.505	0.460	**0.480**	bdl	bdl	0.0004	bdl	bdl	bdl	bdl	bdl	**0.0004**	0.0006	0.0010	0.0028	0.0012	0.0008	0.0034	**0.0016**	0.165	0.191	**0.178**
Tm	0.083	0.075	0.075	0.078	**0.078**	bdl	bdl	n.a.	n.a.	n.a.	n.a.	n.a.	n.a.	**n.a.**	bdl	bdl	bdl	n.a.	n.a.	n.a.	**bdl**	0.031	0.023	**0.027**
Yb	0.669	0.660	0.641	0.563	**0.619**	bdl	0.0012	0.0004	0.0004	0.0007	0.0003	0.0004	bdl	**0.0006**	0.0005	0.0006	bdl	0.0003	0.0003	0.0009	**0.0005**	0.175	0.172	**0.174**
Lu	0.108	0.113	0.108	0.110	**0.110**	bdl	bdl	0.0001	0.0001	bdl	0.0003	0.0001	bdl	**0.0001**	bdl	bdl	0.0004	0.0003	bdl	0.0001	**0.0003**	0.029	0.036	**0.033**
Hf	0.423	0.466	0.390	0.436	**0.437**	0.0075	0.010	0.012	0.009	0.013	0.014	0.011	0.011	**0.011**	0.0083	0.007	0.012	0.008	0.012	0.018	**0.011**	0.521	0.490	**0.506**
Ta	0.083	0.044	0.048	0.040	**0.049**	0.0075	0.0091	0.012	0.010	0.010	0.012	0.011	0.010	**0.010**	0.0092	0.013	0.010	0.018	0.019	0.018	**0.014**	0.032	0.049	**0.040**
W	n.a.	n.a.	n.a.	n.a.	**n.a.**	n.a.	n.a.	n.a.	n.a.	n.a.	n.a.	n.a.	n.a.	**n.a.**	bdl	bdl	bdl	n.a.	n.a.	n.a.	**bdl**	n.a.	n.a.	**n.a.**
Pb	0.054	0.093	bdl	0.105	**0.095**	n.a.	n.a.	0.023	0.026	0.029	0.022	0.025	0.075	**0.033**	n.a.	n.a.	n.a.	0.034	0.032	0.035	**0.034**	0.167	0.327	**0.247**
Th	0.009	0.010	0.010	0.012	**0.011**	bdl	bdl	0.0001	bdl	0.0004	0.0008	0.0059	bdl	**0.0018**	n.a.	n.a.	n.a.	0.0008	0.0019	0.0016	**0.0014**	bdl	0.010	**0.010**
U	0.023	0.025	0.024	0.021	**0.023**	bdl	0.0001	bdl	0.0001	0.0004	0.0001	0.0014	0.0001	**0.0004**	0.0004	0.0004	0.0005	0.0001	bdl	0.0002	**0.0003**	0.020	0.021	**0.021**

Table 4.3 *(continued)*

	F-8 olivine							F-8 orthopyroxene						F-8 clinopyroxene					F-8 garnet					
							average						**average**					**average**							
Element	F8-Ol-2	F8-Ol-3	F8-Ol-4	F8-ol1	F8-ol4	F8-ol6	**ol F-8**	F8opx1	F8opx2	F8opx-2	F8opx-3	F8opx-1	**opx F-8**	F8cpx1	F8cpx2	F8Cpx1	F8Cpx2	**cpx F-8**	F8-Gt1	F8-Gt3	F8-Gt4	F8grt1a	F8gt1b	F8gt2b
Li	bdl	bdl	bdl	1.42	1.16	1.19	**1.26**	0.601	0.644	bdl	bdl	0.720	**0.655**	0.390	bdl	0.141	0.220	**0.250**	0.283	bdl	bdl	0.480	bdl	bdl
B	1.14	1.20	1.16	n.a.	n.a.	n.a.	**1.17**	0.900	0.850	0.958	0.894	1.10	**0.940**	n.a.	n.a.	0.290	0.430	**0.360**	n.a.	n.a.	n.a.	0.500	0.557	0.462
Sc	n.a.	n.a.	n.a.	2.26	2.05	2.07	**2.13**	0.556	0.580	0.730	0.740	1.14	**0.749**	16.6	16.1	15.5	16.6	**16.2**	105	107	106	123	125	123
V	6.68	6.74	6.63	5.90	5.88	5.66	**6.25**	36.3	37.3	39.2	39.1	38.7	**38.1**	243	232	255	251	**245**	297	297	292	334	295	312
Co	145	143	142	137	139	140	**141**	72.5	74.1	58.9	59.0	61.5	**65.2**	22.4	22.5	22.2	22.3	**22.4**	39.2	37.6	37.7	48.0	41.2	40.8
Ni	n.a.	n.a.	n.a.	3018	3035	3026	**3026**	n.a.	n.a.	n.a.	n.a.	n.a.	**n.a.**	498	490	413	408	**453**	62.4	59.8	59.0	63.0	65.3	65.5
Cu	n.a.	n.a.	n.a.	n.a.	n.a.	n.a.	**n.a.**	n.a.	n.a.	n.a.	n.a.	n.a.	**n.a.**	1.51	1.35	1.73	1.72	**1.58**	0.160	bdl	bdl	0.690	0.145	0.179
Zn	n.a.	n.a.	n.a.	n.a.	n.a.	n.a.	**n.a.**	n.a.	n.a.	n.a.	n.a.	n.a.	**n.a.**	11.0	10.7	10.0	10.3	**10.5**	9.08	9.80	10.2	12.5	9.48	9.70
Ga	0.117	0.127	0.117	n.a.	n.a.	n.a.	**0.120**	1.53	1.56	1.71	1.73	1.76	**1.66**	n.a.	n.a.	n.a.	n.a.	**n.a.**	n.a.	n.a.	n.a.	7.09	6.99	7.22
Ge	0.616	0.588	0.582	n.a.	n.a.	n.a.	**0.595**	1.29	1.30	1.36	1.37	1.31	**1.33**	n.a.	n.a.	n.a.	n.a.	**n.a.**	n.a.	n.a.	n.a.	n.a.	n.a.	n.a.
Rb	bdl	bdl	bdl	0.0087	bdl	bdl	**0.0087**	0.0024	0.0012	bdl	bdl	bdl	**0.0018**	0.084	0.073	bdl	0.029	**0.062**	0.041	0.082	0.047	0.255	0.021	0.022
Sr	bdl	0.012	0.010	bdl	0.074	bdl	**0.032**	0.401	0.459	0.429	0.430	0.415	**0.427**	159	158	167	166	**162**	0.471	0.541	0.400	0.551	0.480	0.495
Y	0.0019	0.0131	0.0045	0.012	0.0038	0.0029	**0.0064**	0.028	0.030	0.035	0.033	0.031	**0.031**	1.05	0.99	1.37	1.35	**1.19**	10.4	10.5	10.1	12.3	15.3	15.3
Zr	0.072	0.273	0.118	0.272	0.108	0.096	**0.157**	0.110	0.117	0.134	0.121	0.104	**0.117**	4.57	3.93	3.43	3.95	**3.97**	21.9	21.0	20.4	23.9	29.2	28.7
Nb	0.018	0.022	0.021	0.023	0.016	0.013	**0.019**	0.024	0.027	0.020	0.022	0.024	**0.023**	0.062	0.056	0.112	0.105	**0.083**	0.117	0.160	0.149	0.126	0.153	0.185
Mo	n.a.	n.a.	n.a.	n.a.	n.a.	n.a.	**n.a.**	n.a.	n.a.	n.a.	n.a.	n.a.	**n.a.**	n.a.	n.a.	n.a.	n.a.	**n.a.**	n.a.	n.a.	n.a.	n.a.	0.353	0.405
Cs	n.a.	n.a.	n.a.	bdl	0.0018	bdl	**0.0018**	n.a.	n.a.	n.a.	n.a.	n.a.	**n.a.**	bdl	bdl	bdl	bdl	**bdl**	bdl	0.0053	bdl	0.0167	bdl	bdl
Ba	n.a.	n.a.	n.a.	0.095	bdl	0.085	**0.090**	n.a.	n.a.	n.a.	n.a.	n.a.	**n.a.**	2.23	0.82	0.91	1.17	**1.28**	0.169	0.040	bdl	0.091	bdl	bdl
La	bdl	0.0001	bdl	bdl	0.0004	0.0001	**0.0002**	0.0059	0.0087	0.0067	0.0084	0.0094	**0.0078**	2.14	2.19	3.87	3.27	**2.87**	0.046	0.049	0.035	0.074	0.050	0.062
Ce	0.0005	0.0008	0.0008	0.0002	0.0017	bdl	**0.0008**	0.030	0.040	0.031	0.032	0.031	**0.033**	8.46	8.91	8.56	8.87	**8.70**	0.475	0.581	0.523	0.587	0.691	0.777
Pr	n.a.	n.a.	n.a.	n.a.	n.a.	n.a.	**n.a.**	n.a.	n.a.	n.a.	n.a.	n.a.	**n.a.**	1.35	1.37	n.a.	n.a.	**1.36**	0.151	0.165	0.163	0.174	n.a.	n.a.
Nd	bdl	0.0016	0.0013	bdl	0.0004	bdl	**0.0011**	0.027	0.036	0.035	0.037	0.037	**0.034**	6.58	6.25	7.80	7.41	**7.01**	1.45	1.51	1.41	1.61	1.79	1.88
Sm	bdl	bdl	0.0015	bdl	0.0009	0.0018	**0.0014**	0.010	0.009	0.012	0.013	bdl	**0.011**	1.18	1.10	1.21	1.22	**1.18**	0.953	0.935	0.868	1.01	1.10	1.15
Eu	0.0003	0.0002	0.0003	bdl	0.0004	bdl	**0.0003**	0.0024	0.0021	0.0034	0.0032	0.0030	**0.0028**	0.325	0.268	0.328	0.306	**0.307**	0.395	0.400	0.370	0.389	0.457	0.479
Gd	0.0003	0.0013	0.0014	0.0015	0.0002	0.0003	**0.0008**	0.0084	0.0071	0.0074	0.0095	0.0065	**0.0078**	0.712	0.609	0.864	0.798	**0.746**	1.36	1.27	1.26	1.51	1.75	1.80
Tb	0.0001	0.0006	bdl	bdl	bdl	bdl	**0.0003**	0.0012	0.0013	0.0016	0.0011	0.0015	**0.0013**	0.071	0.068	0.071	0.069	**0.070**	0.250	0.248	0.203	0.278	0.289	0.293
Dy	0.0002	0.0010	0.0012	bdl	bdl	0.0016	**0.0010**	0.0063	0.0087	0.0051	0.0072	0.0033	**0.0061**	0.260	0.322	0.349	0.343	**0.319**	1.78	1.75	1.73	2.13	2.28	2.28
Ho	0.0001	0.0003	bdl	n.a.	n.a.	n.a.	**0.0002**	0.0013	0.0012	0.0020	0.0014	0.0008	**0.0013**	0.047	0.045	0.052	0.053	**0.049**	0.407	0.392	0.378	0.495	0.538	0.529
Er	bdl	0.0029	0.0006	0.0026	0.0008	bdl	**0.0017**	0.0031	0.0028	0.0046	0.0064	0.0028	**0.0039**	0.088	0.082	0.102	0.109	**0.095**	1.22	1.18	1.13	1.39	1.66	1.57
Tm	bdl	0.0003	0.0003	n.a.	n.a.	n.a.	**0.0003**	0.0005	0.0007	0.0006	0.0005	bdl	**0.0006**	0.009	0.012	0.011	0.010	**0.011**	0.206	0.175	0.169	0.249	0.218	0.202
Yb	bdl	0.0027	0.0021	0.0018	0.0005	0.0005	**0.0015**	0.0024	0.0035	0.0050	0.0035	bdl	**0.0036**	0.055	0.038	0.058	0.051	**0.050**	1.53	1.42	1.42	1.76	1.80	1.63
Lu	bdl	0.0004	bdl	0.0003	0.0001	0.0001	**0.0002**	0.0006	0.0004	0.0005	0.0006	bdl	**0.0005**	0.0049	0.0040	0.0065	0.0068	**0.0056**	0.238	0.208	0.202	0.269	0.302	0.276
Hf	0.0030	0.0074	0.0036	0.0080	0.0030	0.0044	**0.0049**	0.0037	0.0039	0.0065	0.0057	0.0059	**0.0051**	0.244	0.208	0.232	0.232	**0.229**	0.602	0.522	0.512	0.672	0.790	0.765
Ta	0.0021	0.0016	0.0017	0.0033	0.0013	0.0007	**0.0018**	0.0020	0.0016	0.0033	0.0025	0.0052	**0.0029**	bdl	0.0024	bdl	0.0079	**0.0052**	0.015	0.017	bdl	0.018	0.011	0.010
W	n.a.	n.a.	n.a.	n.a.	n.a.	n.a.	**n.a.**	bdl	bdl	bdl	bdl	0.061	**0.061**	n.a.	n.a.	0.028	0.003	**0.016**	n.a.	n.a.	n.a.	n.a.	0.147	0.029
Pb	n.a.	n.a.	n.a.	0.019	bdl	0.016	**0.017**	n.a.	n.a.	n.a.	n.a.	n.a.	**n.a.**	0.576	0.543	0.615	0.565	**0.575**	0.340	2.410	2.830	0.026	0.007	0.007
Th	0.0006	bdl	bdl	0.048	bdl	bdl	**0.024**	n.a.	n.a.	n.a.	n.a.	n.a.	**n.a.**	0.020	0.021	0.047	0.028	**0.029**	0.020	0.019	0.016	0.035	0.026	0.032
U	0.0001	0.0001	bdl	0.0014	0.0002	bdl	**0.0004**	0.0005	0.0005	0.0004	0.0003	0.0020	**0.0007**	0.0052	0.0045	0.005	0.0057	**0.0051**	0.034	0.035	0.033	0.035	0.055	0.057

Table 4.3 *(continued)*

	F-8		F-9					F-9				**F-9**	F-9											
	garnet	**average**	olivine				**average**	orthopyroxene			**average**	**cpx**	garnet							**average**				
Element	F8gt3b	**grt F-8**	F9-Ol-1	F9-ol1	F9-ol2	F9-ol4	**ol F-9**	F9Opx2	F9opx3	F9opx5	**opx F-9**	**cpx F-9**	F9-Gt1	F9-Gt2	F9-Gt3	F9-Gt4	F9-Gt5	F9-Gt6	F9-Gt7	**grt F-9**	F10-ol1	F10-ol2	F10-ol4	F10-ol3
Li	bdl	**0.382**	bdl	bdl	1.90	1.54	**1.72**	n.a.	0.710	0.700	**0.705**	**0.256**	bdl	bdl	bdl	bdl	bdl	bdl	bdl	**bdl**	2.15	2.00	2.10	2.76
B	0.493	**0.503**	1.19	n.a.	n.a.	n.a.	**1.19**	0.985	n.a.	n.a.	**0.985**	**0.440**	1.51	1.72	1.57	1.47	1.73	1.89	1.79	**1.67**	n.a.	n.a.	n.a.	0.750
Sc	123	**116**	n.a.	5.02	2.35	2.16	**3.18**	n.a.	2.81	2.73	**2.77**	**14.9**	88.2	86.4	87.8	87.3	87.0	90.0	90.2	**88.1**	2.11	2.05	2.02	2.23
V	305	**304**	6.50	4.86	5.25	5.76	**5.59**	37.1	36.3	38.1	**37.1**	**299**	250	254	238	247	250	245	257	**249**	4.66	4.88	4.18	5.75
Co	41.3	**40.8**	143	143	138	137	**141**	58.7	61.1	60.0	**59.9**	**21.5**	25.9	26.0	24.1	24.8	25.0	25.5	26.7	**25.4**	144	147	149	168
Ni	65.8	**63.0**	n.a.	2876	2962	2944	**2927**	n.a.	874	857	**866**	**444**	35.2	43.2	33.4	38.3	37.2	38.0	39.3	**37.8**	3329	3368	3401	n.a.
Cu	0.165	**0.268**	n.a.	n.a.	n.a.	n.a.	**n.a.**	n.a.	n.a.	n.a.	**n.a.**	**4.19**	bdl	bdl	0.445	0.820	bdl	bdl	bdl	**0.633**	n.a.	n.a.	n.a.	4.17
Zn	10.2	**10.1**	n.a.	n.a.	n.a.	n.a.	**n.a.**	n.a.	n.a.	n.a.	**n.a.**	**16.1**	6.78	8.24	6.50	6.37	6.59	6.72	6.94	**6.88**	n.a.	n.a.	n.a.	81.3
Ga	7.19	**7.12**	0.12	n.a.	n.a.	n.a.	**0.12**	1.90	n.a.	n.a.	**1.90**	**n.a.**	n.a.	n.a.	n.a.	n.a.	n.a.	n.a.	n.a.	**n.a.**	n.a.	n.a.	n.a.	n.a.
Ge	n.a.	**n.a.**	0.53	n.a.	n.a.	n.a.	**0.53**	1.27	n.a.	n.a.	**1.27**	**n.a.**	n.a.	n.a.	n.a.	n.a.	n.a.	n.a.	n.a.	**n.a.**	n.a.	n.a.	n.a.	n.a.
Rb	0.020	**0.070**	bdl	bdl	bdl	0.0049	**0.0049**	0.015	0.026	0.024	**0.022**	**bdl**	0.075	0.067	0.059	0.059	0.076	0.060	0.093	**0.070**	0.0047	bdl	bdl	bdl
Sr	0.486	**0.489**	0.010	bdl	bdl	0.052	**0.031**	0.419	0.534	0.612	**0.522**	**149**	0.446	0.451	0.470	0.459	0.508	0.428	0.653	**0.488**	0.039	0.068	0.069	0.009
Y	14.9	**12.7**	0.0041	0.0060	0.0116	0.0137	**0.0088**	0.020	0.033	0.027	**0.027**	**1.14**	7.15	7.17	7.23	6.85	7.08	6.69	6.46	**6.95**	0.0018	0.0112	0.0033	0.0076
Zr	28.8	**24.8**	0.066	0.121	0.251	0.221	**0.165**	0.104	0.173	0.210	**0.162**	**8.42**	42.3	41.5	43.8	43.4	43.5	41.7	42.0	**42.6**	0.135	0.227	0.151	0.190
Nb	0.168	**0.151**	0.035	0.018	0.030	0.027	**0.027**	0.092	0.104	0.101	**0.099**	**0.474**	0.608	0.644	0.626	0.615	0.709	0.600	0.619	**0.632**	0.046	0.030	0.045	0.028
Mo	0.269	**0.342**	n.a.	n.a.	n.a.	n.a.	**n.a.**	n.a.	n.a.	n.a.	**n.a.**	**n.a.**	n.a.	n.a.	n.a.	n.a.	n.a.	n.a.	n.a.	**n.a.**	n.a.	n.a.	n.a.	n.a.
Cs	bdl	**0.0110**	n.a.	bdl	0.0034	0.0013	**0.0023**	n.a.	bdl	bdl	**bdl**	**bdl**	bdl	bdl	bdl	bdl	bdl	bdl	0.006	**0.006**	bdl	bdl	bdl	bdl
Ba	bdl	**0.1001**	n.a.	bdl	bdl	bdl	**bdl**	n.a.	0.458	1.10	**0.779**	**1.77**	bdl	bdl	bdl	bdl	0.0132	bdl	0.104	**0.058**	bdl	bdl	bdl	bdl
La	0.055	**0.053**	0.0003	bdl	bdl	0.0006	**0.0005**	0.007	0.015	0.033	**0.019**	**4.02**	0.078	0.079	0.078	0.067	0.081	0.089	0.083	**0.079**	0.0031	bdl	bdl	0.0007
Ce	0.720	**0.622**	0.0009	bdl	0.0002	0.0008	**0.0006**	0.034	0.108	0.116	**0.086**	**15.5**	0.760	0.794	0.819	0.791	0.799	0.768	0.806	**0.791**	0.0092	0.0001	0.0005	bdl
Pr	n.a.	**0.163**	n.a.	n.a.	n.a.	n.a.	**n.a.**	n.a.	n.a.	n.a.	**n.a.**	**n.a.**	0.252	0.260	0.265	0.266	0.285	0.243	0.251	**0.260**	n.a.	n.a.	n.a.	0.0005
Nd	1.83	**1.64**	0.0018	bdl	0.0022	bdl	**0.0020**	0.037	0.054	0.056	**0.049**	**9.08**	2.32	2.30	2.39	2.34	2.30	2.21	2.23	**2.30**	0.0047	0.0008	bdl	0.0069
Sm	1.10	**1.02**	bdl	0.0011	0.0004	0.0010	**0.0008**	0.014	0.015	0.013	**0.014**	**1.59**	1.31	1.21	1.21	1.44	1.28	1.21	1.22	**1.27**	0.0005	bdl	bdl	0.0044
Eu	0.470	**0.423**	bdl	bdl	bdl	bdl	**bdl**	0.0026	0.0032	0.0040	**0.0033**	**0.330**	0.418	0.455	0.432	0.416	0.497	0.401	0.425	**0.435**	bdl	0.0007	bdl	0.0012
Gd	1.73	**1.53**	0.0012	0.0029	0.0039	0.0018	**0.0025**	0.0084	0.011	0.010	**0.010**	**0.903**	1.40	1.57	1.53	1.41	1.61	1.51	1.42	**1.49**	n.a.	n.a.	n.a.	bdl
Tb	0.281	**0.263**	0.0001	n.a.	n.a.	n.a.	**0.0001**	0.0013	n.a.	n.a.	**0.0013**	**0.074**	0.237	0.251	0.252	0.233	0.258	0.235	0.224	**0.241**	n.a.	n.a.	n.a.	0.0006
Dy	2.20	**2.02**	0.0010	0.0077	0.0018	0.0028	**0.0033**	0.0055	0.0078	0.0059	**0.0064**	**0.335**	1.51	1.61	1.61	1.54	1.68	1.49	1.48	**1.56**	bdl	bdl	0.0020	0.0004
Ho	0.527	**0.467**	0.0002	n.a.	n.a.	n.a.	**0.0002**	0.0008	n.a.	n.a.	**0.0008**	**0.050**	0.274	0.283	0.270	0.265	0.300	0.272	0.250	**0.273**	n.a.	n.a.	n.a.	0.0001
Er	1.62	**1.39**	bdl	0.0026	bdl	0.0010	**0.0018**	0.0015	0.0051	0.0038	**0.0035**	**0.084**	0.680	0.680	0.667	0.631	0.674	0.599	0.594	**0.646**	bdl	0.0017	0.0008	0.0012
Tm	0.207	**0.204**	bdl	n.a.	n.a.	n.a.	**n.a.**	bdl	n.a.	n.a.	**bdl**	**0.0082**	0.084	0.080	0.081	0.081	0.094	0.081	0.087	**0.084**	n.a.	n.a.	n.a.	bdl
Yb	1.67	**1.60**	0.0008	bdl	0.0016	0.0013	**0.0012**	0.0012	0.0024	0.0016	**0.0017**	**0.043**	0.522	0.591	0.541	0.524	0.585	0.471	0.477	**0.530**	0.0002	0.0016	0.0001	bdl
Lu	0.274	**0.253**	0.0001	0.0003	0.0005	0.0004	**0.0003**	bdl	bdl	bdl	**bdl**	**0.0053**	0.085	0.079	0.072	0.084	0.081	0.067	0.069	**0.077**	0.0001	bdl	0.0001	0.0001
Hf	0.752	**0.659**	0.0024	0.0024	0.0070	0.0065	**0.0046**	0.008	0.012	0.010	**0.010**	**0.620**	1.08	1.00	1.07	1.05	1.09	1.12	1.01	**1.06**	0.0048	0.0092	0.0057	0.0081
Ta	0.010	**0.014**	0.0011	bdl	0.0014	0.0010	**0.0012**	0.0046	0.0097	0.0085	**0.0076**	**0.019**	0.022	bdl	0.023	0.025	0.040	0.026	bdl	**0.027**	0.0047	0.0027	0.0051	0.0023
W	bdl	**0.088**	n.a.	n.a.	n.a.	n.a.	**n.a.**	bdl	n.a.	n.a.	**bdl**	**0.220**	n.a.	n.a.	n.a.	n.a.	n.a.	n.a.	n.a.	**n.a.**	n.a.	n.a.	n.a.	n.a.
Pb	0.007	**0.804**	n.a.	0.0116	0.0184	0.0314	**0.020**	n.a.	0.083	0.070	**0.077**	**0.727**	0.017	0.055	0.046	0.085	0.235	0.015	0.015	**0.067**	0.824	3.13	0.127	0.956
Th	0.027	**0.025**	0.0010	0.0352	0.0001	bdl	**0.0121**	n.a.	0.117	0.004	**0.061**	**0.023**	0.014	bdl	0.020	0.018	0.022	bdl	0.024	**0.019**	0.117	0.074	bdl	0.00
U	0.049	**0.042**	bdl	bdl	bdl	bdl	**bdl**	0.0005	0.0009	0.0014	**0.0009**	**0.0092**	0.040	0.043	0.048	0.046	0.056	0.048	0.041	**0.046**	0.0001	bdl	0.0001	0.0007

Table 4.3 *(continued)*

	F-10 olivine			average	F-10 orthopyroxene					average	F-10 cpx		average	F-10 garnet		average	F-11 olivine					average	F-11 orthopyroxene	
Elemen	F10-ol5	F10-ol6	F10-ol7	**ol F-10**	F10opx1	F10opx3	F10opx5	F10Opx2	F10Opx3	**opx F-10**	F10cpx2	F10cpx4	**cpxF10**	F10gt1	F10gt2	**grt F10**	F11-ol1	F11-ol2	F11-ol3	F11-ol4	F11-ol5	**ol F-11**	F11opx3	F11opx2
Li	2.60	2.80	2.59	**2.43**	1.59	1.36	1.37	1.19	1.21	**1.34**	0.83	1.87	**1.35**	0.164	bdl	**0.164**	1.71	1.72	1.81	1.58	1.57	**1.68**	1.07	0.95
B	0.740	0.690	0.610	**0.698**	0.430	0.353	0.344	n.a.	n.a.	**0.376**	7.86	7.13	**7.50**	2.60	2.49	**2.55**	n.a.	n.a.	n.a.	n.a.	n.a.	**n.a.**	n.a.	n.a.
Sc	2.18	2.08	2.11	**2.11**	3.31	3.00	2.86	2.18	2.25	**2.72**	20.9	18.5	**19.7**	83.2	88.3	**85.7**	1.24	1.28	1.28	1.21	1.24	**1.25**	2.57	2.57
V	5.73	5.83	5.71	**5.25**	36.5	35.3	34.6	31.8	31.7	**34.0**	310	330	**320**	202	187	**195**	5.36	5.79	5.37	4.94	5.41	**5.37**	39.7	40.6
Co	160	170	158	**156**	64.8	63.6	63.2	60.1	59.7	**62.3**	25.9	25.7	**25.8**	43.8	43.0	**43.4**	143	148	151	150	150	**148**	66.7	66.3
Ni	n.a.	n.a.	n.a.	**3366**	940	928	937	935	932	**934**	n.a.	n.a.	**n.a.**	63.2	61.5	**62.4**	2883	2951	3123	3113	3012	**3016**	984	983
Cu	3.93	4.34	3.82	**4.07**	3.13	2.68	2.57	n.a.	n.a.	**2.79**	1.21	4.69	**2.95**	bdl	bdl	**bdl**	n.a.	n.a.	n.a.	n.a.	n.a.	**n.a.**	n.a.	n.a.
Zn	75.9	86.1	74.0	**79.3**	38.7	41.1	41.2	n.a.	n.a.	**40.3**	10.2	12.2	**11.2**	10.8	11.0	**10.9**	n.a.	n.a.	n.a.	n.a.	n.a.	**n.a.**	n.a.	n.a.
Ga	n.a.	n.a.	n.a.	**n.a.**	n.a.	n.a.	n.a.	n.a.	n.a.	**n.a.**	n.a.	n.a.	**n.a.**	n.a.	n.a.	**n.a.**	n.a.	n.a.	n.a.	n.a.	n.a.	**n.a.**	n.a.	n.a.
Ge	n.a.	n.a.	n.a.	**n.a.**	n.a.	n.a.	n.a.	n.a.	n.a.	**n.a.**	n.a.	n.a.	**n.a.**	n.a.	n.a.	**n.a.**	n.a.	n.a.	n.a.	n.a.	n.a.	**n.a.**	n.a.	n.a.
Rb	bdl	bdl	bdl	**0.0047**	0.073	0.013	0.069	0.087	bdl	**0.060**	0.254	0.136	**0.195**	0.043	0.307	**0.175**	bdl	bdl	bdl	bdl	bdl	**bdl**	bdl	bdl
Sr	0.009	0.010	0.005	**0.030**	0.317	0.293	0.365	0.576	0.361	**0.382**	143	145	**144**	0.221	2.62	**1.42**	0.044	0.0072	0.0077	0.0062	bdl	**0.016**	0.780	0.420
Y	0.0081	bdl	bdl	**0.0064**	0.024	0.023	0.027	0.016	0.015	**0.021**	1.42	0.91	**1.16**	6.35	6.65	**6.50**	0.0015	0.0008	0.0018	0.0010	0.0016	**0.0013**	0.015	0.014
Zr	0.158	0.112	0.094	**0.152**	0.195	0.197	0.227	0.233	0.239	**0.218**	16.8	12.9	**14.8**	46.4	49.2	**47.8**	0.049	0.052	0.048	0.040	0.045	**0.047**	0.170	0.111
Nb	0.029	0.033	0.030	**0.034**	0.020	0.018	0.025	0.022	0.024	**0.022**	0.591	0.232	**0.412**	0.143	0.160	**0.151**	0.049	0.049	0.049	0.047	0.051	**0.049**	0.065	0.058
Mo	n.a.	n.a.	n.a.	**n.a.**	n.a.	n.a.	n.a.	n.a.	n.a.	**n.a.**	n.a.	n.a.	**n.a.**	n.a.	n.a.	**n.a.**	n.a.	n.a.	n.a.	n.a.	n.a.	**n.a.**	n.a.	n.a.
Cs	bdl	bdl	bdl	**bdl**	0.0062	bdl	bdl	0.0062	bdl	**0.0062**	bdl	bdl	**bdl**	bdl	0.006	**0.006**	bdl	bdl	bdl	bdl	bdl	**bdl**	bdl	bdl
Ba	bdl	0.0087	bdl	**0.0087**	0.034	0.019	0.039	0.058	0.031	**0.036**	3.20	2.93	**3.07**	0.246	1.85	**1.05**	0.440	0.050	0.043	0.020	0.028	**0.116**	1.56	0.022
La	0.0003	0.0010	0.0003	**0.0011**	0.0031	0.0056	0.0051	0.0049	0.0052	**0.0048**	2.94	1.66	**2.30**	bdl	0.054	**0.054**	0.0002	0.0002	bdl	0.0002	0.0002	**0.0002**	0.035	0.0068
Ce	0.0009	0.0004	0.0011	**0.0020**	0.020	0.020	0.026	0.027	0.022	**0.023**	9.06	6.72	**7.89**	0.157	0.211	**0.184**	0.0023	0.0003	0.0001	0.0008	0.0003	**0.0008**	0.076	0.025
Pr	0.0001	0.0012	bdl	**0.0006**	0.0054	0.0049	0.0056	n.a.	n.a.	**0.0053**	1.43	1.27	**1.35**	0.067	0.072	**0.069**	n.a.	n.a.	n.a.	n.a.	n.a.	**n.a.**	n.a.	n.a.
Nd	0.0055	0.0079	bdl	**0.0051**	0.027	0.024	0.032	0.032	0.032	**0.029**	7.46	6.60	**7.03**	0.812	0.720	**0.766**	0.0014	bdl	bdl	0.0014	bdl	**0.0014**	0.047	0.029
Sm	bdl	bdl	0.0022	**0.0024**	0.014	0.0062	0.015	0.010	0.010	**0.011**	1.76	1.71	**1.74**	0.716	0.724	**0.720**	0.0004	0.0002	0.0002	bdl	0.0012	**0.0005**	0.0058	0.0113
Eu	0.0006	bdl	bdl	**0.0008**	0.0026	0.0037	0.0030	0.0033	0.0037	**0.0033**	0.481	0.404	**0.443**	0.304	0.280	**0.292**	0.0001	0.0004	bdl	bdl	bdl	**0.0003**	0.0038	0.0052
Gd	0.0039	0.0053	bdl	**0.0046**	0.011	0.014	0.0060	0.0089	0.0083	**0.010**	1.17	1.03	**1.10**	1.16	1.26	**1.21**	bdl	bdl	0.0002	bdl	bdl	**0.0002**	0.0087	0.0045
Tb	0.0013	0.0007	0.0002	**0.0007**	0.0020	0.0016	0.0027	n.a.	n.a.	**0.0021**	0.104	0.105	**0.105**	0.189	0.222	**0.206**	n.a.	n.a.	n.a.	n.a.	n.a.	**n.a.**	n.a.	n.a.
Dy	bdl	0.0037	bdl	**0.0021**	0.0077	0.0085	0.0049	0.0043	0.0027	**0.0056**	0.421	0.308	**0.365**	1.26	1.31	**1.28**	0.0001	0.0001	bdl	bdl	0.0006	**0.0003**	0.0051	0.0055
Ho	0.0002	0.0003	bdl	**0.0002**	0.0010	0.0015	0.0014	n.a.	n.a.	**0.0013**	0.072	0.054	**0.063**	0.251	0.255	**0.253**	n.a.	n.a.	n.a.	n.a.	n.a.	**n.a.**	n.a.	n.a.
Er	bdl	bdl	0.0004	**0.0010**	0.0017	0.0018	0.0010	0.0022	0.0012	**0.0016**	0.095	0.042	**0.069**	0.613	0.713	**0.663**	0.0003	bdl	0.0003	bdl	0.0003	**0.0003**	0.0008	0.0026
Tm	0.0002	bdl	bdl	**0.0002**	bdl	bdl	bdl	n.a.	n.a.	**bdl**	n.a.	0.0073	**0.0073**	0.093	0.090	**0.092**	n.a.	n.a.	n.a.	n.a.	n.a.	**n.a.**	n.a.	n.a.
Yb	bdl	bdl	bdl	**0.0007**	bdl	bdl	0.0022	0.0018	0.0016	**0.0019**	0.048	0.032	**0.040**	0.712	0.723	**0.718**	bdl	0.0004	0.0002	0.0002	0.0001	**0.0002**	0.0021	bdl
Lu	0.0012	bdl	bdl	**0.0004**	bdl	bdl	0.0003	0.0005	bdl	**0.0004**	0.0071	0.0063	**0.0067**	0.116	0.116	**0.116**	0.0001	0.0002	0.0001	0.0001	bdl	**0.0001**	0.0004	0.0004
Hf	0.0097	0.0060	bdl	**0.0072**	0.013	0.015	0.012	0.009	0.011	**0.012**	0.766	0.885	**0.826**	0.973	1.12	**1.05**	0.0017	0.0022	0.0009	0.0010	0.0011	**0.0014**	0.0073	0.0050
Ta	0.0013	0.0028	0.0023	**0.0030**	0.0045	0.0023	0.0030	0.0020	0.0017	**0.0027**	0.041	0.014	**0.027**	0.012	0.019	**0.015**	0.0029	0.0027	0.0034	0.0029	0.0026	**0.0029**	0.0092	0.0051
W	n.a.	n.a.	n.a.	**n.a.**	n.a.	n.a.	n.a.	n.a.	n.a.	**n.a.**	n.a.	n.a.	**n.a.**	n.a.	n.a.	**n.a.**	n.a.	n.a.	n.a.	n.a.	n.a.	**n.a.**	n.a.	n.a.
Pb	2.51	2.90	0.26	**1.26**	0.253	0.150	0.217	0.888	0.460	**0.394**	0.807	0.858	**0.833**	0.236	0.117	**0.177**	0.036	0.052	0.380	0.028	0.125	**0.124**	0.072	0.0171
Th	bdl	0.0003	bdl	**0.048**	0.0008	0.0118	0.0010	0.0005	0.0005	**0.0029**	0.204	0.071	**0.138**	bdl	0.009	**0.009**	0.0001	0.0001	0.0012	0.030	0.120	**0.030**	0.0040	0.0009
U	0.0007	0.0002	bdl	**0.0004**	0.0009	0.0016	bdl	0.0003	0.0002	**0.0007**	0.080	0.025	**0.052**	0.011	0.013	**0.012**	bdl	bdl	bdl	bdl	bdl	**bdl**	0.0020	0.0010

Table 4.3 *(continued)*

	F-11		F-11			F-11								F-12					F-12					F-12
	opx	**average**	clinopyroxene		**average**	garnet							**average**	olivine				**average**	orthopyroxene				**average**	cpx.
Element	F11opx4	**opxF-11**	F11cpx1	F11cpx2	**F11cpx**	F11-Gt1	F11-Gt2	F11-Gt3	F11-Gt4	F11-Gt6	F11-Gt7	F11-Gt8	**F11-grt**	F12-ol1	F12-ol2	F12-ol4	F12-ol5	**ol F-12**	F12-opx	F12-opx	F12-opx	F12-opx	**opx F-12**	F12-Cpx1
Li	0.970	**0.950**	0.960	0.950	**0.955**	0.462	bdl	bdl	bdl	bdl	bdl	bdl	**0.462**	1.44	1.19	1.39	1.19	**1.3**	0.716	0.662	0.713	0.604	**0.674**	0.680
B	n.a.	**n.a.**	4.60	5.28	**4.94**	1.69	1.55	1.38	1.43	1.18	1.17	1.07	**1.35**	n.a.	n.a.	n.a.	n.a.	**n.a.**	n.a.	n.a.	n.a.	n.a.	**n.a.**	13.6
Sc	2.51	**2.57**	16.9	16.6	**16.7**	130	134	129	132	117	117	114	**125**	2.09	2.11	2.36	2.42	**2.25**	2.55	2.58	2.60	2.28	**2.50**	20.6
V	40.1	**40.6**	316	322	**319**	295	301	289	280	293	293	283	**291**	8.90	8.80	8.64	8.78	**8.78**	55.4	57.5	57.8	58.7	**57.3**	468
Co	66.0	**66.3**	27.7	27.4	**27.5**	40.0	40.0	39.2	38.8	39.4	39.4	38.4	**39.3**	139	140	132	134	**136**	54.4	56.2	56.1	54.7	**55.4**	24.4
Ni	981	**983**	n.a.	n.a.	**n.a.**	66.2	65.5	64.1	61.9	62.9	63.2	61.4	**63.6**	2924.9	2932.6	2889	2883.1	**2907**	798	814	826	799	**809**	489
Cu	n.a.	**n.a.**	5.04	5.23	**5.14**	0.516	bdl	0.509	0.219	0.286	0.161	bdl	**0.338**	n.a.	n.a.	n.a.	n.a.	**n.a.**	n.a.	n.a.	n.a.	n.a.	**n.a.**	1.08
Zn	n.a.	**n.a.**	12.6	11.7	**12.15**	11.4	11.2	11.1	11.2	11.1	11.4	11.1	**11.2**	n.a.	n.a.	n.a.	n.a.	**n.a.**	n.a.	n.a.	n.a.	n.a.	**n.a.**	11.5
Ga	n.a.	**n.a.**	n.a.	n.a.	**n.a.**	n.a.	n.a.	n.a.	n.a.	n.a.	n.a.	n.a.	**n.a.**	n.a.	n.a.	n.a.	n.a.	**n.a.**	n.a.	n.a.	n.a.	n.a.	**n.a.**	n.a.
Ge	n.a.	**n.a.**	n.a.	n.a.	**n.a.**	n.a.	n.a.	n.a.	n.a.	n.a.	n.a.	n.a.	**n.a.**	n.a.	n.a.	n.a.	n.a.	**n.a.**	n.a.	n.a.	n.a.	n.a.	**n.a.**	n.a.
Rb	bdl	**bdl**	0.051	0.088	**0.070**	0.066	0.043	0.043	0.058	0.025	0.034	0.031	**0.043**	bdl	bdl	bdl	bdl	**bdl**	bdl	bdl	0.013	0.018	**0.015**	0.146
Sr	0.420	**0.420**	128	129	**128**	0.455	0.380	0.372	0.478	0.373	0.353	0.342	**0.393**	bdl	bdl	0.088	bdl	**0.088**	0.628	0.644	0.691	0.776	**0.685**	266
Y	0.016	**0.014**	0.61	0.56	**0.59**	7.42	7.56	7.29	7.35	6.27	6.19	6.07	**6.88**	0.0034	0.0032	0.0024	0.0031	**0.0030**	0.023	0.021	0.025	0.022	**0.023**	1.17
Zr	0.100	**0.111**	3.13	3.10	**3.12**	37.3	38.4	36.4	36.5	32.1	31.7	30.5	**34.7**	0.077	0.081	0.076	0.074	**0.077**	0.175	0.178	0.200	0.192	**0.186**	9.23
Nb	0.057	**0.058**	0.219	0.214	**0.217**	0.452	0.458	0.444	0.460	0.461	0.418	0.409	**0.443**	0.0017	0.0029	0.0027	0.0023	**0.0024**	0.0029	0.0026	0.0041	0.0051	**0.0037**	0.035
Mo	n.a.	**n.a.**	n.a.	n.a.	**n.a.**	n.a.	n.a.	n.a.	n.a.	n.a.	n.a.	n.a.	**n.a.**	n.a.	n.a.	n.a.	n.a.	**n.a.**	n.a.	n.a.	n.a.	n.a.	**n.a.**	n.a.
Cs	bdl	**bdl**	bdl	bdl	**bdl**	bdl	bdl	bdl	bdl	bdl	bdl	bdl	**bdl**	bdl	bdl	bdl	bdl	**bdl**	bdl	0.0025	bdl	0.0071	**0.0048**	bdl
Ba	bdl	**0.022**	0.617	0.695	**0.656**	0.010	bdl	bdl	0.033	0.158	0.021	0.018	**0.048**	bdl	0.036	bdl	bdl	**0.036**	0.017	0.028	0.163	0.412	**0.155**	0.798
La	0.0062	**0.0068**	1.97	1.97	**1.97**	0.032	0.039	0.037	0.038	0.041	0.036	0.030	**0.036**	0.0001	bdl	bdl	0.0001	**0.0001**	0.006	0.007	0.012	0.016	**0.010**	3.16
Ce	0.026	**0.025**	7.25	7.27	**7.26**	0.394	0.408	0.403	0.406	0.418	0.392	0.395	**0.402**	0.0014	bdl	0.0001	0.0003	**0.0006**	0.027	0.030	0.034	0.049	**0.035**	12.6
Pr	bdl	**bdl**	1.15	1.12	**1.13**	0.141	0.142	0.130	0.131	0.125	0.127	0.121	**0.131**	n.a.	n.a.	n.a.	n.a.	**n.a.**	n.a.	n.a.	n.a.	n.a.	**n.a.**	2.35
Nd	0.029	**0.029**	5.12	5.18	**5.15**	1.32	1.36	1.36	1.25	1.13	1.21	1.12	**1.25**	bdl	0.0003	0.0003	bdl	**0.0003**	0.043	0.049	0.056	0.064	**0.053**	14.5
Sm	0.007	**0.011**	1.01	1.01	**1.01**	0.918	0.912	0.894	0.835	0.761	0.797	0.737	**0.836**	0.0003	bdl	0.0007	0.0011	**0.0007**	0.012	0.020	0.024	0.011	**0.017**	2.82
Eu	0.0041	**0.0052**	0.274	0.252	**0.263**	0.365	0.402	0.381	0.381	0.348	0.349	0.312	**0.363**	0.0002	bdl	bdl	0.0002	**0.0002**	0.0043	0.0031	0.0041	0.0076	**0.0048**	0.568
Gd	0.0049	**0.0045**	0.632	0.699	**0.666**	1.37	1.41	1.32	1.33	1.16	1.13	1.1	**1.26**	0.0002	0.0005	0.0002	bdl	**0.0003**	0.0081	0.0085	0.0083	0.0090	**0.0085**	1.34
Tb	bdl	**bdl**	0.077	0.064	**0.070**	0.228	0.221	0.216	0.208	0.164	0.194	0.179	**0.201**	n.a.	n.a.	n.a.	n.a.	**n.a.**	n.a.	n.a.	n.a.	n.a.	**n.a.**	0.146
Dy	0.0021	**0.0055**	0.201	0.307	**0.254**	1.42	1.50	1.45	1.40	1.25	1.17	1.20	**1.34**	bdl	0.0005	bdl	bdl	**0.0005**	0.0070	0.0066	0.0093	0.0054	**0.0071**	0.520
Ho	bdl	**bdl**	0.027	0.036	**0.031**	0.279	0.276	0.264	0.275	0.224	0.238	0.237	**0.256**	n.a.	n.a.	n.a.	n.a.	**n.a.**	n.a.	n.a.	n.a.	n.a.	**n.a.**	0.064
Er	0.0011	**0.0026**	0.017	0.028	**0.023**	0.771	0.824	0.818	0.767	0.628	0.637	0.641	**0.727**	0.0003	0.0001	bdl	bdl	**0.0002**	0.0022	0.0017	0.0023	0.0035	**0.0024**	0.090
Tm	bdl	**bdl**	0.0011	0.0011	**0.0011**	0.119	0.125	0.114	0.114	0.102	0.101	0.101	**0.111**	n.a.	n.a.	n.a.	n.a.	**n.a.**	n.a.	n.a.	n.a.	n.a.	**n.a.**	0.0081
Yb	0.0012	**0.0012**	0.046	0.029	**0.037**	0.916	0.951	0.995	0.911	0.771	0.797	0.820	**0.880**	bdl	0.0003	0.0001	0.0002	**0.0002**	0.0014	0.0009	0.0009	0.0018	**0.0012**	0.025
Lu	bdl	**bdl**	0.0082	0.0055	**0.0069**	0.160	0.163	0.158	0.154	0.121	0.129	0.118	**0.143**	bdl	bdl	0.0001	0.0004	**0.0002**	0.0003	0.0003	bdl	0.0007	**0.0004**	0.0010
Hf	0.0053	**0.0050**	0.255	0.222	**0.239**	0.789	0.836	0.748	0.762	0.664	0.667	0.652	**0.731**	0.0031	0.0036	0.0040	0.0041	**0.0037**	0.009	0.012	0.011	0.011	**0.011**	0.876
Ta	0.0065	**0.0051**	0.012	0.017	**0.014**	0.050	0.051	0.056	0.042	0.042	0.048	0.039	**0.047**	bdl	0.0002	bdl	bdl	**0.0002**	bdl	bdl	0.0002	0.0001	**0.0001**	0.0037
W	n.a.	**n.a.**	n.a.	n.a.	**n.a.**	n.a.	n.a.	n.a.	n.a.	n.a.	n.a.	n.a.	**n.a.**	n.a.	n.a.	n.a.	n.a.	**n.a.**	n.a.	n.a.	n.a.	n.a.	**n.a.**	n.a.
Pb	0.009	**0.017**	0.442	0.424	**0.433**	0.126	0.189	0.361	0.920	1.18	4.09	1.80	**1.24**	0.019	0.036	0.138	0.128	**0.080**	0.297	0.405	0.088	0.021	**0.263**	0.590
Th	0.0008	**0.0009**	0.032	0.028	**0.030**	bdl	0.0093	0.013	bdl	0.0099	0.013	0.0141	**0.012**	0.001	0.128	bdl	0.002	**0.043**	0.0064	0.0005	0.0003	0.0025	**0.0024**	0.050
U	0.0002	**0.0010**	bdl	bdl	**bdl**	0.019	0.078	0.024	0.022	0.022	0.023	0.022	**0.030**	bdl	bdl	bdl	bdl	**bdl**	0.0008	0.0004	0.0004	0.0013	**0.0007**	0.012

Table 4.3 *(continued)*

	F-12 clinopyroxene				average	F-12 rutile			average	F-12 garnet										average	F-13 olivine		
Element	F12cpx2	F12cpx3	F12cpx5	F12cpx6	**F12 cpx**	F12-Rt1	F12-Rt2	F12-Rt3	**F12-rt**	F12-Gt1	F12-Gt2	F12-Gt3	F12-Gt4	F12-Gt5	F12-Gt7	F12-Gt8	F12-Gt9	F12-Gt10	F12-G11	**F12 grt**	F13-ol2	F13-ol3	F13-ol5
Li	0.400	bdl	0.393	0.456	**0.482**	bdl	bdl	bdl	**bdl**	0.171	bdl	bdl	bdl	bdl	bdl	bdl	bdl	bdl	bdl	**0.171**	2.21	2.24	3.28
B	9.80	4.80	7.60	6.15	**8.39**	bdl	0.344	0.215	**0.280**	2.19	1.67	1.40	1.30	1.30	1.15	1.12	1.14	1.31	1.19	**1.38**	n.a.	n.a.	n.a.
Sc	20.7	20.2	19.0	18.4	**19.8**	20.5	20.8	20.2	**20.5**	85.8	82.4	83.7	83.6	85.3	92.5	91.0	92.8	92.8	92.1	**88.2**	2.74	2.51	4.26
V	448	348	408	392	**413**	4396	4678	4656	**4577**	395	382	369	367	370	357	357	372	366	364	**370**	5.19	6.37	3.62
Co	24.1	20.3	23.1	22.7	**22.9**	11.0	13.0	12.3	**12.1**	38.7	37.9	37.5	37.2	37.7	36.4	36.7	36.5	36.9	37.0	**37.2**	155	153	167
Ni	453	394	471	450	**451**	886	1659	1295	**1280**	64.2	60.2	59.9	58.9	58.9	56.5	56.8	57.1	57.3	57.2	**58.7**	3278	3238	3380
Cu	1.41	0.750	0.770	0.860	**0.974**	320	314	347	**327**	4.41	1.25	3.14	1.42	5.89	n.a.	n.a.	n.a.	n.a.	n.a.	**3.22**	n.a.	n.a.	n.a.
Zn	11.5	10.9	10.9	11.3	**11.2**	74.3	78.2	86.6	**79.7**	10.3	10.3	10.2	10.1	10.1	10.5	10.4	10.9	10.7	10.9	**10.4**	n.a.	n.a.	n.a.
Ga	n.a.	n.a.	n.a.	n.a.	**n.a.**	n.a.	n.a.	n.a.	**n.a.**	n.a.	n.a.	n.a.	n.a.	n.a.	n.a.	n.a.	n.a.	n.a.	n.a.	**n.a.**	n.a.	n.a.	n.a.
Ge	n.a.	n.a.	n.a.	n.a.	**n.a.**	n.a.	n.a.	n.a.	**n.a.**	n.a.	n.a.	n.a.	n.a.	n.a.	n.a.	n.a.	n.a.	n.a.	n.a.	**n.a.**	n.a.	n.a.	n.a.
Rb	0.145	0.153	0.091	0.116	**0.130**	0.0073	0.0060	0.0048	**0.0060**	0.044	0.029	0.025	0.025	0.025	0.038	0.023	0.044	0.023	0.036	**0.031**	bdl	0.0051	bdl
Sr	261	249	251	251	**256**	0.476	bdl	bdl	**0.476**	0.618	0.589	0.552	0.563	0.578	0.642	0.613	0.664	0.660	0.625	**0.610**	bdl	bdl	bdl
Y	1.23	1.14	1.04	1.00	**1.12**	0.035	0.031	0.052	**0.039**	8.00	7.41	7.36	7.50	7.58	8.37	8.01	8.44	8.53	8.44	**7.96**	0.010	0.016	0.006
Zr	9.00	8.81	8.60	7.89	**8.71**	167	170	167	**168**	38.8	37.0	37.0	36.6	37.9	40.7	39.2	41.3	40.7	40.8	**39.0**	0.080	0.141	0.050
Nb	0.023	0.016	0.357	0.039	**0.094**	54.4	61.8	31.8	**49.3**	0.055	0.041	0.034	0.040	0.041	0.026	0.031	0.036	0.027	0.042	**0.037**	0.028	0.018	0.039
Mo	n.a.	n.a.	n.a.	n.a.	**n.a.**	0.019	0.019	0.020	**0.019**	n.a.	n.a.	n.a.	n.a.	n.a.	n.a.	n.a.	n.a.	n.a.	n.a.	**n.a.**	n.a.	n.a.	n.a.
Cs	bdl	bdl	bdl	bdl	**bdl**	bdl	bdl	bdl	**bdl**	bdl	bdl	bdl	0.0048	bdl	bdl	bdl	bdl	bdl	0.0062	**0.006**	0.0028	0.0013	bdl
Ba	0.581	0.539	0.577	0.701	**0.639**	bdl	bdl	bdl	**bdl**	0.010	bdl	bdl	bdl	0.012	bdl	bdl	0.010	bdl	bdl	**0.011**	bdl	bdl	bdl
La	3.12	2.85	2.93	2.81	**2.97**	bdl	bdl	bdl	**bdl**	0.030	0.024	0.025	0.029	0.034	0.032	0.023	0.036	0.026	0.024	**0.028**	0.0001	0.0005	bdl
Ce	12.3	10.7	12.2	11.8	**11.9**	bdl	bdl	bdl	**bdl**	0.344	0.341	0.313	0.315	0.332	0.338	0.324	0.366	0.339	0.353	**0.337**	0.0015	0.0014	bdl
Pr	2.30	2.01	2.18	2.13	**2.19**	bdl	bdl	bdl	**bdl**	0.143	0.136	0.136	0.133	0.137	0.129	0.137	0.155	0.149	0.146	**0.140**	n.a.	n.a.	n.a.
Nd	13.8	11.9	12.3	11.7	**12.8**	bdl	bdl	bdl	**bdl**	1.84	1.59	1.46	1.55	1.58	1.73	1.59	1.85	1.81	1.71	**1.67**	bdl	0.0034	0.0020
Sm	2.49	2.14	2.16	2.13	**2.35**	bdl	bdl	bdl	**bdl**	1.15	1.07	1.07	0.98	1.07	1.12	1.09	1.08	1.18	1.23	**1.10**	0.0004	0.0007	bdl
Eu	0.545	0.388	0.446	0.442	**0.478**	bdl	bdl	bdl	**bdl**	0.442	0.384	0.353	0.364	0.373	0.402	0.396	0.434	0.403	0.403	**0.395**	0.0002	bdl	0.0018
Gd	1.40	0.94	0.92	0.94	**1.11**	bdl	bdl	bdl	**bdl**	1.38	1.34	1.28	1.22	1.28	1.38	1.19	1.37	1.39	1.33	**1.32**	0.0036	0.0026	0.0013
Tb	0.128	0.101	0.098	0.099	**0.114**	bdl	bdl	bdl	**bdl**	0.261	0.235	0.239	0.228	0.224	0.244	0.233	0.260	0.251	0.250	**0.243**	n.a.	n.a.	n.a.
Dy	0.556	0.395	0.450	0.406	**0.465**	bdl	bdl	bdl	**bdl**	1.81	1.66	1.71	1.58	1.74	1.79	1.79	1.89	1.92	1.85	**1.77**	0.0006	bdl	bdl
Ho	0.071	0.055	0.054	0.049	**0.058**	bdl	bdl	bdl	**bdl**	0.327	0.300	0.316	0.311	0.309	0.343	0.332	0.327	0.360	0.358	**0.328**	n.a.	n.a.	n.a.
Er	0.076	0.056	0.073	0.074	**0.074**	bdl	bdl	bdl	**bdl**	0.769	0.743	0.672	0.656	0.735	0.816	0.736	0.794	0.839	0.826	**0.759**	0.0020	0.0035	0.0027
Tm	0.0082	0.0059	0.0071	0.0056	**0.0070**	bdl	bdl	bdl	**bdl**	0.082	0.087	0.080	0.077	0.090	0.101	0.088	0.103	0.099	0.076	**0.088**	n.a.	n.a.	n.a.
Yb	0.009	0.006	0.021	0.017	**0.016**	bdl	bdl	bdl	**bdl**	0.549	0.538	0.462	0.476	0.514	0.533	0.529	0.559	0.540	0.519	**0.522**	bdl	0.0044	0.0007
Lu	0.0048	bdl	0.0018	bdl	**0.0025**	bdl	bdl	bdl	**bdl**	0.073	0.075	0.062	0.073	0.074	0.069	0.069	0.074	0.076	0.073	**0.072**	bdl	0.0002	0.0004
Hf	0.980	0.659	0.708	0.626	**0.770**	13.0	13.2	12.9	**13.0**	1.16	1.06	1.06	1.01	1.05	1.13	1.04	1.18	1.15	1.11	**1.09**	bdl	0.0061	0.0007
Ta	0.003	bdl	0.035	bdl	**0.014**	3.51	3.48	3.66	**3.55**	bdl	bdl	bdl	bdl	bdl	bdl	bdl	bdl	bdl	bdl	**bdl**	0.0019	0.0021	0.0027
W	n.a.	n.a.	n.a.	n.a.	**n.a.**	n.a.	n.a.	n.a.	**n.a.**	n.a.	n.a.	n.a.	n.a.	n.a.	n.a.	n.a.	n.a.	n.a.	n.a.	**n.a.**	n.a.	n.a.	n.a.
Pb	0.574	0.510	0.560	0.623	**0.571**	0.951	0.229	0.170	**0.450**	0.311	0.156	0.550	0.489	0.389	0.429	0.177	0.860	0.530	0.400	**0.429**	0.019	0.023	0.026
Th	0.050	0.050	0.039	0.047	**0.047**	bdl	bdl	bdl	**bdl**	0.012	0.011	0.171	0.121	0.090	0.085	0.010	0.874	0.017	0.472	**0.186**	0.094	0.118	0.0002
U	0.0076	0.0071	0.0085	0.0067	**0.0084**	0.113	0.115	0.117	**0.115**	0.020	0.015	0.015	0.017	0.018	0.016	0.013	0.022	0.015	0.016	**0.017**	bdl	0.0002	0.0004

Table 4.3 *(continued)*

	F-13			F-13				F-13							F-13						F-14			
	olivine		**average**	orthopyroxene			**average**	clinopyroxene						**average**	garnet					**average**	olivine			
Element	F13ol11	F13ol12	**ol F-13**	F13opx2	F13opx3	F13opx4	**opx F-13**	F13cpx1	F13cpxt2	F13cpx3	F13cpx4	F13cpx1	F13cpx2	**F13 cpx**	F13-Gt1	F13-Gt2	F13-Gt3	F13-Gt4	F13-Gt5	**F13 grt**	F14ol3	F14ol5	F14ol6	F14ol10
Li	2.03	2.17	**2.39**	1.13	1.42	1.12	**1.22**	0.990	0.840	n.a.	n.a.	n.a.	n.a.	**0.915**	0.426	bdl	bdl	0.207	0.283	**0.305**	1.88	1.56	1.56	1.70
B	n.a.	n.a.	**n.a.**	n.a.	n.a.	n.a.	**n.a.**	5.39	5.93	4.81	8.46	6.45	7.16	**6.37**	4.70	4.43	4.11	4.18	4.30	**4.34**	n.a.	n.a.	n.a.	n.a.
Sc	1.36	1.48	**2.47**	2.13	2.64	2.79	**2.52**	18.7	18.3	17.0	18.0	19.3	19.0	**18.4**	144	143	142	142	135	**141**	2.01	1.94	1.98	1.22
V	4.99	5.39	**5.11**	30.2	41.3	44.2	**38.5**	280	286	298	302	322	341	**305**	331	331	335	340	400	**348**	5.70	5.25	5.65	6.25
Co	143	158	**155**	56.5	65.8	70.3	**64.2**	28.0	27.6	26.9	27.3	30.9	30.4	**28.5**	63.1	62.6	63.3	63.6	77.2	**66.0**	153	150	151	174
Ni	2980	2979	**3171**	853	957	1026	**945**	498	502	493	535	n.a.	n.a.	**507**	100	100	105	97	122	**105**	3308	3224	3248	3412
Cu	n.a.	n.a.	**n.a.**	n.a.	n.a.	n.a.	**n.a.**	2.43	3.09	bdl	2.07	2.11	2.33	**2.41**	bdl	0.430	bdl	0.360	0.560	**0.450**	n.a.	n.a.	n.a.	n.a.
Zn	n.a.	n.a.	**n.a.**	n.a.	n.a.	n.a.	**n.a.**	12.9	13.4	17.9	12.3	17.9	14.3	**14.8**	15.1	16.1	16.2	17.1	20.6	**17.0**	n.a.	n.a.	n.a.	n.a.
Ga	n.a.	n.a.	**n.a.**	n.a.	n.a.	n.a.	**n.a.**	n.a.	n.a.	n.a.	n.a.	n.a.	n.a.	**n.a.**	n.a.	n.a.	n.a.	n.a.	n.a.	**n.a.**	n.a.	n.a.	n.a.	n.a.
Ge	n.a.	n.a.	**n.a.**	n.a.	n.a.	n.a.	**n.a.**	n.a.	n.a.	n.a.	n.a.	n.a.	n.a.	**n.a.**	n.a.	n.a.	n.a.	n.a.	n.a.	**n.a.**	n.a.	n.a.	n.a.	n.a.
Rb	bdl	bdl	**0.0051**	bdl	bdl	bdl	**bdl**	0.038	0.065	0.122	0.070	0.358	0.398	**0.175**	0.059	0.035	0.037	0.032	0.048	**0.042**	0.0044	bdl	bdl	bdl
Sr	0.0064	0.0085	**0.0075**	0.245	0.308	0.343	**0.299**	87.2	86.3	85.4	85.4	92.1	90.9	**87.9**	0.267	0.264	0.250	0.219	0.272	**0.254**	0.0700	0.0550	0.1980	bdl
Y	0.0054	0.0052	**0.0086**	0.043	0.050	0.055	**0.049**	2.30	2.28	1.94	2.32	2.08	2.11	**2.17**	24.5	23.9	23.5	23.5	22.0	**23.5**	bdl	bdl	0.0026	0.0014
Zr	0.064	0.073	**0.082**	0.113	0.124	0.136	**0.124**	5.03	4.88	4.50	4.64	5.05	5.87	**5.00**	42.8	41.5	40.5	40.4	38.2	**40.7**	0.0081	bdl	0.0071	0.0087
Nb	0.018	0.022	**0.025**	0.037	0.038	0.043	**0.039**	0.220	0.197	0.244	0.223	0.262	0.318	**0.244**	0.350	0.373	0.318	0.342	0.397	**0.356**	0.033	0.041	0.036	0.040
Mo	n.a.	n.a.	**n.a.**	n.a.	n.a.	n.a.	**n.a.**	n.a.	n.a.	n.a.	n.a.	n.a.	n.a.	**n.a.**	n.a.	n.a.	n.a.	n.a.	n.a.	**n.a.**	n.a.	n.a.	n.a.	n.a.
Cs	bdl	bdl	**0.0021**	bdl	bdl	bdl	**bdl**	bdl	0.012	bdl	bdl	0.025	0.025	**0.021**	bdl	bdl	bdl	bdl	bdl	**bdl**	bdl	bdl	bdl	bdl
Ba	0.0058	bdl	**0.0058**	0.044	0.134	0.069	**0.082**	0.561	0.538	0.580	0.585	1.601	0.859	**0.787**	bdl	bdl	bdl	0.022	bdl	**0.022**	bdl	bdl	bdl	bdl
La	0.0009	bdl	**0.0005**	0.0062	0.0064	0.0054	**0.0060**	1.83	1.87	1.73	1.88	1.98	1.81	**1.85**	0.031	0.025	bdl	0.025	bdl	**0.027**	0.0001	bdl	bdl	bdl
Ce	0.0002	0.0007	**0.0009**	0.015	0.021	0.021	**0.019**	5.63	5.57	5.73	5.80	6.37	6.03	**5.86**	0.207	0.204	0.202	0.200	0.240	**0.211**	0.0005	bdl	bdl	bdl
Pr	n.a.	n.a.	**n.a.**	n.a.	n.a.	n.a.	**n.a.**	0.936	0.879	0.919	0.918	0.978	0.962	**0.932**	0.070	0.069	0.077	0.068	0.095	**0.076**	n.a.	n.a.	n.a.	n.a.
Nd	0.0016	bdl	**0.0023**	0.018	0.026	0.030	**0.024**	4.67	4.42	4.90	4.58	4.61	4.78	**4.66**	0.933	0.952	0.764	0.790	0.863	**0.860**	0.0002	bdl	0.0002	bdl
Sm	0.0016	0.0002	**0.0007**	0.015	0.011	0.016	**0.014**	1.53	1.23	1.00	1.50	1.43	1.47	**1.36**	1.116	0.927	0.824	0.940	0.772	**0.916**	bdl	bdl	bdl	0.0005
Eu	bdl	0.0001	**0.0007**	0.0060	0.0057	0.0052	**0.0056**	0.420	0.423	0.419	0.411	0.423	0.406	**0.417**	0.476	0.482	0.435	0.441	0.417	**0.450**	bdl	bdl	bdl	bdl
Gd	0.0007	0.0011	**0.0019**	0.0087	0.014	0.013	**0.012**	1.29	1.14	1.18	1.25	1.14	1.16	**1.19**	2.38	2.07	2.27	2.08	2.23	**2.21**	bdl	bdl	0.0006	0.0004
Tb	n.a.	n.a.	**n.a.**	n.a.	n.a.	n.a.	**n.a.**	0.175	0.149	0.147	0.156	0.153	0.152	**0.155**	0.412	0.469	0.423	0.402	0.468	**0.435**	n.a.	n.a.	n.a.	n.a.
Dy	0.0002	bdl	**0.0004**	0.011	0.013	0.010	**0.012**	0.721	0.726	0.626	0.693	0.690	0.662	**0.686**	3.96	3.92	3.78	3.77	3.54	**3.79**	bdl	bdl	bdl	bdl
Ho	n.a.	n.a.	**n.a.**	n.a.	n.a.	n.a.	**n.a.**	0.108	0.090	0.111	0.106	0.108	0.114	**0.106**	0.933	0.928	0.865	0.896	0.865	**0.897**	n.a.	n.a.	n.a.	n.a.
Er	bdl	0.0003	**0.0021**	0.0046	0.0061	0.0061	**0.0056**	0.281	0.222	0.088	0.215	0.224	0.180	**0.202**	3.10	2.89	2.73	2.84	2.66	**2.84**	bdl	0.0002	0.0002	bdl
Tm	n.a.	n.a.	**n.a.**	n.a.	n.a.	n.a.	**n.a.**	0.029	0.021	0.011	0.022	0.014	0.028	**0.021**	0.471	0.443	0.457	0.433	0.429	**0.447**	n.a.	n.a.	n.a.	n.a.
Yb	0.0019	0.0017	**0.0022**	0.0062	0.0055	0.0051	**0.0056**	0.185	0.131	0.064	0.133	0.132	0.098	**0.124**	3.58	3.35	3.35	3.39	2.98	**3.33**	0.0002	bdl	0.0005	0.0004
Lu	0.0002	0.0002	**0.0002**	0.0006	0.0008	0.0005	**0.0006**	0.019	0.016	0.012	0.016	0.014	0.014	**0.015**	0.583	0.527	0.502	0.530	0.488	**0.526**	bdl	bdl	bdl	0.0001
Hf	0.0023	0.0013	**0.0026**	0.0073	0.0064	0.0083	**0.0073**	0.367	0.408	0.317	0.331	0.420	0.470	**0.386**	1.16	0.91	1.03	1.04	0.93	**1.01**	bdl	bdl	0.0002	0.0001
Ta	0.0008	0.0011	**0.0017**	0.0037	0.0047	0.0041	**0.0042**	0.022	0.032	0.013	0.022	0.029	0.025	**0.024**	bdl	0.058	bdl	bdl	bdl	**0.058**	0.0024	0.0042	0.0033	0.00138
W	n.a.	n.a.	**n.a.**	n.a.	n.a.	n.a.	**n.a.**	n.a.	n.a.	n.a.	n.a.	n.a.	n.a.	**n.a.**	n.a.	n.a.	n.a.	n.a.	n.a.	**n.a.**	n.a.	n.a.	n.a.	n.a.
Pb	0.018	0.014	**0.020**	0.020	0.045	0.023	**0.029**	0.408	0.396	0.442	0.336	0.554	0.500	**0.439**	bdl	bdl	bdl	bdl	0.054	**0.054**	0.042	0.050	0.032	0.022
Th	0.0002	0.135	**0.0695**	0.0007	0.0011	0.0007	**0.0008**	0.028	0.042	0.021	0.031	0.048	0.035	**0.034**	0.026	bdl	bdl	bdl	bdl	**0.026**	0.0006	bdl	bdl	0.153
U	0.0020	bdl	**0.0009**	0.0002	0.0004	0.0008	**0.0005**	bdl	bdl	bdl	0.015	bdl	0.014	**0.015**	0.019	0.023	0.024	0.016	0.019	**0.020**	0.0004	0.0008	bdl	0.0010

Table 4.3 *(continued)*

	F-14 olivine		average	F-14 orthopyroxene		average	F-14 clinopyroxene		average	F-14 garnet						average	F-15 olivine				average	F-15 orthopyroxene		
Element	F14-ol1	F14-ol12	**ol F-14**	F14-opx	F14-opx	**opx F-14**	F14-Cpx	F14-Cpx	**F14-cpx**	F14grt1	F14grt2	F14grt3	F14grt4	F14grt5	F14grt6	**grt F-14**	F15-Ol1	F15-Ol2	F15-Ol3	F15-Ol5	**ol F-15**	F15opx	F15opx	F15opx3
Li	1.78	1.95	**1.74**	0.950	0.940	**0.945**	0.610	bdl	**0.610**	bdl	bdl	bdl	bdl	bdl	bdl	**bdl**	1.32	1.27	1.16	1.15	**1.23**	0.790	0.750	0.660
B	n.a.	n.a.	**n.a.**	n.a.	n.a.	**n.a.**	16.4	10.1	**13.3**	4.28	5.96	4.53	5.09	4.43	3.64	**4.66**	n.a.	n.a.	n.a.	n.a.	**n.a.**	n.a.	n.a.	n.a.
Sc	1.23	1.21	**1.60**	1.91	2.20	**2.06**	12.5	11.2	**11.9**	140	143	142	142	144	144	**142**	0.910	0.910	0.860	0.910	**0.898**	1.74	1.74	1.74
V	6.1	5.47	**5.74**	34.1	38.6	**36.4**	186	169	**178**	414	436	412	443	410	396	**419**	5.42	4.73	5.28	4.90	**5.08**	36.9	37.9	37.8
Co	172	172	**162**	63.8	70.5	**67.1**	33.2	30.3	**31.8**	47.5	47.2	47.4	47.3	44.4	44.9	**46.5**	140	140	140	142	**141**	57.7	58.8	59.3
Ni	3292	3401	**3314**	965	1049	**1007**	713	651	**682**	n.a.	n.a.	n.a.	n.a.	82.8	76.1	**79.5**	2866	2984	2991	2988	**2957**	877	891	890
Cu	n.a.	n.a.	**n.a.**	n.a.	n.a.	**n.a.**	4.48	12.14	**8.31**	bdl	bdl	bdl	bdl	bdl	bdl	**bdl**	n.a.	n.a.	n.a.	n.a.	**n.a.**	n.a.	n.a.	n.a.
Zn	n.a.	n.a.	**n.a.**	n.a.	n.a.	**n.a.**	55.9	37.0	**46.4**	14.1	13.3	13.7	12.5	12.4	12.5	**13.1**	n.a.	n.a.	n.a.	n.a.	**n.a.**	n.a.	n.a.	n.a.
Ga	n.a.	n.a.	**n.a.**	n.a.	n.a.	**n.a.**	n.a.	n.a.	**n.a.**	n.a.	n.a.	n.a.	n.a.	n.a.	n.a.	**n.a.**	n.a.	n.a.	n.a.	n.a.	**n.a.**	n.a.	n.a.	n.a.
Ge	n.a.	n.a.	**n.a.**	n.a.	n.a.	**n.a.**	n.a.	n.a.	**n.a.**	n.a.	n.a.	n.a.	n.a.	n.a.	n.a.	**n.a.**	n.a.	n.a.	n.a.	n.a.	**n.a.**	n.a.	n.a.	n.a.
Rb	bdl	bdl	**0.004**	0.031	0.028	**0.030**	0.506	0.084	**0.295**	0.305	0.206	0.214	0.246	0.193	0.238	**0.234**	bdl	bdl	bdl	bdl	**bdl**	0.014	0.130	0.030
Sr	0.006	0.013	**0.068**	0.155	0.244	**0.200**	55.3	56.3	**55.8**	0.105	0.152	0.110	0.147	0.155	0.161	**0.138**	bdl	bdl	bdl	0.0048	**0.0048**	0.310	0.480	0.410
Y	bdl	0.0005	**0.0015**	0.0072	0.0062	**0.0067**	0.259	0.212	**0.236**	3.99	4.15	4.02	3.02	3.29	3.90	**3.73**	0.0018	0.0009	0.0007	0.0016	**0.0013**	0.017	0.016	0.015
Zr	0.0047	0.0086	**0.0074**	0.016	0.013	**0.014**	0.687	0.212	**0.450**	6.35	6.33	6.26	5.98	6.18	6.32	**6.24**	0.019	0.012	0.018	0.017	**0.017**	0.051	0.036	0.037
Nb	0.036	0.037	**0.037**	0.044	0.065	**0.055**	0.299	0.160	**0.230**	0.703	0.685	0.711	0.731	0.703	0.675	**0.701**	0.063	0.058	0.060	0.052	**0.058**	0.066	0.064	0.057
Mo	n.a.	n.a.	**n.a.**	n.a.	n.a.	**n.a.**	n.a.	n.a.	**n.a.**	n.a.	n.a.	n.a.	n.a.	n.a.	n.a.	**n.a.**	n.a.	n.a.	n.a.	n.a.	**n.a.**	n.a.	n.a.	n.a.
Cs	bdl	0.0061	**0.0061**	0.0046	bdl	**0.0046**	0.022	bdl	**0.022**	bdl	bdl	bdl	bdl	bdl	bdl	**bdl**	bdl	bdl	bdl	0.002	**0.002**	bdl	0.004	bdl
Ba	0.0080	0.0201	**0.0141**	0.034	0.044	**0.039**	2.83	1.05	**1.94**	bdl	bdl	bdl	bdl	bdl	bdl	**bdl**	0.011	0.037	0.007	0.013	**0.017**	0.090	1.39	1.15
La	0.0010	0.0024	**0.0011**	0.0058	0.0063	**0.0061**	2.47	2.03	**2.25**	0.079	0.065	0.069	0.066	0.072	0.077	**0.071**	0.0002	bdl	0.0005	bdl	**0.0003**	0.006	0.0059	0.0044
Ce	0.0019	0.0038	**0.0021**	0.016	0.018	**0.017**	6.49	5.02	**5.76**	0.570	0.556	0.541	0.529	0.529	0.503	**0.538**	0.0002	0.0005	0.0007	0.0011	**0.0006**	0.018	0.022	0.017
Pr	n.a.	n.a.	**n.a.**	n.a.	n.a.	**n.a.**	0.681	0.522	**0.602**	0.135	0.132	0.117	0.129	0.111	0.119	**0.124**	n.a.	n.a.	n.a.	n.a.	**n.a.**	n.a.	n.a.	n.a.
Nd	0.0015	0.0030	**0.0012**	0.012	0.014	**0.013**	2.06	1.73	**1.90**	0.844	0.790	0.730	0.763	0.787	0.778	**0.782**	bdl	0.0010	0.0015	0.0006	**0.0010**	0.024	0.030	0.020
Sm	0.0020	0.0026	**0.0017**	bdl	0.0037	**0.0037**	0.217	0.220	**0.219**	0.288	0.299	0.323	0.251	0.322	0.337	**0.303**	bdl	0.0005	0.0009	0.0007	**0.0007**	0.0090	0.0084	0.0082
Eu	0.0003	0.0006	**0.0004**	bdl	0.0012	**0.0012**	0.069	0.050	**0.060**	0.126	0.117	0.103	0.122	0.115	0.106	**0.115**	bdl	bdl	bdl	bdl	**bdl**	0.0035	0.0030	0.0029
Gd	0.0013	bdl	**0.0008**	bdl	0.0022	**0.0022**	0.191	0.148	**0.170**	0.487	0.436	0.428	0.461	0.413	0.424	**0.442**	0.0012	bdl	0.0007	0.0004	**0.0007**	0.0050	0.0049	0.0052
Tb	n.a.	n.a.	**n.a.**	n.a.	n.a.	**n.a.**	0.011	0.015	**0.013**	0.084	0.092	0.088	0.083	0.076	0.081	**0.084**	n.a.	n.a.	n.a.	n.a.	**n.a.**	n.a.	n.a.	n.a.
Dy	0.0005	0.0002	**0.0003**	0.0016	0.0004	**0.0010**	0.052	0.070	**0.061**	0.605	0.643	0.664	0.497	0.560	0.620	**0.598**	0.0004	0.0002	0.0004	0.0008	**0.0005**	0.0040	bdl	0.0018
Ho	n.a.	n.a.	**n.a.**	n.a.	n.a.	**n.a.**	0.012	0.008	**0.010**	0.156	0.153	0.156	0.109	0.116	0.154	**0.140**	n.a.	n.a.	n.a.	n.a.	**n.a.**	n.a.	n.a.	n.a.
Er	bdl	bdl	**0.0002**	0.0013	0.0009	**0.0011**	0.017	0.007	**0.012**	0.541	0.539	0.513	0.346	0.372	0.486	**0.466**	0.0009	bdl	0.0002	0.0002	**0.0004**	0.0014	0.0017	0.0021
Tm	n.a.	n.a.	**n.a.**	n.a.	n.a.	**n.a.**	bdl	0.0014	**0.0014**	0.094	0.099	0.095	0.068	0.071	0.088	**0.086**	n.a.	n.a.	n.a.	n.a.	**n.a.**	n.a.	n.a.	n.a.
Yb	0.0001	0.0003	**0.0003**	bdl	0.0015	**0.0015**	0.018	0.010	**0.014**	0.717	0.802	0.764	0.580	0.577	0.769	**0.702**	bdl	0.0003	0.0011	0.0002	**0.0005**	0.0017	0.0022	0.0019
Lu	0.0001	0.0001	**0.0001**	0.0002	bdl	**0.0002**	0.0011	0.0014	**0.0013**	0.135	0.148	0.129	0.106	0.115	0.142	**0.129**	0.0002	0.0002	0.0003	bdl	**0.0002**	0.0003	0.0003	0.0003
Hf	0.0002	0.0010	**0.0004**	0.0004	0.0003	**0.0004**	bdl	0.017	**0.017**	0.185	0.176	0.173	0.165	0.160	0.199	**0.176**	0.0005	0.0004	0.0007	0.0008	**0.0006**	0.0032	0.0034	0.0017
Ta	0.0006	0.0018	**0.0023**	0.0028	0.0046	**0.0037**	0.016	bdl	**0.016**	0.057	0.062	0.051	0.061	0.063	0.063	**0.059**	0.0028	0.0043	0.0037	0.0031	**0.0035**	0.0090	0.0090	0.0070
W	n.a.	n.a.	**n.a.**	n.a.	n.a.	**n.a.**	n.a.	n.a.	**n.a.**	n.a.	n.a.	n.a.	n.a.	n.a.	n.a.	**n.a.**	n.a.	n.a.	n.a.	n.a.	**n.a.**	n.a.	n.a.	n.a.
Pb	0.048	0.010	**0.034**	0.045	0.032	**0.039**	0.579	0.706	**0.643**	0.062	0.056	0.055	0.074	0.066	0.070	**0.064**	0.240	0.010	0.017	0.036	**0.076**	0.026	0.073	0.036
Th	0.0003	0.0390	**0.0482**	0.0009	0.0011	**0.0010**	0.047	0.026	**0.036**	0.039	0.043	0.042	0.040	0.040	0.034	**0.039**	0.410	0.100	0.560	0.180	**0.313**	0.0012	0.0012	0.011
U	0.0040	0.0010	**0.0014**	0.0003	0.0002	**0.0003**	0.011	0.008	**0.010**	0.035	0.035	0.034	0.036	0.030	0.029	**0.033**	0.001	0.0001	0.0001	bdl	**0.000**	bdl	bdl	bdl

Table 4.3 *(continued)*

	F-15	F-15			F-15						F-16				F-16				F-16					
	average	clinopyroxene		**average**	garnet					**average**	olivine			**average**	orthopyroxene			**average**	clinopyroxene					**average**
Element	**opx F-15**	F15cpx1	F15cpx2	**F15cpx**	F15Gt1	F15Gt2	F15Gt3	F15Gt4	F15Gt5	**F15-grt**	F16ol2	F16ol3	F16ol10	**ol F-16**	F16opx1	F16opx2	F16opx4	**F16opx**	F16cpx1	F16cpx2	F16cpx3	F16cpx4	F16cpx5	**F16 cpx**
Li	**0.733**	1.04	bdl	**1.04**	0.098	bdl	bdl	bdl	bdl	**0.098**	2.64	2.15	1.63	**2.14**	0.460	1.38	1.03	**0.957**	0.900	0.460	0.840	0.723	0.539	**0.692**
B	**n.a.**	6.38	4.71	**5.55**	2.73	2.30	2.18	1.39	1.41	**2.00**	n.a.	n.a.	n.a.	**n.a.**	n.a.	n.a.	n.a.	**n.a.**	4.58	4.18	3.69	3.89	6.07	**4.48**
Sc	**1.74**	13.3	13.1	**13.2**	108	107	108	101	97	**104**	2.08	1.92	1.06	**1.69**	1.73	1.98	2.07	**1.93**	12.5	12.7	12.2	12.0	12.3	**12.3**
V	**37.5**	318	348	**333**	255	245	244	250	244	**248**	3.84	4.56	3.87	**4.09**	17.2	29.9	31.5	**26.2**	176	177	179	167	167	**173**
Co	**58.6**	23.6	23.0	**23.3**	39.6	38.8	38.9	38.8	38.6	**38.9**	154	152	166	**157**	54.3	65.6	71.7	**63.9**	23.6	23.4	24.2	22.3	22.4	**23.2**
Ni	**886**	n.a.	n.a.	**n.a.**	57.7	55.8	56.0	55.0	54.9	**55.9**	3403	3370	3235	**3336**	840	999	1066	**968**	516	524	542	518	515	**523**
Cu	**n.a.**	bdl	1.76	**1.76**	bdl	bdl	bdl	bdl	bdl	**bdl**	n.a.	n.a.	n.a.	**n.a.**	n.a.	n.a.	n.a.	**n.a.**	1.26	1.79	1.16	2.04	1.37	**1.52**
Zn	**n.a.**	7.90	9.17	**8.54**	9.62	9.41	9.52	10.35	10.8	**9.94**	n.a.	n.a.	n.a.	**n.a.**	n.a.	n.a.	n.a.	**n.a.**	12.1	12.1	12.5	10.8	12.4	**12.0**
Ga	**n.a.**	n.a.	n.a.	**n.a.**	n.a.	n.a.	n.a.	n.a.	n.a.	**n.a.**	n.a.	n.a.	n.a.	**n.a.**	n.a.	n.a.	n.a.	**n.a.**	n.a.	n.a.	n.a.	n.a.	n.a.	**n.a.**
Ge	**n.a.**	n.a.	n.a.	**n.a.**	n.a.	n.a.	n.a.	n.a.	n.a.	**n.a.**	n.a.	n.a.	n.a.	**n.a.**	n.a.	n.a.	n.a.	**n.a.**	n.a.	n.a.	n.a.	n.a.	n.a.	**n.a.**
Rb	**0.058**	0.477	0.151	**0.314**	0.038	0.044	0.062	0.052	0.041	**0.047**	0.0057	bdl	bdl	**0.0057**	bdl	0.079	0.019	**0.049**	0.072	0.048	0.051	0.025	0.052	**0.050**
Sr	**0.400**	130	131	**130**	0.241	0.236	0.230	0.236	0.223	**0.233**	bdl	bdl	bdl	**bdl**	0.270	0.380	0.370	**0.340**	102	101	101	98.1	97.8	**99.8**
Y	**0.016**	0.698	0.746	**0.722**	8.46	8.45	8.45	7.60	7.24	**8.04**	0.0030	0.0038	0.0024	**0.0031**	0.019	0.030	0.032	**0.027**	1.46	1.46	1.40	1.39	1.41	**1.42**
Zr	**0.041**	1.49	1.75	**1.62**	14.4	13.9	14.3	13.2	12.2	**13.6**	0.017	0.017	0.021	**0.018**	0.031	0.042	0.048	**0.040**	1.71	1.72	1.65	1.59	1.73	**1.68**
Nb	**0.062**	0.364	0.423	**0.394**	0.488	0.450	0.452	0.463	0.436	**0.458**	0.040	0.041	0.043	**0.041**	0.046	0.058	0.051	**0.052**	0.263	0.303	0.266	0.274	0.271	**0.275**
Mo	**n.a.**	n.a.	n.a.	**n.a.**	n.a.	n.a.	n.a.	n.a.	n.a.	**n.a.**	n.a.	n.a.	n.a.	**n.a.**	n.a.	n.a.	n.a.	**n.a.**	n.a.	n.a.	n.a.	n.a.	n.a.	**n.a.**
Cs	**0.0040**	bdl	bdl	**bdl**	bdl	bdl	bdl	bdl	bdl	**bdl**	bdl	0.0016	bdl	**0.0016**	bdl	0.0056	bdl	**0.0056**	bdl	bdl	bdl	bdl	bdl	**bdl**
Ba	**0.88**	7.24	4.11	**5.68**	bdl	bdl	bdl	0.018	0.018	**0.018**	bdl	0.093	bdl	**0.093**	0.109	0.021	0.370	**0.167**	0.264	0.243	0.332	0.215	0.313	**0.273**
La	**0.0054**	1.92	2.10	**2.01**	0.021	0.018	0.021	0.025	0.016	**0.020**	0.0019	0.0029	bdl	**0.0024**	0.0041	0.0046	0.0062	**0.0050**	1.66	1.71	1.71	1.62	1.70	**1.68**
Ce	**0.019**	6.63	7.22	**6.93**	0.241	0.222	0.233	0.243	0.239	**0.236**	0.0086	0.0111	bdl	**0.0098**	0.019	0.019	0.023	**0.020**	7.69	7.77	7.82	7.19	7.24	**7.54**
Pr	**n.a.**	1.08	1.14	**1.11**	0.095	0.085	0.087	0.097	0.086	**0.090**	n.a.	n.a.	n.a.	**n.a.**	n.a.	n.a.	n.a.	**n.a.**	1.28	1.27	1.28	1.24	1.22	**1.26**
Nd	**0.025**	5.35	5.84	**5.60**	1.021	0.960	0.987	0.871	0.826	**0.933**	bdl	0.0024	bdl	**0.0024**	0.014	0.020	0.019	**0.018**	5.93	5.95	5.87	5.54	5.67	**5.79**
Sm	**0.0085**	0.97	1.21	**1.09**	0.694	0.719	0.669	0.584	0.626	**0.658**	0.0008	bdl	bdl	**0.0008**	0.0075	0.0043	0.0088	**0.0069**	0.764	0.695	0.790	0.698	0.729	**0.735**
Eu	**0.0031**	0.258	0.292	**0.275**	0.289	0.282	0.275	0.259	0.260	**0.273**	0.0004	0.0001	bdl	**0.0003**	0.0010	0.0020	bdl	**0.0015**	0.167	0.165	0.172	0.152	0.165	**0.164**
Gd	**0.0050**	0.531	0.529	**0.530**	0.990	0.930	0.960	0.830	0.810	**0.904**	bdl	0.0008	bdl	**0.0008**	0.0071	0.0045	0.0025	**0.0047**	0.395	0.472	0.417	0.397	0.416	**0.419**
Tb	**n.a.**	0.065	0.066	**0.066**	0.177	0.169	0.168	0.161	0.144	**0.164**	n.a.	n.a.	n.a.	**n.a.**	n.a.	n.a.	n.a.	**n.a.**	0.056	0.059	0.051	0.055	0.043	**0.053**
Dy	**0.0029**	0.193	0.196	**0.195**	1.45	1.33	1.40	1.22	1.19	**1.32**	bdl	0.0007	0.0006	**0.0006**	0.0066	0.0056	0.0057	**0.0060**	0.361	0.318	0.310	0.305	0.307	**0.320**
Ho	**n.a.**	0.030	0.039	**0.034**	0.328	0.328	0.325	0.289	0.278	**0.310**	n.a.	n.a.	n.a.	**n.a.**	n.a.	n.a.	n.a.	**n.a.**	0.057	0.065	0.064	0.055	0.063	**0.061**
Er	**0.0017**	0.048	0.018	**0.033**	1.11	1.04	1.03	0.93	0.87	**1.00**	0.0015	bdl	0.0004	**0.0010**	0.0016	0.0045	0.0034	**0.0032**	0.125	0.161	0.162	0.120	0.145	**0.143**
Tm	**n.a.**	0.0027	0.0025	**0.0026**	0.180	0.185	0.169	0.155	0.143	**0.166**	n.a.	n.a.	n.a.	**n.a.**	n.a.	n.a.	n.a.	**n.a.**	0.018	0.013	0.016	0.013	0.016	**0.015**
Yb	**0.0019**	0.033	0.038	**0.035**	1.36	1.35	1.41	1.22	1.10	**1.29**	0.0018	0.0011	0.0009	**0.0013**	0.0057	0.0037	0.0047	**0.0047**	0.071	0.071	0.086	0.090	0.079	**0.079**
Lu	**0.0003**	0.0057	0.0132	**0.0095**	0.236	0.227	0.231	0.192	0.184	**0.214**	0.0004	0.0002	0.0001	**0.0002**	bdl	0.0007	0.0007	**0.0007**	0.009	0.014	0.012	0.011	0.011	**0.011**
Hf	**0.0028**	0.182	0.124	**0.153**	0.412	0.349	0.366	0.315	0.331	**0.355**	bdl	0.0003	0.0006	**0.0004**	bdl	0.0011	0.0020	**0.0016**	0.087	0.101	0.077	0.078	0.062	**0.081**
Ta	**0.0083**	0.029	0.045	**0.037**	0.059	0.042	0.041	0.048	0.045	**0.047**	0.0063	0.0053	0.0033	**0.0049**	0.0049	0.0070	0.0061	**0.0060**	0.028	0.025	0.030	0.027	0.030	**0.028**
W	**n.a.**	n.a.	n.a.	**n.a.**	n.a.	n.a.	n.a.	n.a.	n.a.	**n.a.**	n.a.	n.a.	n.a.	**n.a.**	n.a.	n.a.	n.a.	**n.a.**	n.a.	n.a.	n.a.	n.a.	n.a.	**n.a.**
Pb	**0.045**	0.386	2.04	**1.21**	0.075	0.090	0.114	0.769	0.910	**0.392**	0.028	0.029	0.023	**0.027**	0.017	0.026	0.018	**0.020**	0.20	0.21	0.21	0.19	0.27	**0.22**
Th	**0.0045**	0.057	0.057	**0.057**	0.014	0.012	0.010	bdl	0.009	**0.011**	0.0005	0.0087	bdl	**0.0046**	0.0008	0.0009	0.0004	**0.0007**	0.019	0.025	0.023	0.020	0.021	**0.021**
U	**bdl**	bdl	0.022	**0.022**	0.021	0.017	0.019	0.017	0.017	**0.018**	bdl	bdl	bdl	**bdl**	0.0003	bdl	bdl	**0.0003**	0.0037	0.0049	0.0048	0.0053	0.0034	**0.0044**

Table 4.3 *(continued)*

	F-16												554-XM46			554-XM46			554-XM46			554-XM46			
	garnet											**average**	olivine		**average**	orthopyroxene		**average**	garnet		**average**	olivine			**average**
Element	F16gt1	F16gt2	F16gt3	F16gt4	F16gt5	F16gt6	F16gt8	F16gt9	F16gt10	F16gt11	F16gt12	**F16 grt**	554Ol1	554Ol2	**ol 554**	554opx1	554opx2	**opx 554**	554grt1	554grt2	**grt 554**	556Ol1	556Ol2	556Ol3	**ol 556**
Li	bdl	bdl	bdl	bdl	bdl	bdl	bdl	bdl	bdl	bdl	bdl	**bdl**	1.44	1.43	**1.43**	0.670	0.714	**0.692**	bdl	bdl	**bdl**	1.42	1.46	1.45	**1.44**
B	1.49	1.41	1.40	1.35	1.37	1.51	1.25	1.10	1.32	1.32	1.28	**1.35**	0.990	0.850	**0.920**	0.820	0.720	**0.770**	0.450	0.470	**0.460**	0.810	0.830	0.770	**0.803**
Sc	83.4	82.1	81.7	82.9	94.2	93.4	79.3	75.5	78.4	79.8	83.4	**83.1**	0.356	0.360	**0.358**	0.479	0.500	**0.490**	150	151	**151**	0.378	0.366	0.373	**0.372**
V	143	146	144	140	146	147	151	148	152	151	150	**147**	5.97	6.08	**6.03**	31.6	33.1	**32.3**	411	410	**410**	6.24	6.33	6.37	**6.31**
Co	40.7	41.2	40.8	41.5	40.4	40.5	42.0	42.1	42.4	42.4	42.0	**41.5**	166	165	**165**	87.1	91.8	**89.4**	47.8	48.3	**48.0**	170	176	174	**173**
Ni	56.4	57.3	56.5	57.4	55.7	56.5	58.8	58.2	59.5	58.8	58.1	**57.6**	n.a.	n.a.	**n.a.**	n.a.	n.a.	**n.a.**	81.2	81.4	**81.3**	n.a.	n.a.	n.a.	**n.a.**
Cu	bdl	bdl	bdl	bdl	bdl	bdl	bdl	bdl	bdl	bdl	bdl	**bdl**	n.a.	n.a.	**n.a.**	n.a.	n.a.	**n.a.**	bdl	bdl	**bdl**	n.a.	n.a.	n.a.	**n.a.**
Zn	11.2	11.1	11.0	11.4	11.2	11.3	12.1	12.6	12.5	12.0	11.5	**11.6**	n.a.	n.a.	**n.a.**	n.a.	n.a.	**n.a.**	13.3	13.1	**13.2**	n.a.	n.a.	n.a.	**n.a.**
Ga	n.a.	n.a.	n.a.	n.a.	n.a.	n.a.	n.a.	n.a.	n.a.	n.a.	n.a.	**n.a.**	0.153	0.151	**0.152**	1.38	1.18	**1.28**	6.02	5.94	**5.98**	0.158	0.162	0.161	**0.160**
Ge	n.a.	n.a.	n.a.	n.a.	n.a.	n.a.	n.a.	n.a.	n.a.	n.a.	n.a.	**n.a.**	0.551	0.548	**0.550**	1.34	1.35	**1.34**	n.a.	n.a.	**n.a.**	0.553	0.567	0.543	**0.554**
Rb	0.029	0.026	0.030	0.029	0.036	0.037	0.041	0.048	0.037	0.026	0.031	**0.033**	0.0012	0.0011	**0.0012**	0.072	0.028	**0.050**	bdl	bdl	**bdl**	0.0019	bdl	0.0048	**0.0034**
Sr	0.135	0.128	0.134	0.131	0.144	0.149	0.128	0.117	0.121	0.137	0.142	**0.133**	0.0055	0.0084	**0.0070**	0.802	0.319	**0.561**	0.284	0.288	**0.286**	bdl	0.0030	0.0061	**0.0045**
Y	11.9	12.5	12.3	12.2	14.0	14.4	11.6	10.9	11.3	11.8	12.4	**12.3**	bdl	bdl	**bdl**	0.0023	0.0026	**0.0024**	1.44	1.38	**1.41**	0.0005	bdl	bdl	**0.0005**
Zr	10.4	8.76	8.64	9.62	12.5	10.5	10.1	8.88	9.94	10.0	9.67	**9.92**	0.133	0.137	**0.135**	0.148	0.071	**0.109**	5.76	5.39	**5.58**	0.0043	0.0042	0.0031	**0.0038**
Nb	0.320	0.313	0.314	0.302	0.325	0.354	0.315	0.296	0.318	0.321	0.321	**0.318**	0.021	0.019	**0.020**	0.109	0.073	**0.091**	1.02	1.03	**1.02**	0.035	0.042	0.037	**0.038**
Mo	n.a.	n.a.	n.a.	n.a.	n.a.	n.a.	n.a.	n.a.	n.a.	n.a.	n.a.	**n.a.**	n.a.	n.a.	**n.a.**	n.a.	n.a.	**n.a.**	0.580	0.470	**0.525**	n.a.	n.a.	n.a.	**n.a.**
Cs	bdl	bdl	bdl	bdl	bdl	bdl	bdl	bdl	bdl	0.006	bdl	**0.006**	n.a.	n.a.	**n.a.**	n.a.	n.a.	**n.a.**	bdl	bdl	**bdl**	n.a.	n.a.	n.a.	**n.a.**
Ba	bdl	bdl	bdl	bdl	bdl	bdl	0.013	bdl	bdl	bdl	bdl	**0.013**	n.a.	n.a.	**n.a.**	n.a.	n.a.	**n.a.**	bdl	bdl	**bdl**	n.a.	n.a.	n.a.	**n.a.**
La	0.013	0.012	bdl	bdl	0.013	0.010	0.017	bdl	0.012	0.014	0.012	**0.013**	0.0007	0.0010	**0.0008**	0.070	0.007	**0.038**	0.061	0.059	**0.060**	bdl	0.0003	0.0017	**0.0010**
Ce	0.159	0.164	0.169	0.169	0.171	0.170	0.165	0.166	0.161	0.169	0.172	**0.167**	0.0016	0.0023	**0.0020**	0.156	0.028	**0.092**	0.704	0.697	**0.701**	0.0002	0.0007	0.0028	**0.0012**
Pr	0.058	0.061	0.063	0.066	0.077	0.067	0.067	0.072	0.061	0.061	0.060	**0.065**	n.a.	n.a.	**n.a.**	n.a.	n.a.	**n.a.**	n.a.	n.a.	**n.a.**	n.a.	n.a.	n.a.	**n.a.**
Nd	0.611	0.626	0.651	0.647	0.759	0.783	0.674	0.535	0.610	0.648	0.644	**0.653**	0.0004	bdl	**0.0004**	0.052	0.015	**0.034**	1.35	1.33	**1.34**	0.0002	bdl	0.0007	**0.0004**
Sm	0.370	0.304	0.298	0.337	0.399	0.391	0.304	0.265	0.342	0.339	0.322	**0.334**	0.0007	bdl	**0.0007**	0.0056	0.0023	**0.0039**	0.377	0.385	**0.381**	bdl	bdl	0.0005	**0.0005**
Eu	0.142	0.125	0.125	0.113	0.144	0.139	0.110	0.108	0.129	0.105	0.123	**0.124**	0.0001	bdl	**0.0001**	0.0008	0.0007	**0.0008**	0.121	0.124	**0.123**	bdl	bdl	bdl	**bdl**
Gd	0.464	0.446	0.549	0.535	0.614	0.596	0.533	0.492	0.528	0.506	0.450	**0.519**	0.0002	bdl	**0.0002**	0.0024	0.0014	**0.0019**	0.354	0.354	**0.354**	0.0001	0.0001	bdl	**0.0001**
Tb	0.131	0.127	0.127	0.132	0.165	0.160	0.137	0.129	0.126	0.140	0.140	**0.138**	bdl	bdl	**bdl**	0.0002	bdl	**0.0002**	0.039	0.039	**0.039**	bdl	bdl	bdl	**bdl**
Dy	1.48	1.51	1.39	1.48	1.73	1.69	1.35	1.42	1.39	1.43	1.54	**1.49**	bdl	bdl	**bdl**	0.0010	0.0002	**0.0006**	0.245	0.225	**0.235**	bdl	bdl	bdl	**bdl**
Ho	0.407	0.433	0.437	0.434	0.487	0.510	0.413	0.377	0.413	0.409	0.439	**0.433**	bdl	bdl	**bdl**	0.0001	0.0001	**0.0001**	0.048	0.045	**0.046**	bdl	bdl	bdl	**bdl**
Er	1.51	1.62	1.54	1.59	1.72	1.78	1.49	1.40	1.44	1.48	1.45	**1.55**	bdl	0.0003	**0.0003**	0.0002	0.0002	**0.0002**	0.160	0.152	**0.156**	0.0002	0.0002	0.0003	**0.0002**
Tm	0.262	0.268	0.272	0.264	0.289	0.294	0.234	0.221	0.239	0.253	0.250	**0.259**	bdl	bdl	**bdl**	bdl	bdl	**bdl**	0.027	0.026	**0.027**	bdl	bdl	bdl	**bdl**
Yb	2.11	2.17	2.07	2.09	2.28	2.34	1.94	1.76	1.97	2.01	2.00	**2.07**	bdl	0.0001	**0.0001**	0.0002	bdl	**0.0002**	0.313	0.289	**0.301**	bdl	bdl	0.0003	**0.0003**
Lu	0.336	0.343	0.330	0.324	0.367	0.372	0.321	0.275	0.311	0.325	0.326	**0.330**	bdl	bdl	**bdl**	bdl	bdl	**bdl**	0.070	0.070	**0.070**	bdl	bdl	bdl	**bdl**
Hf	0.207	0.146	0.124	0.158	0.208	0.188	0.186	0.149	0.159	0.164	0.180	**0.170**	0.0026	0.0026	**0.0026**	0.0029	0.0005	**0.0017**	0.130	0.089	**0.109**	0.0001	bdl	0.0002	**0.0001**
Ta	0.035	0.042	0.036	0.035	0.046	0.046	0.035	0.040	0.038	0.028	0.032	**0.038**	0.0018	0.0018	**0.0018**	0.0109	0.0080	**0.0095**	0.115	0.108	**0.111**	0.0021	0.0025	0.0022	**0.0023**
W	n.a.	n.a.	n.a.	n.a.	n.a.	n.a.	n.a.	n.a.	n.a.	n.a.	n.a.	**n.a.**	n.a.	n.a.	**n.a.**	0.0013	0.0043	**0.0028**	bdl	0.012	**0.012**	n.a.	n.a.	n.a.	**n.a.**
Pb	0.045	0.016	0.026	0.047	0.059	0.023	0.045	0.072	0.120	0.052	0.042	**0.050**	bdl	bdl	**bdl**	n.a.	n.a.	**n.a.**	bdl	bdl	**bdl**	0.0002	bdl	bdl	**0.0002**
Th	bdl	bdl	bdl	bdl	bdl	0.0087	bdl	bdl	bdl	bdl	bdl	**0.0087**	n.a.	n.a.	**n.a.**	n.a.	n.a.	**n.a.**	0.037	0.038	**0.038**	n.a.	n.a.	n.a.	**n.a.**
U	0.0078	0.0093	0.0106	0.0094	0.0083	0.0108	0.0064	0.0118	0.0078	0.0111	0.0065	**0.0091**	bdl	bdl	**bdl**	0.0029	0.0004	**0.0016**	0.046	0.047	**0.047**	bdl	bdl	bdl	**bdl**

Table 4.3 *(continued)*

	556	556-XM48			695			695	695			865	865			882				882		
	opx	garnet		**average**	orthopyroxene		**average**	cpx	garnet		**average**	**opx**	garnet		**average**	orthopyroxene			**average**	garnet		**average**
Element	**556opx1**	556grt1	556grt2	**grt 556**	695opx1	695opx2	**opx 695**	**cpx-1**	695grt1	695grt2	**grt 695 a**	**865opx1**	865grt1	865grt2	**grt 865**	882opx1	882opx2	opx882-3	**opx 882**	882gt1	882gt2	**grt 882**
Li	**0.816**	bdl	bdl	**bdl**	0.683	0.665	**0.674**	**0.253**	bdl	bdl	**bdl**	**0.699**	bdl	bdl	**bdl**	0.469	0.460	0.446	**0.458**	bdl	bdl	**bdl**
B	**6.45**	0.290	0.350	**0.320**	0.820	0.870	**0.845**	**0.490**	0.360	0.410	**0.385**	**0.680**	0.440	0.460	**0.450**	0.890	0.840	n.a.	**0.865**	0.460	0.450	**0.455**
Sc	**bdl**	155	153	**154**	0.564	0.555	**0.560**	**14.7**	146	146	**146**	**0.473**	118	117	**118**	n.a.	n.a.	4.78	**4.78**	182	182	**182**
V	**37.7**	444	456	**450**	37.7	37.0	**37.3**	**242**	373	380	**377**	**34.4**	327	327	**327**	21.9	21.5	24.6	**22.7**	291	286	**288**
Co	**89.9**	45.1	44.7	**44.9**	86.2	88.9	**87.5**	**23.6**	43.7	44.2	**44.0**	**91.5**	48.3	48.2	**48.2**	83.7	84.2	n.a.	**83.9**	38.8	38.0	**38.4**
Ni	**n.a.**	76.2	76.6	**76.4**	n.a.	n.a.	**n.a.**	**423**	69.2	69.8	**69.5**	**n.a.**	76.4	75.5	**75.9**	n.a.	n.a.	875	**875**	61.5	61.3	**61.4**
Cu	**n.a.**	bdl	bdl	**bdl**	n.a.	n.a.	**n.a.**	**2.22**	bdl	bdl	**bdl**	**n.a.**	bdl	bdl	**bdl**	n.a.	n.a.	1.23	**1.23**	bdl	bdl	**bdl**
Zn	**n.a.**	12.5	12.9	**12.7**	n.a.	n.a.	**n.a.**	**10.6**	12.2	13.0	**12.6**	**n.a.**	12.4	12.8	**12.6**	n.a.	n.a.	24.6	**24.64**	10.9	10.5	**10.7**
Ga	**1.78**	7.46	7.31	**7.39**	1.63	2.11	**1.87**	**2.63**	8.03	8.11	**8.07**	**0.94**	4.05	4.13	**4.09**	1.34	1.34	1.41	**1.36**	5.58	5.22	**5.40**
Ge	**1.16**	n.a.	n.a.	**n.a.**	1.50	1.47	**1.49**	**n.a.**	n.a.	n.a.	**n.a.**	**1.02**	n.a.	n.a.	**n.a.**	1.13	1.10	n.a.	**1.11**	n.a.	n.a.	**n.a.**
Rb	**0.399**	0.025	bdl	**0.025**	0.0077	0.0078	**0.0077**	**0.035**	bdl	bdl	**bdl**	**0.014**	bdl	bdl	**bdl**	bdl	bdl	bdl	**bdl**	bdl	bdl	**bdl**
Sr	**11.3**	0.246	0.258	**0.252**	0.504	0.756	**0.630**	**201**	0.724	0.695	**0.710**	**0.43**	0.400	0.388	**0.394**	0.703	0.696	0.676	**0.692**	2.09	2.09	**2.09**
Y	**21.4**	3.42	3.53	**3.48**	0.011	0.010	**0.011**	**0.403**	6.63	6.67	**6.65**	**0.010**	8.03	7.96	**8.00**	0.0053	0.0046	0.0074	**0.0057**	6.35	6.34	**6.35**
Zr	**14.3**	7.28	7.61	**7.45**	0.067	0.063	**0.065**	**2.57**	41.4	41.1	**41.2**	**0.073**	55.3	55.4	**55.3**	0.043	0.041	0.069	**0.051**	43.7	43.1	**43.4**
Nb	**1.42**	1.07	1.11	**1.09**	0.042	0.037	**0.039**	**0.115**	0.422	0.419	**0.421**	**0.047**	0.441	0.453	**0.447**	0.217	0.219	0.227	**0.221**	2.44	2.42	**2.43**
Mo	**n.a.**	0.660	0.490	**0.575**	n.a.	n.a.	**n.a.**	**0.177**	0.490	0.540	**0.515**	**n.a.**	0.440	0.430	**0.435**	n.a.	n.a.	0.224	**0.224**	0.480	0.540	**0.510**
Cs	**n.a.**	bdl	0.0042	**0.0042**	n.a.	n.a.	**n.a.**	**0.0019**	bdl	bdl	**bdl**	**n.a.**	bdl	bdl	**bdl**	n.a.	n.a.	0.0010	**0.0010**	bdl	bdl	**bdl**
Ba	**n.a.**	bdl	0.0076	**0.0076**	n.a.	n.a.	**n.a.**	**0.941**	0.0067	0.0118	**0.0093**	**n.a.**	bdl	bdl	**bdl**	n.a.	n.a.	0.041	**0.041**	0.011	0.020	**0.015**
La	**3.47**	0.078	0.081	**0.080**	0.024	0.017	**0.021**	**3.30**	0.085	0.086	**0.085**	**0.006**	0.017	0.016	**0.016**	0.0081	0.0084	0.0087	**0.0084**	0.182	0.194	**0.188**
Ce	**10.1**	0.845	0.844	**0.845**	0.075	0.052	**0.063**	**15.3**	1.18	1.17	**1.17**	**0.024**	0.3	0.3	**0.3**	0.040	0.040	0.047	**0.042**	2.52	2.52	**2.52**
Pr	**n.a.**	n.a.	n.a.	**n.a.**	n.a.	n.a.	**n.a.**	**n.a.**	n.a.	n.a.	**n.a.**	**n.a.**	n.a.	n.a.	**n.a.**	n.a.	n.a.	n.a.	**n.a.**	n.a.	n.a.	**n.a.**
Nd	**7.57**	1.22	1.24	**1.23**	0.040	0.034	**0.037**	**8.10**	2.95	2.90	**2.93**	**0.026**	1.64	1.65	**1.65**	0.042	0.042	0.045	**0.043**	7.55	7.49	**7.52**
Sm	**2.24**	0.339	0.365	**0.352**	0.0081	0.0095	**0.0088**	**0.946**	1.29	1.27	**1.28**	**0.0063**	1.20	1.24	**1.22**	0.0093	0.0078	0.0071	**0.0080**	2.84	2.87	**2.86**
Eu	**0.682**	0.124	0.136	**0.130**	0.0025	0.0024	**0.0025**	**0.217**	0.450	0.452	**0.451**	**0.0017**	0.495	0.495	**0.495**	0.0014	0.0017	0.0015	**0.0016**	0.778	0.777	**0.778**
Gd	**2.51**	0.434	0.450	**0.442**	0.0052	0.0055	**0.0053**	**0.476**	1.44	1.45	**1.45**	**0.0069**	1.91	1.93	**1.92**	0.0038	0.0034	0.0013	**0.0028**	2.10	2.08	**2.09**
Tb	**0.366**	0.062	0.065	**0.064**	0.0005	0.0008	**0.0006**	**0.034**	0.194	0.190	**0.192**	**0.0009**	0.248	0.259	**0.254**	0.0003	0.0004	bdl	**0.0003**	0.206	0.205	**0.206**
Dy	**2.42**	0.491	0.489	**0.490**	0.0048	0.0034	**0.0041**	**0.126**	1.21	1.24	**1.22**	**0.0047**	1.62	1.61	**1.62**	0.0007	0.0013	0.0029	**0.0016**	1.17	1.14	**1.15**
Ho	**0.518**	0.110	0.119	**0.115**	0.0005	0.0005	**0.0005**	**0.014**	0.230	0.230	**0.230**	**0.0006**	0.279	0.284	**0.282**	0.0002	bdl	bdl	**0.0002**	0.210	0.217	**0.214**
Er	**1.57**	0.361	0.422	**0.392**	0.0013	0.0006	**0.0010**	**0.032**	0.634	0.644	**0.639**	**0.0011**	0.668	0.677	**0.673**	0.0006	0.0007	0.0005	**0.0006**	0.582	0.588	**0.585**
Tm	**0.182**	0.061	0.066	**0.064**	0.0002	0.0002	**0.0002**	**0.0041**	0.088	0.091	**0.089**	**bdl**	0.073	0.077	**0.075**	bdl	bdl	bdl	**bdl**	0.076	0.077	**0.076**
Yb	**0.578**	0.611	0.634	**0.623**	0.0012	0.0014	**0.0013**	**0.015**	0.825	0.802	**0.814**	**bdl**	0.569	0.563	**0.566**	0.0006	0.0005	bdl	**0.0005**	0.623	0.637	**0.630**
Lu	**0.071**	0.130	0.134	**0.132**	0.0001	0.0001	**0.0001**	**0.0023**	0.165	0.155	**0.160**	**0.0004**	0.098	0.103	**0.100**	bdl	0.0001	0.0003	**0.0002**	0.109	0.113	**0.111**
Hf	**0.349**	0.185	0.184	**0.185**	0.0027	0.0023	**0.0025**	**0.155**	0.923	0.925	**0.924**	**0.0030**	1.24	1.26	**1.25**	0.0015	0.0020	bdl	**0.0017**	1.01	1.05	**1.03**
Ta	**0.076**	0.098	0.109	**0.103**	0.0048	0.0151	**0.0099**	**0.0037**	0.026	0.027	**0.027**	**0.0047**	0.034	0.034	**0.034**	0.060	0.056	0.091	**0.069**	0.487	0.491	**0.489**
W	**0.46**	bdl	0.025	**0.025**	0.0040	0.0111	**0.0076**	**0.021**	0.0034	bdl	**0.0034**	**bdl**	0.016	bdl	**0.016**	0.0007	0.0002	bdl	**0.0004**	0.005	0.036	**0.021**
Pb	**n.a.**	0.0085	bdl	**0.0085**	n.a.	n.a.	**n.a.**	**0.492**	0.012	bdl	**0.012**	**n.a.**	bdl	bdl	**bdl**	n.a.	n.a.	0.0077	**0.0077**	0.013	0.011	**0.012**
Th	**n.a.**	0.057	0.059	**0.058**	n.a.	n.a.	**n.a.**	**0.034**	0.034	0.034	**0.034**	**n.a.**	0.0038	0.0047	**0.0043**	n.a.	n.a.	0.0015	**0.0015**	0.077	0.074	**0.076**
U	**0.38**	0.050	0.052	**0.051**	0.0009	0.0026	**0.0017**	**0.0057**	0.064	0.062	**0.063**	**0.0006**	0.026	0.025	**0.026**	0.0005	0.0006	0.0007	**0.0006**	0.120	0.130	**0.125**

Table 4.4 *Major element composition of Finsch peridotites calculated from composition of mineral major elements and modal mineral abundance and normalized to 100%*

	Whole rock																	
	F-1	**F-2**	**F-3**	**F-4**	**F-5**	**F-6**	**F-7**	**F-8**	**F-9**	**F-10**	**F-11**	**F-12**	**F-13**	**F-14**	**F-15**	**F-16**	**695**	**882**
SiO_2	44.31	41.51	41.92	44.05	47.60	45.19	46.99	41.33	43.50	46.45	43.87	44.09	45.68	43.94	44.79	46.25	43.33	43.07
K_2O	<0.01	<0.01	<0.01	<0.01	0.01	0.01	<0.01	<0.01	<0.01	<0.01	<0.01	0.01	<0.01	<0.01	<0.01	<0.01	0.02	<0.01
Na_2O	0.09	0.03	0.05	0.05	0.05	0.11	0.03	0.03	0.03	0.10	0.06	0.12	0.16	0.03	0.11	0.15	0.01	0.01
CaO	1.05	0.19	0.41	0.66	0.66	1.52	0.53	0.29	0.26	0.99	0.56	1.15	1.88	0.46	1.58	1.82	0.31	0.18
MnO	0.14	0.11	0.10	0.13	0.11	0.13	0.12	0.11	0.11	0.12	0.13	0.11	0.14	0.12	0.13	0.12	0.12	0.10
MgO	43.57	50.10	50.05	45.93	43.76	43.30	44.06	49.88	47.61	42.64	45.97	44.62	40.69	46.51	43.14	41.76	48.07	49.68
Cr_2O_3	0.43	0.24	0.26	0.49	0.42	0.62	0.66	0.22	0.28	0.56	0.38	0.54	0.45	0.32	0.65	0.29	0.13	0.41
P_2O_5	0.01	0.01	<0.01	0.01	0.01	0.01	0.01	0.01	<0.01	0.01	0.01	0.01	0.01	0.01	0.01	0.01	<0.01	<0.01
FeO	7.79	6.95	6.22	7.32	6.06	7.16	5.83	7.24	7.51	6.67	7.80	6.54	7.70	7.61	6.66	6.99	7.48	5.99
Al_2O_3	2.26	0.48	0.65	1.02	1.04	1.63	1.48	0.51	0.36	2.13	0.86	1.45	2.95	0.65	2.63	2.29	0.27	0.32
TiO_2	0.06	0.01	0.01	0.02	0.01	0.03	0.02	0.03	0.02	0.04	0.03	1.10	0.09	0.02	0.03	0.01	0.01	<0.01
NiO	0.29	0.36	0.33	0.33	0.28	0.29	0.28	0.35	0.31	0.28	0.32	0.26	0.26	0.32	0.28	0.28	0.26	0.25
Total	100.0	100.0	100.0	100.0	100.0	100.0	100.0	100.0	100.0	100.0	100.0	100.0	100.0	100.0	100.0	100.0	100.0	100.0

Table 4.5 *Recalculated trace element compositions of Finsch peridotites (from the LA-ICP-MS)*

	Whole rock																	
Element	**F-1**	**F-2**	**F-3**	**F-4**	**F-5**	**F-6**	**F-7**	**F-8**	**F-9**	**F-10**	**F-11**	**F-12**	**F-13**	**F-14**	**F-15**	**F-16**	**695**	**882**
Li	1.48	1.05	1.45	1.61	1.16	1.11	0.796	1.21	1.52	1.84	1.49	1.07	1.77	1.52	1.02	1.64	n.a	n.a
B	1.33	1.31	0.708	1.51	1.30	1.71	1.45	1.17	1.17	0.897	n.a	n.a	n.a	n.a	n.a	n.a	0.120	0.063
Sc	8.50	5.04	4.74	9.13	5.45	10.2	8.69	4.99	3.87	10.5	6.62	8.73	20.8	5.97	14.0	9.79	1.64	3.35
Ti	363	45.0	101	141	42.6	182	60.6	120	143	348	195	6590	781	90.2	197	85.1	40.7	25.1
V	46.2	16.5	16.9	28.0	29.5	48.6	35.8	16.2	15.5	37.3	27.1	102	73.9	25.1	55.6	35.0	10.4	7.09
Co	130	131	126	133	109	118	106	135	125	115	128	108	115	139	109	113	12.2	7.28
Rb	0.006	0.009	0.010	0.018	0.041	0.014	0.009	0.010	0.008	0.041	0.003	0.009	0.019	0.018	0.027	0.031	n.a	n.a
Sr	1.92	0.12	1.74	0.13	1.46	6.04	0.28	0.87	0.12	2.86	1.77	8.93	5.38	0.375	5.96	6.60	1.50	0.101
Y	1.08	0.235	0.306	0.169	0.142	0.333	0.192	0.330	0.150	0.643	0.286	0.568	3.08	0.116	1.00	1.21	0.071	0.108
Zr	1.72	0.760	0.797	1.09	1.18	1.68	1.89	0.79	1.00	4.93	1.48	4.63	5.46	0.198	1.73	1.02	0.439	0.743
Nb	0.052	0.095	0.022	0.067	0.044	0.088	0.096	0.023	0.050	0.048	0.068	0.501	0.083	0.061	0.124	0.086	0.010	0.062
Cs	n.a	n.a	n.a	0.002	0.003	0.001	n.a	n.a	0.002	0.002	n.a	n.a	0.002	0.006	n.a	0.003	n.a	n.a
Ba	0.006	n.a	0.021	0.045	0.101	0.093	n.a	0.093	0.13	1.06	0.104	0.061	0.073	0.028	0.211	0.078	n.a	0.004
La	0.029	0.006	0.014	0.005	0.014	0.094	0.003	0.016	0.004	0.048	0.028	0.105	0.116	0.015	0.109	0.113	0.027	0.004
Ce	0.121	0.054	0.081	0.032	0.074	0.347	0.030	0.075	0.023	0.167	0.116	0.434	0.383	0.050	0.377	0.516	0.127	0.047
Pr	0.021	n.a	0.020	n.a	0.016	n.a	n.a	0.011	n.a	0.033	0.020	0.084	0.065	0.007	0.065	0.088	n.a	n.a
Nd	0.140	0.079	0.146	0.091	0.133	0.312	0.179	0.078	0.055	0.210	0.123	0.557	0.394	0.036	0.386	0.442	0.091	0.132
Sm	0.064	0.030	0.050	0.046	0.059	0.082	0.133	0.033	0.028	0.103	0.049	0.156	0.200	0.012	0.133	0.079	0.021	0.049
Eu	0.030	0.011	0.016	0.017	0.018	0.027	0.045	0.012	0.009	0.037	0.019	0.043	0.083	0.004	0.046	0.023	0.006	0.013
Gd	0.111	0.035	0.052	0.051	0.054	0.069	0.122	0.043	0.033	0.138	0.060	0.126	0.351	0.015	0.136	0.076	0.018	0.036
Tb	0.022	0.005	0.009	0.007	0.007	0.010	0.012	0.007	0.005	0.022	0.009	0.020	0.064	0.003	0.023	0.016	0.002	0.004
Dy	0.175	0.035	0.062	0.037	0.033	0.062	0.054	0.053	0.035	0.130	0.058	0.135	0.518	0.019	0.169	0.157	0.014	0.020
Ho	0.043	0.008	0.012	0.006	0.006	0.013	0.007	0.012	0.006	0.025	0.011	0.024	0.119	0.004	0.039	0.043	0.002	0.004
Er	0.135	0.028	0.033	0.018	0.013	0.040	0.013	0.037	0.015	0.065	0.030	0.053	0.370	0.014	0.122	0.150	0.007	0.010
Tm	0.022	0.004	0.004	0.003	0.002	0.006	n.a	0.005	0.002	0.009	0.004	0.006	0.057	0.003	0.020	0.024	0.001	0.001
Yb	0.169	0.033	0.030	0.023	0.013	0.050	0.013	0.042	0.012	0.069	0.036	0.035	0.426	0.022	0.157	0.193	0.008	0.011
Lu	0.025	0.006	0.005	0.005	0.002	0.009	0.002	0.007	0.002	0.011	0.006	0.005	0.067	0.004	0.026	0.031	0.002	0.002
Hf	0.049	0.021	0.024	0.029	0.030	0.040	0.045	0.022	0.026	0.121	0.034	0.233	0.153	0.006	0.050	0.021	0.011	0.018
Ta	0.005	0.011	0.002	0.009	0.006	0.011	0.013	0.002	0.002	0.005	0.005	0.036	0.011	0.004	0.011	0.010	0.002	0.015
Pb	0.227	0.045	0.195	0.056	0.147	0.229	0.048	0.039	0.018	0.773	0.153	0.163	0.052	0.039	0.162	0.041	0.004	0.001
Th	0.003	0.003	0.002	0.001	0.001	0.044	0.002	0.012	0.010	0.023	0.024	0.039	0.045	0.038	0.211	0.004	0.001	0.001
U	0.002	0.002	0.001	0.002	0.002	0.005	0.002	0.002	0.001	0.002	0.001	0.003	0.004	0.002	0.003	0.001	0.001	0.002

n.a. - not analysed in all important minerals

Table 4.6 *P-T calculations for Finsch peridotites*

Sample	F-1	F-2		F-3		F-4	F-5	F-6	F-7		F-8
T preset	1200	1150	1100	1100	1100	1150	1100	1200	1150	1100	1200
P preset	55	47	47	50	50	50	50	50	50	50	50
Type	grt hzb	grt dunite		grt dunite		grt hzb	grt hzb	grt hzb	grt hzb		grt dunite
Paragenesis	ol,opx,cpx,grt	ol,opx,grt		ol,opx,cpx,grt		ol,opx,cpx,grt	ol,opx,cpx,grt	ol,opx,cpx,grt	ol,opx,grt		ol,opx,cpx,grt
Comment		grt with Fe^{3+}		cpx core	cpx-rim				grt with Fe^{3+}		
Thermobarometers, calculated with preset temperature or pressure T (°C), p (Kbar)											
T [BKN]	1204			1178	1054	1164	1149	1199			1189
T [KB]Ca in ol-cpx	1202			1130	1118	1183	1162	1215			1148
T [Krogh]	1148			1085	1025	1127	1073	1118			1126
T [O'Neill]	1139	1191	1066	1096	1121	1116	1131	1149	1169	1109	1110
T [Harley]	1135	1108	1058	1082	1078	1069	1079	1094	1104	1067	1085
T [BK]grt-opx (Mg-Fe)	1310	1237	1285	1263	1270	1310	1293	1292	1248	1284	1285
T [EG]	1197			1137	1079	1152	1113	1157			1162
T [Ca-in-opx]	1160	1098	1098	1095	1095	1127	1109	1143	1037	1037	1118
T [Na-in-px]	1248			1168	1285	1198	1201	1245			1218
T [NTcpx]	1152			1098	1015	1127	1118	1157			1136
T [Canil]	1141		1094	1057		1123	1099	1124		1085	1091
T [Griffin]	1257		1167	1102		1222	1177	1224		1151	1161
T [OW]											
p [BKN]	57	49	47	48	50	51	50	53	52	49	56
p [KB]	55			46	54	44	40	47			60
p [NG]	56	53	51	51	53	54	52	54	56	54	57
p [NTcpx]	57			50	53	55	52	55			53
Thermobarometer combinations (solved iteratively) T (°C), p (Kbar)											
T [BKN/BKN]	1209			1184	1045	1169	1154	1207			1200
p [BKN/BKN]	57			53	45	52	53	54			56
T [BKN/KB]	1206			1200	1036	1154	1142	1191			1211
p [KB/BKN]	56			62	39	45	46	46			62
T [Krogh/BKN]	1136			1071	991	1126	1061	1106			1133
p [BKN/Krogh]	52			47	42	50	47	47			52
T [O'Neill/BKN]	1125	1214	1053	1085	1114	1112	1138	1148	1187	1108	1111
p [BKN/O'Neill]	52	53	44	47	48	49	52	50	54	50	50
T [Harley/BKN]	1106	1109	1034	1057	1045	1036	1062	1058	1098	1041	1071
p [BKN/Harley]	50	47	43	46	45	45	47	44	49	46	48
T [NTcpx]	1152			1097	1012	1136	1124	1165			1138
p [NTcpx]	55			49	48	54	53	54			51

T [BKN] - two-pyroxene- Brey and Köhler, 1990; T [KB] Ca in ol/cpx - Köhler and Brey, 1990; T [Krogh] – cpx/grt (Fe-Mg) - Krogh, 1988; T [O'Neill] – ol/grt (Fe-Mg) - O'Neill and Wood, 1979; T [Harley] opx/grt (Fe-Mg) - Harley, 1984; T [BK] - grt/opx (Mg-Fe) - Brey and Köhler, 1990; T [EG]-cpx/grt(Fe-Mg) – Ellis and Green, 1979; T [Ca-in-opx] - Brey and Köhler, 1990; T [Na-in-px] – Brey and Köhler, 1990; T [NTcpx] - Nimis and Taylor, 2000; T [Canil] -Ni in grt – Canil 1999; T [Griffin]] -Ni in grt – Griffin et al., 1989b; T [OW] – ol/sp (Fe-Mg) – O'Neill and Wall, 1987; p [BKN] – grt/opx - Brey and Köhler, 1990; p [KB] – Ca in ol - Köhler and Brey, 1990; p [NG] – grt/opx –Nickel and Green, 1985; p [NTcpx] - Nimis and Taylor, 2000.

Table 4.6 *(continued)*

Sample	F-9		F-10	F-11		F-12	F-13	F-14	F-15	F-16	F-22	F-23	
Tpreset	1150	1100	1100	1200	1200	1200	1200	1200	1200	1200	1100	1000	900
Ppreset	47	45	50	55	55	55	55	50	50	60	50	50	30
Type	grt hzb		grt hzb	grt hzb		grt hzb	grt lhz	grt hzb	grt lhz	grt lhz	grt hzb	sp per.	
Paragenesis	ol,opx,cpx,grt		ol,opx,cpx,grt	ol,opx,cpx,grt		ol,opx,cpx,grt	ol,opx,cpx,grt	ol,opx,cpx,grt	ol,opx,cpx,grt	ol,opx,cpx,grt	ol,opx,grt	ol,opx,sp	
Comment	grt with Fe^{3+}			cpx-rim	cpx-core								
Thermobarometers, calculated with preset temperature or pressure T (°C), p (Kbar)													
T [BKN]			1183	1237	1225	1190	1210	1179	1185	1210			
T [KB]Ca ol-cpx			1155	1195	1230	1179	1194	1161	1190	1204			
T [Krogh]			1102	1178	1164	1132	1155	1110	1088	1128			
T [O'Neill]	1147	1073	1096	1136	1136	1113	1179	1118	1124	1186	1082		
T [Harley]	1070	1025	1087	1119	1119	1085	1154	1087	1100	1183	1061		
T [BK]	1274	1294	1303	1336	1336	1336	1273	1302	1283	1301	1307		
T [EG]			1155	1206	1194	1170	1209	1136	1142	1192			
T [Ca-in-opx]	1095	1126	1099	1167	1167	1131	1170	1149	1109	1168	1103		
T [Na-in-px]			1185	1251	1253	1199	1253	1236	1201	1215			
T [NTcpx]			1111	1185	1173	1105	1146	1169	1141	1167			
T [Canil]		997	1096		1100	1084	1217	1172	1073	1079			
T [Griffin]		998	1172		1178	1150	1411	1320	1130	1141			
T [OW]												992	949
p [BKN]	48	48	47	53	53	59	57	57	55	59	50		
p [KB]			41	56	50	59	56	57	52	59			
p [NG]	56	55	49	55	55	60	56	58	56	59	52		
p [NTcpx]			48	56	55	56	57	57	53	52			
Thermobarometer combinations (solved iteratively) T (°C), p (Kbar)													
T [BKN/BKN]			1188	1239	1225	1198	1216	1191	1195	1210			
p [BKN/BKN]			52	56	55	59	58	56	55	60			
T [BKN/KB]			1199	1263	1222	1196	1220	1188	1183	1213			
p [KB/BKN]			58	67	54	58	60	55	49	62			
T [Krogh/BKN]			1084	1158	1138	1132	1147	1116	1076	1092			
p [BKN/Krogh]			46	50	49	55	53	52	47	52			
T [O'Neill/BKN]	1155	1080	1075	1102	1102	1105	1180	1128	1126	1179	1076		
p [BKN/O'Neill]	49	45	45	47	47	53	55	52	50	58	49		
T [Harley/BKN]	1054	1016	1048	1047	1047	1054	1140	1085	1087	1163	1039		
p [BKN/Harley]	44	43	44	43	43	50	53	50	48	57	46		
T [NTcpx]			1107	1186	1172	1099	1143	1183	1143	1145			
p [NTcpx]			48	55	54	52	54	57	51	50			

.

Table 4.6 *(continued)*

Sample	**F-24**	**F-25a**	**F-25b**	**F-25c**	**F-25d**	**F-26**	**865**	**554-XM46**	**556-XM48**	**882**	**695**
Tpreset	1100	1100	1200	1200	1100	1200	1150	1150	1150	1000	1200
Ppreset	50	50	55	60	50	55	60	65	55	45	55
Type	grt hzb	grt hzb	grt lhz	grt hzb	grt hzb	grt lhz	grt hzb	grt hzb	grt hzb	grt-sp dunite	grt hzb
Paragenesis	ol,opx,grt	ol,opx,grt	ol,opx,cpx,grt	ol,opx,cpx,grt	ol,opx,grt	ol,opx,cpx,grt	ol,opx,grt	ol,opx,grt	ol,opx,grt	ol,opx,grt	ol,opx,cpx,grt
Comment											
Thermobarometers, calculated with preset temperature or pressure T (°C), p (Kbar)											
T [BKN]			1233	1257		1225					1196
T [KB]Ca in ol-cpx			1211	1243		1188					1165
T [Krogh]			1140	1153		1139					1135
T [O'Neill]	1119	1071	1111	1143	1108	1150	1161	1145	1191	1049	1173
T [Harley]	1072	1050	1122	1156	1072	1124	1132	1123	1090	996	1082
T [BK]grt-opx (Mg-Fe)	1294	1344	1321	1330	1310	1304	1365	1399	1349	1320	1367
T [EG]			1190	1205		1191					1161
T [Ca-in-opx]	1107	1128	1157	1170	1099	1142	1139	1200	1209		1148
T [Na-in-px]			1238	1242		1212					1196
T [NTcpx]			1190	1204		1180					1150
T [Canil]											
T [Griffin]											
T [OW]											
p [BKN]	52	51	56	56	47	55	59	65	54	44	56
p [KB]			53	52		57					61
p [NG]	55	54	55	56	53	55	62	65	60	53	57
p [MC]	57	57	60	61	55	61	60	62	61	49	62
p [NTcpx]			53	50		52					55
Thermobarometer combinations (solved iteratively) T (°C), p (Kbar)											
T [BKN/BKN]			1241	1255		1229					1198
p [BKN/BKN]			59	59		57					56
T [BKN/KB]			1246	1265		1247					1214
p [KB/BKN]			61	64		66					64
T [Krogh/BKN]			1118	1105		1113					1116
p [BKN/Krogh]			50	49		49					51
T [O'Neill/BKN]	1134	1064	1080	1096	1096	1132	1176	1143	1148	1053	1169
p [BKN/O'Neill]	54	48	48	49	47	51	58	65	56	46	54
T [Harley/BKN]	1071	1028	1075	1079	1034	1074	1141	1104	1044	984	1024
p [BKN/Harley]	50	46	47	48	44	47	62	62	52	43	45
T [NTcpx]			1183	1180		1169					1144
p [NTcpx]			52	50		50					53

Table 4.7 *Fe^{2+} and Fe^{3+} composition of Finsch garnets (Mössbauer), and recalculated oxygen fugacity for Finsch peridotites*

sample	corrFe^{3+}/ΣFe	Fe^{3+}/ΣFe	errFe^{3+}/ΣFe	Fe^{2+}	Fe^{3+}	Δlogfo2
F-1	0.0739	0.0998	0.0082	0.412	0.033	-3.76
F-2	0.0612	0.0830	0.0046	0.346	0.023	-3.17
F-3	0.0586	0.0796	0.0019	0.322	0.020	-3.16
F-5	0.0584	0.0794	0.0022	0.355	0.022	-3.67
F-6	0.0660	0.0894	0.0027	0.394	0.028	-3.58
F-7	0.0508	0.0692	0.0013	0.347	0.019	-3.65
F-8	0.0622	0.0844	0.0029	0.361	0.024	-3.77
F-9	0.0736	0.0994	0.0026	0.379	0.030	-2.53
F-11	0.0675	0.0913	0.0016	0.408	0.029	-4.06
F-12	0.0595	0.0808	0.0048	0.372	0.024	-3.81
F-14	0.0785	0.1057	0.0027	0.391	0.033	-3.67
F-15	0.0559	0.0761	0.0109	0.363	0.021	-3.92
F-16	0.0521	0.0709	0.0030	0.400	0.022	-4.64
865	0.0431	0.0589	0.0045	0.345	0.016	-4.71
695	0.0616	0.0836	0.0024	0.377	0.025	-3.46

Table 5.1 *Lu-Hf and Sm-Nd isotope composition of Finsch peridotites*

	$^{176}Lu/^{177}Hf$	$^{176}Hf/^{177}Hf$	εHf	Lu (ID) ppm	Hf (ID) ppm	$^{147}Sm/^{144}Nd$	$^{143}Nd/^{144}Nd$	εNd	Sm (ID) ppm	Nd (ID) ppm
opx										
opx F-2	0.00160	0.282407	-12.9	0.0004	0.038	0.08001	0.51202	-12.0	0.030	0.23
opx F-7	0.00119	0.282586	-6.6	0.0002	0.021	0.10393	0.51227	-7.1	0.024	0.14
opx F-9	0.00147	0.282257	-18.2	0.0004	0.035	0.07781	0.51210	-10.5	0.033	0.26
opx F-11	0.00401	0.282695	-2.7	0.0004	0.014	0.09657	0.51236	-5.5	0.018	0.11
opx F-12	0.00175	0.281961	-28.7	0.0003	0.022	0.09669	0.51228	-6.9	0.026	0.16
opx 695-1	0.01414	0.282327	-15.7	0.0016	0.016	0.08001	0.51202	-12.0	0.023	0.17
opx 695-2	0.00284	0.282371	-14.2	0.0003	0.016	0.08035	0.51203	-11.8	0.022	0.17
opx 882	0.00293	0.282408	-12.9	0.0001	0.007	0.08881	0.51189	-14.7	0.014	0.09
cpx										
cpx F-6	0.00382	0.282976	7.2	0.003	0.12	0.08962	0.51245	-3.7	0.73	4.9
cpx F-8	0.00406	0.283717	33.4	0.006	0.22	0.09880	0.51259	-1.0	1.12	6.8
cpx F-11	0.00251	0.282873	3.6	0.003	0.19	0.11170	0.51252	-2.3	0.86	4.8
cpx F-12	0.00050	0.281566	-42.6	0.003	0.75	0.10592	0.51252	-2.3	2.07	11.8
cpx F-15	0.00513	0.283952	41.7	0.005	0.13	0.10153	0.51273	1.9	0.92	5.4
cpx F-16-1	0.01396	0.287679	173.5	0.010	0.10	0.08083	0.51240	-4.6	0.72	5.4
cpx F-16-2	0.01303	0.287304	160.3	0.010	0.11	0.07305	0.51224	-7.9	0.71	5.9
cpx 695	0.00251	0.282742	-1.1	0.003	0.16	0.07251	0.51219	-8.7	0.88	7.4
grt										
grt F-2	0.06312	0.283813	36.8	0.19	0.43	0.21250	0.51217	-9.2	0.90	2.56
grt F-6	0.03573	0.283101	11.6	0.15	0.61	0.33994	0.51265	0.1	0.66	1.29
grt F-7	0.00820	0.281934	-29.6	0.03	0.59	0.41418	0.51258	-1.0	1.64	2.39
grt F-8	0.05117	0.283987	43.0	0.26	0.72	0.37868	0.51287	4.5	0.89	1.55
grt F-9-1	0.00992	0.282132	-22.6	0.03	0.44	0.32459	0.51279	3.0	1.80	3.73
grt F-9-2	0.00985	0.282129	-22.7	0.13	1.88	0.29171	0.51279	3.1	1.79	3.72
grt F-11	0.02547	0.282939	5.9	0.16	0.89	0.39944	0.51275	2.3	0.88	1.34
grt F-12	0.00857	0.281576	-42.3	0.12	0.22	0.41082	0.51274	2.1	1.11	1.80
grt F-14	0.09853	0.284949	77.0	0.12	0.17	0.21853	0.51249	-2.8	0.26	0.72
grt F-15-1	0.07525	0.284197	50.4	0.24	0.45	0.37971	0.51298	6.6	0.64	1.02
grt F-15-2	0.07553	0.284220	51.2	0.04	0.47	0.36921	0.51296	6.2	0.62	1.02
grt F-16-1	0.27987	0.290410	270.1	0.40	0.11	0.29189	0.51242	-4.3	0.37	0.77
grt F-16-2	0.27548	0.290199	262.6	0.40	0.20	0.29184	0.51236	-5.4	0.37	0.77
grt 554	0.10233	0.284655	66.6	0.06	0.09	0.18568	0.51257	-1.4	0.35	1.13
grt 556	0.09550	0.284470	60.1	0.11	0.17	0.17966	0.51266	0.5	0.32	1.07
grt 695	0.02492	0.282842	2.5	0.13	0.75	0.26945	0.51233	-6.0	0.99	2.22
grt 865-1	0.01113	0.281968	-28.4	0.08	1.06	0.46278	0.51296	6.2	1.05	1.36
grt 865-2	0.01171	0.281990	-27.7	0.09	1.04	0.46173	0.51299	6.8	1.03	1.35
grt 882	0.01658	0.282546	-8.0	0.10	0.89	0.23380	0.51185	-15.3	2.50	6.47
rt										
rt F-12-1		0.281605	-41.3							
rt F-12-2		0.281565	-42.7							
WR										
WR F-6	0.02982	0.283078	10.8			0.13761	0.51249	-2.8		
WR F-8	0.04777	0.283968	42.3			0.23165	0.51272	1.6		
WR F-11	0.02389	0.282935	5.7			0.31079	0.51257	-1.4		
WR F-12 (rt)	0.00050	0.281599	-41.5							
WR F-12	0.00326	0.281569	-42.5			0.16996	0.51257	-1.4		
WR F-15	0.07229	0.284187	50.0			0.20809	0.51283	3.7		
WR F-16	0.13817	0.288688	209.2			0.08591	0.51224	-7.7		
WR 695	0.02264	0.282835	2.2			0.14416	0.51225	-7.6		

„-1 and -2“ = repeated dissolution and measurement.

Table 6.1 Major element composition of olivine from polymict peridotite

	matrix olivine																				Porfir. ol from B and C		
No.	Ol-1	Ol-2	Ol-3	Ol-4	Ol-5	Ol-6	Ol-7	Ol-8	Ol-9	Ol-10	Ol-11	Ol-12	Ol-13	Ol-14	Ol-15	Ol-16	Ol-17	Ol-18	Ol-19	Ol-20	Ol-4-1	Ol-4-2	Ol-4-3
comm.	Ca in ol	Ca in ol	Ca in ol	Ca in ol	Ca in ol	Ca in ol	Ca in ol	Ca in ol	Ca in ol	Ca in ol	Ca in ol	Ca in ol	Ca in ol	Ca in ol	Ca in ol	Ca in ol	Ca in ol	Ca in ol	Ca in ol	Ca in ol	Ca in ol	Ca in ol	Ca in ol
SiO_2	41.07	41.02	40.89	40.48	40.61	40.47	40.92	40.87	40.78	40.98	40.84	40.71	40.78	40.65	40.87	40.65	40.92	40.54	40.67	40.80	41.13	41.23	41.20
TiO_2																							
Al_2O_3																							
FeO*	7.75	8.80	9.36	9.26	9.91	10.13	9.86	10.14	9.76	9.76	9.71	9.55	9.37	9.65	9.66	11.54	9.51	9.43	10.27	9.59	7.45	7.43	7.44
MnO	0.11	0.11	0.11	0.10	0.12	0.11	0.13	0.12	0.12	0.12	0.11	0.12	0.13	0.13	0.10	0.12	0.11	0.10	0.11	0.11	0.10	0.10	0.11
MgO	51.09	50.47	49.68	49.81	49.36	49.23	49.59	49.47	49.63	49.52	49.48	49.53	49.61	49.37	49.74	48.25	49.82	49.42	49.10	49.65	51.28	51.33	51.33
CaO	0.03	0.03	0.04	0.03	0.03	0.04	0.03	0.04	0.04	0.04	0.04	0.04	0.03	0.04	0.03	0.04	0.03	0.03	0.04	0.03	0.03	0.03	0.03
Na_2O																							
K_2O																							
Cr_2O_3																							
NiO	0.39	0.40	0.39	0.37	0.39	0.34	0.39	0.39	0.39	0.39	0.37	0.37	0.38	0.39	0.40	0.28	0.38	0.41	0.37	0.38	0.40	0.38	0.39
Total	100.44	100.84	100.47	100.06	100.42	100.31	100.92	101.02	100.71	100.80	100.55	100.31	100.30	100.22	100.80	100.87	100.77	99.93	100.56	100.56	100.38	100.50	100.51
4 O																							
Si	0.9942	0.9939	0.9966	0.9910	0.9934	0.9916	0.9954	0.9943	0.9937	0.9971	0.9961	0.9949	0.9959	0.9950	0.9944	0.9954	0.9955	0.9944	0.9945	0.9946	0.9950	0.9957	0.9953
Ti																							
Al																							
Fe^{tot}	0.1569	0.1783	0.1908	0.1896	0.2027	0.2076	0.2006	0.2063	0.1989	0.1986	0.1981	0.1952	0.1914	0.1975	0.1966	0.2363	0.1935	0.1934	0.2100	0.1955	0.1507	0.1501	0.1503
Mn	0.0022	0.0023	0.0023	0.0021	0.0024	0.0023	0.0028	0.0024	0.0025	0.0024	0.0022	0.0024	0.0027	0.0026	0.0020	0.0025	0.0022	0.0020	0.0022	0.0023	0.0019	0.0021	0.0023
Mg	1.8438	1.8231	1.8051	1.8178	1.7999	1.7983	1.7984	1.7941	1.8028	1.7962	1.7990	1.8045	1.8060	1.8015	1.8042	1.7614	1.8069	1.8072	1.7899	1.8047	1.8493	1.8480	1.8486
Ca	0.0009	0.0009	0.0009	0.0009	0.0009	0.0010	0.0008	0.0011	0.0009	0.0009	0.0009	0.0009	0.0009	0.0009	0.0009	0.0010	0.0009	0.0009	0.0009	0.0009	0.0008	0.0008	0.0009
Na																							
K																							
Cr																							
Ni	0.0077	0.0076	0.0078	0.0077	0.0073	0.0076	0.0066	0.0075	0.0076	0.0076	0.0076	0.0073	0.0073	0.0074	0.0076	0.0079	0.0054	0.0075	0.0080	0.0073	0.0074	0.0077	0.0074
Total	3.0058	3.0061	3.0034	3.0090	3.0066	3.0084	3.0046	3.0057	3.0063	3.0029	3.0039	3.0051	3.0041	3.0050	3.0056	3.0046	3.0045	3.0056	3.0055	3.0054	3.0050	3.0043	3.0047
Mg#	92.16	91.09	90.44	90.56	89.88	89.65	89.97	89.69	90.06	90.04	90.08	90.24	90.42	90.12	90.18	88.17	90.33	90.33	89.50	90.23	92.46	92.49	92.48
Fo	92.05	90.98	90.34	90.46	89.77	89.55	89.84	89.58	89.95	89.94	89.98	90.13	90.30	90.00	90.09	88.06	90.23	90.24	89.40	90.12	92.37	92.39	92.38
Fa	7.83	8.90	9.55	9.43	10.11	10.34	10.02	10.30	9.92	9.94	9.91	9.75	9.57	9.87	9.81	11.82	9.66	9.66	10.49	9.76	7.53	7.50	7.51

"Ca in ol" - longer measurement on Ca peak (see Chapter 2 for details);
* - Total Fe as FeO;
4 O - formula calculated on 4 oxygen;

Table 6.1 (contnued)

	Porfir. ol from B and C																					
No.	Ol-4-4	Ol-5-2	Ol-5-3	Ol-5-4	Ol-3-1	Ol-3-2	Ol-3-3	Ol-3-4	Ol-3-5	Ol-3-6	Ol-3-7	Ol-3-8	Ol-3-9	Ol-3-10	Ol-1-1	Ol-1-2	Ol-1-3	Ol-1-4	Ol-1-5	Ol-1-6	Ol-1-7	Ol-1-8
comm.	Ca in ol	Ca in ol	Ca in ol	Ca in ol	Ca in ol	Ca in ol	Ca in ol	Ca in ol	Ca in ol	Ca in ol	Ca in ol	Ca in ol	Ca in ol	Ca in ol	Ca in ol	Ca in ol	Ca in ol	Ca in ol	Ca in ol	Ca in ol	Ca in ol	Ca in ol
SiO_2	40.85	41.22	41.25	41.11	41.19	40.84	40.68	40.62	40.43	40.34	40.99	40.74	40.48	40.38	40.61	40.68	40.94	40.85	40.61	40.94	40.84	40.80
TiO_2																						
Al_2O_3																						
FeO*	7.76	7.08	6.98	7.09	7.03	10.80	10.82	10.89	10.74	10.89	10.72	10.64	10.55	10.52	10.73	9.04	9.10	9.07	9.05	9.02	9.01	8.94
MnO	0.09	0.10	0.08	0.08	0.09	0.11	0.11	0.14	0.12	0.13	0.11	0.11	0.14	0.11	0.12	0.12	0.12	0.12	0.10	0.11	0.11	0.12
MgO	50.96	51.71	51.38	51.59	51.56	49.03	48.73	48.80	48.60	48.49	49.15	48.98	48.63	48.37	48.75	50.07	50.23	50.26	49.93	50.19	50.00	49.86
CaO	0.03	0.02	0.02	0.02	0.02	0.08	0.08	0.08	0.08	0.08	0.07	0.07	0.08	0.07	0.08	0.07	0.06	0.06	0.05	0.06	0.05	0.06
Na_2O																						
K_2O																						
Cr_2O_3																						
NiO	0.40	0.41	0.42	0.41	0.41	0.36	0.35	0.36	0.36	0.36	0.38	0.39	0.38	0.39	0.37	0.38	0.36	0.37	0.37	0.38	0.36	0.39
Total	100.10	100.54	100.13	100.30	100.30	101.21	100.78	100.89	100.32	100.29	101.43	100.93	100.25	99.85	100.66	100.35	100.81	100.73	100.11	100.70	100.37	100.17
4 O																						
Si	0.9928	0.9940	0.9979	0.9937	0.9952	0.9942	0.9951	0.9932	0.9936	0.9926	0.9956	0.9944	0.9947	0.9962	0.9943	0.9920	0.9935	0.9923	0.9925	0.9943	0.9948	0.9960
Ti																						
Al																						
Fe^{tot}	0.1577	0.1428	0.1412	0.1433	0.1421	0.2199	0.2213	0.2227	0.2207	0.2241	0.2178	0.2172	0.2168	0.2170	0.2197	0.1844	0.1847	0.1843	0.1850	0.1832	0.1835	0.1825
Mn	0.0019	0.0020	0.0015	0.0016	0.0017	0.0022	0.0024	0.0030	0.0025	0.0026	0.0023	0.0024	0.0029	0.0024	0.0025	0.0024	0.0024	0.0024	0.0021	0.0023	0.0022	0.0025
Mg	1.8463	1.8589	1.8530	1.8590	1.8571	1.7794	1.7770	1.7788	1.7805	1.7787	1.7797	1.7822	1.7814	1.7789	1.7794	1.8202	1.8171	1.8201	1.8192	1.8172	1.8157	1.8145
Ca	0.0009	0.0006	0.0006	0.0006	0.0006	0.0020	0.0021	0.0021	0.0020	0.0022	0.0019	0.0019	0.0020	0.0019	0.0020	0.0018	0.0015	0.0014	0.0014	0.0015	0.0014	0.0015
Na																						
K																						
Cr																						
Ni	0.0077	0.0077	0.0079	0.0082	0.0080	0.0080	0.0070	0.0069	0.0071	0.0071	0.0071	0.0075	0.0076	0.0075	0.0077	0.0073	0.0074	0.0070	0.0073	0.0071	0.0074	0.0070
Total	3.0072	3.0060	3.0021	3.0063	3.0048	3.0058	3.0049	3.0068	3.0064	3.0074	3.0044	3.0056	3.0053	3.0038	3.0057	3.0080	3.0065	3.0077	3.0075	3.0057	3.0052	3.0040
Mg#	92.13	92.87	92.92	92.84	92.89	89.00	88.92	88.87	88.97	88.81	89.10	89.14	89.15	89.13	89.01	90.80	90.77	90.81	90.77	90.84	90.82	90.86
Fo	92.04	92.77	92.85	92.77	92.81	88.90	88.82	88.74	88.86	88.69	88.99	89.03	89.02	89.02	88.90	90.69	90.66	90.70	90.67	90.74	90.72	90.75
Fa	7.86	7.13	7.08	7.15	7.10	10.99	11.06	11.11	11.02	11.17	10.89	10.85	10.83	10.86	10.98	9.19	9.21	9.18	9.22	9.15	9.17	9.13

Table 6.1 (contnued)

	Porfir. ol from B and C								
No.	Ol-2-1	Ol-2-2	Ol-8-1	Ol-9-1	Ol-10-1	Ol-11-1	Ol-12-1	Ol-13-1	Ol-14-1
comm.	Ca in ol	Ca in ol							
SiO_2	41.12	40.73	40.59	41.11	40.43	39.99	40.35	40.05	40.21
TiO_2			0.01	0.02	0.02	0.02	0.03	0.02	0.02
Al_2O_3			0.01	0.02	0.02	0.01	0.02	0.02	0.02
FeO*	8.92	9.03	7.31	6.98	9.73	11.52	8.45	9.98	9.29
MnO	0.11	0.10	0.09	0.10	0.13	0.13	0.11	0.10	0.08
MgO	50.40	49.78	50.50	51.22	49.04	47.68	50.43	49.19	49.54
CaO	0.06	0.06	0.01	0.03	0.04	0.04	0.04	0.04	0.04
Na_2O			0.01	0.01	<0.01	0.01	0.02	0.02	0.01
K_2O			0.01	<0.01	<0.01	<0.01	<0.01	<0.01	<0.01
Cr_2O_3			0.03	0.06	0.03	0.02	0.04	0.04	0.03
NiO	0.38	0.39	0.46	0.40	0.37	0.47	0.39	0.43	0.41
Total	101.00	100.09	99.04	99.95	99.81	99.89	99.87	99.89	99.64
4 O									
Si	0.9951	0.9953	0.9953	0.9966	0.9941	0.9916	0.9869	0.9866	0.9892
Ti			0.0001	0.0003	0.0004	0.0004	0.0005	0.0004	0.0004
Al			0.0003	0.0004	0.0007	0.0002	0.0005	0.0005	0.0006
Fe^{tot}	0.1805	0.1845	0.1500	0.1416	0.2000	0.2389	0.1728	0.2056	0.1911
Mn	0.0023	0.0021	0.0019	0.0021	0.0027	0.0027	0.0023	0.0020	0.0017
Mg	1.8182	1.8135	1.8461	1.8511	1.7979	1.7627	1.8391	1.8064	1.8170
Ca	0.0017	0.0016	0.0003	0.0008	0.0011	0.0012	0.0011	0.0011	0.0009
Na			0.0006	0.0007		0.0003	0.0008	0.0009	0.0004
K			0.0003						
Cr			0.0006	0.0011	0.0005	0.0004	0.0007	0.0008	0.0005
Ni	0.0072	0.0075	0.0091	0.0079	0.0072	0.0093	0.0076	0.0085	0.0082
Total	3.0049	3.0047	3.0046	3.0026	3.0048	3.0077	3.0123	3.0128	3.0100
Mg#	90.97	90.76	92.49	92.90	89.99	88.07	91.41	89.78	90.48
Fo	90.86	90.67	92.40	92.80	89.87	87.95	91.31	89.69	90.41
Fa	9.02	9.23	7.51	7.10	10.00	11.92	8.58	10.21	9.51

Table 6.2 Major element composition of orthopyroxene from polymict peridotite

	In vein-like A																							
No.	1Opx-1	1Opx-2	1Opx-3	1Opx-4	1Opx-5	1Opx-6	1Opx-7	1Opx-8	1Opx-9	1Opx-10	1Opx-11	1Opx-12	1Opx-13	1Opx-14	1Opx-15	1Opx-16	1Opx-17	1Opx-18	1Opx-19	1Opx-20	1Opx-21	1Opx-22	1Opx-23	1Opx-24
comment																								
SiO_2	56.24	56.96	56.33	55.09	56.10	56.44	55.85	56.11	55.39	55.06	55.29	55.65	55.72	55.64	56.48	55.58	55.13	56.51	55.74	56.37	55.67	57.91	57.60	57.72
TiO_2	0.26	0.18	0.28	0.32	0.29	0.28	0.30	0.29	0.32	0.36	0.30	0.24	0.25	0.34	0.21	0.33	0.32	0.23	0.31	0.22	0.31	0.22	0.26	0.26
Al_2O_3	1.51	1.73	1.78	2.87	2.46	1.76	2.96	2.46	3.21	3.00	2.33	2.25	2.15	2.44	1.73	2.81	2.45	1.81	2.75	1.92	2.69	1.05	1.22	1.20
Cr_2O_3	0.75	0.70	0.80	1.29	1.10	0.75	0.85	0.74	1.01	0.89	0.73	0.71	0.81	0.81	0.75	1.35	0.98	0.61	1.32	0.62	0.67	0.30	0.43	0.49
FeO*	6.64	6.38	6.44	6.82	6.86	7.05	6.90	7.30	6.69	6.88	6.97	6.99	7.06	7.03	6.81	6.61	6.97	6.99	6.85	7.04	7.09	7.12	7.07	6.86
MnO	0.12	0.15	0.15	0.16	0.17	0.15	0.14	0.14	0.14	0.16	0.16	0.18	0.13	0.15	0.20	0.12	0.15	0.08	0.13	0.14	0.14	0.13	0.15	0.15
NiO	0.08	0.09	0.07	0.09	0.06	0.06	0.06	0.08	0.08	0.07	0.07	0.07	0.06	0.05	0.06	0.11	0.07	0.06	0.08	0.07	0.06	0.07	0.05	0.04
MgO	33.36	33.93	32.42	31.86	32.49	32.90	32.72	32.62	32.48	32.34	32.99	33.21	33.27	32.92	33.21	32.12	32.15	33.40	32.11	33.26	32.96	32.78	32.69	32.41
CaO	1.10	0.65	1.84	1.33	1.24	1.05	0.91	1.05	1.02	1.24	0.87	0.87	0.81	0.92	1.06	1.37	0.94	0.95	1.33	0.84	0.61	0.86	0.99	1.10
Na_2O	0.21	0.18	0.31	0.27	0.26	0.21	0.27	0.22	0.28	0.27	0.17	0.19	0.20	0.18	0.17	0.35	0.20	0.16	0.28	0.14	0.15	0.12	0.18	0.21
K_2O	0.01	<0.01	0.06	0.02	0.01	0.02	<0.01	<0.01	<0.01	0.03	<0.01	<0.01	<0.01	<0.01	0.01	0.01	0.24	<0.01	<0.01	<0.01	<0.01	<0.01	<0.01	<0.01
Total	100.30	100.94	100.48	100.11	101.04	100.66	100.97	101.00	100.64	100.29	99.88	100.35	100.46	100.48	100.70	100.76	99.60	100.80	100.89	100.63	100.36	100.57	100.65	100.43
6 O																								
Si	1.9470	1.9523	1.9491	1.9177	1.9319	1.9491	1.9217	1.9333	1.9129	1.9120	1.9252	1.9285	1.9292	1.9259	1.9480	1.9207	1.9286	1.9463	1.9241	1.9449	1.9265	1.9924	1.9827	1.9893
Ti	0.0067	0.0046	0.0072	0.0083	0.0074	0.0072	0.0079	0.0074	0.0084	0.0095	0.0079	0.0063	0.0065	0.0088	0.0055	0.0085	0.0084	0.0058	0.0079	0.0058	0.0082	0.0057	0.0067	0.0067
Al	0.0617	0.0697	0.0727	0.1178	0.0999	0.0714	0.1200	0.0999	0.1307	0.1228	0.0958	0.0917	0.0877	0.0995	0.0704	0.1146	0.1009	0.0735	0.1118	0.0782	0.1097	0.0427	0.0496	0.0486
Cr	0.0206	0.0188	0.0218	0.0356	0.0301	0.0203	0.0230	0.0201	0.0275	0.0243	0.0202	0.0194	0.0221	0.0223	0.0205	0.0370	0.0270	0.0167	0.0359	0.0170	0.0184	0.0081	0.0118	0.0132
Fe^{tot}	0.1922	0.1829	0.1864	0.1986	0.1976	0.2036	0.1986	0.2104	0.1932	0.1998	0.2028	0.2027	0.2045	0.2035	0.1964	0.1909	0.2040	0.2012	0.1978	0.2032	0.2053	0.2048	0.2036	0.1978
Mn	0.0035	0.0042	0.0043	0.0047	0.0050	0.0043	0.0040	0.0040	0.0040	0.0047	0.0046	0.0052	0.0039	0.0043	0.0060	0.0035	0.0044	0.0023	0.0039	0.0040	0.0041	0.0038	0.0045	0.0044
Ni	0.0021	0.0025	0.0019	0.0025	0.0016	0.0017	0.0016	0.0021	0.0023	0.0019	0.0019	0.0020	0.0017	0.0014	0.0017	0.0029	0.0020	0.0018	0.0021	0.0020	0.0017	0.0019	0.0013	0.0010
Mg	1.7216	1.7336	1.6723	1.6533	1.6678	1.6937	1.6783	1.6755	1.6721	1.6741	1.7119	1.7152	1.7168	1.6987	1.7073	1.6542	1.6765	1.7145	1.6521	1.7107	1.6998	1.6812	1.6771	1.6646
Ca	0.0409	0.0240	0.0682	0.0495	0.0458	0.0388	0.0336	0.0387	0.0377	0.0460	0.0326	0.0324	0.0299	0.0343	0.0393	0.0508	0.0351	0.0351	0.0490	0.0312	0.0225	0.0318	0.0365	0.0405
Na	0.0139	0.0122	0.0207	0.0180	0.0174	0.0143	0.0178	0.0144	0.0184	0.0181	0.0116	0.0126	0.0137	0.0119	0.0117	0.0235	0.0136	0.0109	0.0190	0.0093	0.0102	0.0079	0.0123	0.0141
K	0.0006		0.0027	0.0007	0.0003	0.0008				0.0015					0.0003	0.0003	0.0105							
Total	4.0115	4.0049	4.0076	4.0066	4.0047	4.0054	4.0070	4.0061	4.0079	4.0147	4.0146	4.0160	4.0163	4.0104	4.0070	4.0069	4.0111	4.0083	4.0036	4.0063	4.0064	3.9804	3.9860	3.9803
Mg#	89.96	90.46	89.97	89.28	89.41	89.27	89.42	88.84	89.64	89.34	89.41	89.43	89.35	89.30	89.68	89.65	89.15	89.50	89.31	89.38	89.22	89.14	89.17	89.38
Ca#	2.32	1.37	3.92	2.91	2.67	2.24	1.96	2.26	2.20	2.67	1.87	1.86	1.71	1.98	2.25	2.98	2.05	2.00	2.88	1.79	1.31	1.86	2.13	2.37

* - Total Fe as FeO;

6 O - formula calculated on 6 oxygen;

Table 6.2 (continued)

	In vein-like A		opx from B and C																				
No.	1Opx-25	1Opx-26	opx A-1	Opx A-2	Opx A-3	Opx A-4	Opx A-5	Opx A-6	Opx A-7	Opx A-8	Opx A-9	opx B-1	opx B-2	opx B-3	opx B-4	opx B-5	opx B-6	opx B-7	opx B-8	opx B-9	opx B-10	opx C-1	opx C-2
comme	core	core	core	core	core	core	core	core	core	core	rim	core	core	core	core	core	core	rim	rim	rim	rim	core	core
SiO_2	56.86	57.66	57.97	58.03	57.93	57.85	57.84	57.30	58.16	58.54	57.30	57.60	57.66	57.52	57.99	57.81	58.51	56.70	56.85	56.67	58.08	58.11	58.11
TiO_2	0.22	0.24	<0.01	<0.01	0.02	<0.01	0.01	0.01	<0.01	0.05	0.22	0.03	0.04	0.02	0.03	0.02	0.02	0.21	0.05	0.18	0.03	<0.01	0.01
Al_2O_3	2.18	1.14	0.81	0.81	0.81	0.80	0.78	0.82	0.86	0.91	1.38	0.71	0.71	0.69	0.69	0.73	0.76	1.26	0.73	1.66	0.73	0.87	0.83
Cr_2O_3	0.40	0.29	0.41	0.43	0.45	0.42	0.47	0.42	0.48	0.51	0.49	0.38	0.39	0.36	0.40	0.38	0.37	0.52	0.36	0.54	0.39	0.32	0.30
FeO*	6.71	6.93	4.17	4.14	4.12	4.05	4.15	4.09	4.08	4.18	6.26	5.20	5.10	5.10	5.06	5.05	5.10	6.82	5.54	5.99	5.57	3.83	3.75
MnO	0.12	0.12	0.08	0.09	0.11	0.12	0.10	0.11	0.09	0.10	0.13	0.15	0.12	0.13	0.11	0.14	0.13	0.16	0.14	0.12	0.11	0.12	0.08
NiO	0.08	0.06	0.10	0.10	0.12	0.08	0.10	0.11	0.12	0.14	0.11	0.13	0.12	0.15	0.13	0.12	0.15	0.08	0.12	0.17	0.12	0.13	0.11
MgO	32.72	33.19	36.15	36.32	36.30	36.14	36.03	35.90	36.24	36.76	35.12	35.11	34.94	35.29	35.23	35.27	35.82	33.33	34.57	33.53	34.87	36.77	36.62
CaO	0.66	1.02	0.34	0.35	0.34	0.32	0.36	0.50	0.37	0.38	0.71	0.94	0.97	0.86	0.94	0.94	0.94	1.08	0.89	1.26	0.96	0.38	0.37
Na_2O	0.16	0.16	0.14	0.15	0.16	0.13	0.19	0.15	0.16	0.17	0.17	0.16	0.12	0.12	0.13	0.15	0.13	0.22	0.15	0.29	0.14	0.14	0.14
K_2O	<0.01	<0.01	<0.01	<0.01	<0.01	<0.01	<0.01	0.03	0.01	0.01	0.01	<0.01	<0.01	<0.01	<0.01	0.01	<0.01	<0.01	<0.01	<0.01	0.01	<0.01	<0.01
Total	100.12	100.81	100.16	100.42	100.34	99.91	100.04	99.44	100.58	101.76	101.91	100.41	100.20	100.24	100.71	100.61	101.94	100.37	99.40	100.41	100.99	100.67	100.32
6 O																							
Si	1.9630	1.9803	1.9777	1.9752	1.9737	1.9777	1.9765	1.9715	1.9760	1.9681	1.9459	1.9745	1.9784	1.9736	1.9792	1.9758	1.9736	1.9608	1.9720	1.9535	1.9808	1.9710	1.9757
Ti	0.0057	0.0062			0.0004		0.0003	0.0003		0.0013	0.0056	0.0008	0.0011	0.0004	0.0008	0.0005	0.0005	0.0053	0.0013	0.0046	0.0006		0.0003
Al	0.0885	0.0463	0.0325	0.0323	0.0325	0.0324	0.0313	0.0332	0.0344	0.0360	0.0553	0.0285	0.0285	0.0277	0.0278	0.0292	0.0304	0.0512	0.0299	0.0673	0.0293	0.0346	0.0333
Cr	0.0109	0.0079	0.0111	0.0115	0.0121	0.0113	0.0127	0.0113	0.0128	0.0135	0.0132	0.0103	0.0105	0.0099	0.0107	0.0103	0.0098	0.0143	0.0098	0.0147	0.0104	0.0086	0.0079
Fe^{tot}	0.1938	0.1991	0.1190	0.1179	0.1174	0.1158	0.1186	0.1177	0.1159	0.1175	0.1778	0.1491	0.1463	0.1464	0.1444	0.1443	0.1439	0.1972	0.1607	0.1727	0.1589	0.1086	0.1066
Mn	0.0036	0.0034	0.0023	0.0026	0.0030	0.0033	0.0029	0.0032	0.0026	0.0029	0.0038	0.0042	0.0034	0.0038	0.0033	0.0040	0.0038	0.0047	0.0041	0.0036	0.0031	0.0035	0.0023
Ni	0.0022	0.0016	0.0027	0.0027	0.0032	0.0022	0.0027	0.0030	0.0032	0.0037	0.0031	0.0036	0.0032	0.0041	0.0035	0.0033	0.0040	0.0022	0.0034	0.0047	0.0033	0.0036	0.0030
Mg	1.6838	1.6987	1.8384	1.8429	1.8436	1.8417	1.8353	1.8413	1.8354	1.8423	1.7779	1.7942	1.7871	1.8050	1.7925	1.7970	1.8011	1.7182	1.7876	1.7230	1.7727	1.8591	1.8560
Ca	0.0245	0.0375	0.0124	0.0129	0.0123	0.0119	0.0132	0.0182	0.0134	0.0138	0.0257	0.0347	0.0358	0.0315	0.0343	0.0344	0.0339	0.0399	0.0331	0.0464	0.0350	0.0138	0.0135
Na	0.0109	0.0106	0.0092	0.0101	0.0106	0.0086	0.0122	0.0098	0.0104	0.0113	0.0109	0.0107	0.0083	0.0079	0.0087	0.0097	0.0086	0.0144	0.0100	0.0193	0.0090	0.0093	0.0093
K								0.0014	0.0005	0.0003	0.0006					0.0004					0.0005		
Total	3.9871	3.9917	4.0053	4.0081	4.0088	4.0049	4.0057	4.0109	4.0046	4.0107	4.0198	4.0106	4.0026	4.0103	4.0052	4.0089	4.0096	4.0082	4.0119	4.0098	4.0036	4.0121	4.0079
Mg#	89.68	89.51	93.92	93.99	94.01	94.08	93.93	93.99	94.06	94.00	90.91	92.33	92.43	92.50	92.54	92.57	92.60	89.70	91.75	90.89	91.77	94.48	94.57
Ca#	1.44	2.16	0.67	0.70	0.66	0.64	0.71	0.98	0.72	0.74	1.42	1.90	1.96	1.72	1.88	1.88	1.85	2.27	1.82	2.62	1.94	0.74	0.72

Table 6.2 (continued)

	opx from B and C																						
No.	opx C-3	opx C-4	opx C-5	opx C-6	opx C-7	opx C-8	opx C-9	opx C-10	opx C-11	opx C-12	opx C-13	opx C-14	opx C-15	opx C-16	opx C-17	opx D-1	opx D-2	opx D-3	opx D-4	opx D-5	opx D-6	opx D-7	opx D-8
comme	core	core	core	core	core	core	core	rim	rim	rim	rim	rim	rim	rim	rim	core	core	core	core	core	rim	rim	rim
SiO_2	58.19	58.02	58.21	58.45	58.32	58.28	58.22	55.59	55.89	57.18	57.34	56.53	57.29	56.90	56.43	57.18	57.54	57.16	57.09	57.30	56.90	57.12	57.04
TiO_2	<0.01	0.01	0.01	<0.01	<0.01	<0.01	0.02	0.26	0.25	0.18	0.18	0.28	0.28	0.23	0.21	0.23	0.26	0.21	0.24	0.24	0.19	0.20	0.20
Al_2O_3	0.88	0.87	0.84	0.85	0.86	0.85	0.86	2.48	1.94	1.26	1.33	1.92	1.43	1.57	2.14	0.84	0.83	0.81	0.80	0.84	1.64	1.48	1.70
Cr_2O_3	0.32	0.33	0.31	0.29	0.26	0.28	0.34	0.73	0.65	0.37	0.42	0.66	0.31	0.45	0.84	0.09	0.09	0.09	0.09	0.09	0.82	0.48	0.47
FeO*	3.74	3.80	3.82	3.79	3.77	3.81	3.80	6.17	6.10	5.48	5.23	6.10	5.05	6.13	5.99	8.44	8.42	8.41	8.48	8.34	6.34	6.51	6.61
MnO	0.08	0.10	0.09	0.07	0.06	0.07	0.10	0.12	0.15	0.14	0.11	0.14	0.12	0.14	0.15	0.13	0.16	0.16	0.17	0.17	0.12	0.13	0.11
NiO	0.11	0.13	0.09	0.12	0.09	0.10	0.11	0.12	0.12	0.11	0.13	0.12	0.12	0.08	0.11	0.09	0.11	0.08	0.10	0.10	0.12	0.13	0.17
MgO	36.59	36.71	36.48	36.66	36.28	36.52	36.45	33.69	33.84	34.97	34.87	33.87	34.90	33.63	32.99	32.73	32.71	32.63	32.50	32.71	33.61	33.16	32.96
CaO	0.39	0.38	0.39	0.38	0.36	0.38	0.37	0.60	0.93	0.71	0.79	0.92	0.70	1.01	1.33	1.04	1.03	1.00	1.04	1.01	1.07	1.52	1.65
Na_2O	0.15	0.13	0.13	0.11	0.14	0.14	0.14	0.17	0.22	0.16	0.19	0.20	0.16	0.22	0.31	0.23	0.22	0.20	0.23	0.25	0.21	0.28	0.33
K_2O	<0.01	<0.01	<0.01	<0.01	<0.01	0.01	<0.01	0.01	<0.01	<0.01	0.01	<0.01	<0.01	<0.01	<0.01	<0.01	<0.01	<0.01	<0.01	<0.01	0.01	0.01	<0.01
Total	100.45	100.48	100.36	100.73	100.14	100.44	100.45	99.94	100.09	100.57	100.64	100.74	100.36	100.38	100.49	101.03	101.38	100.75	100.74	101.04	101.02	101.02	101.23
6 O																							
Si	1.9758	1.9712	1.9783	1.9784	1.9843	1.9788	1.9770	1.9255	1.9347	1.9588	1.9607	1.9420	1.9614	1.9594	1.9450	1.9747	1.9794	1.9788	1.9781	1.9778	1.9520	1.9614	1.9567
Ti	0.0000	0.0003	0.0003	0.0000	0.0000	0.0000	0.0004	0.0068	0.0064	0.0045	0.0047	0.0072	0.0072	0.0060	0.0053	0.0061	0.0066	0.0055	0.0064	0.0063	0.0048	0.0052	0.0052
Al	0.0353	0.0347	0.0336	0.0339	0.0346	0.0341	0.0346	0.1013	0.0792	0.0507	0.0536	0.0777	0.0577	0.0638	0.0869	0.0343	0.0337	0.0332	0.0328	0.0341	0.0662	0.0600	0.0686
Cr	0.0086	0.0088	0.0083	0.0077	0.0070	0.0075	0.0092	0.0201	0.0178	0.0101	0.0114	0.0179	0.0084	0.0122	0.0229	0.0025	0.0025	0.0023	0.0024	0.0025	0.0223	0.0130	0.0126
Fe^{tot}	0.1062	0.1080	0.1086	0.1073	0.1073	0.1082	0.1079	0.1787	0.1766	0.1570	0.1496	0.1753	0.1446	0.1765	0.1727	0.2438	0.2422	0.2435	0.2457	0.2407	0.1819	0.1870	0.1896
Mn	0.0022	0.0030	0.0025	0.0020	0.0018	0.0020	0.0030	0.0034	0.0045	0.0039	0.0033	0.0039	0.0035	0.0041	0.0044	0.0038	0.0046	0.0046	0.0050	0.0048	0.0034	0.0038	0.0031
Ni	0.0031	0.0034	0.0024	0.0032	0.0025	0.0028	0.0029	0.0034	0.0033	0.0031	0.0035	0.0032	0.0033	0.0022	0.0031	0.0024	0.0029	0.0023	0.0027	0.0027	0.0034	0.0036	0.0047
Mg	1.8520	1.8592	1.8481	1.8498	1.8401	1.8484	1.8451	1.7396	1.7462	1.7858	1.7774	1.7345	1.7812	1.7264	1.6951	1.6850	1.6774	1.6839	1.6786	1.6830	1.7188	1.6974	1.6854
Ca	0.0140	0.0138	0.0141	0.0138	0.0130	0.0137	0.0135	0.0222	0.0343	0.0262	0.0288	0.0337	0.0255	0.0373	0.0489	0.0383	0.0381	0.0371	0.0387	0.0374	0.0391	0.0559	0.0606
Na	0.0102	0.0088	0.0086	0.0074	0.0090	0.0093	0.0095	0.0112	0.0150	0.0106	0.0124	0.0133	0.0107	0.0145	0.0207	0.0157	0.0147	0.0135	0.0154	0.0164	0.0139	0.0189	0.0217
K						0.0004		0.0004			0.0004										0.0004	0.0003	
Total	4.0074	4.0112	4.0048	4.0035	3.9996	4.0052	4.0031	4.0126	4.0180	4.0107	4.0058	4.0087	4.0035	4.0024	4.0050	4.0066	4.0021	4.0047	4.0058	4.0057	4.0062	4.0065	4.0082
Mg#	94.58	94.51	94.45	94.52	94.49	94.47	94.48	90.68	90.82	91.92	92.24	90.82	92.49	90.72	90.75	87.36	87.38	87.37	87.23	87.49	90.43	90.08	89.89
Ca#	0.75	0.74	0.76	0.74	0.70	0.74	0.73	1.26	1.93	1.45	1.59	1.91	1.41	2.11	2.80	2.22	2.22	2.16	2.25	2.17	2.22	3.19	3.47

Table 6.2 (continued)

	opx from B and C																							
No.	opx D-9	opx E-1	opx E-2	opx E-3	opx E-4	opx E-5	opx F-1	opx F-2	opx F-3	opx F-4	opx G-1	opx G-2	opx G-3	opx G-4	opx H-1	opx H-2	opx H-3	opx H-4	opx I-1	opx I-3	opx I-4	opx I-2	opx I-5	opx I-6
comme	rim	core	core	core	core	rim	core	core	rim	rim	rim	rim	core	core	core	core	core	core	rim	rim	rim	core	core	core
SiO_2	57.17	57.98	58.36	58.36	58.02	57.16	58.54	58.14	56.52	57.21	56.52	57.21	58.54	58.14	57.08	57.25	57.15	57.50	56.90	56.75	56.37	58.67	58.55	58.51
TiO_2	0.22	0.05	0.05	0.07	0.03	0.08	0.01	0.03	0.28	0.22	0.28	0.22	0.01	0.03	0.24	0.22	0.23	0.18	0.29	0.25	0.23	0.15	0.15	0.15
Al_2O_3	1.68	0.87	0.83	0.83	0.82	1.23	0.81	0.82	2.05	1.12	2.05	1.12	0.81	0.82	1.57	1.65	1.58	1.29	1.40	1.29	1.39	0.64	0.68	0.66
Cr_2O_3	0.47	0.39	0.37	0.40	0.35	0.53	0.33	0.29	0.84	0.37	0.84	0.37	0.33	0.29	0.76	0.78	0.67	0.63	0.30	0.27	0.24	0.35	0.39	0.43
FeO*	6.50	4.25	4.21	4.27	4.31	5.27	4.24	4.26	6.41	6.42	6.41	6.42	4.24	4.26	6.28	6.28	6.33	6.32	6.13	6.98	7.53	4.10	4.15	4.05
MnO	0.12	0.12	0.12	0.10	0.11	0.10	0.11	0.11	0.15	0.14	0.15	0.14	0.11	0.11	0.13	0.13	0.14	0.14	0.15	0.14	0.13	0.09	0.10	0.13
NiO	0.13	0.10	0.09	0.13	0.11	0.12	0.11	0.13	0.13	0.10	0.13	0.10	0.11	0.13	0.06	0.10	0.08	0.09	0.14	0.10	0.10	0.12	0.12	0.10
MgO	33.01	36.14	36.47	36.14	36.35	35.17	37.08	36.57	34.18	34.57	34.18	34.57	37.08	36.57	33.41	33.55	33.73	34.19	34.33	32.89	32.70	36.71	36.57	36.48
CaO	1.52	0.42	0.41	0.41	0.42	0.55	0.42	0.42	0.94	1.04	0.94	1.04	0.42	0.42	1.12	1.07	0.98	1.00	1.08	1.30	1.47	0.57	0.60	0.59
Na_2O	0.33	0.13	0.14	0.15	0.13	0.15	0.10	0.10	0.23	0.20	0.23	0.20	0.10	0.10	0.31	0.37	0.34	0.29	0.17	0.25	0.30	0.14	0.15	0.15
K_2O	<0.01	0.01	<0.01	<0.01	<0.01	0.01	<0.01	<0.01	0.01	<0.01	0.01	<0.01	<0.01	<0.01	<0.01	0.01	<0.01	<0.01	0.02	0.01	<0.01	0.01	<0.01	0.01
Total	101.14	100.45	101.07	100.84	100.67	100.37	101.75	100.89	101.76	101.40	101.76	101.40	101.75	100.89	100.95	101.40	101.25	101.62	100.91	100.24	100.45	101.56	101.45	101.27
6 O																								
Si	1.9603	1.9741	1.9743	1.9787	1.9721	1.9597	1.9681	1.9710	1.9279	1.9548	1.9279	1.9548	1.9681	1.9710	1.9581	1.9559	1.9548	1.9594	1.9513	1.9658	1.9559	1.9755	1.9743	1.9756
Ti	0.0056	0.0013	0.0011	0.0017	0.0007	0.0021	0.0003	0.0008	0.0071	0.0057	0.0071	0.0057	0.0003	0.0008	0.0062	0.0055	0.0060	0.0045	0.0074	0.0066	0.0060	0.0038	0.0037	0.0039
Al	0.0677	0.0348	0.0330	0.0330	0.0329	0.0497	0.0321	0.0328	0.0824	0.0452	0.0824	0.0452	0.0321	0.0328	0.0633	0.0663	0.0635	0.0517	0.0564	0.0526	0.0570	0.0253	0.0270	0.0264
Cr	0.0128	0.0104	0.0099	0.0107	0.0094	0.0144	0.0086	0.0077	0.0227	0.0101	0.0227	0.0101	0.0086	0.0077	0.0206	0.0211	0.0181	0.0169	0.0081	0.0073	0.0064	0.0094	0.0104	0.0115
Fe^{tot}	0.1864	0.1210	0.1191	0.1211	0.1225	0.1511	0.1192	0.1208	0.1829	0.1835	0.1829	0.1835	0.1192	0.1208	0.1802	0.1794	0.1811	0.1801	0.1758	0.2022	0.2185	0.1155	0.1170	0.1144
Mn	0.0034	0.0034	0.0035	0.0028	0.0032	0.0030	0.0031	0.0031	0.0042	0.0042	0.0042	0.0042	0.0031	0.0031	0.0038	0.0038	0.0040	0.0039	0.0042	0.0040	0.0037	0.0026	0.0028	0.0036
Ni	0.0035	0.0027	0.0024	0.0035	0.0031	0.0033	0.0029	0.0035	0.0035	0.0028	0.0035	0.0028	0.0029	0.0035	0.0016	0.0029	0.0023	0.0025	0.0039	0.0028	0.0029	0.0033	0.0032	0.0028
Mg	1.6873	1.8343	1.8391	1.8266	1.8418	1.7975	1.8584	1.8481	1.7380	1.7609	1.7380	1.7609	1.8584	1.8481	1.7085	1.7086	1.7198	1.7367	1.7549	1.6983	1.6914	1.8426	1.8383	1.8361
Ca	0.0558	0.0155	0.0149	0.0148	0.0154	0.0203	0.0150	0.0154	0.0345	0.0382	0.0345	0.0382	0.0150	0.0154	0.0412	0.0390	0.0360	0.0367	0.0398	0.0481	0.0547	0.0207	0.0215	0.0212
Na	0.0221	0.0084	0.0094	0.0096	0.0088	0.0100	0.0067	0.0068	0.0149	0.0130	0.0149	0.0130	0.0067	0.0068	0.0205	0.0246	0.0225	0.0188	0.0110	0.0171	0.0200	0.0090	0.0100	0.0096
K		0.0006	0.0000			0.0003			0.0006		0.0006					0.0004			0.0008	0.0004		0.0004		0.0003
Total	4.0049	4.0065	4.0067	4.0025	4.0099	4.0114	4.0144	4.0100	4.0187	4.0184	4.0194	4.0184	4.0146	4.0105	4.0041	4.0075	4.0087	4.0113	4.0142	4.0057	4.0164	4.0081	4.0083	4.0059
Mg#	90.05	93.81	93.92	93.78	93.76	92.25	93.97	93.86	90.48	90.56	90.48	90.56	93.97	93.86	90.46	90.50	90.47	90.60	90.89	89.36	88.56	94.10	94.02	94.13
Ca#	3.20	0.84	0.80	0.80	0.83	1.12	0.80	0.83	1.95	2.12	1.95	2.12	0.80	0.83	2.35	2.23	2.05	2.07	2.22	3.13	2.75	1.11	1.16	1.14

Table 6.2 (continued)

	opx from B and C																								
No.	opx K-1	opx K-2	opx K-3	opx L-1	opx L-2	opx L-3	opx6-1	opx6-2	opx6-3	opx6-4	opx6-5	opx6-6	opx6-7	opx6-8	opx6-9	opx6-10	opx6-11	opx6-12	opx6-13	opx6-14	opx8-1	opx8-2	opx9-1	opx9-2	opx9-3
comme	core	core	core	core	core	rim	core	core	core	core	core	core	core	core	core	core	core	core	core	rim	core	rim	core	rim	rim
SiO_2	57.15	57.44	57.61	56.92	57.09	57.63	57.80	57.61	57.49	57.71	57.58	57.14	57.62	57.72	57.50	57.31	57.25	57.16	57.32	57.07	56.08	55.77	56.68	56.96	55.30
TiO_2	0.16	0.18	0.19	0.22	0.20	0.23	0.14	0.14	0.16	0.15	0.15	0.15	0.16	0.15	0.16	0.15	0.15	0.16	0.15	0.16	0.22	0.22	0.20	0.25	0.20
Al_2O_3	1.34	1.35	1.31	1.23	1.35	1.31	1.08	1.07	1.12	1.06	1.12	1.12	1.08	1.11	1.09	1.13	1.09	1.11	1.16	1.08	1.37	1.89	0.90	0.97	2.42
Cr_2O_3	0.27	0.25	0.22	0.24	0.33	0.25	0.28	0.29	0.29	0.29	0.29	0.30	0.30	0.28	0.28	0.29	0.28	0.30	0.29	0.28	0.21	0.54	0.57	0.58	1.15
FeO*	6.23	6.44	6.43	7.69	7.77	7.59	5.31	5.37	5.23	5.29	5.42	5.31	5.28	5.34	5.37	5.36	5.29	5.33	5.27	5.46	7.40	6.43	4.43	4.69	6.24
MnO	0.12	0.11	0.13	0.14	0.14	0.12	0.12	0.09	0.12	0.15	0.13	0.13	0.10	0.14	0.15	0.14	0.10	0.12	0.11	0.13	0.12	0.12	0.13	0.13	0.16
NiO	0.14	0.16	0.12	0.11	0.14	0.17	0.15	0.13	0.15	0.16	0.13	0.13	0.16	0.14	0.15	0.15	0.12	0.15	0.16	0.08	0.12	0.13	0.12	0.12	0.13
MgO	33.50	33.40	33.48	33.30	32.70	33.98	33.56	33.61	33.86	33.56	33.68	33.62	33.52	33.78	33.82	33.81	33.72	33.78	33.75	33.87	32.53	33.51	35.16	35.04	32.69
CaO	1.66	1.70	1.67	0.98	1.40	0.89	1.45	1.50	1.52	1.48	1.52	1.44	1.46	1.44	1.46	1.47	1.45	1.51	1.50	1.47	1.27	0.73	0.80	0.83	1.35
Na_2O	0.30	0.34	0.35	0.24	0.30	0.18	0.25	0.27	0.29	0.29	0.27	0.29	0.25	0.26	0.27	0.26	0.26	0.24	0.26	0.24	0.27	0.17	0.30	0.29	0.29
K_2O	<0.01	<0.01	<0.01	<0.01	<0.01	<0.01	<0.01	<0.01	<0.01	<0.01	<0.01	<0.01	<0.01	<0.01	0.01	<0.01	<0.01	<0.01	<0.01	<0.01	<0.01	0.01	<0.01	<0.01	<0.01
Total	100.87	101.37	101.51	101.08	101.44	102.34	100.15	100.09	100.23	100.13	100.28	99.64	99.94	100.36	100.26	100.07	99.71	99.85	99.97	99.84	99.58	99.53	99.29	99.86	99.94
6 O																									
Si	1.9633	1.9649	1.9672	1.9603	1.9623	1.9582	1.9870	1.9830	1.9766	1.9852	1.9794	1.9767	1.9852	1.9813	1.9773	1.9748	1.9779	1.9738	1.9759	1.9720	1.9603	1.9417	1.9614	1.9616	1.9238
Ti	0.0040	0.0047	0.0048	0.0058	0.0053	0.0059	0.0036	0.0037	0.0041	0.0038	0.0038	0.0038	0.0042	0.0039	0.0041	0.0040	0.0038	0.0041	0.0038	0.0042	0.0058	0.0058	0.0053	0.0065	0.0053
Al	0.0542	0.0543	0.0526	0.0498	0.0546	0.0526	0.0436	0.0434	0.0455	0.0429	0.0454	0.0457	0.0440	0.0448	0.0442	0.0458	0.0446	0.0451	0.0471	0.0439	0.0563	0.0774	0.0366	0.0394	0.0992
Cr	0.0074	0.0067	0.0060	0.0064	0.0090	0.0067	0.0076	0.0079	0.0078	0.0079	0.0079	0.0082	0.0081	0.0077	0.0076	0.0078	0.0077	0.0081	0.0079	0.0076	0.0057	0.0149	0.0155	0.0159	0.0318
Fe^{tot}	0.1790	0.1842	0.1836	0.2215	0.2234	0.2157	0.1527	0.1547	0.1503	0.1522	0.1559	0.1535	0.1521	0.1532	0.1545	0.1544	0.1528	0.1539	0.1520	0.1578	0.2162	0.1873	0.1281	0.1351	0.1817
Mn	0.0036	0.0031	0.0036	0.0040	0.0041	0.0033	0.0035	0.0025	0.0035	0.0043	0.0036	0.0039	0.0030	0.0041	0.0045	0.0040	0.0028	0.0036	0.0031	0.0037	0.0035	0.0034	0.0037	0.0037	0.0046
Ni	0.0038	0.0044	0.0032	0.0031	0.0039	0.0045	0.0041	0.0035	0.0041	0.0043	0.0036	0.0035	0.0045	0.0038	0.0042	0.0042	0.0033	0.0041	0.0044	0.0023	0.0034	0.0037	0.0033	0.0032	0.0037
Mg	1.7155	1.7032	1.7042	1.7096	1.6755	1.7211	1.7197	1.7246	1.7349	1.7208	1.7256	1.7338	1.7215	1.7283	1.7335	1.7364	1.7366	1.7387	1.7343	1.7441	1.6948	1.7389	1.8135	1.7987	1.6952
Ca	0.0611	0.0623	0.0611	0.0363	0.0516	0.0326	0.0535	0.0553	0.0562	0.0546	0.0559	0.0536	0.0537	0.0529	0.0537	0.0543	0.0537	0.0559	0.0554	0.0544	0.0476	0.0273	0.0298	0.0307	0.0503
Na	0.0198	0.0225	0.0233	0.0163	0.0198	0.0115	0.0169	0.0181	0.0195	0.0190	0.0177	0.0198	0.0169	0.0172	0.0180	0.0175	0.0177	0.0163	0.0173	0.0163	0.0184	0.0113	0.0199	0.0193	0.0194
K															0.0003							0.0006			
Total	4.0117	4.0103	4.0096	4.0131	4.0095	4.0121	3.9922	3.9967	4.0025	3.9950	3.9990	4.0024	3.9930	3.9972	4.0019	4.0031	4.0010	4.0036	4.0014	4.0062	4.0121	4.0123	4.0172	4.0140	4.0150
Mg#	90.55	90.24	90.27	88.53	88.24	88.86	91.84	91.77	92.03	91.88	91.71	91.87	91.88	91.86	91.82	91.83	91.91	91.87	91.94	91.70	88.68	90.28	93.40	93.01	90.32
Ca#	3.44	3.53	3.46	2.08	2.99	1.86	3.02	3.11	3.14	3.08	3.14	3.00	3.03	2.97	3.00	3.03	3.00	3.11	3.10	3.02	2.73	1.55	1.61	1.68	2.88

Table 6.2 (continued)

	opx from B and C																							
No.	opx14-1	opx14-2	opx14-3	opx14-4	opx14-5	opx14-6	opx15-1	opx15-2	opx15-3	opx16-1	opx16-2	opx16-3	opx17-1	opx17-2	opx17-3	opx17-4	opx20-1	opx20-2	opx20-3	opx20-4	opx22-1	opx22-2	opx22-3	opx22-4
comme	core	core	core	core	core	core	core	core	rim	core	core	rim	core	core	core	rim	core	core	rim	rim	core	core	rim	rim
SiO_2	56.57	56.63	56.80	56.87	56.40	56.78	57.07	56.96	56.54	57.43	56.51	56.01	57.65	57.25	57.11	56.84	57.83	57.74	58.01	58.15	57.88	58.15	56.53	57.92
TiO_2	0.18	0.18	0.19	0.19	0.19	0.21	0.12	0.12	0.20	0.28	0.27	0.25	0.04	0.04	0.04	0.20	0.01	0.01	0.01	0.01	0.03	0.03	0.20	0.07
Al_2O_3	1.28	1.23	1.16	1.23	1.29	1.28	0.73	0.75	1.09	0.75	0.78	1.76	0.70	0.69	0.72	1.61	0.82	0.88	0.86	0.87	0.63	0.67	2.50	0.85
Cr_2O_3	0.15	0.14	0.15	0.16	0.14	0.15	0.22	0.23	0.26	0.38	0.37	0.52	0.41	0.41	0.42	0.35	0.35	0.35	0.33	0.33	0.46	0.43	1.15	0.38
FeO*	6.55	6.43	6.39	6.60	6.60	6.61	5.15	5.20	5.50	4.62	4.65	6.42	4.24	4.33	4.40	6.38	5.14	5.09	5.14	5.15	4.76	4.86	5.99	4.44
MnO	0.18	0.10	0.12	0.11	0.12	0.10	0.10	0.09	0.13	0.13	0.12	0.14	0.08	0.13	0.10	0.12	0.13	0.15	0.16	0.11	0.14	0.15	0.14	0.11
NiO	0.12	0.14	0.14	0.14	0.12	0.11	0.09	0.12	0.15	0.11	0.12	0.11	0.12	0.11	0.14	0.13	0.15	0.13	0.11	0.13	0.08	0.09	0.13	0.12
MgO	33.27	33.51	33.46	33.19	33.57	33.44	35.08	35.14	34.70	34.96	34.93	33.76	35.55	35.64	35.63	33.87	33.91	33.60	33.61	33.44	34.54	34.82	32.01	36.37
CaO	1.65	1.69	1.67	1.65	1.69	1.47	0.66	0.70	0.82	1.02	0.96	0.55	0.60	0.56	0.60	0.95	1.51	1.55	1.53	1.51	0.41	0.41	1.20	0.43
Na_2O	0.28	0.32	0.30	0.28	0.31	0.27	0.15	0.13	0.15	0.22	0.25	0.12	0.12	0.13	0.14	0.26	0.13	0.11	0.10	0.11	0.18	0.13	0.25	0.11
K_2O	<0.01	<0.01	0.01	0.01	0.01	0.01	<0.01	<0.01	<0.01	0.01	<0.01	<0.01	<0.01	<0.01	<0.01	<0.01	0.01	<0.01	<0.01	<0.01	<0.01	<0.01	<0.01	<0.01
Total	100.24	100.37	100.39	100.42	100.45	100.43	99.37	99.44	99.53	99.91	98.98	99.65	99.51	99.30	99.30	100.72	99.98	99.63	99.86	99.82	99.11	99.72	100.10	100.79
6 O																								
Si	1.9594	1.9583	1.9628	1.9654	1.9513	1.9611	1.9737	1.9702	1.9589	1.9744	1.9635	1.9456	1.9817	1.9747	1.9714	1.9539	1.9900	1.9931	1.9970	2.0014	1.9991	1.9965	1.9537	1.9680
Ti	0.0048	0.0047	0.0050	0.0050	0.0051	0.0056	0.0030	0.0030	0.0051	0.0073	0.0071	0.0066	0.0010	0.0011	0.0010	0.0051	0.0002	0.0003	0.0003	0.0002	0.0007	0.0007	0.0051	0.0017
Al	0.0521	0.0502	0.0473	0.0500	0.0527	0.0521	0.0300	0.0306	0.0444	0.0302	0.0319	0.0721	0.0284	0.0281	0.0292	0.0652	0.0334	0.0360	0.0348	0.0354	0.0257	0.0269	0.1017	0.0342
Cr	0.0042	0.0039	0.0041	0.0043	0.0039	0.0042	0.0061	0.0063	0.0071	0.0103	0.0102	0.0143	0.0111	0.0112	0.0114	0.0096	0.0095	0.0096	0.0090	0.0091	0.0125	0.0118	0.0314	0.0101
Fe^{tot}	0.1899	0.1859	0.1845	0.1906	0.1910	0.1910	0.1489	0.1504	0.1594	0.1328	0.1352	0.1865	0.1220	0.1250	0.1269	0.1834	0.1478	0.1470	0.1478	0.1482	0.1374	0.1394	0.1732	0.1262
Mn	0.0052	0.0030	0.0036	0.0033	0.0036	0.0029	0.0030	0.0025	0.0037	0.0038	0.0037	0.0042	0.0024	0.0038	0.0031	0.0035	0.0039	0.0044	0.0047	0.0033	0.0042	0.0043	0.0041	0.0030
Ni	0.0035	0.0039	0.0040	0.0038	0.0033	0.0030	0.0025	0.0034	0.0040	0.0030	0.0035	0.0030	0.0033	0.0031	0.0040	0.0036	0.0042	0.0036	0.0029	0.0036	0.0022	0.0025	0.0036	0.0032
Mg	1.7180	1.7268	1.7232	1.7094	1.7311	1.7216	1.8085	1.8114	1.7920	1.7913	1.8088	1.7480	1.8216	1.8326	1.8334	1.7354	1.7392	1.7287	1.7246	1.7153	1.7781	1.7819	1.6492	1.8422
Ca	0.0611	0.0627	0.0619	0.0611	0.0627	0.0545	0.0243	0.0259	0.0304	0.0374	0.0359	0.0203	0.0219	0.0207	0.0221	0.0352	0.0558	0.0572	0.0563	0.0558	0.0152	0.0149	0.0443	0.0157
Na	0.0188	0.0215	0.0201	0.0190	0.0208	0.0179	0.0102	0.0088	0.0103	0.0146	0.0172	0.0082	0.0080	0.0088	0.0096	0.0171	0.0085	0.0075	0.0069	0.0072	0.0122	0.0087	0.0170	0.0074
K			0.0002	0.0003	0.0003	0.0002				0.0004							0.0002							
Total	4.0170	4.0207	4.0167	4.0121	4.0258	4.0142	4.0103	4.0127	4.0154	4.0056	4.0169	4.0087	4.0015	4.0090	4.0121	4.0120	3.9927	3.9875	3.9844	3.9796	3.9872	3.9877	3.9832	4.0117
Mg#	90.05	90.28	90.33	89.97	90.06	90.01	92.39	92.33	91.83	93.10	93.04	90.36	93.72	93.61	93.53	90.44	92.17	92.16	92.11	92.05	92.83	92.74	90.50	93.59
Ca#	3.44	3.50	3.47	3.45	3.50	3.07	1.33	1.41	1.67	2.05	1.94	1.15	1.19	1.12	1.19	1.99	3.11	3.20	3.16	3.15	0.85	0.83	2.62	0.85

Table 6.2 (continued)

	opx from B and C									
No.	opx23-1	opx23-2	opx23-3	opx24-1	opx24-2	opx25-1	opx25-2	opx29-1	opx29-2	opx29-3
comme	core	core	core	core	core	core	core	core	core	core
SiO_2	56.96	56.52	56.88	57.39	57.19	58.17	58.59	57.87	57.58	57.89
TiO_2	0.18	0.18	0.18	0.29	0.28	0.08	0.05	0.19	0.19	0.19
Al_2O_3	1.36	1.28	1.28	0.85	0.87	0.52	0.60	1.52	1.47	1.52
Cr_2O_3	0.18	0.18	0.18	0.22	0.22	0.52	0.52	0.19	0.19	0.18
FeO*	6.35	6.27	6.37	5.71	5.88	3.06	3.14	6.61	6.48	6.71
MnO	0.13	0.11	0.12	0.14	0.13	0.11	0.11	0.12	0.09	0.13
NiO	0.12	0.13	0.13	0.12	0.14	0.08	0.11	0.15	0.11	0.11
MgO	32.29	32.45	32.23	33.27	33.42	36.06	36.02	32.21	32.04	32.12
CaO	1.48	1.53	1.50	1.04	1.08	0.52	0.46	1.54	1.50	1.46
Na_2O	0.35	0.37	0.36	0.27	0.27	0.15	0.16	0.50	0.46	0.46
K_2O	<0.01	<0.01	0.01	<0.01	<0.01	<0.01	<0.01	<0.01	<0.01	0.01
Total	99.41	99.01	99.23	99.29	99.47	99.28	99.77	100.89	100.12	100.76
6 O										
Si	1.9826	1.9764	1.9837	1.9912	1.9838	1.9925	1.9965	1.9862	1.9894	1.9887
Ti	0.0047	0.0047	0.0047	0.0075	0.0073	0.0020	0.0013	0.0048	0.0050	0.0048
Al	0.0556	0.0527	0.0528	0.0348	0.0355	0.0212	0.0241	0.0615	0.0598	0.0615
Cr	0.0050	0.0049	0.0050	0.0060	0.0060	0.0140	0.0140	0.0050	0.0052	0.0050
Fe^{tot}	0.1848	0.1834	0.1859	0.1656	0.1705	0.0875	0.0895	0.1898	0.1872	0.1928
Mn	0.0038	0.0031	0.0035	0.0040	0.0037	0.0033	0.0033	0.0035	0.0027	0.0037
Ni	0.0035	0.0038	0.0035	0.0033	0.0038	0.0023	0.0030	0.0040	0.0030	0.0030
Mg	1.6752	1.6914	1.6754	1.7207	1.7282	1.8410	1.8292	1.6477	1.6497	1.6450
Ca	0.0554	0.0573	0.0560	0.0387	0.0400	0.0192	0.0168	0.0565	0.0555	0.0536
Na	0.0237	0.0250	0.0241	0.0181	0.0184	0.0100	0.0106	0.0332	0.0310	0.0304
K			0.0004							0.0002
Total	3.9943	4.0026	3.9950	3.9899	3.9973	3.9930	3.9884	3.9922	3.9886	3.9886
Mg#	90.06	90.22	90.01	91.22	91.02	95.46	95.33	89.67	89.81	89.51
Ca#	3.20	3.28	3.23	2.20	2.26	1.03	0.91	3.31	3.26	3.16

Table 6.3 Major element composition of garnet, rutile and ilmenite from polymict peridotite

	vein like A - garnet												garnet from B and C												
No.	Agrt-1	Agrt-2	Agrt-3	Agrt-4	Agrt-5	Agrt-6	Agrt-7	Agrt-8	Agrt-9	Agrt-10	Agrt-11	Agrt-12	grt-1-1	grt-1-2	grt-1-3	grt-2-1	grt-2-2	grt-2-3	grt-2-4	grt-2-5	grt-2-6	grt-2-7	grt-3-1	grt-3-2	grt-3-3
comment													core	core	core	core	core	core	core	rim	rim	rim	core	core	core
SiO_2	41.66	41.95	41.89	41.88	41.58	42.25	41.66	42.39	42.16	42.17	42.36	42.48	41.98	41.88	42.34	42.42	42.41	41.80	41.50	41.50	42.10	41.47	41.82	41.70	41.36
TiO_2	1.31	0.63	0.68	1.33	1.00	0.84	0.63	0.87	0.82	0.66	0.89	0.75	0.63	0.59	0.59	0.56	1.31	0.50	0.88	0.76	0.84	0.93	0.57	0.97	1.34
Al_2O_3	22.56	23.19	23.17	22.08	22.71	22.18	21.88	21.93	20.61	21.04	22.20	22.43	21.51	22.27	23.63	21.10	22.64	22.12	23.05	22.52	23.21	23.13	21.72	22.16	21.80
Cr_2O_3	1.25	1.04	0.91	0.77	0.79	2.21	3.88	2.72	4.22	3.98	2.05	1.75	3.27	2.62	0.93	0.92	0.87	2.51	0.88	1.62	0.94	0.87	3.06	1.51	0.95
FeO*	8.40	8.59	8.49	9.04	8.73	8.37	8.07	8.06	8.24	8.23	8.41	8.46	8.04	8.06	6.90	6.80	7.70	7.86	7.83	8.01	8.09	8.11	8.03	8.12	7.84
MnO	0.32	0.29	0.27	0.32	0.33	0.28	0.35	0.27	0.29	0.30	0.32	0.31	0.30	0.32	0.25	0.39	0.29	0.32	0.32	0.31	0.29	0.25	0.33	0.36	0.30
NiO	0.02	0.02	0.01	0.02	0.01	0.01	0.01	0.01	0.01	<0.01	0.02	<0.01	<0.01	<0.01	0.03	0.01	<0.01	<0.01	<0.01	<0.01	0.01	<0.01	<0.01	0.02	0.01
MgO	21.44	21.25	21.44	21.45	21.19	21.63	20.58	21.97	20.85	21.21	21.09	21.72	21.82	21.66	23.76	26.09	22.84	21.79	22.44	21.95	22.63	22.60	21.84	21.40	23.75
CaO	3.20	3.47	3.52	3.67	3.77	2.98	3.82	3.03	3.91	3.33	3.53	3.20	2.92	3.24	1.74	1.92	2.75	3.02	2.50	2.85	2.19	2.03	2.89	3.52	2.37
Na_2O	0.06	0.06	0.07	0.07	0.06	0.08	0.05	0.07	0.05	0.08	0.09	0.06	0.08	0.08	0.05	0.04	0.07	0.02	0.06	0.08	0.09	0.06	0.05	0.12	0.11
K_2O	0.02	<0.01	<0.01	<0.01	<0.01	<0.01	<0.01	<0.01	<0.01	<0.01	<0.01	<0.01	<0.01	<0.01	<0.01	0.02	<0.01	<0.01	<0.01	<0.01	<0.01	<0.01	<0.01	<0.01	0.01
Total	100.24	100.50	100.45	100.63	100.17	100.82	100.95	101.31	101.15	101.00	100.97	101.16	100.54	100.73	100.22	100.26	100.89	99.94	99.45	99.61	100.39	99.45	100.32	99.89	99.85
O 12																									
Si	2.9508	2.9614	2.9575	2.9646	2.9524	2.9765	2.9505	2.9726	2.9857	2.9831	2.9835	2.9806	2.9717	2.9567	2.9578	2.9750	2.9659	2.9677	2.9448	2.9518	2.9582	2.9415	2.9656	2.9656	2.9321
Ti	0.0700	0.0337	0.0362	0.0707	0.0535	0.0443	0.0336	0.0456	0.0436	0.0351	0.0469	0.0393	0.0337	0.0314	0.0310	0.0296	0.0689	0.0266	0.0470	0.0408	0.0442	0.0497	0.0304	0.0519	0.0714
Al	1.8832	1.9296	1.9275	1.8418	1.9001	1.8413	1.8265	1.8126	1.7200	1.7544	1.8430	1.8553	1.7946	1.8531	1.9453	1.7443	1.8657	1.8507	1.9279	1.8879	1.9216	1.9338	1.8153	1.8572	1.8215
Cr	0.0699	0.0579	0.0508	0.0432	0.0442	0.1228	0.2174	0.1508	0.2361	0.2226	0.1144	0.0969	0.1829	0.1464	0.0514	0.0511	0.0482	0.1412	0.0492	0.0912	0.0525	0.0488	0.1715	0.0850	0.0534
Fe^{tot}	0.4974	0.5072	0.5014	0.5348	0.5182	0.4931	0.4782	0.4730	0.4882	0.4866	0.4955	0.4967	0.4758	0.4759	0.4033	0.3987	0.4504	0.4666	0.4644	0.4768	0.4756	0.4809	0.4763	0.4830	0.4650
Mn	0.0190	0.0175	0.0162	0.0191	0.0196	0.0165	0.0210	0.0158	0.0172	0.0180	0.0193	0.0186	0.0177	0.0189	0.0145	0.0231	0.0173	0.0191	0.0194	0.0189	0.0171	0.0150	0.0200	0.0217	0.0179
Ni	0.0010	0.0010	0.0003	0.0012	0.0006	0.0005	0.0005	0.0005	0.0007		0.0013				0.0019	0.0007					0.0006			0.0014	0.0008
Mg	2.2634	2.2360	2.2560	2.2635	2.2423	2.2717	2.1721	2.2963	2.2012	2.2363	2.2146	2.2715	2.3023	2.2792	2.4735	2.7275	2.3806	2.3062	2.3729	2.3277	2.3695	2.3889	2.3082	2.2689	2.5092
Ca	0.2431	0.2627	0.2664	0.2783	0.2865	0.2251	0.2901	0.2279	0.2966	0.2521	0.2661	0.2406	0.2216	0.2449	0.1306	0.1440	0.2063	0.2300	0.1902	0.2170	0.1651	0.1546	0.2195	0.2683	0.1798
Na	0.0085	0.0083	0.0097	0.0096	0.0087	0.0103	0.0065	0.0091	0.0065	0.0103	0.0124	0.0086	0.0108	0.0112	0.0068	0.0057	0.0094	0.0022	0.0076	0.0113	0.0124	0.0077	0.0075	0.0165	0.0150
K	0.0014															0.0017									0.0010
Total	8.0075	8.0152	8.0219	8.0269	8.0262	8.0023	7.9974	8.0044	7.9958	7.9984	7.9970	8.0082	8.0111	8.0177	8.0161	8.1012	8.0128	8.0110	8.0234	8.0233	8.0167	8.0214	8.0142	8.0197	8.0670
Mg#	81.98	81.51	81.82	80.89	81.23	82.16	81.96	82.92	81.85	82.13	81.72	82.06	82.87	82.73	85.98	87.25	84.09	83.17	83.63	83.00	83.28	83.24	82.89	82.45	84.37
Ca#	9.70	10.51	10.56	10.95	11.33	9.02	11.78	9.03	11.87	10.13	10.73	9.58	8.78	9.70	5.02	5.01	7.97	9.07	7.42	8.53	6.51	6.08	8.68	10.58	6.69
Cr#	3.58	2.91	2.57	2.29	2.27	6.25	10.64	7.68	12.07	11.26	5.84	4.96	9.25	7.32	2.57	2.85	2.52	7.09	2.49	4.61	2.66	2.46	8.63	4.38	2.85

* - Total Fe as FeO;

12, 3, 2 O - formula calculated on 12, 3, 2 oxygen;

Table 6.3 (continued)

	garnet from B and C																								
No.	grt-4-1	grt-4-2	grt-5-1	grt-5-2	grt-5-3	grt-6-1	grt-6-2	grt-6-3	grt-6-4	grt-7-1	grt-7-2	grt-7-3	grt-7-4	grt-8-1	grt-8-2	grt-8-3	grt-8-4	grt-8-5	grt-8-6	grt-8-7	grt-9-1	grt-9-2	grt-10-1	grt-10-2	grt-10-3
commer	core	core	core	core	rim	core	core	core	rim	core	core	core	rim	core	core	core	core	core	core	rim	core	core	core	core	core
SiO_2	41.75	42.21	41.26	40.85	41.25	41.21	41.02	41.77	40.55	41.38	41.28	41.31	41.37	40.32	40.44	41.19	40.83	40.55	41.10	40.62	41.59	41.19	41.63	41.64	41.63
TiO_2	0.59	0.99	0.67	0.62	0.47	0.56	0.56	0.56	0.91	0.93	0.71	0.94	0.65	0.07	0.06	0.06	0.06	0.06	0.05	0.05	0.92	0.76	0.01	0.01	0.01
Al_2O_3	21.96	23.17	22.64	22.89	22.85	21.62	22.01	21.90	19.72	22.69	21.77	22.48	21.14	19.03	19.02	19.22	19.26	19.16	19.02	19.09	22.94	22.91	20.52	20.47	20.54
Cr_2O_3	2.91	0.70	0.80	0.66	1.57	1.62	1.58	1.58	5.10	1.20	2.76	1.20	3.76	6.86	6.94	6.83	6.81	6.88	6.84	6.81	0.78	0.84	5.50	5.42	5.37
FeO*	7.49	6.69	10.62	10.93	9.03	7.92	8.02	7.92	7.59	9.09	8.03	8.85	8.34	6.75	6.85	6.89	6.85	6.89	7.02	6.78	8.34	8.42	6.37	6.15	6.29
MnO	0.28	0.19	0.32	0.34	0.31	0.22	0.25	0.26	0.32	0.31	0.32	0.29	0.32	0.39	0.35	0.37	0.39	0.40	0.36	0.38	0.28	0.29	0.35	0.27	0.30
NiO	0.01	0.05	0.02	0.01	<0.01	0.05	0.03	0.03	0.02	0.01	0.02	<0.01	<0.01	<0.01	<0.01	<0.01	<0.01	<0.01	0.01	<0.01	<0.01	0.03	<0.01	<0.01	0.01
MgO	22.67	23.81	19.83	19.60	21.08	22.00	22.17	22.19	20.43	22.05	22.09	21.55	21.47	19.80	19.95	19.69	19.65	19.63	19.82	19.71	22.68	22.11	20.88	20.84	20.62
CaO	2.38	2.15	4.40	4.37	3.69	3.71	3.65	3.66	5.29	3.27	3.29	3.25	3.39	5.95	5.99	6.16	6.07	6.22	6.00	6.12	2.69	2.61	5.46	5.44	5.43
Na_2O	0.02	0.03	0.10	0.09	0.07	0.14	0.10	0.12	0.06	0.07	0.05	0.04	0.05	0.03	0.03	0.01	0.02	0.01	0.02	0.01	0.07	0.09	0.03	<0.01	0.01
K_2O	<0.01	<0.01	<0.01	<0.01	<0.01	<0.01	<0.01	<0.01	<0.01	<0.01	<0.01	0.01	<0.01	<0.01	<0.01	<0.01	0.01	<0.01	<0.01	<0.01	<0.01	<0.01	<0.01	<0.01	<0.01
Total	100.06	99.99	100.66	100.37	100.31	99.04	99.40	99.99	99.97	101.00	100.32	99.91	100.50	99.22	99.65	100.42	99.94	99.80	100.26	99.57	100.30	99.26	100.75	100.24	100.21
O 12																									
Si	2.9551	2.9563	2.9462	2.9301	2.9340	2.9587	2.9358	2.9669	2.9283	2.9209	2.9332	2.9424	2.9463	2.9427	2.9402	2.9670	2.9557	2.9445	2.9677	2.9527	2.9355	2.9388	2.9615	2.9712	2.9729
Ti	0.0316	0.0523	0.0360	0.0333	0.0251	0.0302	0.0303	0.0301	0.0495	0.0494	0.0380	0.0504	0.0346	0.0036	0.0032	0.0033	0.0034	0.0032	0.0026	0.0028	0.0490	0.0410	0.0005	0.0005	0.0006
Al	1.8321	1.9124	1.9054	1.9349	1.9152	1.8290	1.8566	1.8329	1.6781	1.8874	1.8233	1.8867	1.7748	1.6370	1.6299	1.6320	1.6437	1.6395	1.6183	1.6356	1.9085	1.9265	1.7199	1.7215	1.7291
Cr	0.1626	0.0387	0.0450	0.0377	0.0881	0.0921	0.0895	0.0887	0.2909	0.0669	0.1548	0.0675	0.2119	0.3956	0.3989	0.3889	0.3900	0.3947	0.3905	0.3912	0.0436	0.0472	0.3094	0.3057	0.3031
Fe^{tot}	0.4433	0.3919	0.6343	0.6558	0.5371	0.4753	0.4799	0.4703	0.4581	0.5367	0.4772	0.5271	0.4970	0.4122	0.4164	0.4151	0.4145	0.4186	0.4241	0.4121	0.4920	0.5027	0.3791	0.3668	0.3757
Mn	0.0168	0.0112	0.0191	0.0204	0.0186	0.0133	0.0149	0.0159	0.0194	0.0186	0.0190	0.0173	0.0191	0.0241	0.0216	0.0228	0.0239	0.0247	0.0220	0.0232	0.0170	0.0176	0.0209	0.0166	0.0180
Ni	0.0006	0.0028	0.0013	0.0004		0.0031	0.0019	0.0015	0.0011	0.0003	0.0013								0.0007			0.0016			0.0004
Mg	2.3914	2.4859	2.1111	2.0954	2.2348	2.3538	2.3648	2.3488	2.1988	2.3201	2.3392	2.2874	2.2791	2.1541	2.1623	2.1139	2.1203	2.1252	2.1331	2.1359	2.3856	2.3518	2.2139	2.2165	2.1946
Ca	0.1808	0.1617	0.3370	0.3359	0.2812	0.2857	0.2799	0.2787	0.4092	0.2472	0.2501	0.2478	0.2590	0.4655	0.4668	0.4753	0.4708	0.4842	0.4644	0.4767	0.2035	0.1998	0.4158	0.4156	0.4153
Na	0.0033	0.0047	0.0133	0.0129	0.0094	0.0188	0.0141	0.0162	0.0081	0.0101	0.0069	0.0059	0.0074	0.0044	0.0046	0.0017	0.0026	0.0009	0.0031	0.0012	0.0089	0.0118	0.0045	0.0003	0.0012
K												0.0007					0.0005								
Total	8.0175	8.0181	8.0494	8.0567	8.0440	8.0599	8.0678	8.0504	8.0417	8.0575	8.0430	8.0333	8.0294	8.0396	8.0443	8.0200	8.0255	8.0355	8.0268	8.0317	8.0438	8.0393	8.0255	8.0147	8.0109
Mg#	84.36	86.38	76.90	76.16	80.62	83.20	83.13	83.32	82.76	81.21	83.06	81.27	82.10	83.94	83.85	83.59	83.65	83.54	83.41	83.83	82.90	82.39	85.38	85.80	85.38
Ca#	7.03	6.11	13.77	13.82	11.18	10.82	10.58	10.61	15.69	9.63	9.66	9.77	10.21	17.77	17.76	18.36	18.17	18.56	17.88	18.25	7.86	7.83	15.81	15.79	15.91
Cr#	8.15	1.98	2.31	1.91	4.40	4.80	4.60	4.62	14.77	3.42	7.83	3.45	10.67	19.46	19.66	19.24	19.18	19.40	19.44	19.30	2.23	2.39	15.25	15.08	14.92

Table 6.3 (continued)

	garnet from B and C																								
No.	grt-10-4	grt-10-5	grt-11-1	grt-11-2	grt-11-3	grt-11-4	grt-11-5	grt-11-6	grt-11-7	grt-11-8	grt-11-9	grt-11-1	grt-11-1	grt-11-1	grt-12-1	grt-12-2	grt-12-3	grt-12-4	grt-12-5	grt-12-6	grt-25-1	grt-25-2	grt-26-1	grt-26-2	grt-26-3
commer	rim	rim	core	core	core	core	core	core	core	core	core	core	rim	rim	core	core	core	core	core	rim	core	core	core	rim	core
SiO_2	41.76	41.68	41.20	41.28	41.43	41.14	42.19	42.19	42.05	41.90	42.02	42.24	42.70	42.48	42.59	42.51	42.70	42.39	42.75	42.41	42.25	42.39	41.87	41.92	42.63
TiO_2	<0.01	0.01	0.05	0.04	0.05	0.04	0.03	0.02	0.05	0.06	0.05	0.04	0.66	0.66	0.05	0.05	0.05	0.05	0.05	0.89	0.25	0.27	0.90	0.89	0.89
Al_2O_3	20.71	20.75	20.59	20.64	20.76	20.36	20.26	20.29	20.12	20.01	20.27	20.23	21.85	21.82	19.38	19.32	19.24	19.35	19.36	21.49	20.25	20.37	21.55	21.58	21.89
Cr_2O_3	5.47	5.45	4.87	4.92	5.07	5.21	4.83	4.94	5.16	5.23	4.84	4.75	2.78	2.53	7.45	7.46	7.48	7.48	7.42	2.72	4.75	4.78	0.90	0.89	0.89
FeO*	6.27	6.22	7.13	7.11	7.20	7.11	7.00	6.90	6.96	6.99	7.08	7.01	7.57	7.65	4.73	4.84	4.86	4.84	4.72	7.99	6.14	6.21	9.07	9.17	9.00
MnO	0.31	0.35	0.34	0.34	0.36	0.35	0.33	0.37	0.35	0.35	0.32	0.35	0.26	0.28	0.26	0.22	0.28	0.24	0.24	0.32	0.27	0.26	0.31	0.30	0.28
NiO	0.02	0.02	<0.01	<0.01	0.02	<0.01	0.01	0.03	0.01	<0.01	0.03	0.01	<0.01	0.04	<0.01	0.03	<0.01	0.01	0.01	0.02	0.03	0.02	0.03	<0.01	0.01
MgO	21.02	20.94	20.61	20.70	20.83	20.73	21.11	20.96	20.99	20.77	21.10	21.28	23.38	22.63	23.48	23.64	23.31	23.73	23.54	21.33	21.14	21.25	20.16	20.33	20.87
CaO	5.49	5.57	5.13	5.13	5.24	5.22	5.17	5.17	5.20	5.33	5.14	5.09	2.69	3.04	2.26	2.25	2.23	2.22	2.35	3.38	4.75	4.86	4.27	4.28	4.25
Na_2O	0.04	0.01	0.03	0.02	0.04	0.03	0.04	0.04	0.04	0.05	0.03	0.04	0.05	0.08	0.02	0.02	0.01	0.00	0.02	0.06	0.06	0.06	0.12	0.14	0.09
K_2O	<0.01	0.01	0.01	<0.01	<0.01	<0.01	<0.01	<0.01	<0.01	<0.01	<0.01	<0.01	<0.01	<0.01	0.01	<0.01	<0.01	<0.01	<0.01	0.01	<0.01	<0.01	<0.01	<0.01	<0.01
Total	101.08	101.02	99.98	100.21	100.98	100.19	101.02	100.94	101.03	100.75	100.97	101.09	101.97	101.22	100.25	100.34	100.16	100.32	100.45	100.63	99.90	100.47	99.19	99.52	100.80
O 12																									
Si	2.9586	2.9556	2.9572	2.9562	2.9473	2.9511	2.9929	2.9946	2.9875	2.9869	2.9854	2.9937	2.9678	2.9766	3.0068	3.0004	3.0175	2.9930	3.0109	2.9964	3.0115	3.0056	3.0108	3.0063	3.0112
Ti		0.0006	0.0025	0.0023	0.0025	0.0023	0.0017	0.0011	0.0027	0.0033	0.0027	0.0023	0.0347	0.0347	0.0028	0.0026	0.0026	0.0025	0.0026	0.0474	0.0136	0.0146	0.0488	0.0482	0.0470
Al	1.7288	1.7338	1.7423	1.7419	1.7405	1.7213	1.6939	1.6973	1.6847	1.6811	1.6973	1.6898	1.7899	1.8020	1.6121	1.6070	1.6028	1.6105	1.6069	1.7898	1.7011	1.7023	1.8263	1.8235	1.8228
Cr	0.3062	0.3056	0.2766	0.2788	0.2854	0.2954	0.2709	0.2772	0.2898	0.2948	0.2719	0.2662	0.1528	0.1402	0.4156	0.4164	0.4178	0.4177	0.4132	0.1522	0.2674	0.2677	0.0513	0.0505	0.0496
Fe^{tot}	0.3713	0.3690	0.4281	0.4260	0.4285	0.4264	0.4153	0.4096	0.4135	0.4167	0.4207	0.4155	0.4400	0.4483	0.2793	0.2856	0.2873	0.2859	0.2782	0.4720	0.3661	0.3685	0.5456	0.5499	0.5318
Mn	0.0186	0.0211	0.0207	0.0209	0.0216	0.0214	0.0201	0.0221	0.0213	0.0212	0.0193	0.0207	0.0151	0.0166	0.0157	0.0129	0.0168	0.0141	0.0142	0.0191	0.0163	0.0154	0.0187	0.0184	0.0167
Ni	0.0014	0.0011			0.0009		0.0004	0.0017	0.0007		0.0017	0.0004		0.0020		0.0015		0.0006	0.0007	0.0012	0.0017	0.0013	0.0017		0.0006
Mg	2.2195	2.2128	2.2055	2.2099	2.2084	2.2166	2.2324	2.2178	2.2231	2.2072	2.2348	2.2483	2.4225	2.3639	2.4709	2.4870	2.4549	2.4975	2.4712	2.2465	2.2462	2.2457	2.1608	2.1726	2.1976
Ca	0.4165	0.4228	0.3946	0.3937	0.3994	0.4015	0.3929	0.3932	0.3958	0.4071	0.3913	0.3865	0.2003	0.2282	0.1713	0.1704	0.1690	0.1681	0.1772	0.2562	0.3628	0.3693	0.3294	0.3286	0.3218
Na	0.0052	0.0020	0.0047	0.0026	0.0048	0.0039	0.0051	0.0051	0.0059	0.0064	0.0036	0.0051	0.0063	0.0103	0.0031	0.0024	0.0015	0.0004	0.0022	0.0079	0.0080	0.0084	0.0161	0.0199	0.0129
K		0.0009	0.0013												0.0007					0.0006					
Total	8.0262	8.0253	8.0336	8.0324	8.0395	8.0400	8.0256	8.0196	8.0251	8.0246	8.0286	8.0285	8.0294	8.0228	7.9784	7.9863	7.9701	7.9904	7.9775	7.9893	7.9947	7.9989	8.0096	8.0186	8.0120
Mg#	85.67	85.71	83.74	83.84	83.75	83.87	84.32	84.41	84.32	84.12	84.16	84.40	84.63	84.06	89.84	89.70	89.52	89.73	89.88	82.64	85.99	85.90	79.84	79.80	80.52
Ca#	15.80	16.04	15.18	15.12	15.32	15.33	14.97	15.06	15.11	15.57	14.90	14.67	7.64	8.80	6.48	6.41	6.44	6.31	6.69	10.24	13.91	14.12	13.23	13.14	12.77
Cr#	15.05	14.99	13.70	13.80	14.09	14.65	13.79	14.04	14.68	14.92	13.81	13.61	7.86	7.22	20.49	20.58	20.68	20.60	20.46	7.84	13.58	13.59	2.73	2.70	2.65

Table 6.3 (continued)

	garnet from B and C																											
No.	grt-26-4	grt-13-1	grt-13-2	grt-13-3	grt-13-4	grt-13-5	grt-13-6	grt-14-1	grt-14-2	grt-15-1	grt-15-2	grt-15-3	grt-16-1	grt-16-2	grt-16-3	grt-16-4	grt-16-5	grt-16-6	grt-17-1	grt-17-2	grt-17-3	grt-17-4	grt-18-1	grt-18-2	grt-18-3	grt-19-1
commer	core	core	core	core	core	rim	rim	core	core	core	core	rim	core	core	core	core	rim	rim	core	core	core	rim	core	core	rim	rim
SiO_2	42.58	42.42	42.56	42.63	42.59	41.93	42.01	42.11	42.29	41.66	41.60	42.00	41.78	41.87	42.19	42.02	42.43	42.73	42.03	42.03	42.09	42.01	42.43	42.10	41.98	42.52
TiO_2	0.82	0.35	0.35	0.34	0.37	0.72	0.72	0.11	0.11	0.90	0.85	0.89	0.01	0.02	0.01	0.06	0.59	0.61	0.08	0.07	0.07	0.08	0.22	0.36	0.55	0.66
Al_2O_3	21.87	19.86	19.81	19.89	19.98	21.83	21.94	20.99	21.13	21.90	21.91	21.70	20.96	20.92	21.03	20.78	21.35	21.72	20.69	20.61	20.80	20.72	19.95	19.81	19.50	20.24
Cr_2O_3	0.82	4.61	4.62	4.60	4.63	2.46	2.75	4.08	4.08	0.68	0.63	2.60	4.22	4.19	4.24	4.23	3.30	2.88	4.74	4.92	4.80	4.77	6.11	5.90	5.82	4.82
FeO*	9.16	6.61	6.64	6.81	7.20	7.89	7.69	7.15	7.06	10.04	9.89	7.95	7.08	7.03	7.13	7.18	7.80	7.77	6.49	6.44	6.49	6.50	6.17	6.14	6.16	7.65
MnO	0.29	0.31	0.27	0.24	0.24	0.26	0.31	0.35	0.39	0.28	0.26	0.28	0.37	0.33	0.38	0.40	0.30	0.32	0.35	0.31	0.33	0.32	0.33	0.31	0.31	0.28
NiO	0.01	<0.01	0.03	0.03	0.03	<0.01	0.03	<0.01	0.01	0.01	0.01	0.01	<0.01	<0.01	<0.01	<0.01	0.03	<0.01	0.04	<0.01	0.01	<0.01	<0.01	<0.01	0.02	<0.01
MgO	20.36	20.75	20.99	20.77	20.79	21.55	21.60	19.97	19.91	19.72	20.07	21.42	19.95	19.85	20.10	19.82	21.25	21.45	20.72	20.53	20.67	20.88	21.31	21.16	20.70	21.04
CaO	4.23	4.82	4.84	4.83	4.86	3.32	3.22	5.43	5.38	4.14	4.03	3.56	5.37	5.21	5.33	5.23	3.45	3.09	4.83	4.94	4.82	4.80	4.03	4.21	4.70	3.53
Na_2O	0.11	0.03	0.04	0.05	0.06	0.06	0.04	0.04	0.02	0.11	0.08	0.07	0.02	0.01	0.01	0.02	0.07	0.05	0.04	0.03	0.05	0.03	0.05	0.10	0.09	0.04
K_2O	<0.01	<0.01	<0.01	<0.01	<0.01	<0.01	<0.01	<0.01	<0.01	<0.01	<0.01	0.01	<0.01	<0.01	0.01	<0.01	0.01	<0.01	<0.01	0.01	<0.01	<0.01	<0.01	<0.01	<0.01	0.01
Total	100.25	99.77	100.16	100.21	100.74	100.02	100.30	100.23	100.39	99.46	99.32	100.49	99.75	99.43	100.44	99.74	100.60	100.62	100.02	99.88	100.14	100.11	100.60	100.10	99.84	100.77
O 12																										
Si	3.0248	3.0324	3.0317	3.0358	3.0234	2.9771	2.9732	3.0036	3.0094	2.9974	2.9934	2.9735	2.9954	3.0074	3.0029	3.0124	3.0011	3.0112	2.9979	3.0019	2.9976	2.9930	3.0079	3.0015	3.0060	3.0132
Ti	0.0436	0.0188	0.0185	0.0183	0.0197	0.0383	0.0382	0.0059	0.0061	0.0487	0.0461	0.0474	0.0007	0.0013	0.0006	0.0030	0.0316	0.0322	0.0043	0.0037	0.0039	0.0042	0.0119	0.0193	0.0296	0.0353
Al	1.8312	1.6729	1.6633	1.6696	1.6716	1.8268	1.8302	1.7648	1.7716	1.8571	1.8582	1.8107	1.7712	1.7712	1.7645	1.7558	1.7798	1.8037	1.7393	1.7347	1.7460	1.7401	1.6669	1.6647	1.6459	1.6902
Cr	0.0462	0.2606	0.2599	0.2588	0.2599	0.1381	0.1540	0.2303	0.2293	0.0387	0.0356	0.1455	0.2390	0.2377	0.2389	0.2400	0.1845	0.1604	0.2675	0.2779	0.2702	0.2684	0.3427	0.3328	0.3295	0.2699
Fe^{tot}	0.5442	0.3954	0.3958	0.4054	0.4274	0.4685	0.4551	0.4263	0.4202	0.6040	0.5949	0.4709	0.4246	0.4225	0.4242	0.4304	0.4614	0.4578	0.3871	0.3848	0.3863	0.3870	0.3656	0.3662	0.3689	0.4531
Mn	0.0174	0.0188	0.0162	0.0146	0.0145	0.0158	0.0183	0.0213	0.0236	0.0170	0.0159	0.0168	0.0224	0.0198	0.0229	0.0240	0.0181	0.0190	0.0214	0.0188	0.0197	0.0195	0.0198	0.0187	0.0190	0.0165
Ni	0.0007		0.0019	0.0017	0.0015		0.0016		0.0008	0.0007	0.0005	0.0007					0.0016	0.0001	0.0025	0.0000	0.0005	0.0000	0.0000	0.0000	0.0012	0.0000
Mg	2.1552	2.2112	2.2285	2.2049	2.1994	2.2811	2.2785	2.1231	2.1114	2.1149	2.1523	2.2604	2.1319	2.1252	2.1325	2.1181	2.2405	2.2531	2.2025	2.1857	2.1942	2.2176	2.2512	2.2487	2.2093	2.2219
Ca	0.3220	0.3695	0.3695	0.3687	0.3695	0.2523	0.2444	0.4148	0.4101	0.3192	0.3107	0.2700	0.4123	0.4010	0.4068	0.4014	0.2611	0.2336	0.3693	0.3778	0.3680	0.3667	0.3059	0.3216	0.3609	0.2677
Na	0.0149	0.0044	0.0053	0.0072	0.0079	0.0084	0.0053	0.0050	0.0023	0.0160	0.0114	0.0091	0.0022	0.0011	0.0018	0.0024	0.0097	0.0065	0.0049	0.0048	0.0074	0.0036	0.0065	0.0132	0.0128	0.0055
K												0.0006			0.0005		0.0011			0.0005						0.0012
Total	8.0002	7.9842	7.9907	7.9853	7.9949	8.0063	7.9989	7.9952	7.9851	8.0140	8.0193	8.0057	7.9998	7.9872	7.9958	7.9879	7.9905	7.9777	7.9967	7.9906	7.9939	8.0002	7.9784	7.9869	7.9830	7.9746
Mg#	79.84	84.83	84.92	84.47	83.73	82.96	83.35	83.28	83.40	77.78	78.35	82.76	83.39	83.41	83.41	83.11	82.92	83.11	85.05	85.03	85.03	85.14	86.03	85.99	85.69	83.06
Ca#	13.00	14.32	14.22	14.33	14.38	9.96	9.69	16.35	16.26	13.11	12.62	10.67	16.21	15.87	16.02	15.93	10.44	9.39	14.36	14.74	14.36	14.19	11.96	12.51	14.04	10.75
Cr#	2.46	13.48	13.51	13.42	13.46	7.03	7.76	11.54	11.46	2.04	1.88	7.44	11.89	11.83	11.92	12.02	9.39	8.17	13.33	13.81	13.40	13.36	17.05	16.66	16.68	13.77

Table 6.3 (continued)

	garnet from B and C																							
No.	grt-19-2	grt-19-3	grt-20-1	grt-20-2	grt-20-3	grt-20-4	grt-20-5	grt-20-6	grt-20-7	grt-20-8	grt-20-9	grt-20-10	grt-20-11	grt-20-12	grt-20-13	grt-20-14	grt-20-15	grt-20-16	grt-20-17	grt-20-18	grt-20-19	grt-20-20	grt-21-1	grt-21-2
commer	core	core	core	core	core	core	core	core	core	core	core	core	core	rim	rim	rim	rim	rim	rim	rim	rim	rim	core	core
SiO_2	42.26	42.37	41.93	41.91	41.44	41.78	42.80	42.56	42.44	42.60	42.08	42.35	42.36	41.77	42.30	42.25	42.27	41.78	42.05	41.89	42.02	41.78	41.30	41.29
TiO_2	0.14	0.14	0.01	0.01	0.01	<0.01	0.02	<0.01	0.01	<0.01	0.01	0.03	0.02	0.95	0.60	0.69	0.67	1.67	1.00	1.52	1.30	1.28	0.14	0.15
Al_2O_3	19.56	19.39	22.39	22.40	22.32	22.31	22.24	22.35	22.54	22.38	22.47	22.24	22.52	20.73	21.50	22.51	22.69	22.32	23.10	22.21	22.72	22.62	20.92	21.04
Cr_2O_3	6.09	6.04	3.17	3.22	3.23	3.22	3.17	3.15	3.21	3.13	3.07	3.04	3.07	3.25	3.23	1.90	1.82	0.76	0.85	0.76	0.68	0.72	4.62	4.63
FeO*	6.52	6.45	5.77	5.88	5.78	5.72	5.81	5.91	5.89	5.84	5.76	5.83	5.92	7.98	8.03	8.10	8.01	8.56	8.22	8.57	8.66	8.65	5.98	5.88
MnO	0.37	0.36	0.31	0.23	0.23	0.26	0.23	0.22	0.25	0.24	0.31	0.27	0.27	0.28	0.29	0.31	0.31	0.30	0.25	0.28	0.30	0.33	0.26	0.26
NiO	<0.01	0.01	<0.01	0.02	0.03	<0.01	<0.01	<0.01	0.01	0.01	<0.01	<0.01	<0.01	0.01	<0.01	0.01	0.01	0.01	0.02	0.01	0.04	0.04	0.01	0.02
MgO	20.06	20.45	22.32	22.19	22.34	22.27	21.99	21.82	22.12	22.06	22.03	21.73	22.18	21.17	22.07	22.21	22.29	22.17	21.91	21.93	21.89	21.94	21.94	21.68
CaO	5.06	5.11	4.18	4.10	4.19	4.13	4.25	4.32	4.32	4.42	4.40	4.47	4.44	3.67	2.38	2.42	2.40	2.96	2.92	2.92	2.84	2.66	4.61	4.56
Na_2O	0.06	0.02	0.00	0.02	0.01	0.02	0.02	0.01	0.02	0.01	0.02	0.03	0.03	0.02	0.03	0.06	0.00	0.07	0.09	0.07	0.03	0.05	0.03	0.04
K_2O	<0.01	<0.01	<0.01	<0.01	<0.01	<0.01	0.01	<0.01	0.01	<0.01	<0.01	<0.01	<0.01	0.01	<0.01	<0.01	<0.01	<0.01	<0.01	<0.01	<0.01	<0.01	<0.01	<0.01
Total	100.13	100.34	100.08	100.00	99.58	99.71	100.53	100.34	100.81	100.70	100.15	99.99	100.80	99.85	100.43	100.45	100.48	100.59	100.41	100.15	100.49	100.08	99.82	99.54
O 12																								
Si	3.0245	3.0252	2.9586	2.9604	2.9416	2.9583	3.0017	2.9926	2.9730	2.9857	2.9672	2.9898	2.9691	2.9853	2.9899	2.9757	2.9735	2.9466	2.9610	2.9652	2.9627	2.9585	2.9468	2.9514
Ti	0.0077	0.0074	0.0006	0.0005	0.0007		0.0009		0.0003		0.0006	0.0016	0.0009	0.0512	0.0319	0.0364	0.0354	0.0885	0.0529	0.0809	0.0688	0.0679	0.0075	0.0081
Al	1.6496	1.6315	1.8624	1.8649	1.8677	1.8617	1.8386	1.8519	1.8609	1.8489	1.8673	1.8503	1.8599	1.7461	1.7910	1.8685	1.8811	1.8557	1.9167	1.8528	1.8881	1.8873	1.7593	1.7724
Cr	0.3447	0.3407	0.1767	0.1797	0.1810	0.1803	0.1756	0.1750	0.1775	0.1732	0.1711	0.1696	0.1701	0.1836	0.1803	0.1056	0.1014	0.0426	0.0473	0.0424	0.0381	0.0404	0.2608	0.2616
Fe^{tot}	0.3901	0.3851	0.3407	0.3476	0.3434	0.3386	0.3406	0.3474	0.3448	0.3425	0.3397	0.3442	0.3467	0.4768	0.4744	0.4771	0.4712	0.5050	0.4842	0.5074	0.5107	0.5124	0.3565	0.3513
Mn	0.0226	0.0219	0.0184	0.0140	0.0136	0.0157	0.0136	0.0128	0.0146	0.0145	0.0183	0.0162	0.0160	0.0168	0.0176	0.0184	0.0187	0.0178	0.0147	0.0166	0.0181	0.0199	0.0156	0.0158
Ni		0.0006		0.0012	0.0014				0.0008	0.0006				0.0008		0.0008	0.0007	0.0003	0.0013	0.0008	0.0021	0.0022	0.0008	0.0011
Mg	2.1394	2.1766	2.3473	2.3366	2.3639	2.3504	2.2982	2.2873	2.3096	2.3047	2.3151	2.2862	2.3169	2.2553	2.3250	2.3320	2.3368	2.3309	2.2991	2.3143	2.3002	2.3158	2.3335	2.3098
Ca	0.3878	0.3907	0.3160	0.3103	0.3187	0.3135	0.3191	0.3256	0.3245	0.3323	0.3321	0.3384	0.3336	0.2812	0.1803	0.1823	0.1808	0.2235	0.2206	0.2212	0.2143	0.2021	0.3527	0.3492
Na	0.0081	0.0030	0.0003	0.0026	0.0016	0.0031	0.0030	0.0014	0.0025	0.0008	0.0024	0.0037	0.0037	0.0024	0.0037	0.0078	0.0004	0.0093	0.0123	0.0096	0.0046	0.0062	0.0038	0.0053
K							0.0007		0.0005					0.0005										
Total	7.9745	7.9827	8.0213	8.0179	8.0340	8.0219	7.9920	7.9943	8.0089	8.0033	8.0140	8.0005	8.0168	8.0000	7.9944	8.0046	7.9999	8.0203	8.0103	8.0110	8.0077	8.0127	8.0374	8.0261
Mg#	84.58	84.97	87.33	87.05	87.31	87.41	87.09	86.82	87.01	87.06	87.20	86.91	86.98	82.55	83.05	83.01	83.22	82.19	82.60	82.02	81.83	81.88	86.75	86.80
Ca#	15.35	15.22	11.87	11.72	11.88	11.77	12.19	12.46	12.32	12.60	12.55	12.90	12.59	11.09	7.20	7.25	7.18	8.75	8.75	8.72	8.52	8.03	13.13	13.13
Cr#	17.28	17.27	8.67	8.79	8.84	8.83	8.72	8.63	8.71	8.57	8.39	8.39	8.38	9.51	9.15	5.35	5.12	2.24	2.41	2.24	1.98	2.09	12.91	12.86

Table 6.3 (continued)

	garnet from B and C																							
No.	grt-21-3	grt-21-4	grt-21-5	grt-21-6	grt-21-7	grt-21-8	grt-21-9	grt-21-10	grt-21-11	grt-21-12	grt-21-13	grt-22-1	grt-22-2	grt-23-1	grt-23-2	grt-24-1	grt-24-2	grt-24-3	grt-24-4	grt-L27-1	grt-L27-2	grt-L27-3	grt-L27-4
commer	core	core	core	rim	rim	rim	rim	rim	rim	rim	rim	core	core	core	core	core	core	core	core	core	core	core	core
SiO_2	41.00	41.83	42.61	41.18	41.23	40.47	40.96	41.48	42.08	42.39	42.61	42.20	42.26	41.55	41.76	40.09	40.56	40.78	40.38	42.81	43.16	42.53	42.87
TiO_2	0.16	0.18	0.18	0.78	0.64	0.75	1.12	0.95	1.74	1.33	1.23	0.19	0.20	0.19	0.19	0.06	0.05	0.07	0.07	0.77	0.78	0.77	0.77
Al_2O_3	21.23	21.33	21.05	22.60	22.87	22.17	21.47	22.36	21.28	21.85	22.28	20.65	20.61	20.44	20.68	19.03	19.11	18.94	18.92	21.60	21.31	21.29	21.38
Cr_2O_3	4.41	4.23	4.09	1.22	1.25	1.45	1.16	1.65	1.01	1.02	0.77	4.82	4.83	4.84	4.85	7.02	7.04	6.96	6.99	1.81	1.82	1.81	1.84
FeO*	5.98	6.02	5.94	8.51	8.34	8.26	8.01	8.45	8.68	8.41	8.00	6.77	6.66	6.61	6.63	6.39	6.38	6.37	6.32	7.70	7.45	7.56	7.52
MnO	0.31	0.28	0.31	0.32	0.36	0.33	0.34	0.32	0.28	0.30	0.27	0.37	0.34	0.38	0.35	0.30	0.32	0.30	0.29	0.27	0.25	0.26	0.24
NiO	0.01	0.02	0.02	0.02	0.01	0.02	0.02	0.01	0.04	0.02	<0.01	0.02	<0.01	<0.01	<0.01	0.02	0.01	0.01	0.01	0.01	0.04	<0.01	0.03
MgO	22.00	21.74	22.27	21.78	21.78	21.50	20.58	21.80	22.57	22.31	23.18	20.23	20.22	20.61	20.42	21.82	21.91	21.56	21.32	21.48	21.45	21.58	21.53
CaO	4.62	4.66	4.50	3.23	3.34	4.09	4.83	3.08	2.95	3.07	2.39	5.49	5.52	5.55	5.49	4.47	4.56	4.57	4.54	4.36	4.32	4.25	4.31
Na_2O	0.02	0.06	0.05	0.07	0.05	0.10	0.18	0.04	0.10	0.08	0.06	0.03	0.04	0.04	0.01	0.02	0.02	0.02	0.01	0.08	0.09	0.08	0.09
K_2O	0.01	<0.01	<0.01	0.01	<0.01	0.06	0.06	0.01	<0.01	<0.01	<0.01	<0.01	<0.01	<0.01	0.01	<0.01	0.01	<0.01	<0.01	<0.01	<0.01	0.01	0.01
Total	99.75	100.35	101.02	99.74	99.86	99.21	98.75	100.15	100.81	100.82	100.82	100.77	100.68	100.21	100.39	99.24	99.96	99.58	98.85	100.89	100.68	100.13	100.57
O 12																							
Si	2.9277	2.9633	2.9920	2.9350	2.9327	2.9126	2.9606	2.9443	2.9670	2.9810	2.9810	2.9971	3.0021	2.9709	2.9774	2.9118	2.9232	2.9471	2.9406	3.0120	3.0378	3.0136	3.0225
Ti	0.0086	0.0095	0.0000	0.0420	0.0340	0.0406	0.0610	0.0508	0.0920	0.0704	0.0645	0.0099	0.0108	0.0102	0.0103	0.0035	0.0025	0.0036	0.0036	0.0407	0.0413	0.0410	0.0408
Al	1.7869	1.7806	0.0073	1.8988	1.9173	1.8799	1.8290	1.8702	1.7690	1.8110	1.8370	1.7288	1.7254	1.7228	1.7382	1.6290	1.6230	1.6132	1.6236	1.7911	1.7677	1.7780	1.7766
Cr	0.2491	0.2367	0.3380	0.0689	0.0702	0.0826	0.0664	0.0927	0.0563	0.0567	0.0425	0.2708	0.2713	0.2737	0.2735	0.4034	0.4012	0.3977	0.4021	0.1007	0.1013	0.1014	0.1026
Fe^{tot}	0.3572	0.3569	0.0183	0.5075	0.4960	0.4973	0.4844	0.5015	0.5120	0.4950	0.4680	0.4019	0.3954	0.3956	0.3951	0.3884	0.3847	0.3847	0.3850	0.4531	0.4385	0.4480	0.4434
Mn	0.0188	0.0171	2.3320	0.0195	0.0215	0.0201	0.0209	0.0195	0.0165	0.0176	0.0157	0.0221	0.0205	0.0229	0.0213	0.0187	0.0193	0.0186	0.0177	0.0161	0.0149	0.0156	0.0143
Ni	0.0008	0.0009	0.2270	0.0014	0.0006	0.0013	0.0012	0.0006	0.0025	0.0010		0.0010				0.0009	0.0004	0.0004	0.0008	0.0006	0.0023		0.0017
Mg	2.3413	2.2957	0.0000	2.3142	2.3095	2.3063	2.2175	2.3067	2.3720	2.3390	2.4170	2.1419	2.1403	2.1967	2.1699	2.3626	2.3535	2.3228	2.3144	2.2530	2.2507	2.2795	2.2629
Ca	0.3536	0.3538	0.3490	0.2464	0.2544	0.3154	0.3744	0.2340	0.2230	0.2310	0.1800	0.4174	0.4201	0.4251	0.4196	0.3482	0.3521	0.3538	0.3538	0.3287	0.3258	0.3227	0.3256
Na	0.0028	0.0080	1.7430	0.0100	0.0065	0.0134	0.0246	0.0054	0.0131	0.0106	0.0081	0.0041	0.0054	0.0053	0.0019	0.0034	0.0032	0.0034	0.0016	0.0109	0.0123	0.0110	0.0123
K	0.0005			0.0005		0.0055	0.0058	0.0005							0.0005		0.0008					0.0009	0.0009
Total	8.0472	8.0225	0.0011	8.0443	8.0426	8.0749	8.0457	8.0262	8.0234	8.0133	8.0138	7.9952	7.9914	8.0231	8.0075	8.0700	8.0639	8.0453	8.0437	8.0437	8.0437	8.0437	8.0437
Mg#	86.76	86.54	86.98	82.02	82.32	82.26	82.07	82.14	82.25	82.53	83.78	84.20	84.41	84.74	84.60	85.88	85.95	85.79	85.74	83.26	83.69	83.58	83.62
Ca#	13.12	13.35	12.66	9.62	9.92	12.03	14.44	9.21	8.59	8.99	6.93	16.31	16.41	16.21	16.20	12.85	13.01	13.22	13.26	12.73	12.64	12.40	12.58
Cr#	12.24	11.73	11.52	3.50	3.53	4.21	3.50	4.72	3.08	3.04	2.26	13.54	13.59	13.71	13.59	19.85	19.82	19.78	19.85	5.32	5.42	5.40	5.46

Table 6.3 (continued)

	garnet from B and C																					
No.	grt-L27-5	grt-L25-1	grt-L25-2	grt-L25-3	grt-L25-4	grt-L26-1	grt-L26-2	grt-L21-1	grt-L21-2	grt-L21-3	grt-L21-4	grt-L5-1	grt-L5-2	grt-L5-3	grt-L5-4	grt-L5-5	grt-L5-6	grt-L5-7	grt-L5-8	grt-L14-1	grt-L14-2	grt-L14-3
commer	rim	core	core	core	core	core	core	core	core	core	core	core	core	core	core	core	rim	rim	rim	rim	rim	rim
SiO_2	42.05	41.43	42.40	42.76	42.09	42.08	42.15	41.99	41.70	42.04	41.98	42.12	42.37	42.26	42.13	42.15	41.91	42.23	42.23	41.71	42.62	42.59
TiO_2	0.92	0.21	0.20	0.22	0.23	0.72	0.71	0.84	0.92	0.07	0.84	0.29	0.28	0.36	0.58	0.70	0.84	0.86	0.91	0.87	0.46	0.49
Al_2O_3	21.10	23.35	23.64	23.26	23.22	21.17	21.19	20.97	21.02	20.48	20.86	22.86	22.95	22.95	22.69	22.58	21.12	21.26	21.01	21.03	22.21	22.70
Cr_2O_3	2.97	0.28	0.27	0.40	0.47	2.04	2.02	3.11	2.62	4.78	3.20	0.09	0.12	0.10	0.10	0.12	2.69	2.67	2.81	2.55	1.80	1.07
FeO*	8.02	11.19	11.09	11.29	11.25	8.87	8.69	7.90	7.82	6.62	8.07	9.73	9.74	9.71	9.75	9.71	7.80	7.80	7.80	7.91	8.27	8.39
MnO	0.29	0.36	0.38	0.41	0.36	0.24	0.27	0.29	0.29	0.35	0.30	0.25	0.27	0.27	0.29	0.29	0.31	0.29	0.26	0.28	0.34	0.37
NiO	0.01	<0.01	0.03	0.03	0.01	<0.01	0.01	<0.01	0.01	0.02	0.03	<0.01	<0.01	0.01	0.01	0.01	0.05	0.05	0.01	0.01	<0.01	0.04
MgO	21.26	19.07	18.65	18.14	18.39	20.95	20.57	21.99	22.13	21.29	21.58	20.01	20.13	20.14	20.29	20.33	21.91	22.04	21.94	21.82	21.11	20.98
CaO	3.65	4.15	4.03	4.14	4.19	4.27	4.21	3.49	3.39	4.96	3.67	4.75	4.72	4.68	4.37	4.18	3.52	3.44	3.43	3.65	4.36	4.29
Na_2O	0.06	0.05	0.06	0.06	0.04	0.03	0.06	0.06	0.07	0.06	0.06	0.06	0.08	0.12	0.13	0.12	0.05	0.07	0.07	0.06	0.09	0.12
K_2O	<0.01	<0.01	<0.01	0.01	<0.01	<0.01	<0.01	0.01	<0.01	0.01	<0.01	<0.01	<0.01	0.01	<0.01	<0.01	<0.01	<0.01	<0.01	<0.01	0.01	0.02
Total	100.33	100.09	100.73	100.72	100.26	100.36	99.88	100.68	100.00	100.76	100.58	100.17	100.67	100.60	100.40	100.21	100.26	100.74	100.52	99.90	101.30	101.08
O 12																						
Si	2.9870	2.9704	3.0104	3.0398	3.0101	2.9960	3.0114	2.9720	2.9690	2.9810	2.9790	2.9990	3.0020	2.9960	2.9930	2.9970	2.9750	2.9810	2.9880	2.9740	2.9940	2.9940
Ti	0.0491	0.0113	0.0107	0.0118	0.0124	0.0385	0.0381	0.0444	0.0493	0.0034	0.0447	0.0157	0.0151	0.0192	0.0311	0.0374	0.0450	0.0458	0.0482	0.0465	0.0241	0.0259
Al	1.7665	1.9730	1.9782	1.9488	1.9571	1.7764	1.7843	1.7500	1.7640	1.7120	1.7450	1.9180	1.9160	1.9180	1.9000	1.8930	1.7670	1.7690	1.7520	1.7670	1.8390	1.8800
Cr	0.1668	0.0159	0.0152	0.0225	0.0266	0.1148	0.1141	0.1740	0.1470	0.2680	0.1800	0.0052	0.0067	0.0058	0.0057	0.0065	0.1510	0.1490	0.1570	0.1440	0.1000	0.0596
Fe^{tot}	0.4764	0.6709	0.6585	0.6712	0.6728	0.5281	0.5192	0.4680	0.4660	0.3930	0.4790	0.5800	0.5770	0.5760	0.5790	0.5780	0.4630	0.4600	0.4620	0.4720	0.4860	0.4930
Mn	0.0174	0.0219	0.0229	0.0247	0.0218	0.0145	0.0163	0.0171	0.0176	0.0209	0.0181	0.0149	0.0163	0.0162	0.0176	0.0174	0.0187	0.0172	0.0155	0.0170	0.0202	0.0222
Ni	0.0006		0.0017	0.0017	0.0006		0.0006		0.0007	0.001	0.0014			0.0005	0.0007		0.003	0.0028	0.0005	0.0006		0.0021
Mg	2.2514	2.0382	1.9740	1.9224	1.9606	2.2236	2.1908	2.3200	2.3480	2.2510	2.2830	2.1240	2.1250	2.1280	2.1480	2.1560	2.3180	2.3190	2.3140	2.3190	2.2100	2.1980
Ca	0.2778	0.3188	0.3066	0.3153	0.3210	0.3257	0.3223	0.2650	0.2590	0.3770	0.2790	0.3620	0.3580	0.3550	0.3330	0.3190	0.2680	0.2600	0.2600	0.2790	0.3280	0.3230
Na	0.0083	0.0070	0.0083	0.0083	0.0055	0.0041	0.0083	0.0080	0.0102	0.0080	0.0085	0.0089	0.0103	0.0158	0.0184	0.0159	0.0067	0.0092	0.0097	0.0075	0.0126	0.0164
K				0.0010				0.0010		0.0006				0.0006							0.0012	0.0021
Total	8.0437	8.0273	7.9863	7.9675	7.9885	8.0219	8.0054	8.0185	8.0308	8.0153	8.0177	8.0277	8.0264	8.0305	8.0265	8.0202	8.0154	8.0130	8.0069	8.0266	8.0139	8.0142
Mg#	82.53	75.23	74.99	74.12	74.45	80.81	80.84	83.21	83.44	85.14	82.66	78.55	78.65	78.70	78.77	78.86	83.35	83.45	83.36	83.09	81.97	81.68
Ca#	10.98	13.52	13.44	14.09	14.07	12.78	12.82	10.25	9.93	14.35	10.89	14.56	14.42	14.30	13.42	12.89	10.36	10.08	10.10	10.74	12.92	12.81
Cr#	8.63	0.80	0.76	1.14	1.34	6.07	6.01	9.04	7.69	13.54	9.35	0.27	0.35	0.30	0.30	0.34	7.87	7.77	8.22	7.54	5.16	3.07

Table 6.3 (continued)

	garnet from B and C																				
No.	grt-L14-4	grt-L14-5	grt-L14-6	grt-L14-7	grt-L14-8	grt-L14-9	grt-L14-10	grt-L14-11	grt-L14-12	grt-L14-13	grt-L14-14	grt-L14-15	grt-L16-1	grt-L16-2	grt-L16-3	grt-L16-4	grt-L16-5	grt-L16-6	grt-L16-7	grt-L16-8	grt-L15-1
commer	rim	rim	core	core	core	core	core	core	core	core	core	core	core	core	core	core	core	core	core	core	core
SiO_2	42.59	42.33	41.52	41.45	41.29	41.20	41.47	41.35	41.45	41.59	41.12	41.49	41.90	42.73	42.87	42.70	42.73	42.61	42.70	42.78	42.00
TiO_2	0.50	0.62	0.20	0.25	0.21	0.21	0.21	0.20	0.21	0.22	0.18	0.22	0.76	0.65	0.64	0.64	0.63	0.65	0.62	0.64	0.02
Al_2O_3	22.56	22.41	22.93	22.91	22.91	22.87	22.92	22.93	22.99	23.18	22.71	22.87	21.40	21.20	21.29	21.13	21.11	21.24	21.17	21.29	20.61
Cr_2O_3	0.98	0.82	0.19	0.17	0.20	0.19	0.15	0.21	0.19	0.17	0.17	0.21	2.32	1.98	2.05	2.20	2.17	2.16	2.18	2.15	4.24
FeO*	8.60	9.22	15.89	16.04	16.07	15.91	16.02	16.04	16.06	16.09	16.03	15.98	7.61	7.35	7.37	7.36	7.37	7.40	7.34	7.37	7.08
MnO	0.35	0.34	0.32	0.33	0.30	0.33	0.33	0.33	0.32	0.35	0.31	0.31	0.27	0.27	0.26	0.29	0.27	0.26	0.27	0.27	0.34
NiO	<0.01	0.03	0.02	0.03	0.04	0.03	<0.01	<0.01	<0.01	0.02	0.02	<0.01	<0.01	0.03	0.02	0.01	0.02	<0.01	0.02	0.05	0.05
MgO	20.81	20.51	16.48	16.58	16.53	16.47	16.60	16.49	16.69	16.72	16.52	16.65	21.96	21.92	21.99	21.99	21.88	21.84	22.01	21.99	20.51
CaO	4.33	4.13	3.23	3.13	3.18	3.17	3.17	3.15	3.17	3.16	3.17	3.17	3.55	4.31	4.33	4.36	4.39	4.43	4.32	4.34	5.39
Na_2O	0.11	0.14	0.10	0.09	0.08	0.09	0.11	0.10	0.12	0.09	0.07	0.10	0.07	0.11	0.09	0.09	0.10	0.11	0.11	0.08	0.02
K_2O	0.02	<0.01	<0.01	0.02	<0.01	0.01	<0.01	0.02	0.01	0.01	0.03	<0.01	<0.01	<0.01	<0.01	<0.01	<0.01	<0.01	<0.01	<0.01	<0.01
Total	100.91	100.60	100.93	101.05	100.85	100.53	101.04	100.88	101.25	101.62	100.39	101.07	99.84	100.60	100.91	100.81	100.68	100.73	100.76	101.01	100.33
O 12																					
Si	3.0000	2.9980	3.0030	2.9970	2.9930	2.9940	2.9980	2.9950	2.9910	2.9910	2.9940	2.9980	2.9800	3.0130	3.0140	3.0070	3.0140	3.0040	3.0080	3.0070	2.9950
Ti	0.0263	0.0332	0.0110	0.0138	0.0114	0.0114	0.0115	0.0108	0.0113	0.0121	0.0100	0.0117	0.0404	0.0345	0.0340	0.0337	0.0333	0.0342	0.0330	0.0340	0.0008
Al	1.8730	1.8710	1.9550	1.9530	1.9570	1.9590	1.9530	1.9580	1.9560	1.9640	1.9500	1.9480	1.7940	1.7620	1.7640	1.7540	1.7550	1.7650	1.7580	1.7640	1.7330
Cr	0.0547	0.0462	0.0110	0.0098	0.0113	0.0108	0.0083	0.0119	0.0109	0.0098	0.0098	0.0122	0.1300	0.1110	0.1140	0.1230	0.1210	0.1200	0.1220	0.1190	0.2390
Fe^{tot}	0.5070	0.5460	0.9610	0.9700	0.9740	0.9670	0.9690	0.9720	0.9690	0.9670	0.9760	0.9650	0.4530	0.4330	0.4330	0.4330	0.4350	0.4360	0.4330	0.4330	0.4230
Mn	0.0209	0.0202	0.0193	0.0201	0.0186	0.0204	0.0205	0.0205	0.0195	0.0216	0.0190	0.0189	0.0161	0.0160	0.0157	0.0173	0.0161	0.0152	0.0160	0.0161	0.0205
Ni		0.0019	0.0012	0.0019	0.0025	0.0019				0.0014	0.0014			0.0017	0.0009	0.0004	0.0011		0.0009	0.0028	0.0012
Mg	2.1850	2.1650	1.7770	1.7870	1.7860	1.7840	1.7890	1.7800	1.7960	1.7920	1.7930	1.7930	2.3280	2.3040	2.3040	2.3090	2.3010	2.2950	2.3110	2.3040	2.1800
Ca	0.3270	0.3130	0.2510	0.2430	0.2470	0.2460	0.2460	0.2440	0.2450	0.2440	0.2480	0.2450	0.2700	0.3260	0.3260	0.3290	0.3310	0.3350	0.3260	0.3270	0.4120
Na	0.0150	0.0189	0.0144	0.0124	0.0115	0.0123	0.0159	0.0134	0.0162	0.0120	0.0103	0.0140	0.0094	0.0151	0.0124	0.0117	0.0135	0.0153	0.0150	0.0113	0.0031
K	0.0021			0.0015		0.0010		0.0018	0.0013	0.0011	0.0026										
Total	8.0089	8.0134	8.0039	8.0080	8.0123	8.0068	8.0112	8.0056	8.0149	8.0149	8.0115	8.0058	8.0209	8.0163	8.0180	8.0181	8.0210	8.0197	8.0229	8.0182	8.0076
Mg#	81.17	79.86	64.90	64.82	64.71	64.85	64.87	64.68	64.95	64.95	64.75	65.01	83.71	84.18	84.18	84.21	84.10	84.04	84.22	84.18	83.75
Ca#	13.02	12.63	12.38	11.97	12.15	12.12	12.09	12.06	12.00	11.98	12.15	12.02	10.39	12.40	12.40	12.47	12.58	12.74	12.36	12.43	15.90
Cr#	2.84	2.41	0.56	0.50	0.57	0.55	0.42	0.60	0.55	0.50	0.50	0.62	6.76	5.93	6.07	6.55	6.45	6.37	6.49	6.32	12.12

Table 6.3 (continued)

	garnet from B and C																					
No.	grt-L15-2	grt-L15-3	grt-L15-4	grt-L15-5	grt-L15-6	grt-L15-7	grt-L15-8	grt-L15-9	grt-L15-1	grt-L24-1	grt-L24-2	grt-L24-3	grt-L24-4	grt-L24-5	grt-L24-6	grt-L24-7	grt-L24-8	grt-L24-9	grt-L9-1	grt-L9-2	grt-L9-3
commer	core	core	core	core	core	core	core	core	rim	core	core	core	core	core	core	core	rim	rim	core	core	core
SiO_2	42.24	42.19	42.11	41.96	42.27	42.10	42.16	42.12	41.73	42.53	42.67	42.77	42.63	42.61	42.65	42.54	42.29	42.21	42.21	42.14	42.13
TiO_2	0.03	<0.01	0.01	0.03	0.01	0.02	0.02	0.04	0.96	0.05	0.06	0.09	0.05	0.06	0.05	0.07	0.69	0.73	0.02	0.02	<0.01
Al_2O_3	20.78	20.82	20.86	20.76	20.65	20.71	20.60	20.61	20.83	18.76	18.93	19.02	19.01	18.93	19.04	19.03	20.97	19.94	20.94	20.87	21.14
Cr_2O_3	4.18	4.22	4.25	4.22	4.24	4.32	4.25	4.30	2.75	7.28	7.34	7.36	7.34	7.32	7.24	7.18	3.64	4.75	3.98	3.90	3.86
FeO*	7.13	7.05	7.07	7.11	7.11	7.06	7.13	7.10	8.08	4.72	4.76	4.70	4.83	4.71	4.73	4.77	7.70	7.60	6.89	6.91	6.97
MnO	0.37	0.36	0.35	0.36	0.34	0.33	0.34	0.35	0.30	0.21	0.27	0.22	0.30	0.25	0.22	0.23	0.29	0.29	0.36	0.36	0.34
NiO	<0.01	<0.01	<0.01	0.03	<0.01	0.04	0.01	0.02	<0.01	<0.01	0.04	0.03	<0.01	0.02	<0.01	0.01	0.02	0.02	0.02	<0.01	<0.01
MgO	20.76	20.75	20.67	20.47	20.57	20.54	20.41	20.58	21.86	24.42	24.57	24.46	24.33	24.27	24.36	24.37	22.64	22.66	20.98	20.74	20.94
CaO	5.36	5.40	5.38	5.33	5.40	5.38	5.58	5.36	3.54	2.27	2.19	2.25	2.38	2.50	2.43	2.38	2.97	2.63	5.31	5.29	5.31
Na_2O	0.03	0.04	0.02	0.02	0.03	0.03	0.04	0.04	0.07	0.04	0.04	0.03	0.02	0.03	0.05	0.02	0.08	0.09	0.02	0.03	0.01
K_2O	<0.01	0.01	<0.01	<0.01	<0.01	<0.01	<0.01	<0.01	<0.01	<0.01	<0.01	0.01	<0.01	0.02	0.01	<0.01	0.02	0.01	<0.01	<0.01	0.01
Total	100.95	100.89	100.78	100.33	100.68	100.59	100.60	100.59	100.11	100.30	100.90	100.98	100.92	100.76	100.82	100.64	101.32	100.95	100.83	100.34	100.81
O 12																					
Si	2.9920	2.9910	2.9890	2.9920	3.0030	2.9950	3.0000	2.9960	2.9730	3.0030	2.9960	2.9990	2.9940	2.9970	2.9960	2.9930	2.9720	2.9840	2.9890	2.9980	2.9840
Ti	0.0016		0.0005	0.0015	0.0007	0.0011	0.0011	0.0020	0.0514	0.0027	0.0032	0.0049	0.0027	0.0034	0.0026	0.0039	0.0367	0.0386	0.0011	0.0013	
Al	1.7360	1.7400	1.7450	1.7450	1.7290	1.7360	1.7280	1.7280	1.7490	1.5610	1.5670	1.5720	1.5740	1.5700	1.5770	1.5790	1.7370	1.6610	1.7480	1.7500	1.7640
Cr	0.2340	0.2370	0.2380	0.2380	0.2380	0.2430	0.2390	0.2420	0.1550	0.4070	0.4080	0.4080	0.4080	0.4070	0.4020	0.3990	0.2020	0.2650	0.2230	0.2190	0.2160
Fe^{tot}	0.4220	0.4180	0.4200	0.4240	0.4220	0.4200	0.4240	0.4220	0.4810	0.2790	0.2790	0.2750	0.2840	0.2770	0.2780	0.2810	0.4530	0.4490	0.4080	0.4110	0.4130
Mn	0.0224	0.0216	0.0209	0.0216	0.0206	0.0200	0.0205	0.0213	0.0178	0.0125	0.0159	0.0129	0.0179	0.0149	0.0129	0.0136	0.0175	0.0171	0.0213	0.0217	0.0201
Ni				0.0017		0.0023	0.0006	0.0014			0.0009	0.0011		0.0005		0.0016	0.0012	0.0007	0.001		
Mg	2.1930	2.1930	2.1870	2.1760	2.1780	2.1770	2.1650	2.1830	2.3210	2.5690	2.5720	2.5560	2.5480	2.5440	2.5510	2.5560	2.3720	2.3870	2.2150	2.1990	2.2100
Ca	0.4070	0.4100	0.4090	0.4070	0.4110	0.4100	0.4250	0.4090	0.2710	0.1720	0.1650	0.1690	0.1790	0.1890	0.1830	0.1790	0.2230	0.1990	0.4030	0.4030	0.4030
Na	0.0047	0.0054	0.0032	0.0021	0.0036	0.0047	0.0052	0.0051	0.0090	0.0057	0.0053	0.0046	0.0024	0.0043	0.0069	0.0022	0.0107	0.0122	0.0027	0.0044	0.0019
K		0.0010										0.0007		0.0017	0.0007		0.0016	0.0012			0.0006
Total	8.0127	8.0160	8.0126	8.0089	8.0059	8.0091	8.0084	8.0098	8.0282	8.0119	8.0123	8.0025	8.0100	8.0071	8.0094	8.0083	8.0251	8.0136	8.0121	8.0074	8.0120
Mg#	83.86	83.99	83.89	83.69	83.77	83.83	83.62	83.80	82.83	90.20	90.21	90.29	89.97	90.18	90.17	90.10	83.96	84.17	84.45	84.25	84.25
Ca#	15.65	15.75	15.76	15.76	15.87	15.85	16.41	15.78	10.46	6.28	6.03	6.20	6.56	6.92	6.69	6.54	8.59	7.70	15.39	15.49	15.42
Cr#	11.88	11.99	12.00	12.00	12.10	12.28	12.15	12.28	8.14	20.68	20.66	20.61	20.59	20.59	20.31	20.17	10.42	13.76	11.31	11.12	10.91

Table 6.3 (continued)

	garnet from B and C														rutile from part A			ilmenite from part A						
No.	grt-L9-4	grt-L9-5	grt-L9-6	grt-L9-7	grt-L9-8	grt-L9-9	grt-L22-1	grt-L22-3	grt-L22-4	grt-L22-5	grt-L22-6	grt-L22-7	grt-L22-8	grt22-9	GS6-rt1	GS6-rt2	GS6-rt3	GS1ilm1	GS1ilm2	6-ilm1	6-ilm2	6-ilm3	8-ilm1	8-ilm2
commer	core	core	core	core	core	core	core	core	core	core	core	core	rim	rim										
SiO_2	42.24	42.41	42.42	42.40	42.30	42.20	42.54	42.46	42.37	42.18	42.17	42.06	41.85	41.61	0.08	0.08	0.04	0.13	0.15	0.08	0.10	0.06	0.07	0.07
TiO_2	0.02	<0.01	<0.01	0.02	0.03	0.02	0.03	0.01	0.02	<0.01	0.01	0.03	0.96	0.95	94.43	93.43	95.61	54.78	54.84	54.81	55.35	55.41	54.88	54.97
Al_2O_3	21.06	20.88	21.02	20.97	20.95	20.85	20.91	20.97	20.86	20.88	20.92	20.79	20.58	20.59	<0.02	<0.02	<0.02	0.50	0.70	0.56	0.53	0.49	0.62	0.59
Cr_2O_3	3.87	4.02	3.99	3.94	4.00	3.98	3.93	3.92	4.06	4.13	4.05	4.07	3.01	3.00	2.86	2.93	1.45	1.76	1.72	1.68	1.62	1.60	1.90	1.79
FeO*	6.89	6.81	6.88	6.89	6.87	6.86	6.92	6.93	7.00	6.95	7.08	7.09	7.89	7.93	0.33	0.35	0.51	27.46	27.45	26.40	26.54	26.56	27.14	27.14
MnO	0.34	0.35	0.35	0.34	0.33	0.33	0.35	0.35	0.33	0.36	0.36	0.35	0.29	0.30	<0.02	<0.02	<0.02	0.26	0.26	0.27	0.26	0.25	0.21	0.25
NiO	<0.01	<0.01	0.01	0.02	<0.01	0.02	<0.01	0.02	0.02	0.05	0.01	0.03	<0.01	0.03	<0.02	<0.02	<0.02	0.17	0.17	0.20	0.15	0.19	0.16	0.19
MgO	20.72	20.86	21.07	20.70	20.77	20.80	21.09	21.13	20.90	21.03	21.11	20.92	21.72	21.60	0.04	0.02	0.01	14.40	14.48	15.10	15.15	15.08	14.45	14.61
CaO	5.21	5.30	5.27	5.35	5.26	5.31	4.98	4.95	5.01	5.02	5.01	4.99	3.62	3.60	0.01	<0.02	0.01	0.03	0.02	0.03	0.03	0.04	0.03	0.02
Na_2O	0.03	0.02	0.01	0.03	0.02	0.03	0.03	0.03	0.04	0.03	0.05	0.03	0.09	0.09	<0.02	<0.02	0.02	0.03	0.01	0.02	0.08	0.00	0.04	0.02
K_2O	0.01	<0.01	0.01	<0.01	0.01	<0.01	<0.01	0.01	<0.01	<0.01	<0.01	<0.01	<0.01	<0.01	<0.01	<0.01	<0.01	<0.01	<0.01	<0.01	<0.01	<0.01	<.01	<.01
Total	100.42	100.72	101.08	100.71	100.60	100.46	100.84	100.84	100.68	100.69	100.83	100.43	100.04	99.72	97.76	96.81	97.64	99.51	99.80	99.15	99.81	99.68	99.50	99.64
O 12															O 2			O 3						
Si	3.0000	3.0040	2.9950	3.0040	3.0000	2.9980	3.0070	3.0020	3.0030	2.9910	2.9870	2.9920	2.9830	2.9770	0.0011	0.0011	0.0005	0.0030	0.0034	0.0018	0.0024	0.0014	0.0017	0.0015
Ti	0.0013			0.0008	0.0015	0.0009	0.0013	0.0006	0.0009		0.0005	0.0018	0.0513	0.0510	0.9732	0.9726	0.9846	0.9474	0.9446	0.9468	0.9493	0.9519	0.9478	0.9479
Al	1.7630	1.7430	1.7490	1.7510	1.7510	1.7460	1.7420	1.7470	1.7420	1.7450	1.7470	1.7430	1.7290	1.7370				0.0136	0.0189	0.0151	0.0142	0.0131	0.0167	0.0159
Cr	0.2170	0.2250	0.2230	0.2210	0.2240	0.2240	0.2200	0.2190	0.2270	0.2320	0.2270	0.2290	0.1700	0.1700	0.0310	0.0321	0.0157	0.0319	0.0312	0.0305	0.0291	0.0290	0.0345	0.0325
Fe^{tot}	0.4090	0.4030	0.4060	0.4080	0.4070	0.4080	0.4090	0.4100	0.4150	0.4120	0.4190	0.4220	0.4700	0.4750	0.0038	0.0040	0.0058	0.5281	0.5259	0.5072	0.5062	0.5074	0.5211	0.5203
Mn	0.0203	0.0213	0.0209	0.0201	0.0199	0.0200	0.0211	0.0209	0.0199	0.0216	0.0216	0.0210	0.0176	0.0180				0.0050	0.0050	0.0052	0.0051	0.0049	0.0040	0.0049
Ni			0.0004	0.001		0.0009		0.0019	0.0012	0.0019	0.0025	0.0010		0.0018				0.0031	0.0030	0.0037	0.0028	0.0035	0.0030	0.0035
Mg	2.1940	2.2020	2.2180	2.1860	2.1960	2.2030	2.2220	2.2270	2.2080	2.2230	2.2290	2.2180	2.3080	2.3040	0.0009	0.0004	0.0002	0.4934	0.4942	0.5170	0.5149	0.5135	0.4947	0.4991
Ca	0.3960	0.4020	0.3990	0.4060	0.4000	0.4040	0.3770	0.3750	0.3800	0.3810	0.3810	0.3810	0.2760	0.2760	0.0002		0.0001	0.0007	0.0006	0.0008	0.0008	0.0009	0.0006	0.0005
Na	0.0036	0.0025	0.0011	0.0041	0.0033	0.0039	0.0045	0.0039	0.0055	0.0040	0.0063	0.0038	0.0120	0.0128			0.0005	0.0013	0.0005	0.0009	0.0034	0.0001	0.0017	0.0007
K	0.0006		0.0010		0.0012			0.0006																
Total	8.0042	8.0028	8.0124	8.0020	8.0027	8.0087	8.0039	8.0073	8.0025	8.0115	8.0209	8.0126	8.0169	8.0226	1.0102	1.0103	1.0074	2.0276	2.0272	2.0291	2.0284	2.0258	2.0258	2.0268
Mg#	84.29	84.53	84.53	84.27	84.36	84.37	84.45	84.45	84.18	84.36	84.18	84.02	83.08	82.91				48.30	48.45	50.48	50.42	50.30	48.70	48.96
Ca#	15.29	15.44	15.25	15.66	15.41	15.50	14.51	14.41	14.68	14.63	14.60	14.66	10.68	10.70										
Cr#	10.96	11.43	11.31	11.21	11.34	11.37	11.21	11.14	11.53	11.73	11.50	11.61	8.95	8.91										

Table 6.4 Major element composition of cpx from polymict peridotite

	vein like part A																			
sample	**Acpx-1**	**Acpx-2**	**Acpx-3**	**Acpx-4**	**Acpx-5**	**Acpx-6**	**Acpx-7**	**Acpx-8**	**Acpx-9**	**Acpx-10**	**Acpx-11**	**Acpx-12**	**Acpx-13**	**Acpx-14**	**Acpx-15**	**Acpx-16**	**Acpx-17**	**Acpx-18**	**Acpx-19**	**Acpx-20**	**Acpx-21**
SiO_2	54.89	55.24	55.06	54.81	55.22	55.43	54.86	55.44	54.80	56.34	55.83	56.08	54.34	54.19	54.15	54.19	54.26	55.09	54.59	54.18	54.47
TiO_2	0.36	0.36	0.37	0.35	0.34	0.34	0.33	0.34	0.34	0.34	0.34	0.35	1.20	1.53	0.40	0.33	0.52	0.33	0.32	0.35	0.32
Al_2O_3	2.04	2.15	2.18	1.83	2.03	2.04	1.99	1.98	2.02	1.98	1.94	2.01	2.40	1.99	2.34	2.08	3.58	2.00	1.92	2.44	1.89
FeO*	3.29	3.35	3.42	3.45	3.40	3.52	3.38	3.53	3.39	3.47	3.39	3.46	4.25	4.37	3.62	3.46	3.69	3.45	3.48	3.46	3.42
MnO	0.09	0.09	0.09	0.13	0.10	0.08	0.09	0.09	0.10	0.09	0.11	0.13	0.14	0.14	0.10	0.09	0.10	0.11	0.12	0.11	0.11
MgO	16.34	16.13	16.48	16.64	16.02	16.27	16.08	16.22	16.15	16.21	16.14	16.02	16.25	17.23	17.15	16.44	16.50	16.51	16.66	16.52	16.23
CaO	20.07	20.13	19.76	20.07	19.78	19.92	19.84	19.75	19.78	19.92	19.85	19.77	18.80	18.77	19.29	20.14	18.63	19.68	19.65	19.21	19.68
Na_2O	2.09	2.25	2.11	1.88	2.09	2.02	2.08	2.05	2.07	2.02	2.00	2.01	1.56	1.27	1.67	1.68	2.20	1.97	1.70	1.82	2.13
K_2O	0.01	0.01	0.01	0.01	0.01	0.01	0.02	0.01	0.01	0.01	0.03	0.02	0.01	<0.01	0.02	0.03	0.02	0.02	0.02	0.02	0.07
Cr_2O_3	1.08	1.14	1.14	1.00	1.03	1.02	1.01	1.03	1.04	1.02	1.02	1.03	0.97	0.70	1.14	1.09	1.71	0.93	0.93	0.96	0.92
NiO	0.01	0.02	<0.01	0.01	0.01	0.05	0.04	<0.01	0.01	0.03	0.02	0.03	0.02	0.03	0.04	<0.01	0.04	0.05	<0.01	0.05	<0.01
Total	100.28	100.87	100.63	100.17	100.03	100.69	99.72	100.46	99.70	101.42	100.67	100.90	99.94	100.23	99.91	99.54	101.24	100.14	99.39	99.13	99.21
O 6																					
Si	1.9748	1.9760	1.9734	1.9756	1.9941	1.9891	1.9867	1.9939	1.9843	2.0078	2.0055	2.0087	1.9706	1.9602	1.9561	1.9686	1.9332	1.9855	1.9843	1.9723	1.9791
Al	0.0866	0.0906	0.0922	0.0779	0.0863	0.0862	0.0849	0.0841	0.0863	0.0830	0.0822	0.0848	0.1025	0.0848	0.0996	0.0890	0.1503	0.0848	0.0824	0.1045	0.0810
Ti	0.0096	0.0098	0.0099	0.0094	0.0091	0.0091	0.0090	0.0092	0.0092	0.0092	0.0092	0.0095	0.0327	0.0418	0.0107	0.0091	0.0139	0.0090	0.0089	0.0097	0.0086
Cr	0.0309	0.0321	0.0323	0.0286	0.0295	0.0290	0.0290	0.0294	0.0296	0.0287	0.0290	0.0290	0.0279	0.0200	0.0325	0.0313	0.0482	0.0265	0.0266	0.0277	0.0263
Ni	0.0002	0.0005		0.0003	0.0004	0.0013	0.0011		0.0003	0.0009	0.0005	0.0007	0.0007	0.0010	0.0011		0.0010	0.0014		0.0015	
Fe^{tot}	0.0991	0.1002	0.1027	0.1039	0.1027	0.1057	0.1024	0.1062	0.1026	0.1033	0.1017	0.1037	0.1290	0.1323	0.1092	0.1052	0.1099	0.1040	0.1058	0.1054	0.1038
Mg	0.8764	0.8602	0.8808	0.8939	0.8627	0.8703	0.8678	0.8697	0.8716	0.8613	0.8642	0.8555	0.8785	0.9289	0.9236	0.8900	0.8763	0.8871	0.9026	0.8967	0.8789
Mn	0.0027	0.0026	0.0028	0.0039	0.0030	0.0025	0.0028	0.0026	0.0029	0.0027	0.0032	0.0040	0.0044	0.0044	0.0031	0.0028	0.0029	0.0034	0.0037	0.0034	0.0033
Ca	0.7734	0.7715	0.7587	0.7750	0.7651	0.7659	0.7696	0.7612	0.7673	0.7605	0.7639	0.7586	0.7304	0.7274	0.7464	0.7837	0.7112	0.7599	0.7650	0.7493	0.7660
Na	0.1457	0.1558	0.1468	0.1312	0.1466	0.1402	0.1459	0.1430	0.1454	0.1394	0.1392	0.1398	0.1095	0.0894	0.1169	0.1185	0.1522	0.1375	0.1196	0.1287	0.1498
K	0.0007	0.0006	0.0004	0.0004	0.0006	0.0005	0.0007	0.0006	0.0005	0.0004	0.0012	0.0007	0.0005		0.0008	0.0015	0.0008	0.0008	0.0010	0.0009	0.0032
Total	3.9997	3.9989	4.0111	4.0000	4.0036	4.0000	3.9959	3.9989	4.0000	3.9971	4.0000	3.9951	3.9865	3.9903	4.0000	4.0030	4.0000	4.0087	3.9999	4.0000	3.9968
En	50.04	49.59	50.48	50.31	49.77	49.89	49.80	49.99	49.97	49.85	49.87	49.69	50.42	51.81	51.82	49.95	51.54	50.56	50.79	51.10	50.17
Fs	5.81	5.93	6.04	6.07	6.09	6.21	6.04	6.25	6.05	6.14	6.06	6.26	7.66	7.62	6.30	6.07	6.64	6.12	6.16	6.20	6.11
Wo	44.15	44.48	43.48	43.62	44.14	43.91	44.16	43.76	43.99	44.01	44.08	44.06	41.92	40.57	41.88	43.98	41.83	43.31	43.05	42.70	43.72
Mg#	89.60	89.32	89.31	89.24	89.09	88.94	89.19	88.88	89.20	89.04	89.17	88.82	86.82	87.17	89.16	89.17	88.59	89.20	89.18	89.18	89.14
Ca#	46.88	47.28	46.28	46.44	47.00	46.81	47.00	46.67	46.82	46.89	46.92	47.00	45.40	43.92	44.69	46.82	44.80	46.14	45.88	45.52	46.57

* - Total Fe as FeO;

12 O - formula calculated on 12 oxygen;

Table 6.4 (continued)

	vein like part A			cpx from part B and C																	
sample	**Acpx-22**	**Acpx-23**	**Acpx-24**	**Cpx-1**	**Cpx-2**	**Cpx-3**	**Cpx-4**	**Cpx-5**	**Cpx-6**	**Cpx-7**	**Cpx-8**	**Cpx-9**	**Cpx-10**	**Cpx-11**	**Cpx-12**	**Cpx-13**	**Cpx-14**	**Cpx-15**	**Cpx-16**	**Cpx-17**	**Cpx-18**
SiO_2	54.48	54.56	55.20	54.53	54.49	54.18	54.24	54.83	54.42	54.81	54.36	54.84	54.62	54.67	54.69	54.56	54.71	54.81	54.40	54.62	54.48
TiO_2	0.34	0.32	0.32	0.34	0.36	0.36	0.40	0.34	0.38	0.34	0.38	0.40	0.36	0.33	0.36	0.35	0.39	0.39	0.35	0.36	0.38
Al_2O_3	2.40	1.95	1.96	1.78	1.96	2.01	2.09	1.87	2.00	1.90	2.38	1.94	1.97	1.91	1.94	1.78	1.93	1.82	1.77	1.79	1.67
FeO*	3.48	3.44	3.49	3.06	3.19	3.24	3.36	3.15	3.20	3.24	3.15	3.16	3.19	3.22	3.23	3.14	3.21	3.17	3.12	3.18	3.23
MnO	0.08	0.11	0.11	0.10	0.07	0.09	0.09	0.07	0.11	0.08	0.11	0.08	0.08	0.10	0.10	0.10	0.09	0.11	0.09	0.09	0.10
MgO	16.43	16.13	16.50	16.14	16.21	16.28	16.39	15.95	16.04	15.98	16.50	16.08	15.92	16.09	16.07	16.57	16.03	16.11	16.16	16.26	16.49
CaO	19.52	19.78	19.77	20.07	19.61	19.97	19.36	19.90	19.90	20.00	19.16	19.88	19.84	19.95	19.83	19.92	19.77	19.86	20.16	20.16	19.89
Na_2O	2.00	1.91	2.13	1.81	1.77	1.73	1.81	1.82	1.87	1.92	1.86	1.88	1.94	1.96	1.88	1.66	1.94	1.86	1.71	1.63	1.75
K_2O	0.01	0.03	0.04	0.01	0.02	0.05	0.02	<0.01	0.05	0.02	0.03	0.02	0.01	0.02	0.01	0.02	0.02	0.01	0.03	0.01	0.03
Cr_2O_3	0.92	0.92	0.94	1.10	1.08	1.11	1.10	1.10	1.16	1.11	1.16	1.18	1.10	1.09	1.15	1.05	1.05	1.06	1.06	1.05	1.02
NiO	0.01	0.03	0.02	0.04	0.02	0.04	0.04	0.03	0.05	0.01	0.05	0.04	0.03	0.05	0.03	0.05	0.03	0.02	0.02	0.03	0.03
Total	99.67	99.19	100.47	99.01	98.79	99.05	98.92	99.07	99.20	99.43	99.16	99.53	99.05	99.41	99.30	99.19	99.17	99.24	98.86	99.19	99.09
O 6																					
Si	1.9709	1.9875	1.9807	1.9917	1.9941	1.9776	1.9812	2.0030	1.9842	1.9936	1.9784	1.9934	1.9935	1.9873	1.9917	1.9880	1.9938	1.9973	1.9904	1.9935	1.9871
Al	0.1025	0.0839	0.0827	0.0768	0.0845	0.0865	0.0900	0.0804	0.0859	0.0815	0.1021	0.0831	0.0847	0.0818	0.0833	0.0762	0.0829	0.0781	0.0763	0.0769	0.0717
Ti	0.0092	0.0089	0.0086	0.0093	0.0100	0.0098	0.0110	0.0095	0.0103	0.0094	0.0103	0.0109	0.0099	0.0090	0.0098	0.0096	0.0107	0.0108	0.0095	0.0099	0.0103
Cr	0.0262	0.0264	0.0266	0.0317	0.0313	0.0321	0.0318	0.0316	0.0335	0.0319	0.0335	0.0340	0.0317	0.0314	0.0331	0.0301	0.0302	0.0306	0.0305	0.0304	0.0295
Ni	0.0003	0.0010	0.0005	0.0011	0.0007	0.0011	0.0011	0.0008	0.0013	0.0004	0.0016	0.0011	0.0008	0.0015	0.0009	0.0014	0.0008	0.0007	0.0007	0.0009	0.0009
Fe^{tot}	0.1053	0.1048	0.1048	0.0935	0.0976	0.0989	0.1026	0.0962	0.0976	0.0986	0.0959	0.0961	0.0974	0.0979	0.0984	0.0957	0.0978	0.0966	0.0955	0.0971	0.0985
Mg	0.8860	0.8757	0.8829	0.8788	0.8844	0.8858	0.8925	0.8686	0.8718	0.8665	0.8952	0.8713	0.8662	0.8719	0.8725	0.9001	0.8709	0.8751	0.8815	0.8847	0.8966
Mn	0.0025	0.0035	0.0034	0.0030	0.0021	0.0027	0.0029	0.0021	0.0033	0.0026	0.0034	0.0026	0.0023	0.0031	0.0032	0.0030	0.0027	0.0035	0.0028	0.0028	0.0031
Ca	0.7567	0.7718	0.7600	0.7854	0.7689	0.7810	0.7577	0.7789	0.7774	0.7794	0.7471	0.7742	0.7758	0.7770	0.7737	0.7777	0.7719	0.7754	0.7903	0.7883	0.7773
Na	0.1401	0.1352	0.1479	0.1282	0.1256	0.1224	0.1282	0.1289	0.1322	0.1354	0.1312	0.1325	0.1373	0.1381	0.1327	0.1173	0.1371	0.1314	0.1213	0.1153	0.1238
K	0.0004	0.0013	0.0020	0.0005	0.0007	0.0021	0.0011		0.0025	0.0008	0.0013	0.0008	0.0004	0.0007	0.0007	0.0008	0.0011	0.0007	0.0012	0.0004	0.0012
Total	4.0000	3.9957	4.0000	4.0083	3.8975	4.0000	4.0133	4.0000	3.9852	4.0000	4.0035	4.0000	4.0000	3.9965	3.8895	3.9190	4.0000	4.0000	4.0101	4.0000	4.0050
En	50.62	49.88	50.42	49.91	50.45	50.09	50.83	49.75	49.82	49.60	51.40	49.96	49.73	49.83	49.92	50.67	49.95	49.99	49.80	49.90	50.50
Fs	6.16	6.17	6.18	5.48	5.69	5.74	6.01	5.63	5.77	5.79	5.70	5.66	5.73	5.77	5.81	5.56	5.77	5.72	5.55	5.63	5.72
Wo	43.23	43.96	43.40	44.61	43.86	44.16	43.15	44.61	44.42	44.61	42.90	44.39	44.54	44.40	44.27	43.78	44.28	44.29	44.65	44.47	43.78
Mg#	89.16	89.00	89.09	90.11	89.86	89.71	89.42	89.83	89.63	89.55	90.02	89.83	89.68	89.62	89.57	90.12	89.65	89.74	89.97	89.86	89.82
Ca#	46.06	46.85	46.26	99.86	99.91	99.86	99.86	99.90	99.83	99.95	99.79	99.85	99.89	99.80	99.88	99.82	99.89	99.91	99.91	99.89	99.88

Table 6.5 Trace element composition of opx from polymict peridotite

	vein-like A							from B and C													
Element	**Aopx1**	**Aopx2**	**Aopx3**	**Aopx4**	**Aopx5**	**Aopx6**	**Aopx7**	**opx2**	**opx3**	**opx5**	**opx6**	**opx7**	**opx8**	**opx9**	**opx10**	**opx11**	**opx12**	**opx13**	**opx14**	**opx15**	**opx16**
Li	4.91	6.35	15.04	na	na	na	na	1.32	1.33	1.97	1.76	1.59	1.32	1.87	1.45	1.71	1.52	1.54	1.61	1.39	1.81
B	0.459	0.465	0.467	na	na	na	na	0.197	0.181	0.770	0.460	0.216	0.212	0.214	0.221	0.280	0.222	0.198	0.208	0.225	0.355
Sc	10.0	8.2	10.7	9.0	13.5	4.4	4.3	5.8	5.1	4.8	4.1	4.5	5.1	5.3	4.2	6.7	6.5	4.3	4.4	10.2	5.2
Ti	na	na	na	na	2112	255	268	na	na	na	na	na	na	na	na	na	na	na	na	na	na
V	133	92.2	172	135	216	51.4	49.5	61.1	58.0	64.0	41.2	64.5	64.2	60.3	51.8	33.1	32.6	61.1	63.5	40.7	43.0
Co	72.1	67.4	82.7	na	na	na	na	77.2	75.9	65.2	65.2	67.0	76.1	77.1	72.3	57.0	57.1	70.9	74.0	68.9	80.9
Cu	2.27	2.14	3.63	3.23	3.39	6.80	4.88	3.68	3.74	5.22	3.26	5.76	12.61	9.97	4.74	1.47	1.18	5.54	4.80	2.54	3.22
Zn	60.9	46.6	63.8	61.1	60.7	48.0	46.3	60.3	58.2	45.6	34.0	53.4	81.8	65.5	51.1	38.9	38.7	51.3	59.2	55.9	106
Rb	4.51	1.30	12.25	0.65	0.13	bdl	0.98	0.010	0.085	0.101	0.683	bdl	0.229	0.059	bdl	0.335	0.222	bdl	0.175	0.230	0.214
Sr	14.16	17.27	18.65	4.63	3.51	1.68	8.01	1.70	2.55	1.07	4.12	0.82	3.31	2.63	2.37	3.52	2.81	1.70	1.83	5.50	1.65
Y	0.240	0.252	0.288	0.201	0.242	0.149	0.177	0.434	0.412	0.170	0.059	0.234	0.570	0.422	0.298	0.198	0.226	0.235	0.290	0.407	0.273
Zr	7.63	4.91	6.74	2.65	4.27	0.349	0.910	1.21	1.14	0.700	0.700	0.780	1.71	0.800	0.570	1.13	1.46	0.500	0.660	1.58	1.63
Nb	1.54	0.78	1.35	0.31	0.19	0.04	0.40	0.035	0.113	0.053	0.263	0.027	0.093	0.048	0.032	0.183	0.321	0.040	0.028	0.176	0.066
Cs	na	na	na	bdl	0.020	bdl	0.094	bdl	0.006	0.027	0.052	bdl	0.014	0.010	bdl	0.068	0.024	bdl	0.026	0.026	na
Ba	na	na	na	4.16	1.35	bdl	6.45	0.061	0.629	0.284	3.820	0.013	0.996	0.264	0.010	0.373	2.54	0.043	0.062	0.626	na
La	1.48	1.61	1.10	0.38	0.22	0.03	0.47	0.033	0.104	0.042	0.252	0.012	0.132	0.060	0.039	0.046	0.183	0.032	0.022	0.055	0.048
Ce	2.95	2.87	2.34	0.768	0.405	0.133	0.933	0.186	0.388	0.119	0.737	0.056	0.312	0.216	0.212	0.148	0.504	0.148	0.115	0.143	0.172
Pr	na	na	na	0.083	0.048	0.021	0.108	0.029	0.044	0.018	0.063	0.014	0.052	0.041	0.037	0.020	0.056	0.025	0.024	0.023	na
Nd	1.02	1.01	0.884	0.353	0.201	0.199	0.430	0.183	0.215	0.102	0.274	0.082	0.269	0.254	0.241	0.112	0.242	0.144	0.153	0.106	0.151
Sm	0.16	0.15	0.14	0.08	0.05	0.04	0.07	0.071	0.072	0.043	0.041	0.032	0.110	0.109	0.093	0.040	0.071	0.052	0.059	0.043	0.046
Eu	0.05	0.05	0.05	0.02	0.02	bdl	0.02	0.019	0.014	0.014	0.012	0.012	0.033	0.027	0.023	0.012	0.012	0.018	0.017	0.013	0.021
Gd	0.11	0.09	0.11	0.08	na	na	0.10	0.107	0.085	0.044	0.020	0.059	0.148	0.096	0.083	0.046	0.063	0.054	0.066	0.061	0.058
Tb	0.01	0.01	0.02	na	na	na	na	0.020	0.016	0.009	bdl	0.014	0.031	0.024	0.014	0.010	0.009	0.009	0.014	0.014	0.012
Dy	0.064	0.061	0.068	0.050	0.060	0.044	0.031	0.072	0.093	0.044	0.014	0.060	0.146	0.094	0.072	0.034	0.045	0.051	0.057	0.077	0.057
Ho	0.0099	0.0106	0.0172	na	na	na	na	0.0159	0.0151	0.0073	0.0012	0.0105	0.029	0.018	0.014	0.0098	0.011	0.010	0.014	0.016	0.014
Er	0.027	0.024	0.031	0.038	0.029	bdl	0.019	0.035	0.031	0.018	0.0026	0.0307	0.073	0.060	0.033	0.026	0.031	0.022	0.038	0.046	0.031
Tm	0.0020	0.0019	0.0052	na	na	na	na	0.0061	0.0035	0.0035	0.0004	0.0049	0.014	0.0072	0.0039	0.0045	0.0036	0.0052	0.0045	0.0081	0.0027
Yb	0.016	0.015	0.026	bdl	0.025	bdl	bdl	0.026	0.022	0.016	0.0030	0.020	0.052	0.048	0.019	0.025	0.023	0.025	0.028	0.032	0.027
Lu	0.0039	0.0032	0.0032	bdl	bdl	0.0057	bdl	0.0042	0.0023	0.0028	bdl	0.0035	0.016	0.0086	0.0059	0.0039	0.0051	0.0031	0.0043	0.0063	0.0027
Hf	na	na	na	0.210	0.321	bdl	bdl	0.048	0.0450	0.0460	0.0113	0.0470	0.089	0.0440	0.0229	0.0450	0.0540	0.0332	0.0420	0.0520	na
Ta	na	na	na	0.0090	bdl	bdl	0.011	0.0041	0.0145	0.0051	0.0182	0.0053	0.015	0.0050	0.0031	0.0320	0.0370	0.0035	bdl	0.0330	na
Pb	na	na	na	0.046	0.026	bdl	0.074	0.024	0.019	0.034	0.057	0.053	0.667	0.731	0.015	0.015	0.036	0.013	0.018	0.014	na
Th	na	na	na	0.032	0.024	bdl	0.057	0.0011	0.0164	0.0136	0.0300	bdl	0.097	0.0046	0.0010	0.0072	0.0228	0.0009	bdl	0.0070	na
U	bdl	0.057	0.027	0.0089	bdl	bdl	0.025	0.0002	0.0026	0.0025	0.0072	0.0007	0.088	0.0051	0.0008	0.0115	0.0132	bdl	0.0040	0.0038	0.0022

bdl - below detection limit

na - not analysed

Table 6.5 (continued)

from B and C						
Element	**opx17**	**opx18**	**opx19**	**opx20**	**opx21**	**opx22**
Li	2.02	0.772	bdl	bdl	bdl	bdl
B	0.437	0.356	4.63	4.31	4.62	4.36
Sc	3.8	4.2	6.4	4.2	4.0	4.3
Ti	na	na	na	na	na	na
V	32.8	45.0	56.3	66.1	64.8	51.5
Co	106.2	58.1	68.5	67.9	68.7	75.7
Cu	4.50	0.41	3.57	3.58	3.61	3.69
Zn	147.2	26.6	45.8	60.1	58.2	58.7
Rb	0.740	bdl	0.240	0.014	bdl	bdl
Sr	5.30	0.376	2.83	2.41	1.71	4.00
Y	0.146	0.006	0.239	0.262	0.244	0.288
Zr	0.771	0.321	1.95	1.16	0.910	0.960
Nb	0.175	0.113	0.157	0.091	0.033	0.027
Cs	na	na	na	na	na	na
Ba	na	na	na	na	na	na
La	0.202	0.013	0.174	0.086	0.026	0.047
Ce	0.465	0.052	0.377	0.279	0.136	0.234
Pr	na	na	na	na	na	na
Nd	0.200	0.062	0.214	0.234	0.163	0.275
Sm	0.051	0.017	0.059	0.072	0.064	0.083
Eu	0.012	0.006	0.024	0.025	0.022	0.030
Gd	0.034	0.009	0.057	0.058	0.055	0.077
Tb	0.007	0.002	0.010	0.012	0.012	0.012
Dy	0.040	bdl	0.060	0.049	0.062	0.071
Ho	0.0070	0.0003	0.013	0.012	0.012	0.013
Er	0.018	bdl	0.026	0.027	0.025	0.028
Tm	0.0028	bdl	0.0039	0.0034	0.0030	0.0051
Yb	0.015	bdl	0.021	0.022	0.023	0.032
Lu	0.0021	bdl	0.0033	0.0037	0.0037	0.0028
Hf	na	na	0.083	0.042	0.033	0.046
Ta	na	na	0.0060	0.0052	0.0028	0.0020
Pb	na	na	na	na	na	na
Th	na	na	na	na	na	na
U	0.0081	0.0009	0.0069	0.0025	0.0010	0.0010

Table 6.6 Trace element composition of grt from polymict peridotite

grt from B and C																					
	grt 20												grt 24								
	grt20-1	grt20-2	grt20-3	grt20-4	grt20-5	grt20-6	grt20-7	grt20-8	grt20-9	grt20-10	grt20-11	grt20-12	grt24-1	grt24-2	grt24-4	grt24-5	grt24-6	grt24-3	grt24-7	grt24-8	grt24-9
comm.	core	core	core	core	core	core	core	core	core	rim	rim	rim	core	core	core	core	core	rim	rim	rim	rim
T Canil (°C)		1039											1126								
T Griffin (°C)		1069											1226								
Li	0.134	bdl	bdl	bdl	bdl	bdl	0.06	bdl	bdl	bdl	7.59	bdl	bdl	0.079	bdl	0.06	bdl	bdl	0.829	0.696	0.775
B	10.0	9.15	7.99	6.83	6.06	6.09	4.88	1.49	1.52	1.45	8.19	2.25	4.52	3.73	1.52	2.02	2.16	1.53	2.36	3.79	5.87
Sc	53.5	52.4	54.1	53.3	54.3	55.6	69.5	79.8	79.4	78.0	102	95.6	109	96.1	118	121	120	115	117	142	157
Ti	74.8	56.6	56.9	55.5	58.7	96.1	64.1	70.3	67.7	88.7	7490	11441	437	424	478	510	561	467	523	11398	12831
V	186	188	185	183	185	177	185	200	199	194	257	264	274	278	282	313	292	281	304	356	404
Co	40.3	38.6	38.3	37.7	38.2	37.6	37.5	44.0	44.1	43.8	56.7	58.4	39.9	39.9	47.1	48.7	47.2	47.2	46.6	77.8	103
Ni	49.4	45.4	45.5	45.2	44.7	44.3	44.6	50.7	50.2	50.4	96.2	114	66.6	65.3	76.4	80.3	73.5	76.3	73.9	134	175
Cu	2.64	bdl	bdl	0.33	bdl	bdl	bdl	bdl	bdl	bdl	1.59	0.502	bdl	0.149	bdl	0.104	bdl	bdl	0.317	0.973	1.01
Zn	8.64	8.55	8.21	8.72	8.56	8.48	9.67	10.3	10.1	9.77	20.7	18.7	11.6	10.7	11.9	13.8	12.0	11.6	14.3	28.7	36.0
Ga	na	na	na	na	na	na	na	4.40	4.65	4.36	14.3	17.9	na	na	3.55	3.48	3.52	3.55	3.04	18.0	23.7
Ge	na	na	na	na	na	na	na	1.38	1.42	1.39	2.36	2.24	na	na	1.59	1.66	1.60	1.53	1.67	2.75	4.02
Rb	0.079	0.057	0.046	0.043	0.049	0.027	0.018	bdl	bdl	bdl	0.835	bdl	0.036	0.042	0.016	0.043	0.055	0.033	0.196	0.157	0.206
Sr	0.461	0.337	0.342	0.321	0.381	0.300	0.346	0.592	0.528	0.398	14.6	0.331	0.584	0.588	0.657	0.695	4.28	0.657	3.80	2.28	2.90
Y	3.41	3.04	3.13	3.08	3.13	3.32	4.14	4.75	4.73	4.65	22.5	27.1	1.59	1.47	1.91	1.89	2.22	1.67	1.93	33.7	38.4
Zr	4.44	2.76	1.93	1.81	3.38	7.02	4.72	5.97	1.92	7.93	216	363	20.5	17.9	22.6	24.4	24.8	21.6	24.1	335	342
Nb	0.151	0.142	0.138	0.149	0.161	0.148	0.155	0.195	0.226	0.184	1.36	0.676	0.273	0.244	0.326	0.576	0.435	0.33	5.37	0.938	0.694
Mo	na	na	na	na	na	na	na	bdl	bdl	0.038	0.112	bdl	na	na	0.0774	0.339	0.054	0.03	0.45	0.589	0.483
Cs	bdl	bdl	bdl	bdl	bdl	bdl	0.0029	bdl	bdl	bdl	0.254	bdl	bdl	bdl	bdl	bdl	bdl	bdl	0.037	bdl	0.024
Ba	bdl	bdl	bdl	0.004	0.007	bdl	0.003	bdl	bdl	bdl	10.8	0.347	bdl	0.013	bdl	bdl	0.635	bdl	0.404	1.143	0.898
La	0.036	0.020	0.025	0.027	0.032	0.015	0.019	0.047	0.050	0.021	1.62	0.031	0.027	0.029	0.028	0.030	0.263	0.030	2.13	0.207	0.237
Ce	0.459	0.379	0.375	0.427	0.458	0.322	0.330	0.613	0.599	0.376	3.69	0.359	0.316	0.341	0.370	0.393	0.784	0.364	4.60	0.793	0.672
Pr	0.162	0.141	0.142	0.140	0.149	0.128	0.148	na	na	na	na	na	0.135	0.127	na	na	na	na	na	na	na
Nd	1.45	1.27	1.34	1.28	1.46	1.23	1.51	2.17	1.83	1.80	1.95	1.42	1.63	1.45	1.84	1.87	1.96	1.88	2.71	1.95	1.54
Sm	0.565	0.464	0.370	0.340	0.478	0.526	0.607	0.772	0.407	0.760	1.05	1.33	1.32	1.14	1.48	1.50	1.53	1.51	1.87	1.81	1.48
Eu	0.139	0.117	0.080	0.067	0.121	0.165	0.146	0.185	0.061	0.195	0.522	0.657	0.686	0.593	0.767	0.798	0.759	0.758	0.856	0.957	0.757
Gd	0.291	0.132	0.097	0.084	0.185	0.328	0.227	0.306	0.094	0.346	2.171	3.02	1.67	1.41	1.70	1.82	1.71	1.64	1.88	3.74	3.74
Tb	0.037	0.025	0.021	0.025	0.033	0.043	0.029	0.034	0.023	0.039	0.485	0.628	0.156	0.150	0.173	0.188	0.178	0.164	0.190	0.765	0.758
Dy	0.330	0.267	0.299	0.263	0.294	0.334	0.323	0.402	0.400	0.406	4.06	4.91	0.558	0.479	0.624	0.603	0.657	0.547	0.762	5.89	6.34
Ho	0.112	0.105	0.101	0.105	0.103	0.107	0.133	0.160	0.151	0.149	0.933	1.10	0.059	0.053	0.067	0.068	0.083	0.061	0.078	1.44	1.49
Er	0.508	0.448	0.457	0.499	0.484	0.474	0.597	0.716	0.709	0.668	2.93	3.30	0.105	0.103	0.141	0.146	0.214	0.135	0.105	3.98	4.89
Tm	0.113	0.098	0.104	0.094	0.099	0.105	0.122	0.146	0.142	0.138	0.440	0.484	0.018	0.013	0.019	0.022	0.026	0.017	0.026	0.578	0.709
Yb	0.960	0.860	0.890	0.870	0.870	0.880	1.07	1.31	1.30	1.27	3.14	3.38	0.138	0.138	0.144	0.152	0.170	0.148	0.159	4.86	5.08
Lu	0.171	0.139	0.170	0.158	0.160	0.162	0.201	0.231	0.227	0.223	0.479	0.501	0.029	0.020	0.031	0.029	0.034	0.027	0.035	0.666	0.769
Hf	0.079	0.039	0.060	0.022	0.064	0.108	0.085	0.113	0.044	0.125	4.91	8.17	0.386	0.344	0.434	0.485	0.484	0.424	0.444	8.16	8.47
Ta	0.018	0.015	0.016	0.016	0.013	0.014	0.015	0.024	0.023	0.018	0.063	0.123	0.020	0.021	0.023	0.018	0.023	0.024	0.557	0.099	0.052
Pb	0.265	0.012	0.0094	0.015	0.011	0.022	0.012	0.038	bdl	0.014	0.130	0.017	0.0065	0.043	0.024	0.025	bdl	0.026	0.227	0.289	0.148
Th	0.011	0.0048	0.0042	0.0043	0.0066	bdl	0.0044	0.0077	0.0073	0.0048	0.205	0.019	0.0093	0.012	0.011	0.014	0.041	0.011	1.41	0.033	0.037
U	0.027	0.016	0.024	0.018	0.019	0.019	0.019	0.027	0.023	0.019	0.080	0.048	0.026	0.028	0.027	0.028	0.042	0.027	0.030	0.053	0.039

T Canil (°C) - Canil, 1999

T Griffin (°C) - Griffin et al., 1989b

Table 6.6 (continued)

grt from B and C																				
	grt 21											grt 23	grt L5			grt 16				
	grt21--1	grt21--2	grt21--3	grt21--4	grt21--5	grt21--6	grt21--7	grt21--8	grt21--9	grt21--10	grt21--11	grt23-1	grt-L5-1	grt-L5-2	grt-L5-3	grt16-1	grt16-2	grt16-3	grt16-4	grt16-5
comme	core	core	core	core	core	core	rim	rim	rim	rim	rim					core	core	rim	rim	rim
T Canil (°C)		1047										1036	1129			1027				
T Griffin (°C)		1083										1063	1233			1048				
Li	bdl	bdl	0.06	bdl	bdl	0.042	0.370	9.52	bdl	1.33	1.46	1.63	0.321	0.236	0.223	0.075	0.068	0.941	0.050	0.212
B	5.05	4.79	4.54	1.42	1.52	1.55	3.03	6.65	2.31	3.32	3.61	4.34	4.26	3.23	3.49	5.18	4.75	7.31	1.32	2.13
Sc	78.2	79.2	81.8	72.4	76.8	81.2	79.2	139	79	129	135	113	43.6	42.3	44.0	99.2	106	68.6	63.8	104
Ti	1028	1021	1054	994	1031	1189	1216	12449	1129	10176	8854	1529	3901	2010	2030	136	146	92.5	88.7	6207
V	154	154	156	163	170	185	169	368	176	370	361	190	133	129	126	215	198	144	134	257
Co	37.4	37.6	37.6	41.3	44.2	44.0	47.0	88.5	45.2	68.4	64.5	39.6	50.8	49.9	50.2	41.5	42.4	37.3	29.7	50.0
Ni	46.5	46.0	46.2	52.1	53.8	52.6	59.2	134	55.3	106	106	46.2	74.0	71.7	71.1	44.1	44.4	40.0	31.1	80.2
Cu	0.257	bdl	bdl	bdl	bdl	0.081	bdl	1.51	0.116	0.765	0.677	0.590	1.05	0.308	0.475	0.610	bdl	bdl	bdl	0.395
Zn	10.1	10.2	10.1	8.69	10.0	11.8	12.4	22.1	12.3	25.5	25.7	10.9	25.1	25.8	25.7	10.2	10.5	10.6	6.57	15.5
Ga	na	na	na	3.37	3.70	3.50	3.61	27.8	3.58	17.1	18.9	na	na	na	na	na	na	3.04	2.18	13.2
Ge	na	na	na	1.46	1.61	1.62	1.46	3.74	bdl	3.03	2.80	na	na	na	na	na	na	1.56	0.987	1.92
Rb	0.031	0.044	0.030	0.031	0.033	0.025	0.081	0.394	0.067	0.277	0.300	0.225	bdl	bdl	bdl	0.044	0.035	0.115	0.057	0.027
Sr	0.279	0.308	0.291	0.257	0.308	0.323	0.391	19.1	0.344	2.30	2.39	6.56	0.253	0.267	0.272	0.625	0.693	1.02	0.424	0.189
Y	5.00	4.97	5.19	4.64	5.03	5.37	5.55	38.2	5.36	33.2	27.3	6.74	9.73	9.03	9.48	5.47	5.56	3.72	3.58	19.8
Zr	53.9	53.8	56.7	50.1	53.8	58.3	60.3	394	58.1	263	225	141	27.1	13.0	13.3	37.1	43.7	27.0	24.5	150
Nb	0.200	0.201	0.209	0.208	0.249	0.394	0.358	1.51	0.421	0.518	0.524	0.649	0.078	0.100	0.100	0.351	0.357	0.486	0.362	0.240
Mo	bdl	na	na	bdl	0.047	0.27	0.273	0.470	0.295	0.314	0.373	na	na	na	na	na	na	1.75	0.147	0.232
Cs	bdl	bdl	0.0052	bdl	bdl	0.0023	bdl	0.253	bdl	0.055	0.097	0.056	bdl	bdl	bdl	bdl	bdl	bdl	0.0073	bdl
Ba	0.0028	0.0048	bdl	bdl	bdl	0.0049	0.040	5.86	0.015	1.27	0.802	6.39	0.0035	0.0057	0.011	0.011	0.0046	0.103	0.0085	0.018
La	0.015	0.014	0.016	0.013	0.016	0.019	0.013	1.54	0.017	0.159	0.277	0.303	0.010	0.013	0.015	0.036	0.029	0.075	0.020	0.012
Ce	0.207	0.201	0.209	0.222	0.237	0.261	0.226	4.00	0.252	0.657	0.781	0.972	0.132	0.173	0.178	0.802	0.670	0.729	0.526	0.169
Pr	0.104	0.099	0.100	na	na	na	na	na	na	na	na	0.222	0.053	0.064	0.055	0.340	0.311	na	na	na
Nd	1.35	1.38	1.36	1.37	1.49	1.55	1.24	2.88	1.46	1.46	1.37	2.33	0.601	0.519	0.512	3.60	3.45	2.50	2.51	0.859
Sm	1.25	1.32	1.35	1.32	1.40	1.50	1.54	1.89	1.42	1.44	1.44	1.78	0.467	0.349	0.308	1.57	1.62	1.09	1.03	0.718
Eu	0.625	0.628	0.610	0.599	0.627	0.678	0.603	0.904	0.652	0.722	0.612	0.794	0.261	0.208	0.185	0.426	0.513	0.293	0.295	0.445
Gd	1.84	1.94	2.10	1.76	1.88	1.96	2.09	3.77	1.96	3.21	2.99	2.36	0.950	0.730	0.750	1.30	1.30	0.708	0.741	1.83
Tb	0.244	0.255	0.274	0.234	0.241	0.263	0.279	0.864	0.271	0.742	0.679	0.294	0.206	0.159	0.174	0.193	0.192	0.112	0.122	0.408
Dy	1.29	1.25	1.31	1.19	1.27	1.36	1.47	7.47	1.39	6.00	4.98	1.60	1.59	1.37	1.40	1.28	1.14	0.968	0.756	3.53
Ho	0.181	0.191	0.198	0.178	0.187	0.202	0.198	1.32	0.194	1.36	1.14	0.266	0.355	0.332	0.352	0.262	0.207	0.143	0.135	0.773
Er	0.452	0.426	0.465	0.410	0.435	0.499	0.509	4.95	0.516	4.28	3.50	0.650	1.14	1.11	1.16	0.740	0.558	0.337	0.364	2.64
Tm	0.070	0.069	0.069	0.065	0.067	0.079	0.086	0.712	0.072	0.616	0.522	0.090	0.180	0.176	0.183	0.108	0.089	0.052	0.067	0.395
Yb	0.614	0.592	0.641	0.592	0.599	0.675	0.771	5.58	0.591	4.25	3.51	0.740	1.28	1.31	1.38	0.800	0.682	0.512	0.444	2.72
Lu	0.117	0.113	0.125	0.109	0.116	0.130	0.123	0.786	0.123	0.655	0.502	0.108	0.199	0.205	0.210	0.128	0.119	0.113	0.077	0.418
Hf	1.05	1.10	1.14	1.01	1.05	1.21	1.24	9.30	1.21	6.04	5.66	2.34	0.521	0.276	0.267	0.690	0.740	0.535	0.493	3.67
Ta	0.029	0.024	0.030	0.023	0.021	0.026	0.015	0.144	0.030	0.045	0.033	0.036	0.0073	0.014	0.013	0.023	0.027	0.030	0.017	0.0078
Pb	0.014	0.014	0.012	0.0070	0.0072	0.016	bdl	0.178	0.012	0.025	0.030	0.157	0.011	0.010	0.010	0.053	0.0082	bdl	bdl	bdl
Th	0.022	0.0023	0.0043	0.0028	0.0025	0.0028	bdl	0.259	0.0028	0.031	0.034	0.041	0.0032	0.0039	0.0043	0.0091	0.0058	0.0073	0.010	0.0049
U	0.012	0.011	0.011	0.012	0.012	0.013	0.019	0.110	0.014	0.034	0.029	0.020	0.0046	0.0092	0.0086	0.033	0.028	0.012	0.021	0.011

Table 6.6 (continued)

grt from B and C																					
	grt 13					grt 14				grt 22		grt L9	grt 25		grt 26		grt 17	grt 18	grt L14	grt L15
	grt13-1	grt13-2	grt13-3	grt13-4	grt13-5	grt14-1	grt14-2	grt14-3	grt14-4	grt-22-1	grt-22-2	grt-L9-3	grt-25-1	grt-25-2	grt-26-1	grt-26-2	grt-17-1	grt-18-1	grt-L14-1	grt-L15-1
comme	core	core	core	rim	rim	core	rim	rim	rim	core	rim									
T Canil (°C)		1229				1032				1044		1026	1217		1240		1031	1097		1017
T Griffin (°C)		1435				1057				1078		1047	1409		1459		1055	1172		1031
Li	0.179	0.171	bdl	0.134	0.541	0.085	bdl	bdl	0.138	0.075	0.086	0.420	0.156	0.327	0.417	0.496	0.356	0.298	1.62	0.146
B	4.24	4.01	0.98	1.79	3.43	3.75	1.74	3.06	2.26	4.84	4.18	3.74	3.65	3.71	2.67	3.45	3.01	3.75	2.77	3.23
Sc	89.9	98.3	96.9	71.1	99.6	92.2	103	104	103	83.1	93.5	88.3	102	72.3	60.9	72.7	79.4	105	43.3	99.6
Ti	2385	2491	2734	2669	5401	782	933	888	914	127	616	73	1945	6156	5218	6484	555	2482	1392	116
V	274	274	285	206	226	215	227	237	228	189	192	202	259	233	235	239	201	233	90.1	203
Co	41.8	41.8	47.8	36.9	54.9	41.7	48.9	58.3	45.7	40.6	42.0	41.3	40.4	50.2	51.1	51.3	39.3	41.9	72.6	40.6
Ni	103	105	120	90.4	98.9	45.4	54.8	65.0	50.4	42.8	54.1	44.1	104	114	114	116	45.2	62.3	49.9	41.9
Cu	0.500	0.366	0.356	0.346	0.451	0.305	0.227	bdl	0.054	0.600	0.293	1.27	0.442	0.610	0.920	0.750	0.500	0.840	0.580	0.405
Zn	14.7	15.0	14.8	16.5	17.5	9.99	11.8	13.7	11.3	9.22	11.2	10.4	13.4	24.3	26.0	26.6	8.74	10.2	92.1	9.62
Ga	na	na	10.2	7.08	13.0	na	3.79	4.90	3.03	na	na	na	na	na	na	na	na	na	na	na
Ge	na	na	2.06	1.49	1.93	na	1.75	2.14	1.651	na	na	na	na	na	na	na	na	na	na	na
Rb	0.032	0.033	bdl	0.081	0.374	0.036	0.069	0.104	0.118	0.032	0.041	0.050	0.030	bdl	0.013	0.017	0.028	0.057	bdl	0.032
Sr	0.647	1.03	0.747	0.549	2.48	0.614	1.25	1.43	2.26	0.471	0.501	0.950	0.515	0.538	1.21	0.616	0.547	0.595	0.495	1.01
Y	10.0	11.0	10.8	8.27	19.2	1.93	2.40	2.53	2.54	3.17	4.88	2.76	9.48	18.8	15.5	19.2	9.78	2.01	18.3	1.74
Zr	29.6	32.8	33.0	26.2	105	71.1	88.1	89.6	86.1	63.1	76.4	39.8	15.2	58.1	43.7	62.8	129	35.4	5.93	35.5
Nb	0.180	0.208	0.231	0.272	0.352	0.248	0.567	0.520	0.537	0.263	0.293	0.395	0.234	0.147	0.125	0.163	0.265	0.140	0.051	0.458
Mo	na	na	0.0423	0.25	0.366	na	0.381	0.585	0.409	na	na	na	na	na	na	na	na	na	na	na
Cs	bdl	bdl	bdl	bdl	0.083	bdl	bdl	0.024	0.023	bdl	0.006	0.011	bdl	bdl	bdl	bdl	bdl	0.0059	bdl	0.0041
Ba	0.005	10.6	bdl	bdl	0.703	0.025	11.0	0.229	0.605	0.012	0.050	0.333	bdl	bdl	0.056	0.071	0.047	0.052	bdl	0.164
La	0.036	0.041	0.045	0.037	0.345	0.020	0.059	0.032	0.199	0.021	0.025	0.061	0.033	0.032	0.040	0.033	0.033	0.038	0.002	0.052
Ce	0.432	0.451	0.479	0.409	0.791	0.500	0.813	0.760	0.827	0.449	0.467	0.745	0.362	0.320	0.325	0.307	0.335	0.202	0.065	0.791
Pr	0.134	0.140	na	na	na	0.233	na	na	na	0.241	0.260	0.294	0.123	0.096	0.088	0.095	0.142	0.073	0.030	0.370
Nd	1.30	1.45	1.48	1.19	0.668	2.87	3.60	3.82	3.46	2.98	2.89	3.02	1.25	0.940	0.780	0.980	1.75	0.940	0.418	3.62
Sm	0.920	1.000	1.027	0.748	0.705	1.12	1.17	1.04	1.17	1.56	1.59	1.40	0.850	0.920	0.678	0.890	1.87	0.710	0.660	1.50
Eu	0.421	0.440	0.438	0.322	0.352	0.305	0.405	0.353	0.363	0.584	0.615	0.439	0.361	0.468	0.361	0.492	1.00	0.272	0.411	0.468
Gd	1.50	1.72	1.66	1.25	1.91	0.700	1.02	0.898	0.899	1.68	1.81	1.05	1.35	1.97	1.61	2.09	3.27	0.800	1.75	0.980
Tb	0.284	0.296	0.287	0.193	0.427	0.090	0.083	0.067	0.103	0.211	0.242	0.112	0.250	0.424	0.348	0.441	0.504	0.105	0.384	0.100
Dy	1.84	1.95	1.99	1.51	3.49	0.399	0.599	0.414	0.553	0.870	1.14	0.670	1.63	3.19	2.67	3.31	2.55	0.590	3.09	0.425
Ho	0.386	0.418	0.417	0.330	0.796	0.075	0.102	0.095	0.101	0.121	0.198	0.105	0.354	0.720	0.600	0.720	0.367	0.080	0.690	0.070
Er	1.16	1.23	1.19	0.91	2.51	0.245	0.259	0.312	0.333	0.338	0.500	0.251	1.09	2.15	1.82	2.16	0.800	0.199	2.09	0.186
Tm	0.173	0.189	0.191	0.129	0.384	0.041	0.027	0.063	0.058	0.042	0.071	0.042	0.171	0.319	0.281	0.342	0.097	0.026	0.318	0.035
Yb	1.25	1.38	1.38	1.13	2.73	0.344	0.415	0.425	0.555	0.341	0.574	0.345	1.28	2.36	1.94	2.36	0.630	0.186	2.36	0.313
Lu	0.196	0.213	0.211	0.163	0.394	0.069	0.077	0.060	0.081	0.065	0.097	0.058	0.197	0.340	0.297	0.363	0.087	0.037	0.358	0.063
Hf	0.770	0.880	0.857	0.722	2.72	1.33	1.60	2.23	1.76	1.01	1.54	0.740	0.386	1.43	0.980	1.55	2.00	0.560	0.116	0.630
Ta	0.016	0.015	0.014	0.010	0.010	0.020	0.037	0.031	0.030	0.021	0.020	0.043	0.022	0.012	0.020	0.013	0.021	0.0076	0.0011	0.022
Pb	0.024	0.0075	0.0056	bdl	0.029	0.024	0.052	bdl	0.025	0.019	0.023	0.823	0.0068	0.0059	0.164	0.015	0.039	0.057	0.012	0.084
Th	0.012	0.0082	0.0062	0.0021	0.060	0.036	0.025	0.0080	0.019	0.0079	0.0061	0.0089	0.0075	0.0080	0.011	0.0055	0.0041	0.0070	bdl	0.0067
U	0.013	0.014	0.016	0.005	0.021	0.023	0.030	0.022	0.037	0.022	0.021	0.027	0.011	0.010	0.007	0.0064	0.017	0.011	0.0007	0.033

Table 6.6 (continued)

grt from B and C																	grt from vein-like A				
	grt L16	**grt 8**	**grt 10**	**grt 11**	**grt L21**	**grt L22**		**grt L23**	**grt L24**		**grt L25**	**grt L26**	**grt L27**		**grt L28**	**grt L29**					
	grt-L16-1	**grt-8-1**	**grt-10-1**	**grt-11-1**	**grt-L21-1**	**L22-1**	**L22-2**	**grt-L23-2**	**grt-L24-1**	**grt-L24-2**	**grtL25-1**	**grt-L26-1**	**L27-1**	**L27-2**	**grtL28-2**	**grtL29-1**	**grtA-1**	**grtA-2**	**grtA-3**	**grtA-4**	**grtA-5**
comment																					
T Canil	1215	1025	1056	1059	1025	1032		1075	1151		1310	1329	1070		1060	1297					
T Griffi	1405	1046	1098	1104	1045	1057		1133	1276		1618	1664	1123		1107	1588					
Li	0.551	0.074	0.059	0.172	0.069	bdl	bdl	bdl	bdl	bdl	bdl	bdl	bdl	bdl	bdl	bdl	0.349	0.570	bdl	7.59	bdl
B	3.66	4.67	5.50	4.73	4.18	1.36	0.932	0.744	0.899	0.881	1.01	0.830	1.19	0.896	1.01	1.19	7.98	1.41	1.24	8.19	2.25
Sc	81.1	94.3	86.3	116	88.3	45.6	47.3	97.1	62.5	61.8	74.9	69.3	112	114	86.8	80.5	78.3	105	72.2	102	95.6
Ti	4274	379	102	345	376	1683	1703	382	1582	1619	5247	5559	525	548	432	4069	170	23317	18155	7490	11441
V	211	222	199	228	169	66.8	68.2	148	148	154	258	244	210	207	214	247	238	337	306	257	264
Co	42.9	40.8	42.1	42.8	41.5	81.0	81.9	42.9	71.3	71.7	57.4	50.9	44.2	44.9	46.2	49.7	53.0	56.5	55.7	56.7	58.4
Ni	103	43.9	51.1	51.9	43.7	45.6	45.2	56.3	79.8	79.6	148	158	54.9	54.7	52.3	141	142	86.5	100	96.2	114
Cu	0.499	0.224	0.580	bdl	0.610	0.789	0.497	0.421	bdl	0.087	0.528	0.619	bdl	bdl	bdl	0.415	0.95	1.18	0.871	1.59	0.50
Zn	15.1	9.37	8.48	10.4	9.22	93.8	100	8.16	20.3	21.3	28.7	19.4	8.71	9.23	9.68	16.7	16.2	19.2	18.8	20.7	18.7
Ga	na	na	na	na	na	8.88	8.93	1.95	8.83	9.04	13.64	12.74	2.39	2.40	3.66	12.2	na	21	22.9	14.3	17.9
Ge	na	na	na	na	na	1.85	1.92	1.23	1.66	1.64	2.05	1.82	1.50	1.49	1.46	1.85	na	2.41	1.70	2.36	2.24
Rb	0.028	0.062	0.045	0.041	0.026	bdl	bdl	bdl	bdl	bdl	bdl	bdl	bdl	bdl	bdl	bdl	0.082	0.018	bdl	0.835	bdl
Sr	0.507	1.63	0.682	0.76	0.365	1.46	2.59	2.34	0.201	0.208	0.908	0.569	0.422	0.463	0.809	0.664	0.654	0.448	0.284	14.6	0.331
Y	16.5	3.10	1.33	8.25	8.89	15.5	16.6	2.06	9.29	8.89	16.0	16.4	9.14	9.31	1.63	15.2	25.3	34.6	26.3	22.5	27.1
Zr	37.5	56.3	42.8	89.1	122	7.90	8.36	17.3	17.4	19.4	34.2	41.7	111	113	38.5	37.1	415	578	387	216	363
Nb	0.146	0.485	0.242	0.504	0.208	0.077	0.090	0.384	0.117	0.113	0.212	0.219	0.271	0.253	0.386	0.128	1.52	2.54	1.13	1.36	0.676
Mo	na	na	na	na	na	0.065	0.082	0.064	0.054	0.057	bdl	0.040	0.055	0.071	0.066	0.034	na	0.045	0.082	0.112	bdl
Cs	0.0052	0.0027	0.003	0.0055	bdl	bdl	bdl	bdl	bdl	bdl	bdl	bdl	bdl	bdl	bdl	bdl	0.0092	bdl	bdl	0.254	bdl
Ba	0.006	2.000	0.040	0.081	0.020	bdl	0.171	bdl	bdl	bdl	bdl	bdl	bdl	bdl	bdl	0.060	0.396	0.019	bdl	10.8	0.347
La	0.025	0.081	0.055	0.052	0.016	0.033	0.238	0.077	0.009	0.007	0.072	0.036	0.016	0.019	0.042	0.044	0.062	0.065	0.043	1.62	0.031
Ce	0.259	0.835	0.804	0.437	0.363	0.434	0.782	2.055	0.164	0.167	0.686	0.382	0.341	0.389	0.714	0.180	0.520	0.946	0.589	3.69	0.359
Pr	0.090	0.378	0.394	0.215	0.159	na	na	na	na	na	na	na	na	na	na	na	0.173	na	na	na	na
Nd	0.870	4.20	5.78	2.63	2.19	1.66	1.71	3.83	0.787	0.784	1.34	1.08	3.60	4.08	3.03	0.521	1.83	3.25	2.16	1.95	1.42
Sm	0.720	2.01	2.65	2.10	2.06	1.11	1.21	0.876	0.587	0.580	0.792	0.791	2.60	2.64	1.24	0.549	1.49	2.50	1.79	1.05	1.33
Eu	0.371	0.579	0.697	0.940	0.990	0.695	0.679	0.327	0.277	0.275	0.377	0.421	1.09	1.13	0.300	0.318	0.715	1.24	0.886	0.522	0.657
Gd	1.47	1.39	1.41	2.67	3.10	1.66	1.82	0.977	0.897	0.890	1.56	1.69	3.48	3.52	0.649	1.323	2.970	4.710	3.580	2.171	3.020
Tb	0.319	0.167	0.113	0.361	0.441	0.302	0.326	0.127	0.174	0.174	0.330	0.349	0.491	0.483	0.065	0.306	0.620	0.929	0.717	0.485	0.628
Dy	2.69	0.77	0.44	2.04	2.37	2.43	2.57	0.603	1.41	1.37	2.61	2.76	2.60	2.46	0.380	2.414	4.89	7.20	5.32	4.06	4.91
Ho	0.610	0.132	0.047	0.300	0.346	0.591	0.612	0.082	0.347	0.334	0.604	0.624	0.367	0.363	0.062	0.574	1.09	1.51	1.13	0.933	1.10
Er	1.94	0.343	0.094	0.700	0.750	2.00	2.08	0.156	1.13	1.07	1.89	1.90	0.793	0.758	0.190	1.784	3.210	4.27	3.08	2.93	3.30
Tm	0.299	0.050	0.012	0.095	0.072	0.331	0.349	0.016	0.188	0.184	0.298	0.292	0.096	0.093	0.029	0.282	0.490	0.614	0.424	0.440	0.484
Yb	2.14	0.405	0.095	0.513	0.530	2.75	2.78	0.097	1.48	1.39	2.22	2.100	0.551	0.589	0.306	2.09	3.380	4.31	2.83	3.14	3.38
Lu	0.340	0.063	0.026	0.089	0.082	0.444	0.453	0.018	0.234	0.218	0.326	0.319	0.080	0.087	0.059	0.306	0.471	0.587	0.384	0.479	0.501
Hf	0.930	1.09	0.690	1.51	1.91	0.106	0.108	0.363	0.302	0.368	0.885	1.02	2.08	2.02	0.694	0.976	9.920	13.9	9.34	4.91	8.17
Ta	0.016	0.033	0.038	0.045	0.019	0.011	0.010	0.019	0.014	0.016	0.015	0.018	0.014	0.017	0.018	0.006	0.359	0.668	0.219	0.063	0.123
Pb	0.0053	0.075	0.167	0.110	0.025	0.025	0.024	0.043	0.0034	0.0037	bdl	0.005	0.014	0.019	0.013	bdl	bdl	0.065	0.079	0.130	0.017
Th	0.0053	0.012	0.010	0.0089	0.0047	0.0017	0.021	0.031	0.0015	0.0009	0.0086	0.0056	0.0042	0.0046	0.0067	0.0066	0.043	0.083	0.040	0.205	0.019
U	0.0093	0.033	0.047	0.017	0.021	0.0030	0.011	0.087	0.0055	0.0058	0.013	0.011	0.026	0.028	0.029	0.0044	0.069	0.179	0.095	0.080	0.048

Table 6.7 P-T calculation for neoblastic grt-opx-ol paragenesis from polymict peridotite

Sample	grt-21, ol6, opx17	grt-21, ol6, opx17	grt-21, opx17	Grt2-Opx-8	Grt2-Opx-8	grtL-5, opxGS7a-2	grtL14-opx5	grtL-16-opx C
Locality	Boshof	Boshof	Boshof	Boshof	Boshof	Boshof	Boshof	Boshof
Type	polymict	polymict	polymict	polymict	polymict	polymict	polymict	polymict
T_{PRESET}	1100	1100	1100	1100	1100	1100	1100	1100
p_{PRESET}	35	35	35	35	35	35	35	35
Paragenesis	grt, ol, opx	grt, opx	grt, ol, opx	grt, opx	grt, opx	grt, opx	grt, opx	grt, opx
T [O'Neill]	1176	1057	1057					
T [Harley]	1129	1001	1222	1071	1091	1176	1077	1222
T [BK] Mg-Fe (gt-opx)	1122	1240	1060	1198	1186	1137	1167	1091
p [BKN]	41.9	39.2	28.2	35.4	34.3	33.3	35.4	36.1
p [NG]	43.9	40.8	30.6	37.8	36.5	35.6	37.8	38.4
p [MC]	41.1	41.5	34.0	37.8	35.7	38.5	37.7	40.8

T [O'Neill] – ol/grt (Fe-Mg) - O'Neill and Wood, 1979; T [Harley] opx/grt (Fe-Mg) - Harley, 1984; T [BK] - grt/opx (Mg-Fe) - Brey and Köhler, 1990;
p [BKN] – grt/opx - Brey and Köhler, 1990; p [NG] – grt/opx – Nickel and Green, 1985; p [MC] - grt/opx - McGregor, 1974.

SUPPLEMENTS

Acknowledgements

After five years of work on this PhD and when it is finally completed, I would like to thank to all of you that have directly or indirectly followed and supported me and my project.

First of all I would like to acknowledge Gerhard Brey for seeing and believing in my potential and selecting me to work on this project. Many thanks for your supervision, for lively discussions on the data and for being optimistic about the obtained results, even when I was dissatisfied. Thank you for organising my financial support at the beginning of my stay in Frankfurt and during the last months, and also for keeping the pleasant atmosphere at the institute, during the working time and during many parties and "Grill" sessions. I would also like to express my gratitude for you organising my field trip to the South Africa, for the sample collection, and for all conferences and meetings in Germany, China, Australia you let me go, and where I had the opportunity to present and discuss my on going project with other researches.

Stefan, I would like to thank you for teaching me to work on a Neptune, for helpful discussions about my obtained results, and for many ours you have spent on reading and correcting this manuscript. Many thanks for the German translation of the "Zusammenfassung". I would also like to thank you for all the nice time we spent together; which made me feel much more comfortable here in Germany.

Alan, your enthusiasm about oxidation state of the mantle went on me to. That is how I decided to do the Mössbauer analyses on my garnets. Therefore, I would like to thank you for analysing garnets (by Mössbauer) for my work and the helpful discussions of that data.

Many thanks to Heidi and Yann for the technical support (EPMA and LA-ICP-MS, respectively) and useful advices during the measurement time and processing the data. Thank you for sharing your knowledge, that goes beyond the simple measurement (setting the instrument, standardisation, dealing with the technical problems, …).

Frank, thank you for support by investigating the polymict breccia.

Dmitri, several good tips and instructions about my rutile bearing sample and in preparation of mineral separates helped a lot to be sufficient in my further work. Thanks for that and for many interesting discussions.

Part of the samples I worked on where supplied from other working groups, and I would like to use this opportunity to thank F. Viljoen (Johannesburg), T. Stachel (Edmonton) and H. Grütter (Vancouver) for providing these samples to me. Also, many thanks for discussions. At this place I would like to thank J. vA. Robey for the nice three day tour on the Kimberley mine dumps (South Africa), where Gerhard and I have enlarged our sample collection.

I gratefully acknowledge J. Harris for organising my visit to the Finsch mine dump and for his personal help in collecting subcalcic garnets (on his knees). Many thanks also to J. Ekkerd and the De Beers company for their support during field work at the Finsch mine.

An euch alle, die ich während meiner 5 Jahre am Mineralogiesche Institute Frankfurt getroffen habe: Axel, Kai, Soodabhe, Michael, Anna, Heidi, Yann, Franz, Jan, Thomas, Sabine, Chris, Adele, Vadim, Andrei, Sina, Iris, Holger, Stephan, Pedro, Aleksandra, Margaret, Alex, Bana, Eveline, Silvia, Klaus, Carolina… - vielen, vielen Dank für die freundliche (freundschaftliche) Atmosphäre und eure Unterstützung in all dieses Jahren. Anna, herzlichen Dank, dass du mir die erste Schritte im „clean lab" beigebracht hast, und für die stetige Unterstützung bei der Laborarbeit. Außerdem, danke ich dir dafür, meine Deutsche-Finnische Mutter zu sein. Jan, vielen Dank für alle durchgesägten Xenolithe und alle Dick- und Dünnschliffe, die du für mich und meine Arbeit angefertigt hast. Thomas, du hast mich immer gerettet, wenn ich irgendwelche Computerprobleme hatte – vielen Dank!

Soodabeh, thank you for being a good friend, always ready to help, listen and give an advice. You, being also a foreigner in Germany, but with the longer residence here, have helped me a lot to understand German habits and therefore made my stay in Frankfurt more comfortable.

Many thanks to Axel for giving me good advices in several fields, including e.g. chromatographic procedures or dealing with the German administration. Sharing office for almost three years with you

and Kai made my stay at this Institute more cheerful, especially when you made jokes about "my German" and my afternoon snacks ☺.

Michael and Sabine, you took me as a friend and showed me to feel the life of the German family. It is very pleasant and refreshing doing things with you, grill parties, going to the cinema, "Palmengarden", … Michael thank, you for proceeding and measuring Li isotopes in orthopyroxenes from my samples.

Iris, thank you for being a friend during my stay in Germany and for the pleasant sharing accommodation during our conference visits. Also, thank you for giving me a lift home, with all my suitcases, on my first arrival in Frankfurt.

Такође бих желела да се захавлим Владици који ме је увео у свет „литосферског омотача" - без тебе никада не бих дошла до Франкфурта и не бих радила на овако обимном и узбудљивом пројекту. Пуно хвала на интересовању, коментарима и дискусији везаним за мој докторат. Владице, Кристина, од срца вам захваљујем на речима подршке и пријатељству током свих ових година. Крис, жао ми је што ниси успела да ме посетиш за сво ово време – то ћемо морати да надокнадимо.

Пуно хвала свим мојим пријатељима у Србији: Мими, Сандри и Милошу, Аци и Марији, Милану, Ђури, Аци П., који су били и остали добри пријатељи свих ових година. Ваше кратке посете Франкфурту и наши кратки сусрети у Србији су ме увек увесељавали, освежавали и давали снаге да наставим. Пуно вам хвала на интересовању и пријатељству.

Захвална сам и вама пријатељима из Србије, сада расутим по Европи: Милици, Дејану и Ирени, Зорану, Мирјани и Млађану, Владани, што сте увек били спремни да помогнете било корисним саветима, било опуштајућим разговорима или добром српском кухињом. Ви и сами знате да није лако бити далеко од „куће" и да је увек пријатно осетити мало српске топлине у белом свету. Дејане, хвала на дискусији и заинтересованости везаној за мој пројекат.

Александра, франкфуртски староседеоче српског порекла, хвала и теби на шаци топлог разговора и савета, али и на помоћи када ми је то било важно (вожња до лекара, зубара, ...).

На крају бих желела да се захвалим и мојој породици. Вера, Власто, Мићо, пуно вам хвала што сте увек били уз мене, макар и у мислима, и што сте увек имали речи подршке, савета и љубави. То ми је уливало снагу свих ових година. Без вас сигуно не бих постала оваква особа. Знам да сте поносни на мене што сам завршила овај докторат, што мене такође чини још поноснијом.

This research and my stay in Frankfurt were carried out with the financial support of the Royal Family Karadjordjevic foundation, of the "Deutsche Austausch Dienst" (DAAD) and the "Deutsche Forschungsgemeinschaft" (DFG).

CV:

Personal details:

Name: **Lazarov**
First name: **Marina**
Sex: Female
Address: Am Wiesenrain 14
60431 Frankfurt am Main,
Germany
Telephone: 069/798-40151
E-mail: marina@em.uni-frankfurt.de
Date of birth: 29.06.1978.
City of birth: Pancevo,
Country of birth: Serbia (former Yugoslavia)

Education:

2003-2008 PhD program at the J.W. Goethe University in Frankfurt am Main, Germany.
Department: Mineralogy (*Petrology and Geochemistry).* Project title: "Archean to present day evolution of the lithospheric mantle beneath the Kaapvaal craton - Processes recorded in subcalcic garnets, peridotites and polymict breccia "
Supervisor: Prof. Dr. G. Brey

2002-2003 MSc program at Faculty of Mining and Geology at the University of Belgrade, Serbia
Department: Petrology of igneous and metamorphic rocks
Supervisor: Prof. Dr. V. Cvetkovic

1997-2002 Graduated from the Faculty of Mining and Geology at the University of Belgrade, Serbia
Section: Geology,
Department: Petrology and Geochemistry,
Final thesis*:* "Characteristics of the mantel xenoliths enclosed in Paleogene basanites from Sokobanja, East Serbia"
Supervisor: Prof. Dr. V. Cvetkovic

1993-1997 Secondary school "Uros Predic" in Pancevo, Serbia.

Awarded grants:

Oct. 2004- July. 2005 DAAD scholarship for studies at the Institute of Mineralogy, J.W. Goethe University, Frankfurt, Germany.

Sept. 2003- Sept. 2004 One-year grant from the Royal Family Karadjordjevic Foundation for studies at the Institute of Mineralogy, J.W. Goethe University, Frankfurt, Germany.

2002 By the Royal Family Karadjordjevic Foundation as one of 100 best students in all fields from all Universities in Yugoslavia (Serbia). I was the only awarded student from the Faculty of Mining and Geology for that year.

2002 Best student at the Faculty of Mining and Geology, Belgrade, Serbia.

2001 By the Royal Norwegian Embassy as one of 500 best students in all fields from all Universities in Serbia.

Profesional experience:

July 2005- March 2008 „Wissenschaftliche Mitarbeiterin" at the University of Frankfurt, Institute of Geosciences (funded by the Deutsche Forschungsgemeinschaft).

List of Publication:

- Lazarov, M., Brey, G.P., Weyer, S., Time steps of depletion and enrichment in the Kaapvaal craton as recorded by subcalcic garnets from Finsch (SA) (submitted to Earth and Planetary Science Letters).
- Cvetkovic, V., Lazarov, M., Downes, H. and Prelevic, D., 2007. Modification of the subcontinental mantle beneath East Serbia: Evidence from orthopyroxene-rich xenoliths. Lithos, 94(1-4): 90-110.
- Cvetkovic, V., Downes, H., Prelevic, D., Lazarov, M. and Resimic-Saric, K., 2007. Geodynamic significance of ultramafic xenoliths from Eastern Serbia: Relics of sub-arc oceanic mantle? Journal of Geodynamics, 43(4-5): 504-527.
- Cvetkovic, V., Downes, H., Prelevic, D., Jovanovic, M., Lazarov, M., 2004. Characteristics of the lithospheric mantle beneath East Serbia inferred from ultramafic xenoliths in Palaeogene basanites, Contrib. Mineral. Petrol. 148, 335-357.

***Abstracts and extended abstracts at international conferences*:**

- Lazarov, M., Brey, G.P., Harris, J.W. and Weyer, S., 2007. Timing of mantle depletion and enrichment from single subcalcic garnet grains (Finsch mine, SA). Geochimica Et Cosmochimica Acta, 71(15): A551-A551.
- Lazarov, M., Brey, G. and Lahaye, Y., 2006. Mapping of the Kaapvaal craton lithosphere with garnets from a polymict peridotite. Geochimica Et Cosmochimica Acta, 70(18): A345-A345.
- Downes, H., Cvetkovic, V., Hock, V., Prelevic, D. and Lazarov, M., 2006. Refertilization of highly depleted lithospheric mantle (Balkan peninsula, SE Europe): Evidence from peridotite xenoliths. Geochimica Et Cosmochimica Acta, 70(18): A146-A146.
- Lazarov, M., Brey, G., Lahaye, Y., 2005. Explosive brecciation and chemical overprint of deep mantle section, Berichte der Deutschen Mineralogischen Ges., Beih. Z. Eur. J. Mineral. Vol. 17, 82.
- Lazarov, M., Weyer S., Bouman, C., Schwieters, J., Brey, G., 2004. Hf-isotope measurements at ppt concentration levels with multi ion counting ICP-MS, Geochemica et Cosmochemica Acta, 68, International V.M. Goldschmidt Conference.
- Lazarov, M., Brey, G., 2004. The deep roots of the Kaapvaal craton: evidence from the Finsch xenoliths, Berichte der Deutschen Mineralogischen Ges., Beih. Z. Eur. J. Mineral. Vol.16, 81.
- Cvetković, V., Poli, G. Resimic-Šaric, K., Prelević, D., Lazarov, M., 2002. Tertiary post-collision granitoid of Mt. Kopaonik (Serbia) - petrogenetic constraints based on new geochemical data. Proceedings of the XVIIth Congress of CBGA, Bratislava, September 1-4, CD-version.